



UNIVERSIDAD NACIONAL AUTÓNOMA DE MÉXICO
FACULTAD DE QUÍMICA

**COMPUESTOS DE Cu(II) CON LOS HETEROCICLOS
ALOPURINOL, HIPOXANTINA, 6-MERCAPTOPURINA,
PIRAZOL Y 3,5-DIMETILPIRAZOL.**

TESIS QUE PRESENTA

RODOLFO ACEVEDO CHÁVEZ

PARA OBTENER EL GRADO DE:

DOCTOR EN CIENCIAS QUÍMICAS

(QUÍMICA INORGÁNICA)

1997

M-249897



Universidad Nacional
Autónoma de México

Dirección General de Bibliotecas de la UNAM

Biblioteca Central



UNAM – Dirección General de Bibliotecas
Tesis Digitales
Restricciones de uso

DERECHOS RESERVADOS ©
PROHIBIDA SU REPRODUCCIÓN TOTAL O PARCIAL

Todo el material contenido en esta tesis esta protegido por la Ley Federal del Derecho de Autor (LFDA) de los Estados Unidos Mexicanos (México).

El uso de imágenes, fragmentos de videos, y demás material que sea objeto de protección de los derechos de autor, será exclusivamente para fines educativos e informativos y deberá citar la fuente donde la obtuvo mencionando el autor o autores. Cualquier uso distinto como el lucro, reproducción, edición o modificación, será perseguido y sancionado por el respectivo titular de los Derechos de Autor.

Supervisor de Tesis Doctoral:

Dr. Roberto Escudero Derat.
Instituto de Investigaciones en Materiales, UNAM.

JURADO

Presidente: Dr. Jacobo Gómez Lara.
Universidad Nacional Autónoma de México.

Primer Vocal: Dra. Lena Ruíz Azuara.
Universidad Nacional Autónoma de México.

Segundo Vocal: Dr. Hugo Torrens Miquel.
Universidad Nacional Autónoma de México.

Tercer Vocal: Dr. Tetsuya Ogura Fujii.
Universidad Autónoma de Guadalajara.

Secretario: Dr. Anatoli Iatsimirski.
Universidad Nacional Autónoma de México.

Suplente: Dr. Gunther Geissler Dahlheim.
Universidad Autónoma de Puebla.

Suplente: Dra. Leticia Lomas Romero.
Universidad Autónoma Metropolitana.



CONTENIDO

Reconocimientos.

Precisiones.

Resumen.

CAPÍTULO I. Antecedentes.

CAPÍTULO II. Problemas, Considerandos y Propuesta.

CAPÍTULO III. Objetivos.

CAPÍTULO IV. Metodologías.

CAPÍTULO V. Resumen de Resultados y Discusión.

- Va.** Algunos estudios sobre la preparación y caracterización del compuesto polinuclear $\text{Cu(II)(alopurinolato}^-\text{)(OH}^-\text{)}$.
- Vb.** Estudios sobre la preparación y caracterización de los compuestos polinucleares $\text{Cu(II)(pirazolato}^-\text{)(OH}^-\text{)}$ y $\text{Cu(II)(3,5-dimetilpirazolato}^-\text{)(OH}^-\text{)}$.
- Vc.** Algunos estudios sobre la preparación en medio acuoso ácido y la caracterización de compuestos de Cu(II) con los ligantes heterocíclicos respectivos alopurinol e hipoxantina.
- Vd.** Estudios sobre la preparación y caracterización del compuesto polinuclear $\text{Cu(II)(6-mercaptopurinolato}^{2-}\text{)}$.
- Ve.** Estudios sobre la preparación en CH_3OH y la caracterización de compuestos de Cu(II) con los heterociclos respectivos alopurinol, hipoxantina y 6-mercaptopurina. Parte I.
- Vf.** Estudios sobre la preparación en CH_3OH y la caracterización de compuestos de Cu(II) con los heterociclos respectivos alopurinol, hipoxantina y 6-mercaptopurina. Parte II.
- Vg.** Estudios teóricos preliminares a nivel de Teoría de Funcionales de la Densidad, sobre la Estabilidad Energética, las Propiedades Moleculares y de Estructura Electrónica de algunos Tautómeros Cetónicos de los Heterociclos Alopurinol e Hipoxantina.
- Vh.** Estudios teóricos a nivel de Teoría de Funcionales de la Densidad, sobre la Estabilidad Energética, las Propiedades Moleculares y de Estructura Electrónica de los Tautómeros del Heterociclo Hipoxantina.

CAPÍTULO VI. Conclusiones y Sugerencias.

CAPÍTULO VII. Manuscritos Anexos.

1. Rodolfo Acevedo-Chávez, Maria Eugenia Costas and Roberto Escudero Derat. *Antiferromagnetic Coupling in the Polinuclear Compound $[Cu(II)(Alopurinolate)(OH^-)]_n$.*
2. Rodolfo Acevedo-Chávez, Maria Eugenia Costas and Roberto Escudero Derat. *Antiferromagnetic coupling in the Cyclic Octanuclear Compound $[Cu(II)(\mu-3,5\text{-dimethylpyrazolate})(\mu-OH)]$ and its analogue $[Cu(II)(\mu\text{-pyrazolate})(\mu-OH)]$.*
3. Rodolfo Acevedo-Chávez, Maria Eugenia Costas and Roberto Escudero Derat. *Allopurinol- and Hypoxanthine- Copper(II) Compounds. Spectral and Magnetic Studies of Novel Dinuclear Coordination Compounds with Bridging Hypoxanthine.*
4. Rodolfo Acevedo-Chávez, Maria Eugenia Costas and Roberto Escudero Derat. *Magnetic Study of the Novel Polynuclear Compound $[Cu(II)(6\text{-mercaptapurinolate}^{2-})_n$.*
5. Rodolfo Acevedo-Chávez and Maria Eugenia Costas. *Spectral and Magnetic Characterization of Novel Cu(II) Coordination Compounds Synthesized in Methanolic Medium with the Heterocycles Allopurinol, Hypoxanthine and 6-mercaptapurine. Part I.*
6. Rodolfo Acevedo-Chávez and Maria Eugenia Costas. *Spectral and Magnetic Characterization of Novel Cu(II) Coordination Compounds Synthesized in Methanolic Medium with the Heterocycles Allopurinol, Hypoxanthine and 6-mercaptapurine. Part I.*
7. María Eugenia Costas, Estrella Ramos and Rodolfo Acevedo-Chávez. *Density Functional Study of Purine-type Heterocycles: Allopurinol and Hypoxanthine.*
8. María Eugenia Costas and Rodolfo Acevedo-Chávez. *DFT Study of the Neutral Hypoxanthine Tautomeric Forms.*

RECONOCIMIENTOS.

Las reacciones Químicas de centros metálicos con heterociclos y la caracterización de los compuestos de coordinación respectivos, es uno de los temas que desarrolla Rodolfo Acevedo Chávez en la Universidad Autónoma de Puebla desde 1989, y como parte de su trabajo académico.

Los estudios magnéticos experimentales de los compuestos de Cu(II) abordados en este trabajo, han sido efectuados bajo la supervisión y colaboración del Dr. Roberto Escudero Derat, supervisor de la Tesis Doctoral, en el Instituto de Investigaciones en Materiales, UNAM.

Los estudios magnéticos teóricos de los compuestos de Cu(II) referidos y los estudios teóricos sobre los heterociclos centrales en este trabajo, han sido efectuados en colaboración con la Dra. María Eugenia Costas Basin, en la Facultad de Química, UNAM.

Por su espíritu indeclinable de trabajo, de ayuda siempre incondicional y desinteresada, y de colaboración que supera lo notable, dichos investigadores de la UNAM aparecen intachablemente en los manuscritos que han resultado de un programa de investigación y de varios estudios de colaboración, los cuales constituyen la columna vertebral de este trabajo de Tesis Doctoral.

Rodolfo Acevedo Chávez
Marzo, 1997.

PRECISIONES.

- ◆ La síntesis química de los compuestos de coordinación estudiados en este trabajo fue realizada en un cubículo del Centro de Química, ICUAP.
- ◆ La mayoría de las determinaciones instrumentales correspondientes, fue realizada en laboratorios de otras Instituciones Públicas de Educación Superior del país, ó en laboratorios comerciales.
- ◆ La etapa última de la caracterización de los compuestos, y la escritura de los manuscritos correspondientes (y que aparecen en este trabajo), fueron realizados en la Facultad de Química de la UNAM. La etapa última de caracterización y la totalidad de los manuscritos, fueron producto de una estancia sabática en el Departamento de Física y Química Teórica, de la Facultad de Química de la UNAM.
- ◆ Los estudios teóricos que aparecen en este trabajo, fueron resultado también de dicha estancia sabática, y fueron realizados con recursos de cómputo de la DGSCA, UNAM.
- ◆ La escritura de los manuscritos de los estudios teóricos, así como del trabajo de Tesis, fueron realizados en una extensión de la estancia sabática en el Departamento de Física y Química Teórica, de la Facultad de Química de la UNAM.

La edición final de este trabajo, estuvo a cargo de la Dra. María Eugenia Costas Basin (Departamento de Física y Química Teórica, de la Facultad de Química de la UNAM), quien ha sido anfitriona en la estancia sabática y extensión de la estancia académica, y colaboradora de proyectos.

Rodolfo Acevedo Chávez
Marzo, 1997.



RESUMEN.

Los heterociclos alopurinol, hipoxantina y 6-mercaptapurina son moléculas de interés diverso. La presencia en sus estructuras de varios átomos que pueden reaccionar con ácidos de Lewis, y el hecho mismo de presentar en disolución procesos tautoméricos, le confiere a estos sistemas propiedades fisicoquímicas de gran complejidad, así como también, y por ejemplo, una riqueza notable en sus reacciones con centros metálicos de transición.

Con la intención de explorar la conducta de estos tres heterociclos ante un centro metálico de transición común y bajo condiciones experimentales de reacción modificadas en forma sistemática, se realizaron las reacciones respectivas Metal-Heterociclo en dos disolventes (H_2O , $pH=1$; CH_3OH). En éstas, se modificó en forma sistemática la naturaleza del contraión ($X=Cl^-$, Br^- , NO_3^- , SO_4^{2-} , ClO_4^- y $CH_3CO_2^-$) presente en las sales metálicas. También se exploraron en forma sistemática las reacciones de sustitución heterocíclica, y las de competencia heterocíclica simultánea ante el centro metálico.

De las reacciones realizadas y para el caso del alopurinol ($=L_1$) se obtuvieron los compuestos del tipo $Cu(II)(L_1)_2(X)_2$ ($X=Cl^-$, Br^- , NO_3^-), $Cu(II)(L_1)_4(ClO_4^-)_2$, $Cu(II)(L_1)(SO_4^{2-})(H_2O)$ y $Cu(II)(L_1^-)(OH^-)$. En relación a este último compuesto y en otro estudio, se obtuvieron los compuestos $Cu(II)(pirazolato^-)(OH^-)$ y $Cu(II)(3,5-dimetilpirazolato^-)(OH^-)$. En relación a la hipoxantina ($=L_2$), se obtuvieron los compuestos del tipo $Cu(II)(L_2)_2(X)_2$ ($X=Cl^-$, Br^- , NO_3^- , ClO_4^-), $[Cu(II)(L_2)_2(X)]_2^{2+}(X)_2$ ($X=NO_3^-$, ClO_4^-), $[Cu(II)(L_2)_2(X)]_2$ ($X=SO_4^{2-}$), $Cu(II)(L_2)(SO_4^{2-})(H_2O)$ y $Cu(II)(L_2^-)(CH_3CO_2^-)$. Por último y en relación a la 6-mercaptapurina ($=L_3$), se obtuvieron los compuestos del tipo $Cu(II)(L_3)_n(X)_2$ ($X=Cl^-$, $n=1$; $X=Br^-$, $n=2$) y $Cu(II)(L_3^{2-})$.

Así también y de las reacciones realizadas, la capacidad de competencia heterocíclica por el centro metálico y la capacidad coordinante a $Cu(II)$ sigue el orden general $L_3 > L_1 > L_2$. Los estudios permiten proponer que los heterociclos alopurinol e hipoxantina se coordinan a $Cu(II)$ por átomos de N (N(2) para L_1 , N(1) y N(2) para L_1^- ; N(7), N(3) y N(7), N(3) y N(9) para L_2) presentando ambos la forma cetónica. Para la 6-mercaptapurina, la participación del átomo S exocíclico es preponderante en la coordinación metálica sugerida (S(6) ($X=Cl^-$), S(6) y N(7) ($X=Br^-$) con la forma tiona en ambos casos; S(6), N(7), N(9) para L_3^{2-}).

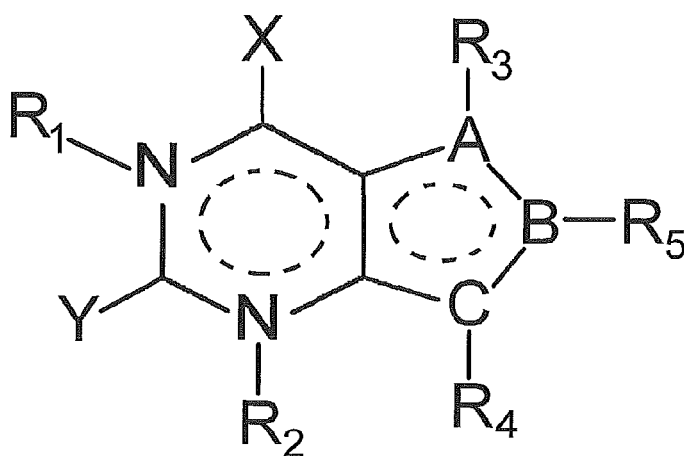
Los estudios espectrales y magnéticos permiten plantear la existencia predominante de acoplamiento antiferromagnético muy débiles entre espines de $Cu(II)$ para los productos del tipo $Cu(II)(L)_2(X)_2$ ($L=alopurinol$ ó $hipoxantina$; $X=Cl^-$, Br^- , NO_3^- , ó ClO_4^-), $Cu(II)(L_1)_4(ClO_4^-)_2$, $Cu(II)(L)(SO_4^{2-})(H_2O)$ ($L=alopurinol$ ó $hipoxantina$), $Cu(II)(L_2^-)(CH_3CO_2^-)$, $Cu(II)(L_3)_n(X)_2$ y $Cu(II)(L_3^{2-})$. En dicha conducta magnética, los ligantes aniónicos no heterocíclicos (y en algunos casos los heterocíclicos también) son considerados a participar en la construcción de las trayectorias respectivas de intercambio magnético. Los mismos estudios permiten plantear la existencia de acoplamiento antiferromagnético intensos para los sistemas $Cu(II)(L_1^-)(OH^-)$, $Cu(II)(pirazolato^-)(OH^-)$, $Cu(II)(3,5-dimetilpirazolato^-)(OH^-)$, $[Cu(II)(L_2)_2(X)]_2^{2+}(X)_2$ y $[Cu(II)(L_2)_2(X)]_2$. Para los tres primeros sistemas, la construcción de la trayectoria respectiva del intercambio magnético se asocia a los heterociclos y grupos OH^- . Para los dos tipos de sistemas restantes, dicha trayectoria se asocia al heterociclo hipoxantina.

Por último, los cálculos teóricos realizados sobre los heterociclos alopurinol, hipoxantina y 6-mercaptapurina, permiten plantear que los tautómeros energéticamente más estables son $\underline{\text{N}}(1)\text{-H}/\underline{\text{N}}(5)\text{-H}$ y $\underline{\text{N}}(2)\text{-H}/\underline{\text{N}}(5)\text{-H}$ para el alopurinol, $\underline{\text{N}}(1)\text{-H}/\underline{\text{N}}(7)\text{-H}$ y $\underline{\text{N}}(1)\text{-H}/\underline{\text{N}}(9)\text{-H}$ para la hipoxantina y la 6-mercaptapurina. Estos tautómeros también son predominantes en disolución, y la mayoría de ellos se presentan en los compuestos de Cu(II) obtenidos. Los cálculos teóricos han permitido obtener también información referente a otras propiedades moleculares y de estructura electrónica, que pudieran estar asociadas parcialmente a su conducta en disolución, así como a sus reacciones con centros metálicos de transición.

CAPÍTULO I

Antecedentes.

Los estudios que constituyen este trabajo, están asociados a heterociclos que corresponden a varios grupos. Entre ellos, se pueden citar a las azinas, los azoles ó las pirimidinas. En particular, los heterociclos presentan en su estructura pirimidinas unidas a azoles. En la figura siguiente se muestra la estructura general simplificada de este tipo de sistemas.



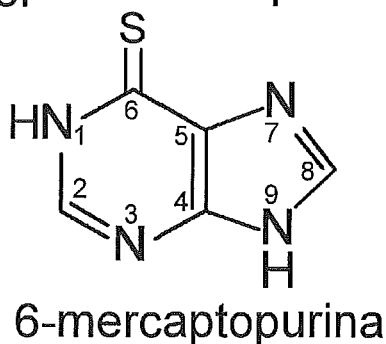
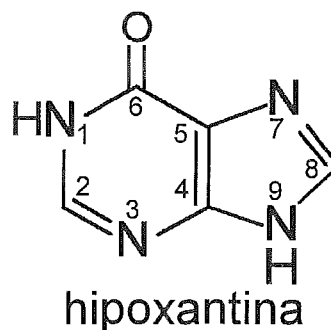
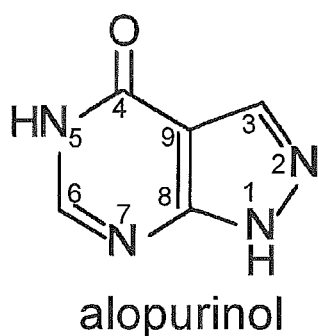
$X, Y = O, S, Se, \dots$

$A, B, C = C, N$

$R_i = H, \dots$

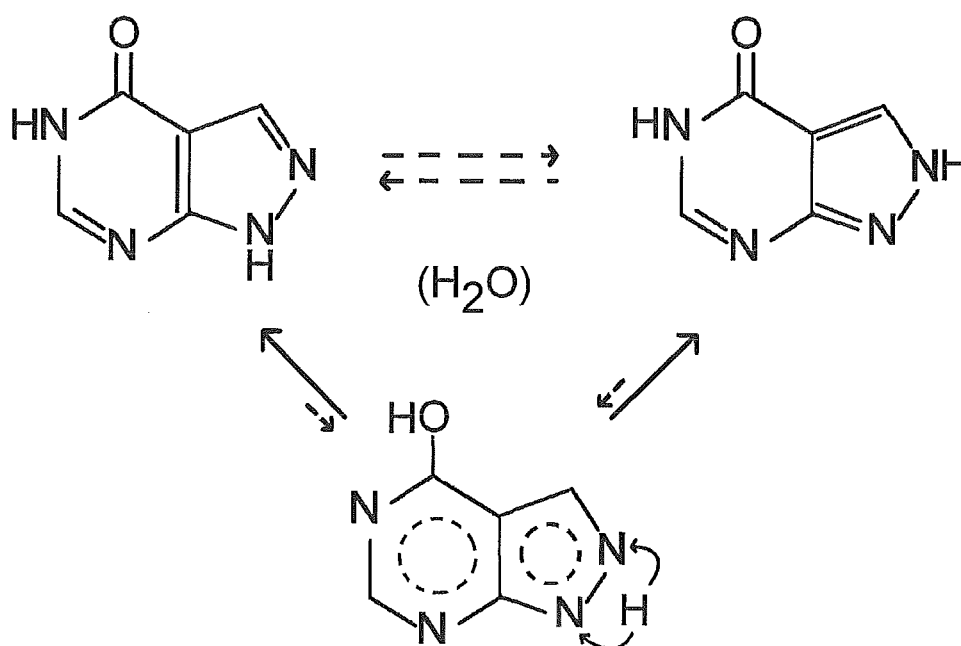
Este tipo de heterociclos son de interés notable en temas diversos. Algunos ejemplos son: en síntesis heterocíclica¹, en estudios biomédicos², en investigaciones sobre ácidos nucleicos y código genético^{3,4}, en estudios sobre secuencia, estructura y función de ácidos nucleicos⁵, en estudios farmacológicos⁶⁻⁸, en estudios sobre sitios catalíticos y mecanismos de catálisis enzimática⁹⁻¹⁴, en estudios fisicoquímicos en estado gaseoso y en disolución^{15,16}, como sistemas ideales a ser empleados en estudios teóricos sobre fenómenos en disolución¹⁷, y en química de coordinación¹⁸.

Los tres heterociclos de estudio central en este trabajo se presentan en la figura siguiente, bajo las formas cetónica (alopurinol e hipoxantina) y tiona (6-mercaptopurina), y tautómeros $\underline{N}(1)\text{-H}/\underline{N}(5)\text{-H}$ y $\underline{N}(1)\text{-H}/\underline{N}(9)\text{-H}$.

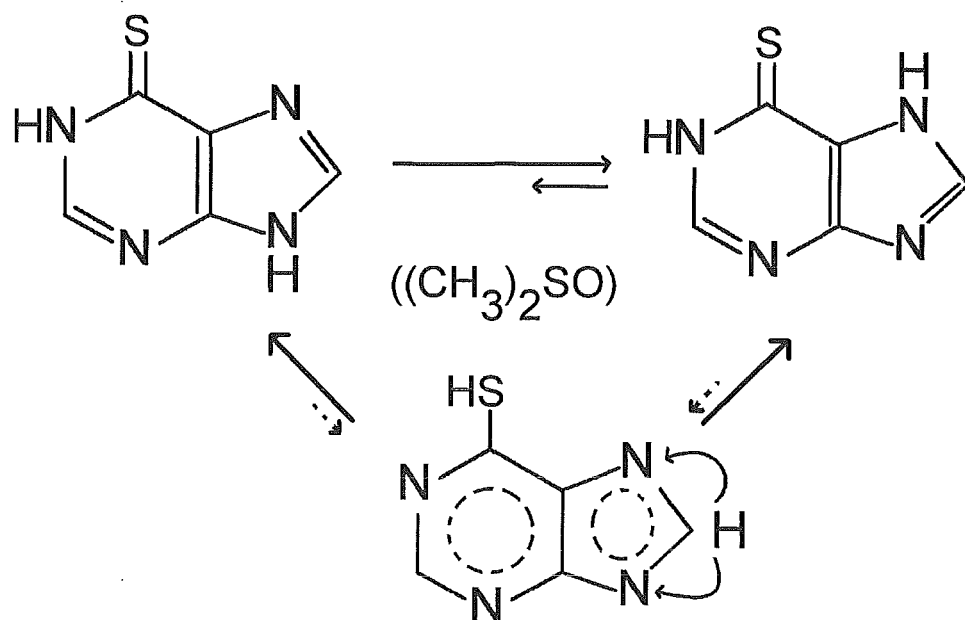
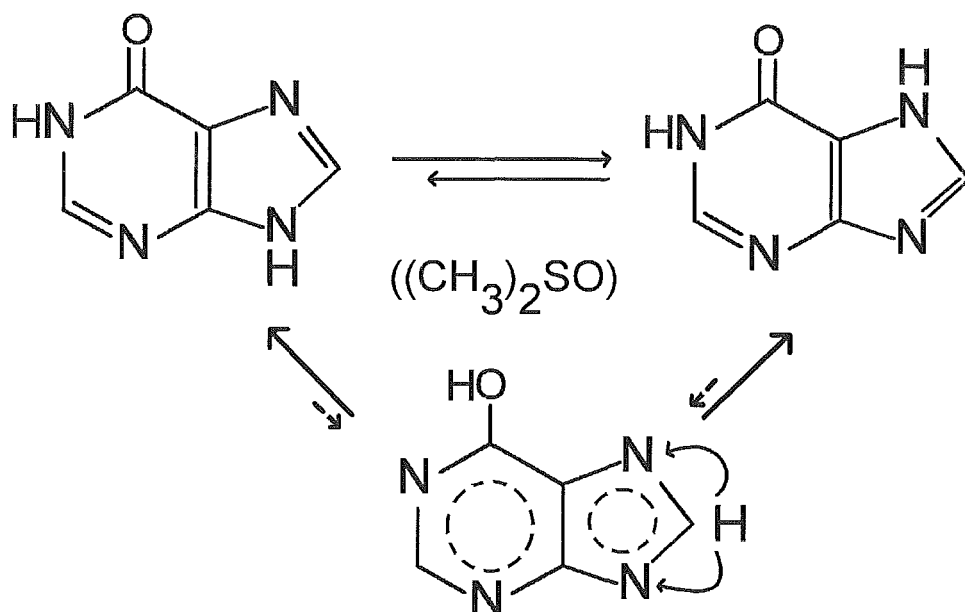


Aquí es necesario aclarar, que el tautomerismo que involucra tanto al intercambio de un átomo de H entre el átomo exocíclico y un átomo de N del anillo pirimidínico, como al intercambio de un átomo de H entre átomos de N en el anillo de cinco miembros, es parte de la característica inherente a los heterociclos pertenecientes a los grupos ya citados y mostrados en la primera figura.

En particular y para el caso del alopurinol, este fenómeno ha sido evidenciado en estudios espectroscópicos del heterociclo en disolución¹⁹⁻²¹. En la figura siguiente se ilustra esquemáticamente el equilibrio tautomérico y las especies predominantes del alopurinol en disolución acuosa.



El tautomerismo también ha sido evidenciado en estudios espectroscópicos de disoluciones de hipoxantina^{15,22,23} y de 6-mercaptapurina^{15,23,24-27}. En las dos figuras siguientes se ilustra esquemáticamente los equilibrios y las especies predominantes de estos dos heterociclos en disoluciones de $(\text{CH}_3)_2\text{SO}$.



En relación al tema del tautomerismo en este tipo de heterociclos, y en particular para el alopurinol, la hipoxantina y la 6-mercaptapurina, los estudios apuntan a que las poblaciones relativas de las especies predominantes son dependientes de la constante dieléctrica del disolvente. Sin embargo y para cada uno de estos heterociclos no parecen existir a la fecha estudios sistemáticos al respecto. Tampoco se sabe cabalmente cuál es el efecto de la temperatura sobre el fenómeno, ni mucho menos sobre el mecanismo de éste, y a qué factores se asocia.

El tautomerismo en estos tres heterociclos, ha sido tema de estudios teóricos, predominando en éstos los cálculos de energías moleculares y de propiedades de ciertos tautómeros en estado aislado.

Para el alopurinol, los cálculos²⁸⁻³² teóricos permiten sugerir que los dos tautómeros energéticamente más estables del heterociclo neutro y aislado, son el $\underline{\text{N}}(1)\text{-H}/\underline{\text{N}}(5)\text{-H}$ y el $\underline{\text{N}}(2)\text{-H}/\underline{\text{N}}(5)\text{-H}$. Cálculos teóricos considerando efectos del disolvente H_2O ²⁹, y cálculos teóricos realizados en la interpretación de estudios espectroscópicos del alopurinol en disolución acuosa³⁰, apuntan al mismo resultado.

En el caso de la hipoxantina, los estudios teóricos^{22,28,29,31-41} permiten sugerir que los dos tautómeros energéticamente más estables del heterociclo neutro y aislado, son el $\underline{\text{N}}(1)\text{-H}/\underline{\text{N}}(7)\text{-H}$ y el $\underline{\text{N}}(1)\text{-H}/\underline{\text{N}}(9)\text{-H}$. Estudios teóricos considerando efectos del disolvente H_2O ^{29,40} están de acuerdo con los mismos resultados.

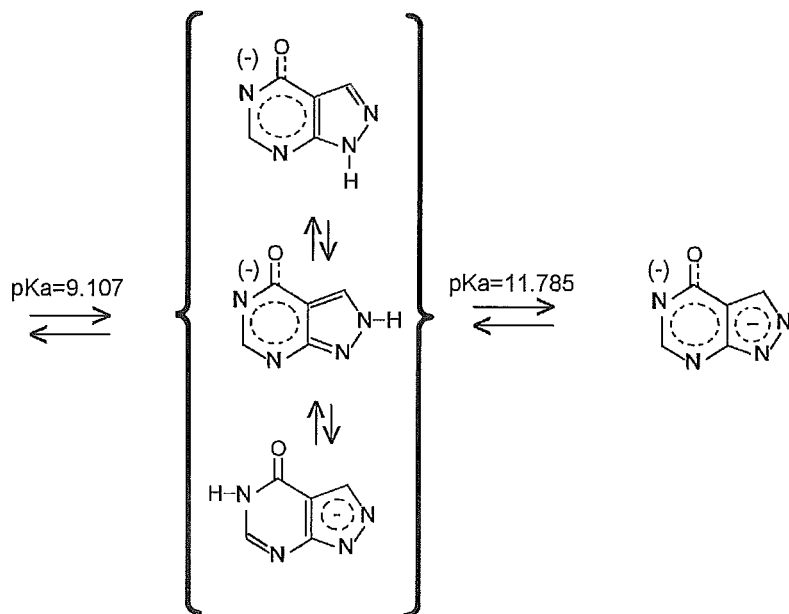
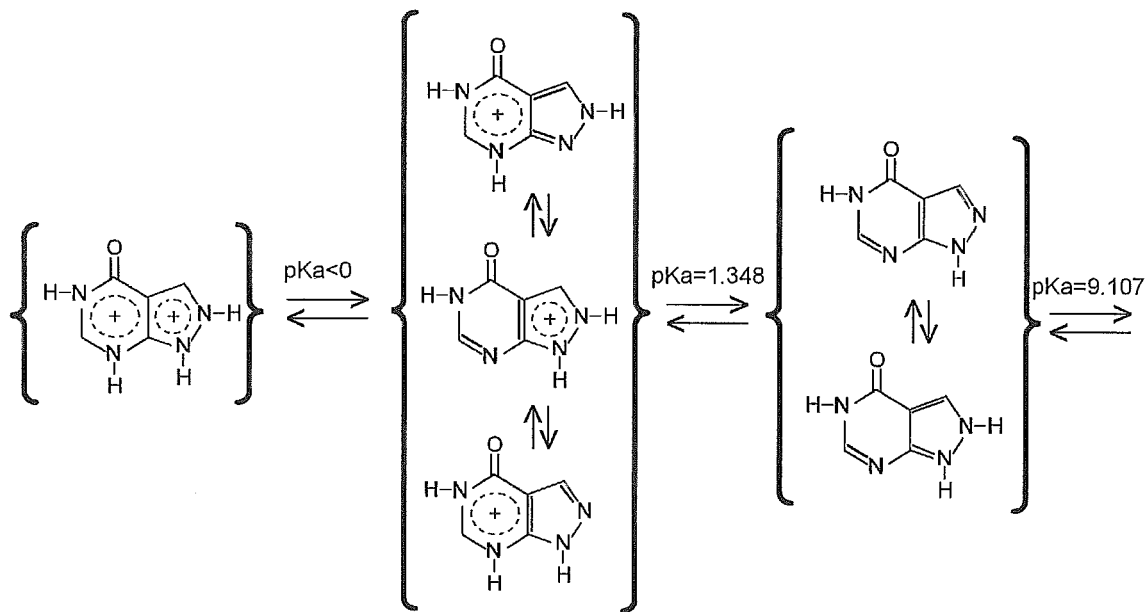
Por último y en relación a la 6-mercaptapurina, los estudios teóricos^{22,27,37,42} permiten sugerir que los dos tautómeros energéticamente más estables del heterociclo en estado neutro y aislado, son el $\underline{\text{N}}(1)\text{-H}/\underline{\text{N}}(7)\text{-H}$ y el $\underline{\text{N}}(1)\text{-H}/\underline{\text{N}}(9)\text{-H}$. Estudios teóricos²⁷ realizados en la interpretación de estudios espectroscópicos de la 6-mercaptapurina en disolución acuosa, están de acuerdo con dichos resultados.

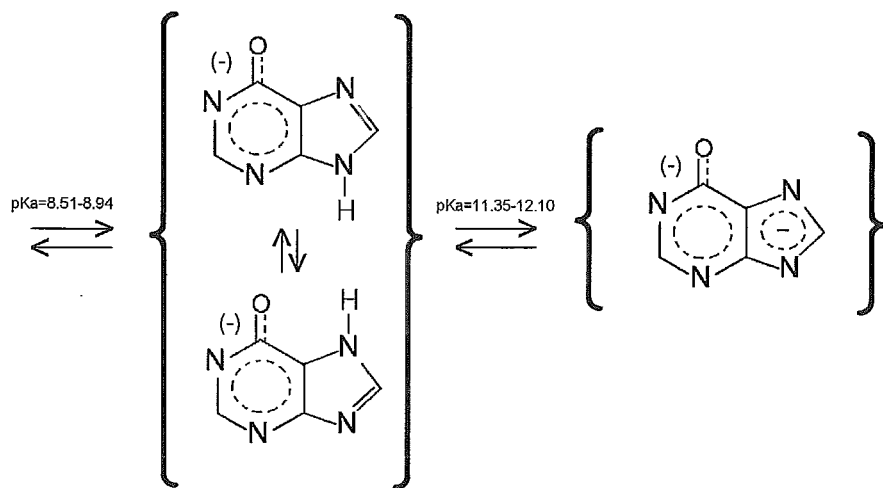
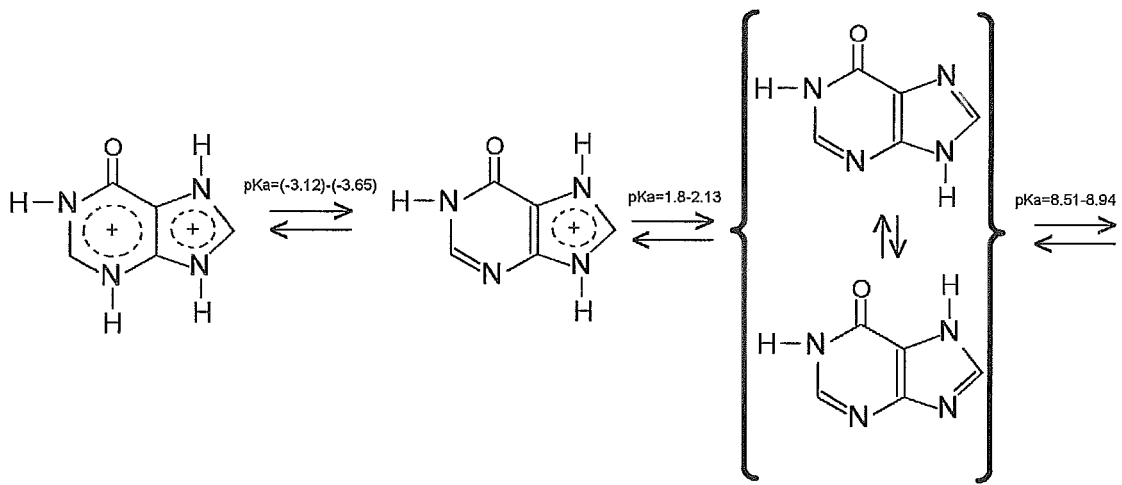
En relación también a este tema, y en particular respecto al efecto que tiene la constante dieléctrica del medio, el análisis de los resultados experimentales y teóricos, permite considerar que un medio de constante dieléctrica elevada favorece la estabilidad de aquellos tautómeros que en estado aislado presentan el valor mayor del vector momento dipolo eléctrico. Así, los tautómeros respectivos del alopurinol, hipoxantina y 6-mercaptapurina $\underline{\text{N}}(1)\text{-H}/\underline{\text{N}}(5)\text{-H}$, $\underline{\text{N}}(1)\text{-H}/\underline{\text{N}}(9)\text{-H}$ y $\underline{\text{N}}(1)\text{-H}/\underline{\text{N}}(9)\text{-H}$, los cuales poseen valores del vector momento dipolo eléctrico (3.65 D, 5.19 D y 5.90 D) comparativamente mayores que los asociados a sus contrapartes tautoméricas de estabilidad energética comparable ($\underline{\text{N}}(2)\text{-H}/\underline{\text{N}}(5)\text{-H}$, 0.93 D; $\underline{\text{N}}(1)\text{-H}/\underline{\text{N}}(7)\text{-H}$, 1.80 D; $\underline{\text{N}}(1)\text{-H}/\underline{\text{N}}(7)\text{-H}$, 0.74 D)^{32,41,42}, se ven relativamente favorecidos en su contribución a la población relativa tautomérica en sus disoluciones acuosas respectivas. Este efecto ha sido evidenciado experimentalmente⁴³ y deducido también de cálculos teóricos⁴⁴⁻⁴⁶, a partir de estudios sobre heterociclos relacionados.

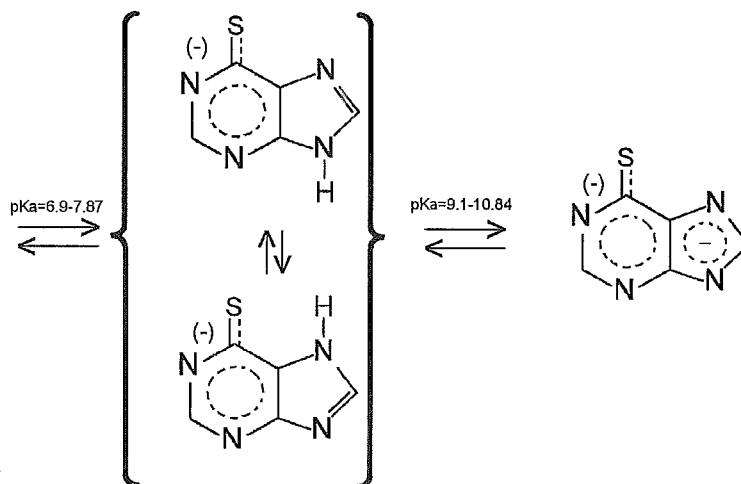
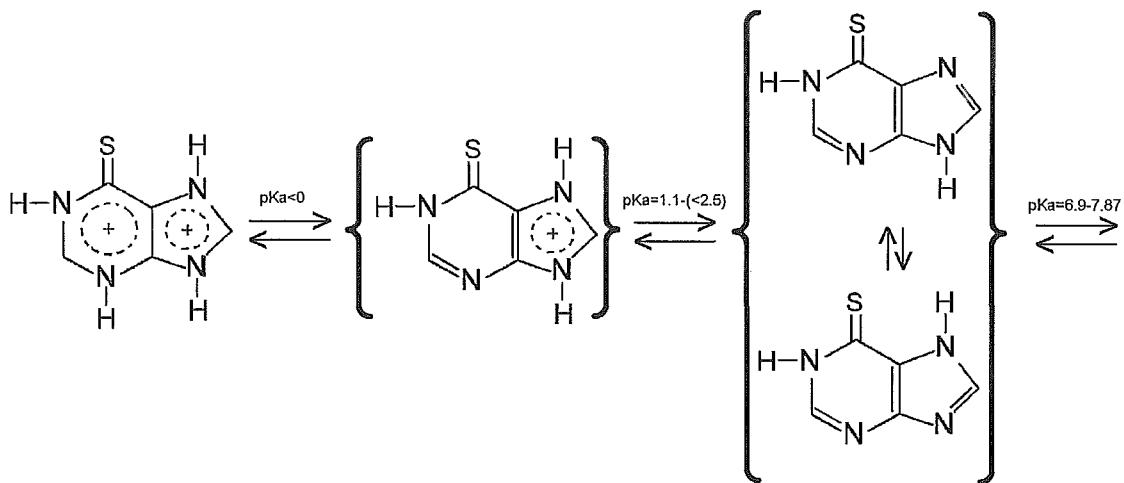
Otra de las características de los tres heterociclos considerados en este trabajo, es el de presentar una conducta ácido-base frente al protón. Dicha conducta está asociada íntimamente al fenómeno del tautomerismo en cada heterociclo. De hecho, las constantes de estabilidad termodinámica L-H^+ correspondientes a los diferentes equilibrios de la protonación heterocíclica respectiva, son constantes globales; cada una en realidad está pesada por las contribuciones de las constantes asociadas a los equilibrios correspondientes en que intervienen los tautómeros predominantes.

Sobre una revisión de los estudios llevados a cabo respecto a los equilibrios L-H^+ para los heterociclos alopurinol^{20,21,47}, hipoxantina^{23,24,47-54} y 6-mercaptapurina^{23,24,55-61},

es posible realizar una propuesta de disociación protónica en H₂O para cada heterociclo, considerando también los equilibrios tautoméricos de las especies predominantes en cada etapa de los equilibrios L-H⁺. Estas se presentan en los tres esquemas siguientes.



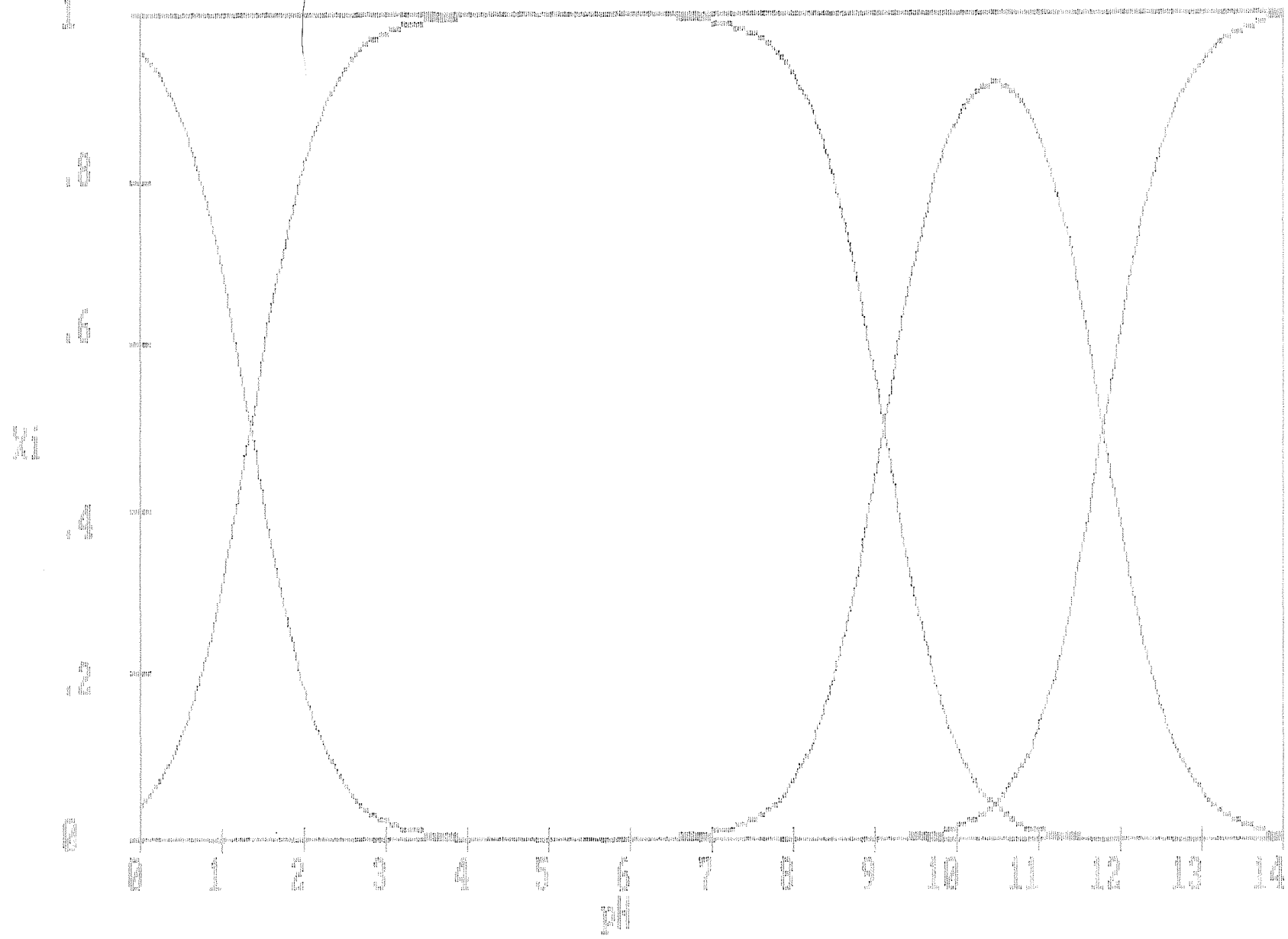




En las tres figuras siguientes, se presentan los diagramas de predominio de especies en función del pH, considerando tan solo las constantes globales de estabilidad termodinámica para los equilibrios $L-H^+$ de cada heterociclo.

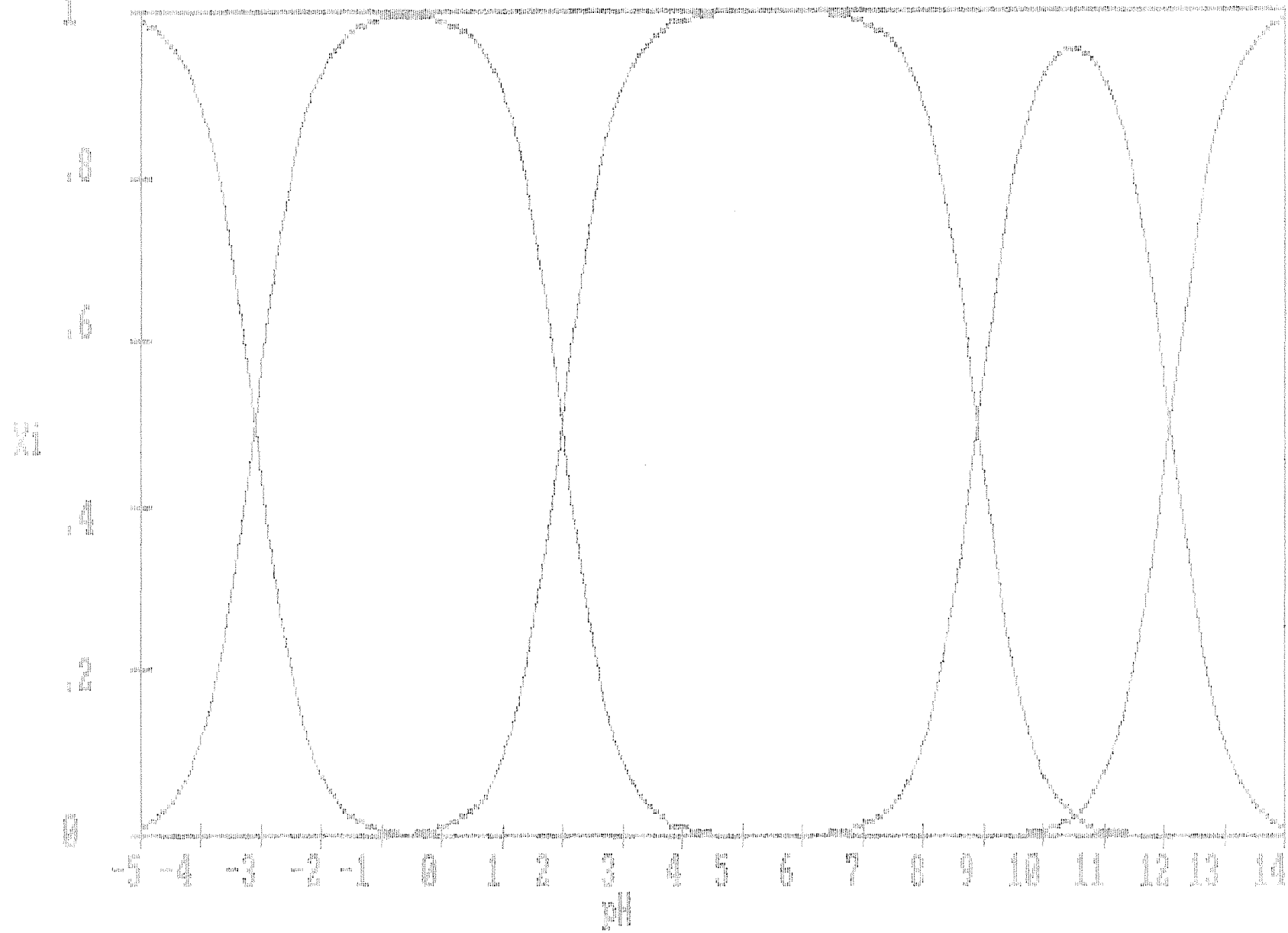
NO. TUBOS

Distribución de especies algueales en función del pH



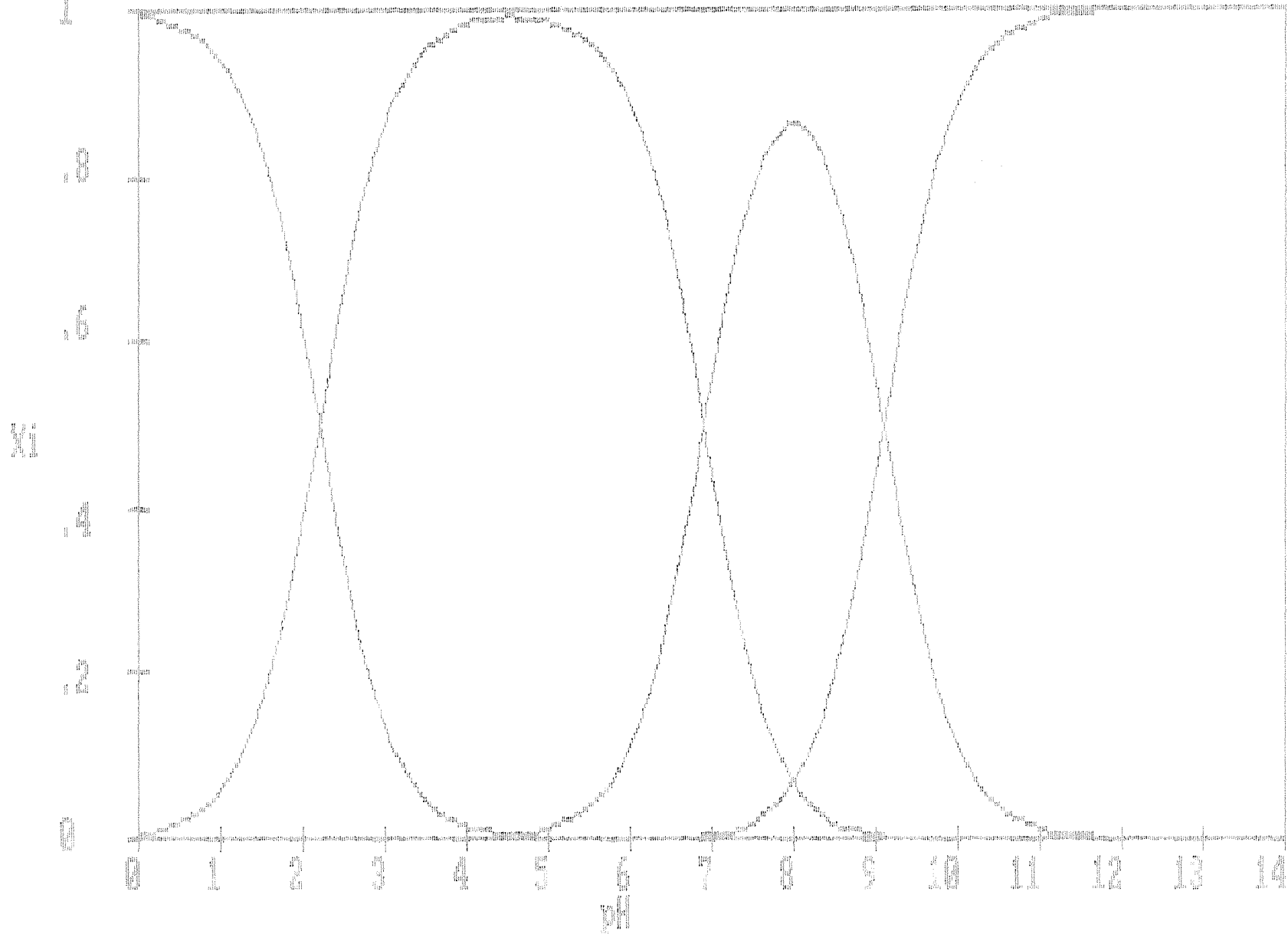
100-1000P

Distribucion de especies hipoxantina en funcion del pH



100-100MP

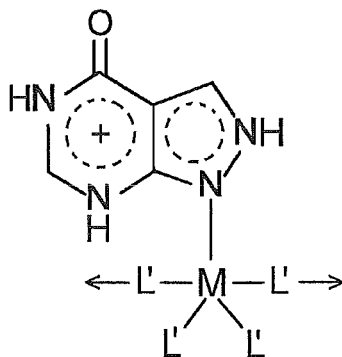
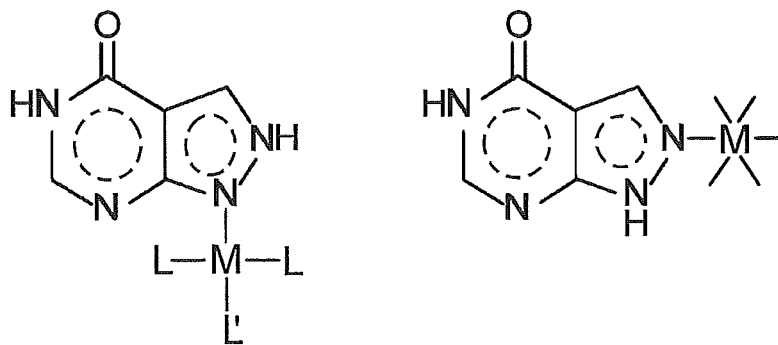
Distribución de especies G-MP en función del pH

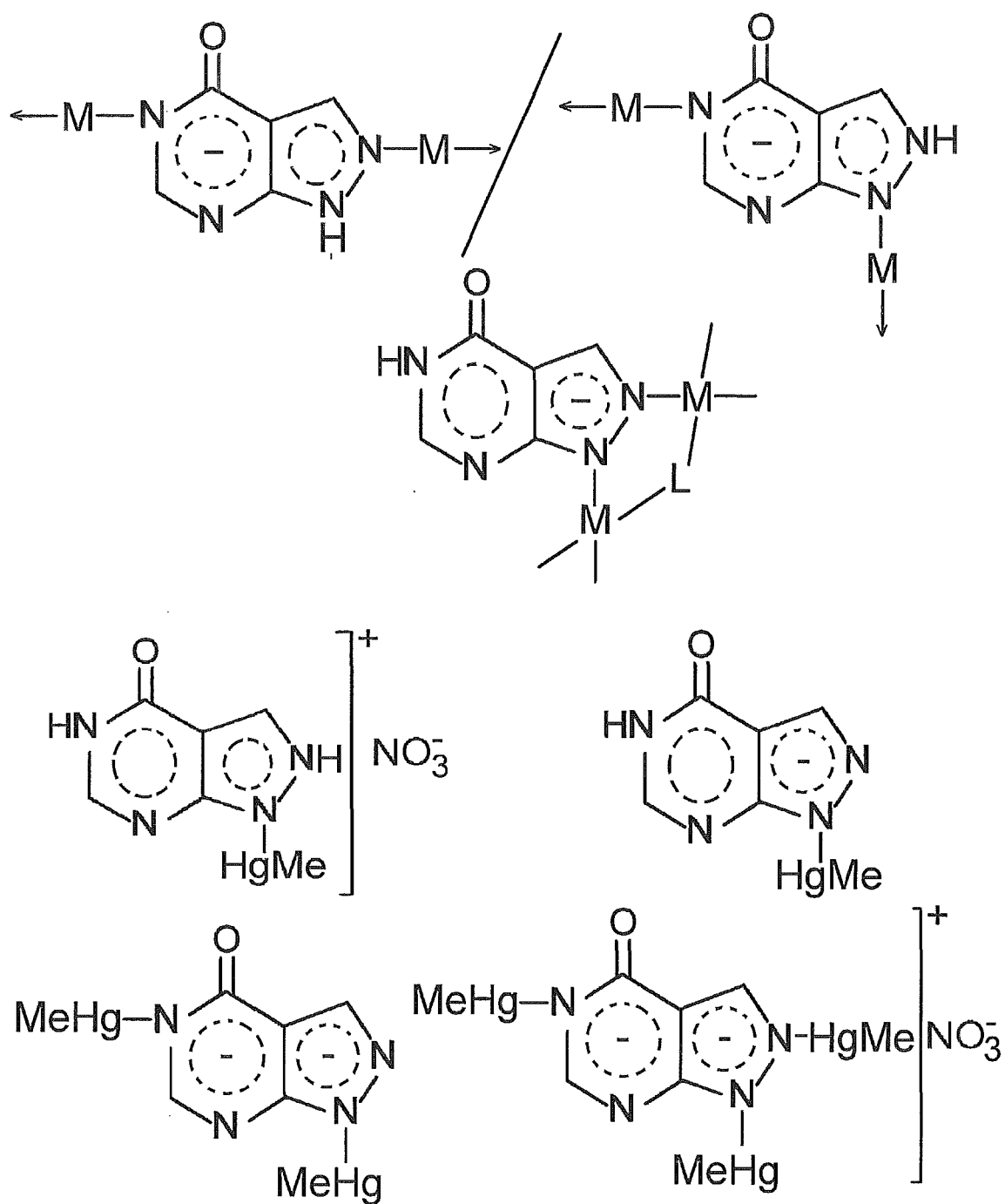


Como parte de las propiedades de los heterociclos de estudio en este trabajo, se encuentra su capacidad de coordinación metálica.

En relación al alopurinol, los estudios reportados por otros grupos⁶²⁻⁷² sobre las reacciones químicas Metal-Heterociclo, así como sobre el aislamiento y caracterización de los compuestos de coordinación correspondientes, permiten plantear la coordinación metálica del heterociclo por átomos de N. De éstos, e independientemente de la carga formal del alopurinol, destacan los átomos de N del anillo pirazólico. Para el alopurinol neutro coordinado destaca la existencia de las formas tautoméricas N(1)-H/N(5)-H y N(2)-H/N(5)-H. En relación a los sitios sucesivos de coordinación metálica del alopurinol, destacan los efectuados con el empleo del catión $[HgMe]^+$. Aquí, la coordinación sucesiva se presenta en los átomos N(1), N(5) y N(2), que en alguna medida sería la secuencia de protonación del heterociclo. Este sistema metálico parece ser un buen modelo en el análisis de los equilibrios $L-H^+$ de heterociclos relacionados.

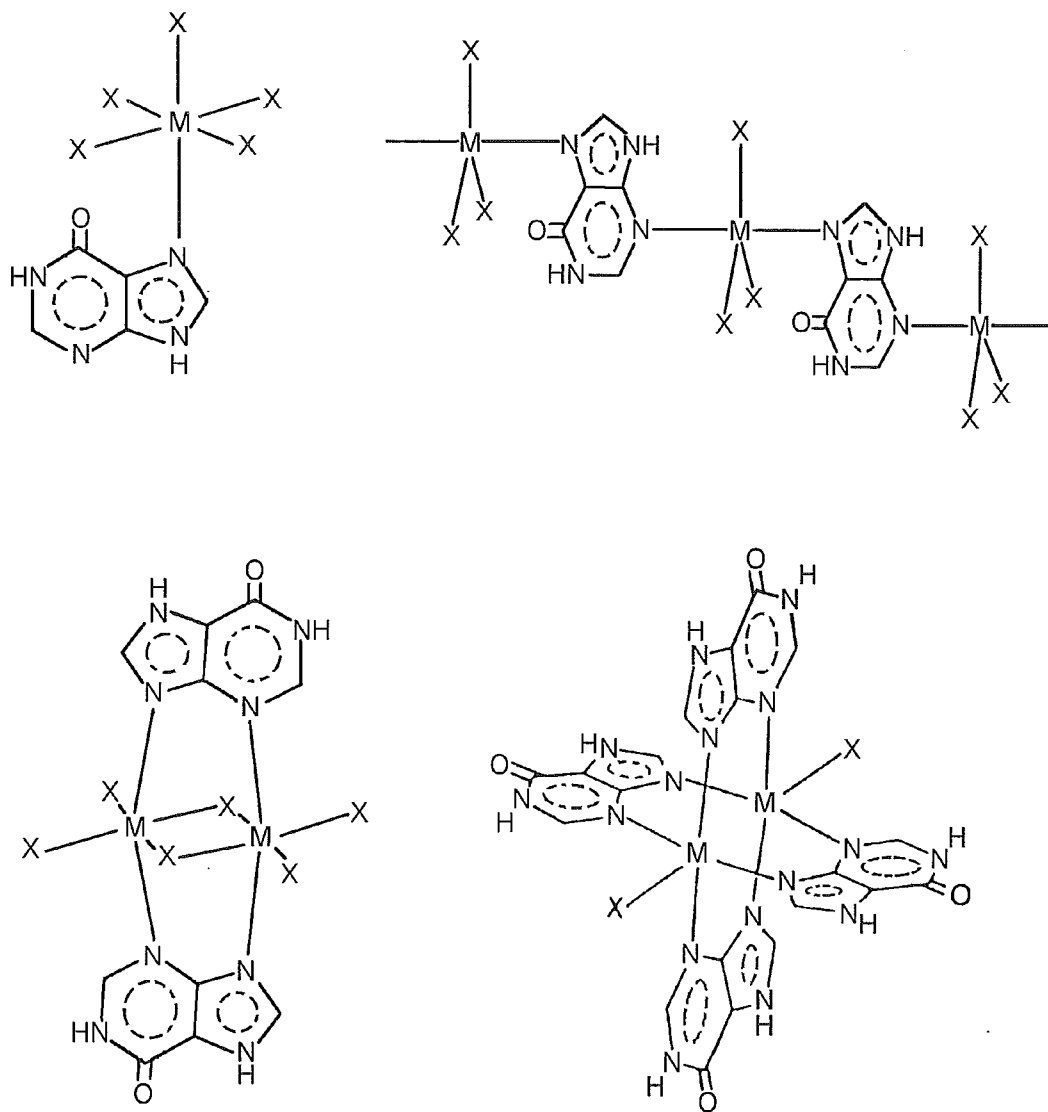
En las figuras que siguen se muestran esquemáticamente los modos de coordinación metálica del alopurinol, derivados de los estudios referidos anteriormente.





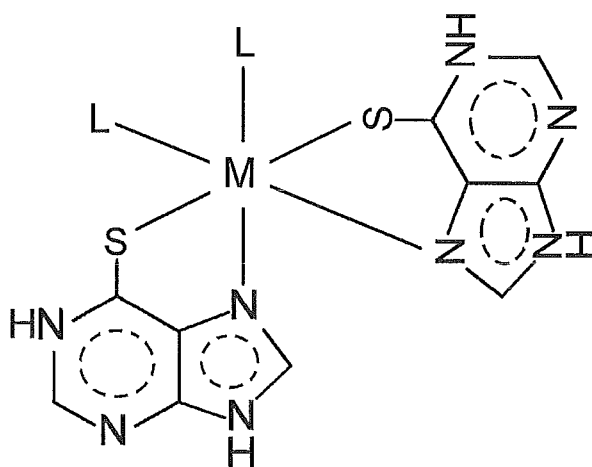
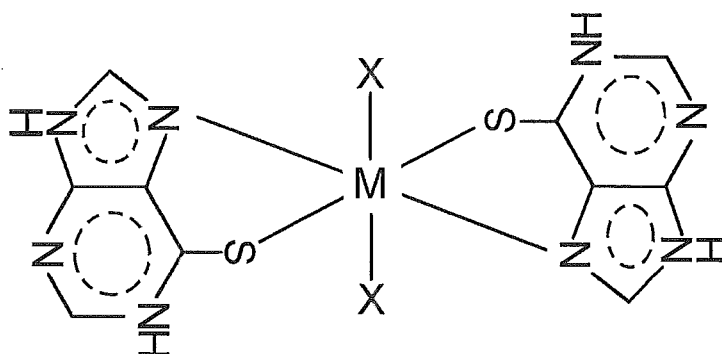
En relación a la hipoxantina, los estudios reportados por otros grupos^{18,73-78} permiten plantear que al igual al alopurinol, la hipoxantina se coordina por átomos de N. De estos, e independientemente de la carga formal del heterociclo, participa siempre alguno de los dos átomos de N del anillo imidazólico. Para la hipoxantina neutra coordinada, destaca la existencia de los tautómeros N(1)-H/N(9)-H y N(1)-H/N(7)-H. A diferencia del alopurinol neutro (el cual se coordina en forma monodentada por alguno de los dos átomos de N del anillo pirazólico), la hipoxantina neutra muestra a la fecha una

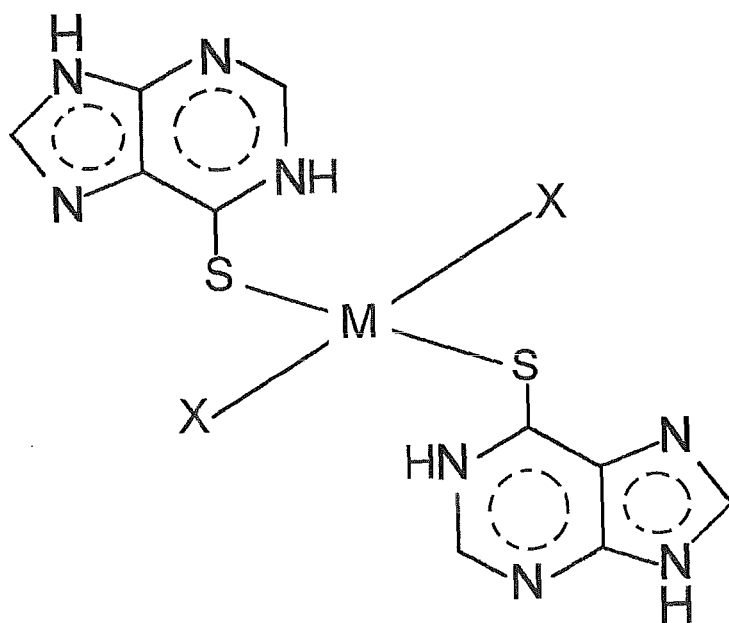
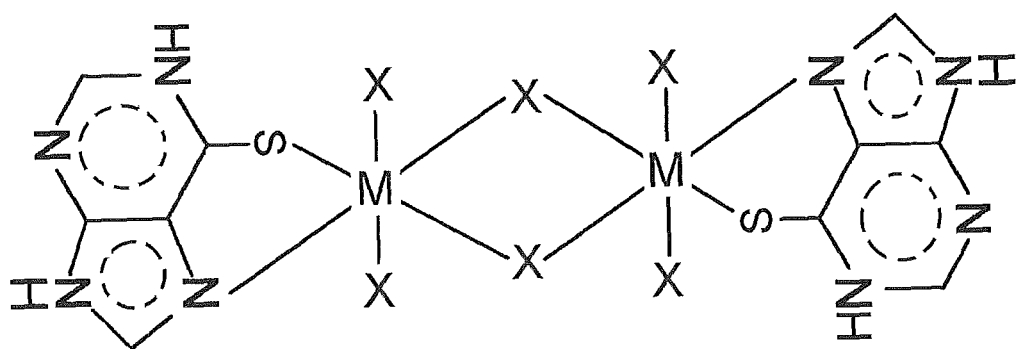
conducta coordinante más rica, coordinándose por el átomo N(7) ó por los átomos N(3) y N(7) (tautómero N(1)-H/N(9)-H) o bien por los átomos N(3) y N(9) (tautómero N(1)-H/N(7)-H). En la figura que sigue se ilustran esquemáticamente los modos de coordinación metálica de la hipoxantina, derivados de los estudios referidos arriba.

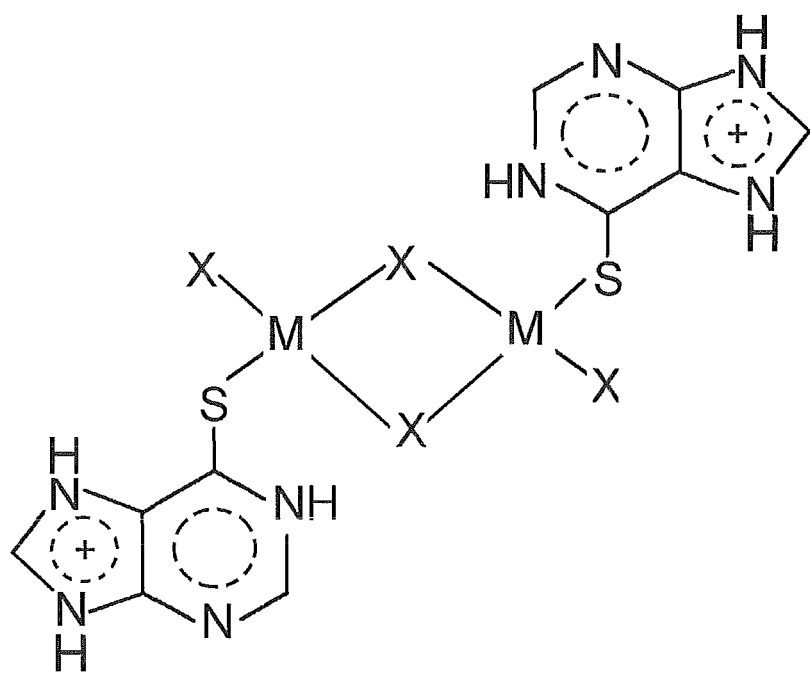
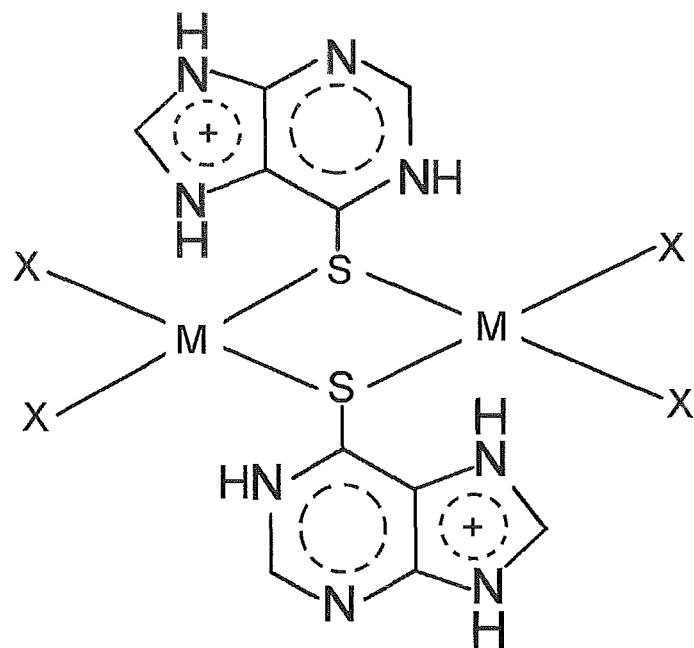


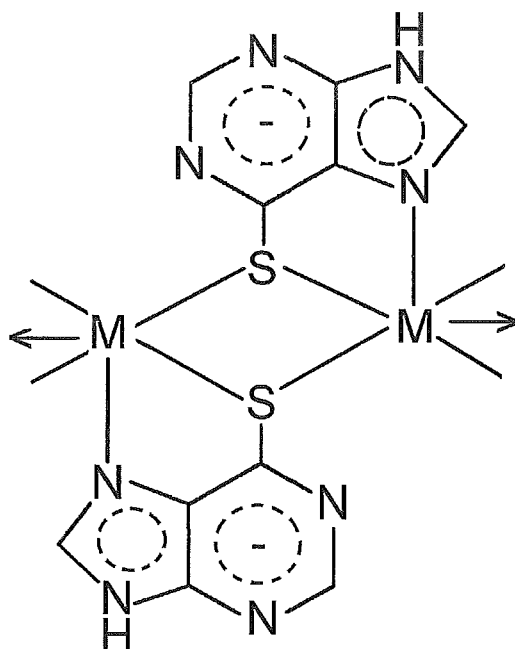
Por último y en relación a la 6-mercaptapurina, los estudios reportados a la fecha por otros grupos¹⁸, permiten plantear que en dicho heterociclo participa siempre el átomo S(6) como sitio de coordinación metálica. Para la 6-mercaptapurina neutra coordinada, el único tautómero presente ha sido el N(1)-H/N(9)-H. Es interesante también el hecho de que el heterociclo presenta modos de enlace metálico más complejos, a medida que su desprotonación se ve incrementada. Por último, analizando las posiciones protonadas del heterociclo coordinado, en función de su carga formal, se desprende la existencia de un cierto paralelismo con el propuesto para los equilibrios L-H⁺ de la 6-mercaptapurina libre en H₂O.

En las figuras que siguen se ilustran los modos de coordinación metálica presentados a la fecha por la 6-mercaptapurina.









De este panorama actual sobre la química de coordinación de los tres heterociclos, resalta la diversidad y heterogeneidad de las condiciones experimentales de reacción para cada uno de ellos. No obstante esto, parecen existir ciertas tendencias, como la referente a la coordinación metálica preponderante del alopurinol y la hipoxantina, a través de átomos de N, y no por el átomo O exocíclico, ó la referente a la 6-mercaptopurina, que siempre se coordina con la participación del átomo S exocíclico.

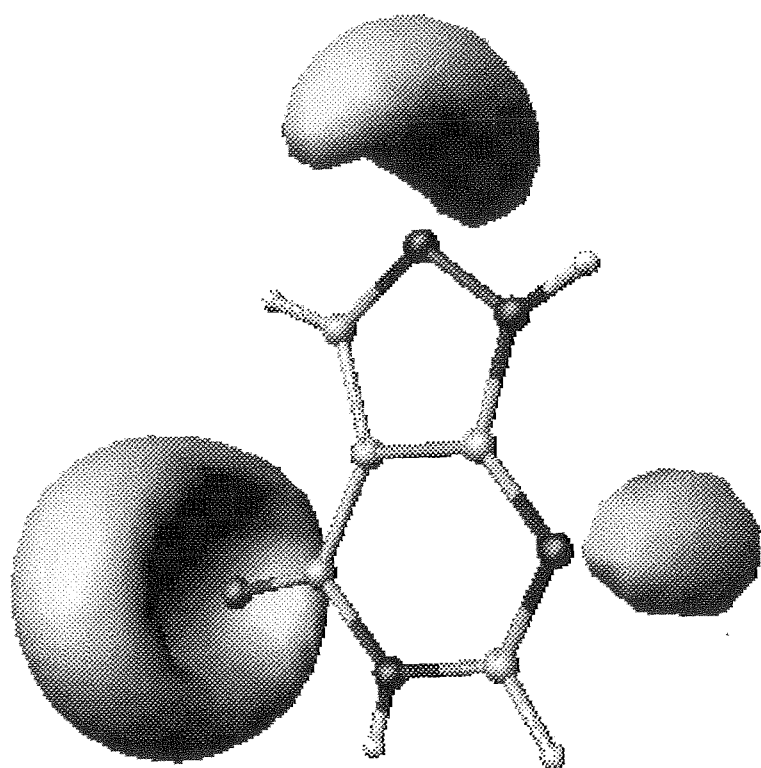
De los estudios resalta también la inexistencia de un paralelismo entre la estabilidad termodinámica hacia el protón y la estabilidad termodinámica hacia un metal de transición, para un sitio de coordinación particular en un heterociclo.

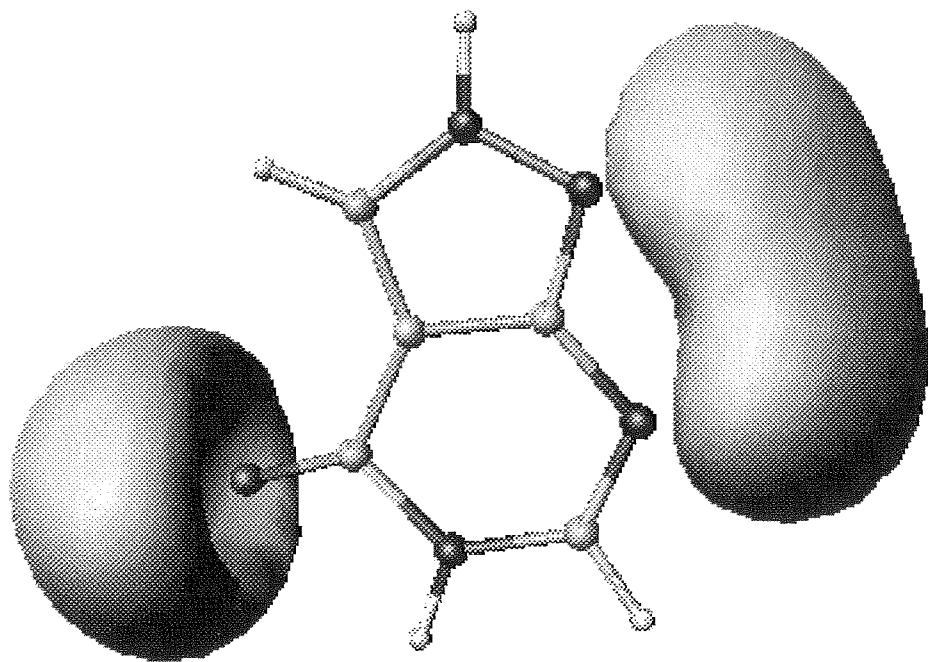
Respecto al tema del tautomerismo, los heterociclos coordinados presentan la forma cetónica (alopurinol e hipoxantina) y la forma tiona (6-mercaptopurina). Para el alopurinol y la hipoxantina neutros, los tautómeros existentes son respectivamente N(1)-H/N(5)-H ó N(2)-H/N(5)-H, y N(1)-H/N(9)-H ó N(1)-H/N(7)-H, que son los tautómeros energéticamente más estables en los cálculos teóricos de los heterociclos aislados, y los deducidos como predominantes en estudios de disoluciones de los heterociclos libres. Aquí es necesario decir, que no obstante que en disoluciones de los heterociclos libres de alopurinol y de hipoxantina, coexistan en equilibrio los dos grupos de tautómeros, los estudios reportados anteriormente (en particular, los estudios cristalográficos) no indican la existencia de dos formas tautoméricas del heterociclo en un compuesto de coordinación, o producto. Pareciera ser que la reacción del heterociclo (en equilibrio tautomérico) con el centro metálico, desplaza el equilibrio tautomérico, hacia una especie u otra; los factores a nivel molecular que pudieran conducir a esta fenomenología, no han sido explorados a la fecha.

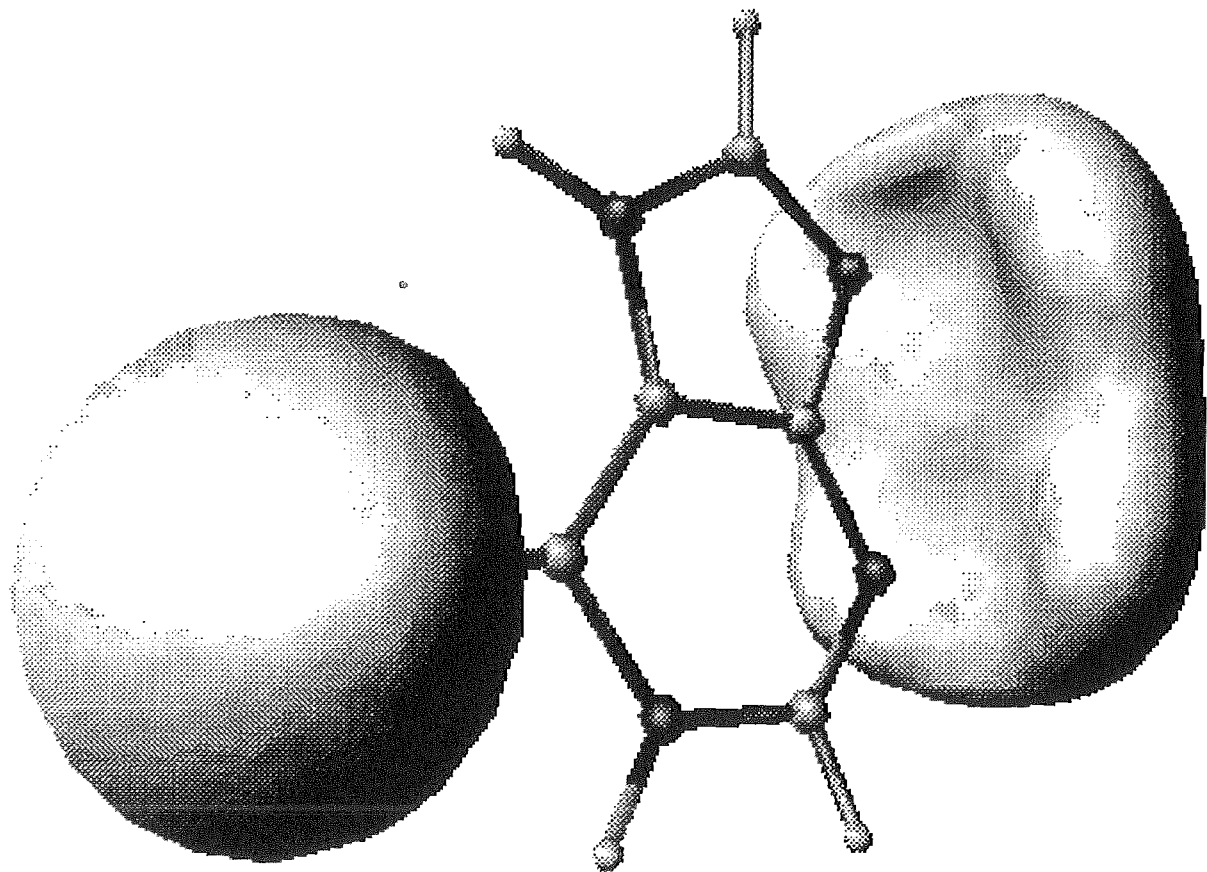
Para la 6-mercaptopurina neutra, el tautómero existente es el N(1)-H/N(9)-H, independientemente de que el heterociclo se coordine por S(6), ó por S(6) y N(7). Aquí también, no obstante que tanto los estudios teóricos como los experimentales sobre disoluciones del heterociclo libre, coinciden en que los tautómeros energéticamente más

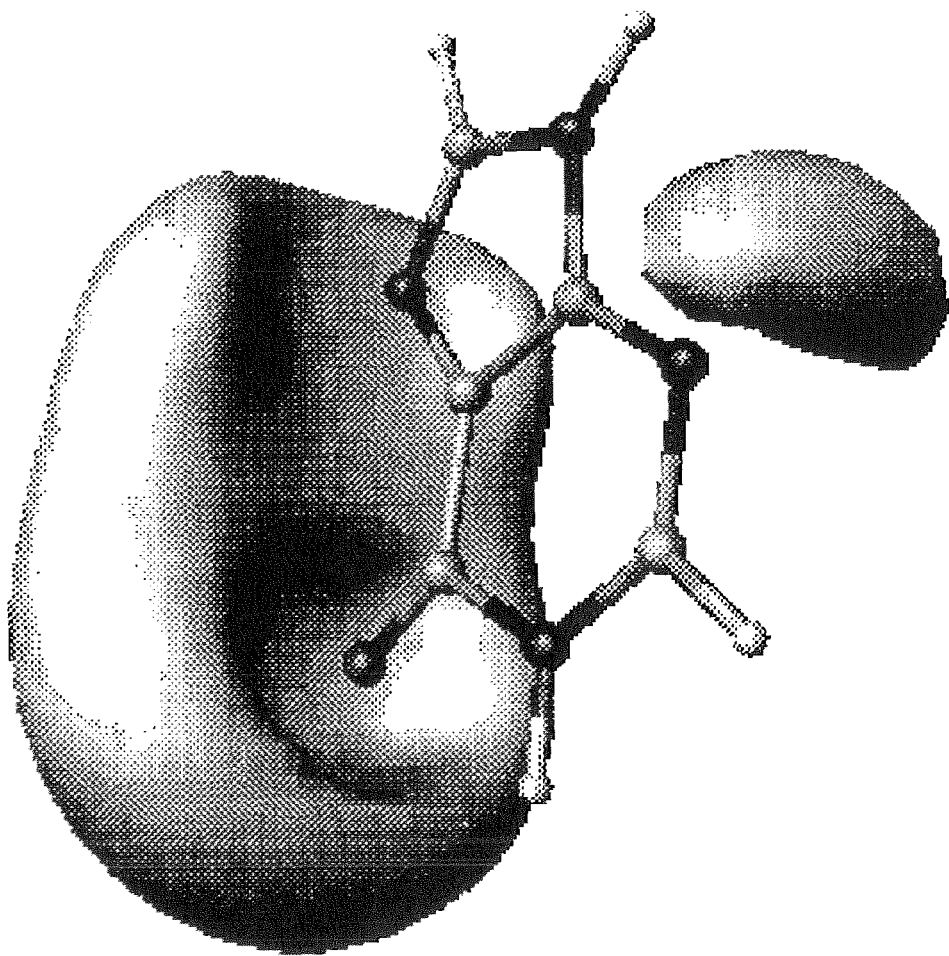
estables del heterociclo son el $\underline{\text{N}}(1)\text{-H}/\underline{\text{N}}(7)\text{-H}$ y el $\underline{\text{N}}(1)\text{-H}/\underline{\text{N}}(9)\text{-H}$, la reacción del heterociclo con el centro metálico, parece desplazar el equilibrio tautomérico, ahora (y a diferencia del alopurinol y la hipoxantina) a favor de solo una de las especies. De nueva cuenta, parece que el átomo $\underline{\text{S}}(6)$ y su participación en la coordinación metálica, es el factor de mayor contribución en dicha conducta.

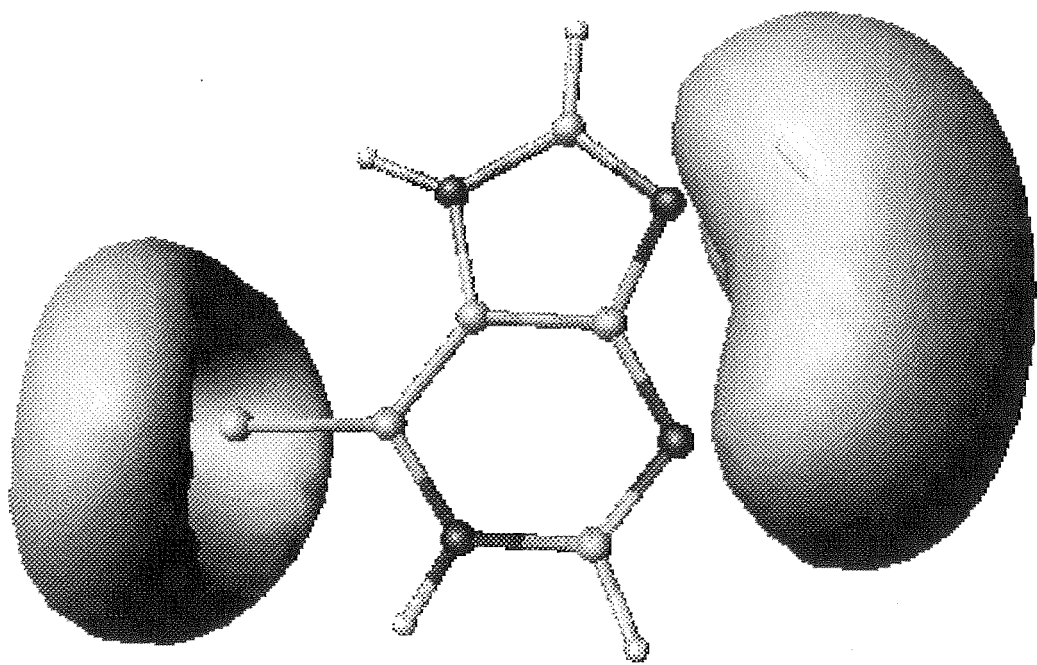
En una primera aproximación al esclarecimiento de la naturaleza de algunos factores que pudieran influir sobre la clase de átomos participantes en la coordinación metálica de los heterociclos (átomos de $\underline{\text{N}}$ en los casos del alopurinol e hipoxantina; el átomo $\underline{\text{S}}(6)$ como preponderante en el caso de la 6-mercaptopurina), se han realizado cálculos teóricos (a nivel de la Teoría de Funcionales de la Densidad) del potencial electrostático molecular para los dos tautómeros energéticamente más estables de los tres heterociclos con carga formal cero^{32,41,42}. Las superficies de isopotencial atractivo (-20 kcal/mol) hacia una carga positiva de prueba, se presentan a continuación y respectivamente para los dos tautómeros del alopurinol, la hipoxantina y la 6-mercaptopurina.

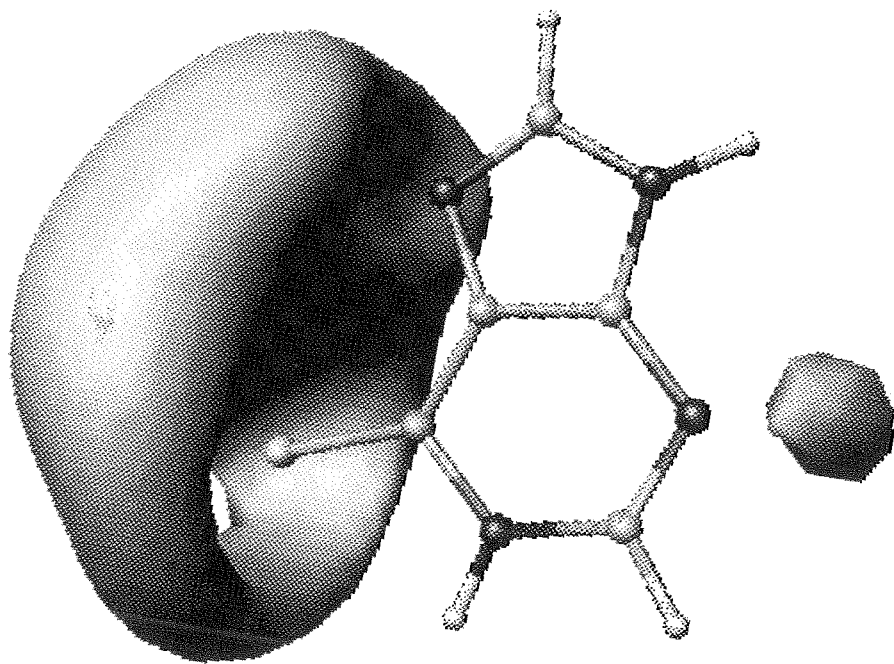












Los diagramas en tres dimensiones del potencial electrostático molecular para los dos tautómeros tanto del alopurinol como de la hipoxantina, si bien no contradicen la conducta coordinante mostrada hasta ahora por los átomos de N de los tautómeros respectivos, tampoco excluyen al O como sitio coordinante potencial, conducta no evidenciada hasta la fecha en la química de coordinación de estos dos heterociclos con carga formal cero, ó la del átomo N(7) en los tautómeros del alopurinol, también y hasta la fecha no evidenciada.

Lo mismo es aplicable al caso de los dos tautómeros de la 6-mercaptapurina: el potencial electrostático molecular (a dicho valor) no contradice la conducta coordinante experimental mostrada por el átomo S(6), ó incluso la del átomo N(7). Sin embargo, tampoco excluye al átomo N(3) (tautómero N(1)-H/N(9)-H) ó al par N(3)/N(9) (para el tautómero N(1)-H/N(7)-H) como sitios coordinantes potenciales, los cuales no han sido evidenciados a la fecha en la química de coordinación del heterociclo neutro.

Entendido el potencial electrostático molecular como una propiedad ante interacciones puramente electrostáticas, ésta debe ser considerada en su dimensión real, asumiendo en todo caso que aquellas regiones moleculares (ó átomos) con potenciales electrostáticos atractivos más favorables, pudieran ser las zonas potencialmente preferenciales en la aproximación de cationes; otros factores, relacionados a la estructura electrónica de los heterociclos, y a las condiciones experimentales de reacción, pueden influir decisivamente en la construcción y formación de enlaces químicos metal-heterociclo con un carácter covalente y selectivo.

Referencias.

1. Y. Tominaga, Y. Honkawa, M. Hara y A. Hosomi, *J. Heterocyclic Chem.*, **27**, 775 (1990).
2. R.J. Quinn, P.J. Scammells y D.J. Tucker, *Aust. J. Chem.*, **44**, 753 (1991).
3. C. Switzer, S.E. Moroney y S.A. Benner, *J. Am. Chem. Soc.*, **111**, 8322 (1989).
4. J.A. Piccirilli, T. Krauch, S.E. Moroney y S.A. Benner, *Nature*, **343**, 33 (1990).
5. P.J. Hagerman e I. Tinoco, Jr., *Current Opinion in Struct. Biol.*, **6**, 277 (1996).
6. C. Hansch, *J. Chem. Educ.*, **51**, 360 (1974).
7. U. Kela y R. Vijayvardiya, *Biochem. J.*, **193**, 799 (1981).
8. H.B. Cottam, G.R. Revankar y R.K. Robins, *Nucleic Acid Res.*, **11**, 871 (1983).
9. F. Bergmann, H. Kwietny, G. Levin y D.J. Brown, *J. Am. Chem. Soc.*, **82**, 598 (1960).
10. T.R. Hawkes, G.N. George y R.C. Bray, *Biochem. J.*, **218**, 961 (1984).
11. R.K. Robins, G.R. Revankar, D.E. O'Brien, R.H. Springer, T. Novinson, A. Albert, K. Senga, J.P. Miller y D.G. Streeter, *J. Heterocyclic Chem.*, **22**, 601 (1985).
12. R. Hille, G.N. George, M.K. Eidsness y S.P. Cramer, *Inorg. Chem.*, **28**, 4018 (1989).
13. J.H. Kim y R. Hille, *J. Inorg. Biochem.*, **55**, 295 (1994).
14. R. Hille, *Biochim. Biophys. Acta*, **1184**, 143 (1994).
15. M.T. Chenon, R.J. Pugmire, D.M. Grant, R.P. Panzica y L.B. Townsend, *J. Am. Chem. Soc.*, **97**, 4636 (1975).
16. K. Szczepaniak, M. Szczesniak y W.B. Person, *Chem. Phys. Lett.*, **153**, 39 (1988).
17. V.I. Danilov, J.S. Kwiatkowski, B. Lesyng y V.I. Potter, *Int. J. Quantum Chem: Quantum Biology Symposium*, **8**, 359 (1981).
18. *CRC Handbook of Nucleobase Complexes*; J.R. Lusty, Ed., CRC Press, Boca Raton, Florida, 1990; Vol. I y referencias.

19. M.T. Chenon, R.J. Pugmire, D.M. Grant, R.P. Panzica y L.B. Townsend, *J. Heterocyclic Chem.*, **10**, 431 (1973).
20. F. Bergmann, A. Frank y Z. Neiman, *J. Chem. Soc. Perkin I*, 2795 (1979).
21. W.S. Sheldrick y P. Bell, *Inorg. Chim. Acta*, **137**, 181 (1987).
22. B. Pullman y A. Pullman, *Adv. Heterocyclic Chem.*, **13**, 77 (1971) y referencias.
23. D. Lichtenberg, F. Bergmann y Z. Neiman, *Isr. J. Chem.*, **10**, 805 (1972).
24. D.J. Brown y S.F. Mason, *J. Chem. Soc.*, 682 (1957).
25. J.S. Kwiatkowski, *J. Mol. Struct.*, **8**, 471 (1971).
26. L.M. Twanmoh, H.B. Wood, Jr. y J.S. Driscoll, *J. Heterocyclic Chem.*, **10**, 187 (1973).
27. C. Santhosh y P.C. Mishra, *Spectrochim. Acta*, **49A**, 985 (1993).
28. M. Nonella, G. Hänggi y E. Dubler, *J. Mol. Struct. (Theochem.)*, **279**, 173 (1993).
29. B. Hernández, F.J. Luque y M. Orozco, *J. Org. Chem.*, **61**, 5964 (1996).
30. M.K. Shukla y P.C. Mishra, *Spectrochim. Acta*, **52A**, 1547 (1996).
31. N. El-Bakali Kassimi y A.J. Thakkar, *J. Mol. Struct. (Theochem.)*, **366**, 185 (1996).
32. María Eugenia Costas, Estrella Ramos y Rodolfo Acevedo Chávez, *Density Functional Study of Purine-type Heterocycles: Hypoxanthine y Allopurinol*. Remitido para su publicación. (Anexo 7).
33. J. Lin, C. Yu, S. Peng, I. Akiyama, K. Li, L.K. Lee y P.R. LeBreton, *J. Phys. Chem.*, **84**, 1006 (1980).
34. N. Olaru y Z. Simon, *Rev. Roum. Biochim.*, **18**, 51 (1981).
35. Z.B. Maksić, K. Rupnik y A. Veseli, *Z. Naturforsch.*, **38a**, 866 (1983).
36. L. Lazo, A.M. Tejo, J.L. Pousa, O.M. Sorarrain y H.A. Roncaglia, *Z. Phys. Chemie, Leipzig*, **266**, 143 (1985).
37. J.J. Aaron, M.D. Gaye, C. Párkányi, N.S. Cho y L. Von Szentpály, *J. Mol. Struct.*, **156**, 119 (1987).
38. G.G. Sheina, S.G. Stepanian, E.D. Radchenko y Y.P. Blagoi, *J. Mol. Struct.*, **158**, 275 (1987).
39. Y. Ohta, K. Nishimoto, H. Tanaka, Y. Baba y A. Kagemoto, *Bull. Chem. Soc. Jpn.*, **62**, 2441 (1989).
40. T. Leo, F. Accion, D. Escolar y J. Tortajada, *An. Quim. Sp.*, **87**, 14 (1991).
41. María Eugenia Costas y Rodolfo Acevedo Chávez, *DFT Study of the Neutral Hypoxanthine Tautomeric Forms*. Remitido para su publicación (Anexo 8).
42. María Eugenia Costas y Rodolfo Acevedo Chávez. Resultados no comunicados.
43. D.M. Cheng, L.S. Kan, P.O.P. Ts'o, C.G. Prettre y B. Pullman, *J. Am. Chem. Soc.*, **102**, 525 (1980).
44. K. Szczepaniak y M. Szczesniak, *J. Mol. Struct.*, **156**, 29 (1987).
45. W.B. Person, K. Szczepaniak, M. Szczesniak, J.S. Kwiatkowski, L. Hernández y R. Czerminski, *J. Mol. Struct.*, **194**, 239 (1989).
46. M.J. Nowak, L. Lapinski y J.S. Kwiatkowski, *Chem. Phys. Lett.*, **157**, 14 (1989).
47. P.W. Linder, M.J. Stanford y D.R. Williams, *J. Inorg. Nucl. Chem.*, **38**, 1847 (1976).
48. J.J. Christensen, J.H. Rytting y R.M. Izatt, *Biochemistry*, **9**, 4907 (1970).
49. R.M. Izatt, J.J. Christensen y J.H. Rytting, *Chem. Rev.*, **71**, 439 (1971).
50. R.L. Benoit, D. Boulet, L. Séguin y M. Fréchette, *Can. J. Chem.*, **63**, 1228 (1985).
51. R.L. Benoit y M. Fréchette, *Can. J. Chem.*, **63**, 3053 (1985).
52. R.L. Benoit y M. Fréchette, *Thermochim. Acta*, **127**, 125 (1988).
53. R. Tauler, J.F. Cid y E. Casassas, *J. Inorg. Biochem.*, **39**, 277 (1990).

54. E. Casassas, R. Gargallo, I. Giménez, A. Izquierdo-Ridorsa y R. Tauler, *J. Inorg. Biochem.*, **56**, 187 (1994).
55. E.M. Scoran y M. Cefola, *Arch. Biochem. Biophys.*, **97**, 146 (1962).
56. J. Brigando y D. Colaitis, *Bull. Soc. Chim. Fr.*, No 10, 3440 (1969).
57. M.M. Taqui Khan y C.R. Krishnamoorthy, *J. Inorg. Nucl. Chem.*, **33**, 1417 (1971).
58. *Stability Constants of Metal-Ion Complexes*; D.D. Perrin, Ed., Pergamon Press, Oxford, England, 1979; Part B (Organic Ligands) y referencias.
59. E.P. Serjeant y B. Dempsey, *Ionisation Constants of Organic Acids in Aqueous Solution*. IUPAC Chemical Data Series No. 23. Pergamon Press, LTD, England, 1979.
60. E. Dubler y E. Gyr, *Inorg. Chem.*, **27**, 1466 (1988).
61. R. Bilewicz y E. Muszalska, *J. Electroanal. Chem.*, **300**, 147 (1991).
62. W.S. Sheldrick y P. Bell, *Z. Naturforsch.*, **42b**, 195 (1987).
63. W.S. Sheldrick y P. Bell, *Inorg. Chim. Acta*, **137**, 181 (1987).
64. W.S. Sheldrick y B. Günther, *Inorg. Chim. Acta*, **151**, 237 (1988).
65. G. Hänggi, H. Schmalte y E. Dubler, *Inorg. Chem.*, **27**, 3131 (1988).
66. G. Hänggi, H. Schmalte y E. Dubler, *Acta Cryst.*, **C44**, 1560 (1988).
67. W.S. Sheldrick, P. Bell y H.J. Häusler, *Inorg. Chim. Acta*, **163**, 181 (1989).
68. R. Acevedo-Chávez y N. Barba-Behrens, *Transition Met. Chem.*, **15**, 434 (1990).
69. G. Hänggi, H. Schmalte y E. Dubler, *Acta Cryst.*, **C47**, 1609 (1991).
70. W.S. Sheldrick y G. Heeb, *Inorg. Chim. Acta*, **190**, 241 (1991).
71. G. Hänggi, H. Schmalte y E. Dubler, *J. Chem. Soc. Dalton Trans.*, 941 (1993).
72. C.M. Mikulski, M.E. Holman, G. Tener, T. Dobson, S. Eang, W. Welsh, Y. Nujoma y N.M. Karayannis, *Transition Met. Chem.*, **18**, 262 (1993).
73. E. Dubler, G. Hänggi y H. Schmalte, *Inorg. Chem.*, **29**, 2518 (1990).
74. B.T. Khan, K. Venkatasubramanian, K. Najmuddin, S. Shamsuddin y S.M. Zakeeruddin, *Inorg. Chim. Acta*, **179**, 117 (1991).
75. C.M. Mikulski, K. Udell, D.L. Staley y N.M. Karayannis, *Transition Met. Chem.*, **17**, 159 (1992).
76. G. Hänggi, H. Schmalte y E. Dubler, *Acta Cryst.*, **C48**, 1008 (1992).
77. D.J. Radanović, Z.D. Matović, G. Ponticelli, P. Scano e I.A. Efimenko, *Transition Met. Chem.*, **19**, 646 (1994).
78. I.A. Efimenko, A.P. Kurbakova, Z.D. Matović y G. Ponticelli, *Transition Met. Chem.*, **19**, 640 (1994).

CAPÍTULO II

Problemas, Considerandos
y
Propuesta.

I. Problemas.

De los estudios experimentales reportados por otros autores y que conciernen a compuestos de coordinación con los heterociclos alopurinol, hipoxantina y 6-mercaptopurina, destaca la heterogeneidad de los sistemas metálicos seleccionados, así como de las condiciones experimentales de reacción para su síntesis. También y a este respecto, en muchos estudios no se explica si la especie caracterizada en sólido, es la única aislada del sistema de reacción.

Lo anterior tiene importancia enorme, dado que la obtención, y en su caso separación, de un sistema metal-heterociclo particular (incluyendo aquí y entre otros rasgos no solo la estequiometría metal-heterociclo y la carga formal de ellos, sino el estado tautomérico del ligante y su modo específico de coordinación metálica) están dadas por la interrelación de las estabilidades termodinámica y cinética de las especies involucradas en los equilibrios presentes en la disolución, así como de los equilibrios sólido↔líquido, todo lo cual está relacionado estrechamente a las propiedades fisicoquímicas del disolvente, y a la temperatura.

II. Considerandos.

En relación a estos problemas y en un intento de establecer ciertas bases para un estudio metodológico, es pertinente formular ciertas consideraciones mínimas.

A. Sobre la estabilidad termodinámica ligante-H⁺.

A este respecto, es pertinente señalar que tanto el alopurinol como la hipoxantina, presentan estabilidades termodinámicas globales L-H⁺ muy similares para sus estados diferentes de protonación. A diferencia de ellos, la 6-mercaptopurina presenta estabilidades homólogas relativamente menores, sobre todo para los estados de desprotonación mayor. Es decir, la 6-mercaptopurina es relativamente menos estable a la protonación en las mismas condiciones básicas para los tres heterociclos.

Las diferencias acotadas arriba entre la hipoxantina y la 6-mercaptopurina, aunadas a su carácter isoestructural, permiten considerar la influencia que tiene el átomo de S sobre el carácter de base comparativamente más débil de la 6-mercaptopurina.

Para la 6-mercaptopurina y en comparación con la hipoxantina, existen por tanto y en principio posibilidades comparativamente mayores de sufrir procesos de disociación protónica por efecto de la temperatura, de una constante dieléctrica del medio elevada, por la presencia de otros ligantes con estabilidades termodinámicas L-H⁺ apreciables, ó incluso por su coordinación a un centro metálico.

La coordinación metálica heterocíclica puede ser un factor importante en las diferencias de las estabilidades termodinámicas L-H⁺ para el alopurinol y la hipoxantina. La presencia en el primero de un anillo pirazólico (dos átomos de N vecinos) y la coordinación a través de uno de estos dos átomos de N, le conferirá propiedades de base más débil al alopurinol coordinado, en particular al átomo de N protonado y vecino al sitio de coordinación.

B. Sobre la estabilidad termodinámica de los tautómeros.

Los tres heterociclos en estudio presentan en forma predominante la misma clase de tautomerismo (forma cetónica, tautomerismo prototrópico en los anillos de cinco miembros; forma tiona, tautomerismo en el anillo de cinco miembros) para un estado de protonación y carga formal determinado, en particular aquellos intermedios a los extremos de protonación o desprotonación.

No obstante, las poblaciones relativas tautoméricas de cada heterociclo en un estado de carga formal determinado, pueden cambiar en función de la constante dieléctrica del medio, y en relación a éste, por la temperatura. Este efecto no tiene que ser del mismo tipo y de la misma magnitud para los tres heterociclos en un estado particular. Si bien, entre hipoxantina y 6-mercaptopurina existe un carácter isoestructural, la presencia de átomos exocíclicos diferentes será el factor de mayor contribución en sus estructuras y propiedades moleculares. Así también, y en relación al alopurinol y la hipoxantina, su carácter isomérico respecto a la disposición de los átomos de N en los anillos de cinco miembros, será el factor de mayor peso en las propiedades ya referidas. En particular, un factor importante puede ser el valor del momento dipolo eléctrico.

De esta manera y para un heterociclo en disolución con una carga formal determinada, aquellos tautómeros de él que posean valores mayores del vector momento dipolo eléctrico se verán favorecidos en forma relativa a medida que se incremente la constante dieléctrica del medio. Aquí también es necesario considerar la influencia que puede tener un átomo metálico coordinado a un heterociclo, en un sitio determinado, sobre el favorecimiento de un tautómero específico.

En los tres heterociclos se ha detectado este rasgo. Aquí es importante remarcar que para un heterociclo dado y un sitio de coordinación potencial particular, no existe necesariamente una correspondencia directa entre las estabilidades termodinámicas $L-H^+$ y $L-M^{n+}$.

III. Propuesta.

Los heterociclos alopurinol, hipoxantina y 6-mercaptopurina se caracterizan por ser sistemas ácido-base ante el protón, y presentar el fenómeno de tautomerismo. No obstante, los modos de coordinación metálica de ellos, sus cargas formales (estados de protonación) así como las formas tautoméricas en los compuestos de coordinación respectivos, estarán asociados a:

- Las condiciones de reacción experimental.

Aquí la constante de estabilidad termodinámica metal-heterociclo (M-L) de un sistema particular está relacionada íntimamente a las homólogas y correspondientes a otros equilibrios simultáneos, que pudieran involucrar por ejemplo, a los sistemas $L-H^+$, $M-OH^-$ y $M-X$ (u otros sistemas ácido-base), así como a las propiedades fisicoquímicas de la disolución, o su temperatura.

- La disposición estructural de los átomos de N, a su posición relativa respecto al átomo exocíclico, así como a las propiedades electrónicas de ambos.

Las constantes de estabilidad termodinámica L-cación están asociadas a estos factores estructurales y electrónicos.

Para el caso del alopurinol, un factor preponderante pudiera ser el desempeñado por la disposición y propiedades electrónicas de los átomos de N en el anillo pirazólico. La vecindad de éstos posibilitaría no solo la existencia de formas tautoméricas diferentes en el heterociclo neutro monocoordinado, sino también y dado el caso, el descenso suficiente de la estabilidad termodinámica $L-H^+$ asociada a un sitio vecino a la coordinación metálica, así como la desprotonación subsecuente de éste como resultado de su participación como sitio de coordinación metálica, posibilitando la existencia del heterociclo monoaniónico como ligante exobidentado en compuestos de coordinación.

Para el caso de los derivados purínicos hipoxantina y 6-mercaptopurina, el factor preponderante lo ejercerían las propiedades electrónicas y por tanto capacidades coordinantes de los átomos exocíclicos O(6) y S(6).

CAPÍTULO III

Objetivos.

I. Estudios Experimentales.

Para la confrontación de la propuesta formulada previamente, y que se refiere a la conducta experimental de los heterociclos alopurinol, hipoxantina y 6-mercaptopurina, se estableció como objetivos:

- La realización de reacciones químicas centro metálico de transición-heterociclo bajo un espectro de condiciones experimentales modificadas sistemáticamente.
- El análisis de la conducta coordinante y de tautomerismo de los heterociclos centrales de estudio, así como de la relación entre dichas características y las propiedades estructurales, espectrales y magnéticas de los compuestos de coordinación correspondientes.

I. Estudios Teóricos.

Como parte del problema teórico referente a la conducta fenomenológica de los heterociclos en estudio, se estableció como objetivo:

- El análisis teórico de la estabilidad energética relativa, de la estructura molecular y electrónica, así como de propiedades moleculares asociadas a la reactividad química de los tautómeros más estables.

CAPÍTULO IV

Metodologías.

I. Metodología en la preparación de los compuestos de coordinación.

- Para la realización de los objetivos, se establecieron los parámetros siguientes:

A. Sistemas.

Centro Metálico: se eligió a Cu(II), por su reactividad ante ligantes coordinantes por O, S y N. Al poseer un estado de espín electrónico $S=1/2$, se favorece el estudio espectral y magnético de sus compuestos de coordinación.

Esfera de coordinación de Cu(II): no se estableció una esfera predeterminada para el centro metálico al utilizar ligantes con características específicas. Por el contrario, se eligió que el centro Cu(II) presentara una esfera de coordinación lábil, para favorecer las reacciones Cu(II)-heterociclo.

Contraiones en las sales de Cu(II): se modificó la naturaleza de los contraiones, con la intención de explorar su influencia sobre las reacciones metal-heterociclo y los compuestos metálicos respectivos.

Heterociclos: se eligió como heterociclos centrales de estudio al alopurinol, la hipoxantina y la 6-mercaptapurina. Para modelar ciertos rasgos de la conducta coordinante del anillo pirazólico presente en el alopurinol, se eligió a los heterociclos pirazol y 3,5-dimetilpirazol.

B. Condiciones de reacción.

Estequiometrías metal-heterociclo: se eligió como base una relación equimolar. Para ciertos estudios que así lo sugirieran, se modificó ésta a favor del metal, ó a favor del heterociclo.

Disolventes: se estableció la modificación de la constante dieléctrica del disolvente. Los disolventes elegidos fueron el H₂O y el CH₃OH. La elección de éstos en esta fase del programa de estudio obedeció a la solubilidad restringida de los heterociclos centrales en disolventes con constantes dieléctricas aún menores.

pH: para el disolvente H₂O, se estableció la modificación del pH, y así explorar su efecto sobre las reacciones de competencia entre H⁺ y Cu(II) por los heterociclos, así como de otros grupos (aniones de sales metálicas y OH⁻) por los cationes referidos.

Temperatura de reacción: cuando se estimara necesario, se adoptaría la temperatura de ebullición del sistema de reacción.

Esquemas de reacciones químicas: para las reacciones respectivas Cu(II)-heterociclo central, se modificó sistemáticamente el disolvente y la naturaleza del contraión presente en las sales metálicas. Para el caso del H₂O, el pH fue también otra variable. Los sistemas de reacción respectivos fueron mantenidos hasta su equilibrio químico estimado. Para las reacciones respectivas de sustitución heterocíclica en la esfera de

coordinación de Cu(II), el primer compuesto de coordinación formado a través del equilibrio Cu(II)-heterociclo, fue llevado a reaccionar con un segundo heterociclo de competencia. Los sistemas de reacción respectivos fueron mantenidos hasta su equilibrio químico estimado. Para las reacciones respectivas de competencia heterocíclica por Cu(II), los ligantes fueron solvatados y posteriormente llevados a reaccionar con el centro metálico. Los sistemas de reacción respectivos fueron mantenidos hasta su equilibrio químico estimado.

II. Metodología en la caracterización de los compuestos obtenidos.

Los compuestos de Cu(II) obtenidos de los esquemas de reacción referidos, fueron caracterizados con base en su Microanálisis elemental, la Espectroscopía vibracional IR, la Espectroscopía electrónica, el Análisis Térmico, el Patrón de difracción de rayos X por el método de polvos, la Espectroscopía de resonancia de espín electrónico (banda X), y las mediciones de Susceptibilidades magnéticas en función de la temperatura y el campo magnético externo aplicado.

III. Metodología en los estudios teóricos de los heterociclos libres.

Los estudios teóricos fueron realizados a nivel de la Teoría de Funcionales de la Densidad. En ellos las estructuras heterocíclicas fueron optimizadas empleando criterios de convergencia en el valor de la energía total y en el gradiente de la energía con respecto a la estructura, así como en su caso, su correspondencia a la de puntos estacionarios. Los cálculos incluyeron las propiedades siguientes: energía molecular total, parámetros estructurales, de índice de valencia, densidad de carga total, potencial molecular electrostático, vector momento dipolo eléctrico, energía y propiedades de la función de onda asociada a diferentes orbitales moleculares y los valores de las constantes tautoméricas en función de la temperatura; se calculó también en algunos casos, el primer potencial de ionización vertical y la primera afinidad electrónica vertical, los espectros vibracionales IR tautoméricos, y los espectros vibracionales IR de especies tautoméricas conjuntas en fase gaseosa con poblaciones relativas diferentes.

CAPÍTULO V

Resumen de Resultados

Y

Discusión.

Capítulo Va

**Algunos estudios sobre la preparación
y caracterización del compuesto polinuclear
Cu(II)(alopurinolato⁻)(OH⁻).**

En esta primera etapa de los estudios propuestos, se exploraron las reacciones de Cu(II) con el alopurinol, bajo condiciones experimentales variadas. Los disolventes principales fueron H₂O (pH variable), (CH₃)₂SO y CH₃OH. En las reacciones se modificó la naturaleza del contraión metálico en las sales de Cu(II). Bajo las condiciones experimentales impuestas, el compuesto con fórmula mínima Cu(II)(alopurinolato⁻)(OH⁻) fue el producto aislado. Los estudios de caracterización han permitido proponer que el compuesto es de naturaleza polinuclear, con los ligantes alopurinolato⁻ y OH⁻ como grupos puente a los centros de Cu(II). La caracterización magnética del producto sólido ha permitido plantear la existencia de un acoplamiento antiferromagnético intenso en el material. En este acoplamiento los ligantes puente han sido postulados a desempeñar el papel central en el intercambio magnético detectado.

Respecto a la formación de Cu(II)(alopurinolato⁻)(OH⁻) desde etapas iniciales diferentes de reacción, pareciera ser que las estabilidades cinética y termodinámica notables referentes a la formación de dicho compuesto están asociadas simultáneamente a más de un denominador común. Uno de ellos, es el relacionado con las propiedades fisicoquímicas del disolvente (constante dieléctrica), ó en su caso, al contenido de H₂O; disolventes con constante dieléctrica elevada (H₂O) ó disolventes menos disociantes pero no anhidros, favorecen la disociación protónica del heterociclo bajo estudio. Aquí, el grupo OH⁻ parece desempeñar el papel crucial. Este proceso pareciera favorecerse aún más bajo la presencia de contraiones metálicos con estabilidades termodinámicas apreciables hacia el H⁺, de tal manera que son bases competitivas por el protón frente al alopurinol. Para el caso del H₂O, es notable también el efecto que tiene el incremento de la concentración del grupo OH⁻ sobre la disociación del alopurinol.

Un segundo denominador común parece ser el asociado a la disposición de los átomos de N en el anillo heterocíclico de cinco miembros. A este respecto, una coordinación metálica monodentada inicial del heterociclo a través de uno de los dos átomos de N se traduciría tanto en un descenso en la estabilidad termodinámica átomo de N(vecino)-H⁺, como en su correspondiente disociación protónica (por la presencia de otras bases que compiten por el protón y/ó por la proximidad de otro centro metálico) y la subsecuente coordinación heterocíclica exobidentada. En estos procesos sugeridos, la temperatura parece desempeñar un papel catalizador en la disociación protónica del heterociclo, como se desprende de algunas de las variantes de las reacciones exploradas.

A esta complejidad de factores se sumaría el del tautomerismo N(1)-H/N(2)-H en el anillo de cinco miembros. En relación a este proceso y su vinculación posible al problema de las interacciones de los tautómeros con los centros metálicos y sus consecuencias, cabe señalar que estudios teóricos realizados¹ sobre los tautómeros N(1)-H/N(5)-H y N(2)-H/N(5)-H del alopurinol neutro, han permitido plantear que para ambos tautómeros los orbitales moleculares frontera (HOMO y LUMO) son del tipo II e independientes (en su distribución sobre los átomos de N del anillo pirazólico) del estado tautomérico. Ambos tautómeros poseen también un OM tipo σ de enlace, que es independiente también de dichos estados tautoméricos. Estos resultados permitirían sospechar que para cualquiera de los dos tautómeros mas estables, la posible interacción inicial de un centro metálico con un átomo de N involucrado en el tautomerismo no requeriría necesariamente que éste estuviera desprotonado.

En relación a esto, no es desmesurado el considerar además la existencia de equilibrios de intercambio metal-protón (equilibrios metalo-protónicos) en las etapas

iniciales de las reacciones exploradas. Estos equilibrios, sumados a los factores señalados arriba, favorecerían la desprotonación del anillo pirazólico y su participación como ligante puente. De hecho, estos equilibrios han sido evidenciados en estudios sobre compuestos de coordinación con ligantes pirazoles sustituidos^{2,3}.

Por otra parte, y en relación a las propiedades magnéticas del producto $\text{Cu(II)(alopurinolato}^{\ominus})(\text{OH}^{\ominus})$, éstas han sido descritas satisfactoriamente a través del modelo dinuclear de espines $S=1/2$ acoplados⁴. Los resultados obtenidos han permitido considerar la existencia de un acoplamiento antiferromagnético intenso de los espines electrónicos provenientes de los átomos metálicos. En este análisis el acoplamiento magnético intermolecular es despreciable. De esta forma, las propiedades magnéticas de bulo han sido asociadas al acoplamiento intramolecular. El tipo e intensidad de este acoplamiento magnético resultante pudiera asociarse a la existencia de una trayectoria suficientemente eficiente para el superintercambio magnético. En ella, los ligantes puente alopurinolato⁻ y OH⁻ parecen desempeñar el papel central.

En relación a este problema, estudios posteriores⁵ que han considerado en el análisis magnético a un modelo octanuclear⁶ de espines $S=1/2$ acoplados, han permitido describir exitosamente las propiedades magnéticas experimentales, no existiendo contraposición con el carácter de los parámetros magnéticos reportados previamente.

En el anexo 1 se presenta una exposición detallada sobre la preparación, la caracterización espectral, y la caracterización magnética preliminar de este compuesto de Cu(II).

Referencias.

1. María Eugenia Costas, Estrella Ramos y Rodolfo Acevedo Chávez. *Density Functional Study of Purine-type Heterocycles: Hypoxanthine and Allopurinol*. Remitido para su publicación (Anexo 7).
2. N.F. Borkett y M.I. Bruce, *J. Organometal. Chem.*, **65**, C51 (1974).
3. G.W. Bushnell, K.R. Dixon, D.T. Eadie y S.R. Stobart, *Inorg. Chem.*, **20**, 1545 (1981).
4. A. Rajca, *Chem. Rev.*, **94**, 871 (1994).
5. Rodolfo Acevedo Chávez, María Eugenia Costas y Roberto Escudero Derat. *Antiferromagnetic Coupling in the Cyclic Octanuclear Compound [Cu(II)(μ -3,5-dimethylpyrazolate)(OH⁻)] and its analogue [Cu(II)(μ -pyrazolate)(OH)]*. Remitido para su publicación (Anexo 2).
6. J.C. Bonner y M.E. Fisher, *Phys. Rev. A*, **135**, 640 (1964).

Capítulo Vb

**Estudios sobre la preparación y caracterización
de los compuestos polinucleares
Cu(II)(pirazolato⁻)(OH⁻) y Cu(II)(3,5-dimetilpirazolato⁻)(OH⁻).**

En relación a los resultados anteriores y con el objetivo tanto de modelar la conducta coordinante del heterociclo alopurinol ante Cu(II), como de analizar el papel desempeñado por el anillo pirazólico en el intercambio magnético entre centros de Cu(II), se sintetizaron tanto el compuesto polinuclear Cu(II)(pirazolato⁻)(OH⁻) como el compuesto octanuclear Cu(II)(3,5,-dimetilpirazolato⁻)(OH⁻)₈^{1,2}. Para el primero se establecieron condiciones experimentales que favorecieran la desprotonación del heterociclo y la participación del grupo OH⁻. Para el segundo, se siguieron condiciones experimentales muy similares a las reportadas^{1,2}.

La caracterización espectral de los compuestos está en concordancia con la participación respectiva de los heterociclos pirazolato⁻ y 3,5-dimetilpirazolato⁻, así como del grupo OH⁻, como ligantes puente a los centros de Cu(II). Ambos compuestos resultaron ser en consecuencia homólogos al compuesto Cu(II)(alopurinolato⁻)(OH⁻), y sistemas adecuados para los objetivos señalados anteriormente. Las propiedades magnéticas experimentales de ambos productos fueron descritas exitosamente a través del empleo de un modelo octanuclear de espines S=1/2 acoplados. Del análisis magnético, se deriva la existencia de un acoplamiento antiferromagnético intenso en ambos sólidos, predominantemente asociado al intercambio magnético respectivo a nivel intramolecular.

Analizando los valores de los parámetros magnéticos respectivos para estos dos compuestos de Cu(II), y comparándolos con los correspondientes al sistema Cu(II)(alopurinolato⁻)(OH⁻) y que fue estudiado con el mismo modelo magnético, se podría sugerir que los tres compuestos de Cu(II) son homólogos estructurales y magnéticos. De esta forma y en relación a Cu(II)(alopurinolato⁻)(OH⁻), se puede considerar que en la coordinación exobidentada del heterociclo a través de los átomos de N del anillo pirazólico, el papel preponderante en la trayectoria del superintercambio magnético desempeñada por el alopurinolato⁻ descansa en el anillo pirazólico de éste.

En relación a los estudios magnéticos de estos tres compuestos de Cu(II) y a los valores del parámetro de acoplamiento magnético (J), éstos permiten proponer la existencia de una trayectoria de superintercambio magnético comparativamente menos eficiente para el caso del compuesto de Cu(II) con el heterociclo puente 3,5-dimetilpirazolato⁻. Ello pudiera estar asociado en parte a las repulsiones intermoleculares derivadas de la presencia de los grupos metilo, lo que aparentemente repercutiría en una distorsión mayor dentro del anillo octanuclear, como se observa en la estructura reportada^{1,2}.

En el anexo 2 se presenta una exposición detallada tanto sobre la preparación, como sobre la caracterización espectral y magnética de los dos compuestos de Cu(II) polinucleares con los ligantes puente respectivos pirazolato⁻ y OH⁻, y 3,5-dimetilpirazolato⁻ y OH⁻.

Referencias.

1. G.A. Ardizzoia, M.A. Angaroni, G. La Monica, F. Cariati, M. Moret y N. Masciocchi, *J. Chem. Soc. Chem. Commun.*, 1021 (1990).
2. G.A. Ardizzoia, M.A. Angaroni, G. La Monica, F. Cariati, S. Cenini, M. Moret y N. Masciocchi, *Inorg. Chem.*, **30**, 4347 (1991).

Capítulo Vc

**Algunos estudios sobre la preparación en medio acuoso ácido
y la caracterización de compuestos de Cu(II)
con los ligantes heterocíclicos respectivos
alopurinol e hipoxantina.**

Como continuación a los estudios precedentes y con el objetivo de explorar la Química de coordinación de los heterociclos isómeros alopurinol e hipoxantina ante Cu(II) en medio acuoso y a pH variable, en una primera etapa se eligió un valor de pH suficientemente bajo (=1.0) en un afán de dificultar tanto la disociación protónica del alopurinol, como la presencia y participación del grupo OH⁻ en la formación de compuestos respectivos de Cu(II) con los ligantes heterocíclicos, así como también la presencia significativa de especies de nuclearidad diversa del sistema Cu(OH)₂ en las reacciones a explorar.

En relación a lo anterior, dicho valor de pH conduciría también a que en las disoluciones acuosas de los heterociclos libres, las especies predominantes fueran las monocatónicas, con los anillos de cinco miembros protonados. Esto daría oportunidad a estudiar también la capacidad de coordinación metálica de sitios de N protonados y en disposiciones diferentes en los anillos referidos. En un afán de profundizar un poco más en el conocimiento de la Química de coordinación de dichos heterociclos, en esta etapa se exploró también la capacidad competitiva de ellos frente a Cu(II), modificando el orden de su participación en la reacción de competencia por el metal. En toda esta primera etapa, se modificó la naturaleza de los contraiones presentes en las sales de Cu(II), con la finalidad de explorar su influencia sobre la naturaleza de los productos obtenidos, y de ser posible, sobre algunas de sus propiedades.

De las reacciones individuales metal-heterociclo y para el caso del alopurinol, se obtuvo el compuesto metálico Cu(II)(alopurinol)₂(Cl)₂ en la totalidad virtual de las reacciones exploradas. Solo con el empleo de CH₃CO₂⁻ como contraión en la sal metálica, se obtuvo al compuesto Cu(II)(alopurinolato⁻)(OH⁻) ya comentado. Para el caso de la hipoxantina, se obtuvieron los sistemas metálicos Cu(II)(hipoxantina)₂(X)₂ (X=Cl⁻ ó Br⁻) y Cu(II)(hipoxantina)₂(X)_n (X=NO₃⁻ ó ClO₄⁻, n=2; X=SO₄²⁻, n=1).

En relación a las reacciones de competencia heterocíclica por el centro de Cu(II), es notable la capacidad de competencia y de coordinación metálica mostrada por el alopurinol sobre la hipoxantina. Para este tipo de reacciones, no se obtuvieron compuestos de Cu(II) con ligantes heterocíclicos mixtos.

Respecto a la preparación de los compuestos, son notables las estabilidades cinética y termodinámica asociadas a la formación del compuesto metálico Cu(II)(alopurinol)₂(Cl)₂. Solamente y bajo la presencia de un ligante (CH₃CO₂⁻) con una estabilidad termodinámica apreciable frente a H⁺, el alopurinol fue desprotonado a las condiciones del pH experimental. Lo opuesto sucede para el caso de los compuestos de Cu(II) con hipoxantina; en éstos es notable la presencia de los contraiones metálicos que fueron incorporados como sales de Cu(II) a las reacciones, no obstante la concentración comparativamente mayor de Cl⁻, como consecuencia del sistema amortiguante de pH empleado. También y en oposición a la conducta mostrada por el alopurinol, la hipoxantina no se encuentra desprotonada en ninguno de sus compuestos de Cu(II) respectivos.

Con la información obtenida de la realización de estas reacciones, es difícil discernir sobre la naturaleza de los factores que inciden en la estabilidad cinética y termodinámica de los productos referidos. Lo que es evidente, es que la disposición de los átomos de N en los anillos de cinco miembros es un factor determinante, pero no lo es en cuanto a las contribuciones diversas en que se traduce dicho rasgo.

Respecto a la caracterización de los compuestos obtenidos, los estudios han permitido sugerir que en todos los casos los ligantes heterocíclicos se coordinan por

átomos de N. Para los dos compuestos con alopurinol, se ha propuesto a átomos de N del anillo pirazólico: N(2) en Cu(II)(alopurinol)₂(Cl)₂, y N(1) y N(2) en Cu(II)(alopurinolato⁻)(OH⁻). Para el primer caso esta propuesta de coordinación metálica correspondería a la existencia del alopurinol en la forma tautomérica N(1)-H/N(5)-H, la cual ha sido considerada como la energéticamente más estable en cálculos teóricos¹ y una de las dos formas predominantes y coexistentes en equilibrio tautomérico en estudios espectroscópicos de disoluciones del heterociclo libre². La propuesta sobre la existencia del alopurinol coordinado en la forma tautomérica N(1)-H/N(5)-H estaría en concordancia con el valor teórico del vector momento dipolo eléctrico comparativamente mayor para este tautómero (3.65 D) en relación al tautómero N(2)-H/N(5)-H (0.93 D), y al efecto que tiene el incremento de la constante dieléctrica del medio sobre el aumento de la estabilidad de aquel tautómero que en estado aislado presenta la magnitud mayor de dicho vector^{1i,3}.

Para el segundo caso, la propuesta de coordinación metálica correspondería a la existencia del alopurinolato⁻ en la forma tautomérica cetónica y protonación en el átomo N(5). La protonación de este átomo parece ser un rasgo importante en el alopurinol monoaniónico coordinado, dado que los estudios experimentales sobre la disociación protónica del heterociclo libre no han considerado a esta forma tautomérica como importante en los equilibrios tautoméricos del heterociclo en disolución con dicha carga formal. Aquí, la vecindad de los átomos de N en el anillo pirazólico parece desempeñar el papel central, al posibilitar la coordinación del heterociclo a través de dicho anillo, y la desprotonación del mismo bajo condiciones experimentales favorables.

De esta forma, la coordinación metálica del alopurinol a través del anillo pirazólico, y la existencia simultánea de bases suficientemente fuertes en la mezcla de reacción (que favorecerían la desprotonación del mismo), posibilitan la estabilización de una forma tautomérica no favorecida en el caso del heterociclo libre monoaniónico.

En relación a los compuestos de Cu(II) con hipoxantina, se ha propuesto la coordinación metálica del heterociclo a través del átomo N(7) del anillo imidazólico en los compuestos del tipo Cu(II)(hipoxantina)₂(X)₂ (X=Cl⁻ ó Br⁻). Aquí, esta propuesta de coordinación metálica correspondería a la existencia de la hipoxantina en la forma tautomérica N(1)-H/N(9)-H, la cual y en cálculos teóricos^{1i,1iii,1iv,4} ha sido considerada prácticamente de la misma estabilidad energética que la forma N(1)-H/N(7)-H. El valor teórico del vector momento dipolo eléctrico para la forma N(1)-H/N(9)-H (5.186 D), es comparativamente mayor que el correspondiente a la forma N(1)-H/N(7)-H (1.798 D). En este caso también, un aumento en la constante dieléctrica del medio incrementaría la estabilidad del tautómero N(1)-H/N(9)-H. De hecho, ya en estudios espectroscópicos en (CD₃)₂SO sobre las poblaciones relativas de estos dos tautómeros, se ha deducido una relación prácticamente equimolar entre ambos⁵. Una constante dieléctrica aún mayor favorecería el incremento de la población relativa del N(1)-H/N(9)-H sobre el N(1)-H/N(7)-H, lo cual estaría en concordancia con la propuesta hecha sobre la coordinación heterocíclica para los dos compuestos de Cu(II) aquí discutidos.

También y en relación a los compuestos de Cu(II) con hipoxantina, se ha propuesto la coordinación del heterociclo a través de los átomos N(3) y N(9) para los compuestos del tipo Cu(II)(hipoxantina)₂(X)_n ya referidos, los cuales presentarían una estructura tipo acetato de Cu(II). Aquí, y en oposición a los dos compuestos de Cu(II) precedentes, el heterociclo se encontraría coordinado en la forma tautomérica N(1)-H/N(7)-H. La presencia de esta forma tautomérica obliga a pensar que en el problema del

tautomerismo en disolución de la hipoxantina neutra, así como en el referente al cambio de las poblaciones relativas tautoméricas con la constante dieléctrica y de la estabilidad preferencial de un tautómero sobre otro en la coordinación metálica, pueden entrar en juego otros factores.

Con respecto a este problema, cálculos teóricos recientes⁴ⁱⁱ sobre los dos tautómeros (N(1)-H/N(7)-H y N(1)-H/N(9)-H) han mostrado que en relación al potencial electrostático molecular, las regiones que involucran a los átomos desprotonados de N y O son favorecidas para una interacción potencial tipo electrostática con especies catiónicas, en concordancia también con las propiedades de los vectores respectivos del momento dipolo eléctrico. En relación a las propiedades de las funciones de onda asociadas a los orbitales moleculares (OM), ambos tautómeros presentan un OM de enlace tipo σ , y un OM (HOMO) tipo Π , los cuales son independientes (en su distribución molecular) del estado tautomérico. Las propiedades de los HOMO podrían tener implicaciones potenciales en el problema de la reactividad, puesto que inducirían a pensar entre otros aspectos, que un átomo de N podría verse involucrado en etapas iniciales de interacción con un metal de transición, no obstante que estuviera protonado. Esto permitiría sospechar que un tautómero dado no necesariamente se coordinaría a través y por ejemplo, de los átomos desprotonados de N que presente dicha forma.

En resumen, y de acuerdo a los cálculos teóricos, ambas formas tautoméricas son susceptibles de participar en interacciones electrostáticas con cationes, *vía* sus átomos desprotonados; ambas también presentan una estructura electrónica tal que posibilita su participación (a través de sus HOMO) en procesos de transferencia de densidad de carga electrónica con orbitales tipo *d* de centros metálicos de transición, *vía* la participación de regiones heterocíclicas que involucran (por ejemplo) átomos de N, desprotonados ó no.

Aquí y en relación a estos tres casos, la naturaleza del contraión ($X=\text{NO}_3^-$, SO_4^{2-} , ClO_4^-) parece ser determinante en la conducta experimental obtenida. También aquí el compuesto del tipo $\text{Cu(II)(hipoxantina)}_2(X)_2$ ha sido obtenido como especie minoritaria (y en donde se ha propuesto la coordinación del heterociclo en la forma tautomérica N(1)-H/N(9)-H). Con esta información es difícil sugerir la naturaleza de la influencia que ejerce el tipo de contraión presente en la sal de Cu(II) en relación al predominio de una forma tautomérica coordinada sobre otra, ó la presencia de ambas en compuestos de Cu(II) diferentes y aislados de la misma disolución en equilibrio químico.

Por otra parte, y con respecto a las propiedades físicas de los compuestos de Cu(II) obtenidos en este estudio, y que contienen respectivamente a los ligantes alopurinol e hipoxantina con carga formal cero, destacan las propiedades espectrales y magnéticas. Para los sistemas del tipo $\text{Cu(II)(L)}_2(X)_2$ (L=alopurinol, $X=\text{Cl}^-$; L=hipoxantina, $X=\text{Cl}^-$ ó Br^-) los estudios magnéticos han permitido plantear la existencia de un acoplamiento antiferromagnético débil entre espines electrónicos de átomos de Cu(II), sugiriéndose que los ligantes halógeno son los participantes preponderantes en la trayectoria del superintercambio magnético respectivo. En estos estudios, los modelos magnéticos utilizados han sido una herramienta notablemente selectiva para la elaboración de las propuestas estructurales de los compuestos de Cu(II), destacando aquí el modelo de cadena lineal de espines $S=1/2$ acoplados.

Para los sistemas del tipo $\text{Cu(II)(hipoxantina)}_2(X)_n$ ($X=\text{NO}_3^-$, SO_4^{2-} , ClO_4^-) los estudios magnéticos han permitido plantear la existencia de un acoplamiento antiferromagnético intenso entre un par de espines electrónicos de átomos de Cu(II), ésto en concordancia con los estudios de REE a las temperaturas de 300 y 77 K. De dichos estudios se ha

propuesto que los ligantes hipoxantina (coordinados a dos átomos de Cu(II) a través de los átomos N(3) y N(9)) desempeñan el papel central en la trayectoria del superintercambio magnético respectivo. Aquí, el modelo magnético de un par de espines $S=1/2$ acoplados, ha sido exitoso en la descripción de las propiedades magnéticas de bulto de los productos sólidos respectivos.

En relación a estos estudios, en el anexo 3 se presenta una exposición detallada sobre la preparación y caracterización espectral y magnética de los compuestos de Cu(II) respectivos.

Referencias.

1. i) B. Hernández, F.J. Luque y M. Orozco, *J. Org. Chem.*, **61**, 5964 (1996); ii) M.K. Shukla y P.C. Mishra, *Spectrochim. Acta Part A*, **52**, 1547 (1996); iii) N. El-Bakali Kassimi y A.J. Thakkar, *J. Mol. Struct.(Theochem.)*, **366**, 185 (1996); iv) María Eugenia Costas, Estrella Ramos y Rodolfo Acevedo Chávez. *Density Functional Study of purine-type Heterocycles: Hypoxanthine and Allopurinol*. Remitido para su publicación (Anexo 7).
2. i) M.T. Chenon, R.J. Pugmire, D.M. Grant, R.P. Panzica y L.B. Townsend, *J. Heterocyclic Chem.*, **10**, 431 (1973); ii) F. Bergmann, A. Frank y Z. Neiman, *J. Chem. Soc., Perkin I*, 2795 (1979); iii) W.S. Sheldrick y P. Bell, *Inorg. Chim. Acta*, **137**, 181 (1987); iv) W.S. Sheldrick y B. Günther, *Inorg. Chim. Acta*, **151**, 237 (1988).
3. i) D.M. Cheng, L.S. Kan, P.O.P. Tso, C.G. Prettre y B. Pullman, *J. Am. Chem. Soc.*, **102**, 525 (1980), ii) K. Szczepaniak y M. Szczesniak, *J. Mol. Struct.*, **156**, 29 (1987); iii) W.B. Person, K. Szczepaniak, M. Szczesniak, J.S. Kwiatkowski, L. Hernández y R. Czerminski, *J. Mol. Struct.*, **194**, 239 (1989); iv) M.J. Nowak, L. Lapinski y J.S. Kwiatkowski, *Chem. Phys. Lett.*, **157**, 14 (1989).
4. i) T. Leo, F. Accion, D. Escolar y J. Tortajada, *An. Quim. Sp.*, **87**, 14 (1991); ii) María Eugenia Costas y Rodolfo Acevedo Chávez, *DFT Study of the Neutral Hypoxanthine Tautomeric Forms*. Remitido para su publicación (Anexo 8).
5. M.T. Chenon, R.J. Pugmire, D.M. Grant, R.P. Panzica y L.B. Townsend, *J. Am. Chem. Soc.*, **97**, 4636 (1975).

Capítulo Vd

Estudios sobre la preparación y caracterización
del compuesto polinuclear
Cu(II)(6-mercaptopurinolato²⁻).

Como extensión a los estudios precedentes y efectuados a pH=1, se intentó explorar la capacidad de competencia heterocíclica hacia Cu(II) por parte del alopurinol y la hipoxantina, ahora en presencia de un nuevo ligante heterocíclico, como es la 6-mercaptopurina. La presencia del átomo S(6) en este heterociclo le confiere tanto una capacidad notable de coordinación metálica como una diversidad de modos de enlace hacia los centros metálicos. Los estudios de competencia heterocíclica por el centro Cu(II) fueron efectuados en una primera etapa en disolución acuosa y valores de pH=1.0, 4.0, 7.0 y 13.0. La intención fue explorar el efecto de las propiedades fisicoquímicas del disolvente (constante dieléctrica elevada) y el valor del pH, sobre la estabilidad termodinámica de un sistema particular Cu(II)-heterociclo (formado en una primera etapa de reacción) bajo la presencia de otro heterociclo en competencia por el mismo centro metálico.

Las reacciones de competencia por Cu(II) fueron efectuadas bajo el mismo esquema seguido en los estudios a pH=1. Para cada tipo de reacción y valor de pH fue modificada sistemáticamente la naturaleza del contraión presente en las sales de Cu(II) ($X = \text{Cl}^-$, Br^- , NO_3^- , SO_4^{2-} , ClO_4^- , CH_3CO_2^-). En esta primera etapa y a diferencia de las reacciones análogas efectuadas en los estudios a pH=1, la temperatura fue la de ebullición de la mezcla de reacción; esto fue hecho con la intención de compensar en alguna medida la solubilidad escasa de los sistemas Cu(II)-heterociclo formados en la primera etapa de reacción y favorecer por tanto la posible competencia del segundo heterociclo, sobre todo y a medida que el pH se ve incrementado. La medida fue adoptada también para favorecer la disociación protónica de los heterociclos en competencia por el centro metálico.

Los mismos estudios de competencia heterocíclica por Cu(II) fueron efectuados en una segunda etapa, modificando las propiedades fisicoquímicas del disolvente, empleando en ésta uno con valores menores en su constante dieléctrica y en su constante de autodisociación protónica. Aquí fue elegido el CH_3OH , para no disminuir drásticamente la solubilidad de los heterociclos. Los estudios en esta segunda etapa fueron efectuados bajo las mismas condiciones experimentales que las de la primera etapa, con la diferencia de emplear tan solo a los contraiones $X = \text{NO}_3^-$, SO_4^{2-} , ClO_4^- y CH_3CO_2^- .

De todas las reacciones de competencia heterocíclica efectuadas en estas dos etapas, un solo producto fue aislado, del tipo $\text{Cu(II)(6-mercaptopurinolato}^{2-})$. Este resultado hace pensar que la independencia de la naturaleza del producto respecto a los contraiones metálicos empleados, es consecuencia del grado apreciable de disociación protónica del heterociclo 6-mercaptopurina. En este proceso pudieran haber influido tanto la temperatura, como las propiedades fisicoquímicas del disolvente (para el caso del H_2O), ó el contenido de ésta (para el caso del CH_3OH).

El hecho de que se obtenga este estado dianiónico formal para el heterociclo en el caso de las reacciones efectuadas a pH=1 (y no obstante la existencia de dos valores de $\text{pK}_a > 6.0$ en el heterociclo libre en H_2O) permite sospechar que la interacción del centro de Cu(II) con aquel, es otro factor importante en dicho proceso de disociación protónica. Aquí, el descenso de valores de pK_a cuando menos en seis unidades, bajo la presencia de Cu(II), es un hecho notable en la fisicoquímica y la química de coordinación de la 6-mercaptopurina.

La capacidad competitiva notable por el Cu(II) mostrada por la 6-mercaptopurina en estos estudios, pudiera atribuirse tanto a la participación del átomo exocíclico S en la

coordinación metálica, a su disposición en la estructura de la molécula (que posibilita por ejemplo, la formación simultánea de enlaces metálicos por S(6) y N(7)), así como a la capacidad heterocíclica comparativamente mayor de disociación protónica. Destaca el hecho de que incluso a valores de pH notablemente elevados, no existe participación del grupo OH^- en el producto, lo cual permite hablar de la existencia de estabilidades cinética y termodinámica peculiares sobre la formación de dicho compuesto de Cu(II). La simple estequiometría metal-ligante de éste, es un indicio a favor de estas características.

La caracterización espectral y magnética del compuesto estarían en correspondencia con su carácter polinuclear, fungiendo la 6-mercaptopurina como ligante puente a centros de Cu(II). En esta propuesta el heterociclo dianiónico participaría (a través de su átomo de S y de los dos átomos de N del anillo imidazólico) en puentes bidireccionales, construyendo con los átomos metálicos una malla aproximadamente bidimensional. Este ha sido el primer caso de los hasta ahora discutidos, en donde uno de los heterociclos centrales de estudio se encuentra bidesprotonado, y por tanto en ausencia de un estado tautomérico prototrópico determinado en el anillo de cinco miembros.

En la caracterización magnética del producto sólido, dos modelos magnéticos han sido exitosos en la descripción de las propiedades magnéticas de bulto del compuesto de Cu(II). Tanto el modelo de cadena lineal de espines $S=1/2$ acoplados (incluyendo en éste la aproximación de campo medio para interacciones intermoleculares), como el modelo tetranuclear de espines $S=1/2$ acoplados con simetría C_{2v} arrojan la existencia de un acoplamiento antiferromagnético muy débil entre pares de espines electrónicos de átomos de Cu(II) para las dos direcciones de la malla propuesta. En el análisis magnético los grupos puente del heterociclo aparecen como los más importantes en la construcción de las trayectorias respectivas de superintercambio magnético. La magnitud del acoplamiento magnético pudiera atribuirse en parte a las distorsiones en los planos que contienen a los átomos de Cu(II).

En el anexo 4 se presenta una exposición detallada sobre la preparación, la caracterización espectral y magnética del sistema polinuclear Cu(II)(6-mercaptopurinolato²⁻).

Capítulo Ve

Estudios sobre la preparación en CH₃OH y la caracterización de compuestos de Cu(II) con los heterociclos respectivos alopurinol, hipoxantina y 6-mercaptopurina. Parte I.

Como extensión a los estudios precedentes (efectuados en disolución acuosa y pH variable, así como en CH₃OH) sobre reacciones de competencia entre el alopurinol, la hipoxantina y la 6-mercaptapurina por Cu(II), se consideró pertinente complementar el estudio sobre la química de coordinación de los heterociclos en CH₃OH, tanto en sus reacciones respectivas Cu(II)-heterociclo, como en las de competencia heterocíclica por el centro metálico, ampliando la serie de contraiones (X=Cl⁻, Br⁻, NO₃⁻) presentes en las sales metálicas. El esquema general de las reacciones fue análogo a los seguidos en los estudios de los subcapítulos Vc y Vd; todas las reacciones se efectuaron a la misma temperatura que en Vd.

Con respecto a las reacciones individuales Cu(II)-heterociclo, aquí se presentaron diferencias notables para el caso del alopurinol (y en comparación a los estudios de los subcapítulos Va y Vc), obteniéndose compuestos del tipo Cu(II)(alopurinol)₂(X)₂ (X=Cl⁻, Br⁻ y NO₃⁻). Aquí pareciera que las propiedades fisicoquímicas del disolvente (constante dieléctrica menor con respecto a la del H₂O), juegan un papel importante en el mantenimiento de la carga formal cero en el heterociclo, posibilitando compartir la esfera de coordinación metálica con los contraiones de las sales metálicas.

Para el caso de la hipoxantina, aquí se obtuvieron sistemas del tipo Cu(II)(hipoxantina)₂(X)₂ (X=Cl⁻, Br⁻, NO₃⁻), el cual es homólogo al de compuestos de Cu(II) con hipoxantina obtenidos y comentados en el subcapítulo Vc.

Por último, y para el caso de la 6-mercaptapurina, se obtuvieron compuestos de los tipos Cu(II)(6-mercaptapurina)_n(X)₂ (X=Cl⁻, n=1; Br⁻, n=2) y Cu(II)(6-mercaptapurinolato²⁻). Aquí también, la presencia del ligante heterocíclico con carga formal cero posibilita la presencia de los contraiones metálicos en la esfera de coordinación de los compuestos de Cu(II) respectivos, hecho contrario al que se presenta en el sistema Cu(II)(6-mercaptapurinolato²⁻). En relación a estos dos compuestos, pareciera que la naturaleza de los contraiones juega un papel importante en el estado de carga formal del heterociclo, y en la estequiometría de los compuestos de Cu(II).

En relación a las reacciones de competencia heterocíclica por Cu(II), la 6-mercaptapurina es el ligante con la capacidad mayor de sustitución heterocíclica, desplazando al alopurinol ó a la hipoxantina de los compuestos Cu(II)(L)₂(NO₃⁻)₂. Por otra parte y para los compuestos con X=Cl⁻ ó Br⁻, los tres heterociclos (como segundos heterociclos respectivos incorporados a los sistemas de reacción) no presentan capacidad de sustitución heterocíclica. La capacidad de la 6-mercaptapurina descrita anteriormente pudiera ser argumentada en términos de la capacidad de coordinación relativamente menor del grupo NO₃⁻; esta característica, asociada a la disociación protónica del heterociclo, favorecen la formación del sistema polinuclear Cu(II)(6-mercaptapurinolato²⁻).

Por último y cuando los heterociclos son llevados a competir simultáneamente por el centro metálico, la 6-mercaptapurina presenta la capacidad mayor de competencia heterocíclica y de coordinación metálica. La reactividad mayor de este heterociclo, pudiera estar asociada aquí al papel desempeñado por el átomo S(6), el cual es el sitio más reactivo del ligante, en su química de coordinación metálica explorada hasta ahora. De los estudios de competencia heterocíclica por el metal, no se obtuvieron compuestos de Cu(II) con ligantes heterocíclicos mixtos.

La caracterización espectral de los compuestos de Cu(II) con alopurinol, permite sugerir la existencia del heterociclo coordinado en forma monodentada por N(2) y en la forma tautomérica N(1)-H/N(5)-H. Para los compuestos de Cu(II) con hipoxantina, la

caracterización correspondiente permite sugerir la existencia del heterociclo coordinado en forma monodentada por N(7) y en la forma tautomérica N(1)-H/N(9)-H. Por último y para los compuestos de Cu(II) con la 6-mercaptapurina en forma neutra, se propone coordinada por S(6) y N(7) (para el caso de X=Cl⁻), y por S(6) (cuando X=Br⁻). En ambos casos, se sugiere la presencia del heterociclo coordinado en la forma N(1)-H/N(9)-H. Aquí cabe señalar que la existencia del tautomerismo N(7)-H/N(9)-H de la forma tiona de la 6-mercaptapurina neutra ha sido evidenciado en estudios espectroscópicos de disoluciones de dicho heterociclo¹⁻⁷.

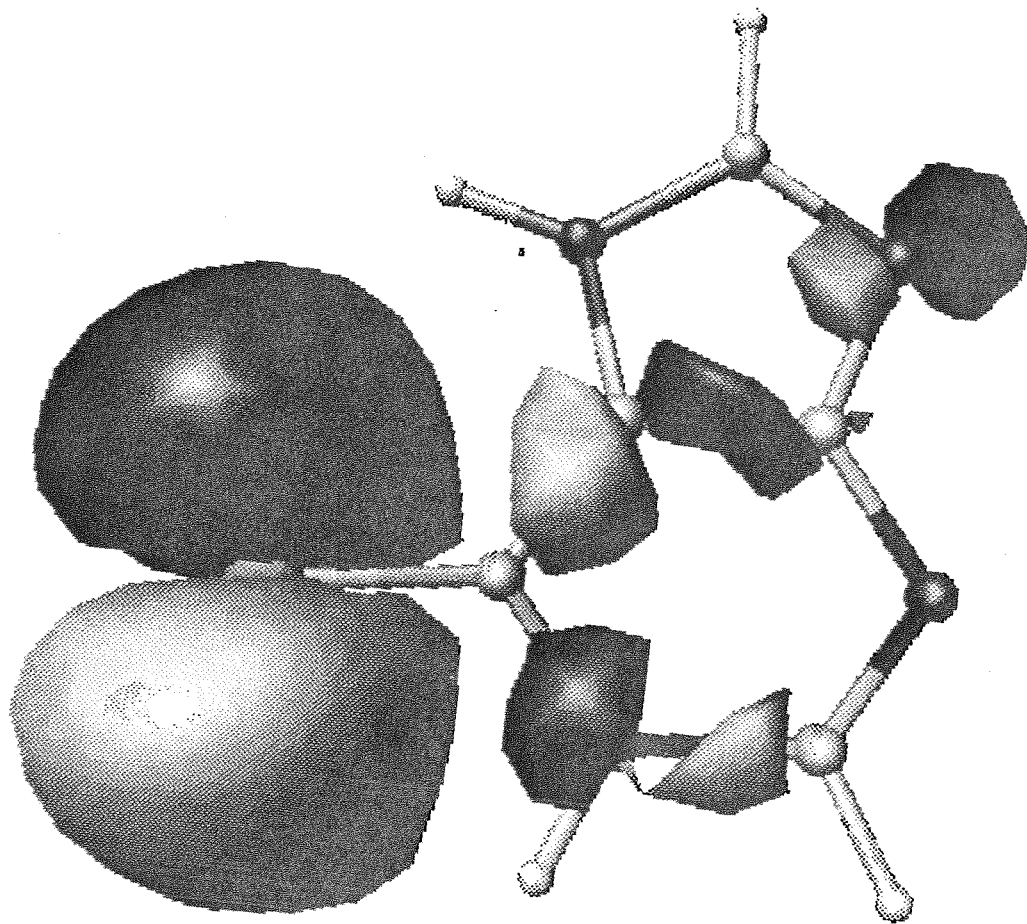
Respecto a la estabilidad energética de los tautómeros de la 6-mercaptapurina en forma tiona y en estado aislado, los estudios teóricos⁶⁻⁸ han revelado que el tautómero N(1)-H/N(7)-H es relativamente más estable ($\Delta E=3.03$ kcal/mol) que el N(1)-H/N(9)-H. Los cálculos teóricos⁸ arrojan para el tautómero N(1)-H/N(7)-H un valor para el vector momento dipolo eléctrico (0.74 D) comparativamente menor que el correspondiente y asociado al tautómero N(1)-H/N(9)-H (5.90 D).

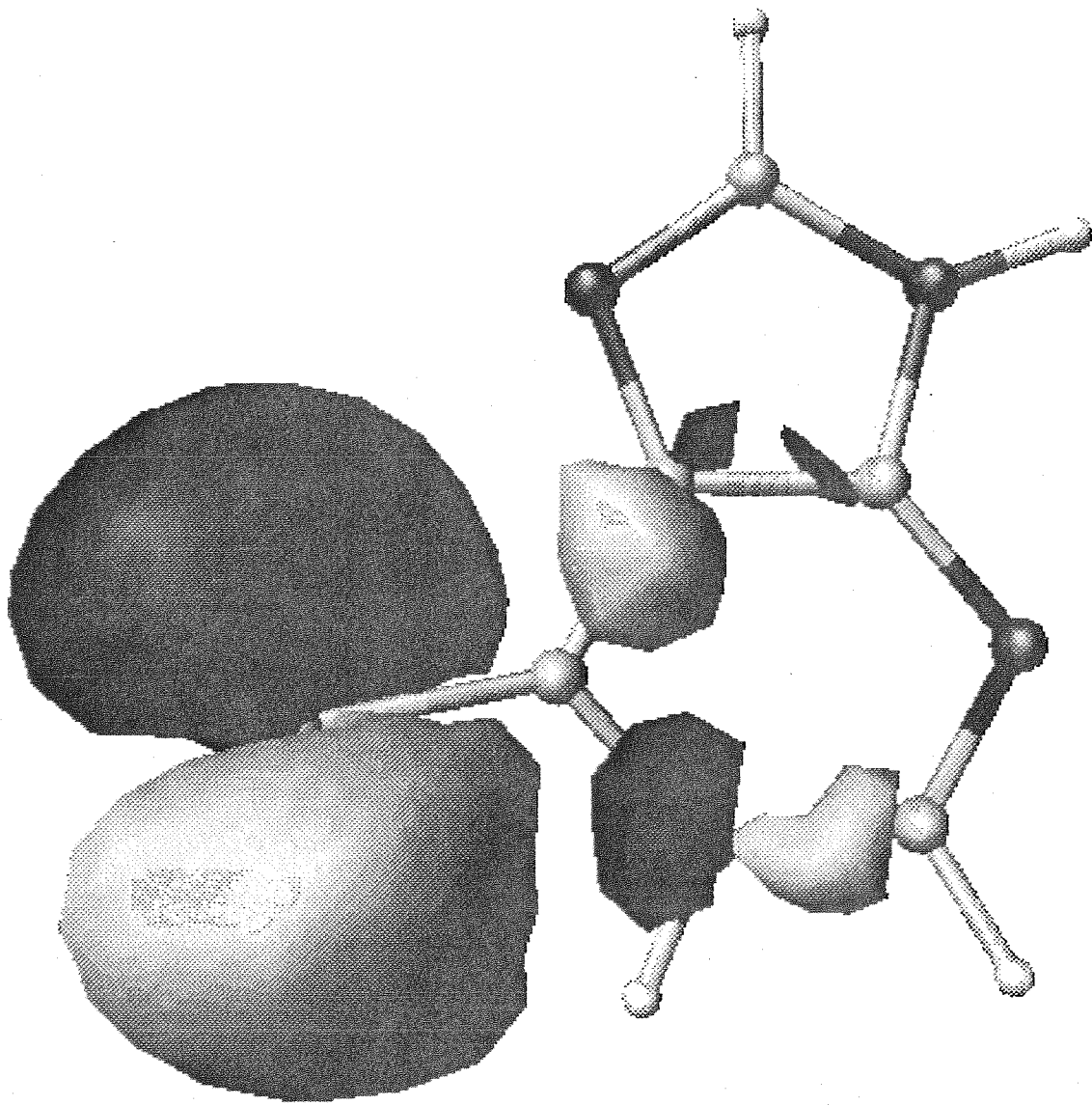
Por otra parte, en los estudios espectroscópicos en (CD₃)₂SO⁵, la población relativa de los tautómeros favorece al N(1)-H/N(7)-H sobre el N(1)-H/N(9)-H, siendo la relación aproximada de 4/1. Para el caso del disolvente H₂O, la población relativa parece favorecer al tautómero N(1)-H/N(9)-H^{1-4,6,7}. De esta forma, un incremento importante en la constante dieléctrica del medio parece favorecer la población relativa de aquel tautómero que en estado aislado presenta el valor mayor del vector momento dipolo eléctrico. El cambio de la población tautomérica relativa de la 6-mercaptapurina con la constante dieléctrica del disolvente, aunado a la participación del átomo S(6) como sitio preferencial de coordinación metálica del heterociclo, pudieran ser factores que contribuyeran al favorecimiento del tautómero N(1)-H/N(9)-H en la 6-mercaptapurina coordinada.

De esta forma y para los tres heterociclos en estudio, la caracterización permite sugerir que éstos se encuentran coordinados respectivamente en aquella forma tautomérica que en estado aislado presenta el valor mayor del vector momento dipolo eléctrico.

En un intento por racionalizar la conducta coordinante experimental mostrada por el átomo S presente en la 6-mercaptapurina, y que pudiera ser el factor decisivo en la participación de otros átomos del heterociclo como sitios de coordinación, se realizaron cálculos teóricos⁸ de algunas propiedades para los tautómeros N(1)-H/N(7)-H y N(1)-H/N(9)-H del heterociclo libre.

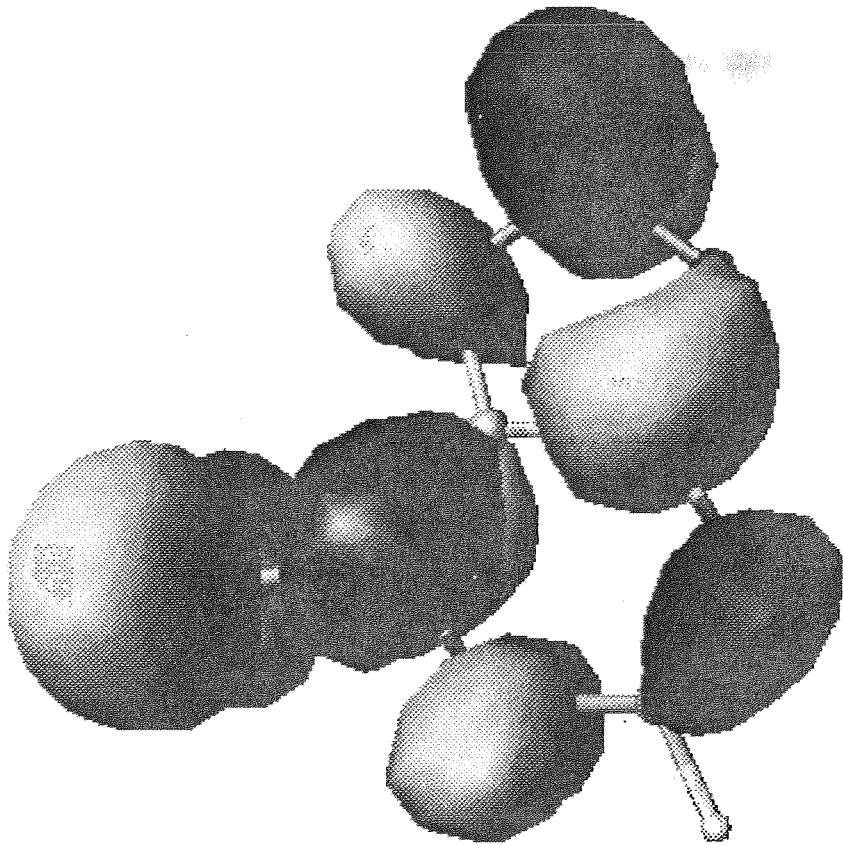
De los cálculos, es importante resaltar que en ambos tautómeros la función de onda asociada a los HOMO presenta propiedades de simetría y de contribución atómica, diferentes a las mostradas por la función homóloga para los dos tautómeros energéticamente más estables tanto del alopurinol como de la hipoxantina. Las dos figuras siguientes ilustran las propiedades de la función para el HOMO ($\Psi \pm 0.025$) de los dos tautómeros de la 6-mercaptapurina en su forma tiona.

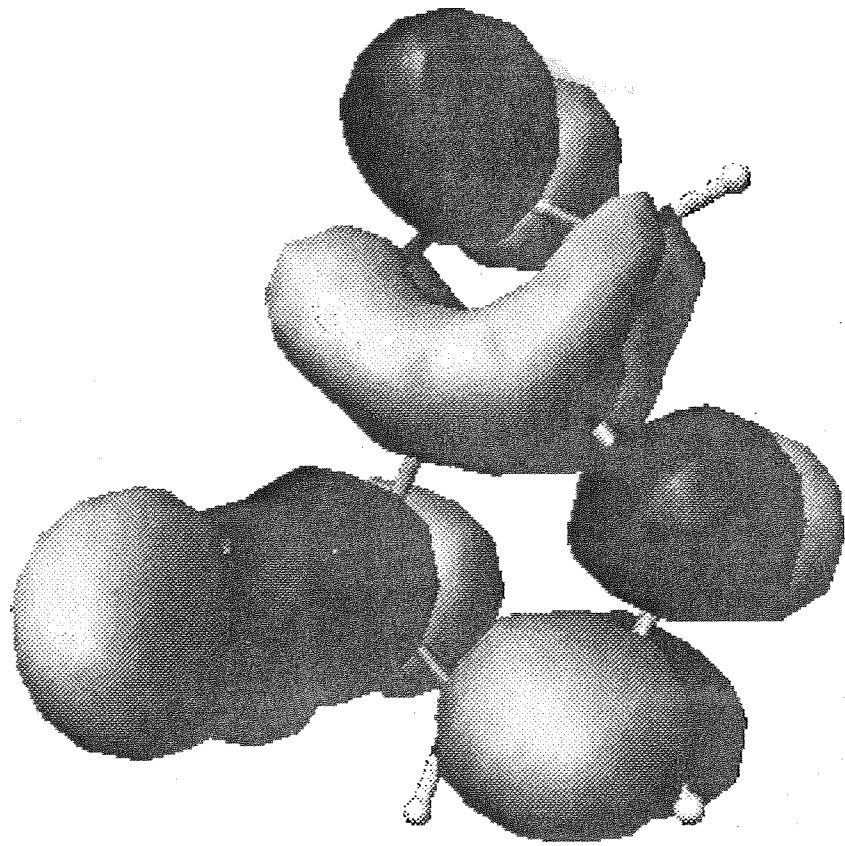




En las figuras se observa que la función se distribuye a nivel del plano molecular, y la contribución atómica más importante es por parte del $\underline{S}(6)$. La función sobre dicho átomo parece tener al menos una contribución tipo p en el plano molecular. Las propiedades de la función sobre dicho átomo exocíclico no cambian notablemente con la forma tautomérica. Es interesante notar que para los dos tautómeros, la función de onda asociada al OM inmediato inferior en energía tiene las mismas propiedades que la asociada a los HOMO para los dos tautómeros del alopurinol y los dos tautómeros de la hipoxantina (Anexos 7 y 8). Por tanto, las propiedades asociadas al HOMO de ambos tautómeros de la 6-mercaptopurina, pudieran ser parte de los factores contribuyentes a la reactividad comparativamente mayor del átomo $\underline{S}(6)$ respecto a los átomos $\underline{O}(4)$ y $\underline{O}(6)$ presentes en el alopurinol y la hipoxantina.

En relación a lo anterior y a las propiedades de la función de onda asociada al LUMO de ambos tautómeros de la 6-mercaptopurina, éstas se muestran en las figuras siguientes.





En ellas se observa que la función (en el nivel ± 0.025) tiene un plano nodal (sobre el plano molecular), y que su contribución atómica y distribución no muestran cambios apreciables con la forma tautomérica. En ambos casos el átomo $\underline{S}(6)$ contribuye a la función del LUMO, teniendo cuando menos una contribución tipo p perpendicular al plano molecular. En resumen y para este heterociclo, en ambos tautómeros el átomo $\underline{S}(6)$ contribuye a la función de onda de los OM frontera, que son a los que se asocian fundamentalmente las propiedades de transferencia de densidad de carga electrónica del heterociclo en sus reacciones químicas.

Por otra parte, y en relación a la caracterización magnética de los compuestos de Cu(II) obtenidos en este estudio, las propiedades magnéticas de bulto fueron analizadas con algunos modelos magnéticos. De los elegidos, sólo el modelo de cadena lineal de espines $S=1/2$ acoplados, describió exitosamente la conducta magnética de cada compuesto. En el tratamiento respectivo de los datos experimentales con este modelo, se incluyó la aproximación de campo medio con la finalidad de explorar la posible descripción de acoplamientos magnéticos entre cadenas.

Para todos los compuestos de Cu(II) los resultados de la caracterización magnética permiten sugerir la existencia de un acoplamiento antiferromagnético muy débil entre los espines electrónicos asociados a pares de átomos de Cu(II) que forman un arreglo lineal. En este análisis magnético las cadenas respectivas estarían formadas a través de la participación de los ligantes aniónicos ($X=Cl^-$, Br^- y NO_3^-) como grupos puente a átomos metálicos vecinos. Del mismo análisis magnético se desprende la existencia de acoplamientos magnéticos muy débiles entre cadenas. Para el compuesto polinuclear del tipo Cu(II)(6-mercaptopurinolato²⁻), el análisis magnético (subcapítulo Vd) empleando el modelo de cadena lineal con la aproximación de campo medio, ó bien el tetranuclear en una simetría C_{2v} , permite sugerir la existencia de un acoplamiento antiferromagnético muy débil entre espines electrónicos asociados a átomos de Cu(II), alineados en dos direcciones en una malla bidimensional distorsionada. Para los compuestos con $X=Br^-$, la intensidad de los acoplamientos magnéticos respectivos es ligeramente mayor que para cuando $X=Cl^-$, sugiriéndose la influencia posible de la polarizabilidad comparativamente mayor del Br^- en dicha conducta magnética. Para los compuestos con $X=Cl^-$, Br^- ó NO_3^- , estos ligantes son convocados a participar como preponderantes en las trayectorias respectivas del superintercambio magnético. Para el compuesto Cu(II)(6-mercaptopurinolato²⁻) el heterociclo coordinado desempeñaría el papel central en la construcción de dicha trayectoria. La intensidad del acoplamiento magnético resultante obtenido en los casos de $X=Cl^-$, Br^- ó NO_3^- , permite considerar la posibilidad de que existan solamente interacciones débiles entre los ligantes aniónicos coordinados a un centro, y los centros vecinos; otra posibilidad es la referente a que los ángulos M-X-M son de tal magnitud que provocan una ortogonalidad apreciable entre los orbitales contribuyentes a la trayectoria del superintercambio magnético (de hecho, se han obtenido relaciones lineales entre el valor del parámetro J de intercambio magnético y el valor del ángulo M-X-M; en estos últimos, existen valores tales de dicho ángulo, que el valor de J es cero). Con los estudios realizados es difícil discernir sobre el peso específico de estas posibilidades, ó incluso la existencia de otras.

Por último, la intensidad del acoplamiento magnético resultante obtenido en el compuesto de Cu(II) con el heterociclo dianiónico, pudiera deberse en parte a las distorsiones en la esfera de coordinación de los átomos de Cu(II).

En el anexo 5 se presenta una exposición detallada de la preparación, así como de la caracterización espectral y magnética de los compuestos de Cu(II) obtenidos en este estudio.

Referencias.

1. D.J. Brown y S.F. Mason, *J. Chem. Soc.*, 682 (1957).
2. J.S. Kwiatkowski, *J. Mol. Struct.*, **8**, 471 (1971).
3. D. Lichtenberg, F. Bergmann y Z. Neiman, *Isr. J. Chem.*, **10**, 805 (1972).
4. L.M. Twanmoh, H.B. Wood, Jr. y J.S. Driscoll, *J. Heterocyclic Chem.*, **10**, 187 (1973).
5. M.T. Chenon, R.J. Pugmire, D.M. Grant, R.P. Panzica y L.B. Townsend, *J. Am. Chem. Soc.*, **97**, 4636 (1975).
6. C. Santhosh y P.C. Mishra, *Spectrochim. Acta*, **49A**, 985 (1993).
7. B. Pullman y A. Pullman, *Adv. Heterocyclic Chem.*, **13**, 77 (1971).
8. María Eugenia Costas y Rodolfo Acevedo Chávez. Estudios no publicados.

Capítulo Vf

Estudios sobre la preparación en CH₃OH y la caracterización de compuestos de Cu(II) con los heterociclos respectivos alopurinol, hipoxantina y 6-mercaptopurina. Parte II.

Como continuación a los estudios del subcapítulo precedente, aquí se exploraron tanto las reacciones Cu(II)-heterociclo para los ligantes respectivos alopurinol, hipoxantina y 6-mercaptapurina, como las reacciones competitivas de dichos heterociclos por el centro metálico, empleando el mismo disolvente y condiciones de temperatura para dichas reacciones, pero ampliando la serie de los contraiones metálicos a $X = \text{SO}_4^{2-}$, ClO_4^- y CH_3CO_2^- .

En relación a las reacciones químicas Cu(II)-heterociclo, en todos los casos se formaron compuestos de Cu(II) con los heterociclos respectivos. Para el alopurinol, se obtuvieron los compuestos del tipo $\text{Cu(II)(alopurinolato}^-\text{)(OH}^-\text{)}$ (cuando se empleó $X = \text{SO}_4^{2-}$ ó CH_3CO_2^-), $\text{Cu(II)(alopurinol)}_4(\text{ClO}_4^-)_2$, y $\text{Cu(II)(alopurinol)(SO}_4^{2-}\text{)(H}_2\text{O)}$ (cuando se limitó la presencia de H_2O en el disolvente de la reacción respectiva). Para la hipoxantina, se obtuvieron compuestos del tipo $\text{Cu(II)(hipoxantina)(SO}_4^{2-}\text{)(H}_2\text{O)}$, $\text{Cu(II)(hipoxantina)}_2(\text{ClO}_4^-)_2$ y $\text{Cu(II)(hipoxantinato}^-\text{)(CH}_3\text{CO}_2^-)$. Por último, y para la 6-mercaptapurina, de todas las reacciones se obtuvo el compuesto del tipo $\text{Cu(II)(6-mercaptapurinolato}^{2-}\text{)}$, descrito y discutido en los subcapítulos Vd y Ve.

En relación a las reacciones Cu(II)-alopurinol, es notable la influencia que tienen la estabilidad termodinámica hacia el protón por parte de los contraiones metálicos empleados, la presencia de H_2O en el disolvente y la temperatura de la reacción, sobre la carga formal del heterociclo y la presencia de otros grupos aniónicos coordinados al centro metálico en los compuestos obtenidos. Así, en aquellas reacciones con X como base conjugada relativamente fuerte hacia el protón ($X = \text{SO}_4^{2-}$ ó CH_3CO_2^-), y presencia de H_2O en el disolvente, se favorece la disociación protónica del heterociclo, y la presencia del grupo OH^- en el compuesto de Cu(II) resultante.

En relación a las reacciones Cu(II)-hipoxantina, la influencia de los factores citados arriba se detecta solamente en el caso $X = \text{CH}_3\text{CO}_2^-$, favoreciéndose la disociación protónica del heterociclo por primera vez. A diferencia de lo ocurrido con el alopurinol, aquí y para el caso de la hipoxantina monoaniónica, el contraión original es el que comparte la esfera de coordinación metálica del Cu(II). Los resultados obtenidos de las reacciones Cu(II)-alopurinol y Cu(II)-hipoxantina, muestran una vez más la estabilidad relativamente mayor hacia el estado de protonación con carga formal cero por parte de la hipoxantina. Por último y en relación a las reacciones Cu(II)-6-mercaptapurina, aquí se obtuvo solamente al compuesto de Cu(II) con el heterociclo bidesprotonado. Resulta notable la influencia desempeñada al menos por los contraiones poliatómicos ($X = \text{NO}_3^-$, subcapítulo Ve; $X = \text{SO}_4^{2-}$, ClO_4^- y CH_3CO_2^-) en el favorecimiento de la desprotonación heterocíclica. La diversidad de las estabilidades termodinámicas hacia el protón por parte de estas bases conjugadas dificulta el análisis sobre los factores a nivel molecular que dan por resultado la disociación protónica del heterociclo. Pareciera ser que la temperatura es aquí también determinante.

De cualquier forma, resalta también de estos estudios la tendencia relativamente mayor hacia la desprotonación extrema en H_2O por parte de la 6-mercaptapurina y en relación al alopurinol ó a la hipoxantina. Por otra parte, y con respecto a las reacciones de competencia heterocíclica por el centro metálico, los estudios muestran la existencia de una capacidad notable de competencia y de coordinación metálica por parte de la 6-mercaptapurina y la estabilización del compuesto $\text{Cu(II)(6-mercaptapurinolato}^{2-}\text{)}$. De todas las reacciones de competencia heterocíclica por Cu(II) no se obtuvieron compuestos de Cu(II) con ligantes heterocíclicos mixtos.

Acerca de los compuestos de Cu(II) con alopurinol, los estudios de caracterización permiten sugerir la coordinación metálica heterocíclica respectivamente a través de los átomos N(1) y N(2) (para el compuesto Cu(II)(alopurinolato⁻)(OH⁻), discutido en el subcapítulo Va) y N(2) (para los compuestos Cu(II)(alopurinol)(SO₄²⁻)(H₂O) y Cu(II)(alopurinol)₄(ClO₄⁻)₂). Para los compuestos de Cu(II) con hipoxantina la caracterización permite sugerir la coordinación metálica heterocíclica a través de N(3) y N(7) (compuesto Cu(II)(hipoxantina)(SO₄²⁻)(H₂O)), N(7) (compuesto Cu(II)(hipoxantina)₂(ClO₄⁻)₂) y átomos de N (compuesto Cu(II)(hipoxantinato⁻)(CH₃CO₂⁻)). Por último y para el compuesto Cu(II)(6-mercaptopurinolato²⁻), se sugiere (como se discutió en el subcapítulo Vd) la coordinación metálica heterocíclica a través de S(6), N(7) y N(9).

En relación a las formas tautoméricas presentes en los heterociclos neutros alopurinol e hipoxantina coordinados respectivamente a Cu(II), la caracterización está en concordancia con la existencia respectiva de los tautómeros N(1)-H/N(5)-H y N(1)-H/N(9)-H. Para el caso de la hipoxantina neutra y en el compuesto Cu(II)(hipoxantina)(SO₄²⁻)(H₂O), resalta la existencia de su forma tautomérica N(1)-H/N(9)-H y de su coordinación metálica a través de los átomos N(3) y N(7). La participación del átomo N(3) en la coordinación metálica aparece como novedosa, y muestra una vez más la inexistencia de una correspondencia directa entre la estabilidad termodinámica hacia el protón y la estabilidad termodinámica hacia un centro de transición, para un átomo heterocíclico dado.

Como parte de este estudio y en relación a la caracterización magnética de los compuestos de Cu(II) novedosos obtenidos, las propiedades magnéticas de bulto de los productos sólidos han sido descritas exitosamente con el empleo del modelo de cadena lineal de espines $S=1/2$ acoplados, incluyendo en el tratamiento la aproximación de campo medio. Para todos los sistemas se plantea la existencia de acoplamientos antiferromagnéticos muy débiles entre espines electrónicos asociados a átomos de Cu(II) vecinos en un arreglo lineal, así como también la sospecha de la existencia de acoplamientos magnéticos muy débiles entre las cadenas respectivas. En este análisis, los grupos SO₄²⁻, ClO₄⁻ y CH₃CO₂⁻, así como los heterociclos neutros ó aniónicos, son considerados a participar en las trayectorias de superintercambio magnético. Sin embargo y a este nivel del análisis, es difícil discernir sobre el tipo de contribución de cada uno de dichos grupos a los acoplamientos magnéticos, tanto de tipo intracadena como intercadena.

En el Anexo 6 se expone detalladamente la preparación de los compuestos de Cu(II) aquí comentados, así como su caracterización espectral y magnética.

Capítulo Vg

**Estudios teóricos preliminares a nivel de
Teoría de Funcionales de la Densidad, sobre la
Estabilidad Energética, las Propiedades Moleculares y
de Estructura Electrónica de algunos Tautómeros Cetónicos
de los Heterociclos Alopurinol e Hipoxantina.**

En forma paralela a los estudios realizados y comentados en los subcapítulos precedentes, se llevaron a cabo cálculos teóricos preliminares sobre la estabilidad energética relativa, los parámetros estructurales y de índice de valencia, densidad total de carga electrónica, momento dipolo eléctrico, potencial electrostático molecular, así como de las propiedades de los orbitales moleculares ocupados y de los desocupados inmediatos y de energía superior, para los tautómeros energéticamente más estables del alopurinol y la hipoxantina neutros. La intención fue el explorar tanto la relación entre dichas propiedades y el tautomerismo de cada heterociclo, así como la relación posible entre ellas y algunos rasgos de conducta experimental mostrada por los heterociclos neutros en sus reacciones químicas ante el protón, o ante centros metálicos transicionales.

Los cálculos teóricos revelan que en estado aislado y de estructura optimizada, los dos tautómeros energéticamente más estables para el alopurinol son el $\underline{\text{N}}(1)\text{-H}/\underline{\text{N}}(5)\text{-H}$ y el $\underline{\text{N}}(2)\text{-H}/\underline{\text{N}}(5)\text{-H}$ (el segundo con una $\Delta E \approx 3$ kcal/mol sobre el primero). Para la hipoxantina, los dos tautómeros más estables son el $\underline{\text{N}}(1)\text{-H}/\underline{\text{N}}(7)\text{-H}$ y el $\underline{\text{N}}(1)\text{-H}/\underline{\text{N}}(9)\text{-H}$ (el segundo, con una $\Delta E \approx 1$ kcal/mol sobre el primero). De esta forma, los cálculos indican que el par de tautómeros energéticamente más estables de cada heterociclo, son las formas cetónicas que presentan tautomerismo en los anillos de cinco miembros. Precisamente dicho par de tautómeros de cada heterociclo, es el que se ha podido detectar como especies predominantes en estudios espectroscópicos de disoluciones de dichos compuestos.

Los cálculos de los parámetros estructurales y de índice de valencia revelan que en cada par de tautómeros existen pares atómicos unidos por enlaces químicos con carácter de enlace doble. Para cada par de tautómeros la posición de dichas regiones está relacionada estrechamente al tautomerismo en los anillos de cinco miembros; los átomos de $\underline{\text{N}}$ desprotonados están asociados a uniones químicas con átomos vecinos, con la propiedad acotada arriba. Los cálculos teóricos sobre densidad total de carga electrónica están en correspondencia con dichos resultados. En vector momento dipolo eléctrico está relacionado también estrechamente al tautomerismo en los anillos de cinco miembros.

Aquellas regiones moleculares que involucran a átomos de $\underline{\text{N}}$ desprotonados (ó inclusive, al $\underline{\text{O}}$), están sociadas al extremo negativo del dipolo eléctrico. Las propiedades de este parámetro pudieran tener implicaciones en el problema del tautomerismo de los dos heterociclos en disolución, sugiriéndose que las poblaciones relativas de los tautómeros respectivos tanto del alopurinol como de la hipoxantina en disoluciones con disolventes de constante dieléctrica elevada, pudiera cambiar a favor de aquellos tautómeros con valores mayores del vector momento dipolo eléctrico.

Los cálculos teóricos del potencial electrostático molecular atractivo hacia una carga positiva de prueba revelan que las propiedades de dicho parámetro están asociadas íntimamente al tautomerismo presente en cada heterociclo: aquellas regiones que involucran a átomos de $\underline{\text{N}}$ desprotonados (ó incluso al $\underline{\text{O}}$) están asociadas a los potenciales electrostáticos atractivos mayores. En otras palabras, estas regiones pudieran considerarse como zonas preferenciales en las interacciones electrostáticas de los tautómeros con especies catiónicas.

Por último y en relación a las propiedades de la función de onda asociada a los orbitales moleculares (OM), y en particular para los OM frontera, la función cambia de signo con el plano molecular de cada par tautomérico tanto del alopurinol como de la

hipoxantina. En forma interesante y para la función del HOMO, las contribuciones atómicas a la función, así como su distribución a nivel molecular, son independientes del tautomerismo del alopurinol y la hipoxantina. De otra manera, la función asociada a las propiedades donadoras de densidad de carga electrónica tiene las mismas propiedades de simetría y de contribución atómica independientemente del tautomerismo de los dos heterociclos. Este resultado podría tener también implicaciones en el problema de los dos isómeros, dado que permite plantear la posibilidad de que átomos de N en cada par de tautómeros, puedan participar en procesos de donación de densidad de carga electrónica ante centros metálicos con orbitales *d*, independientemente del estado de protonación ó de desprotonación en que se encuentren.

En relación a la función del LUMO, las contribuciones atómicas a la función, así como su distribución a nivel molecular, presentan ciertos cambios con el tautomerismo de cada heterociclo. Esto implicaría que las propiedades de aceptación de densidad de carga electrónica por parte del alopurinol y la hipoxantina, dependerían en cierta medida del estado tautomérico de cada uno de ellos en su forma cetónica.

En el Anexo 7 se presenta en forma detallada el nivel de los cálculos teóricos realizados, así como los resultados obtenidos.

Capítulo Vh

**Estudios teóricos a nivel de
Teoría de Funcionales de la Densidad, sobre la
Estabilidad Energética, las Propiedades Moleculares y
de Estructura Electrónica de los Tautómeros
del Heterociclo Hipoxantina.**

Como continuación de los estudios teóricos precedentes, en este subcapítulo se presenta el resumen de algunos resultados obtenidos sobre un estudio teórico exhaustivo a nivel de Teoría de Funcionales de la Densidad de todos los tautómeros del heterociclo hipoxantina con carga formal cero. La intención ha sido realizar el refinamiento de los cálculos teóricos previos, extender el estudio a otros tautómeros, así como el calcular otras propiedades y su relación con la temperatura. Cálculos análogos para los heterociclos alopurinol y 6-mercaptapurina se encuentran en desarrollo.

Los estudios teóricos consideraron catorce posibles tautómeros e isómeros de la hipoxantina neutra. En las optimizaciones de geometrías se emplearon criterios de convergencia de campo autoconsistente (10^{-9} Hartrees) y de gradiente de energía con respecto a la geometría (10^{-7} Hartrees/Bohr). Para todas las geometrías optimizadas se verificó su correspondencia a la de puntos estacionarios. Los cálculos teóricos permitieron obtener valores de energía molecular total, parámetros estructurales, índice de valencia, densidad de carga electrónica total, vector momento dipolo eléctrico, potencial electrostático molecular, energías y propiedades de la función de onda asociada a los 35 OM ocupados y 5 OM desocupados de energía menor, primer potencial de ionización y afinidad electrónica verticales, valores de las constantes de equilibrio tautomérico con la temperatura, y espectros vibracionales IR.

Los estudios han permitido confirmar que de todos los tautómeros e isómeros posibles de la hipoxantina neutra, los energéticamente más estables son el N(1)-H/N(7)-H y el N(1)-H/N(9)-H. Así también y para estos dos tautómeros, los resultados sobre diversas propiedades estructurales, índice de valencia, densidad de carga electrónica total, momento dipolo eléctrico, potencial electrostático molecular, y propiedades de la función de onda asociada a los 40 OM de energía menor, no presentan diferencias cualitativas en relación a las homólogas obtenidas en el estudio preliminar (subcapítulo Vg).

Los cálculos sobre el primer potencial de ionización vertical, revelan que estos dos tautómeros son las especies relativamente más reductoras, y permiten sugerir que en el proceso de oxidación se involucran fundamentalmente a los HOMO respectivos, de tipo II. Los cálculos sobre la primera afinidad electrónica vertical revelan que los dos tautómeros más estables son las especies relativamente menos oxidantes, y permiten sugerir que en el proceso de reducción se involucran fundamentalmente a los LUMO respectivos, de tipo II.

Los resultados obtenidos sobre los valores de las constantes de equilibrio tautomérico como función de la temperatura, revelan que a medida que ésta aumenta, lo hace también la población relativa de tautómeros energéticamente menos favorecidos respecto a los dos energéticamente más estables.

El estudio teórico permitió realizar el cálculo y caracterización de los espectros vibracionales IR de cada tautómero, y de su contribución al espectro IR teórico de la hipoxantina en fase gaseosa, en función de la temperatura y de los valores de las constantes de equilibrio tautomérico correspondientes. De esta manera, se ha podido realizar un análisis teórico del espectro vibracional IR experimental de la hipoxantina en matriz de Ar a 11 K, y se ha concluido que los dos tautómeros que contribuyen al IR experimental, son los energéticamente más estables, sin una contribución espectral significativa del tautómero siguiente en estabilidad energética descendente (el tautómero N(9)-H/enol-cis respecto al N(1)). Así también, se realizaron asignaciones (por modos vibracionales contribuyentes) a las absorciones del IR experimental.

En el Anexo 8 se hace una exposición detallada de la metodología en el estudio teórico, así como de todos y cada uno de los cálculos realizados, de los resultados respectivos, y de sus implicaciones sobre la fisicoquímica teórica y experimental del heterociclo.

CAPÍTULO VI

Conclusiones
y
Sugerencias.

Conclusiones.

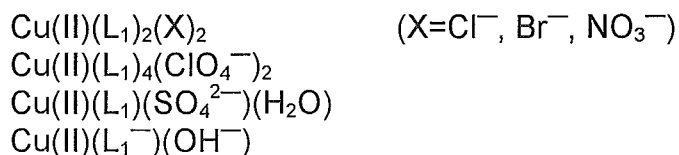
Los estudios realizados sobre las reacciones de los heterociclos alopurinol, hipoxantina y 6-mercaptapurina con el centro metálico Cu(II), así como sobre algunas de las propiedades de los compuestos de coordinación correspondientes, ha sido una primera aproximación sistemática a la exploración de la naturaleza de algunos factores que pudieran intervenir tanto en la química de coordinación de los heterociclos, como en algunas propiedades de los compuestos de Cu(II), y que tienen que ver por ejemplo y particularmente, con procesos de intercambio magnético entre espines electrónicos asociados a los centros metálicos. En estos estudios, algunos compuestos de Cu(II) con heterociclos relacionados fueron preparados y utilizados para profundizar en el análisis de las propiedades magnéticas de uno de los compuestos de coordinación obtenidos en los estudios experimentales.

Así también, los cálculos teóricos realizados sobre los heterociclos centrales de estudio, han permitido obtener información sobre algunas propiedades de los tautómeros energéticamente más estables, y ha sido analizada en un afán de interpretar ciertos aspectos de la información obtenida en los estudios experimentales referidos.

I. Reacciones químicas Cu(II)-heterociclo.

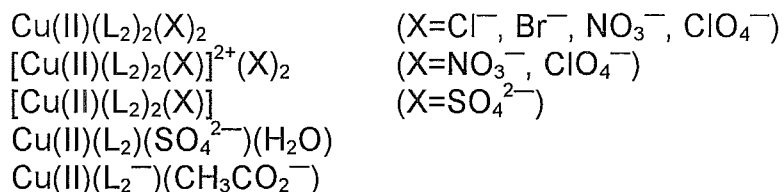
De las reacciones llevadas a cabo en disolución acuosa y en CH₃OH, se obtuvieron los siguientes tipos de compuestos de Cu(II):

a) Con alopurinol (=L₁).

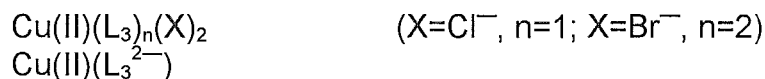


En relación al último, se obtuvieron también los compuestos Cu(II)(pirazolato⁻)(OH⁻) y Cu(II)(3,5-dimetilpirazolato⁻)(OH⁻).

b) Con hipoxantina (=L₂).



c) Con 6-mercaptapurina (=L₃).



Los estudios sobre las reacciones respectivas Cu(II)-heterociclo permiten constatar que existe una influencia apreciable de las condiciones experimentales de reacción sobre la naturaleza del compuesto de coordinación obtenido de una reacción particular Cu(II)-heterociclo. En otras palabras, una misma reacción puede conducir a productos diferentes. En estos estudios, se ha detectado la influencia de la temperatura de reacción, constante dieléctrica del medio, pH, fuerza iónica, tipo de aniones provenientes de las sales metálicas, ó incluso, contenido de H₂O en el disolvente.

De estos mismos estudios se constata que un mismo compuesto de coordinación puede obtenerse por rutas diferentes. Uno de los factores de mayor peso en este resultado, es el asociado a las estabilidades cinética y termodinámica notables y referentes a la formación de dicho compuesto, relacionadas a su vez a la desprotonación del ligante heterocíclico.

Los estudios referidos permiten plantear que los tres heterociclos centrales pueden presentar una conducta diferente frente al mismo centro metálico y condiciones experimentales de reacción comunes. En estas diferencias (concernientes a la carga formal del heterociclo, modo de coordinación metálica y estequiometría Metal-Heterociclo, entre otras) las disposiciones de los átomos potencialmente coordinantes en los heterociclos, sus propiedades electrónicas atómicas, así como moleculares, y las condiciones experimentales de reacción, desempeñan el papel central.

En relación a lo anterior, la secuencia de capacidad de disociación protónica mostrada por los heterociclos coordinados es:



En esta secuencia, juegan un papel preponderante las disposiciones de los átomos coordinantes en los heterociclos, sus propiedades electrónicas, así como el modo de coordinación metálica heterocíclica.

II. Reacciones químicas de sustitución y de competencia heterocíclica por el centro Cu(II).

Los estudios realizados permiten plantear que existe una influencia apreciable de las condiciones experimentales de reacción, así como de las propiedades de los heterociclos, sobre su capacidad de sustitución y de competencia por Cu(II). La secuencia global de capacidad de sustitución y de competencia por el metal, es:



En ésta, un factor decisivo lo desempeña la misma disociación protónica del heterociclo en su coordinación metálica.

III. Coordinación metálica y tautomerismo de los heterociclos.

La caracterización de los compuestos de Cu(II) obtenidos, permite sugerir los sitios de coordinación metálica siguientes:

a) Para el alopurinol ($=L_1$).

N(2) para los compuestos de Cu(II) con alopurinol neutro.

N(1) y N(2) para el compuesto de Cu(II) con el alopurinol monoaniónico.

b) Para la hipoxantina ($=L_2$).

N(7) para los compuestos del tipo $Cu(II)(L_2)_2(X)_2$.

N(3) y N(7) para el compuesto $Cu(II)(L_2)(SO_4^{2-})(H_2O)$.

N(3) y N(9) para los compuestos $[Cu(II)(L_2)_2(X)]^{2+}(X)_2$ y $[Cu(II)(L_2)_2(X)]$.

c) Para la mercaptopurina ($=L_3$).

S(6) para el compuesto $Cu(II)(L_3)_2(Br)_2$.

S(6) y N(7) para el compuesto $Cu(II)(L_3)(Cl)_2$.

S(6), N(7), N(9) para el compuesto $Cu(II)(L_3^{2-})$.

Los estudios estarían asociados a la participación de los heterociclos alopurinol e hipoxantina como ligantes coordinantes por N. Respecto a la 6-mercaptopurina, el papel desempeñado por el átomo S en la coordinación metálica es preponderante. Los cálculos teóricos realizados sobre estos tres heterociclos y en particular sobre sus dos tautómeros respectivos energéticamente más estables, permiten considerar que uno de los factores que pudieran contribuir a la diferencia en las capacidades coordinantes de los átomos exocíclicos O(4), O(6) y S(6), reside en el tipo de contribución orbital de estos átomos a la función de onda de los orbitales moleculares ocupados de energía mayor (HOMO), del mismo tipo (II respecto al plano molecular) para los átomos de O en los HOMO de los tautómeros del alopurinol y de la hipoxantina, y diferente a la mostrada por el S(6) (carácter *p* en el plano molecular) en los HOMO de los tautómeros de la 6-mercaptopurina.

En relación al alopurinol neutro coordinado, los resultados permiten sugerir que éste se encuentra coordinado en la forma tautomérica N(1)-H/N(5)-H, la cual es una de las dos formas energéticamente más estables del heterociclo que se predicen con los estudios teóricos, así como con los estudios espectroscópicos de disoluciones del alopurinol. Respecto al alopurinol monoaniónico coordinado, los resultados permiten sugerir su existencia en la forma cetónica y con el átomo N(5) protonado. Esto podría ser un hecho interesante, dado que en los estudios de disociación protónica del heterociclo libre, la contribución de este tautómero no ha sido considerada como predominante en los equilibrios tautoméricos del alopurinol monoaniónico. Aquí, pareciera que las propiedades del anillo pirazólico, su participación como fragmento de coordinación metálica inicial, y las condiciones experimentales, favorecen su desprotonación bajo la interacción subsecuente con un átomo más de Cu(II).

Con respecto a la hipoxantina neutra coordinada, los resultados permiten sugerir su existencia en las formas tautoméricas $\underline{N}(1)\text{-H}/\underline{N}(7)\text{-H}$ y $\underline{N}(1)\text{-H}/\underline{N}(9)\text{-H}$. Estas dos formas han sido sugeridas a partir de cálculos teóricos como las más estables de la hipoxantina en estado aislado, y evidencias por estudios espectroscópicos como las formas predominantes en disoluciones del heterociclo.

Por último, la capacidad coordinante del átomo $\underline{S}(6)$ en la mercaptopurina pareciera desempeñar un papel determinante en el tipo de tautómero sugerido en los compuestos de Cu(II) con el heterociclo neutro, que es el $\underline{N}(1)\text{-H}/\underline{N}(9)\text{-H}$.

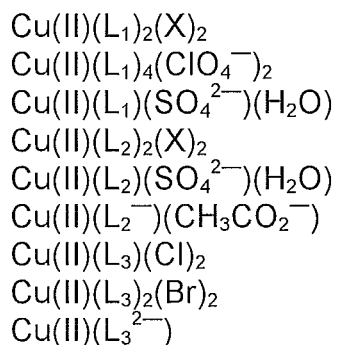
En relación a este punto, se puede concluir que las formas tautoméricas sugeridas en que se encuentran coordinados los tres heterociclos neutros, están influenciadas por factores cuyo peso específico varía entre clases de conductas coordinantes. Para el caso del alopurinol y la hipoxantina (ligantes coordinantes por \underline{N}), la conducta sugerida pareciera estar más asociada a las condiciones experimentales de reacción. Para la 6-mercaptopurina, el factor de mayor contribución parece estar relacionado a las propiedades electrónicas del átomo $\underline{S}(6)$ y su capacidad coordinante.

IV. Acoplamientos magnéticos en los compuestos de Cu(II).

Los estudios espectrales y magnéticos sobre los compuestos de Cu(II) permiten plantear la existencia de dos grupos de acoplamiento magnético, referidos a la intensidad del intercambio correspondiente.

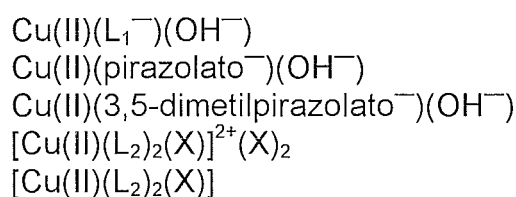
a) Tipos de compuestos de Cu(II) con acoplamientos magnéticos predominantemente muy débiles.

Este grupo lo integran los sistemas:



b) Tipos de compuestos de Cu(II) con acoplamientos magnéticos intensos.

Este grupo lo constituyen los sistemas:



La conducta magnética experimental de la gran mayoría de los compuestos del inciso a) ha sido analizada exitosamente con el empleo del modelo de cadena lineal de espines $S=1/2$ acoplados, incluyendo en el análisis la aproximación de campo medio, con la finalidad de explorar la posibilidad de la existencia de acoplamientos magnéticos entre las cadenas.

La conducta magnética de los compuestos del inciso b) ha sido analizada exitosamente y en forma respectiva por dos tipos de modelos: el del anillo octanuclear de espines $S=1/2$ acoplados, y el dinuclear de espines $S=1/2$ acoplados. En dicho análisis y dado el caso, la aproximación de campo medio fue considerada también.

Los estudios referentes a la mayoría de los compuestos del primer grupo, permiten sugerir que el acoplamiento antiferromagnético entre los espines electrónicos asociados a los centros metálicos, se efectuaría a través de ligantes puente (aniones provenientes de las sales metálicas, aniones y ligantes heterocíclicos, ó heterociclos). Este acoplamiento magnético promedio no se detecta a temperatura ambiental; solo los estudios a $T \rightarrow 0$ K permiten detectarlo, y su intensidad pudiera estar asociada a un conjunto muy complejo de factores, entre ellos, el arreglo estructural entre centros de Cu(II) a lo largo de las cadenas sugeridas.

En relación a los compuestos del segundo grupo, los estudios permiten sugerir que el acoplamiento antiferromagnético entre los espines electrónicos asociados a los centros metálicos en los compuestos del tipo $\text{Cu(II)(L}^-\text{)(OH}^-\text{)}$, se efectúa a través de los ligantes puente aniónicos. Este acoplamiento magnético se detecta a T ambiental, y esto habla de su intensidad. Los tres tipos de compuestos presentan un acoplamiento magnético similar en intensidad, lo que en conjunto con la información obtenida de su caracterización espectral, permite plantear un carácter homólogo para ellos, tanto del tipo estructural como magnético.

Con respecto a los compuestos de los tipos $[\text{Cu(II)(L}_2\text{)}_2\text{(X)}]^{2+}(\text{X})_2$ y $[\text{Cu(II)(L}_2\text{)}_2\text{(X)}]$, los estudios magnéticos permiten sugerir que el acoplamiento antiferromagnético entre el par de espines electrónicos (asociados a dos átomos de Cu(II)) se efectúa a través de los ligantes puente hipoxantina. Este acoplamiento magnético se detecta también a T ambiental. La similitud en la intensidad del acoplamiento magnético en estos sistemas, sumada a la información espectral, permite considerar aquí también la existencia de un carácter homólogo para ellos, en los mismos aspectos ya referidos.

Sugerencias.

Con la intención de profundizar y ampliar los estudios realizados, se pueden sugerir algunas investigaciones tanto experimentales como teóricas.

A. Sobre los sistemas estudiados experimentalmente.

1. Disolución acuosa.

a) Estudios a $\text{pH} < 1$.

Se sugiere la realización (a temperatura ambiental) de los estudios en condiciones de protonación mayor en los tres heterociclos, con la intención de inhibir en mayor medida la existencia de tautomerismos en los anillos de cinco miembros, y explorar la capacidad y conducta coordinante heterocíclica respectiva ante Cu(II) . En estos estudios se implicaría el empleo de ácidos diferentes, y por tanto de bases conjugadas.

b) Estudios a $\text{pH} = 1$.

Se sugiere la realización (a temperatura ambiental) de los estudios que consideran a los tres heterociclos, con la intención de inhibir la disociación protónica de la 6-mercaptopurina, y explorar en dichas condiciones la capacidad y conducta coordinante de los heterociclos ante Cu(II) . En estos estudios se implicaría el uso de especies diferentes en la constitución de la fuerza iónica.

c) Otros valores de pH .

Se sugiere la realización de los estudios aquí abordados, a valores progresivamente ascendentes de pH , con la finalidad de explorar la capacidad y conducta coordinante de los heterociclos bajo estados sucesivos de disociación protónica y presencia ascendente del grupo OH^- . Aquí y para cada valor de pH , se considerarían especies amortiguantes con valores diferentes en sus constantes de estabilidad termodinámica en la formación de compuestos de Cu(II) .

2. $(\text{CH}_3)_2\text{SO}$.

Se sugiere la realización (a temperatura ambiental) de los estudios aquí abordados, con la finalidad de explorar el efecto de la constante dieléctrica del medio sobre la naturaleza de las reacciones Cu(II) -heterociclo, así como sobre la capacidad y conducta coordinante heterocíclica ante Cu(II) .

Se sugiere la realización de estudios espectroscópicos de las reacciones M(II) -heterociclo, con la finalidad de explorar los equilibrios correspondientes, así como las formas tautoméricas de los heterociclos.

3. Heterociclos relacionados.

Se sugiere el empleo de heterociclos sustituidos en posiciones selectivas, como una herramienta en la confrontación de los modos de coordinación metálica sugeridos para los heterociclos abordados y sobre la base de la eliminación de ciertos tipos de tautómeros. Dichos heterociclos podrían ser empleados en la realización de estudios paralelos a los que se han efectuado, ó bien, a los que aquí se proponen.

B. Sobre los sistemas estudiados teóricamente.

1. Refinamientos.

Se sugiere la realización de los cálculos teóricos de los tautómeros de la 6-mercaptapurina, al mismo nivel de refinamiento que para el alopurinol y la hipoxantina, con la intención de homologar la información sobre las propiedades de estos tres heterociclos.

2. Modelos de disolvente.

Se sugiere la realización de cálculos teóricos sobre propiedades de los tautómeros (más estables energéticamente) del alopurinol, la hipoxantina y la 6-mercaptapurina, con diferentes modelos de disolventes, modificando en este estudio la constante dieléctrica del medio. La intención es analizar la influencia de la constante dieléctrica del disolvente sobre la estabilidad energética, las propiedades moleculares y de estructura electrónica de los tautómeros.

3. Reacciones heterociclo-protón.

Se sugiere la realización de cálculos teóricos para determinar energías de protonación y de disociación protónica heterociclo-protón, para los diferentes estados de protonación y tautomerismo de los tres heterociclos en estudio. La intención es analizar las estabildades energéticas, las energías implicadas en las reacciones ácido-base de los tres heterociclos (considerando las contribuciones tautoméricas respectivas), así como sus propiedades moleculares y de estructura electrónica. En este proyecto se estaría considerando el estudio teórico de los heterociclos (en sus estados diferentes de protonación y tautomerismo) bajo la influencia de disolventes de constante dieléctrica modificada sistemáticamente.

4. Propiedades termodinámicas y moleculares de los heterociclos en agua.

Se sugiere la realización de cálculos teóricos de la superficie de potencial de interacción de cada uno de los tres heterociclos (en sus formas tautoméricas más estables) con el agua. Esto se efectuaría con el fin de determinar, por los métodos de simulación por computadora, las propiedades termodinámicas y moleculares de las disoluciones acuosas de los heterociclos referidos.

C. Sobre otros sistemas a estudiar experimentalmente.

1. Sistemas metálicos.

Se sugiere el estudio de las reacciones centro metálico-heterociclo, con el empleo de los centros metálicos del tipo $[M(II)(N,N)(X)_2]^{2+}$ y $[M(II)(N,N,N)X]^{2+}$ ($M(II)=Pd, Pt$; N,N =ligante bidentado por \underline{N} ; N,N,N =ligante tridentado por \underline{N} ; X =ligante lábil con carga formal cero), modificando sistemáticamente las condiciones experimentales de reacción. La intención de este proyecto es explorar la capacidad y conducta coordinante de los heterociclos frente a sitios de selectividad y restricción mayores.

2. Sistemas heterocíclicos.

Se sugiere la incorporación a los estudios sistemáticos, de otros heterociclos análogos estructurales al alopurinol (por ejemplo, los derivados 4-amino ó 4-mercapto), y

a la hipoxantina y 6-mercaptopurina (por ejemplo, la 6-selenopurina), incluyendo sus derivados con sustituciones selectivas. La intención de este proyecto es analizar la influencia de los grupos ó átomos exocíclicos presentes en los heterociclos, sobre la química de coordinación de estos sistemas. Este proyecto podría ser paralelo a los estudios abordados, así como a los que aquí se han sugerido.

D. Sobre otros sistemas a estudiar teóricamente.

1. Sistemas heterocíclicos.

Se sugiere la realización de estudios teóricos sobre los heterociclos relacionados al punto anterior. Este proyecto sería paralelo a los estudios teóricos ya abordados, así como también a los que aquí se han planteado. La intención de este proyecto estaría en relación estrecha con la planteada previamente sobre los estudios teóricos.

2. Compuestos de coordinación.

Se sugiere la realización de estudios teóricos sobre determinados compuestos de coordinación de Cu(II), que presentan respectivamente a los heterociclos alopurinol, hipoxantina y 6-mercaptopurina. La intención en este proyecto es analizar las propiedades principales de la estructura electrónica de los sistemas, y su posible correspondencia con algunos aspectos de la química de coordinación experimental de dichos heterociclos, así como con algunas propiedades experimentales de los compuestos de coordinación respectivos.

ANEXO

1

*Antiferromagnetic Coupling in the Polinuclear
Compound $[\text{Cu}(\text{II})(\text{Alopurinolate})(\text{OH}^-)]_n$.*

Antiferromagnetic Coupling in the Polynuclear Compound [Cu(II) (Allopurinolate) (OH⁻)]_n

Rodolfo Acevedo-Chávez

Centro de Química, Instituto de Ciencias, Benemérita Universidad Autónoma de Puebla, Apartado Postal 1613, Puebla, Puebla, México

and

María Eugenia Costas*¹ and Roberto Escudero-Deratt†

*Facultad de Química, and †Instituto de Investigaciones en Materiales, Universidad Nacional Autónoma de México, México 04510, Distrito Federal, Mexico

Received August 25, 1993; in revised form December 10, 1993; accepted January 10, 1994

Synthetic, spectral, and magnetic studies of the Cu(II) polynuclear coordination compound [Cu(HL)(OH⁻)]_n with bridging OH⁻ and HL (allopurinolate; C₅H₃N₄O⁻) ligands are reported. The compound is obtained from aqueous media (at several pH values and from Cl⁻, Br⁻, NO₃⁻, SO₄²⁻, ClO₄⁻, and CH₃CO₂⁻ Cu(II) salts), from DMSO at ca. 70°C using several of the above salts, and under refluxing methanol employing Cu(SO₄) or Cu(CH₃CO₂)₂. The results suggest that the compound [Cu(HL)(OH⁻)]_n has a polynuclear form in which the bridging allopurinolate is coordinated through the N(1) and N(2) atoms of the pyrazolic moiety. All attempts to grow crystals suitable for X-ray studies were unsuccessful, and an amorphous compound was always obtained. Magnetic studies show the existence of a strong antiferromagnetic coupling, which may be associated with a favorable structural arrangement between the metallic centers and the bridging ligands. This magnetic behavior is remarkable for a Cu(II) polynuclear coordination compound. Spectral and magnetic results together with the coordination modes of the bridging groups let us postulate as a possible arrangement a cyclic polynuclear structure presenting the allopurinolate and OH⁻ bridging ligands in a mutually *trans* configuration. This work is the first EPR spectral and magnetic study reported for a coordination compound with the allopurinol heterocycle as a ligand and, thus for the first example of a polynuclear coordination compound combining allopurinolate and OH⁻ as bridging groups. © 1994 Academic Press, Inc.

INTRODUCTION

Heterocycles with pyrimidine- andazole-type rings fused in their structure are molecules of interest in biochemistry (1), its related areas (2), and coordination chemistry (3-5). This interest is due in part to the fact that

they have several donor atoms, binding arrangements, and structural dispositions, and their coordination compounds have novel spectral and magnetic properties. In particular, several of these heterocycles, purine-type molecules and their structural analogues and isomers, are of special biochemical and biomedical interest, since they are heterocyclic substrates of the Mo metalloenzyme xanthine oxidase, for which oxidation in almost all of these substrates takes place in the Mo center (2). In relation to the structural properties, donor atomic dispositions, and coordinating capability of these heterocycles, a refined understanding of the heterocycle-metallic center interactions is an open field of systematic studies, including kinetic, thermodynamic, structure, and spectral studies, as well as in magnetochemical and quantum mechanical research. Among the compounds that contain these heterocycles, only a few examples have been found (3, 4, 6) that have polynuclear structures. A member of this family, allopurinol (H₂L, 1*H*-pyrazolo[3,4-*d*]pyrimidine-4-one), is a structural isomer of hypoxanthine (6-oxopurine), as is shown in Fig. 1.

Figure 1 shows in **1** a pyrazolic moiety and in **2** an imidazolic moiety as five-membered rings. This characteristic leads to remarkable differences in their behavior with Lewis acids, e.g., transition metal centers. From previous and more recent studies with allopurinol and its derivatives (5-11), and depending on the metallic systems and the experimental conditions, the N atoms of the five-membered ring, and in particular the N(2) atom, are the most favorable coordinating sites of the heterocycle, in agreement with the donor properties (12-14) of N(2). In a previous work (5) the ethanolic synthesis and some properties of the compound [Cu(HL)(OH⁻)]_n were reported. The suggested polynuclear nature of this product and its low magnetic moment at room temperature are

¹ To whom correspondence should be addressed.

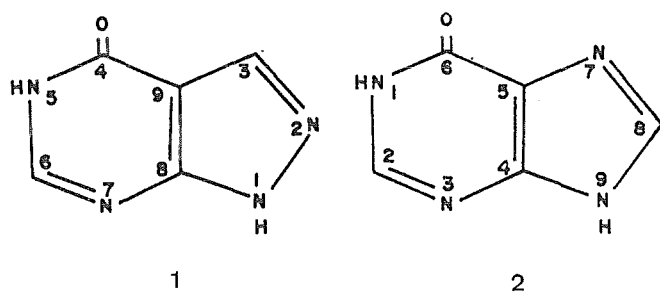


FIG. 1. Formulae and numbering schemes of allopurinol (1) and hypoxanthine (2).

properties that could be associated with an effective magnetic coupling pathway, particularly of an antiferromagnetic character. All these facts prompted us to explore alternative synthetic routes and to carry out a more detailed characterization and magnetic study of this coordination compound.

In this paper, other synthetic routes and spectral (EPR), thermogravimetric, and further magnetic results for $[\text{Cu}(\text{HL})(\text{OH}^-)]_n$ are reported. From these results we propose a possible structural arrangement based on a cyclic framework for $[\text{Cu}(\text{HL})(\text{OH}^-)]_n$. This represents the first example of a polynuclear system with allopurinolate and OH^- as bridging groups.

EXPERIMENTAL

1. Materials

The cupric salts, solvents, and buffer solution reagents were analytical grade products from Aldrich and Merck. Allopurinol was from Sigma. All these products were used without further purification.

2. Synthesis

Aqueous medium. Metallic salts with $X = \text{Cl}^-$, Br^- , NO_3^- , SO_4^{2-} , ClO_4^- , and CH_3CO_2^- , in 1:1, 2:1, 3:1, 1:2, and 1:3 metal:allopurinol molar ratios, were used (mmole scale). pH values were 4, 7, and 13. In all syntheses 1 mmole (136.11 mg) of allopurinol was dissolved in about 100 ml of the respective buffer aqueous solution ($\text{CH}_3\text{COOH}/\text{NaCH}_3\text{CO}_2$ for pH 4, $\text{KH}_2\text{PO}_4/\text{Na}_2\text{HPO}_4$ for pH 7, and KCl/NaOH for pH 13) with stirring and heating. After ligand dissolution, the corresponding cupric salt was added to the colorless solution at room temperature and the reaction mixture was stirred for about 1 hr. The deep blue product obtained was isolated by filtration, washed with water and hot ethanol, and then dried at 110°C for 4 hr. The same product was also obtained for pH 1 (glycine/ HCl) for a 1:1 $\text{Cu}(\text{CH}_3\text{CO}_2^-)_2$:allopurinol molar ratio at boiling temperature.

Methanol medium. In this technique SO_4^{2-} and CH_3

CO_2^- , as counterions and stronger bases, were used. A 1:1 metal:allopurinol molar ratio (mmole scale) was employed. The heterocycle was dissolved in about 100 ml of boiling methanol under reflux. The respective metallic salt was added to the colorless solution, and the mixture was maintained under reflux for 10 days. The corresponding product was isolated by filtration from the hot mixture and washed with hot methanol. The resulting deep blue solid was dried at 110°C for 4 hr. For both techniques, the compounds obtained were preserved in a desiccator under vacuum with CaCl_2 .

Dimethyl sulfoxide medium. In this technique several of the metallic salts employed in the aqueous media synthesis were used. A 1:1 metal:allopurinol molar ratio (mmole scale) was applied. The ligand was dissolved under stirring in ca. 20 ml of DMSO and the respective cupric salt was added. The reaction mixture was maintained at ca. 70°C for several days. The deep blue compound obtained was filtered, washed with hot methanol, dried, and preserved as mentioned above.

3. Physical Measurements

Infrared (IR) spectra were obtained as nujol mulls using CsI plates in the $4000\text{--}200\text{ cm}^{-1}$ range employing a 598 Perkin-Elmer spectrometer. Electronic spectra (350–1100 nm) of the powdered samples were measured by the specular reflectance method in a 160-A Shimadzu spectrometer. Magnetic susceptibility at room temperature was measured by the modified Gouy method using a Johnson Matthey magnetic susceptibility balance and employing $\text{Hg}[\text{Co}(\text{SCN})_4]$ as calibrating agent. Thermogravimetric measurements were carried out in DT-30 Shimadzu equipment using N_2 as the carrier gas and a heating rate of $5^\circ\text{C}/\text{min}$. The variable-temperature magnetic susceptibility measurements were carried out using a SQUID Quantum Design magnetometer, from 5 to 300 K under a magnetic field of 100 G. EPR spectra (X band) of the solid samples were obtained in a 200-D Bruker spectrometer at liquid nitrogen and room temperature. An EPR spectrum (X band) of the frozen solution (DMSO) of the solvated compound was obtained at liquid nitrogen temperature only. The g values obtained were standardized against the absorption of diphenylpicrylhydrazine (DPPH) at $g = 2.0043$. X-ray powder diffraction patterns of allopurinol and several samples of the coordination compound were taken in a XD-5A Shimadzu and a D-500 Siemens diffractometer, the latter using a secondary monochromator with $\text{CuK}\alpha$ radiation. Scanning electronic microscopy of solid $[\text{Cu}(\text{HL})(\text{OH}^-)]_n$ samples, treated under several thermal and pressure conditions, was carried out in JEOL 5400-LV equipment, employing an Ag thin layer as electric conductor medium. Microanalysis confirmation (C, H, N) was performed by the Chemistry Department at the University College, London.

RESULTS AND DISCUSSION

The coordination compound studied was obtained by several synthetic routes and corresponds to the formula $[\text{Cu}(\text{HL})(\text{OH}^-)]_n$ (calculated: 27.8, C; 1.8, H; 25.9, N; found: 27.5, C; 1.9, H; 25.8, N). The reaction was ca. 100% quantitative in all cases. The product is insoluble in common organic solvents and shows a thermogravimetric curve that corresponds to an anhydrous sample, its thermal decomposition starting at around 310°C. The same thermal behavior was observed even when the Cu(II) compound was exposed to humid air. X-ray powder diffraction patterns of several samples of $[\text{Cu}(\text{HL})(\text{OH}^-)]_n$ obtained by different synthetic routes are identical and show remarkable differences with respect to the free heterocycle. The former show scarce, weak, and broader signals, indicative of a poor-crystalline nature. It is important to mention that this poor crystallinity was not overcome by the different product syntheses, by modifying the formation and the precipitation rates, nor by the redissolution attempts of the same compound in several solvents at different temperature conditions. The scanning electronic microscopy results for several samples of solid $[\text{Cu}(\text{HL})(\text{OH}^-)]_n$ do not show the topology and the morphology of a crystalline product. The electronic spectrum of the solid shows a broad band at around 590 nm and a low energy tail of a band in the limit of the blue region. The position of the broad band could be associated with Cu(II) $d-d$ transitions, and the pattern of the spectrum is suggestive of near-planar geometry around Cu(II).

The IR spectrum of $[\text{Cu}(\text{HL})(\text{OH}^-)]_n$ shows a strong band close to 3500 cm^{-1} , which can be assigned to the $\nu(\text{OH}^-)$ bridge (15). It is interesting that the splitting band of the $\nu(\text{OH}^-)$ mode can be associated with the presence of OH^- groups simultaneously bridging two metallic centers in a mutually *cis* configuration; this spectral behavior has been reported (16) for the dinuclear system $[\text{Ni}_2(\text{C}_6\text{F}_5)_4(\text{OH}^-)_2]^{2-}$ and is absent in the spectrum under discussion, suggesting that this type of configuration does not exist for the OH^- groups. The complex and broad signal in the 1130–1010 cm^{-1} region is associated with the $\delta(\text{OH}^-)$ bridge mode. Also, as previously noted (5), the IR spectrum shows bands at 1700 cm^{-1} ($\nu(\text{C}=\text{O})$) and 1610 cm^{-1} ($\delta(\text{N}(\text{5})-\text{H})$), therefore excluding these groups of the organic ligand as coordinating sites in the compound. Signals at 486 cm^{-1} ($\nu(\text{Cu}-\text{OH}^-)$ bridge) and at 295 and 265 cm^{-1} ($\nu(\text{Cu}-\text{N})$) are also shown. The presence of these two latter bands in the low-energy region, attributed to the $\nu(\text{metal}-\text{N})$ mode, is in agreement with the participation of the N atoms of the pyrazolic moiety of allopurinolate as coordinating sites in a bridging fashion (17). In summary, IR data are suggestive of the participation of the pyrazolic fragment of allopurinolate and OH^- as bridging

groups between Cu(II) centers in a polynuclear arrangement.

Although in principle two arrangements of the bridging ligands are feasible (one in the mutually *cis* configuration of the pyrazolic moiety of allopurinolates and the OH^- groups, and the other in the mutually *trans* configuration), the IR data are in agreement with a mutually *trans* configuration, which has been found previously in a triazolic ligand with Cu(II) in a polynuclear system (18), and recently in the interesting cyclic compound $[\text{Cu}(3,5\text{-dmpz}^-)(\text{OH}^-)]_8$ (19).

The room-temperature EPR spectrum of powdered $[\text{Cu}(\text{HL})(\text{OH}^-)]_n$ shows a complex pattern. A reliable assignment of the bands is difficult, but it indicates the existence of strong metal–metal interactions. The approximate g value is 2.27. Although the EPR spectrum at 77 K shows (Fig. 2) a relatively better resolution, its pattern is complicated because, among other features (a nonflat baseline and a long tail at the high-field side of the g_{\perp} feature), it seems to contain overlapped signals in the middle-field region. With a g_{\perp} value of ca. 2.08, the region for g_{\parallel} (ca. 2.4) shows several bumps. This last characteristic could be associated with magnetic impurity signals or exchange averaging of magnetically nonequivalent sites. With this spectral information it is difficult to conclude anything about the possibilities mentioned above. However, the general pattern in the middle-field region could correspond to a predominant axial line shape and principally $d_{x^2-y^2}$ ground state ($g_{\parallel} > g_{\perp} > 2.0$) in a dominant tetragonal stereochemistry (20). The underlying broad signal of the ERP spectrum is suggestive of the existence of Cu(II)–Cu(II) interactions in a polynuclear arrangement.

The EPR spectrum at 77 K of the DMSO frozen solution of the solvated sample shows (Fig. 3) the existence of an anisotropic g tensor, with an axial line shape and values of $g_{\perp} = 2.07$ and $g_{\parallel} = 2.4$. The spectrum exhibits bands in the low-field region related to a hyperfine structure. It is interesting to point out that the EPR pattern (axially symmetric signal) resembles that shown by some copper(II) compounds in solution with a pentacoordinated environment (square pyramidal) in the solid state, e.g., $[\text{Cu}(\text{Cl})(\text{DMF})(\text{HB}((3,5\text{-}i\text{-propyl})_2\text{pz})_3)]$ in DMF frozen solution (77 K), which presents, in solid state, a DMF molecule coordinated to Cu(II) (21). The hyperfine constant value (≈ 130 G) in the EPR spectrum under discussion is related to significant e^- -nuclei coupling. It may be that the ground state of the metallic centers is mainly due to the $d_{x^2-y^2}$ orbitals, although it is possible that the EPR spectrum characteristics could be due to mononuclear species that appear after a dissociative process induced by temperature and solvent nature has taken place.

Since there are no magnetic studies reported for polynuclear coordination compounds with purine-type ligands and their isomers, and since the room-temperature effec-

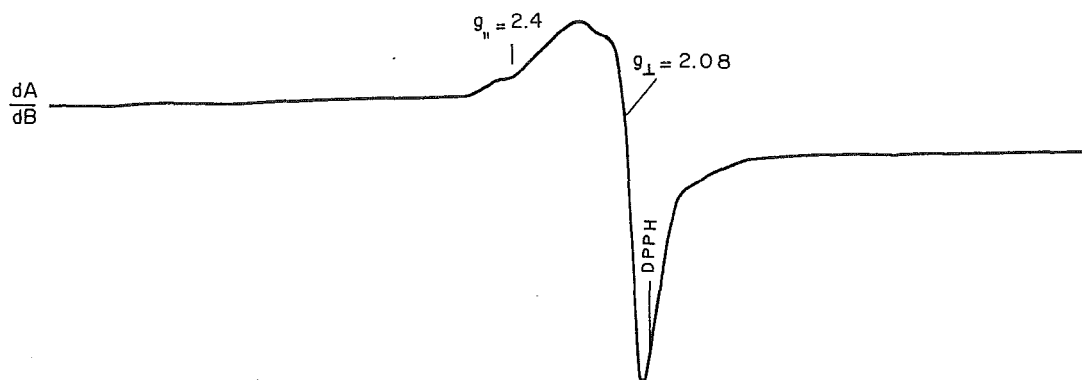


FIG. 2. X-band (9.25 GHz) EPR spectrum at 77 K of solid $[\text{Cu}(\text{HL})(\text{OH}^-)]_n$.

tive magnetic moment of powdered $[\text{Cu}(\text{HL})(\text{OH}^-)]_n$ is $0.9 \mu_B$, it was of great interest to explore its magnetic behavior. Figure 4 presents the experimental molar magnetic susceptibility (per $\text{Cu}(\text{HL})(\text{OH}^-)$) as a function of temperature.

From these results we observe interesting qualitative features, such as the increase of the molar susceptibility close to room temperature, which is suggestive of the existence of a strongly antiferromagnetic coupled system (22). In the low-temperature region a Curie-Weiss behavior is observed, very probably associated with magnetically noncoupled $\text{Cu}(\text{II})$ centers as a magnetic impurity. This result was reproducible for all samples studied.

In a preliminary study, the experimental low-temperature magnetic susceptibility was analyzed employing the Curie-Weiss law. For the range 5–30 K, the parameters $\chi_0 = 4.27 \times 10^{-4}$, $C = 11.06 \times 10^{-3}$, and $\theta = -0.2233$ K were obtained. Also, and for the range 5–80 K, the antiferromagnetic coupling behavior results from the same equation. For this case, we obtained the values $\chi_0 = 4.42 \times 10^{-4}$, $C = 10.73 \times 10^{-3}$, and $\theta = -0.096$ K. This same magnetic characteristic is confirmed when the relation $\chi^{-1}-T$ for the low-temperature region is studied.

In order to study the magnetic properties of $[\text{Cu}$

$(\text{HL})(\text{OH}^-)]_n$, several models were selected, corresponding to two principal categories of systems: (a) dinuclear units for paired spins (23–26) and (b) linear chains of interacting spins, including interchain interactions (27–29). From a fitting process, the expression that corresponds to a Bleaney-Bowers-type equation (i.e., dinuclear systems of paired spins) gave the best results:

$$\chi(T) = \frac{2N\beta^2g^2}{k_B T} \left[3 + \exp\left(\frac{-2J}{k_B T}\right) \right]^{-1} (1 - \rho) + 2n\alpha(1 - \rho) + \rho \frac{N\beta^2g^2}{2k_B T} \quad [1]$$

In this equation, N is the Avogadro number, g the Lande splitting factor, β the Bohr magneton, k_B the Boltzmann constant, T the temperature in Kelvin, J the interaction exchange energy between metallic nearest neighbors, ρ the mole fraction of the magnetically noncoupled $\text{Cu}(\text{II})$ impurity, and $n\alpha$ the temperature-independent paramagnetism term. A fitting of the experimental values with Eq. [1] (Fig. 4) was carried out using as the criterion of best fit the minimum value of $\sum_i (\chi_i^{\text{calc}} - \chi_i^{\text{obs}})^2 / (\chi_i^{\text{calc}})^2$, with the following resulting parameters: $g = 2.25$, $\rho = 0.0097$, $J = -492 \text{ cm}^{-1}$, and $2n\alpha = 480 \times 10^{-6} \text{ emu/mole}$. It is

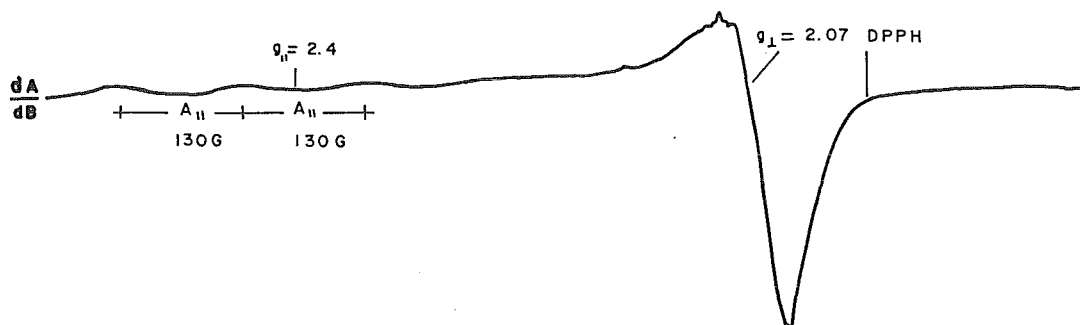


FIG. 3. X-band (9.204 GHz) EPR spectrum of DMSO frozen solution of $[\text{Cu}(\text{HL})(\text{OH}^-)]_n$ at 77 K.

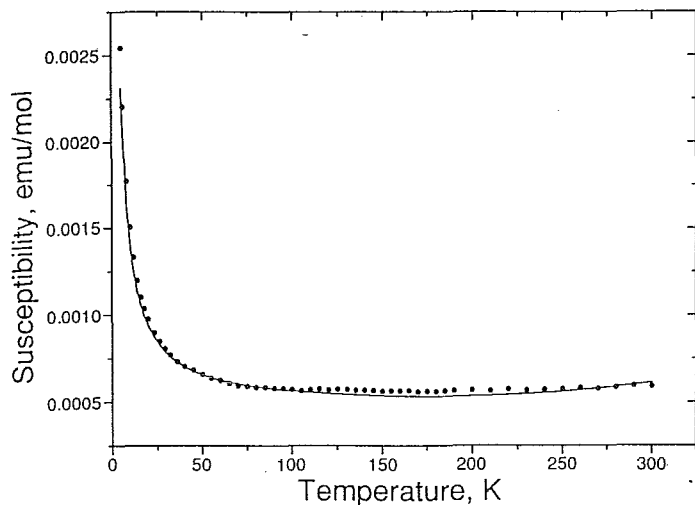


FIG. 4. Experimental (circles) and theoretical (solid line) values of the molar magnetic susceptibility vs temperature of $[\text{Cu}(\text{HL})(\text{OH}^-)]_n$.

interesting that the theoretical g value is in close agreement with the experimental one (2.27). The ρ value is indicative of a very small contribution from magnetically noncoupled Cu(II) centers. The presence and nature of this magnetic impurity were observed in several samples, and they seem to be inherent to the nature of the polynuclear compound. Regarding the J value, its negative character (joined to the same property for θ) may be associated with the existence of a singlet ground state, that is, an antiferromagnetic coupling between the Cu(II) atoms. The magnitude of J is attributed to an appreciable band gap between the ground and the excited states (22). Similar results were obtained when the χT - T behavior was analyzed with Eq. [1] (Fig. 5). In this case, the following

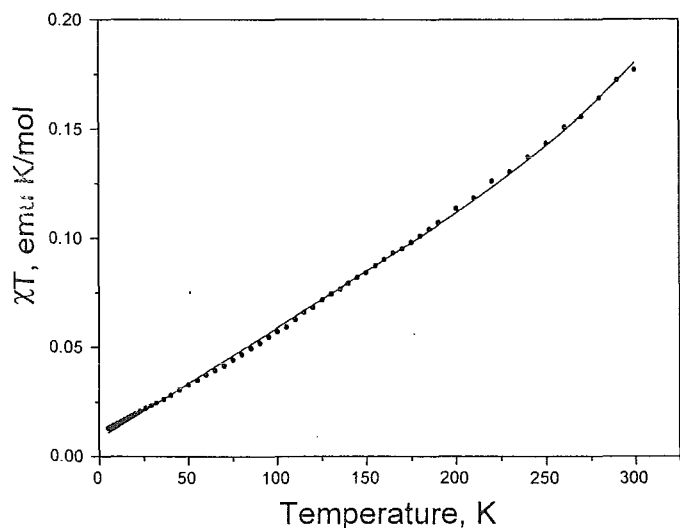


FIG. 5. Experimental (circles) and theoretical (solid line) values of χT vs temperature values of $[\text{Cu}(\text{HL})(\text{OH}^-)]_n$.

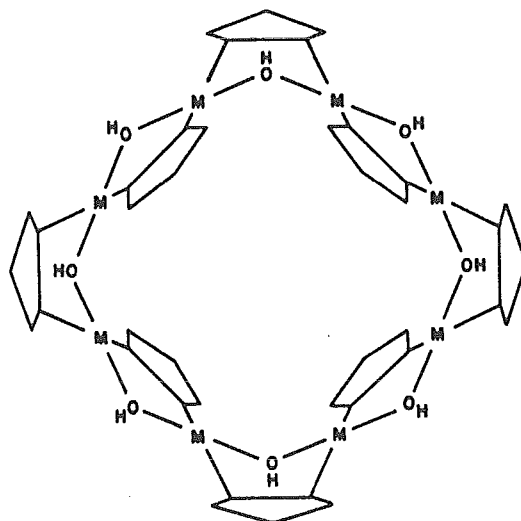


FIG. 6. Schematic drawing of the cyclic framework proposition for $[\text{Cu}(\text{HL})(\text{OH}^-)]_n$ in a mutually *trans* configuration.

results were obtained: $g = 2.24$, $\rho = 0.00857$, $J = -549.7 \text{ cm}^{-1}$, and $2n\alpha = 515.6 \times 10^{-6} \text{ emu/mole}$.

The good fitting shown by our results suggests a remarkable intrachain spin coupling between the Cu(II) centers by the bridging ligands due to an arrangement that makes efficient connection between the magnetic orbitals possible. As has been previously discussed (30), the planarity and efficient overlap between the metallic and the bridging in-phase orbitals gives, in general, this strong antiferromagnetic coupling. In our case it is probable that the participation of the Cu(II) $d_{x^2-y^2}$ orbitals in sigma bonding with N and O atomic orbitals of the bridging groups, and the d_{yz} and/or d_{xz} orbitals of Cu(II) overlapping with $p\pi$ orbitals of N atoms of the pyrazolic moiety of allopurinolate, may be relevant to the J value.

Keeping these aspects in mind as well as the structural and configurational arrangement possibilities for $[\text{Cu}(\text{HL})(\text{OH}^-)]_n$, it is interesting to note that the mutually *trans* configuration is a favorable arrangement for the coordination chemistry of pyrazolate⁻ (pz^-), its derivatives, and OH^- , OR^- , and X^- ligands as bridging groups (14, 16, 19). The fact that the pyrazolic moiety N atoms are participating as a bridge in the coordination of allopurinolate, together with the existence of the bridging OH^- ligand in $[\text{Cu}(\text{HL})(\text{OH}^-)]_n$ and the same metal:ligands stoichiometry with respect to $[\text{Cu}(3,5\text{-dmpz}^-)(\text{OH}^-)]_8$, makes it possible in principle to suggest analogous configurational and structural features in these two coordination compounds. A schematic drawing of this possible structure is shown in Fig. 6.

This possible structure is supported also by the fact that the chemical behavior of the allopurinolate in the compound $[\text{Cu}(\text{HL})(\text{OH}^-)]_n$ is established essentially by

the pyrazolic ring, which is a structural analogue of the 3,5-dmpz⁻ model system ligand.

CONCLUSIONS

Alternative experimental conditions for the synthesis of the polynuclear compound [Cu(HL)(OH⁻)]_n have been established. The critical factors in these routes of synthesis are the presence of water in the reaction media, the nature and basic properties of the counterions, and the pH and temperature. We found that the coordination compound [Cu(HL)(OH⁻)]_n is kinetic and thermodynamically stable toward other competitive reactions (31). Concerning the magnetic studies carried out on [Cu(HL)(OH⁻)]_n, the results show strong antiferromagnetic coupling, and the *J* average value obtained let us suggest the existence of a favorable structural arrangement, in which the disposition and orientation of metallic and bridging donor atomic orbitals are critical for the superexchange coupling pathway. The influence of the pyrimidinic ring of allopurinolate on the magnetic behavior previously discussed was studied by analyzing the magnetic results for the molar susceptibility temperature dependence of [Cu(pz⁻)(OH⁻)]_n obtained under selected conditions (31). This compound shows magnetic properties analogous to those of [Cu(HL)(OH⁻)]_n. This allows us to postulate that the principal heterocyclic ring involved in the magnetic coupling of the metallic centers in [Cu(HL)(OH⁻)]_n is the pyrazolic moiety. On the structural arrangement for [Cu(HL)(OH⁻)]_n the results suggest a possible cyclic framework in a mutually *trans* configuration, in which the superexchange coupling pathway could be favorable. The magnitude of this antiferromagnetic coupling is remarkable for a polynuclear coordination compound. This is the first report of EPR spectral and magnetic studies of an allopurinol coordination compound, and of one of the few polynuclear coordination compounds with these types of heterocycles reported thus far. Also, this is the first example of a polynuclear system with allopurinolate and OH⁻ as bridging groups.

ACKNOWLEDGMENTS

We thank Jorge Ramírez-Salcedo (IFC-UNAM), Max Azomoza-Palacios (UAM-Iztapalapa), Leticia Baños-López (IIM-UNAM), Francisco Morales-Leal (IIM-UNAM), and Rutilo Silva-González (IFBUAP) for the EPR spectra of samples, thermal results, X-ray diffraction patterns, magnetic susceptibility measurements, and scanning electronic microscopy studies, respectively. We also acknowledge Hugo Torres (FQ-UNAM) for his helpful comments on this manuscript. Secretaría

de Educación Pública de México Grants C88-01-0143 and C89-01-0160 are gratefully acknowledged by R. A. Ch. R.E.D. thanks DGAPA (UNAM), CONACyT, and AEO for financial support.

REFERENCES

1. L. Stryer, "Biochemistry," 3rd. ed. Freeman, New York, 1988.
2. R. K. Robins, G. R. Revankar, D. E. O'Brien, R. H. Springer, T. Novinson, A. Albert, K. Senga, J. P. Miller, and D. G. Streeter, *J. Heterocyclic Chem.* **22**, 601 (1985).
3. E. Dubler and E. Gyr, *Inorg. Chem.* **27**, 1466 (1988).
4. E. Dubler, G. Hänggi, and H. Schmalle, *Inorg. Chem.* **29**, 2518 (1990), and references therein.
5. R. Acevedo-Chávez and N. Barba-Behrens, *Transition Met. Chem.* **15**, 434 (1990).
6. W. S. Sheldrick and P. Bell, *Z. Naturforsch. B* **42**, 195 (1987).
7. W. S. Sheldrick and P. Bell, *Inorg. Chim. Acta* **137**, 181 (1987).
8. G. Hänggi, H. Schmalle, and E. Dubler, *Inorg. Chem.* **27**, 3131 (1988).
9. G. Hänggi, H. Schmalle, and E. Dubler, *Acta Crystallogr. Sect. C* **44**, 1560 (1988).
10. W. S. Sheldrick and B. Günther, *Inorg. Chim. Acta* **151**, 237 (1988).
11. G. Hänggi, H. Schmalle, and E. Dubler, *Acta Crystallogr. Sect. C* **47**, 1609 (1991); *J. Chem. Soc. Dalton Trans.*, 941 (1993).
12. A. D. Mighell, C. W. Reimann, and A. Santoro, *Acta Crystallogr. Sect. B* **25**, 595 (1969).
13. C. W. Reimann, A. Santoro, and A. D. Mighell, *Acta Crystallogr. Sect. B* **26**, 521 (1970).
14. S. Trofimenko, *Prog. Inorg. Chem.* **34**, 115 (1986).
15. G. López, J. Ruíz, G. García, C. Vicente, V. Rodríguez, G. Sánchez, J. A. Hermoso, and M. M. Ripoll, *J. Chem. Soc. Dalton Trans.*, 1681 (1992).
16. G. López, G. García, G. Sánchez, J. García, J. Ruíz, J. A. Hermoso, A. Vegas, and M. M. Ripoll, *Inorg. Chem.* **31**, 1518 (1992).
17. J. G. Vos and W. L. Groeneveld, *Inorg. Chim. Acta* **24**, 123 (1977).
18. J. A. J. Jarvis and A. F. Wells, *Acta Crystallogr.* **13**, 1027 (1960).
19. G. A. Ardizzoia, M. A. Angaroni, G. la Monica, F. Cariati, S. Cenini, M. Moret, and N. Masciocchi, *Inorg. Chem.* **30**, 4347 (1991).
20. L. Mishra and A. K. Pandey, *Polyhedron* **11**, 423 (1992).
21. N. Kitajima, K. Fujisawa, and Y. Moro-oka, *J. Am. Chem. Soc.* **112**, 3210 (1990).
22. S. S. Tandon, S. K. Mandal, L. K. Thompson, and R. C. Hynes, *Inorg. Chem.* **31**, 2215 (1992).
23. C. G. Pierpont, L. C. Francesconi, and D. N. Hendrickson, *Inorg. Chem.* **16**, 2367 (1977).
24. M. S. Haddad, S. R. Wilson, D. J. Hodgson, and D. N. Hendrickson, *J. Am. Chem. Soc.* **103**, 384 (1981).
25. I. E. Dickson and R. Robson, *Inorg. Chem.* **13**, 1301 (1974).
26. A. Escuer, R. Vicente, T. Comas, J. Rivas, M. Gomez, and X. Solans, *Inorg. Chim. Acta* **177**, 161 (1990).
27. W. E. Estes, W. E. Hatfield, J. A. C. van Ooijen, and J. Reedijk, *J. Chem. Soc. Dalton Trans.*, 2121 (1980).
28. M. Inoue, S. Emori, and M. Kubo, *Inorg. Chem.* **7**, 1427 (1968).
29. B. C. Gerstein, F. D. Gehring, and R. D. Willett, *J. Appl. Phys.* **43**, 1932 (1972).
30. E. Colacio, J. M. D. Vera, J. P. Costes, R. Kivekäs, J. P. Laurent, J. Ruiz, and M. Sundberg, *Inorg. Chem.* **31**, 774 (1992).
31. R. Acevedo-Chávez, M. E. Costas, and R. Escudero-Derat, in preparation.

ANEXO

2

*Antiferromagnetic Coupling in the Cyclic Octanuclear Compound
[Cu(II)(μ -3,5-dimethylpyrazolate)(μ -OH)]
and its Analogue
[Cu(II)(μ -pyrazolate)(μ -OH)].*

From jssc@chem.purdue.edu Wed Mar 19 06:58 CST 1997
Received: from cv3.chem.purdue.edu by mizton.pquim.unam.mx with SMTP
(16.8/16.2) id AA06654; Wed, 19 Mar 97 06:58:13 -0600
Return-Path: <jssc@chem.purdue.edu>
Received: from [128.210.28.25] by CV3.CHEM.PURDUE.EDU with SMTP;
Wed, 19 Mar 1997 8:07:28 -0500 (EST)
From: "J.S.S.C." <jssc@chem.purdue.edu>
Date: Wed, 19 Mar 97 08:07:58 EST
Message-Id: <1031.jssc@chem.purdue.edu_POPMail/PC_3.2.2>
Reply-To: <jssc@chem.purdue.edu>
X-Popmail-Charset: English
To: costas@mizton.pquim.unam.mx
Subject: Manuscript No. S247
Status: RO

Dear Dr. Costas:

Just a short note to let you know that your manuscript No. S247

Authors: Rodolfo Acevedo-Chavez, MARIA EUGENIA COSTAS, and
Roberto Escudero

Title: Antiferromagnetic Coupling in the Cyclic Octanuclear
Compound...

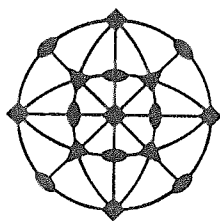
has been accepted for publication in the Journal of Solid State Chemistry.

The referee stated that "the manuscript was carefully revised".

The acceptance notification is being mailed to you today and you should
receive it in the near future.

Respectfully,

Helen Clark
Editorial Assistant
Journal of Solid State Chemistry



Journal of Solid State Chemistry
AN INTERNATIONAL JOURNAL

March 19, 1997

Dr. María Eugenia Costas
Dept. Física y Química Teórica
Universidad Nacional Autónoma de México
Facultad de Química
Cd. Universitaria
México 04510, D.F.
MÉXICO

Dear Dr. Costas:

I am pleased to inform you that your manuscript (No. S247)

Author(s): Rodolfo Acevedo-Chávez, MARIA EUGENIA COSTAS, and Roberto Escudero

Title: Antiferromagnetic Coupling in the Cyclic Octanuclear Compound $[\text{Cu}(\text{II})(\mu\text{-}3,5\text{-dimethylpyrazolate})(\mu\text{-OH})]$ and its Analogue $[\text{Cu}(\text{II})(\mu\text{-pyrazolate})(\mu\text{-OH})]$

has been accepted for publication by the Journal of Solid State Chemistry.

Your manuscript has been forwarded to the Publisher. Page proofs will be sent to you at the earliest possible time. All inquiries concerning processing your manuscript should be addressed to:

Editorial Office
Journal of Solid State Chemistry
525 B Street, Suite 1900
San Diego, California 92101-4495

Sincerely yours,

J.W. Richardson
Associate Editor

JMH:hc

Editor
J.M. Honig

Associate Editor
J.W. Richardson
Department of Chemistry
Purdue University
1393 Brown Building
West Lafayette, Indiana 47907-1393
Tel • (317) 494-5279
FAX • (317) 494-0239
E-mail • jssc@chem.purdue.edu

Book Review Editor
E. Kostiner
Department of Chemistry
University of Connecticut
Box U-60
Storrs, Connecticut 06268

ANEXO

3

*Allopurinol- and Hypoxanthine- Copper(II)
Compounds. Spectral and Magnetic Studies of Novel Dinuclear
Coordination Compounds with Bridging Hypoxanthine.*

**Allopurinol– and Hypoxanthine–Copper(II)
Compounds. Spectral and Magnetic
Studies of Novel Dinuclear Coordination
Compounds with Bridging Hypoxanthine**

Rodolfo Acevedo-Chávez

Centro de Química, Instituto de Ciencias, B. Universidad Autónoma de
Puebla, Apartado Postal 1613, Puebla, Puebla, México

María Eugenia Costas

Facultad de Química, Universidad Nacional Autónoma de México,
México 04510, D.F., México

Roberto Escudero

Instituto de Investigaciones en Materiales, Universidad Nacional
Autónoma de México, México 04510, D.F., México

**Inorganic
Chemistry[®]**

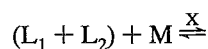
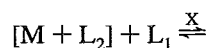
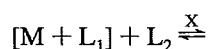
Reprinted from
Volume 35, Number 25, Pages 7430–7439

Table 1. Analytical Results of the Cu(II) Coordination Compounds (L_1 = Allopurinol; L_2 = Hypoxanthine)

compound	color	calcd			found		
		% C	% H	% N	% C	% H	% N
Cu(L_1) ₂ (Cl) ₂ ·H ₂ O	pale green	28.28	2.37	26.38	28.20	2.50	26.10
Cu(L_2) ₂ (Cl) ₂ ·2H ₂ O	blue	27.13	2.73	25.31	27.10	2.60	25.29
Cu(L_2) ₂ (Br) ₂ ·2H ₂ O	green-yellow	22.59	2.27	21.08	22.65	2.60	21.15
Cu(L_2) ₂ (NO ₃) ₂ ·2H ₂ O	deep blue	24.22	2.44	28.25	24.71	2.71	28.40
Cu(L_2) ₂ (SO ₄)·H ₂ O	blue	26.70	2.24	24.91	26.79	2.33	25.04
Cu(L_2) ₂ (ClO ₄) ₂ ·2H ₂ O	blue	21.05	2.12	19.36	21.36	2.13	19.88

To this, 1 mmol of the respective Cu(II) salt ($X = Cl^-$, Br^- , NO_3^- , SO_4^{2-} , or ClO_4^-) previously dissolved in *ca.* 10 mL of buffer solution was added. The reaction mixture was maintained under stirring at room temperature for *ca.* 2 weeks, and then was kept at *ca.* 40 °C and slow evaporation. From this, a solid product was initially formed, isolated, and carefully washed with H₂O ($T = 4$ °C). The solid product was kept at *ca.* 50–60 °C for 48 h, without color changes (see Results and Discussion). For allopurinol and $CH_3CO_2^-$ a blue suspension was formed. The product was isolated, washed with H₂O and kept at 50–60 °C for several days, resulting in a deep blue product. Its characterization was in full agreement with the polynuclear system $Cu^{II}(\text{allopurinolate}^-)(OH^-)$, previously synthesized under several experimental conditions.⁴ For hypoxanthine and $X = Br^-$, a second minor fraction was isolated, which was not characterized. Also for this heterocycle and $X = SO_4^{2-}$ or ClO_4^- , a second solid product was respectively formed, which was isolated and treated as before (see Results and Discussion).

(ii) Competitive Heterocycle-Cu(II) Interactions. Competitive reactions of the heterocycles in study toward the metallic center were systematically performed. The reactions scheme employed was as follows:



The brackets correspond to the previously established chemical equilibria in solution, while the parentheses correspond to the previously dissolved heterocycles, X is the metallic counterion systematically modified ($X = Cl^-$, Br^- , NO_3^- , SO_4^{2-} , ClO_4^- and $CH_3CO_2^-$), $M = Cu(II)$, and L_1 and L_2 represent the heterocyclic ligands allopurinol and hypoxanthine, respectively. All the competitive reactions were performed at the same pH and temperature values. For the first and second type of competitive reactions, the initial step was performed as mentioned in point i; the solution obtained by adding the second heterocyclic ligand was maintained for another 2 weeks. After this time, the respective reaction mixture was maintained at slow evaporation ($T = 40$ °C), and the solid products formed were isolated and treated as before. For the last type of competitive reactions the two ligands previously dissolved in the buffer solution were allowed to react simultaneously with each metallic salt. For this case also each competitive reaction was maintained for the same period of time and treated with the same technique.

It is important to point out that the high chemical complexity of the reaction mixtures and the evaporation conditions from which the different fractions were separated made it very difficult to obtain single crystals for any of the compounds, which could be employed in diffraction studies.

(C) Physical Measurements. Infrared (IR) spectra in the 4000–200 cm^{-1} range (Nujol mulls, CsI windows) were

obtained by using a 599-B Perkin-Elmer spectrometer. IR data in the 600–70 cm^{-1} range (high density polyethylene pellets) were obtained by using a 740 FT IR Nicolet equipment.

Electronic spectra in the 200–1100 nm range (quartz windows and BaSO₄ as reference) of the powdered solid samples were recorded by the specular reflectance method by employing a 160-A Shimadzu spectrometer.

Thermogravimetric studies (room temperature–600 °C) were carried out in a DT-30 Shimadzu equipment by using N₂(g) as carrier fluid and 5 °C/min as heating rate.

X-band EPR spectra of the powdered solid samples (room temperature and 77 K) were recorded by employing a 200-D Bruker spectrometer, with DPPH as reference.

Magnetic susceptibility of powdered samples as a function of temperature at different magnetic fields was obtained with a SQUID MPMS-5 Quantum Design Magnetometer, from 2 to 300 K, and magnetic fields of 100, 1000, 5000, 10000, and 30000 G. The equipment was previously calibrated with very fine standards (Pd, Ni, Al). The magnetic measurements (for each field) were carried out under both increasing and decreasing temperature. Each magnetic measurement was corrected due to the cell and sample diamagnetic contributions and showed an average standard deviation 3 orders of magnitude lower than the respective reading reported.

Microanalyses (C,H,N) were performed at the Chemistry Department of the University College of London, and by means of a 240-C Perkin-Elmer elemental analyzer.

Results and Discussion

(A) Analytical Results. The products isolated and characterized in this study were systematically confirmed by elemental analysis. The results shown in Table 1 are the representative values obtained.

(B) Summary of the Single and Competitive Heterocycle-Cu(II) Interactions. The single and competitive heterocycle-Cu(II) interactions carried out yield several coordination compounds. Table 2 shows these results for the different counterions employed.

In this table, a remarkable preponderance of Cu(allopurinol)₂(Cl)₂·H₂O from the single reactions is observed, irrespective of the metallic counterion employed (except for $X = CH_3CO_2^-$). The higher basicity of $CH_3CO_2^-$ may play a significant role in the heterocyclic ligand deprotonation and in the stabilization of Cu(allopurinolate⁻)(OH⁻), in which the allopurinol is dissociated even at this very low pH value. The behavior, however, is different for hypoxanthine: for the single reactions, a clear influence of the metallic counterion is found due to the formation of several coordination compounds. It is possible that the lower coordination capability of the polyatomic counterions leads to the formation of other products, such as Cu(hypoxanthine)₂(Cl)₂·2H₂O. The most significant case is for $X = CH_3CO_2^-$, in which only this last product was formed. Again, the higher basicity of this anion appears to play a critical role in this behavior. The higher stability of Cu(allopurinol)₂(Cl)₂·H₂O arises again in the competitive heterocycle-Cu(II) interactions,

characteristics suggest the noninvolvement of both the O(6) atom and the N(1)-H group in the metallic bonding. The spectral analysis is in agreement with a noticeable electronic perturbation of endocyclic groups, suggesting the existence of a different metallic bonding behavior of the heterocyclic ligand. In this respect, the IR characteristics of the bands attributed to the C=O and N(1)-H groups suggest the involvement of endocyclic N atoms (possibly the N(3) and N(9) atoms) in addition to those for X = Cl⁻ or Br⁻. The spectral data permit us to propose the noninvolvement of the H₂O molecules in the bonding, as for X = Cl⁻ and Br⁻.

NO₃⁻ IR bands. The IR bands for this system are located in the 1800–600 cm⁻¹ range. The spectral characterization is indicative of the presence of both ionic and coordinated^{9,10} NO₃⁻. The existence of the coordinated NO₃⁻ (C_{2v} symmetry) is deduced from the partial splitting of the complex and strong band in the 1750–1725 cm⁻¹ range (peaks at 1750, 1744, 1740, and 1725 cm⁻¹). This band corresponds to the ν₁ + ν₄ vibrational mode. This same behavior is deduced from the band at 1565 cm⁻¹ (ν₄), and from the partial splitting of the complex band in the 1395–1300 cm⁻¹ range (peaks at 1380, 1360, and 1345 cm⁻¹). The band corresponding to ν₁ might be masked by the band at 1273 cm⁻¹, which in turn is associated with ring, ν_{C-N}, and δ_{N-H} vibrational modes of the coordinated hypoxanthine. Also, ν₂ might be masked by the bands at 980 and 935 cm⁻¹ (assigned to ring and C-H vibrational modes of the same heterocyclic ligand). ν₆ is associated with the band at 830 cm⁻¹. Finally, the bands at 730 and 696 cm⁻¹ might contain the ν₃ and ν₅ vibrational modes, respectively, although they are also attributed to vibrational modes of the heterocyclic ligand. The existence of the ionic NO₃⁻ group is inferred from the band at 1050 cm⁻¹ (ν₁). The bands corresponding to ν₂, ν₃, and ν₄ for the NO₃⁻ group in D_{3h} symmetry might be contained respectively in the bands corresponding to the vibrational modes for the coordinated NO₃⁻. The ν₁ + ν₄ vibrational mode for the ionic NO₃⁻ group might also be contained in the same 1750–1725 cm⁻¹ range. The ν_{Cu-ONO₂} vibrational mode is associated with the band at 343 cm⁻¹, although heterocyclic ligand vibrational modes cannot be discarded. The band at 290 cm⁻¹ is attributed to the ν_{Cu-N} vibrational mode.

(v) Cu^{II}(hypoxanthine)₂(SO₄)·H₂O. Heterocycle IR Bands. The IR information for the 4000–1400 cm⁻¹ range is very similar to that corresponding to X = NO₃⁻; this suggests an analogous metallic bonding behavior for hypoxanthine in both cases, which is corroborated by the related bands (except those corresponding to SO₄²⁻ vibrational modes) appearing in the 1300–600 cm⁻¹ range and by the low-energy IR spectrum. From the spectral analysis, the H₂O molecules show the same behavior for both cases.

SO₄²⁻ IR Bands. The spectral data of the IR active bands are indicative of the existence of coordinated SO₄²⁻. ν₃ shows splitting with broad bands at 1175 and 1100 cm⁻¹. ν₁ can be associated to the broad band at 970 cm⁻¹, without excluding in this band the participation of ring and C-H vibrational modes of the coordinated heterocyclic ligand. ν₄ is associated to the band centered at 623 cm⁻¹, which is also split at 600 cm⁻¹; these bands seem to be also produced by the skeletal and C-H vibrational modes. Finally, the very weak band at 490 cm⁻¹ could be assigned to ν₂. With this spectral information, the participation of the SO₄²⁻ group in a monocoordinated (C_{3v} symmetry) form can be suggested.^{9,10} This metallic coordination might be supported by the band at 348 cm⁻¹, which is attributed

to ν_{M-OSO₃}, and which is also suggested to be produced, in part, by heterocyclic vibrational modes. The metallic bonding of hypoxanthine could be supported by the broad band at 290 cm⁻¹, assigned to the ν_{Cu-N} vibrational mode.

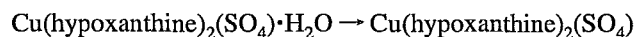
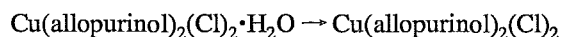
(vi) Cu^{II}(hypoxanthine)₂(ClO₄)₂·2H₂O. Heterocycle IR Bands. The IR data are very similar to that for X = SO₄²⁻; therefore, we can suggest an equivalent behavior for the coordinated hypoxanthine and H₂O molecules in the three cases (X = NO₃⁻, SO₄²⁻, and ClO₄⁻).

ClO₄⁻ IR Bands. The spectral data for this group are in agreement with its existence in both ionic and coordinated forms. For the coordinated ClO₄⁻, the strong and broad band (peaks at 1140, 1116, and 1060 cm⁻¹) is respectively assigned to ν₄ and ν₁ of ClO₄⁻ in a C_{3v} symmetry. The broad and asymmetric band at 932 cm⁻¹ is attributed to the ν₂ of ClO₄⁻ in this same symmetry, although the contribution to this band of ring and C-H vibrational modes is not discarded. ν₃ is associated with the broad band at 680 cm⁻¹. The contribution of ν₅ is attributed to the broad band at 620 cm⁻¹, in addition to the contribution of skeletal and C-H vibrational modes. ν₆ could be associated to the weak band at 500 cm⁻¹. These spectral data are in agreement with the presence of ClO₄⁻ in a monocoordinated form (C_{3v} symmetry).^{9,10} On the other hand, the presence of the ν₃ and ν₄ vibrational modes for ClO₄⁻ in a T_d symmetry could be masked respectively, by the bands attributed to ν₄ and ν₁, and to ν₅ for ClO₄⁻ in a C_{3v} symmetry. The IR activated ν₁ for the ionic ClO₄⁻ could be assigned^{9,10} to the broad and weak band at 860 cm⁻¹. The asymmetric and broad band at 345 and 338 cm⁻¹ could be assigned in part to the ν_{M-OCO₃} vibrational mode. The contribution of the heterocyclic ligand skeletal vibrations in this band must also be considered. The band at 285 cm⁻¹ is assigned to the ν_{Cu-N} vibrational mode.

With the above spectral information, two types of metallic bonding for the heterocycles can be proposed. For the Cu(II) compounds with allopurinol and hypoxanthine respectively (X = Cl⁻ or Br⁻), the first type is through one of the N atoms of the five-membered ring. The second type is deduced for the cases with X = NO₃⁻, SO₄²⁻, and ClO₄⁻, with the involvement of N(3) and N(9) atoms of hypoxanthine. For all the cases, counterions are suggested to be coordinated to the Cu(II) atoms, the polyatomic ones in a monocoordinated form. For the systems with NO₃⁻ and ClO₄⁻ the presence of ionic groups is also proposed. In all the cases, the participation of H₂O molecules in the metallic bonding is excluded.

(D) Thermogravimetric Results. The thermogravimetric results are summarized in Table 3.

For the first and the last compounds, the first mass loss step corresponds respectively to the following processes:



For the other three, this step is in agreement with the sample dryness process. For all the cases, the temperature range in which the initial step takes place is suggestive of the nonexistence of H₂O molecules in the metallic coordination sphere, in agreement with the low-energy IR spectral information. In trying to corroborate our results related to the nature of the H₂O molecules (crystalline lattice type) and the thermal stability

(9) Ferraro, J. R. *Low-frequency vibrations of Inorganic and Coordination Compounds*; Plenum Press: New York, 1971 and references therein.

(10) Nakamoto, K. *Infrared and Raman spectra of Inorganic and Coordination Compounds*, 2nd. ed.; John Wiley & Sons, Inc.: New York, 1978 and references therein.

the same general pattern. The only difference lies in the resolution of the signal for g_{\parallel} (with g components of 2.24 and 2.16), which supports the considerations on the structural features and axial interactions quoted above for the Cu(II) center. Again, under these conditions, a Cu(II)-Cu(II) magnetic coupling is discarded.

The EPR spectrum of $\text{Cu}^{\text{II}}(\text{hypoxanthine})_2(\text{Cl})_2 \cdot 2\text{H}_2\text{O}$ shows (Figure 2b) a signal in the middle magnetic field region, suggestive of an anisotropic g tensor, with $g_1 = 2.025$, $g_2 = 2.103$ and $g_3 = 2.247$ ($R = (g_2 - g_1)/(g_3 - g_2) = 0.5 (< 1.0)$), with no evidence at these conditions of Cu(II)-Cu(II) interactions. The spectral data could be associated to a distorted octahedral rhombic environment for Cu(II). The ground electronic state is suggested to be associated to the $d_{x^2-y^2}$ and d_z^2 orbitals. With a decrease in temperature (77 K, $\nu = 9.264$ GHz) the spectrum gives $g_1 = 2.029$ and $g_2 = 2.072$ and shows a resolution of the signal for g_{\parallel} (with g components of 2.22 and 2.14). This result, joined to the value $g_{\perp} = 2.072$, is associated to axial interactions and to the suggestion of an elongated octahedral rhombic environment for Cu(II). Also, under these conditions, there is no evidence of Cu(II)-Cu(II) interactions.

Finally, the EPR spectrum at room temperature ($\nu = 9.778$ GHz) of the anhydrous $\text{Cu}^{\text{II}}(\text{hypoxanthine})_2(\text{Cl})_2$ was obtained in the hope of corroborating the isostructural character for this system and the former hydrated analogous. For the anhydrous compound, essentially the same pattern is obtained ($g_1 = 2.02$, $g_2 = 2.09$, $g_3 = 2.20$), in agreement with the spectral and thermal results (*i.e.*, the noninvolvement of H_2O molecules in the Cu(II) coordination sphere of $\text{Cu}^{\text{II}}(\text{hypoxanthine})_2(\text{Cl})_2 \cdot 2\text{H}_2\text{O}$).

The EPR spectrum of $\text{Cu}^{\text{II}}(\text{hypoxanthine})_2(\text{Br})_2 \cdot 2\text{H}_2\text{O}$ (Figure 2c) shows differences with respect to the two preceding cases. The spectral pattern consists of a very broad and non symmetric signal ($g_1 = 1.96$, $g_2 = 2.14$, $g_3 = 2.38$), which is associated with an anisotropic g tensor¹⁵ and to the existence of Cu(II)-Cu(II) interactions. With a lowering of the temperature (77 K, $\nu = 9.264$ GHz) the spectrum shows the same general features ($g_1 = 1.98$, $g_2 = 2.15$, $g_3 = 2.36$). Interestingly, a broad and unresolved signal in the low-field region is also detected (600–1500 G), supporting the existence of Cu(II)-Cu(II) interactions, although without excluding its origin due to the presence of magnetic impurities of $S = 1/2$ spins in the ground state.

The analysis of the EPR spectral results described for these three compounds, suggests the structural features for them. For $\text{Cu}^{\text{II}}(\text{allopurinol})_2(\text{Cl})_2 \cdot \text{H}_2\text{O}$, it is possible to consider the existence of mononuclear $\text{Cu}^{\text{II}}(\text{allopurinol})_2(\text{Cl})_2$ units in a distorted square planar geometry, possibly with very weak axial interactions in the crystalline lattice, as is schematically shown in Figure 3.

For $\text{Cu}^{\text{II}}(\text{hypoxanthine})_2(\text{Cl})_2 \cdot 2\text{H}_2\text{O}$ the existence of a distorted octahedral rhombic geometry for Cu(II), with the hypoxanthine and Cl^- ligands in the equatorial plane is proposed. Weak axial interactions occur possibly through the heterocyclic ligand (*i.e.*, the exocyclic O(6) atoms) or through the halogen atoms of neighboring Cu(II) units, this last one in a similar way to that postulated for $\text{Cu}^{\text{II}}(\text{allopurinol})_2(\text{Cl})_2 \cdot \text{H}_2\text{O}$. For $\text{Cu}^{\text{II}}(\text{hypoxanthine})_2(\text{Br})_2 \cdot 2\text{H}_2\text{O}$, it is possible to consider the existence of Cu(II)-Cu(II) interactions through the Br^- ligands, in a similar form to that suggested for $\text{Cu}^{\text{II}}(\text{allopurinol})_2(\text{Cl})_2 \cdot \text{H}_2\text{O}$.

(ii) $\text{Cu}^{\text{II}}(\text{hypoxanthine})_2(\text{NO}_3)_2 \cdot 2\text{H}_2\text{O}$ and analogue compounds ($\text{X} = \text{SO}_4^{2-}$ and ClO_4^-). The EPR spectrum of $\text{Cu}^{\text{II}}(\text{hypoxanthine})_2(\text{NO}_3)_2 \cdot 2\text{H}_2\text{O}$ at room temperature (Figure 4) shows absorptions at resonance fields both well above and below

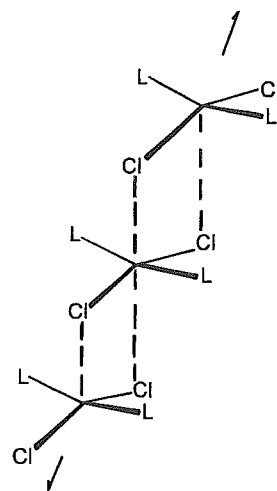


Figure 3. Schematic drawing of the distorted tetracoordinated environment proposed for $\text{Cu}^{\text{II}}(\text{allopurinol})_2(\text{Cl})_2 \cdot \text{H}_2\text{O}$ and its interactions.

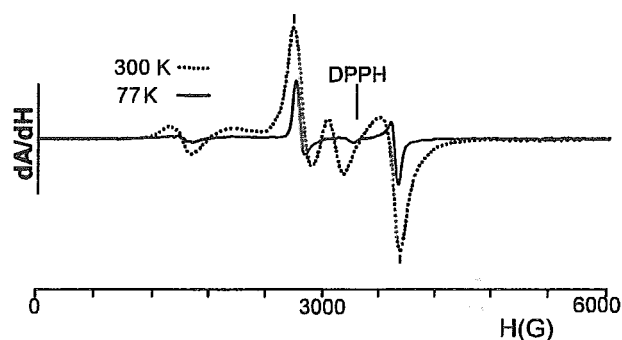


Figure 4. X-band EPR spectra of powdered $\text{Cu}^{\text{II}}(\text{hypoxanthine})_2(\text{NO}_3)_2 \cdot 2\text{H}_2\text{O}$ at room temperature (dotted line) and 77 K (solid line) at $\nu = 9.264$ GHz.

the region (g_{eff} ca. 2) where signals are normally found for Cu(II) with $S = 1/2$ spins in the ground state. In fact, the spectral pattern at 77 K fully resembles the one shown by dinuclear Cu(II) systems with N,N-bridging ligands in a square-pyramidal geometry for the Cu(II) centers, showing ligands bonded in the axial positions.^{16–18}

For the spectrum at room temperature, the pair of bands quoted are assigned to the two $\Delta m = 1$ transitions H_{xy1} and H_{xy2} of a triplet electronic state. From these, the dipolar splitting (dipolar interaction between the electronic spins of the Cu(II) centers) is ca. 1125 G. The g values are $g_{\perp} = 2.09$ and $g_{\parallel} = 2.19$. The spectrum also shows, in the low-field region, the expected absorption $\Delta m = 2$ for dinuclear Cu(II) systems in the same triplet electronic state. In short, the spectrum shows the $\Delta m = 1$ and $\Delta m = 2$ transitions for a triplet state and nearly axial symmetry for Cu(II) in a dinuclear framework. The unpaired spins of the Cu(II) centers are suggested to lie upon the $d_{x^2-y^2}$ orbitals. The E splitting parameter appears to be zero, or at least negligible, due to the fact that the xy bands do not split in the spectra at 300 and 77 K. The spectrum at 77 K shows a general pattern that closely resembles the one shown at low temperature by this type of dinuclear systems. The lowering in the intensities of the signals is in agreement with the depopulation of a $S = 1$ state and the population of a $S = 0$ state associated with the existence of an antiferromagnetic coupling between the unpaired electrons of the Cu(II) atoms in the dinuclear compound. At this temperature, the almost

(16) Goodgame, D. M. L.; Price, K. A. *Nature* **1968**, *220*, 783.

(17) Duerst, R. W.; Baum, S. J.; Kokoszka, G. F. *Nature* **1969**, *222*, 665.

(18) Sonnenfroh, D.; Krellick, R. W. *Inorg. Chem.* **1980**, *19*, 1259 and references therein.

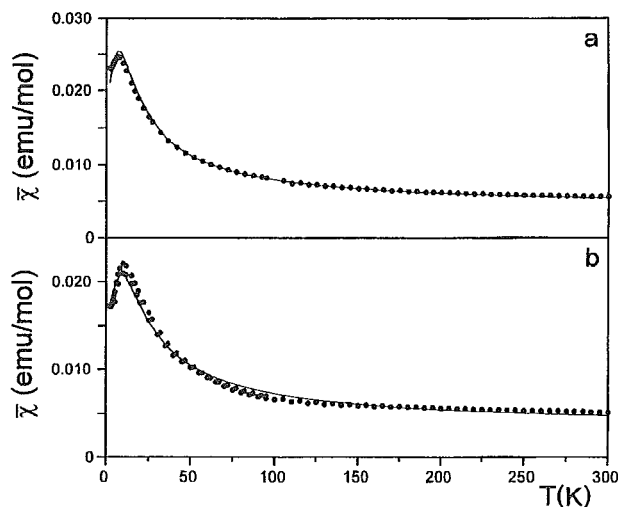


Figure 8. $\bar{\chi}$ (emu/mol) - T (K) curves for powdered (a) $\text{Cu}^{\text{II}}(\text{allopurinol})_2(\text{Cl})_2 \cdot \text{H}_2\text{O}$ ($H = 100$ G) and (b) $\text{Cu}^{\text{II}}(\text{hypoxanthine})_2(\text{Cl})_2 \cdot 2\text{H}_2\text{O}$ ($H = 100$ G). Dotted lines are experimental data; solid lines are theoretical results.

(G) Magnetic Studies Results. In order to study in detail the behavior of the Cu(II) centers, magnetic measurements of the different coordination compounds were made.

(i) $\text{Cu}^{\text{II}}(\text{allopurinol})_2(\text{Cl})_2 \cdot \text{H}_2\text{O}$ and $\text{Cu}^{\text{II}}(\text{hypoxanthine})_2(\text{Cl})_2 \cdot 2\text{H}_2\text{O}$. The molar magnetic susceptibility $\bar{\chi}$ (emu/mol) values as a function of T (K) were obtained at the three magnetic fields of 100, 1000 and 10000 G for both compounds. The results for $H = 100$ G are shown in Figure 8 for (a) $\text{Cu}^{\text{II}}(\text{allopurinol})_2(\text{Cl})_2 \cdot \text{H}_2\text{O}$ and (b) $\text{Cu}^{\text{II}}(\text{hypoxanthine})_2(\text{Cl})_2 \cdot 2\text{H}_2\text{O}$. A very small decrease of $\bar{\chi}$ is observed with the increase of the magnetic field, but without any changes in the general trend of the magnetic response, which in turn is associated in both cases to very weak antiferromagnetic coupling. The presence of a magnetic impurity is excluded in both systems due to the form of the $\bar{\chi} - T$ curves at low temperature (at least up to 2 K).

In order to analyze the magnitude of the magnetic interactions (not detected in the EPR data, not even at 77 K), and considering the distorted geometry and axial interactions suggested for these systems, a linear chain magnetic model of antiferromagnetically coupled $S = 1/2$ spins was selected, for which the $\bar{\chi}$ values can be calculated with the Bonner-Fisher equation

$$\bar{\chi} = \frac{Ng^2\beta^2}{kT} \left[\frac{0.25 + 0.14995x + 0.30094x^2}{1 + 1.9862x + 0.68854x^2 + 6.0626x^3} + \bar{\chi}_0 \right] (1 - \rho) + \frac{Ng^2\beta^2}{2kT} \rho \quad (1)$$

where $x = |J|/kT$ and the other symbols have their usual meaning.

For $\text{Cu}^{\text{II}}(\text{allopurinol})_2(\text{Cl})_2 \cdot \text{H}_2\text{O}$, setting $g = 2.09$ and $\rho = 0$ as fixed parameters, a very good fit was obtained (Figure 8a, solid line). The magnetic parameters obtained are the following: $J = -3.9088 \text{ cm}^{-1}$ and $\bar{\chi}_0 = 0.004167 \text{ emu/mol}$. The fitting process was performed for the other two values of the magnetic field (1000 and 10000 G), and very similar parameters were obtained. When the same fitting procedure was carried out fixing only the g parameter, very similar J and $\bar{\chi}_0$ values were also obtained. Other magnetic models (i.e., a dinuclear magnetic model of coupled $S = 1/2$ spins) were studied, without successful results both in the fitting process and in the physical meaning of the magnetic parameters obtained.

When the same model and eq 1 for $\text{Cu}^{\text{II}}(\text{hypoxanthine})_2(\text{Cl})_2 \cdot 2\text{H}_2\text{O}$ were employed, a good fit was obtained, which is shown

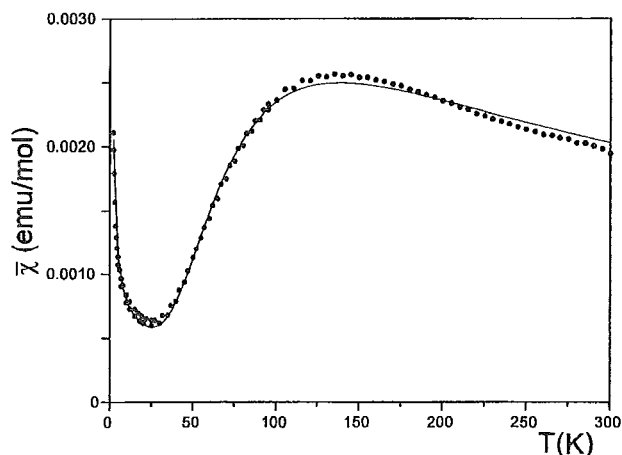


Figure 9. $\bar{\chi}$ (emu/mol) - T (K) curves ($H = 1000$ G) for powdered $\text{Cu}^{\text{II}}(\text{hypoxanthine})_2(\text{Br})_2 \cdot 2\text{H}_2\text{O}$. Dotted line are experimental data; solid line are theoretical results.

as a solid line in Figure 8b. For this process with $g = 2.10$ and $\rho = 0$, the values $J = -4.85 \text{ cm}^{-1}$ and $\bar{\chi}_0 = 0.003534 \text{ emu/mol}$ were obtained. For $H = 10\,000$ G, the same procedure gave $J = -4.69 \text{ cm}^{-1}$ and $\bar{\chi}_0 = 0.001562 \text{ emu/mol}$. With the employment of a dinuclear system of coupled $S = 1/2$ spins, and the Bleaney-Bowers equation, the fitting process was good (for $H = 100$ G), with $J = -5.77 \text{ cm}^{-1}$ and $\bar{\chi}_0 = 0.0034 \text{ emu/mol}$, but with a very low (unphysical) $g (= 1.22)$ value.

The magnitude of the J parameter for both compounds ($J = -3.9088 \text{ cm}^{-1}$ for $\text{Cu}^{\text{II}}(\text{allopurinol})_2(\text{Cl})_2 \cdot \text{H}_2\text{O}$ and $J = -4.85 \text{ cm}^{-1}$ for $\text{Cu}^{\text{II}}(\text{hypoxanthine})_2(\text{Cl})_2 \cdot 2\text{H}_2\text{O}$) is indicative of very weak antiferromagnetic coupling between the unpaired electrons of the Cu(II) centers, without an important dependence on the magnetic field intensity. These magnetic results joined to the spectral information for both systems suggest the participation of certain ligands in the magnetic coupling discussed. From these, the allopurinol and hypoxanthine molecules are excluded, respectively, and the ligands that play an important role in the magnetic coupling pathway could be the Cl^- atoms. Thus, the suggestion of the structural arrangement for both $\text{Cu}^{\text{II}}(\text{allopurinol})_2(\text{Cl})_2 \cdot \text{H}_2\text{O}$ and $\text{Cu}^{\text{II}}(\text{hypoxanthine})_2(\text{Cl})_2 \cdot 2\text{H}_2\text{O}$ would be analogous (Figure 7).

(ii) $\text{Cu}^{\text{II}}(\text{hypoxanthine})_2(\text{Br})_2 \cdot 2\text{H}_2\text{O}$. The $\bar{\chi}(\text{emu/mol}) - T$ (K) values for this compound were obtained at magnetic fields of 1000, 10000, and 30000 G, and only shown for $H = 1000$ G in Figure 9. The general pattern is in agreement with an antiferromagnetic coupling, higher in intensity than that shown for the former two cases. With an increase of the intensity of the magnetic field, a very small lowering of the $\bar{\chi}$ values is obtained, but without a modification of the general trend of the magnetic response. The tail at the low-temperature region, which follows a Curie-Weiss behavior, is associated to a magnetic impurity of non coupled $S = 1/2$ spins.

With respect to the spectral information for this compound, several magnetic models were explored. The first was the dinuclear model of coupled $S = 1/2$ spins with the Bleaney-Bowers equation:

$$\bar{\chi} = \frac{Ng^2\beta^2}{kT} \left[\frac{2}{3 + e^{-2J/kT}} + \bar{\chi}_0 \right] (1 - \rho) + \frac{Ng^2\beta^2}{2kT} \rho \quad (2)$$

The attempts to fit this equation to the experimental data completely revealed a poor agreement between the calculated (with realistic magnetic parameters) and experimental susceptibilities; when the fitting was good, unrealistic parameters (i.e., $g = 1.7$) were obtained. An appreciable improvement was

several axial ones appear to show lower $|J|$ values,¹⁶⁻²⁰ ranging from -127 to -107 cm^{-1} , showing the influence that the anionic character of the heterocyclic ligand has on the decrease of the antiferromagnetic coupling effectiveness between the unpaired electrons of the metallic centers.

With respect to the few (only three) magnetic studies on dinuclear Cu(II) systems reported up to date with 6-oxopurine (hypoxanthine) in neutral form as unique bridging ligand and anions ($\text{X} = \text{Cl}^-$ or Br^-) in the axial positions,^{18,19} the J values range from -142.1 to -105.5 cm^{-1} . There are no reports of homologue dinuclear systems and anionic or cationic 6-oxopurine.

In relation to the three dinuclear Cu(II) compounds reported here with the unique bridging ligand 6-oxopurine, the J values (-141.76 to -142.56 cm^{-1} for $\text{X} = \text{NO}_3^-$; -162.03 to -167.02 cm^{-1} for $\text{X} = \text{SO}_4^{2-}$; and -153.89 to -160.16 cm^{-1} for $\text{X} = \text{ClO}_4^-$) are of the same type as those for the analogue systems with 6-aminopurine or the few reported with 6-oxopurine ($\text{X} = \text{Cl}^-$ or Br^-). The similarity in the J parameter for all these cases is suggestive of strongly related structural features and electronic architecture between them.

In the absence of crystalline data for these dinuclear compounds, we cannot make statements about the nature of the magnetic coupling pathway that produces the antiferromagnetic behavior we have found. For the examples quoted before,¹⁶⁻²⁰ the Cu(II)-Cu(II) distance is such that a direct metal-metal interaction has been discarded, as in the cupric acetate type systems, and a ligand-mediated process is proposed. The similarity of the magnetic behavior they show with respect to the three dinuclear compounds reported here let us suggest that the magnetic coupling pathway in these last ones could be also through the bridging hypoxanthine molecules, in the N(1)-H, N(7)-H tautomeric form.

In order to explore this possibility at a molecular level, we have recently performed exhaustive density functional theory calculations for hypoxanthine and its tautomers, and we have found interesting results for the N(1)-H, N(7)-H tautomeric form. The electrostatic potential with respect to a positive charge, shows an attractive region located at the N(3) and N(9) atoms. The total electron density shows pseudoaromaticity in both rings, and for still high density values ($\rho = 0.27$) these nitrogen atoms are electronically communicated through the fragment N(3)-C(4)-N(9). The molecular orbital analysis is also interesting, because the d-orbitals of two Cu(II) atoms can present respectively potential effective overlap with the N(3) and N(9) atoms: for the σ bonding MO the overlap could be suggested to be with the $d_{x^2-y^2}$ orbitals; the HOMO (Π -type) could overlap with the d_{xz} orbitals, and finally, the LUMO (Π -type located at the C(2), C(4), and C(8) atoms) could overlap with the d_{yz} orbitals, favoring a Π -type backbonding process. The first two overlaps postulated would form σ/Π bonds between the two Cu(II) atoms and the deprotonated nitrogen atoms, which suggest a possible communication between these Cu(II) centers through the fragment N(3)-C(4)-N(9) of the bridging ligands. This communication could be enhanced by the backbonding process from the third type of overlap considered.

Concluding Remarks. In the study reported here, new Cu(II) coordination compounds with the heterocyclic ligands allopurinol and hypoxanthine, respectively, and several anions were synthesized in aqueous solution and at low pH value. In the competitive reactions of these heterocycles by the Cu(II) center, the fact that $\text{Cu}^{\text{II}}(\text{allopurinol})_2(\text{Cl})_2 \cdot \text{H}_2\text{O}$ is the predominant compound is relevant, almost without influence (except for $\text{X} = \text{CH}_3\text{CO}_2^-$) of the metallic counterion employed in the syntheses.

With regard to the Cu(II) compounds with allopurinol and hypoxanthine ($\text{X} = \text{Cl}^-$ or Br^-), respectively, the correspondent characterization supports the existence of both the MN_2X_2 character and nearest neighbor interactions, which lead to a very weak antiferromagnetic coupling. This type of coupling is conceived through both a linear chain (Cu(II) compounds with allopurinol and hypoxanthine with $\text{X} = \text{Cl}^-$), and a dinuclear system (Cu(II) compound with hypoxanthine and $\text{X} = \text{Br}^-$), with the participation of the halogen atoms as bridging ligands.

For the Cu(II) compounds with hypoxanthine and $\text{X} = \text{NO}_3^-$, SO_4^{2-} , or ClO_4^- , the characterization supports the existence of dinuclear units, of the cupric acetate type, with bridging hypoxanthine and polyatomic anions as axial ligands. The unpaired electrons on the pairs of Cu(II) atoms are strongly antiferromagnetically coupled in all these cases. The three systems are incorporated within the few examples reported up to date with this heterocycle as unique bridging ligand in dinuclear Cu(II) compounds.

The magnetic study carried out for the $\text{Cu}^{\text{II}}(\text{N})_2(\text{X})_2$ systems has contributed to the exploration of both the role played by the halogen atoms on the magnetic coupling pathway between the Cu(II) units and some features of their structural arrangements in the crystalline lattices. For the dinuclear $\text{Cu}^{\text{II}}(\text{N})_4(\text{O})_1$ systems the same study let us suggest the role played by the bridging hypoxanthine ligands in the effectiveness of the antiferromagnetic coupling pathway when anionic and polyatomic O-donor groups are simultaneously bonded to Cu(II) centers in axial form.

Noticeable differences in the metallic bonding behavior for the two isomeric heterocyclic ligands have been deduced from the study. This is particularly remarkable for hypoxanthine, where the N(3) and N(9) atoms are in some cases involved in this bonding, irrespective of the strong acid conditions and the N(7)-H/N(9)-H tautomerism for the free ligand in solution. All this could be of potential biochemical significance in the study of their catalytic metal center-ligand interactions, because both heterocycles are substrates of the metalloenzyme xanthine oxidase.^{1,4}

With regard to the Cu(II) compounds studied here, the synthetic dinuclear compounds could be proposed to potentially mimic some physical property of dinuclear copper centers of protein sites,^{21,22} which could contribute to an improved understanding of their biological analogues.

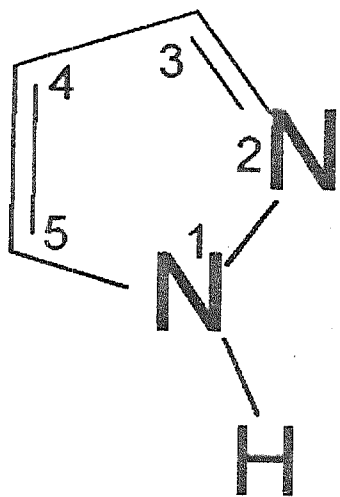
Finally, this study also represents a contribution about the exploration of the chemical behavior of Cu(II) toward two isomeric heterocyclic ligands under systematically modified reaction conditions. Related studies are in progress, in the hope to advance in the correspondent comprehensive understanding of this problem.

Acknowledgment. We thank Max Azomoza-Palacios (UAM-Iztapalapa), Jorge Ramírez-Salcedo (IFC-UNAM), and Francisco Morales-Leal (IIM-UNAM) for the thermal results, the EPR spectra of the Cu(II) compounds and the magnetic susceptibility measurements, respectively. We also acknowledge CONACyT (Grant 3170-E) for partial financial support.

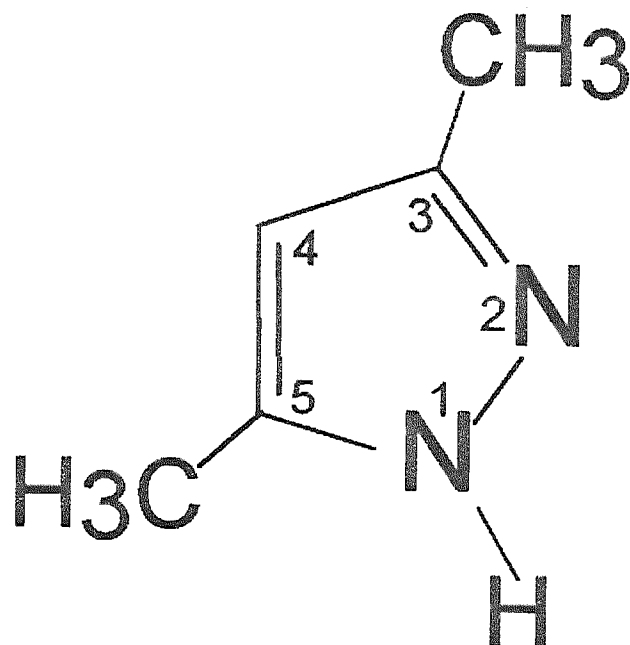
IC9602005

(21) Urbach, F. L. In *Metal Ions in Biological Systems*; Sigel, H., Ed.; Marcel Dekker, Inc.: New York, 1981; Vol. 13.

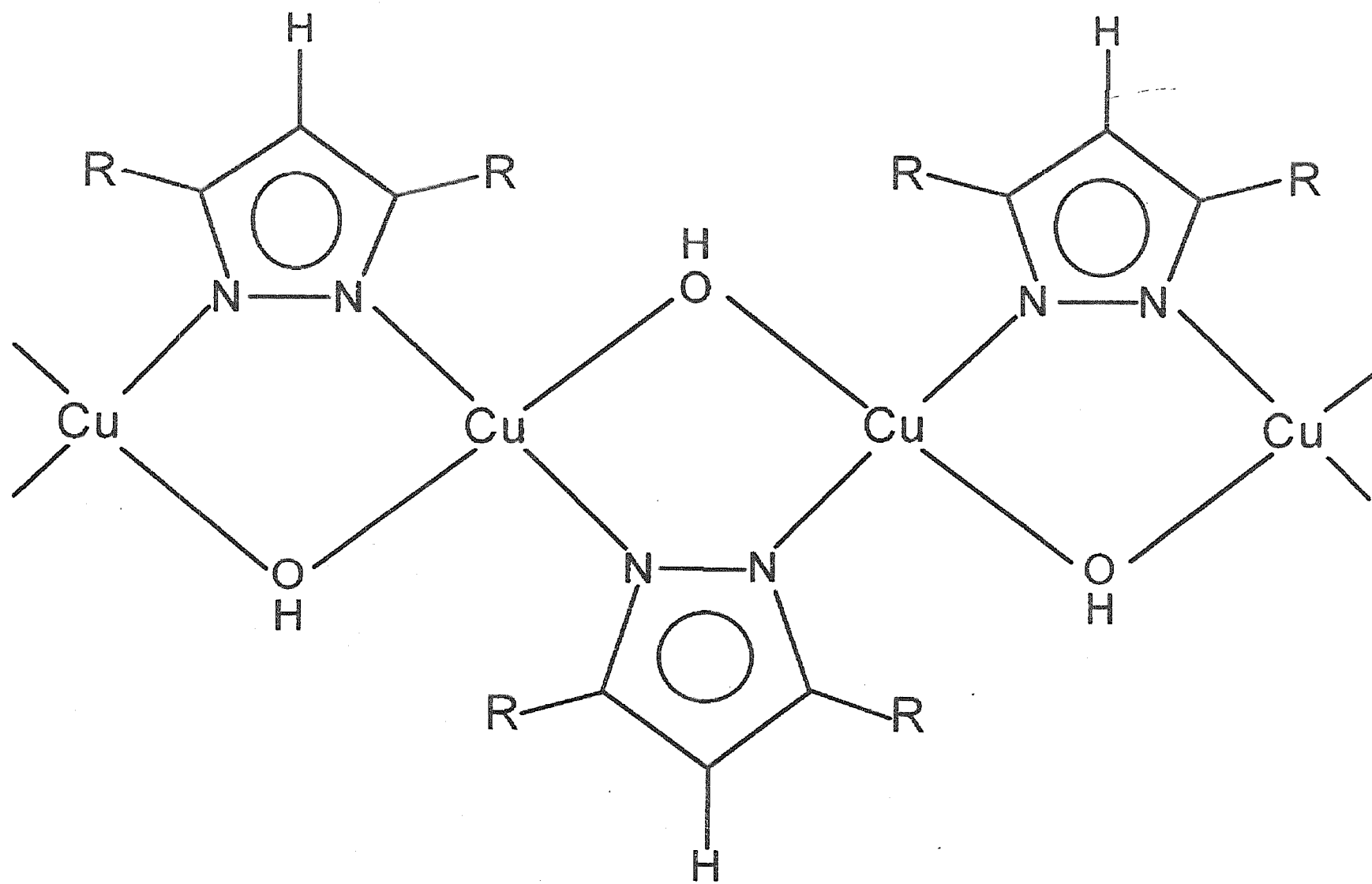
(22) Solomon, E. I.; Balchin, M. J.; Lowery, M. D. *Chem. Rev.* **1992**, *92*, 521.

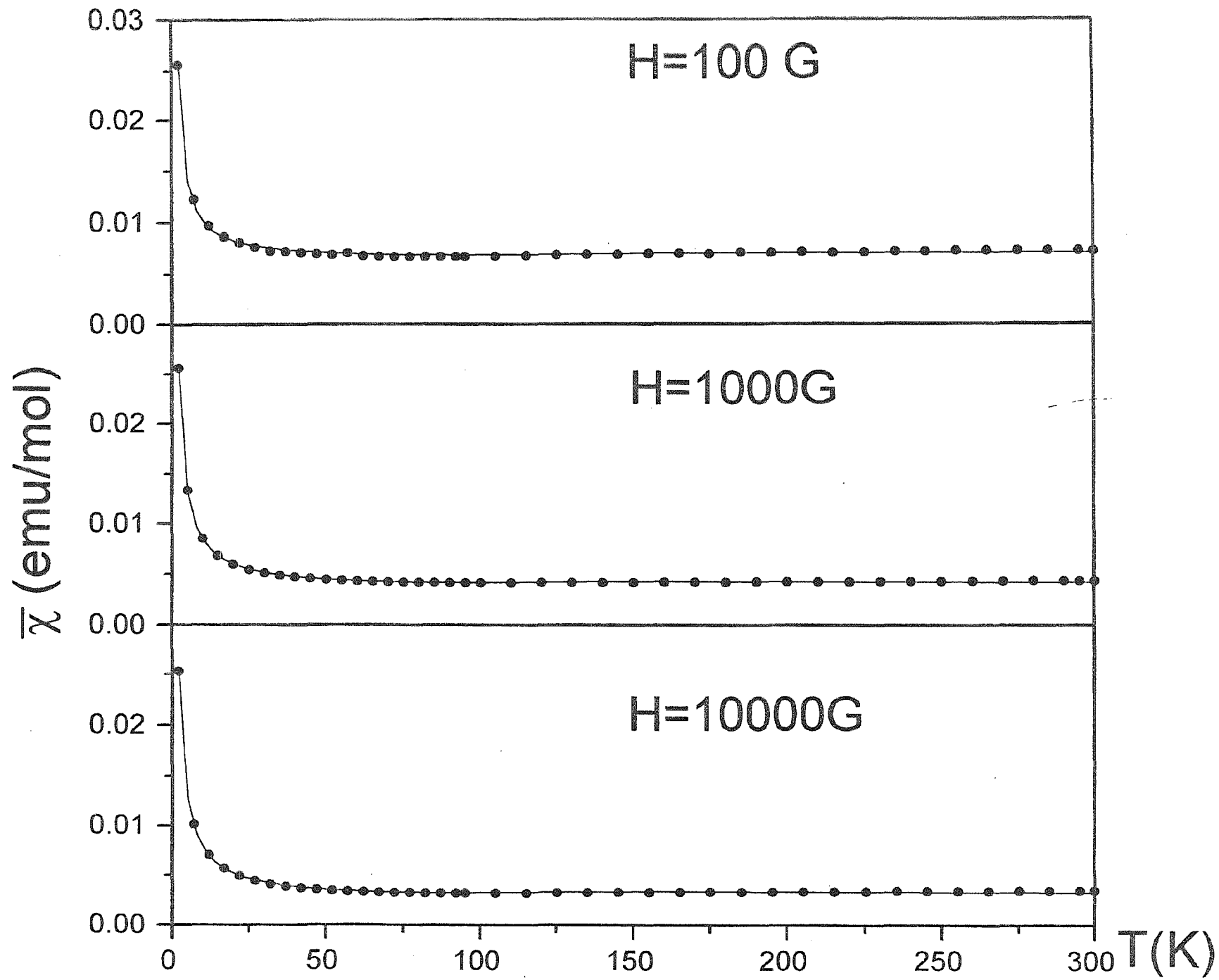


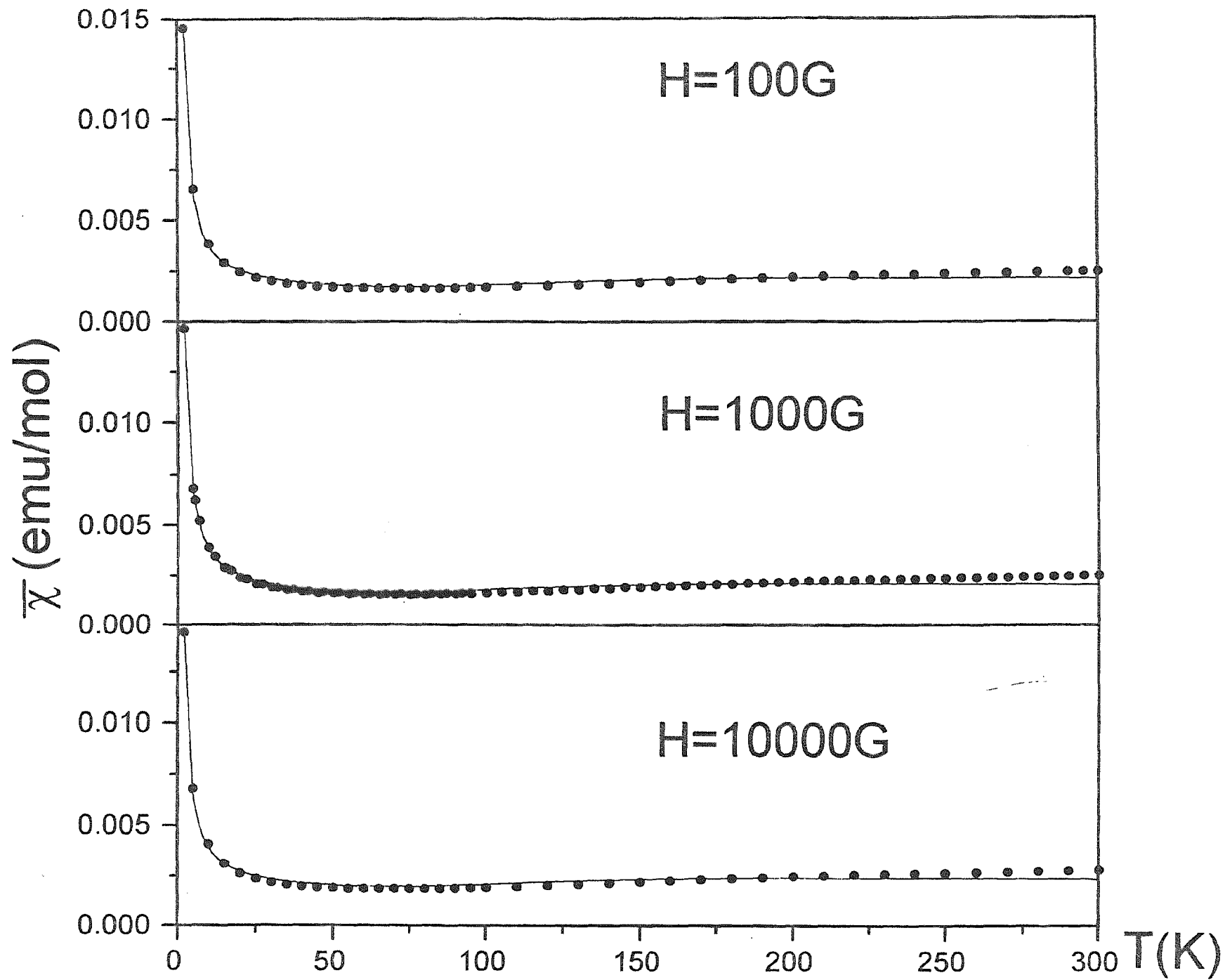
(I)

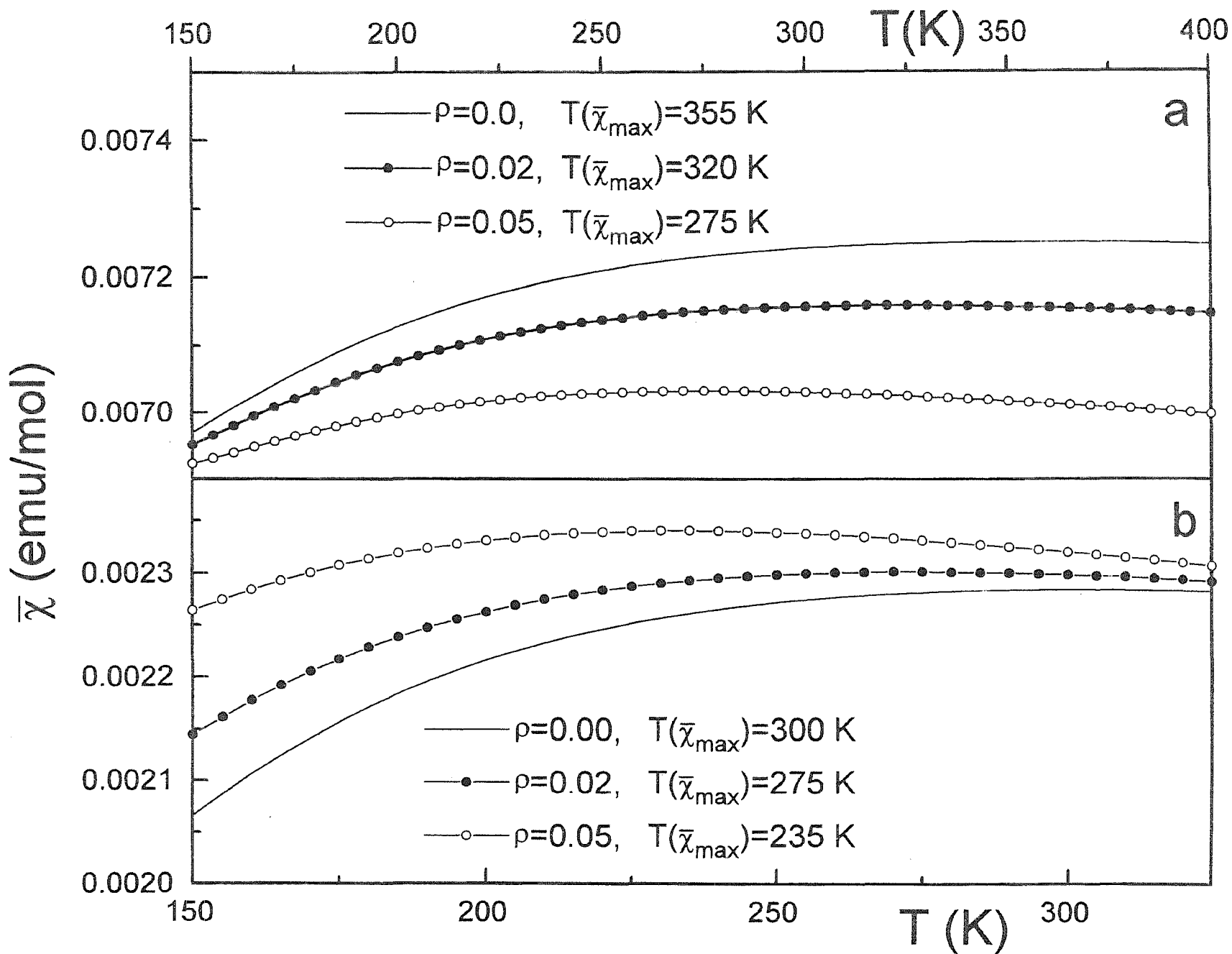


(II)

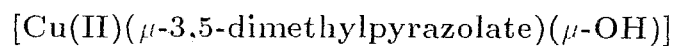








Antiferromagnetic Coupling in the Cyclic Octanuclear Compound



and its Analogue $[\text{Cu(II)}(\mu\text{-pyrazolate})(\mu\text{-OH})]$.

Rodolfo Acevedo-Chávez^a, María Eugenia Costas ^{*,b}, Roberto Escudero^c.

^aCentro de Química, Instituto de Ciencias, B, Universidad Autónoma de Puebla, Apartado Postal 1613, Puebla, Puebla, México.

^bFacultad de Química, Universidad Nacional Autónoma de México, México 04510, D.F., México.

^cInstituto de Investigaciones en Materiales, Universidad Nacional Autónoma de México, México 04510, D.F., México.

* To whom correspondence should be addressed.

ABSTRACT.

The spectral and magnetic characterization of the cyclic octanuclear compound $[\text{Cu}(\text{II})_8(\mu\text{-}3,5\text{-dimethylpyrazolate})_8(\mu\text{-OH})_8]$ and its analogue $[\text{Cu}(\text{II})(\mu\text{-pyrazolate})(\mu\text{-OH})]$ is reported. An octanuclear ring magnetic model describes the magnetic data of the first compound, in agreement with a strong antiferromagnetic coupling between the Cu(II) centers through the mixed bridging ligands. The same results are obtained for its Cu(II) analogue, which let us consider the existence of a structural arrangement of the same type for $[\text{Cu}(\text{II})(\mu\text{-pyrazolate})(\mu\text{-OH})]$.

INTRODUCTION.

As part of a methodology in the coordination chemistry study of the family of the purinic derivatives, their structural analogues and isomers, selective heterocyclic fragments serve as models of certain regions of the whole original molecules. For example, by selecting the heterocycle pyrazole and derivatives, it is possible to study some aspects of the coordination chemistry of the purinic isomer allopurinol in a simpler way. We have been interested in the coordination chemistry of the pyrazolic fragment of allopurinol and we have selected the pyrazole (1) and 3,5-dimethylpyrazole heterocycles (2) (Figure 1) to explore their interactions with metallic atoms (*e.g.*, Cu(II)) under several reaction conditions systematically modified, and to analyze the structural, spectral and magnetic properties of the respective coordination compounds.

Figure 1.

In the progress of our research program the synthesis and structural characterization of the cyclic octanuclear coordination compound $[\text{Cu(II)}_8 (\mu\text{-3,5-dimethylpyrazolate})_8 (\mu\text{-OH})_8]$ were reported (3,4). In these papers the formation of the polynuclear compound $[\text{Cu(II)}(\mu\text{-pyrazolate})(\mu\text{-OH})]$ was also mentioned. However, no detailed information about the synthesis conditions and physical properties was given for the last Cu(II) compound. These aspects prompted us to explore the syntheses for these two coordination compounds (both by the reported and by alternative routes) to perform their spectral and magnetic characterization, and to compare their physical properties with those shown by the related polynuclear compound $[\text{Cu(II)}(\mu\text{-allopurinolate})(\mu\text{-OH})]$ reported before (5).

The magnetic study reported here represents the first analysis ever done of these interesting systems, in which the pyrazolic ligands and OH groups simultaneously bridge the Cu(II) centers.

EXPERIMENTAL.

1. *Materials.*

1H-pyrazole (=pzH), 1H-3.5-dimethylpyrazole (=3.5-dmpzH) and the metallic Cu(II) salts (analytical grade) were commercially supplied. There was no need for further purification.

2. *Synthesis.*

The polynuclear compound $[\text{Cu}(\text{II})(\mu\text{-pz})(\mu\text{-OH})]$ was prepared by dissolving 1 mmol of pzH in *ca.* 50 ml of an aqueous buffer solution at pH=13 (KCl/NaOH) upon stirring at room temperature. 1 mmol of the respective Cu(II) metallic salt ($\text{X}=\text{Cl}^-$, Br^- , NO_3^- , SO_4^{2-} or ClO_4^-), previously dissolved in *ca.* 10 ml of H_2O , was added to the colorless solution previously obtained. The resulting deep blue suspension of each reaction was maintained under stirring at room temperature. All of them changed to a blue-purple color in a few hours. The corresponding reaction mixture was kept under these conditions for *ca.* 24 hours with no observed changes. The suspension was filtered off and the solid product (blue-purple color) was washed first with several portions of H_2O and then with repetitive volumes of $\text{C}_2\text{H}_5\text{OH}$. When kept at *ca.* 100°C for 4 hours each solid showed no changes. The respective colorless filtrate was discarded. When using $\text{X}=\text{CH}_3\text{CO}_2^-$ as the metallic counterion, the deep blue suspension (under stirring for *ca.* 48 hours) changed to a blue-purple suspension, and when it was kept at the same conditions for 48 additional hours, no changes were detected. The reaction mixture and the solid product were treated as above.

Deep purple-black solids were obtained by carrying out the same reactions at boiling temperature (except for $\text{X}=\text{SO}_4^{2-}$). These solids correspond to mixtures of CuO and $\text{Cu}(\text{II})_n(\text{pz})_n(\text{OH})_{n/2}(\text{X})_{n/2}$ in a ratio directly proportional to the reaction time.

The synthesis of $[\text{Cu}(\text{II})_8(\mu\text{-dmpz})_8(\mu\text{-OH})_8]$ required the previous preparation of CuI and its reaction with 3.5-dmpzH, giving the starting cyclic trinuclear Cu(I) coordination compound $[\text{Cu}(\text{I})_3(\mu\text{-3.5-dmpz})_3]$. This reaction was performed as follows: 10.0 mmol of

CuI were dissolved in 80 ml of CH_3CN under stirring at room temperature and $\text{N}_2(\text{g})$ atmosphere (the solvent was previously bubbled with $\text{N}_2(\text{g})$). Sheets of Cu(s) were added to the resulting solution (pale yellow). 10.0 mmol of 3,5-dmpzH first and then 11.0 mmol of $(\text{C}_2\text{H}_5)_3\text{N}$ were incorporated to the reaction mixture, rapidly forming a white suspension, which was maintained under stirring at room temperature and $\text{N}_2(\text{g})$ for half an hour. The mixture was filtered off. A white solid was isolated and washed first with 50 ml of CH_3CN and then with 50 ml of $(\text{CH}_3)_2\text{CO}$. The solid product was kept at 105°C for half an hour, and no changes were observed. The product was found to be insoluble in the common organic solvents, and stable in air and moisture. The IR bands of the product were the same as those quoted for the Cu(I) compound in a crystalline structure determination (6), in which other synthetic method was used. Finally, the cyclic trinuclear compound $[\text{Cu}(\text{I})_3(\mu\text{-dmpz})_3]$ was employed in the synthesis of $[\text{Cu}(\text{II})_8(\mu\text{-dmpz})_8(\mu\text{-OH})_8]$, with a very similar technique to that previously reported (4), as follows: 0.98 g of $[\text{Cu}(\text{I})_3(\mu\text{-dmpz})_3]$ were added to 40 ml of $\text{C}_5\text{H}_5\text{N}$ with 0.5 ml of deionized H_2O . A vigorous stream of $\text{O}_2(\text{g})$ was applied to the reaction mixture under stirring at room temperature. A slow change to deep blue color was observed; no changes were detected in the next 24 hours. The suspension was filtered off, and a deep blue-purple solid was isolated and washed with *ca.* 20 ml of $\text{C}_5\text{H}_5\text{N}$. The product was dried at reduced pressure and room temperature. The original filtrate and the $\text{C}_5\text{H}_5\text{N}$ used in the washing were mixed and evaporated to dryness, getting a second fraction of the same product.

3. Physical Measurements.

Infrared (IR) spectra (Nujol mulls, KBr windows) in the $4000\text{-}400\text{ cm}^{-1}$ range were obtained by using a 750 FT IR Nicolet equipment. For the $4000\text{-}200\text{ cm}^{-1}$ range (Nujol mulls, CsI windows) a 598 Perkin Elmer spectrometer was employed. IR data (high density polyethylene pellets) in the $600\text{-}70\text{ cm}^{-1}$ range were obtained by using a 740 FT IR Nicolet equipment.

-Electronic spectra (200-1100 nm. quartz windows and BaSO₄ as reference) in the solid state of the powdered samples. were recorded by using a 160-A Shimadzu spectrometer.

-Thermogravimetric data (room temperature-800°C) were obtained by using a 2100 Dupont thermobalance. employing N₂(g) as carrier gas and 5°C-min⁻¹ as heating rate.

-X-ray diffraction patterns of the powdered samples were recorded by using a D-500 Siemens diffractometer. by employing a secondary monochromator with CuKα radiation.

-X-band epr spectra of the powdered samples (room temperature and 77 K) were recorded by employing a 200-D Bruker spectrometer. using DPPH as reference.

-The magnetic susceptibility of powdered samples as a function of temperature at different magnetic fields, was measured with a SQUID Quantum Design Magnetometer. from 2 to 300 K, and magnetic fields of 100. 1000 and 10000 G. The magnetic susceptibility data were corrected by the cell and the sample diamagnetic contributions. The magnetometer was previously calibrated with very fine standards (Pd, Ni and Al), and the mean standard deviation of the magnetic susceptibility measurements was three orders of magnitude lower than the studied data. Preliminary magnetic susceptibilities (room temperature) of powdered samples were obtained by using a Johnson Matthey balance and employing Hg[Co(SCN)₄] as reference.

-Microanalysis confirmation (C. H. N) was performed at the Chemistry Department. University College of London.

RESULTS AND DISCUSSION.

[Cu(II)(μ-pz)(μ-OH)].

1. Analytical Results.

Experimental: 24.4 (%C), 2.76 (%H), 18.91 (%N); calculated for Cu(II)(C₃H₃N₂⁻)(OH⁻): 24.4 (%C), 2.73 (%H), 18.98 (%N). These analytical results correspond to the product obtained when X=SO₄²⁻ was employed as the initial Cu(II) metallic counterion, and they are in full agreement with the anionic character of the pyrazolate ligand.

2. Infrared spectrum.

The IR spectral data of several samples of the Cu(II) compound and those corresponding to the free heterocyclic ligand are listed in Table I. The assignments were made based on recent studies (7-11).

Table I.

The overall spectral behavior is in agreement with the existence of the pyrazolate as bridging ligand to Cu(II) centers through the \underline{N} atoms (7-11). The heterocyclic ligand coordination is supported by a strong and sharp band at 330 cm^{-1} , assigned to the ν_{M-N} vibrational mode. The IR data for the OH group indicate its existence as bridging ligand (12-15).

With regard to the geometrical disposition of the pyrazolate and OH ligands in the Cu(II) coordination sphere, the low-energy IR data are in agreement with a mutually-trans configuration, as it is schematically shown in Figure 2.

Figure 2.

3. Electronic spectrum.

The spectra of the samples in the 400-1100 nm range show a broad and asymmetric band centered at 590 nm. The frequency and structure of this band is associated with $d-d$ transitions of Cu(II) in a nearly planar tetracoordinated geometry.

4. X-Ray diffraction pattern.

The powder patterns consist of broad signals in the $7.00-50.00\ 2\theta$ range. This could be suggestive of a poor crystallinity of all the samples analyzed, associated to the synthesis experimental conditions under which the Cu(II) compound was obtained.

5. Epr spectrum.

The X-band ($\nu=9.79\text{ GHz}$) epr spectra at room temperature of all the samples show a very weak, broad and symmetric signal with $g_{av} \simeq 2.14$. These spectra are not resolved

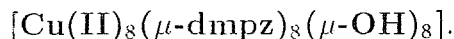
upon decreasing the temperature (77 K). The pattern is associated to the existence of strong Cu(II)-Cu(II) magnetic coupling.

6. Thermogravimetric results.

The thermal results do not show mass loss in the room temperature-200°C range. This suggests the absence of H₂O molecules both in the lattice and in the metallic coordination sphere. The lowering of mass starts at 232°C (98.88% of initial mass) in an abrupt step; then a second one is observed starting at *ca.* 237°C (71.39%), and finally a mass loss in steps from *ca.* 341° (44.12%) up to 800° (23.64%) is obtained. The same results were observed when the samples were in contact with ambient air, confirming the non hygroscopic character of the coordination compound.

7. Preliminary magnetic results.

The effective magnetic moment (μ_{eff}) of samples coming from the several reaction conditions (X=Cl⁻, SO₄²⁻, ClO₄⁻ and CH₃CO₂⁻) was obtained at room temperature, ranging from 0.94 to 1.0 BM/Cu(II) center. The values close to 1.0 BM allow us to suggest the existence of a noticeable Cu(II)-Cu(II) magnetic coupling, in agreement with the epr spectral information.



1. Infrared spectrum.

The IR spectrum of [Cu(II)₈(μ-dmpz)₈(μ-OH)₈] shows a similar pattern with respect to the IR bands of 3,5-dmpz bonded as bridging ligand in the cyclic trinuclear system [Cu(I)₃(μ-3,5-dmpz)₃]. Table II shows the IR bands of the compound under discussion and tentative assignments to them.

Table II.

The IR spectrum of the coordinated heterocycle shows several modifications when compared to the free ligand. The analysis supports the non existence of the N-H group in the

heterocyclic ligand. The same analysis arise the existence of perturbations of the bands associated with endocyclic groups vibrational modes in agreement with the participation of the \underline{N} atoms in their coordination to the Cu(II) centers, and the heterocycle as bridging ligand. The bands appearing at 371 and 320 cm^{-1} are assigned to ν_{M-N} . The IR spectrum also shows bands associated with the $\nu(\text{OH}^-)$ and the $\nu(\text{M-OH}^- \text{ bridge})$ vibrational modes, also in concordance with the structural information reported for this Cu(II) compound.

2. Electronic spectrum.

In the 400-1100 nm range $[\text{Cu(II)}_8(\mu\text{-3,5-dmpz})_8(\mu\text{-OH})_8]$ shows a broad band with a maximum at 580 nm, which can be associated to $d-d$ transitions of Cu(II) in a roughly planar tetracoordinated Cu(II) geometry. The structure and frequency of this band is similar to that shown by the analogue $[\text{Cu(II)}(\mu\text{-pz})(\mu\text{-OH})]$ (590 nm) and it is in agreement with the Cu(II)(N)₂(O)₂ character for both systems.

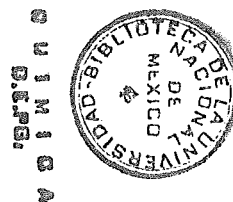
3. Epr spectrum.

At room temperature and $\nu=9.7$ GHz. $[\text{Cu(II)}_8(\mu\text{-3,5-dmpz})_8(\mu\text{-OH})_8]$ is nearly epr silent. This behavior also indicates remarkable magnetic coupling, as in $[\text{Cu(II)}(\mu\text{-pz})(\mu\text{-OH})]$ at the same spectral conditions. The epr spectrum was not resolved upon a temperature decrease (77 K).

4. X-Ray diffraction pattern.

The analyzed samples of the cyclic octanuclear compound $[\text{Cu(II)}_8(\mu\text{-3,5-dmpz})_8(\mu\text{-OH})_8]$ show a powder pattern that resembles in some aspects that of the analogue $[\text{Cu(II)}(\mu\text{-pz})(\mu\text{-OH})]$. The former shows however, signals of sharper and higher intensity character in the 4-30 2θ range. The differences between the two patterns could be attributed in part to the drastic synthesis conditions carried out. Also, the detailed structural and lattice characteristics of both Cu(II) systems are not necessarily the same, and this may also explain that differences.

5. Thermogravimetric results.



$[\text{Cu(II)}_8(\mu\text{-}3.5\text{-dmpz})_8(\mu\text{-OH})_8]$ shows a different thermogravimetric pattern compared to the one shown by its analogue $[\text{Cu(II)}(\mu\text{-pz})(\mu\text{-OH})]$. It shows a first step of mass loss starting at 86.6°C (98.21% of initial mass). The second step starts at 211.6°C (83.2%) and continues in steps from *ca.* 334°C (44.34%) up to 800°C (23.21%). The thermal results for the first mass loss step could be associated with the elimination of $\text{C}_5\text{H}_5\text{N}$ solvent molecules from the sample, related to the dryness conditions carried out for this compound synthesis (in fact, in the synthetic route previously reported(4), two $\text{C}_5\text{H}_5\text{N}$ molecules per octanuclear unit are deduced from the analytical results).

6. Preliminary magnetic results.

$[\text{Cu(II)}_8(\mu\text{-}3.5\text{-dmpz})_8(\mu\text{-OH})_8]$ shows an effective magnetic moment at room temperature of *c.a.* 0.7 BM/Cu(II) center. This low value indicates a strong magnetic coupling between the unpaired electrons of the Cu(II) centers, in agreement with the epr spectrum. This behavior is similar to that deduced for the analogue polynuclear compound $[\text{Cu(II)}(\mu\text{-pz})(\mu\text{-OH})]$.

MAGNETIC STUDIES.

The magnetic susceptibility *versus* temperature measurements were carried out in the 2-300 K range at magnetic fields of 100, 1000 and 10000 G for both compounds.

Figure 3 shows the molar magnetic susceptibility $\bar{\chi}$ (per octanuclear unit) for $[\text{Cu(II)}(\mu\text{-pz})(\mu\text{-OH})]$, as a function of temperature for the three values of the external magnetic field.

Figure 3.

The small but continue increase of the $\bar{\chi}$ values with temperature in the high-temperature region indicates an antiferromagnetic coupling. In the low-temperature region a Curie-Weiss behavior, which may be associated with non coupled $S=1/2$ spins, is observed. As the magnetic field increases, a small decrease in the $\bar{\chi}$ values is observed, with

no modification in the general trend of the magnetic response. The antiferromagnetic coupling is also inferred from the $\bar{\chi}T - T$ plots for the same magnetic fields: a nearly linear lowering of $\bar{\chi}T$ with the temperature decrease is observed. In this representation the three lines for the different H values converge in the limit of low-temperature, and the increase of the magnetic field produces a lowering of the respective slopes. Linear relationships that converge at 100 G are obtained when plotting the experimental magnetization data (M) as a function of the magnetic field (H) for the fixed temperatures 10, 70, 200 and 300 K. The line for $T=10$ K shows a higher slope than that of the others: the slopes for the other three temperatures are very similar, slightly increasing from 70 to 300 K. This behavior corroborates both the non coupled $S=1/2$ spins contribution in the low-temperature region, and the successive population of excited states of higher spin multiplicity for the high-temperature region, which indicates the existence of magnetic coupling in the solid product.

The data were studied employing several magnetic models like the dinuclear, the infinite linear chain and the finite size ring (*i.e.*, octanuclear). The best fitting results were obtained for the octanuclear ring model of $S=1/2$ coupled spins (16), for which the parallel magnetic susceptibility expression, modified to take into account the fraction of non-coupled spins (ρ) and the temperature independent term ($\bar{\chi}_0$) contributions, is:

$$\bar{\chi} = \frac{N\mathcal{J}^2g^2}{4kT} e^{-|J|/kT} \left[\frac{1 - (-\tanh K)^N}{1 + (-\tanh K)^N} \right] (1 - \rho) + \bar{\chi}_0(1 - \rho) + \frac{N\mathcal{J}^2g^2}{2kT} \rho \quad (1)$$

where $K = |J|/2kT$, N is the size of the finite ring (we used $N = 8$) and the other symbols have their usual meaning. In the fitting process, the minimization function used was:

$$\sigma^2 = \sum_{i=1}^N \frac{(\bar{\chi}_{\text{theor}} - \bar{\chi}_{\text{exp}})^2}{N - n}$$

The fitting process (employing Eq. (1)) was very successful and gave the following magnetic parameters for $g = 2.14$: $H = 100\text{G}$: $J = -178.6 \pm 4.28 \text{ cm}^{-1}$, $\rho = 0.045 \pm 1.77 \times 10^{-4}$, $\bar{\chi}_0 = 0.0066 \pm 1.72 \times 10^{-5} \text{ emu/octanuclear unit}$; $H = 1000\text{G}$: $J = -226.7 \pm 20.97$

cm^{-1} , $\rho = 0.051 \pm 4.24 \times 10^{-4}$, $\bar{\chi}_0 = 0.0039 \pm 4.85 \times 10^{-5}$ emu/octanuclear unit; $H = 10000\text{G}$: $J = -218.4 \pm 21.47 \text{ cm}^{-1}$, $\rho = 0.053 \pm 4.73 \times 10^{-4}$, $\bar{\chi}_0 = 0.0029 \pm 5.36 \times 10^{-5}$ emu/octanuclear unit. The J values are consistent with a strong antiferromagnetic coupling between the unpaired electrons of the Cu(II) centers.

The same magnetic model with a mean-field correction was employed to explore the possibility of inter-ring magnetic coupling. The magnetic susceptibility ($\bar{\chi}'$) in this approximation is:

$$\bar{\chi}' = \frac{\bar{\chi}}{1 - (2zJ'/Ng^2\beta^2)\bar{\chi}} \quad (2)$$

where $\bar{\chi}$ is the magnetic susceptibility given by Eq. (1). J' is the inter-ring magnetic coupling parameter, and z is the number of nearest neighboring rings.

From this, a very good fit was obtained for the three fields, with the following magnetic parameters for $g = 2.14$: $H = 100\text{G}$: $J = -191.54 \pm 22.37 \text{ cm}^{-1}$, $zJ' = -0.14 \pm 1.38 \text{ cm}^{-1}$, $\rho = 0.045 \pm 0.0034$, $\bar{\chi}_0 = 0.0067 \pm 8.73 \times 10^{-5}$ emu/octanuclear unit; $H = 1000\text{G}$: $J = -173.6 \pm 7.97 \text{ cm}^{-1}$, $zJ' = -3.73 \pm 0.304 \text{ cm}^{-1}$, $\rho = 0.063 \pm 0.001$, $\bar{\chi}_0 = 0.0038 \pm 2.85 \times 10^{-5}$ emu/octanuclear unit; $H = 10000\text{G}$: $J = -167.5 \pm 10.28 \text{ cm}^{-1}$, $zJ' = -4.43 \pm 0.41 \text{ cm}^{-1}$, $\rho = 0.067 \pm 0.002$, $\bar{\chi}_0 = 0.0027 \pm 4.37 \times 10^{-5}$ emu/octanuclear unit. These parameters correspond to the theoretical curves shown as solid lines in Figure 3. The J values corroborate a strong antiferromagnetic coupling (intra-ring type). The zJ' values makes us think about the possibility of very weak inter-ring magnetic coupling, maybe of antiferromagnetic type.

For $[\text{Cu}(\text{II})_8(\mu\text{-}3,5\text{-dmpz})_8(\mu\text{-OH})_8]$, Figure 4 shows the molar magnetic susceptibility $\bar{\chi}$ (per octanuclear unit) as a function of temperature for the three magnetic fields.

Figure 4.

The general pattern in the high-temperature region also suggests an antiferromagnetic coupling. The behavior in the low-temperature region (Curie-Weiss type) may also be

associated with the presence of non coupled S=1/2 spins. The applied magnetic field leads to a nearly insignificant increase of the $\bar{\chi}$ values, with no changes in the general magnetic response. As in the previous system, the antiferromagnetic coupling is also deduced from the $\bar{\chi}T - T$ plots for the three magnetic fields. In this case, and for a magnetic field value, a $\bar{\chi}T$ lowering and a decrease of the slope starting from *ca.* 130 K are obtained with the temperature decrease. The three curves show the same trend, and they converge at the limit of low-temperature. The increase of the magnetic field produces a slight increase of the corresponding slopes.

The $M - H$ plots for the fixed temperatures 10, 70, 200 and 300 K, show linear relationships which converge at 100 G. The lines show a progressive increase of slope for 70, 200, 300 and 10 K. These slopes are lower than those found for the previously discussed compound. The slope for 10 K also corroborates the non coupled S=1/2 spins contribution in the low-temperature region. The increasing slopes for the 70-300 K range are consistent with the population of excited states of higher spin multiplicity. The slopes of the 10 K lines for both Cu(II) compounds allow us to suggest the presence of a higher contribution of non coupled S=1/2 spins in [Cu(II)(μ -pz)(μ -OH)].

The fitting process was also performed for the model employed before with a mean field correction (Eq. (2)). In this case, the magnetic parameters obtained for $g = 2.20$ were: $H = 100\text{G}$: $J = -173.0 \pm 14.5 \text{ cm}^{-1}$, $zJ' = +7.89 \pm 3.12 \text{ cm}^{-1}$, $\rho = 0.024 \pm 0.0017$, $\bar{\chi}_0 = 0.0014 \pm 5.67 \times 10^{-5} \text{ emu/octanuclear unit}$; $H = 1000\text{G}$: $J = -160.98 \pm 11.66 \text{ cm}^{-1}$, $zJ' = +3.69 \pm 2.39 \text{ cm}^{-1}$, $\rho = 0.027 \pm 0.0015$, $\bar{\chi}_0 = 0.0013 \pm 5.53 \times 10^{-5} \text{ emu/octanuclear unit}$; $H = 10000\text{G}$: $J = -164.45 \pm 17.09 \text{ cm}^{-1}$, $zJ' = +7.88 \pm 4.12 \text{ cm}^{-1}$, $\rho = 0.024 \pm 0.0022$, $\bar{\chi}_0 = 0.0016 \pm 7.07 \times 10^{-5} \text{ emu/octanuclear unit}$. These parameters correspond to the theoretical curves shown as solid lines in Figure 4.

The J values obtained here are also in concordance with a strong antiferromagnetic coupling between the unpaired electrons of the Cu(II) centers. The zJ' values allows us to suggest the existence of very weak inter-ring magnetic coupling, although it could be

suspected to be of a ferromagnetic type. The contribution of the non coupled $S=1/2$ spins in the sample (ρ in Eq. (1)) is lower than the one found for $[\text{Cu}(\text{II})(\mu\text{-pz})(\mu\text{-OH})]$, in agreement with the previous discussion of the $M - H$ plots for both compounds. The differences in such contributions outstand in the form of the $\bar{\chi} - T$ curves in the low-temperature region for the two $\text{Cu}(\text{II})$ compounds studied here.

The significant contribution of non-coupled spins (noticeable at low temperatures as a Curie-Weiss type behavior) affects the magnetic response of the studied compounds, for which in addition the $\bar{\chi}$ values are small. When fitting Eq. (1) to the experimental data, we noticed that the calculated temperature at which the molar magnetic susceptibility should be a maximum, lies well below both the one estimated experimentally, and the one predicted by the pure octanuclear model (Eq. (1) with $\rho = 0$) which is $T(\bar{\chi}_{\text{max}}) = |J|/k$ (16). Note that the last term in Eq. (1) shows the dependence of $\bar{\chi}$ on ρ and T . In order to study the effect of the mole fraction of non-coupled spins on the behavior of the molar magnetic susceptibility, we fitted Eq. (1) with $\rho = 0$ to the experimental data of both compounds at $H = 100$ G for the temperature range 50 – 300 K, and used the J and $\bar{\chi}_0$ values obtained in this way to theoretically calculate the molar magnetic susceptibility curves as a function of ρ with Eq. (1). These are shown in Figure 5 for a) $[\text{Cu}(\text{II})(\mu\text{-pz})(\mu\text{-OH})]$, and b) $[\text{Cu}(\text{II})_8(\mu\text{-3,5-dmpz})_8(\mu\text{-OH})_8]$. As can be seen, the temperature for which $\bar{\chi}$ has a maximum value is lower as ρ is increased. The presence of non-coupled spins, considered as a magnetic impurity, modifies the curves form and the $T(\bar{\chi}_{\text{max}})$ values for both compounds.

Figure 5.

In the next step, we proceeded to fit equation (1) with $\rho = 0$ to the experimental data for the 100-300 K temperature region, in which the effect of the magnetic impurity is not as noticeable as in the low-temperature region. The magnetic results employing this pure octanuclear model are for $[\text{Cu}(\text{II})(\mu\text{-pz})(\mu\text{-OH})]$ with $g = 2.14$: $H = 100$ G,

$J = -331.32 \pm 22.28 \text{ cm}^{-1}$, $\bar{\chi}_0 = 0.0067 \pm 6.56 \times 10^{-5} \text{ emu/mol}$: $H = 1000 \text{ G}$, $J = -363.50 \pm 5.19 \text{ cm}^{-1}$, $\bar{\chi}_0 = 0.0041 \pm 5.52 \times 10^{-6} \text{ emu/mol}$: $H = 10000 \text{ G}$, $J = -346.64 \pm 5.20 \text{ cm}^{-1}$, $\bar{\chi}_0 = 0.0032 \pm 6.30 \times 10^{-6} \text{ emu/mol}$. and for $[\text{Cu(II)}_8(\mu\text{-3.5-dmpz})_8(\mu\text{-OH})_8]$ with $g = 2.20$: $H = 100 \text{ G}$, $J = -231.23 \pm 35.77 \text{ cm}^{-1}$, $\bar{\chi}_0 = 0.0018 \pm 1.09 \times 10^{-4} \text{ emu/mol}$: $H = 1000 \text{ G}$, $J = -227.83 \pm 32.60 \text{ cm}^{-1}$, $\bar{\chi}_0 = 0.0018 \pm 1.04 \times 10^{-4} \text{ emu/mol}$: $H = 10000 \text{ G}$, $J = -247.66 \pm 48.70 \text{ cm}^{-1}$, $\bar{\chi}_0 = 0.0021 \pm 1.31 \times 10^{-4} \text{ emu/mol}$.

Although the fitting results are very good for both compounds and the three magnetic fields, the fact of reducing the number of experimental data make the statistical errors grow. Nevertheless, this procedure let us see that the respective temperature for which $\bar{\chi}$ is a maximum ($|J|/k$) moves to a higher value than the one calculated considering the contribution of non-coupled spins in the whole temperature range.

In order to analyze the possibility of inter-ring interactions, we applied the octanuclear model with a mean-field correction (Eq. (2)) for the same range of temperature (100-300 K) and $\rho = 0$. The fitting results were excellent, as can be seen in Figure 6 for $[\text{Cu(II)}(\mu\text{-pz})(\mu\text{-OH})]$ and Figure 7 for $[\text{Cu(II)}_8(\mu\text{-3.5-dmpz})_8(\mu\text{-OH})_8]$. The magnetic parameters obtained are: for $[\text{Cu(II)}(\mu\text{-pz})(\mu\text{-OH})]$ with $g = 2.14$ and $H = 100 \text{ G}$, $J = -334.77 \pm 9.41 \text{ cm}^{-1}$, $zJ' = -2.86 \pm 1.68 \text{ cm}^{-1}$, $\bar{\chi}_0 = 0.0081 \pm 0.00089 \text{ emu/mol}$; $H = 1000 \text{ G}$, $J = -324.15 \pm 10.11 \text{ cm}^{-1}$, $zJ' = -3.69 \pm 0.83 \text{ cm}^{-1}$, $\bar{\chi}_0 = 0.0047 \pm 0.00014 \text{ emu/mol}$; $H = 10000 \text{ G}$, $J = -311.67 \pm 9.18 \text{ cm}^{-1}$, $zJ' = -4.05 \pm 0.92 \text{ cm}^{-1}$, $\bar{\chi}_0 = 0.0036 \pm 0.00009 \text{ emu/mol}$: for $[\text{Cu(II)}_8(\mu\text{-3.5-dmpz})_8(\mu\text{-OH})_8]$ with $g = 2.20$ and $H = 100 \text{ G}$, $J = -263.78 \pm 2.77 \text{ cm}^{-1}$, $zJ' = 21.20 \pm 0.53 \text{ cm}^{-1}$, $\bar{\chi}_0 = 0.0013 \pm 8.88 \times 10^{-6} \text{ emu/mol}$; $H = 1000 \text{ G}$, $J = -256.14 \pm 2.94 \text{ cm}^{-1}$, $zJ' = 25.33 \pm 0.59 \text{ cm}^{-1}$, $\bar{\chi}_0 = 0.0012 \pm 9.25 \times 10^{-6} \text{ emu/mol}$; $H = 10000 \text{ G}$, $J = -261.89 \pm 4.03 \text{ cm}^{-1}$, $zJ' = 24.06 \pm 0.75 \text{ cm}^{-1}$, $\bar{\chi}_0 = 0.0014 \pm 1.0 \times 10^{-5} \text{ emu/mol}$.

Figure 6.

Figure 7.

The pure octanuclear model with a mean-field correction also predicts higher temperature values for the $\bar{\chi}$ maximum for both Cu(II) compounds. The magnetic coupling parameter J for both compounds, is in agreement with the above results about the proposition of strong antiferromagnetic coupling, slightly higher for [Cu(II)(μ -pz)(μ -OH)]. Also, this model and correction let us suggest the possibility of very weak inter-ring magnetic coupling for both Cu(II) systems, maybe of antiferromagnetic type for [Cu(II)(μ -pz)(μ -OH)] and of ferromagnetic type for [Cu(II)₈(μ -3,5-dmpz)₈(μ -OH)₈]. Based on the spectral and magnetic studies, it is possible to suggest that the Cu(II) compound, with the unsubstituted pyrazolate ligand, shows an analogue structural arrangement to that of the cyclic octanuclear Cu(II) compound with the methylated pyrazolate ligand. The character (ferro or antiferromagnetic) of the inter-ring interactions zJ' is not conclusive, and at this point only the existence of this type of interactions can be suggested.

A very good fitting was also obtained applying the same cyclic octanuclear magnetic model and Eq. (1) with $\rho = 0$ to the magnetic data ($H = 100$ G) of the previously reported polynuclear compound [Cu(II)(allopurinolate)(OH)] (5), with $J = -378.23 \pm 19.0$ cm⁻¹. The J value is of the same character to the ones corresponding to the Cu(II) compounds discussed here, and also in agreement with the structural arrangement suggested before for this Cu(II) system (5).

The dinuclear and the infinite linear chain magnetic models were employed in an attempt to explore the quality of the octanuclear ring magnetic model with respect to others in the description of the magnetic data here presented. The unsuccessful results in the fitting process for these two models lead us to conclude the reliability of the octanuclear ring model for the Cu(II) compounds discussed here.

When comparing the magnetic behavior of polynuclear bis-pyrazolate Cu(II) or Co(II) compounds (17-19) to that of the polynuclear system [Cu(II)(μ -pz)(μ -OH)], the former show lower superexchange magnetic coupling (J ranging from -6 to -105 cm⁻¹). Dinuclear bis-pyrazolate Cu(II) compounds (20-22) show more intense magnetic coupling (J in

the -100 to -214 cm^{-1} range). On the other hand, polynuclear bis-dimethylpyrazolate Cu(II) or Co(II) compounds (11.19.23) (J in the -58 to -66 cm^{-1} range for Cu(II); from -2 to -6.6 cm^{-1} for Co(II)) also show lower magnetic coupling than $[\text{Cu(II)}_8(\mu\text{-}3.5\text{-dmpz})_8(\mu\text{-OH})_8]$. For dinuclear or trinuclear bis-pyrazolate Co(II) systems (24), the antiferromagnetic coupling is very low (J ranging from -1 to -25 cm^{-1}).

The compound $[\text{Cu(II)}(\mu\text{-pz})(\mu\text{-OH})]$ shows magnetic coupling in the same range as that shown by dinuclear Cu(II) compounds with pyrazolic and OR donor groups as bridges (25-28) (J from -32 to > -500 cm^{-1}). With respect to the magnetic behavior of $[\text{Cu(II)}_8(\mu\text{-}3.5\text{-dmpz})_8(\mu\text{-OH})_8]$, only one dinuclear case of this type was found in the literature (25). The magnetic coupling in this case is comparatively lower ($J = -95$ cm^{-1}).

On the other hand, from all the dinuclear Cu(II) compounds quoted above (25-28), it is possible to analyze the influence of the methyl groups in the pyrazolic moiety on the magnetic coupling intensity of the respective systems. The only cases reported (25) (compounds quoted therein as 7a, $J(\text{pz/OR}) = -100$ cm^{-1} ; 7c, $J(\text{dmpz/OR}) = -95$ cm^{-1}) show that the methyl groups do not have a strong influence on the intensity of the magnetic coupling. This influence is lower than the one deduced from the magnetic study of the two Cu(II) compounds presented here.

CONCLUSIONS.

In the present study, we performed the spectral and magnetic characterization of the polynuclear systems $[\text{Cu(II)}(\mu\text{-pz})(\mu\text{-OH})]$ and $[\text{Cu(II)}_8(\mu\text{-}3.5\text{-dmpz})_8(\mu\text{-OH})_8]$. The spectral results allow us to suggest the pyrazolate and OH groups as mutually-trans bridging ligands in the first system. This behavior is shown in $[\text{Cu(II)}_8(\mu\text{-}3.5\text{-dmpz})_8(\mu\text{-OH})_8]$. These systems are remarkable in their strong intra-ring superexchange magnetic coupling.

Finally, the Cu(II) compounds discussed before would be some of the few polynuclear Cu(II) systems which would have some topological relationship with the few octanuclear compounds reported up to now (29-32). They are also the first class of Cu(II) systems

showing those mixed bridging ligands. This paper is the first magnetic study carried out for this type of very complex metallic systems.

ACKNOWLEDGMENTS.

The authors are indebted to Francisco Morales-Leal (IIM, UNAM), Jorge Ramírez-Salcedo (IFC, UNAM), Carmen Vázquez (IIM, UNAM) and Leticia Baños (IIM, UNAM) for the magnetic susceptibility measurements, the epr spectra, the TG measurements and the X-ray diffraction patterns respectively. We thank Maria Elena Solares and Milton Medeiros for reading throughly the manuscript. We also thank CONACyT (Grant 3170-E) for partial financial support. RE is indebted to OAS for financial support.

References

1. J. Berthou, J. Elguero and C. Rérat. *Acta Cryst.* **B26**, 1880 (1970).
2. J.A.S. Smith, B. Wehrle, F.A. Parrilla, H.H. Limbach, M.C.F. Foces, F.H. Cano, J. Elguero, A. Baldy, M. Pierrot, M.M.T. Khurshid and J.B.L. McDouall. *J. Am. Chem. Soc.* **111**, 7304 (1989).
3. G.A. Ardizzoia, M.A. Angaroni, G. La Monica, F. Cariati, M. Moret and N. Masciocchi. *J. Chem. Soc. Chem. Commun.* 1021 (1990).
4. G.A. Ardizzoia, M.A. Angaroni, G. La Monica, F. Cariati, S. Cenini, M. Moret and N. Masciocchi. *Inorg. Chem.* **30**, 4347 (1991).
5. R. Acevedo-Chávez, M.E. Costas and R. Escudero-Derat. *J. Solid State Chem.* **113**, 21 (1994).
6. M.K. Ehlert, S.J. Rettig, A. Storr, R.C. Thompson and J. Trotter. *Can. J. Chem.* **68**, 1444 (1990).
7. J. Pons, X. López, E. Benet, J. Casabó, F. Teixidor and F.J. Sánchez. *Polyhedron* **9**, 2839 (1990).
8. G. López, G. García, G. Sánchez, J. García, J. Ruíz, J.A. Hermoso, A. Vegas and M.M. Ripoll. *Inorg. Chem.* **31**, 1518 (1992).
9. D. Carmona, J. Ferrer, I.M. Marzal, L.A. Oro and S. Trofimenko. *Gazzetta Chim. Italiana* **124**, 35 (1994).
10. D.A. Johnson, A.W. Cordes, B.A.F. Kelley and W.C. Deese. *J. Coord. Chem.* **32**, 1 (1994).
11. A.M.V. Sadus. *Transition Metal Chem.* **20**, 46 (1995).
12. J. Sletten, A. Sørensen, M. Julve and Y. Journaux. *Inorg. Chem.* **29**, 5054 (1990).
13. M. Angaroni, G.A. Ardizzoia, T. Beringhelli, G. La Monica, D. Gatteschi, N. Masciocchi and M. Moret. *J. Chem. Soc. Dalton Trans.* 3305 (1990).
14. G. López, J. Ruíz, G. García, C. Vicente, V. Rodríguez, G. Sánchez, J.A. Hermoso and M.M. Ripoll. *J. Chem. Soc. Dalton Trans.* 1681 (1992).

15. D. Carmona, A. Mendoza, J. Ferrer, F.J. Lahoz and L.A. Oro. *J. Organometallic Chem.* **431**, 87 (1992).
16. J.C. Bonner and M.E. Fisher. *Phys. Rev. A.*, **135**, 640 (1964).
17. M.K. Ehlert, S.J. Rettig, A. Storr, R.C. Thompson and J. Trotter. *Can. J. Chem.* **67**, 1970 (1989).
18. M.K. Ehlert, S.J. Rettig, A. Storr, R.C. Thompson and J. Trotter. *Can. J. Chem.* **69**, 432 (1991).
19. M.K. Ehlert, A. Storr and R.C. Thompson. *Can. J. Chem.* **71**, 1412 (1993).
20. T. Kamiyuki, H. Okawa, N. Matsumoto and S. Kida. *J. Chem. Soc. Dalton Trans.* 195 (1990).
21. J.C. Bayon, P. Esteban, G. Net, P.G. Rasmussen, K.N. Baker, C.W. Hahn and M.M. Gumz. *Inorg. Chem.* **30**, 2572 (1991).
22. J. Pons, X. López, J. Casabó, F. Teixidor, A. Caubet, J. Rius and C. Miravittles. *Inorg. Chim. Acta* **195**, 61 (1992).
23. M.K. Ehlert, A. Storr and R.C. Thompson. *Can. J. Chem.* **70**, 1121 (1992).
24. M.K. Ehlert, S.J. Rettig, A. Storr, R.C. Thompson and J. Trotter. *Can. J. Chem.* **71**, 1425 (1993).
25. W. Mazurek, B.J. Kennedy, K.S. Murray, M.J. O'Connor, J.R. Rodgers, M.R. Snow, A.G. Wedd and P.R. Zwack. *Inorg. Chem.* **24**, 3258 (1985).
26. Y. Nishida and S. Kida. *Inorg. Chem.* **27**, 447 (1988).
27. T.N. Doman, D.E. Williams, J.F. Banks, R.M. Buchanan, H.R. Chang, R.J. Webb and D.N. Hendrickson. *Inorg. Chem.* **29**, 1058 (1990).
28. M.K. Ehlert, S.J. Rettig, A. Storr, R.C. Thompson and J. Trotter. *Can. J. Chem.* **70**, 2161 (1992).
29. J. Galy, A. Mosset, I. Grenthe, I. Puigdomènech, B. Sjöberg and F. Hultén. *J. Am. Chem. Soc.* **109**, 380 (1987).
30. Q. Chen, S. Liu and J. Zubieta. *Inorg. Chem.* **28**, 4433 (1989).

31. P. Gili, P.M. Zarza, G.M. Reyes, J.M. Arrieta and G. Madariaga. *Polyhedron*. **11**, 115 (1992).
32. M.K. Ehlert, S.J. Rettig, R.C. Thompson and J. Trotter. *Inorg. Chem.* **32**, 5176 (1993).

Tables.

Table I. IR data (4000-200 cm^{-1}) and assignments for pzH and $[\text{Cu}(\text{II})(\mu\text{-pz})(\mu\text{-OH})]$. Abbreviations: S, strong; M, medium; W, weak; Sh, shoulder; vb, very broad; b, broad; s, sharp; d, doublet.

Table II. IR data (4000-200 cm^{-1}) and assignments for $[\text{Cu}(\text{II})_8(\mu\text{-dmpz})_8(\mu\text{-OH})_8]$. Abbreviations are the same as Table I. Assignments were made using the references cited in the discussion of $[\text{Cu}(\text{II})(\mu\text{-pz})(\mu\text{-OH})]$.

FIGURE CAPTIONS.

Figure 1. Schematic drawing of 1H-pyrazole (I) and 1H-3,5-dimethylpyrazole (II).

Figure 2. Schematic drawing of the structural arrangement suggested for $[\text{Cu}(\text{II})(\mu\text{-pz})(\mu\text{-OH})]$ ($R=\text{H}$), and partial drawing of the structural arrangement shown by the octanuclear ring $[\text{Cu}(\text{II})_8(\mu\text{-dmpz})_8(\mu\text{-OH})_8]$ ($R=\text{CH}_3$) (References 3 and 4).

Figure 3. Molar magnetic susceptibility $\bar{\chi}$ (per octanuclear unit) as a function of temperature and magnetic field for $[\text{Cu}(\text{II})(\mu\text{-pz})(\mu\text{-OH})]$. Dotted lines are the experimental data and solid lines are theoretical values.

Figure 4. Molar magnetic susceptibility $\bar{\chi}$ (per octanuclear unit) as a function of temperature and magnetic field for $[\text{Cu}(\text{II})_8(\mu\text{-dmpz})_8(\mu\text{-OH})_8]$. Dotted lines are experimental data and solid lines are theoretical values.

Figure 5. $\bar{\chi}$ (emu/mol)- T (K) theoretical curves from Eq. (1) for a) $[\text{Cu}(\text{II})(\mu\text{-pz})(\mu\text{-OH})]$, and b) $[\text{Cu}(\text{II})_8(\mu\text{-dmpz})_8(\mu\text{-OH})_8]$, as a function of the magnetic contribution of the non-coupled $S = 1/2$ spins.

Figure 6. $\bar{\chi}$ (emu/mol) - T (K) values for $[\text{Cu}(\text{II})(\mu\text{-pz})(\mu\text{-OH})]$ and $H = 100, 1000$ and 10000 G. Dotted lines are the experimental data and solid lines are theoretical values from Eq. (2).

Figure 7. $\bar{\chi}$ (emu/mol) - T (K) values for $[\text{Cu}(\text{II})_8(\mu\text{-dmpz})_8(\mu\text{-OH})_8]$ and $H = 100, 1000$ and 10000 G. Dotted lines are the experimental data and solid lines are theoretical values from Eq. (2).

pzH		[Cu(II)(μ -pz)(μ -OH)]	
$\bar{\nu}$ (cm ⁻¹)	Assignments	$\bar{\nu}$ (cm ⁻¹)	Assignments
—	—	3580 <u>M</u> , b 3410 <u>S</u> , b	} ν_{OH^-} bridge
3050 <u>S</u> , vb	{ $\nu_{\text{N-H}}$ $\nu_{\text{C-H}}$	3100 <u>W</u> , b	{ $\nu_{\text{C-H}}$ $\nu_{\text{N-H}}$
1460 <u>M</u> , b	{ ν_{ring} ω $\beta_{\text{N-H}}$	1480 <u>M</u> , s	{ ν_{ring} ω $\beta_{\text{N-H}}$
1400 <u>S</u> , s	{ ν_{ring} ω $\beta_{\text{N-H}}$	1410 <u>S</u> , b	{ ν_{ring} ω $\beta_{\text{N-H}}$
1360 <u>S</u> , d	{ ν_{ring} ω $\beta_{\text{N-H}}$	1370 <u>S</u> , s	{ ν_{ring} ω $\beta_{\text{N-H}}$
1265 <u>W</u> , d	{ ring $\beta_{\text{C-H}}$ $\delta_{\text{C-H}}$ $\beta_{\text{N-H}}$	1270 <u>S</u> , s	{ ring $\beta_{\text{C-H}}$ $\delta_{\text{C-H}}$ $\beta_{\text{N-H}}$
1235 <u>W</u> , d	{ $\beta_{\text{C-H}}$ $\delta_{\text{C-H}}$ $\beta_{\text{N-H}}$ ring	1250 <u>Sh</u>	{ $\delta_{\text{C-H}}$ $\beta_{\text{C-H}}$ ring $\beta_{\text{N-H}}$
1145 <u>S</u> , d	{ $\beta_{\text{C-H}}$ $\delta_{\text{N-H}}$ $\beta_{\text{N-H}}$ ring	1170 <u>S</u> , s	{ $\beta_{\text{C-H}}$ ring $\delta_{\text{N-H}}$ $\beta_{\text{N-H}}$
1045 <u>S</u> , d	{ $\beta_{\text{C-H}}$ $\delta_{\text{C-H}}$	1055 <u>S</u> , b	{ $\beta_{\text{C-H}}$ $\delta_{\text{C-H}}$

Table I.

pZH		[Cu(II)(μ-pz)(μ-OH)]	
$\nu(\text{cm}^{-1})$	Assignments	$\bar{\nu}(\text{cm}^{-1})$	Assignments
935 <u>M</u> .b	$\begin{cases} \beta_{\text{C-H}} \\ \delta_{\text{ring}} \end{cases}$	915 <u>M</u> .b	$\begin{cases} \beta_{\text{C-H}} \\ \delta_{\text{ring}} \end{cases}$
880 <u>M</u> .b	$\begin{cases} \gamma_{\text{C-H}} \\ \gamma_{\text{N-H}} \\ \delta_{\text{C-H}} \end{cases}$	865 <u>M</u> .b	$\begin{cases} \gamma_{\text{C-H}} \\ \delta_{\text{C-H}} \\ \gamma_{\text{N-H}} \end{cases}$
835 <u>M</u> .b	$\begin{cases} \gamma_{\text{C-H}} \\ \gamma_{\text{N-H}} \\ \delta_{\text{C-H}} \end{cases}$	—	—
760 <u>S</u> .b	$\begin{cases} \gamma_{\text{C-H}} \\ \gamma_{\text{N-H}} \\ \delta_{\text{C-H}} \end{cases}$	745 <u>S</u> .s	$\begin{cases} \gamma_{\text{C-H}} \\ \delta_{\text{C-H}} \\ \gamma_{\text{N-H}} \end{cases}$
655 <u>M</u> .s	$\begin{cases} \text{ring} \\ \gamma_{\text{N-H}} \end{cases}$	—	—
615 <u>S</u> .d	$\begin{cases} \text{ring} \\ \delta_{\text{N-H}} \\ \gamma_{\text{N-H}} \end{cases}$	615 <u>S</u> .s	$\begin{cases} \text{ring} \\ \delta_{\text{N-H}} \\ \gamma_{\text{N-H}} \end{cases}$
—	—	535 <u>M</u> .b	$\{\nu_{\text{M-OH}^-} \text{ bridge}\}$
—	—	465 <u>Sh</u>	$\{\nu_{\text{M-OH}^-} \text{ bridge}\}$
—	—	330 <u>S</u> .s	$\{\nu_{\text{M-N}}\}$

Continuation of Table I.

ν (cm^{-1})	Assignments
ca. 3400 <u>M</u> . b	ν_{OH^-} bridge
ca. 3100 <u>M</u> . b	—
2900 <u>W</u> . s	$\nu_{\text{C-H}}$
1538 <u>S</u> . s	ν_{ring}
1418 <u>S</u> . b	ν_{ring}
1340 <u>S</u> . s	ν_{ring}
1140 <u>W</u> . b	$\left\{ \begin{array}{l} \nu_{\text{ring}} \\ \beta_{\text{C-H}} \end{array} \right.$
1040 <u>M</u> . s	$\delta_{\text{C-H}}/\beta_{\text{C-H}}$
890 <u>M</u> . b	$\left\{ \begin{array}{l} \gamma_{\text{C-H}} \\ \delta_{\text{C-H}} \end{array} \right.$
770 <u>M</u> . s	$\left\{ \begin{array}{l} \gamma_{\text{C-H}} \\ \delta_{\text{C-H}} \end{array} \right.$
700 <u>W</u> . s	—
485 <u>M</u> . b	$\nu_{\text{M-OH}^-}$ bridge
460 <u>M</u> . b	$\nu_{\text{M-OH}^-}$ bridge
371 <u>M</u> . b	$\nu_{\text{M-N}}$
320 <u>W</u> . b	$\nu_{\text{M-N}}$

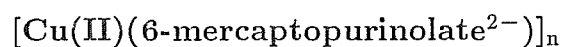
Table II.

ANEXO

4

*Magnetic Study of the Novel Polynuclear
Compound [Cu(II)(6-mercaptopurinolate²⁻)_n].*

Magnetic Study of the Novel Polynuclear Compound



Rodolfo Acevedo-Chávez.

Centro de Química, Instituto de Ciencias, B. Universidad Autónoma de Puebla,
Apartado Postal 1613, Puebla, Puebla, México.

María Eugenia Costas*.

Facultad de Química, Universidad Nacional Autónoma de México,
México 04510, D.F., México.

Roberto Escudero.

Instituto de Investigaciones en Materiales, Universidad Nacional Autónoma de México,
México 04510, D.F., México.

* To whom correspondence should be addressed.

ABSTRACT.

Aqueous and methanolic Cu(II)-6-mercaptapurine interactions yield the novel amorphous polynuclear compound $[\text{Cu(II)(6-mercaptapurinate)}^{2-}]_n$, which is also obtained from diverse Cu(II)-heterocyclic ligand competitive reactions. The kinetic and thermodynamic stabilities inferred for this compound are remarkable. The spectroscopic data let us suggest the involvement of S(6) and N atoms in the imidazolic moiety of the deprotonated ligand in the bonding to Cu(II) atoms, forming a distorted bidimensional metallic network. The magnetic studies show the existence of very weak antiferromagnetic coupling in the magnetic superexchange pathways postulated. This system represents the first example of a 1:1 Metal:6-mercaptapurinate²⁻ system with a *d*-type open shell metallic center. The magnetic study carried out also represents the first example of magnetic characterization for this type of polynuclear Cu(II) compounds.

INTRODUCTION.

Purine derivatives are interesting molecules due to their very rich acid-base physical chemistry, to the variety of coordination sites they show in metal-heterocycle interactions and to the stereochemical, spectral and physical properties of the respective coordination compounds, among other features.

The synthetic (1,2) heterocycle 6-mercaptapurine (Figure 1) is the structural analogue of the Ribonucleic Acid minor base 6-oxapurine (hypoxanthine); it is employed against certain neoplastic diseases, as acute lymphoblastic leukemia (3).

Figure 1

This fact, together with the specific role that several transitional metals play in the Nucleic Acid processes (4), have prompted several research groups to carry out studies related to the bonding behavior of 6-mercaptapurine (and its nucleosides, nucleotides and derivatives) in metal-heterocycle interactions (5). From these studies it is important to arise the key role played by the exocyclic $\underline{\text{S}}(6)$ atom in the metallic bonding of the molecule: as terminal or bridge ligand through the $\underline{\text{S}}(6)$ atom, as chelating ligand through the $\underline{\text{S}}(6)$ and $\underline{\text{N}}(7)$ atoms, or even more and interestingly, as chelating ligand toward a metallic center ($\underline{\text{S}}(6)$ and $\underline{\text{N}}(7)$) and simultaneously bridging (through $\underline{\text{S}}(6)$) adjacent metallic centers in scarce polynuclear coordination compounds (6). To our knowledge, there is no report of a compound where this exocyclic $\underline{\text{S}}$ atom reluctes to bond to transitional centers. This behavior makes it possible to suggest the great electronic exchange capability, and the energetic and spatial disposition of the atomic orbitals of this atom in those interactions.

In our research program related to the study of transition metallic center-purine derivative interactions, we have explored the reactions of 6-mercaptapurine with Cu(II) under several experimental conditions, and we have confirmed the great reactivity and bonding capability of the heterocyclic ligand through the $\underline{\text{S}}(6)$ atom. In this paper we

report several Cu(II)-6-mercaptopurine interactions carried out both in aqueous (at different pH values) and in methanolic media, including competitive reactions of this heterocycle with other ligands (for example, 6-oxopurine or its isomer, allopurinol) toward the Cu(II) coordination sphere. Also, we report here the spectral and magnetic study of the novel polynuclear coordination compound $[\text{Cu}(\text{II})(6\text{-mercaptopurinolate}^{2-})]_n$, which is the unique product in these metal-ligand interactions.

EXPERIMENTAL.

Reagents. The Cu(II) metallic salts ($\text{X}=\text{Cl}^-$, Br^- , NO_3^- , SO_4^{2-} , ClO_4^- and CH_3CO_2^-), 6-mercaptopurine, 6-oxopurine, allopurinol, buffers (glycine/HCl/NaCl for pH=1; $\text{CH}_3\text{CO}_2\text{H}/\text{NaCH}_3\text{CO}_2$ for pH=4; $\text{KH}_2\text{PO}_4/\text{K}_2\text{HPO}_4$ for pH=7 and KOH/KCl for pH=13) and organic solvents were commercially acquired. All were used with no further purification.

Cu(II)-heterocycle interactions.

A) Aqueous medium.

All the reactions were independently carried out at pH values of 1, 4, 7 and 13. Also, for each one of these interactions, the metallic counterion (from Cl^- to CH_3CO_2^-) was systematically changed.

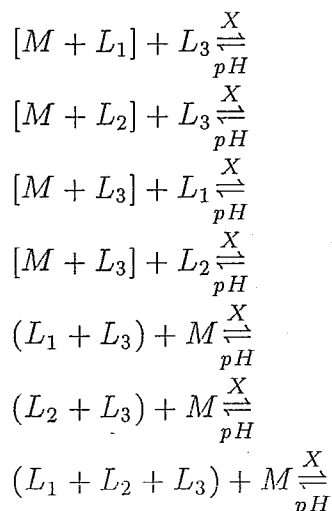
a) Single Cu(II)-6-mercaptopurine interactions.

At each pH value, 1 mmol of 6-mercaptopurine was added to 100 ml of the buffer solution, and the mixture was allowed to boil under stirring and refluxing at atmospheric pressure. 1 mmol of the respective metallic salt (previously dissolved in *c.a.* 10 ml of H_2O) was added to the resulting pale yellow solution, shortly forming a green suspension, which was maintained under those conditions for several days; no changes were observed. The boiling mixture was filtered off, and the solid product (dark green) was exhaustively washed, first with boiling H_2O and then with boiling CH_3OH . The product obtained from each reaction was kept at *c.a.* 100°C for 24 hours. At these conditions, the solid showed a noticeable dark green color, due to the high density of the sample. The original

color was again obtained when each sample was finely powdered. This same product was obtained when 1:2 and 1:3 metal:ligand molar ratios were used for each metallic salt and pH value. The compound synthesized in all these reactions was almost insoluble (at room temperature) in the common organic solvents $(\text{CH}_3)_2\text{CO}$, $\text{C}_2\text{H}_5\text{OH}$, CH_3OH , CH_3CN , CH_3NO_2 and $(\text{CH}_3)_2\text{SO}$. A green-yellow solution was obtained after several days only when the product was kept in $(\text{CH}_3)_2\text{SO}$ under prolonged stirring and slight heating.

b) Competitive Cu(II)-heterocycle interactions.

These were carried out systematically modifying the sequence of the metal-heterocycle interactions at different pH values, as is schematically shown below:



where $M=\text{Cu(II)}$, $L_1=\text{allopurinol}$, $L_2=\text{hypoxanthine}$, $L_3=6\text{-mercaptapurine}$, $X=\text{metallic salt counterion}$, $[M + L_i]=\text{chemical equilibrium between these reagents and } (L_i + L_{ii} + \dots)=\text{solvated ligands}$.

In a typical reaction, 1 mmol of allopurinol was added to 100 ml of the specific buffer solution and the mixture was treated as in (a). 1 mmol of the respective metallic salt was added to this solution, shortly forming (for pH values from 4 to 13) a blue suspension (the final product was reported before (7)) which was maintained under stirring and boiling for several hours; no changes were observed. 1 mmol of 6-mercaptapurine was added to this suspension at the same conditions; the mixture color changed from blue to green with

time. Finally, after several days, the reaction mixture was the same as that obtained in all the cases in (a), and the solid was treated in the same way. The product obtained (8) from the respective Cu(II)-allopurinol interaction in this typical reaction at pH=1 (except for $X=CH_3CO_2^-$), was kept in solution at boiling conditions. The 6-mercaptopurine added to this solution formed the same green suspension, and the solid obtained was treated as before. The Cu(II)-allopurinol interaction yield also the same blue suspension from this typical reaction at pH=1 ($X=CH_3CO_2^-$). The following reaction step was carried out as before, and the same dark green product was also obtained.

In summary, the product was the same (*i.e.*, the dark green powder) from the systematically modified competitive reactions of the heterocyclic ligands (allopurinol and 6-mercaptopurine, hypoxanthine and 6-mercaptopurine or even more, allopurinol, hypoxanthine and 6-mercaptopurine) towards Cu(II) at several pH values and by employing diverse metallic salt counterions.

B) Methanolic medium.

For each one of the reactions carried out in this medium, the metallic salt counterion (from $X=NO_3^-$ to $CH_3CO_2^-$) was systematically modified as in part A.

a) Single Cu(II)- 6-mercaptopurine interactions.

1 mmol of 6-mercaptopurine was dissolved (upon stirring, boiling and refluxing at atmospheric pressure) in 100 ml of CH_3OH . 1 mmol of the respective metallic salt (previously dissolved in *c.a.* 10 ml of CH_3OH) was added to the pale yellow solution. A green suspension was obtained and maintained at these conditions for several days; no further changes were observed. The solid formed (dark green) was isolated, purified and dried as quoted before.

b) Competitive Cu(II)-heterocycle interactions.

These reactions were carried out under the same scheme as in the aqueous medium. In a typical reaction, 1 mmol of 6-oxopurine was dissolved in 100 ml of CH_3OH under stirring, boiling and refluxing at atmospheric pressure. The respective metallic salt was

added to the colorless solution. A blue suspension was obtained which was preserved at the same conditions for several days, with no additional changes observed. Then, 1 mmol of 6-mercaptopurine was added to this product suspension (8), turning to green with time. It was maintained under the experimental conditions quoted before for several days; no changes were detected. The product (dark green) was isolated, purified and dried as previously mentioned.

In summary, all the competitive Cu(II)-heterocycle methanolic interactions carried out yield also the same dark green product.

PHYSICAL MEASUREMENTS.

Infrared (IR) spectra of all the samples were obtained as nujol mulls (CsI plates) in the 4000-200 cm^{-1} range by employing a 598 Perkin Elmer spectrometer. Electronic spectra (350-1100 nm) of the powdered samples were measured by the specular reflectance method in a 160-A Shimadzu equipment, and by using BaSO_4 as reference. Electronic spectra (200-1100 nm) of $(\text{CH}_3)_2\text{SO}$ solutions of the solvated compound were also obtained with the same equipment. Thermogravimetric measurements were carried out in a DT-30 Shimadzu equipment by using $\text{N}_2(\text{g})$ as carrier gas and $5^\circ\text{C}/\text{min}$ as heating rate. The magnetic susceptibility at room temperature was measured by the modified Gouy method using a Johnson Matthey balance and employing $\text{Hg}[\text{Co}(\text{SCN})_4]$ as calibrating agent. The variable field and temperature magnetic susceptibility measurements were carried out by using a SQUID Quantum Design magnetometer from 2 to 300 K and from 10^3 to 5×10^4 G. The magnetic measurements for each magnetic field were performed both increasing and decreasing the temperature. They were corrected considering both the cell and the sample diamagnetic contributions. EPR spectra (X-band) of the powdered samples were obtained in a 200-D Bruker spectrometer at room and liquid nitrogen temperatures. An EPR spectrum (X-band) of the $(\text{CH}_3)_2\text{SO}$ frozen solution of the solvated compound was obtained only at liquid nitrogen temperature. The g values obtained were standardized against the absorption of diphenylpicrylhydrazyl (DPPH) at 2.0043. X-ray powder diffraction patterns

of the organic ligands 6-oxopurine, allopurinol and 6-mercaptapurine and several samples of the Cu(II) coordination compound obtained, were taken in XD-5A Shimadzu and D-500 Siemens diffractometers. Microanalysis determination (C, H, N) was performed by the Chemistry Department at the University College, London, and confirmed employing a 240-C Perkin Elmer equipment.

The samples obtained were previously exposed to atmosphere for several days before performing the analytical and the thermal studies. All the other physical measurements were carried out with the freshly obtained dried samples.

RESULTS AND DISCUSSION.

The Cu(II) coordination compound obtained was the same irrespective of the pH values explored, the metallic salt counterion used, the Metal:ligand molar ratios employed and the sequence in the competitive Cu(II)-heterocycle interactions performed. The same product was obtained by modifying the reaction medium, CH₃OH in this case. This compound appears to be of both remarkable kinetic and thermodynamic stabilities. To our knowledge, there is no example among the purine-type heterocycles with such reactivity and with the specific and selective coordination mode towards Cu(II) as that shown by 6-mercaptapurinolate²⁻ in this study.

a) Analytical results.

All the samples analyzed are in agreement with the formulation: Cu(II)(6-mp²⁻)·H₂O (6-mp²⁻=6-mercaptapurinolate²⁻). Found: 25.55% (C), 1.52% (H), 23.84% (N); expected for Cu(C₅H₂N₄S²⁻)·H₂O: 25.91% (C), 1.73% (H), 24.17% (N).

b) Infrared (IR) results.

The IR bands characterization both of the free ligand 6-mercaptapurine and Cu(II)(6-mp²⁻) was carried out based on related studies (9-16).

The IR spectrum of the free ligand 6-mercaptapurine shows a band at 3425 cm⁻¹ ($\nu_{\text{N-H}}$), which does not exist in the IR spectrum of the coordination compound. This is in agreement with the N-H deprotonation of the organic ligand in the Cu(II) compound.

The bands in the IR spectrum of 6-mercaptapurine associated to ν_{C-H} vibrational modes (3140 and 3090 cm^{-1}), are not clearly shown in the IR spectrum of the Cu(II) compound, and indicate a strong electronic modification in the nearest sites of the C-H groups. The band at 1610 cm^{-1} ($\delta_{N-H}/\nu_{C=C}/\nu_{C=N}$) in the free ligand IR shows a shift to lower energy (1580 cm^{-1}) in the Cu(II) compound IR, in agreement with the deprotonation quoted before and the endocyclic coordination involvement of this ligand.

The band appearing at 1520 cm^{-1} ($\nu_{C=N}/\text{ring vib.}$) in the free ligand IR spectrum is not observed in the IR spectrum of the Cu(II) compound. The 6-mercaptapurine IR band (1410 cm^{-1}) associated to several endocyclic groups vibrational modes ($\nu_{C-N}/\nu_{C-C}/\text{ring vib.}$) is also not present. This same spectral behavior is shown for the band at 1275 cm^{-1} ($\nu_{C-N}/\text{ring vib.}$) in the free ligand IR. Again, these spectral modifications are in agreement with the coordination of 6-mercaptapurine in a deprotonated state through endocyclic sites. The IR spectrum of 6-mercaptapurine shows a band at 1150 cm^{-1} ($\nu_{C=S}/\text{ring vib.}$) which is absent in the Cu(II) compound IR spectrum, and suggests the participation of the exocyclic S(6) atom (together with endocyclic groups) in the metallic bonding. Related to this last proposition, the bands that appear at 1575 cm^{-1} , 1345 cm^{-1} and 1115 cm^{-1} ($\nu_{R-N-C=S}$) in the 6-mercaptapurine IR spectrum, show a noticeable perturbation in the Cu(II) compound IR spectrum, together with the absence of some of them. This spectral pattern is also strongly suggestive of the S(6) atom participation in the metallic bonding of the heterocyclic ligand in the Cu(II) coordination compound. On the other hand, the IR spectrum of the coordination compound in the 1100-600 cm^{-1} range shows remarkable modifications (in frequency and intensity) of bands associated to vibrational modes of both the endocyclic groups (*e.g.*, the C-H groups) and the exocyclic groups (*i.e.*, the C-S group), in agreement with the involvement of the S(6) and N atoms in the metallic bonding of 6-mercaptapurinolate²⁻.

Finally, bands at 317 cm^{-1} , 275 cm^{-1} , 240 cm^{-1} and 216 cm^{-1} appear in the low-energy IR spectrum of the Cu(II) coordination compound. These bands might be related to the ν_{Cu-S} and ν_{Cu-N} vibrational modes.

c) Electronic spectroscopy results.

The electronic spectrum (350-1100 nm) of powdered Cu(II)(6-mp²⁻) shows the low-energy tail of a band that arises in the UV region and continues to the visible region. This is associated both to a Metal- Ligand charge transfer process and to the participation of the S(6) atom of the heterocycle in the metallic bonding. The spectrum also shows a broad band at 715 nm, associated to Cu(II) *d-d* transitions. Unfortunately, the spectral pattern difficults the possible assignment of the Cu(II) stereochemistry.

The electronic spectrum (200-1100 nm) of the Cu(II) coordination compound solvated in (CH₃)₂SO shows a broad and asymmetric band (centered at *c.a.* 278 nm) in the 225-650 nm range, which is assigned as above. The broad band associated to Cu(II) *d-d* transitions appears at *c.a.* 834 nm, and is shifted to lower energy with respect to the analogous band in the spectrum of the solid sample. This lower energy shift might be attributed to changes in the stereochemistry of the Cu(II) coordination sphere, perhaps due to the presence of solvent molecules in it.

d) Thermogravimetric results.

The atmosphere exposed powdered sample shows a mass loss attributed to the process: Cu(II)(6-mp²⁻)·H₂O → Cu(II)(6-mp²⁻). The temperature range (*c.a.* 90- 100°) in which this loss occurs, is also in agreement with the suggestion that the H₂O molecule is not involved in the Cu(II) coordination sphere, as was also inferred from the absence of the ν_{M-OH_2} vibrational mode in the low-energy IR spectrum of the dried Cu(II) compound. Finally, the thermal decomposition of the anhydrous Cu(II) system starts at *c.a.* 320°C and it is attributed to the thermal heterocyclic ligand modification.

e) EPR spectral results.

The X-band ($\nu=9.244$ GHz) epr spectra (Figure 2a) of all the powdered samples of the Cu(II) coordination compound, both at room and liquid nitrogen temperatures, are the same.

Figure 2

The spectral behavior could be associated to the presence of a nearly static structure around Cu(II). This also suggests the existence of very strong Metal-Ligand interactions, including lattice interactions of very short-range. The existence of an anisotropic g tensor can be inferred from Figure 2a; the spectral pattern in full indicates the existence of Cu(II)-Cu(II) magnetic interactions. The estimated g values ($g_{\perp} = 2.09$, $g_{\parallel} = 2.40$), indicate a significant tetragonal geometry on Cu(II). The spectral pattern in the middle-field region corresponds to a predominant axial-type, and principally $d_{x^2-y^2}$ orbitals as electronic ground state ($g_{\parallel} > g_{\perp} > 2.0$) in a dominant tetragonal stereochemistry. The fact that no changes are observed in the EPR data with the decrease of temperature, and the indication of metal-metal interactions, suggest that, at least in this temperature range, there are no changes in the electronic states of the Cu(II)-Cu(II) magnetic coupling.

The X-band ($\nu=9.204$ GHz) EPR spectrum of $(\text{CH}_3)_2\text{SO}$ frozen solution (77 K) of the solvated Cu(II) coordination compound is shown in Figure 2b. The spectral pattern (axial-type) is very different from that in the solid state. For the case in discussion, an anisotropic g tensor, with values of $g_{\perp} = 2.08$ and $g_{\parallel} = 2.40$, is also inferred. The spectrum in the high-field region also indicates the existence of Metal-Metal magnetic interactions. In the low-field region, the four absorptions are attributed to a hyperfine structure; the value (*c.a.* 130 G) is associated to significant e^- -nuclei coupling. It is necessary to point out that the EPR spectral pattern resembles the one shown by some Cu(II) compounds in solution that show a pentacoordinated environment (square pyramidal) in the solid state (17).

Finally, it is possible to propose that the electronic ground state of the Cu(II) centers lies mainly upon the $d_{x^2-y^2}$ orbitals. The spectral characteristics discussed above could also be due to the existence of mononuclear units, as a consequence of a dissociative processes induced by the temperature and the solvent physical chemistry properties.

f) X-ray powder diffraction patterns results.

The X-ray diffraction pattern ($10-70^\circ 2\theta$) of the free organic ligand shows several signals, mainly in the low- 2θ region. However, the respective diffraction pattern ($10-60^\circ 2\theta$) of several powdered samples of the Cu(II) coordination compound, indicate an amorphous character. This could be associated both to the synthesis conditions and to the complex polynuclear character of the Cu(II) compound. Slow evaporations of both aqueous and methanolic filtrates of the original reaction mixtures, yield scarce mass of the same amorphous system.

In summary, with all the experimental results discussed before, the existence of a Cu(II) coordination compound that only shows heterocyclic donor atoms of the deprotonated $6mp^{2-}$ ligand in the metallic coordination sphere can be considered. The spectroscopic data are in concordance with the metallic bonding of the exocyclic $\underline{S}(6)$ atom and endocyclic \underline{N} atoms forming a tetracoordinated Cu(II) environment. With respect to the nature of these last atoms, the donor properties of those corresponding to the imidazolic ring would make them the most favorable ones, because of the high basicity of the $\underline{N}(9)$ atom, and of the adequate stereochemical disposition of the $\underline{N}(7)$ atom in constructing (together with the $\underline{S}(6)$ atom) chelating bonding towards the metallic centers. This metallic bonding mode is characterized by a noticeable Metal-Ligand thermodynamic stability.

In order to obtain a possible structural arrangement for this Cu(II) compound, in agreement with all the results discussed before and with the existence of a polynuclear character, systematically modified molecular models were made. From these, only one arrangement, shown in Figure 3, is selfconsistent.

Figure 3

In this, the Cu(II) atoms are simultaneously bridged by the $\underline{S}(6)$ and the $\underline{N}(7)/\underline{N}(9)$ atoms of the deprotonated ligand. The structural arrangement would not be planar, with

the Cu(II) atoms in a roughly distorted tetracoordinated environment (*i.e.*, flattened tetrahedral geometry). This structural proposition for the novel Cu(II) coordination compound would implicate the existence of an unexplored metallic bonding mode for the heterocyclic ligand, also in a non frequent deprotonation level. This bidimensional network is not frequent in the metal coordination chemistry. Very scarce examples of this class have been reported up to date, being one of them the system $[\text{Cu(II)(imidazolate}^-)_2]_n$ (18-20), in which the monoanionic ligands are bridging the Cu(II) atoms in two directions. Two other examples of this type are the compounds $[\text{Cu(II)(methylpyrazolate}^-)_2]_n$ and $[\text{Cu(II)(chloropyrazolate}^-)_2]_n$, in which the Cu(II) atoms are linked through the N atoms of the pyrazolate⁻ rings (21). In these structures the Cu(II) environments are respectively flattened tetrahedrals (21), or alternating planar tetracoordinated and flattened tetrahedrals (18-20). Also, in all these few examples the 1:2 Metal:Heterocycle molar ratio is present. The Cu(II) compound in discussion here, is the first example of a 1:1 Cu(II):6-mp²⁻ system for which a spectroscopic and magnetic characterization (see below) has been made.

Only one example of the M(II)(6-mp²⁻) type has been reported up to date (14), which corresponds to the formulation $\text{Cd(II)(6-mercaptopurinate}^{2-}) \cdot \text{H}_2\text{O}$. Unfortunately, only a limited study was made without advances in its structural arrangement and in the detailed metallic bonding of the heterocyclic ligand.

g) Magnetic studies results.

The magnetic study of the Cu(II) compound under discussion was made in the 2-300 K range and external magnetic fields of 10^3 , 10^4 , 3×10^4 and 5×10^4 G. When plotting the $\bar{\chi}$ (emu/Cu(II)) values *versus* T (K) for the respective magnetic fields, a small decrease of the magnetic susceptibility with the increase of the magnetic field intensity was observed. The general pattern of the curves is in agreement with a Curie-Weiss behavior; the fitting process of the Curie-Weiss equation, $\chi = \chi_0 + C/(T - \theta)$, to the experimental data was very good, and the θ (< 0) values obtained for all the magnetic fields indicate the existence

of an antiferromagnetic coupling. This type of magnetic coupling is confirmed plotting $\bar{\chi}T$ versus T for all the magnetic field intensities. In this representation a continuous decrease of $\bar{\chi}T$ values with descending T is observed, and at temperatures lower than 100 K, the slope increases. This pattern indicates an antiferromagnetic coupling in the sample analyzed.

We selected the linear chain model of coupled $S = 1/2$ spins to analyze the magnetic features of the structural proposition mentioned before. The magnetic susceptibility is described by the Bonner-Fisher equation:

$$\bar{\chi}_{\text{BF}} = \frac{N\beta^2 g^2}{kT} \left[\frac{0.025 + 0.14995x + 0.30094x^2}{1 + 1.9862x + 0.68854x^2 + 6.0626x^3} + \bar{\chi}_0 \right] (1 - \rho) + \frac{N\beta^2 g^2}{2kT} \rho \quad (1)$$

where $x = |J|/kT$, and the other symbols have their usual meaning. With this equation, a very good fitting process was obtained for the whole temperature and magnetic field ranges. The value of the spectroscopic g tensor (2.09) was maintained constant in this process. The parameters obtained were: $H = 1000$ G: $J = -7.59 \pm 0.15$ cm⁻¹, $\rho = 0.1748 \pm 0.0015$, $\bar{\chi}_0 = 1.549 \times 10^{-3} \pm 1.33 \times 10^{-4}$ emu/tetranuclear unit; $H = 10000$ G: $J = -6.67 \pm 0.17$ cm⁻¹, $\rho = 0.1608 \pm 0.0014$, $\bar{\chi}_0 = 8.09 \times 10^{-5}$ emu/tetranuclear unit; $H = 30000$ G: $J = -4.64 \pm 0.16$ cm⁻¹, $\rho = 0.1090 \pm 0.003$, $\bar{\chi}_0 = 8.09 \times 10^{-5}$ emu/tetranuclear unit; $H = 50000$ G: $J = -4.13 \pm 0.13$ cm⁻¹, $\rho = 0.0720 \pm 0.003$, $\bar{\chi}_0 = 8.09 \times 10^{-5}$ emu/tetranuclear unit. The J values indicate a very weak intensity for the intrachain antiferromagnetic coupling. The ρ values (assumed as the mole fraction of non coupled $S = 1/2$ spins) are consistent with the Curie-Weiss behavior in the low-temperature region.

The presence of the non coupled $S = 1/2$ spins makes it difficult to observe the $\bar{\chi}$ maxima as a function of temperature in the four different magnetic fields curves. The maxima are predicted by equation (1) for $\rho = 0$ (by employing the other fitting parameters mentioned before) to be localized in the 7-13 K range for the four magnetic fields.

This is in concordance with the typical $\bar{\chi} - T$ behavior for a system with a very weak antiferromagnetic coupling.

The structural proposition for the Cu(II) compound also allows us to propose the existence of interchain magnetic interactions, in addition to the intrachain ones. To analyze this possibility, a molecular field approximation was included, for which the magnetic susceptibility is calculated as:

$$\bar{\chi} = \frac{\bar{\chi}_{\text{BF}}}{1 - \frac{2zJ'\bar{\chi}_{\text{BF}}}{N\beta^2g^2}} \quad (2)$$

where $\bar{\chi}_{\text{BF}}$ is the magnetic susceptibility of one linear chain of coupled $S = 1/2$ spins described by equation (1), z is the number of nearest neighboring chains and J' is the interchain mean-field magnetic coupling parameter. The fitting process obtained for this expression was very good, and the magnetic parameters obtained were (for $g = 2.09$ and $z = 4$): $H = 1000$ G: $J = -11.34 \pm 0.27$ cm⁻¹, $J' = -0.45 \pm 0.06$ cm⁻¹, $\rho = 0.21 \pm 0.001$, $\bar{\chi}_0 = 1.09 \times 10^{-3} \pm 3.7 \times 10^{-5}$ emu/tetranuclear unit; $H = 10000$ G: $J = -11.58 \pm 0.19$ cm⁻¹, $J' = -0.67 \pm 0.05$ cm⁻¹, $\rho = 0.21 \pm 0.001$, $\bar{\chi}_0 = 1.90 \times 10^{-4} \pm 2.6 \times 10^{-5}$ emu/tetranuclear unit; $H = 30000$ G: $J = -11.58 \pm 0.31$ cm⁻¹, $J' = -1.56 \pm 0.01$ cm⁻¹, $\rho = 0.22 \pm 0.002$, $\bar{\chi}_0 = 7.59 \times 10^{-5} \pm 3.8 \times 10^{-5}$ emu/tetranuclear unit; $H = 50000$ G: $J = -11.20 \pm 0.34$ cm⁻¹, $J' = -2.54 \pm 0.17$ cm⁻¹, $\rho = 0.21 \pm 0.002$, $\bar{\chi}_0 = 5.65 \times 10^{-5} \pm 4.1 \times 10^{-5}$ emu/tetranuclear unit. The corresponding theoretical values from equation (2) are shown in Figure 4a together with the experimental data for $H = 1000$ G.

Figure 4

The results support the possible existence of both intra and interchain antiferromagnetic coupling throughout the network of the polynuclear Cu(II) coordination compound. The magnetic coupling is very weak (J and J' values) in both types of interactions.

In a further step, the tetranuclear cluster magnetic model of coupled $S = 1/2$ spins in the T_d , D_{2d} , D_2 and C_{2v} symmetries was employed to fit the experimental data. The best results were obtained for the C_{2v} symmetry. In this approximation (22), $J_1 \neq J_2 \neq J_3 = J_4$. J_1 and J_2 would represent the superexchange magnetic coupling parameters for the two diagonal pairs (1-2; 3-4) of Cu(II) centers in a tetranuclear unit of the network shown in Figure 3 (see numbering there); J_3 and J_4 would represent the corresponding magnetic parameters for the pairs (1-3 or 2-4; 1-4 or 2-3) of non diagonal Cu(II) centers bridged only by the $\underline{S}(6)$ or the $\underline{N}-\underline{N}$ donor groups. From the fitting process, the following parameters were obtained (for fixed $g = 2.09$): $H = 1000$ G: $J_1 = -3.22 \pm 1.4$ cm⁻¹, $J_2 = -10.12 \pm 0.96$ cm⁻¹, $J_3 = J_4 = -3.26 \pm 0.47$ cm⁻¹, $\bar{\chi}_0 = 0.00315$ emu/tetranuclear unit, $\rho = 0.97 \pm 0.00097$; $H = 10000$ G: $J_1 = -2.74 \pm 0.46$ cm⁻¹, $J_2 = -9.27 \pm 0.68$ cm⁻¹, $J_3 = J_4 = -3.12 \pm 0.20$ cm⁻¹, $\bar{\chi}_0 = 0.002$ emu/tetranuclear unit, $\rho = 0.97 \pm 0.00073$; $H = 50000$ G: $J_1 = -2.15 \pm 1.56$ cm⁻¹, $J_2 = -7.96 \pm 0.55$ cm⁻¹, $J_3 = J_4 = -2.16 \pm 0.52$ cm⁻¹, $\bar{\chi}_0 = 0.0018$ emu/tetranuclear unit, $\rho = 0.98 \pm 0.00064$.

From these results, an antiferromagnetic coupling between the unpaired electrons of the Cu(II) atoms involved in the constructing tetranuclear unit of the network proposed before, can be suggested. The theoretical values from the corresponding equation (22) are shown in Figure 4b together with the experimental data for $H = 10000$ G. From this approximation, one finds that $J_1 + J_3 + J_4$ is slightly lower than J_2 , in agreement with the low-symmetry considered for the distorted bidimensional metallic network suggested for this Cu(II) compound. From the theoretical model, the possible existence of a more favorable magnetic coupling pathway between the types considered can be established. In this magnetic study, the ρ values are noticeable overestimated in the fitting process.

The two last magnetic models explored can be considered equivalent in the magnetic data description. In fact, both models let us propose the existence of interacting tetranuclear Cu(II) units (the first one through interacting Cu(II) chains; the second one, as distorted tetranuclear Cu(II) units), and the Cu(II)- Cu(II) antiferromagnetic coupling is

inferred. In this coupling, the bridging donor groups appear to be the most favorable ones in constructing the superexchange magnetic coupling pathways. The very weak intensity in the antiferromagnetic coupling would appear to be related (in great measure) to distortions in the planes that contain the Cu(II) atoms (*i.e.*, a distorted bidimensional network). However, at this level of experimental information and magnetic study, it is difficult to state the detailed structural correspondence for each one of the superexchange magnetic coupling parameters (J values). The presence of non coupled $S = 1/2$ spins difficulties the magnetic characterization (*e.g.*, the observation and study of the $\bar{\chi}$ maxima in the $\bar{\chi} - T$ curves). The non coupled spins could be associated in part to the amorphous character of the solid product and the short-range order for the metallic network proposed.

Finally, the molar magnetization (\bar{M}) as a function of the magnetic field at constant temperature was analyzed using the Brillouin function. The good fitting to the experimental data at different constant temperatures let us estimate the respective total spin states S : 0.31 ($T = 2$ K); 0.40 ($T = 5$ K); 0.47 ($T = 10$ K); 0.56 ($T = 20$ K); 0.68 ($T = 50$ K); 0.74 ($T = 100$ K) and 0.80 ($T = 200$ K). Figure 5 shows the case for $T = 10$ K, for which negative magnetic fields were applied to the sample. The magnetization is fully reversible under these experimental magnetic conditions for the whole temperature range.

Figure 5.

A gradual singlet ($S = 0$) state depopulation starting at 2 K and with the increase of temperature is deduced from the S values. Typical $\bar{M} - H$ magnetic patterns corresponding to an antiferromagnetic coupling (23) are also obtained in the 10-200 K range.

CONCLUDING REMARKS.

Several synthetic routes for the novel polynuclear compound $[\text{Cu(II)}(\text{6-mercaptopurinolate}^{2-})_n]$ were explored. This system shows both a metal- ligand stoichiometry and a heterocyclic ligand deprotonation level, scarcely explored in the coordination chemistry of this organic molecule. The Cu(II) compound appears to show noticeable kinetic and

thermodynamic stabilities, also deduced from several Cu(II)-heterocyclic ligand competitive reactions. These stabilities could be associated to the high anionic character of 6-mercaptapurinolate²⁻, and thus to its polycoordinating capability towards the metallic atoms, as it is inferred from the spectroscopic data. These results support the involvement of the exocyclic S(6) atom and N atoms of the imidazolic moiety in the metallic bonding. The Metal:Ligand stoichiometry and polynuclear character of the Cu(II) compound allows us to suggest a 6-mercaptapurine coordination type not explored up to date. This is concerned with its polydirectional metallic bonding mode, which in turn favors the Cu(II)-Cu(II) magnetic interactions in a distorted tetracoordinated geometry for Cu(II). The magnetic studies confirm the existence of magnetic coupling between the unpaired electrons of the Cu(II) atoms, being this of very weak antiferromagnetic character through both classes of superexchange magnetic coupling pathways postulated from the two magnetic models explored. The very weak magnetic coupling in the polynuclear Cu(II) compound studied here, appears to be related both to the structural distortions through the metallic network, and to the restricted short-range order in this, in concordance with the amorphous character of the samples analyzed.

Finally, it is important to arise the high difficulty associated to the study of non crystalline coordination compounds. In this context, the magnetic studies are an unvaluable tool to advance in their characterization and to detect certain phenomena at a molecular level.

ACKNOWLEDGMENTS.

We thank Jorge Ramírez-Salcedo (IFC-UNAM), Max Azomoza-Palacios (UAM-Iztapalapa), Leticia Baños-López (IIM-UNAM) and Francisco Morales-Leal (IIM-UNAM) for the EPR spectra, thermal results, X-ray diffraction patterns and magnetic susceptibility measurements, respectively. We also acknowledge CONACyT (Grant 3170-E) for partial financial support.

References

1. Beaman A.G. and Robins R.K., *J. Am. Chem. Soc.* **83**, 4038 (1961).
2. Brown G.M., *Acta Cryst.* **B25**, 1338 (1969).
3. Arly Nelson J., Carpenter J.W., Rose L.M. and Adamson D.J., *Cancer Res.* **35**, 2872 (1975).
4. *Nuclei Acid-Metal Ion Interactions* (Edited by T.G. Spiro), Vol. 1, John Wiley & Sons, Inc., USA (1980).
5. Lusty J.R., *Handbook of Nucleobase Complexes*, Vol. I, CRC Press, Inc., USA (1990) and references therein.
6. Dubler E. and Gyr E., *Inorg. Chem.* **27**, 1466 (1988).
7. Acevedo-Chávez R., Costas M.E. and Escudero R., *J. Solid State Chemistry* **113**, 21 (1994).
8. Acevedo-Chávez R., Costas M.E. and Escudero R., submitted for publication.
9. Katsaros N. and Grigoratou A., *J. Inorg. Biochem.* **25** 131 (1985).
10. Kottmair N. and Beck W., *Inorg. Chim. Acta* **34**, 137 (1979).
11. Brigando J., Colaitis D. and Morel M., *Bull. Soc. Chim. Fr.* **10**, 3440 (1969).
12. Piperaki P., Katsaros N. and Katakis D., *Inorg. Chim. Acta* **67**, 37 (1982).
13. Barbieri R., Rivarola E., Di Bianca F. and Huber F., *Inorg. Chim. Acta* **57**, 37 (1982).
14. Perelló L., Borrás J., Soto L., Gordo F.J. and Gordo J.C., *Monats. Chem.* **115**, 1377 (1984).
15. Hadjiliadis N. and Theophanides T., *Inorg. Chim. Acta* **15**, 167 (1975).
16. Behrens N.B. and Goodgame D.M.L., *Inorg. Chim. Acta* **46**, 45 (1980).
17. Kitajima N., Fujisawa K. and Moro-oka Y., *J. Am. Chem. Soc.* **112**, 3210 (1990).
18. Jarvis J.A.J. and Wells A.F., *Acta Cryst.* **13**, 1027 (1960).
19. Inoue M., Kishita M. and Kubo M., *Inorg. Chem.*, **4** 626 (1965).
20. Freeman H.C., *Adv. Protein Chem.* **22**, 257 (1967).
21. Sadus A.M.V., *Transition Met. Chem.* **20**, 46 (1995) and references therein.

22. J.W., Estes W.E., Estes E.D., Scaringe R.P. and Hatfield W.E., *Inorg. Chem.* **16**, 1572 (1977).
23. Miller J.S., Epstein A.J. and Reiff W.M., *Chem. Rev.*, **88**, 201 (1988).

Figure Captions.

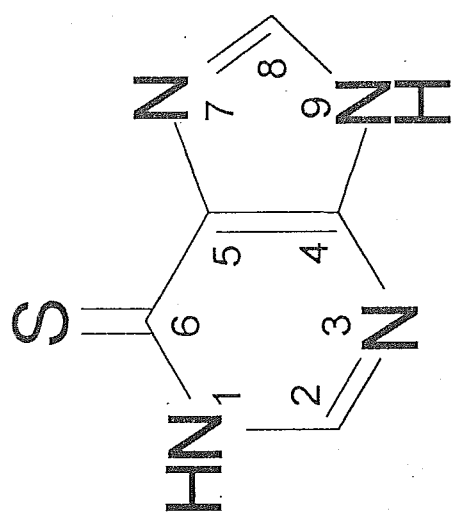
Figure 1. Schematic drawing and numbering of 6-oxopurine (I) and its structural analogue 6-mercaptopurine (II).

Figure 2. X-band EPR spectra of $[\text{Cu}(\text{II})(6\text{-mp}^{2-})]_n$ a) in powdered solid state at 300 K ($\nu=9.244$ GHz) and b) in $(\text{CH}_3)_2\text{SO}$ frozen solution (77 K) ($\nu=9.204$ GHz).

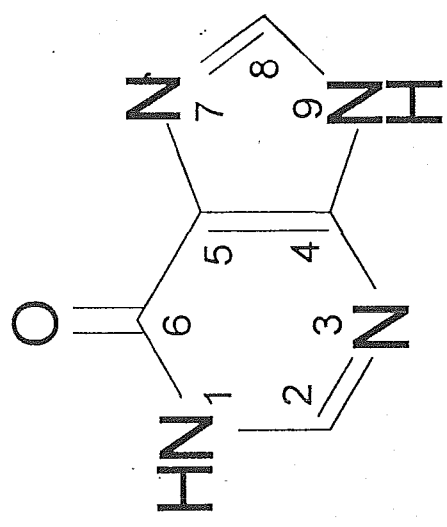
Figure 3. Schematic drawing of the structural arrangement proposition for $[\text{Cu}(\text{II})(6\text{-mp}^{2-})]_n$.

Figure 4. $\bar{\chi}$ (emu/tetranuclear unit) as a function of T (K) for $[\text{Cu}(\text{II})(6\text{-mp}^{2-})]_n$ a) from the linear chain magnetic model with a mean-field approximation ($H = 1000$ G) and b) from the C_{2v} tetranuclear cluster magnetic model ($H = 10000$ G). Dotted lines are experimental data; solid curves are theoretical values.

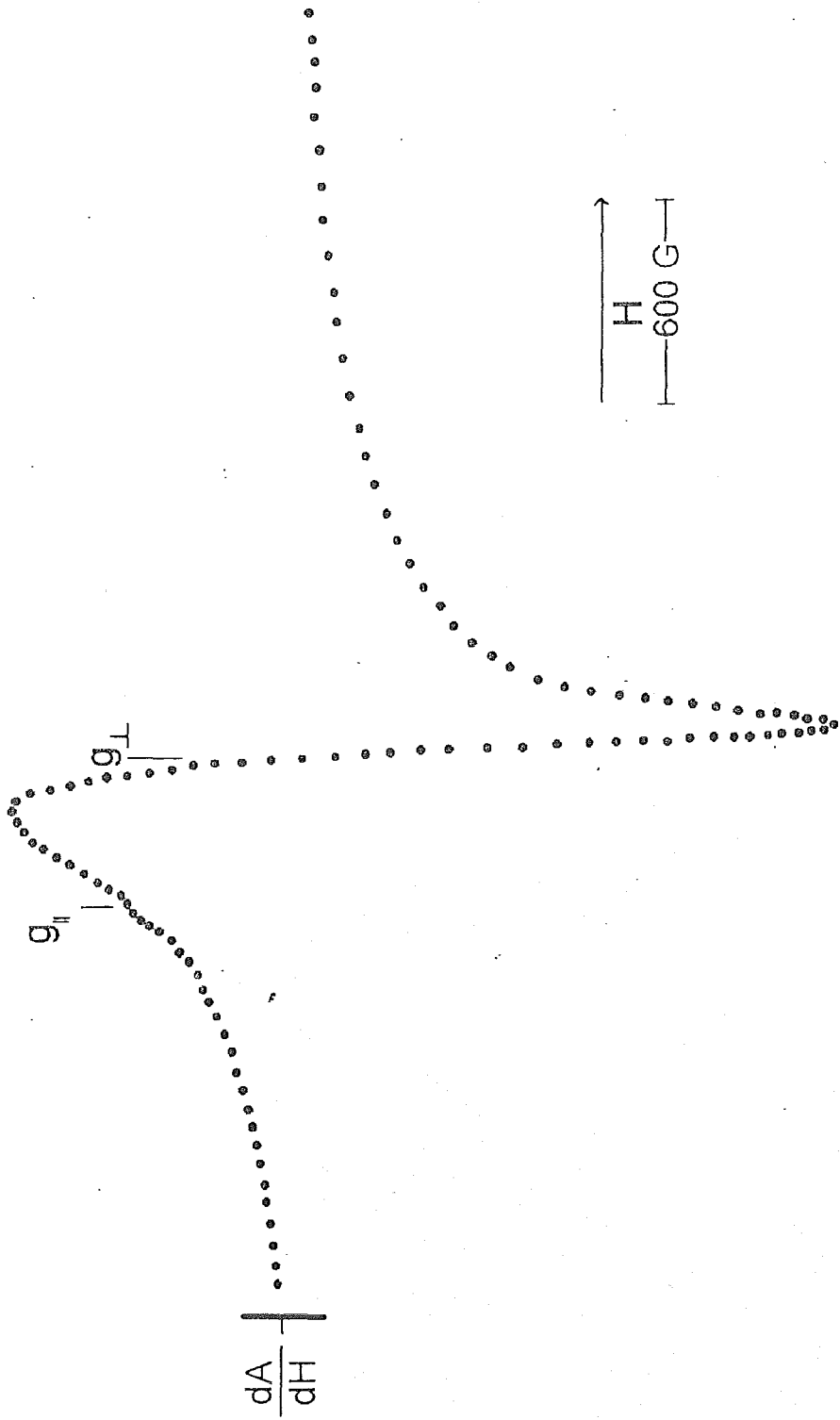
Figure 5. $\bar{M} - H$ plot ($T = 10$ K) of $[\text{Cu}(\text{II})(6\text{-mp}^{2-})]_n$. Dotted line are experimental data; solid line are theoretical values from the Brillouin function.

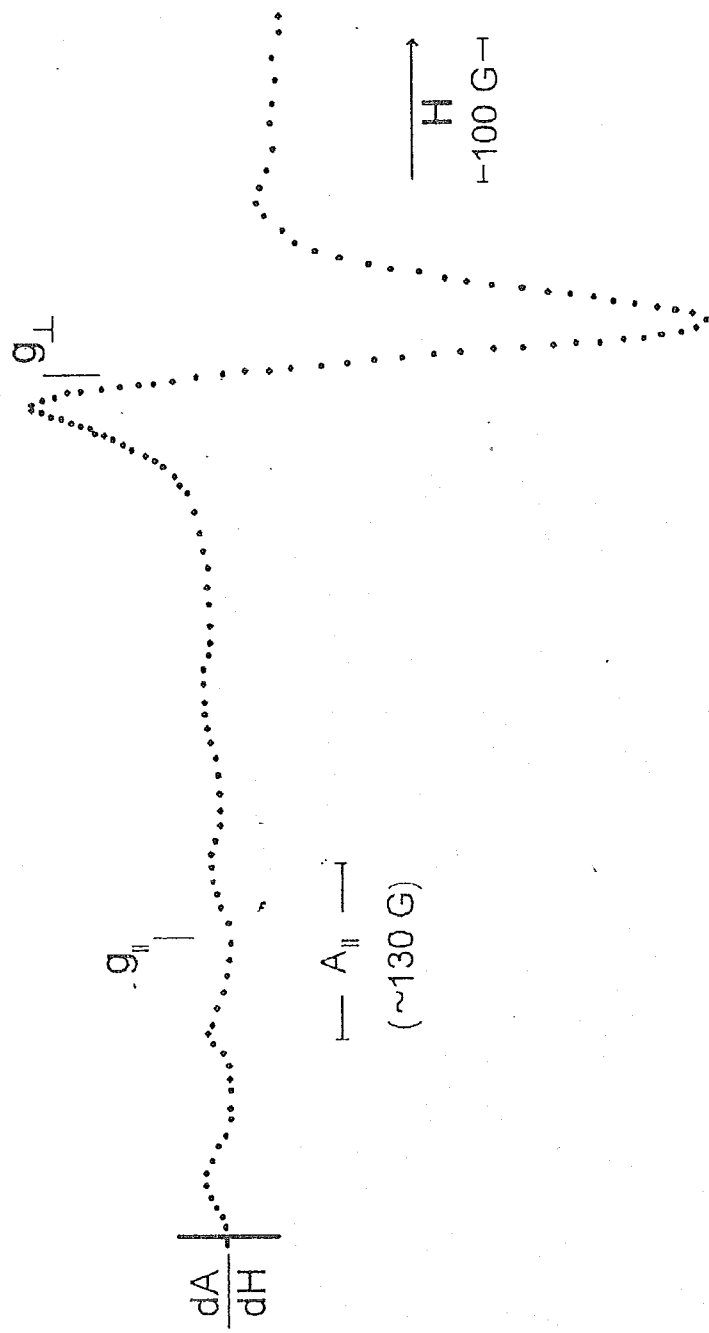


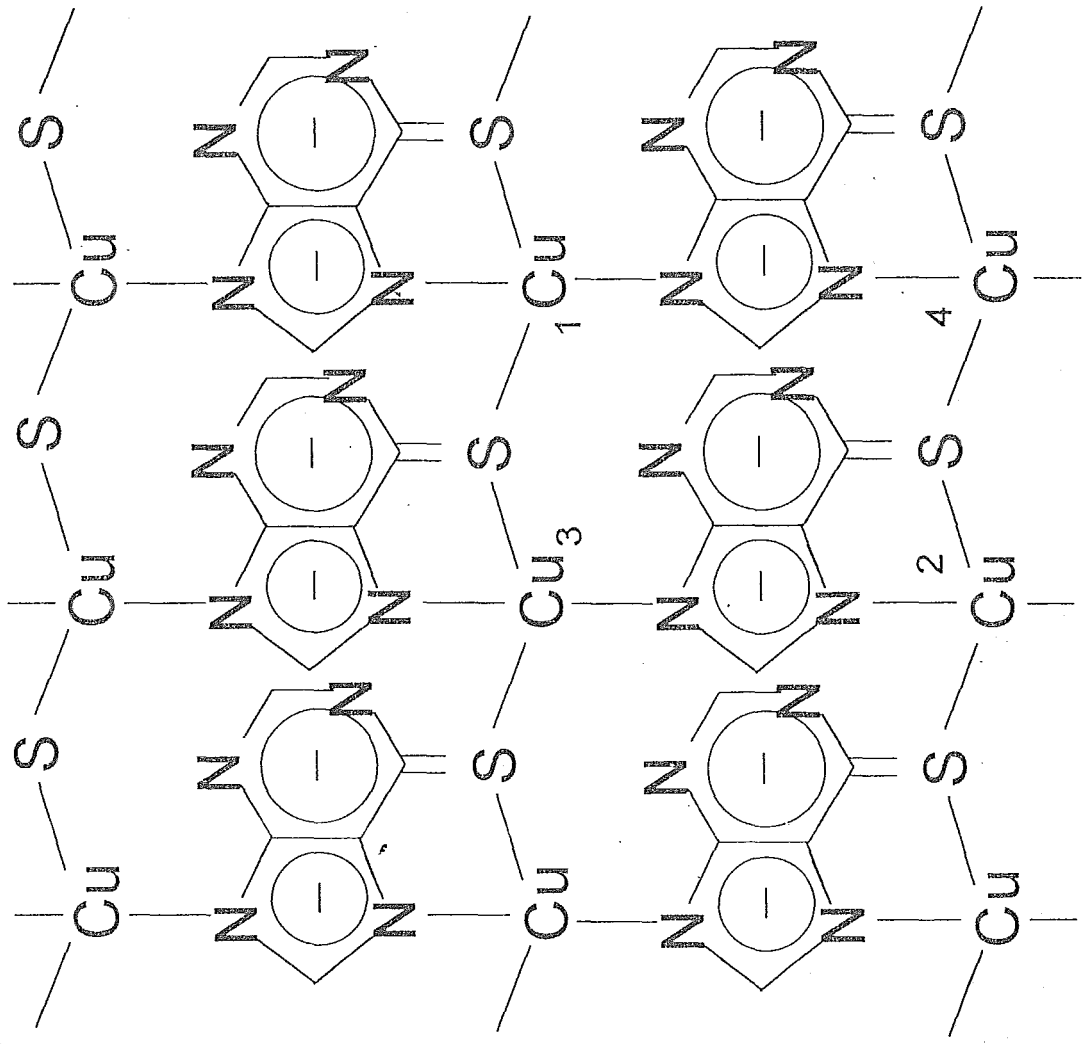
II

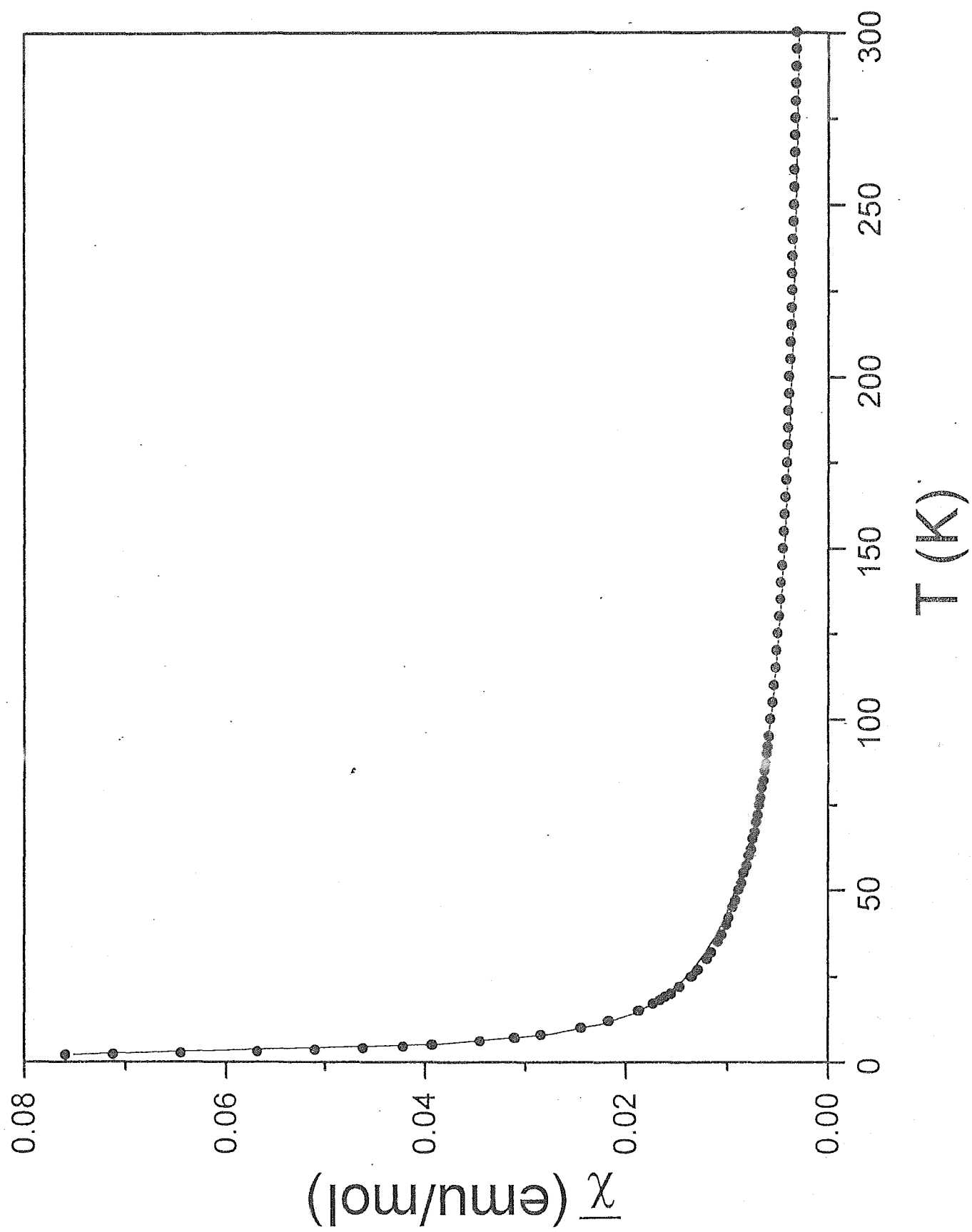


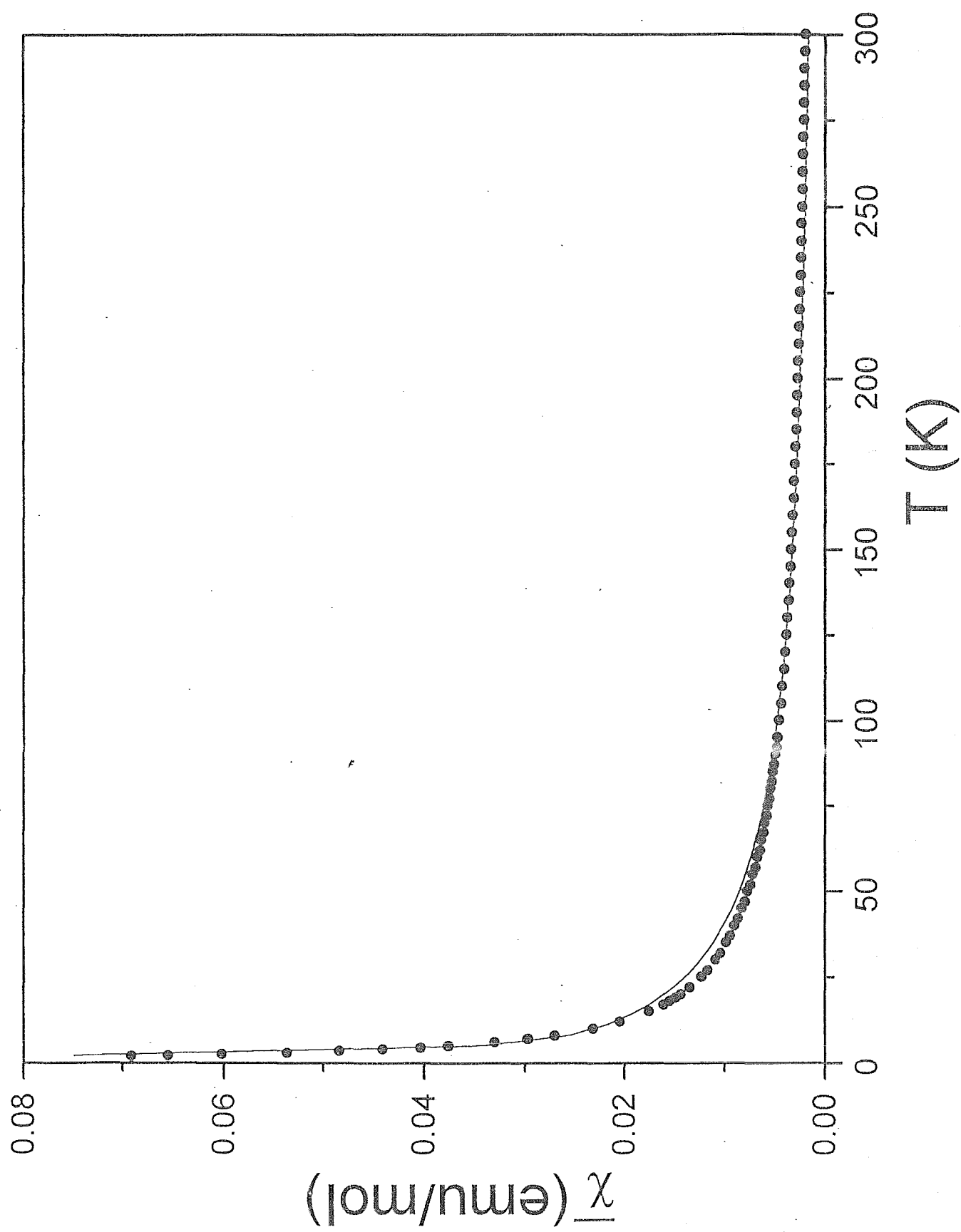
I

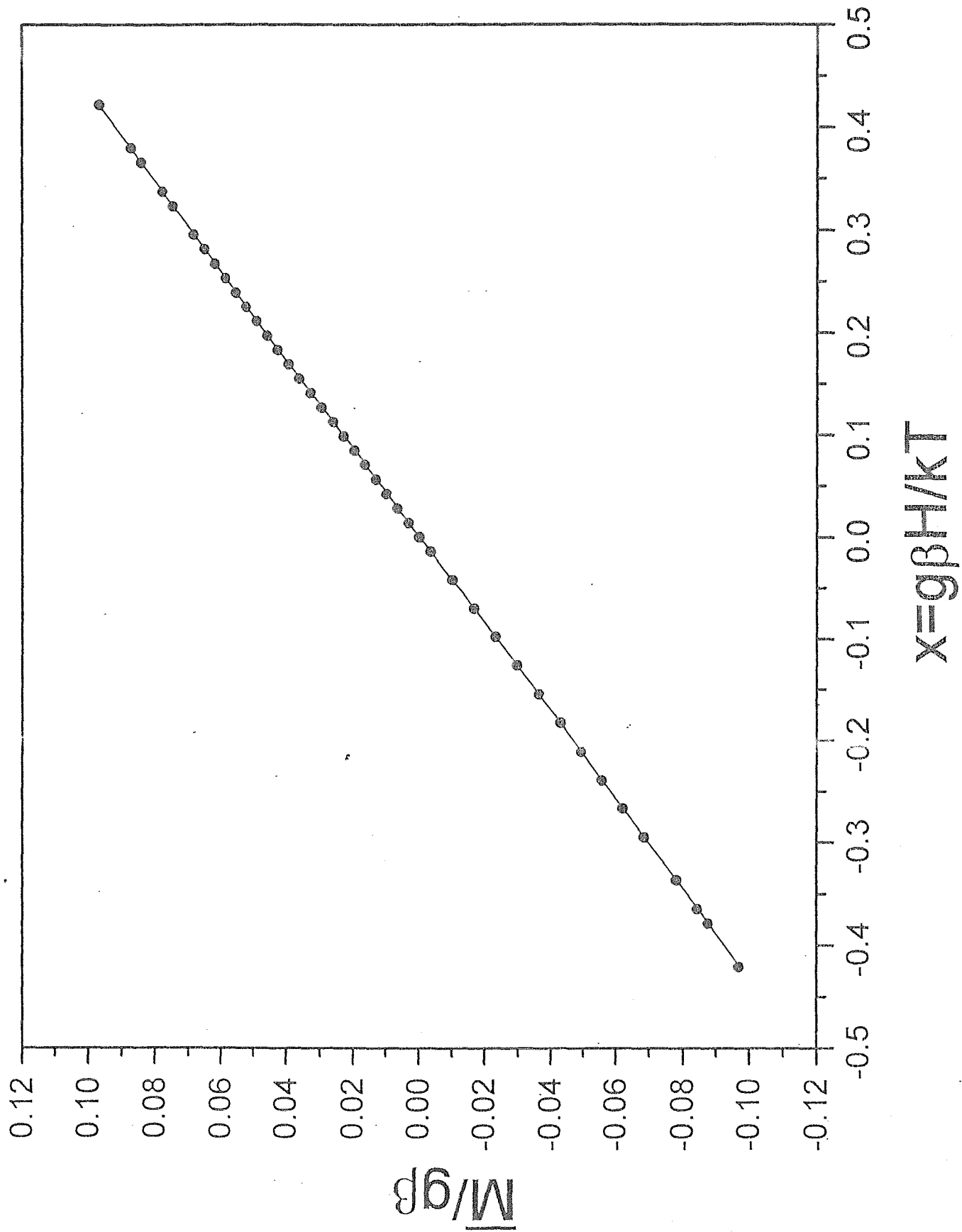














ANEXO

5

*Spectral and Magnetic Characterization of Novel Cu(II) Coordination
Compounds Synthesized in Methanolic Medium with the
Heterocycles Allopurinol, Hypoxanthine and 6-mercaptopurine.
Part I.*

**Spectral and Magnetic Characterization of Novel Cu(II) Coordination
Compounds Synthesized in Methanolic Medium with the Heterocycles
Allopurinol, Hypoxanthine and 6-mercaptopurine. I.**

Rodolfo Acevedo-Chávez.

Centro de Química, Instituto de Ciencias, B. Universidad Autónoma de Puebla,
Apartado Postal 1613, Puebla, Puebla, México.

María Eugenia Costas*.

Facultad de Química, Universidad Nacional Autónoma de México,
México 04510, D.F., México.

* To whom correspondence should be addressed.

Abstract.

Single and competitive heterocyclic ligand - Cu(II) methanolic interactions with allopurinol, hypoxanthine and 6-mercaptopurine, and $X = Cl^-$, Br^- , NO_3^- were carried out. From both the heterocyclic substitution and simultaneously competitive reactions the S(6)-purine derivative shows the higher coordination capacity, even substituting in some cases (NO_3^-) both allopurinol and hypoxanthine of the correspondent coordination spheres. The chromophores $M(II)(N)_2(X)_2$ for allopurinol and hypoxanthine and $M(II)(N)_1(S)_1(X)_2$, $M(II)(S)_2(X)_2$ and $M(II)(N)_2(S)_2$ for the S(6)-purine derivative, were obtained. In these systems and for allopurinol and hypoxanthine, the N(2) and N(7) atoms are the respective metallic coordination sites suggested. For the S(6)-purine derivative, the S(6)/N(7), S(6), and N(7)/N(9)/S(6) atoms are the correspondent metallic bonding sites proposed. The spectral and magnetic characterization of the systems with the neutral heterocycles, is in agreement with the structural suggestion of distorted tetracoordinated environments for Cu(II) and axial interactions with anionic ligands from the nearest neighboring Cu(II) units, in a linear-chain type framework. The magnetic studies are in agreement with the suggestion of very weak both intra and interchain magnetic coupling, the former of antiferromagnetic character. For the Cu(II) compound obtained with the dianionic S(6)-purine derivative a distorted tetracoordinated environment for Cu(II) in a roughly bidimensional framework is suggested, with the same types of magnetic coupling between the Cu(II) units.

I. Introduction.

Allopurinol (1H-pyrazolo[3,4-d]pyrimidine-4-one, I), hypoxanthine (6-oxopurine, II) and 6-mercaptopurine (III) are heterocycles (Figure 1) of interest from both pharmacological and biochemical points of view [1-3]. Having several donor atoms in their structures, these heterocycles are interesting ligands in coordination chemistry [4-6], due to the diversity in metallic bonding sites, Metal-Ligand stoichiometries, structural arrangements and physical properties of the respective coordination compounds. These features depend strongly on the experimental reaction conditions, which are of a great variety in the studies reported up to date.

Figure 1

As part of our research program concerned to heterocycle-metallic center interactions, we have focused our attention on the purine derivative and isomer - Cu(II) interactions, in competitive reactions of these ligands towards the metallic center and under systematically modified reaction conditions. To our knowledge, there are no studies of this type reported in the literature, and we have considered that these represent a good methodology to explore some qualitative aspects of the kinetic and thermodynamic stabilities of these interactions, and their correspondent coordination compounds, and also some of their physical properties.

Here we report certain heterocycle - Cu(II) methanolic interactions for the three ligands mentioned above, both in single and competitive modes. Also we report the correspondent reaction products, and the spectral and magnetic characterization of these new Cu(II) coordination compounds.

II. Experimental.

A) Reagents.

Heterocyclic ligands, metallic salts and solvents were analytical grade and commercially supplied. All were used with no further purification.

B) Heterocycle - Cu(II) interactions.

1) Single heterocycle - Cu(II) interactions.

For this step, the respective heterocycle - Cu(II) interactions were carried out employing 1:1 metal:heterocyclic ligand molar ratios, and CH₃OH as solvent at boiling temperature and refluxing. For each type of heterocycle - Cu(II) reaction, the counterion was changed (X=Cl⁻, Br⁻, NO₃⁻). The reactions yield solid products which were washed with boiling CH₃OH, and kept at *ca.* 100°C for eight hours.

In a typical reaction, 1 mmol of allopurinol was added to 100 ml of CH₃OH, and the mixture was kept at boiling temperature under stirring and refluxing (atmospheric pressure). To the colorless solution obtained, 1 mmol of CuCl₂•2H₂O (previously solvated in *ca.* 5 ml of CH₃OH) was incorporated, and after two hours a scarce pale green solid was formed. Two hours later, a noticeable suspension (pale green color) was obtained, which was maintained at these conditions for another 4.8 days, without changes. The hot suspension was filtered off, and a solid product (pale green-blue color) was isolated, which was washed with several portions (30 ml in total) of boiling CH₃OH. The solid obtained (same color) was kept at 100°C for 8 hours, without changes in color.

Total reaction times and colors of the respective coordination compounds obtained with each of the heterocyclic ligands and metallic counterions are shown in Table 1.

Also, the respective Cu(II) compounds (X=Cl⁻) with allopurinol, hypoxanthine and 6-mercaptapurine were synthesized employing 1:1 metal:heterocycle molar ratios (mmol scale) in 15 ml of (CH₃)₂SO, under stirring at room temperature. The reaction mixtures were maintained at these conditions for 2, 11 and 17 days respectively; to the solutions obtained, 25 ml of CHCl₃:C₂H₅OH (1:1, V:V), 25 ml of C₂H₅OH and 20 ml of C₂H₅OH were added respectively. The respective solid products were formed after several weeks, which were isolated by filtration, exhaustively washed with boiling C₂H₅OH, and kept at 100°C for 8 hours. The respective solid products (pale green-blue, deep blue and dark green) gave the same analytical and spectral results than the Cu(II) compounds (X=Cl⁻) obtained in CH₃OH and here reported.

2) Successively competitive heterocycle - Cu(II) interactions.

For this type of reactions, a Cu(II) coordination compound with a specific heterocyclic ligand was initially synthesized (as described in section 1). The purified compound was microanalytically studied to obtain its empirical formulation. Assuming a mononuclear character for this, a second interaction (coordination compound - second heterocyclic ligand) in a 1:1 molar ratio was explored, at the same conditions as in section 1. The correspondent solid was also treated as before.

In a typical reaction, 1 mmol of allopurinol was solvated under stirring and boiling by refluxing (atmospheric pressure) in 100 ml of CH₃OH. To the colorless solution, 1 mmol of Cu(NO₃)₂•6H₂O (previously dissolved in *ca.* 10 ml of CH₃OH). was added at the above conditions, forming a turquoise-green suspension, which changed to blue-green after 0.5 hours. After 8 hours, the suspension showed a lilac color and was kept at the above experimental conditions for 8 additional days. The hot suspension was filtered off, and the solid product was washed with hot CH₃OH. The lilac solid was kept at 100°C for 6 hours, without changes. Under microanalysis of the product, 1 mmol of this was suspended in 100 ml of CH₃OH, and kept boiling under refluxing. 1 mmol of 6-mercaptopurine was added to this suspension, and at these conditions a gray suspension was quickly formed, which changed to green 17 hours after. By maintaining the suspension at the same above conditions, the green color was kept for 9 days. The hot suspension was filtered off, and the solid was washed with hot CH₃OH. The solid (dark green) was kept at 100°C for 6 hours. The final color was dark green.

Total reaction times for the second step and corresponding to these types of reactions, are listed in Table 1.

3) Simultaneously competitive heterocycle - Cu(II) interactions.

For this type of competitive reactions, the respective heterocyclic ligands were previously solvated in CH₃OH at boiling temperature and refluxing. To the respective solution obtained, the correspondent metallic salt was added. The reaction mixture without changes

with time, was filtered off in hot, and the solid product was washed with hot CH₃OH. The solid product was kept at 100°C for 8 hours.

In a typical reaction, 1 mmol of allopurinol and 1 mmol of 6-mercaptopurine were added to 100 ml of CH₃OH. The mixture was kept boiling under stirring and refluxing (atmospheric pressure), and at these conditions, 1 mmol of CuCl₂•2H₂O (previously dissolved in 5 ml of CH₃OH) was added to the solution obtained before, forming in short a green suspension. After three days, the suspension turned to dark green, without changes with another 3 days of reaction at these conditions. The hot suspension was filtered off, and the dark green solid was washed with several portions of boiling CH₃OH (50 ml in total). The solid of the same color was kept at 100°C for 8 hours, without changes in color.

Reaction times and products obtained for this type of competitive reactions are shown in Table 1.

Table 1.

C) Physical measurements.

-Microanalytical results (C,H,N) were performed in the Chemistry Department at the University College of London. Analytical confirmation was obtained by the Department of Chemistry, University of Sheffield (microanalysis service).

-Infrared (IR) spectra were obtained as Nujol mulls using CsI plates in the 4000-200 cm⁻¹ range and employing a 599-B Perkin Elmer spectrometer. IR data (high density polyethylene pellets) in the 600-70 cm⁻¹ range were obtained using a 740 FT IR Nicolet equipment.

-Electronic spectra (350-1100 nm) of the powdered samples were measured by the specular reflectance method in a 160-A Shimadzu spectrometer, using BaSO₄ as reference.

-Thermogravimetric results were obtained employing a DT-30 Shimadzu equipment using N₂(g) as carrier fluid and 5°C/min as heating rate.

-EPR spectra (X-band) of powdered samples were performed in a 200-D Bruker spectrometer, both at room temperature and 77 K. The *g* values were standardized against the absorption of diphenylpicrylhydrazine (DPPH), at 2.0043.

X-ray powder diffraction patterns of free ligands and their Cu(II) coordination compounds were taken in a XD-5A Shimadzu equipment.

-Magnetic susceptibilities of samples at room temperature were measured using a Johnson Matthey balance and employing $\text{Hg}[\text{Co}(\text{SCN})_4]$ as calibrating agent.

-Magnetic susceptibility as a function of temperature were carried out using a SQUID MPMS-5 Quantum Design Magnetometer, from 2-300 K, and magnetic fields of 100 and 10000 G. The equipment was previously calibrated with very fine standards (Pd, Ni, Al). The magnetic measurements for each sample and magnetic field were carried out both increasing and decreasing temperature. The experimental magnetic data are fully statistically representative (each value has an average standard deviation three orders of magnitude lower than the reported data). The magnetic susceptibilities were corrected by the cell and sample diamagnetic contributions.

For the analytical results, the samples obtained were previously exposed to the atmosphere for several weeks. A similar procedure was applied for the thermal studies. All the other physical measurements were carried out with the freshly obtained samples.

III Results and Discussion.

a) Analytical results.

Table 2 shows the microanalytical results for the Cu(II) coordination compounds obtained in the single and competitive heterocyclic - Cu(II) interactions carried out in this study.

Table 2.

b) Compounds obtained.

i) Single heterocycle - Cu(II) interactions.

For all the single interactions, Cu(II) compounds with the respective heterocyclic ligands were obtained. For almost all these reactions, the metallic counterions exist also as ligands, and only one case shows deprotonation of the heterocyclic ligand, without the presence of the metallic counterion. The 1:2 metal:heterocycle ratio is the favored one in the compounds obtained with allopurinol and hypoxanthine. For the $\underline{\text{S}}(6)$ -purine derivative, the 1:1 and 1:2 stoichiometries are the favored ones.

ii) Successively competitive heterocycle - Cu(II) interactions.

The $\underline{S}(6)$ -purine derivative ligand shows higher substitution capacities in this type of competitive reactions (*e.g.*, $X=\text{NO}_3^-$). The high stability of its interactions towards Cu(II) is also shown by the inertness of the respective coordination compound when trying to substitute it with both allopurinol and hypoxanthine. On the other hand, the three heterocycles as respective second ligands do not show ($X=\text{Cl}^-$ or Br^-) substitution capacities in this type of competitive reactions. The capacity of 6-mercaptopurine to carry out ligand substitution reactions towards allopurinol and hypoxanthine previously bonded to Cu(II) (as in $\text{Cu(II)(L}_i)_2(\text{NO}_3)_2$, $L_i=\text{allopurinol, hypoxanthine}$) could be explained in terms of the lower metallic bonding capacity of the NO_3^- groups (relative to Cl^- or Br^-) in the correspondent coordination spheres. This behavior, joined to the deprotonation of the $\underline{S}(6)$ -purine derivative under these particular experimental conditions, favors the formation of the $\text{Cu(II)(L}_3)_2^{2-}$ system (see analytical results), with high kinetic and thermodynamic stabilities.

iii) Simultaneously competitive heterocycle - Cu(II) interactions.

When the heterocyclic ligands were simultaneously solvated for the reaction towards the metallic center, the $\underline{S}(6)$ -purine derivative shows again the major reactivity and stability in the metallic interactions. In this type of competitive interactions, allopurinol and hypoxanthine show similar competitive and reactive capacities. The higher reactivity and stability in the $\underline{S}(6)$ -purine derivative-Cu(II) interactions, could be associated to the role played by the $\underline{S}(6)$ exocyclic atom, which is the most reactive site of the heterocycle ligand. In fact, this atom always appear as the metallic bonding site in the reactions of this heterocycle towards metallic centers [5].

c) Thermogravimetric results.

Compound 1. The sample analyzed does not show mass loss from room temperature until *ca.* 220°C. From this temperature and above 500°C a noticeable, abrupt and complex pathway of mass loss is obtained. The thermal results below 220°C are in agreement with

the anhydrous character of the Cu(II) compound, $\text{Cu}(\text{L}_1)_2(\text{Cl})_2$. The limit of thermal stability for this anhydrous compound would be *ca* 220°C.

Compound 2. The sample shows a first step of mass loss which starts at room temperature and ends at 120°C. Upon increasing the temperature and starting at *ca.* 250°C an abrupt, complex and considerable step of mass loss above 500°C is observed. The first step is assumed as: $\text{Cu}(\text{L}_2)_2(\text{Cl})_2 \cdot 0.8\text{H}_2\text{O} \rightarrow \text{Cu}(\text{L}_2)_2(\text{Cl})_2$. The temperature range for this step is suggestive of the non involvement of H_2O molecules in the Cu(II) compound coordination sphere. The thermal stability limit for the anhydrous compound appears to be *ca.* 250°C.

Compound 3. The sample shows a first step of mass loss starting from room temperature up to *ca.* 115°C. Upon increasing the temperature, and starting at *ca* 200°C, an abrupt, noticeable and complex mass loss is observed, which continues to a temperature above 500°C. The first step is assumed as: $\text{Cu}(\text{L}_3)_1(\text{Cl})_2 \cdot 0.5\text{H}_2\text{O} \rightarrow \text{Cu}(\text{L}_3)_1(\text{Cl})_2$. The temperature range for this step is suggestive of the non involvement of H_2O molecules in the Cu(II) compound coordination sphere. The thermal stability limit for the anhydrous compound appears to be *ca.* 200°C.

Compound 4. The sample analyzed shows a first step of mass loss which starts at room temperature and ends at 100°C. Upon increasing the temperature and starting at *ca.* 250°C a noticeable, abrupt and complex pathway of mass loss above 500°C is observed. The first step is assumed as: $\text{Cu}(\text{L}_1)_2(\text{Br})_2 \cdot \text{H}_2\text{O} \rightarrow \text{Cu}(\text{L}_1)_2(\text{Br})_2$. The temperature range for this step is suggestive of the non involvement of H_2O molecules in the Cu(II) compound coordination sphere. The thermal stability limit for the anhydrous compound appears to be *ca.* 250°C.

Compound 5. The sample shows a first step of mass loss which starts at room temperature and ends at 115°C. Upon increasing the temperature and starting at *ca.* 285°C a noticeable, abrupt and complex mass loss step is observed above 500°C. The first step is assumed as: $\text{Cu}(\text{L}_2)_2(\text{Br})_2 \cdot 0.5\text{H}_2\text{O} \rightarrow \text{Cu}(\text{L}_2)_2(\text{Br})_2$. The temperature range for this step

is suggestive of the non involvement of H₂O molecules in the Cu(II) compound coordination sphere. The thermal stability limit for the anhydrous compound appears to be *ca.* 285°C.

Compound 6. The sample shows a first step of mass loss which starts at room temperature and ends at 130°C. Upon increasing the temperature and starting at *ca.* 225°C a noticeable, abrupt and complex pathway of mass loss is detected above 500°C. The first step is assumed as: $\text{Cu}(\text{L}_3)_2(\text{Br})_2 \cdot 1/3\text{H}_2\text{O} \rightarrow \text{Cu}(\text{L}_3)_2(\text{Br})_2$. The characteristics of this process would be in agreement with non participation of H₂O molecules in the Cu(II) compound coordination sphere. The thermal stability limit for the anhydrous compound appears to be *ca.* 225°C.

Compound 7. The sample shows a very complex step by step process of mass loss, the first of them starting at 45°C and continuing up to *ca.* 250°C; the second from this last temperature to 320°C, and the last step continuing to a temperature above 500°C. When heating another sample of this compound in this temperature range, the following colors were observed: i) 45°C→250°C: lilac (45°C)→ gray (145°C) → green (200°C) → green-brown (250°C); ii) 250°C→320°C: green-brown (250°C) → dark brown (320°C). Without additional information, it is difficult to point out in detail the nature of these processes. Thermochromic processes could be involved in i), including the limit of thermal stability of the anhydrous compound, perhaps below 250°C.

Compound 8. The sample shows a first step of mass loss which starts at room temperature and ends at 135°C. Upon increasing the temperature and starting at *ca.* 265°C a second step is observed, ending at 355°C. Finally, from this last temperature, a third step is detected, which continues above 500°C. The first step is assumed as: $\text{Cu}(\text{L}_2)_2(\text{NO}_3)_2 \cdot 1.5\text{H}_2\text{O} \rightarrow \text{Cu}(\text{L}_2)_2(\text{NO}_3)_2$. The temperature range for this step is suggestive of the non involvement of H₂O molecules in the Cu(II) compound coordination sphere. The thermal stability limit for the anhydrous compound appears to be *ca.* 265°C.

Compound 9. The sample shows a first step of mass loss which starts at room temperature and ends at 125°C. Upon increasing the temperature a second complex step is observed,

starting at 225°C and ending above 500°C. The first step is associated to the process: $\text{Cu}(\text{L}_3^{2-}) \cdot 0.5\text{H}_2\text{O} \rightarrow \text{Cu}(\text{L}_3^{2-})$. The temperature range for this step is suggestive of the non involvement of H_2O molecules in the $\text{Cu}(\text{II})$ compound coordination sphere. The thermal stability limit for the anhydrous compound appears to be *ca.* 225°C.

d) Infrared spectroscopy results.

The IR bands, the respective assignments for the free heterocyclic ligands allopurinol ($=\text{L}_1$) [7], hypoxanthine ($=\text{L}_2$) [8-15] and 6- mercaptopurine ($=\text{L}_3$) [16-23], and the spectral characterization of their $\text{Cu}(\text{II})$ coordination compounds are listed respectively in Tables 3, 4 y 5.

$\text{Cu}(\text{II})$ coordination compounds with allopurinol ($=\text{L}_1$).

1) $\text{Cu}(\text{L}_1)_2(\text{Cl})_2 \cdot \text{H}_2\text{O}$.

The IR characterization (Table 3) for this compound let us consider the non involvement of the $\text{O}(4)$ exocyclic atom in the metallic bonding. Also, The IR information let us exclude the $\text{N}(5)\text{-H}$ group in that interaction. The spectral information is in agreement with the electronic perturbation of endocyclic regions. The higher perturbation corresponds to vibrational modes of N-H and C-H groups. The spectral information for the $\text{N}(5)\text{-H}$ group let us discard $\text{C}(6)\text{-H}$ as nearest neighbor group in the metallic bonding of allopurinol through the $\text{N}(7)$ atom of the pyrimidinic ring. The spectral characterization let us suggest the participation of the $\text{N}(2)$ atom in the pyrazolic moiety as metallic bonding site of the heterocycle allopurinol, being this suggested as the $\text{N}(1)\text{-H}$ tautomer. In the low-energy region the IR band appearing at 336 cm^{-1} is assigned to $\nu_{\text{Cu-Cl}}$. The complex band with a peak at 320 cm^{-1} and a shoulder at 300 cm^{-1} is associated to $\nu_{\text{Cu-N}}$.

2) $\text{Cu}(\text{L}_1)_2(\text{Br})_2 \cdot 3\text{H}_2\text{O}$.

The IR characterization for this compound let us exclude the involvement of the $\text{O}(4)$ exocyclic atom, the $\text{N}(5)\text{-H}$ group and the $\text{N}(7)$ atom as metallic bonding sites of allopurinol. As for the previous compound, the spectral data are in agreement with the perturbation

and involvement of the pyrazolic moiety in the metallic bonding. The similarity in the IR spectra for the above ($X=\text{Cl}^-$) and this ($X=\text{Br}^-$) let us suggest for the last one an analogue metallic bonding fashion, *i.e.*, through the $\underline{\text{N}}(2)$ of the five-membered ring, and allopurinol in the $\underline{\text{N}}(1)$ - $\underline{\text{H}}$ tautomeric form. In the low-energy region, the IR bands appearing at 326 cm^{-1} and 290 cm^{-1} are attributed to $\nu_{\text{Cu-N}}$. The complex band with peaks at 265 cm^{-1} and 253 cm^{-1} is attributed to $\nu_{\text{Cu-Br}}$.

3) $\text{Cu}(\text{L}_1)_2(\text{NO}_3)_2$.

The IR characterization for the heterocyclic ligand is in agreement with the non participation of the $\underline{\text{O}}(4)$ exocyclic atom as metallic bonding site. This conclusion is also proposed for the $\underline{\text{N}}(5)$ - $\underline{\text{H}}$ group. The general spectral pattern is also (as for $X=\text{Cl}^-$ or Br^-) in concordance with the metallic coordination of allopurinol through the $\underline{\text{N}}(2)$ atom of the five-membered ring, being allopurinol suggested to be in the $\underline{\text{N}}(1)$ - $\underline{\text{H}}$ tautomeric form.

NO_3^- IR bands. The IR spectral pattern for the NO_3^- group is in agreement with its behavior as monocoordinated group. The $(\nu_1 + \nu_4)$ combined band is suggested to be contained in the complex structure of the broad band centered at *ca.* 1675 cm^{-1} , which does not appear in the Cu(II) compounds with allopurinol and $X=\text{Cl}^-$ or Br^- . The new band centered at 1440 , 1290 and 1040 cm^{-1} are assigned to the ν_4 , the activated ν_1 , and the ν_2 vibrational modes respectively. Finally, the new bands centered at 720 and 640 cm^{-1} are attributed to the ν_6 , and ν_3 and ν_5 vibrational modes for the monocoordinated NO_3^- group. The low-energy IR spectrum shows an asymmetric band at 310 cm^{-1} , a second band centered at 300 cm^{-1} and a third and asymmetric band at 285 cm^{-1} . These are suggested to contain both $\nu_{\text{Cu-N}}$ and $\nu_{\text{Cu-ONO}_2^-}$ vibrational modes.

Cu(II) coordination compounds with hypoxanthine (=L₂).

4) $\text{Cu}(\text{L}_2)_2(\text{Cl})_2$

The IR characterization (Table 4) is in agreement with the non involvement of the $\underline{\text{O}}(6)$ exocyclic atom in the metallic bonding of hypoxanthine. This same suggestion is for the $\underline{\text{N}}(1)$ - $\underline{\text{H}}$ group. Again, the higher changes belong to vibrational modes of N-H and C-H

groups. The spectral behavior for the $\underline{N}(1)\text{-H}$ group let us exclude $\underline{C}(2)\text{-H}$ as nearest neighboring group in the metallic coordination through the $\underline{N}(3)$ site. The spectral information is in agreement with the participation of endocyclic groups of the five-membered ring as nearest neighbor and coordination site, respectively. From these, the $\underline{C}(8)\text{-H}$ group belongs to the first type. The second one is between the $\underline{N}(7)$ and $\underline{N}(9)$ atoms. Unfortunately, with this spectral information it is difficult to dilucidate them. In the low-energy IR spectrum, the strong, broad and asymmetric band at 298 cm^{-1} and with peaks at 340 cm^{-1} , 325 cm^{-1} , 312 cm^{-1} and 287 cm^{-1} , could be assigned to the $\nu_{\text{Cu-Cl}}$ and $\nu_{\text{Cu-N}}$ vibrational modes.

5) $\text{Cu}(\text{L}_2)_2(\text{Br})_2$.

The spectral pattern for this compound in the $4000 - 600\text{ cm}^{-1}$ range is very similar to the one shown by $\text{Cu}(\text{L}_2)_2(\text{Cl})_2$. Thus, the same suggestions of the metallic bonding behavior for the heterocycle could be made here. In the low-energy IR spectrum, the strong, broad and asymmetric band at 280 cm^{-1} (showing peaks at 315 and 250 cm^{-1}) could contain the $\nu_{\text{Cu-N}}$ and $\nu_{\text{Cu-Br}}$ vibrational modes.

6) $\text{Cu}(\text{L}_2)_2(\text{NO}_3)_2$.

The IR spectral pattern for this compound is different to the two preceding cases of $\text{Cu}(\text{II})$ compounds with hypoxanthine, in part due to the presence of bands associated to the NO_3^- group. With respect to the metallic bonding behavior of the heterocycle, this appears to be analogue to that of $\text{X}=\text{Cl}^-$ or Br^- , being the noticeable perturbation the one concerning to C-H and N-H vibrational modes of the five-membered ring.

NO_3^- IR bands. The IR spectral pattern of the NO_3^- bands is in agreement with the existence of this group as monocoordinated ligand. The complex structure of the strong and broad band at 1690 cm^{-1} could be also associated to the $(\nu_1 + \nu_4)$ combined vibrational mode. The new band at 1500 cm^{-1} is assigned to the ν_4 vibrational mode. The strong band centered at 1250 cm^{-1} is suggested to contain both ring and $\nu_{\text{C-N}}$ vibrational modes of the heterocyclic ligand, and the ν_1 vibrational mode of the NO_3^- group. The new bands at 995

cm^{-1} and 780 cm^{-1} are associated to the ν_2 and ν_6 vibrational modes, respectively. The new band at 720 cm^{-1} is attributed to the ν_3/ν_6 vibrational modes of monocoordinated NO_3^- . Finally, in the low-energy IR spectrum two strong, broad and asymmetric bands appear at 300 cm^{-1} and 280 cm^{-1} , which are suggested to contain both the $\nu_{\text{Cu}-\text{ONO}_2^-}$ and $\nu_{\text{Cu}-\text{N}}$ vibrational modes.

Cu(II) coordination compounds with 6-mercaptapurine (=L₃).

7) Cu(L₃)(Cl)₂.

The IR characterization (Table 5) of this compound let us consider a noticeable electronic perturbation of the S(6) exocyclic atom and endocyclic regions. With respect to the first one, the bands that appear labeled as I, II and III in the free heterocyclic ligand characterization, are almost absent in the spectrum of the coordination compound in discussion here. Also, the IR data let us consider a noticeable perturbation of C-H vibrational modes. When comparing this spectrum with that for 6-mercaptapurine in $\text{W}(\text{CO})_4(\text{L}_3)$ [24] a noticeable similarity can be observed. For this last compound, a S(6)/N(7) bidentated metallic bonding has been suggested. In consequence, an analogue metallic coordination for 6-mercaptapurine can be proposed for the Cu(II) compound studied here. In the low-energy IR spectrum the broad band of complex structure, centered at *ca.* 324 cm^{-1} , is associated both to the heterocyclic ligand and $\nu_{\text{Cu}-\text{Cl}}$ vibrational modes. The broad and complex band centered at *ca.* 293 cm^{-1} is suggested to contain both heterocyclic ligand and $\nu_{\text{Cu}-\text{N}}$ vibrational modes. Finally, the broad band of complex structure at *ca.* 230 cm^{-1} , could be associated to both heterocycle and $\nu_{\text{Cu}-\text{S}}$ vibrational modes.

8) Cu(L₃)₂(Br)₂.

The IR spectrum of this compound shows a different spectral pattern with respect to the previous case. In particular, the band labeled as I in Table 5, and the band at 1150 cm^{-1} in the free heterocyclic ligand, are those that show a noticeable spectral change in the spectrum under discussion. In addition, the band appearing at 1543 cm^{-1} could be assigned to the $\delta_{\text{N}(1)-\text{H}}$ vibrational mode. Also, bands attributed to certain vibrational

modes of pyrimidinic-type ring and C-N groups (in the 1600- 1000 cm^{-1} range) show important changes. The spectrum shows a noticeable similarity with the one shown by the compound $\text{W}(\text{CO})_5(\text{L}_3)$, where a $\underline{\text{S}}(6)$ metallic bonding has been proposed[24]. With this information, the suggestion of this type of metallic bonding for the heterocyclic ligand in the compound under discussion can be made. In the low-energy IR spectrum the complex band at 230 cm^{-1} is associated to both heterocyclic ligand and $\nu_{\text{Cu-S}}$ vibrational modes. Finally, the broad and strong band centered at 115 cm^{-1} could be assigned to heterocyclic ligand and $\nu_{\text{Cu-Br}}$ vibrational modes.

9) $\text{Cu}(\text{L}_3^{2-}) \cdot 2\text{H}_2\text{O}$.

The IR spectrum of this compound shows noticeable differences with respect to the preceding two cases. In particular, a great spectral modification of the bands labeled as I, II and III in Table 5, is found. Also, a general suppression of the bands due to both several endocyclic and N-H group vibrational modes is observed, and noticeable changes (in intensity and frequency) of bands attributed to several C-H group vibrational modes are shown. This spectral information is in agreement with a substantial electronic change in the coordinated and deprotonated heterocycle. In the metallic bonding, both the $\underline{\text{S}}(6)$ exocyclic atom and endocyclic groups appear to be involved. In the low-energy IR spectrum the broad and asymmetric band at *ca.* 270 cm^{-1} is assigned to $\nu_{\text{Cu-N}}$; the band appearing at 216 cm^{-1} is attributed to $\nu_{\text{Cu-S}}$. This compound is also obtained in aqueous (variable pH values) and DMSO media. A spectral (epr) and exhaustive magnetic characterization has been made [25]. Here, only a few data are quoted.

Table 3.

Table 4.

Table 5.

e) Electronic spectroscopy results.

Cu(II) coordination compounds with allopurinol (=L₁).

1) Cu(L₁)₂(Cl)₂·H₂O.

The electronic spectrum shows a broad and asymmetric band centered at *ca.* 665 nm. A second band of higher intensity and in the blue region is centered at *ca.* 370 nm. The structure of the bands and their positions are suggestive of a distorted tetracoordinated geometry for Cu(II), possibly with weak axial interactions.

2) Cu(L₁)₂(Br)₂·3H₂O.

The electronic spectrum shows two broad bands: one centered at *ca.* 710 nm, and the other (of higher intensity) centered at *ca.* 425 nm. Again, the spectral pattern is suggestive of a distorted tetracoordinated environment for Cu(II), possibly with weak axial interactions. The shift to lower energy of these bands with respect to the previous case (X=Cl⁻), would be in agreement with the coordination of the halogens (X=Cl⁻ or Br⁻) in the respective Cu(II) compounds.

3) Cu(L₁)₂(NO₃)₂.

The spectrum shows a broad and asymmetric band centered at *ca.* 560 nm. A second band (of lower intensity) is centered at *ca.* 375 nm. The spectral pattern would be in agreement with a roughly square planar geometry for the Cu(II) center.

Cu(II) coordination compounds with hypoxanthine (=L₂).

4) Cu(L₂)₂(Cl)₂.

The spectrum shows a broad and asymmetric band centered at *ca.* 625 nm. A second band (of lower intensity) is centered at *ca.* 380 nm. The spectral pattern appears to be in concordance with a distorted tetracoordinated geometry for Cu(II), and possibly weak axial interactions.

5) Cu(L₂)₂(Br)₂.

The spectrum shows a broad and asymmetric band centered at *ca.* 625 nm. A second band (of lower intensity) is centered at *ca.* 375 nm. Again and for this case, a distorted tetracoordinated geometry for Cu(II) and possibly weak axial interactions are suggested.

6) $\text{Cu}(\text{L}_2)_2(\text{NO}_3)_2$.

The spectrum shows a very broad and partially resolved band with maxima at *ca.* 540 nm and *ca.* 625 nm. In the blue region, a tail (of lower intensity) of a band from the near UV is observed. The spectrum would be in concordance with a roughly square planar geometry for Cu(II).

For the three first cases with allopurinol (1, 2 and 3) the thermal studies do not show the presence of H_2O coordinated to the metallic centers, in agreement with the IR spectral studies. These Cu(II) compounds are proposed to be chromophores of the types $\text{Cu}(\text{II})(\text{N})_2(\text{X})_2$ ($\text{X}=\text{Cl}^-$ or Br^-) and $\text{Cu}(\text{II})(\text{N})_2(\text{O})_2$ ($\text{X}=\text{NO}_3^-$). The same can be proposed for the three compounds with hypoxanthine (4, 5 and 6).

When comparing the electronic spectra of the Cu(II) compounds with allopurinol and hypoxanthine, analogue ligand field strengths for these heterocycles are deduced. This result could be associated to a same type of N atoms (of the five-membered rings) involved in the metallic coordination: the $\underline{\text{N}}(2)$ atom of the pyrazolic ring is suggested to be the metallic bonding site for allopurinol in its coordination compound, whereas the pyridine-type $\underline{\text{N}}(7)$ atom in the imidazolic ring, would be the one proposed for hypoxanthine in its coordination compounds studied here.

Cu(II) coordination compounds with 6-mercaptapurine ($=\text{L}_3$).

7) $\text{Cu}(\text{L}_3)(\text{Cl})_2$.

The spectrum shows in all the visible region a lower energy tail of a band that arises in the near UV region, with shoulders at *ca.* 430 and 520 nm. This spectral pattern makes the assignment of the Cu(II) *d-d* transitions quite difficult, and therefore the possible suggestion of the structural features of this Cu(II) compound. However, this spectral pattern is in concordance with the Metal-Ligand charge transfer process, through the involvement of the $\underline{\text{S}}(6)$ exocyclic atom of the 6-mercaptapurine in the metallic bonding.

8) $\text{Cu}(\text{L}_3)_2(\text{Br})_2$.

The spectrum shows a lower energy tail of a band that arises in the near UV region, showing a shoulder at *ca.* 600 nm. As for the above case, the spectral pattern makes the

Cu(II) structural assignment difficult. However, as for $\text{Cu}(\text{L}_3)(\text{Cl})_2$, the spectral pattern is in agreement with the Metal-Ligand charge transfer process, through the participation of the $\underline{\text{S}}(6)$ exocyclic atom of 6-mercaptapurine in the metallic bonding.

9) $\text{Cu}(\text{L}_3^{2-}) \cdot 2\text{H}_2\text{O}$.

The electronic spectrum shows a lower energy tail of a band from the near UV region, associated to the Metal-Ligand charge transfer process by the $\underline{\text{S}}(6)$ exocyclic atom participation in the metallic bonding. The spectrum also shows a weak, broad and asymmetric band centered at *ca.* 715 nm, attributed to Cu(II) *d-d* transitions.

From the spectral information for these three last systems, the involvement of the $\underline{\text{S}}(6)$ exocyclic atom of the heterocyclic ligand in the metallic bonding is supported, in addition to the IR spectral information discussed before. With regard to the dilucidation of the structural features of these three Cu(II) compounds, the epr spectral and magnetic results are helpful tools. For example, and for the system $\text{Cu}(\text{II})(\text{L}_3^{2-})$, a bidimensional polynuclear framework has been deduced [25], where 6-mercaptapurinolate²⁻ has been suggested to act as bridging ligand to Cu(II) atoms through both the $\underline{\text{N}}$ atoms of the imidazolic moieties and the $\underline{\text{S}}(6)$ exocyclic atom.

f) epr spectral results.

Cu(II) coordination compounds with allopurinol (=L₁).

1) $\text{Cu}(\text{L}_1)_2(\text{Cl})_2 \cdot \text{H}_2\text{O}$.

The X-band epr spectrum at room temperature is shown in Figure 2.

Figure 2.

From the epr data, an anisotropic *g* tensor is deduced. The values of the components ($g_1 = 2.04$, $g_2 = 2.07$ and $g_3 = 2.24$) support the suggestion of a distorted tetracoordinated environment for the Cu(II) center, and axial interactions ($g_3 \gg g_2 \approx g_1 > 2.0$). The ground electronic state is associated mainly to the Cu(II) $d_{x^2-y^2}$ orbital [26,27]. When the temperature is decreased (77 K) the epr spectrum does not show changes in the spectral

pattern nor in the values of the g parameter. Finally, there are no evidences of Cu(II)-Cu(II) magnetic interactions both at room temperature and at 77 K. The epr spectrum partially resembles that shown by the compound $\text{Cu}(\text{L}_1)(\text{Cl})_2 \cdot \text{H}_2\text{O}$, synthesized in aqueous medium (pH=1) [28].

2) $\text{Cu}(\text{L}_1)_2(\text{Br})_2 \cdot 3\text{H}_2\text{O}$.

The X-band epr spectrum at room temperature is shown in Figure 3.

Figure 3.

The existence of an anisotropic g tensor ($g_1 = 1.89$, $g_2 = 2.12$ and $g_3 = 2.41$) is deduced from the spectral data. The features of this spectrum let us suggest the existence of Cu(II)-Cu(II) magnetic interactions. The value for $R = (g_2 - g_1)/(g_3 - g_2) = 0.79$ indicates the existence of a distorted tetracoordinated environment of Cu(II) with weak axial interactions. Upon decreasing the temperature (77 K) no changes in the spectrum data are observed.

3) $\text{Cu}(\text{L}_1)_2(\text{NO}_3)_2$.

The X-band epr spectrum at room temperature for this compound is shown in Figure 4.

Figure 4.

From the epr spectrum, the components $g_1 = 2.04$, $g_2 = 2.11$ and $g_3 = 2.17$ are obtained. From those, the value for $R (= 1.058)$ let us suggest a noticeable isotropic character for the g tensor, *i.e.*, the existence of a nearly spherical symmetry for the unpaired electron. Upon decreasing the temperature (=77 K), the components $g_1 = 2.06$, $g_2 = 2.11$ and $g_3 = 2.15$ are obtained. The correspondent value for $R (= 1.16)$ let us consider the existence of a slight lowering of the symmetry for Cu(II).

Cu(II) coordination compounds with hypoxanthine (=L₂).

4) $\text{Cu}(\text{L}_2)_2(\text{Cl})_2$.

The X-band epr spectrum at room temperature for this compound is shown in Figure 5.

Figure 5.

The spectrum corresponds to an almost isotropic g tensor (with components $g_1 = 2.01$, $g_2 = 2.11$ and $g_3 = 2.21$; $R = 1.006$). However, in the low-field region a very weak signal partially shown in the spectrum, is detected, which could be associated to a distortion of the geometry for Cu(II). Upon decreasing the temperature (=77 K) no changes in the general features of the spectrum are observed. The components $g_1 = 2.04$, $g_2 = 2.10$ and $g_3 = 2.17$, with $R = 0.82$, let us suggest a higher distortion for the Cu(II) environment.

5) Cu(L₂)₂(Br)₂.

The X-band epr spectrum at room temperature for this compound is shown in Figure 6.

Figure 6.

The spectrum is in agreement with the existence of an anisotropic g tensor (with components $g_1 = 2.01$, $g_2 = 2.11$ and $g_3 = 2.21$; $R = 0.88$). The value for R is suggestive of a low tetragonality in the geometry for Cu(II). Upon decreasing the temperature (=77 K) the general features of the spectrum do not show changes. For this temperature, the components $g_1 = 2.02$, $g_2 = 2.10$ and $g_3 = 2.20$, with $R = 0.67$, let us suggest a small increase of the tetragonality for the Cu(II) environment.

6) Cu(L₂)₂(NO₃)₂.

The X-band epr spectrum at room temperature for this compound is shown in Figure 7.

Figure 7.

The spectrum corresponds to an anisotropic g tensor. The components $g_1 = 2.03$, $g_2 = 2.10$ and $g_3 = 2.18$ ($R = 0.86$) let us suggest a low tetragonality for Cu(II). Upon decreasing the temperature (=77 K) changes in the spectrum shape are observed. In particular, a

higher anisotropy of the g tensor is detected. With components $g_1 = 2.04$, $g_2 = 2.07$ and $g_3 = 2.19$, and $R = 0.13$, a noticeable increase of the tetragonality for the Cu(II) environment is detected. The spectra for the two temperatures are shown together in Figure 8.

Figure 8.

Cu(II) coordination compounds with 6-mercaptopurine (=L₃).

7) Cu(L₃)(Cl)₂.

The X-band epr spectrum at room temperature for this compound is shown in Figure 9.

Figure 9.

The spectrum shows a broad absorption in the middle-field region, and its features are suggestive of an anisotropic g tensor. The components $g_1 = 2.02$, $g_2 = 2.13$ and $g_3 = 2.24$ ($R = 0.94$), are suggestive of a low tetragonality for Cu(II) [26,27,29]. Besides, the spectrum in the low-field region shows an asymmetric character. The spectral pattern for all the magnetic field values explored appear to suggest the existence of Cu(II)-Cu(II) interactions. Upon lowering the temperature (=77 K) the general spectrum does not show changes. The components $g_1 = 2.02$, $g_2 = 2.12$ and $g_3 = 2.23$, lead to $R = 0.85$, which is suggestive of a small additional decrease of the symmetry for Cu(II) at these conditions.

8) Cu(L₃)₂(Br)₂.

The X-band epr spectrum at room temperature for this compound is shown in Figure 10.

Figure 10.

The spectrum shows an asymmetrical signal in the middle-field region, with components $g_1 = 2.04$, $g_2 = 2.10$ and $g_3 = 2.18$ ($R = 0.85$), which indicates a low tetragonality for Cu(II). Besides this, the spectrum shape both in the low and high-field regions let us

suspect the possibility of Cu(II)-Cu(II) interactions. Upon decreasing the temperature (=77 K) the general spectrum pattern does not show changes. However, the components $g_1 = 2.04$, $g_2 = 2.09$ and $g_3 = 2.16$ ($R = 0.76$), are suggestive of an additional small lowering of the symmetry for Cu(II).

9) $\text{Cu}(\text{L}_3^{2-}) \cdot 2\text{H}_2\text{O}$.

The X-band epr spectrum at room temperature for this compound is shown in Figure 11.

Figure 11.

The epr spectrum shows a broad and asymmetrical signal, in concordance with an anisotropic g tensor. The components $g_1 = 2.03$, $g_2 = 2.12$ and $g_3 = 2.23$, with $R = 0.82$, supports the suggestion of a low tetragonality for Cu(II). Besides this, the spectrum shape both in the low and high-field regions is suggestive of the existence of Cu(II)-Cu(II) interactions. Upon decreasing the temperature (=77 K) the general spectrum pattern does not show changes. However, the components $g_1 = 2.02$, $g_2 = 2.11$ and $g_3 = 2.25$, and $R = 0.59$, let us suggest the existence of an additional increase of tetragonality for Cu(II).

Summary of epr spectral results.

With all the above experimental information for the Cu(II) compounds discussed here, structural arrangement suggestions could be given in advance for them:

Cu(II) coordination compounds with allopurinol (=L₁).

The 1:2 M:Heterocycle stoichiometries together with the existence of monocoordinated counterions, lead to the $\text{M}(\text{N})_2(\text{X})_2$ character for the three compounds. In these, the metallic planes containing the four ligands are suggested to present distortions. Also, axial interactions are proposed, arising possibly from the neighboring Cu(II) units. For one of the three systems ($\text{X}=\text{Br}^-$), the Cu(II)-Cu(II) interactions are evident even at room temperature.

Cu(II) coordination compounds with hypoxanthine (=L₂).

The same structural considerations quoted above could be extended for the three Cu(II) compounds with this heterocyclic ligand. However, the metallic bonding mode suggested for hypoxanthine, and its correspondent spatial disposition in the metallic coordination spheres, could lead to modifications in the interactions with the respective neighboring metallic units.

Cu(II) coordination compounds with 6-mercaptapurine (=L₃).

For these Cu(II) compounds, the 1:2 and 1:1 Metal:Heterocycle stoichiometries (both in neutral and deprotonated forms of the organic ligand) are in concordance with different metallic coordination modes of the S(6)-purine derivative. For both X=Cl⁻ and Br⁻, the chromophores Cu(II)(N)₁(S)₁(X)₂ and Cu(II)(S)₂(X)₂ could interact with neighboring Cu(II) units through bridging halogen atoms, in agreement with the axial interactions quoted before. For the unit Cu(II)(6-mercaptapurinolate²⁻), the previous spectral and magnetic characterization[25] suggest a bidimensional polynuclear framework with the 6-mercaptapurinolate²⁻ ligand bridging Cu(II) atoms in two directions through both the two N atoms of the imidazolic moiety and the S(6) exocyclic atom.

g) Magnetic Results.

Cu(II) coordination compounds with allopurinol (=L₁).

1) Cu(L₁)₂(Cl)₂·H₂O.

The $\bar{\chi}$ (emu/mol) *versus* T (K) experimental data at $H = 10000$ G for this compound are shown (dotted line) in Figure 12.

Figure 12.

Upon increasing the magnetic field from $H = 100$ to 10000 G, a small decrease of the $\bar{\chi}$ values is detected, but without change in the general magnetic response of the sample. From the data, a Curie-Weiss behavior is observed. Employing the correspondent equation $\bar{\chi} = \bar{\chi}_0 + C/(T - \theta)$, an excellent fitting to the experimental data was obtained, with the parameters: $C = 0.4294$ emu K/mol, $\theta = -0.21$ K and $\bar{\chi}_0 = 1.9501 \times 10^{-4}$ emu/mol. The

θ value is in agreement with the suggestion of a very weak magnetic coupling (of antiferromagnetic type) between the unpaired electrons of the metallic centers. When plotting the experimental data as $\bar{\chi}T$ vs. T , a continue decrease of the $\bar{\chi}T$ values with lowering the temperature is obtained until above *ca.* 10 K. Below this temperature, an abrupt increase of the slope is observed. This behavior is in agreement with a very weak antiferromagnetic coupling in the solid product, also deduced from the Curie-Weiss equation.

Considering all the above discussed experimental information for this Cu(II) compound, a linear chain arrangement and the correspondent magnetic model of $S = 1/2$ coupled spins were selected, in an attempt to explore in detail the magnitude of the magnetic coupling between the unpaired electrons of the Cu(II) units. From this magnetic model the correspondent Bonner-Fisher equation was employed:

$$\bar{\chi}_{\text{BF}} = \frac{N\beta^2 g^2}{kT} \left[\frac{0.025 + 0.14995x + 0.30094x^2}{1 + 1.9862x + 0.68854x^2 + 6.0626x^3} + \bar{\chi}_0 \right] (1 - \rho) + \frac{N\beta^2 g^2}{2kT} \rho \quad \dots(1)$$

where $x = |J|/kT$, and the other symbols have their usual meaning. An excellent fit to the experimental data was obtained (Figure 12, solid line). For fixed $g = 2.07$, we obtained $J = -0.1316 \text{ cm}^{-1}$, $\rho = 0.073$ and $\bar{\chi}_0 = 2.0767 \times 10^{-4} \text{ emu/mol}$. The magnitude of J supports the existence of a very weak antiferromagnetic coupling between the Cu(II) units. Further on, we used the Bonner-Fisher equation with a Curie-Weiss correction in the hope to explore the existence of interchain magnetic interactions. From the excellent fitting process to the experimental data, and for $g = 2.07$ we obtained $\theta = -164.7 \pm 21$; this let us suggest the existence of interchain antiferromagnetic coupling. However, when the Bonner-Fisher equation with a mean-field correction was applied, from the excellent fittings carried out qualitatively differences in the interchain magnetic coupling parameter (zJ') were obtained. For example, and for fixed $g = 2.07$, we found $zJ' = +0.48 \text{ cm}^{-1}$; this value could be associated to very weak interchain interactions of ferromagnetic type. The

intrachain magnetic coupling parameter ($J = -0.21\text{cm}^{-1}$), corroborates the intensity and character of the intrachain magnetic coupling.

At this level of study, it is difficult to elucidate the correctness of the physical meaning of the respective values for the θ and zJ' parameters. However, these let us suggest the existence of very weak interchain magnetic coupling. From the magnetic study, full concordance in the existence of very weak intrachain antiferromagnetic coupling is obtained. Attempts to explore other magnetic models were also made. Selecting the dinuclear model of $S = 1/2$ coupled spins, the Bleaney-Bowers equation was employed in the fitting process. From this, excellent fittings were obtained for fixed $g = 2.07$, and both magnetic fields, but with unrealistic physical meaning of all the parameters involved in this equation. These results let us consider the unsuccessful character of the dinuclear model to describe the magnetic properties of the Cu(II) compound in study, and to suggest a more extended framework for this system.

From the spectroscopic and magnetic studies carried out for this Cu(II) compound, a suggestion of the structural features of the Cu(II) units and their mutual interactions is shown in Figure 13.

Figure 13.

In this suggestion, \underline{L} represents the \underline{N} -bonded allopurinol ligands. The interactions between the distorted Cu(II) units occur through the Cl^- ligands. These weak interactions would be in agreement with the very weak intrachain magnetic coupling found, of antiferromagnetic type. In this structural arrangement proposition, interchain magnetic interactions must also be considered.

To our knowledge, there are no reports published by other groups about this Cu(II) system. In previous studies[28], a pale green Cu(II) compound with the same formulation $\text{Cu(II)(L}_1)_2(\text{Cl})_2 \cdot \text{H}_2\text{O}$ was synthesized and characterized. However, its spectral (epr) and

magnetic properties show some differences with the characteristics described here: the system obtained in aqueous (pH=1) solution[28] shows no resolution of the epr signal for the g_{\parallel} component. It also shows a $\bar{\chi}$ maximum value in the low-temperature region (*ca.* 10 K), with values for the intrachain magnetic coupling parameter (J) ranging from -3.88 cm^{-1} to -4.07 cm^{-1} . At this level of study, it is difficult to discern about the factors influencing these differences. Nevertheless, the magnetic properties for both Cu(II) systems have been successfully analyzed employing the linear chain magnetic model of $S = 1/2$ coupled spins, from which very weak both inter and intrachain magnetic couplings have been deduced. Finally, and as part of our research program, the Cu(II) compound studied here has also been previously synthesized in ethanolic medium although only partially characterized[7].

2) $\text{Cu}(\text{L}_1)_2(\text{Br})_2 \cdot 3\text{H}_2\text{O}$.

The $\bar{\chi}$ (emu/mol) *versus* T (K) experimental data at $H = 10000\text{G}$ for this compound are shown (dotted line) in Figure 14.

Figure 14.

Upon increasing the magnetic field from 100 to 10000 G, no changes in both the $\bar{\chi}$ values and the general magnetic response of the sample were observed. From the experimental data a masked shoulder in the low-temperature region is detected, suggesting us the existence of an antiferromagnetic coupling, very weak in intensity. In agreement with this, the magnetic coupling was also pointed out in the epr spectral discussion. Employing the Curie-Weiss equation, a very good fit to the experimental data was obtained, with the parameters: $C = 0.07506 \text{ emu K/mol}$, $\theta = -1.15 \text{ K}$ and $\bar{\chi}_0 = 0.00626 \text{ emu/mol}$. The θ value indicates a very weak antiferromagnetic coupling in the solid product. When plotting the experimental data as $\bar{\chi}T$ *versus* T , a continue decrease of $\bar{\chi}T$ with lowering the temperature is observed. From *ca.* 40 K, an abrupt increase in the slope of the line is detected. This behavior is also suggestive of a very weak antiferromagnetic coupling.

Considering all the above spectroscopic information for this Cu(II) compound, a linear chain arrangement for the Cu(II) units in the solid was postulated. With this scheme and from the correspondent magnetic model, the Bonner-Fisher equation (Eq. (1)) was employed to analyze the magnetic interactions. The fitting process gave for fixed $g = 2.12$, the following parameters: $J = -11.79 \text{ cm}^{-1}$, $\rho = 0.060$ and $\bar{\chi}_0 = 0.00188 \text{ emu/mol}$ were obtained. The theoretical values are shown as a solid line in Figure 14. The magnitude of the J parameter supports the existence of a very weak antiferromagnetic coupling in this Cu(II) compound. This magnetic coupling appears to be slightly higher in intensity than that found in $\text{Cu}(\text{allopurinol})_2(\text{Cl})_2 \cdot \text{H}_2\text{O}$.

With regard to the same magnetic study, the possibility of interchain magnetic coupling for this model of structural arrangement was considered. In this analysis, The Bonner-Fisher equation with the Curie-Weiss correction was applied. From the good fitting process with $g = 2.12$, the following values: $J = -11.80 \text{ cm}^{-1}$, $\theta = -0.163 \text{ K}$, $\rho = 0.061$ and $\bar{\chi}_0 = 0.00189 \text{ emu/mol}$ were obtained. From these results, confirmation of a very weak intrachain antiferromagnetic coupling is deduced ($J < 0$). With respect to the possible interchain magnetic coupling, the θ value is associated to very weak magnetic interactions. However, the error for this parameter (± 3.17) difficulties the correct physical meaning. Continuing with this analysis, and employing the same magnetic model and equation, the correspondent mean-field correction was applied. From the respective excellent fitting process, the parameters (for fixed $g = 2.12$) we obtained are: $J = -13.48 \text{ cm}^{-1}$, $zJ' = -4.46 \text{ cm}^{-1}$, $\rho = 0.074$ and $\bar{\chi}_0 = 0.00116 \text{ emu/mol}$. The zJ' value is here associated to very weak interchain magnetic coupling of antiferromagnetic type. In this last analysis, confirmations of very weak intrachain antiferromagnetic coupling between the unpaired electrons of the Cu(II) units is found. Continuing with the magnetic analysis, the dinuclear magnetic model of $S = 1/2$ coupled spins was also applied to the treatment of the magnetic data. Employing the Bleaney-Bowers equation in the fitting process, unsuccessful results were obtained. This let us discard this model in the description of the experimental

magnetic data. Also, these results let us suggest the successful character of the linear chain magnetic model in the magnetic characterization of the Cu(II) compound in study. From all the spectral and magnetic information, a scheme of the structural features of the Cu(II) units and their interactions arises. This resembles closely the ones suggested for Cu(allopurinol)₂(Cl)₂·H₂O. The distorted Cu(II)(N)₂(Br)₂ units would be interacting through the halogen atoms, leading to very weak magnetic interactions. In this scheme, interchain magnetic interactions must be also considered. The increased intrachain magnetic coupling from X=Cl⁻ to X=Br⁻, would be in part attributed to the higher polarizability of the Br⁻ ligands, which could contribute to higher interactions between their orbitals, with those of the metallic centers from nearest Cu(II) units. Finally, and to our knowledge, there are no studies carried out by other groups and reported in relation to this Cu(II) compound. As part of our research program, this Cu(II) system was also synthesized previously in ethanolic medium although only partially characterized[7].

3) Cu(L₁)₂(NO₃)₂.

The $\bar{\chi}$ (emu/mol) as a function of T (K) experimental data at $H = 100$ G for this compound are shown (dotted line) in Figure 15.

Figure 15.

Upon increasing the magnetic field from 100 to 10000 G, no noticeable changes in the $\bar{\chi}$ values and in the general magnetic response of the sample are observed. From Figure 15, a shoulder in the $\bar{\chi}$ values in the low-temperature region is detected, suggesting us the existence of antiferromagnetic coupling in the compound. Its position (*ca.* 8 K) indicates a very weak intensity of the correspondent magnetic interactions. From the data for the 12-95 K range, and employing the Curie-Weiss equation, values of $\theta = -2.97$ K, $C = 0.0186$ emu K/mol and $\bar{\chi}_0 = 0.0019$ emu/mol were obtained. The θ value supports the existence of very weak antiferromagnetic coupling in the Cu(II) compound. From the $\bar{\chi}T - T$ plot, a continue decrease of the $\bar{\chi}T$ values with decreasing the temperature is obtained. Starting

from *ca.* 13 K, a higher slope of the line for lower temperatures is observed. This behavior also suggests a very weak antiferromagnetic coupling in the solid product.

Considering the possibility of a structural arrangement consisting of a linear chain, the respective magnetic model and the Bonner-Fisher equation was employed in the magnetic analysis. Good fitting process was made for fixed $g = 2.11$, with the resulting parameters: $J = -4.46 \text{ cm}^{-1}$, $\rho = 0.089$ and $\bar{\chi}_0 = 0.0815 \text{ emu/mol}$. The theoretical curve (solid line) is shown in Figure 15. The J value is in concordance with a very weak antiferromagnetic coupling in the compound. Furthermore, the $\bar{\chi}$ values in the low-temperature region (and which follow a Curie-Weiss behavior) were discarded. Employing the same magnetic model and the Bonner-Fisher equation, very good results were obtained in the fitting process for 100 K as upper limit of temperature. From this and for fixed $g = 2.11$ and $\rho = 0$, the parameters: $J = -3.10 \text{ cm}^{-1}$ and $\bar{\chi}_0 = 0.0747 \text{ emu/mol}$ were obtained. In the same form and for $T = 200 \text{ K}$ as upper limit of temperature, very good results ($J = -3.09 \text{ cm}^{-1}$ and $\bar{\chi}_0 = 0.0746 \text{ emu/mol}$) were also obtained. These are shown (solid line) in Figure 16.

Figure 16.

The two last fitting processes confirm the existence of very weak antiferromagnetic coupling in the Cu(II) compound. In order to explore the possibility of interchain magnetic coupling for this structural arrangement suggestion, the Bonner-Fisher equation with the Curie-Weiss correction was employed in the magnetic analysis. From the fitting process, good results were obtained for fixed $g = 2.11$, being $J = -5.72 \text{ cm}^{-1}$, $\rho = 0.104$, $\bar{\chi}_0 = 0.0827 \text{ emu/mol}$ and $\theta = +1.28 \text{ K}$ the values of the parameters obtained for 100 K as the temperature upper limit. In the same way, and for 200 K as the temperature upper limit, the parameters obtained were: $J = -5.68 \text{ cm}^{-1}$, $\rho = 0.102$, $\bar{\chi}_0 = 0.0826 \text{ emu/mol}$ and $\theta = +1.27 \text{ K}$. From these results, confirmation of very weak intrachain antiferromagnetic coupling (J values) is obtained. Interestingly, the θ values let us suspect the possibility of interchain ferromagnetic interactions, very weak in intensity. This same character for θ was

also obtained when the $\bar{\chi}$ values for the low-temperature region were discarded ($\rho = 0$) in the fitting process.

Further on in the magnetic analysis, the Bonner-Fisher equation with a mean-field correction was employed. From the fitting process, good results were obtained for fixed $g = 2.11$. For 100 K as the upper temperature limit, $J = -5.21 \text{ cm}^{-1}$, $zJ' = +2.16 \text{ cm}^{-1}$, $\rho = 0.079$ and $\bar{\chi}_0 = 0.0483 \text{ emu/mol}$ were obtained. In the same form, and for 200 K as the upper temperature limit, $J = -5.24 \text{ cm}^{-1}$, $zJ' = +2.16 \text{ cm}^{-1}$, $\rho = 0.079$ and $\bar{\chi}_0 = 0.0484 \text{ emu/mol}$ were obtained. From these last results, confirmation of very weak both intrachain (J) and interchain (zJ') magnetic coupling is deduced, the last one considered as ferromagnetic in character. This same character for the zJ' parameter was also obtained when the $\bar{\chi}$ values in the low-temperature region were discarded ($\rho = 0$) in the fitting process.

In this analysis, the dinuclear magnetic model of $S = 1/2$ coupled spins was also explored. Using the correspondent Bleaney-Bowers equation in the fitting process, non satisfactory results were obtained. This fact let us discard this magnetic model in the description of the experimental magnetic data. Also, it suggests the successful character of the linear chain magnetic model in the magnetic characterization of the Cu(II) system in study.

With all the spectroscopic and magnetic studies carried out for this compound, it is possible to suggest the essential structural features of the Cu(II) units coordination sphere, and their correspondent interunit interactions. In this scheme, a distorted tetraordinated (roughly square planar) environment for Cu(II) is proposed, through the N-bonded allopurinol molecules and the coordinated NO_3^- groups. In this structural arrangement suggestion, axial interactions must be considered. These could construct roughly linear fragments through the participation of the NO_3^- groups as interacting ligands, in a similar way to that suggested for $\text{Cu}(\text{allopurinol})_2(\text{Cl})_2 \cdot \text{H}_2\text{O}$.

The magnetic study carried out let us consider the existence of very weak intrachain antiferromagnetic coupling. In these magnetic interactions between the unpaired electrons of the

Cu(II) centers, the NO_3^- groups are invoked to be involved in the respective superexchange magnetic coupling pathway. Interestingly, the magnetic results point out the suggestion of very weak ferromagnetic coupling between these chain-type fragments proposed. Finally, and to our knowledge, there are no studies published about this Cu(II) compound. Surprisingly, when the same reaction is carried out in ethanolic medium, the Cu(II) compound synthesized corresponds to the formulation $\text{Cu(II)(L}_1^-)(\text{OH}^-)$ [7]. This last product has been also obtained in both aqueous (several pH values) and DMSO media[4].

Considering the magnetic studies carried out for the three Cu(II) compounds with the heterocyclic ligand allopurinol and the Cl^- , Br^- and NO_3^- coordinated groups ($=\text{Y}$), common structural and magnetic features arise. For these three systems the $\text{Cu(II)(N)}_2(\text{Y})_2$ units show both distorted ($\text{Y} = \text{Cl}^-$ or Br^-) and roughly square planar ($\text{Y} = \text{NO}_3^-$) tetracoordinated environments. In these systems, weak interactions between the nearest neighboring Cu(II) units are deduced. These interactions lead in general to very weak antiferromagnetic coupling between the unpaired electrons of the Cu(II) centers. From the magnetic results an influence of the anion nature on the intensity of the intrachain magnetic coupling is observed. This magnetic response could be in part associated to the stereochemical disposition of the allopurinol ligands; the $\text{N}(2)$ atom as metallic bonding site would contribute to the existence of a less restricted axial interaction. Interestingly, in the structural arrangement suggestion (linear chain-type) for these three Cu(II) compounds, interchain magnetic coupling was suspected, and suggested from the magnetic studies. This magnetic coupling is very weak in all the three cases.

Cu(II) coordination compounds with hypoxanthine ($=\text{L}_2$).

4) $\text{Cu(L}_2)_2(\text{Cl})_2$.

The $\bar{\chi}$ (emu/mol) $-T$ (K) experimental data ($H = 100$ G) for this compound are shown (dotted line) in Figure 17.

Figure 17.

Upon increasing the magnetic field from 100 G to 10000 G, a small decrease of the $\bar{\chi}$ values with temperature but without changes in the general trend of the magnetic response is observed. From Figure 17, a maximum of the $\bar{\chi}$ values in the low-temperature region is observed, which indicates a very weak antiferromagnetic coupling in the sample. Employing the Curie-Weiss equation in a fitting process to the $\bar{\chi}$ data for temperatures higher than the maximum $\bar{\chi}$ value and up to 150 K, very good results were obtained, with the parameters: $C = 0.4729$ emu K/mol, $\theta = -15.52$ K and $\bar{\chi}_0 = 0.02410$ emu/mol. The θ value supports the suggestion of a very weak antiferromagnetic coupling in the product. From the $\bar{\chi}T - T$ data, a continue decrease of the $\bar{\chi}T$ values with lowering the temperature is observed. Starting from *ca.* 15 K a higher slope of the line for the lower temperatures is obtained. This behavior is also suggestive of a very weak antiferromagnetic coupling in the solid product.

Assuming a linear chain arrangement for the Cu(II) compound, the correspondent magnetic model and Bonner-Fisher equation were employed to explore the intensity of the magnetic interactions between the Cu(II) units. From the fitting process (Figure 17, solid line) and fixing $g = 2.11$, the values $J = -5.39$ cm⁻¹, $\rho = 0.0186$ and $\bar{\chi}_0 = 0.0247$ emu/mol were obtained. The J value indicates a very weak antiferromagnetic coupling between the unpaired electrons of the Cu(II) units. In order to explore the possible magnetic interactions between the postulated linear chains, the Bonner-Fisher equation with the Curie-Weiss correction was employed. From the very good fitting obtained, and for $g = 2.11$, the values $J = -5.42$ cm⁻¹, $\rho = 0.017$, $\bar{\chi}_0 = 0.0247$ emu/mol and $\theta = +0.13$ K were obtained for 150 K as the temperature upper limit. By changing this limit, very similar values of the parameters were found. The average J value in this analysis is in concordance with the above result. The θ average value is associated to the existence of very weak interchain interactions. However, the errors (± 1.956) in these values make it difficult to assert the correct physical meaning for this parameter.

Further on with the analysis, the Bonner-Fisher equation with a mean-field correction was considered. From this, the excellent fitting process gave (for fixed $g = 2.11$) the values:

$J = -5.39 \text{ cm}^{-1}$, $zJ' = -0.534 \text{ cm}^{-1}$, $\rho = 0.020$ and $\bar{\chi}_0 = 0.01503 \text{ emu/mol}$. The zJ' value let us consider the existence of very weak magnetic coupling between the chains in this Cu(II) compound. However, and also here, the error for the zJ' value (± 1.718) difficults to give a correct physical meaning to this parameter. Finally, the J value here obtained is in full agreement with its previous calculations, confirming the existence of very weak intrachain antiferromagnetic coupling.

Attempts to explore the experimental information employing the dinuclear magnetic model of $S = 1/2$ coupled spins (through the Bleaney-Bowers equation), considering also the Curie-Weiss and the mean-field corrections to it, were made. The fitting processes were of lower quality than those for the linear chain magnetic model. However, the results obtained for the magnetic parameters let us suggest the existence of very weak both intra and interchain antiferromagnetic couplings.

With all the spectroscopic and magnetic information, a suggestion of the approximate structural arrangement for this compound in the solid state can be made. This consists of Cu(II)(N)₂(Cl)₂ distorted units, axially interacting through halogen atoms with nearest neighboring Cu(II) units, in a similar form to that proposed for the precedent Cu(II) compounds. Very weak interactions in other directions (interchain interactions) must also be considered, although their physical meaning at this level of study is difficult to dilucidate. To our knowledge, the only related systems to the Cu(II) compound discussed here and reported by other research groups, are Cu(II)(L₂)₂(Cl)₂·1/2 H₂O [30] and [Cu(II)(μ-L₂)₂(Cl)]₂·(Cl)₂·6H₂O [31]. Unfortunately, no spectral and magnetic characterization were made for the first one. A dinuclear Cu(II) acetate-type structure has been established for the last one, with a high antiferromagnetic coupling ($J = -105.5 \text{ cm}^{-1}$). Finally, the Cu(II) compound discussed here, was also synthesized by us in aqueous solution (pH=1)[28], as Cu(L₂)₂(Cl)₂·2H₂O and Cu(L₂)₂(Cl)₂, both showing essentially the same spectral and magnetic properties discussed here.

5) Cu(L₂)₂(Br)₂.

The $\bar{\chi}$ (emu/mol) $-T$ (K) experimental data ($H = 100$ G) for this compound are shown (dotted line) in Figure 18.

Figure 18.

Upon increasing the magnetic field from 100 G to 10000 G, no changes in both the $\bar{\chi}$ values with temperature and in the general magnetic response of the sample are observed. In the low-temperature region a maximum of the $\bar{\chi}$ values is observed, which suggests the existence of an antiferromagnetic coupling in the solid sample; the position of this is associated to a very low intensity for this interaction. Employing the Curie-Weiss equation in a fitting process to the $\bar{\chi}$ data at higher temperatures than the T for the $\bar{\chi}$ maximum, and up to 150 K, very good results were obtained: $C = 0.5688$ emu K/mol, $\theta = -16.89$ K and $\bar{\chi}_0 = 2.8746 \times 10^{-4}$ emu/mol. The θ value supports the suggestion of a very weak antiferromagnetic coupling in the solid product. From the $\bar{\chi}T - T$ data, a continue decrease of the $\bar{\chi}T$ values with descending the temperature is observed. Starting from *ca.* 15 K, a much higher slope of the line for the low-temperature region is obtained. This behavior is also suggestive of a very weak antiferromagnetic coupling in the solid product.

With the above spectroscopic information for this compound, a linear chain arrangement was selected to explore the magnetic interactions between the unpaired electrons of the metallic Cu(II) units. From this, the correspondent magnetic model, and the Bonner-Fisher equation were employed. The fitting process to the experimental data, gave excellent results for fixed $g = 2.11$: $J = -4.98$ cm $^{-1}$, $\rho = 0.016$ and $\bar{\chi}_0 = 0.00129$ emu/mol. The theoretical values are also shown in Figure 18 with a solid line. Carrying out the fitting process by excluding the experimental data in the low-temperature region (Curie-Weiss behavior), very good results were obtained, both for 300 K and 150 K as the temperature upper limit. For $g = 2.11$ and $\rho = 0$, the respective J values were -4.38 cm $^{-1}$ and -4.32 cm $^{-1}$. The magnitude of the J parameter is in full agreement with the existence of a very weak antiferromagnetic coupling between the unpaired electrons of the Cu(II)

centers. Assuming the possibility of magnetic interactions between the chains, the Bonner-Fisher equation considering the Curie-Weiss correction was employed. Excellent fitting was obtained for fixed $g = 2.11$ and 150 K as the temperature upper limit: $J = -3.32 \text{ cm}^{-1}$, $\rho = 0.033$, $\theta = -4.75 \text{ K}$ and $\bar{\chi}_0 = 0.0142 \text{ emu/mol}$. The magnitude of the θ parameter suggests the existence of very weak interchain interactions, of antiferromagnetic type. In this magnetic analysis, the J value supports the existence of very weak intrachain antiferromagnetic coupling.

Further on, the Bonner-Fisher equation with a mean-field correction was employed, and an excellent fitting was also obtained for $g = 2.11$ and 150 K as the temperature upper limit: $J = -4.99 \text{ cm}^{-1}$, $zJ' = -3.97 \text{ cm}^{-1}$, $\rho = 0.019$ and $\bar{\chi}_0 = 7.736 \times 10^{-4} \text{ emu/mol}$. A very good fitting was obtained when excluding the low-temperature region (Curie-Weiss behavior), which gave similar values for J and zJ' (-4.09 and -4.51 cm^{-1} , respectively). The zJ' values are also in agreement with the existence of very weak antiferromagnetic coupling between the chains considered. The J values are also in concordance with the previous calculation and physical meaning for this parameter.

Attempts to explore other magnetic models were made. For the dinuclear magnetic model of $S = 1/2$ coupled spins, the correspondent Bleaney-Bowers equation was employed in a fitting process to the experimental data. In this process, non successful results were obtained, which suggest the non realistic level of the dinuclear magnetic model for the magnetic characterization of the Cu(II) compound in study.

With all the spectroscopic and magnetic information a suggestion both for the structural features of the Cu(II) units and their interactions can be made. This appears also to be closely related to that firstly suggested for Cu(II)(allopurinol)₂(Cl)₂·H₂O and also proposed for the precedent compound Cu(II)(hypoxanthine)₂(Cl)₂. For the case in discussion the Cu(II) units connecting mode would be through the Br⁻ ligands. In this scheme, interchain magnetic interactions must also be considered. Comparing the magnetic results

for $\text{Cu}(\text{L}_2)_2(\text{Cl})_2$ and $\text{Cu}(\text{L}_2)_2(\text{Br})_2$, they suggest an analogous character of both the intrachain and interchain antiferromagnetic couplings in those Cu(II) compounds, and thus their closely related structural arrangement.

To our knowledge, the unique related Cu(II) compound reported up to date is the system $\text{Cu}(\text{II})(\text{L}_2)_2(\text{Br})_2 \cdot 2\text{H}_2\text{O}$, which has been related to a dinuclear structure of the Cu(II) acetate-type [32], and which shows a strong ($J = -142.1 \text{ cm}^{-1}$) antiferromagnetic coupling. On the other hand, in previous studies carried out by us in aqueous solution (pH=1)[28], the green-yellow $\text{Cu}(\text{II})(\text{L}_2)_2(\text{Br})_2 \cdot 2\text{H}_2\text{O}$ was obtained. For this system, a very broad and asymmetric absorption band in the epr spectrum was found. The correspondent magnetic studies are in agreement with a higher intramolecular antiferromagnetic coupling ($J = -82.4 \text{ cm}^{-1}$) than that shown by the Cu(II) compound discussed here. For this green-yellow compound the dinuclear system of $S = 1/2$ coupled spins magnetic model was successful, not the linear chain magnetic model. The magnetic characterization of this Cu(II) compound points out the suggestion of the Cu(II) units magnetically interacting through the Br^- bridging ligands, constructing in this way dinuclear units, and these last interacting in the same way, in a reminiscent picture of a cubane-like tetranuclear framework.

6) $\text{Cu}(\text{L}_2)_2(\text{NO}_3)_2$.

The $\bar{\chi}$ (emu/mol) $-T$ (K) experimental data ($H = 10000 \text{ G}$) for this compound are shown (dotted line) in Figure 19.

Figure 19.

Upon increasing the magnetic field from 100 G to 10000 G, no changes in both the $\bar{\chi}$ values with temperature and in the general magnetic response of the sample were obtained. From the data, a maximum of the $\bar{\chi}$ values in the low-temperature region is observed, which indicates the existence of a very weak antiferromagnetic coupling between the unpaired electrons of the Cu(II) units. Using the Curie-Weiss equation in a fitting process to the $\bar{\chi}$

data ($H = 100$ G) at higher temperatures than the T for the $\bar{\chi}$ maximum, good results were obtained. with the parameters: $C = 0.460$ emu K/mol. $\theta = -12.69$ K and $\bar{\chi}_0 = 0.00114$ emu/mol. The θ value supports the suggestion of a very weak antiferromagnetic coupling in the product. From the $\bar{\chi}T - T$ data also at $H = 100$ G, a continue decrease of the $\bar{\chi}T$ values with descending the temperature is observed. Starting from *ca.* 15 K, a much higher slope of the line for the low-temperature region is obtained. This behavior is also suggestive of a very weak antiferromagnetic coupling in the solid product.

Considering the spectral information discussed before for this compound, a linear chain arrangement of interacting Cu(II) units was postulated. From the respective magnetic model, the Bonner-Fisher equation was employed for the magnetic study. From the good fitting process and for fixed $g = 2.10$ and $\rho = 0$ the following parameters were obtained: $J = -3.80$ cm⁻¹ and $\bar{\chi}_0 = 4.53 \times 10^{-4}$ emu/mol. The theoretical values are shown in Figure 19 with a solid line. The J value confirms the existence of a very weak antiferromagnetic coupling in the compound analyzed. Very similar values for the J parameter were also obtained when the Curie-Weiss behavior of the magnetic data (not shown in Figure 19) in the low-temperature region was considered. The fitting process considering the full temperature range (300 K as upper limit) and for $H = 100$ and 10000 G respectively, gave values ranging from -3.89 to -3.72 cm⁻¹ for the J parameter.

Considering the possibility of magnetic interactions between the chains, the Bonner-Fisher equation with the Curie-Weiss correction was employed. From the fitting process, very good results were obtained for both magnetic fields and temperature limits. For example, for $H = 100$ G and fixed $g = 2.10$, the parameters $J = -3.48$ cm⁻¹, $\rho = 0.024$, $\theta = -1.5431$ and $\bar{\chi}_0 = 0.0011$ emu/mol were obtained for 250 K as the temperature upper limit. Very similar values for the parameters J and θ were obtained with this equation and correction, for several temperature ranges and the two magnetic fields. The average θ value suggests very weak interchain interactions of antiferromagnetic type. The overall J value supports the suggestion of very weak intrachain antiferromagnetic coupling.

Further on, the Bonner-Fisher equation with a mean-field correction was employed to explore in detail the interchain interactions, and excellent fittings were obtained for $g = 2.10$ and for both magnetic field values and several temperature upper limits: the J values range from -3.69 cm^{-1} to -4.54 cm^{-1} , confirming the previous calculations for this parameter. However, appreciable errors for the small and positive zJ' values are obtained in this treatment, difficulting the interpretation of its correct physical meaning (the interchain interaction appears to be very weak although of ferromagnetic type). This result is in apparent disagreement with the physical interpretation made for the θ value discussed before. At this level of study it is difficult to dilucidate the physical meaning of the values associated to the interchain magnetic coupling parameter. However, the main results at this respect, would be the suggestion of the existence of very weak interchain magnetic interactions.

Attempts to explore the capability of the dinuclear magnetic model of $S = 1/2$ coupled spins to predict the experimental magnetic behavior of the Cu(II) compound in study were made, in which the Bleaney-Bowers equation (including the Curie-Weiss and the mean-field corrections) was employed in a fitting process to the experimental data. The results were not successful neither in the fitting quality nor in the physical meaning of the values obtained of the magnetic parameters. This last result let us consider the suggestion of a more complex framework for the Cu(II) system in study.

With all the preceding spectroscopic and magnetic information available for this Cu(II) compound, a possibility of the structural features for the Cu(II)(N)₂(O)₂ units and their correspondent magnetic interactions can be made. In this, the roughly square planar Cu(II)(N)₂(O)₂ units could be interacting between them through the NO₃⁻ groups, forming linear chains in a similar way as suggested for Cu(II)(allopurinol)₂(Cl)₂·H₂O. Unfortunately and to our knowledge, there are no studies reported for this Cu(II) compound. At pH=1 we have obtained[28] the compound with the formulation Cu(II)(L₂)₂(NO₃)₂·2H₂O, for which the spectral and magnetic characterization is in full agreement with a

dinuclear structure. Cu(II) acetate-type, with bridging hypoxanthine ligands and NO_3^- groups bonded in the apical positions of the Cu(II) centers. The J parameter obtained for this Cu(II) compound is *ca.* -140 cm^{-1} , and is in full agreement with the dinuclear magnetic model of $S = 1/2$ coupled spins.

Considering the magnetic studies carried out for the three Cu(II) compounds with the heterocyclic ligand hypoxanthine and the Cl^- , Br^- and NO_3^- coordinated groups ($=Y$), common both structural and magnetic features arise, the same as for the analogue Cu(II) compounds with allopurinol. For the systems with hypoxanthine, the $\text{Cu(II)(N)}_2(\text{Y})_2$ units showing both distorted ($Y=\text{Cl}^-$ or Br^-) and nearly square planar ($Y=\text{NO}_3^-$) tetracoordinated geometries are suggested. Also, weak magnetic interactions between the nearest neighboring Cu(II) units are proposed. These interactions lead to very weak antiferromagnetic couplings (of the same level) between the unpaired electrons of the Cu(II) centers. From the magnetic results a non noticeable influence of the anion nature on the intensity of the intrachain magnetic coupling assumed is observed. Perhaps this similarity of magnetic behavior is influenced in part by the stereochemical disposition of the hypoxanthine ligands. It is possible that the N-bonded hypoxanthine molecules could be in a head-tail configuration with respect to the mean plane of the $\text{Cu(II)(N)}_2(\text{Y})_2$ units. In all these three compounds and for the common structural arrangement suggestion, the correspondent magnetic study is in agreement with the existence of very weak interchain magnetic coupling.

Cu(II) coordination compounds with 6-mercaptopurine ($=L_3$).

7) $\text{Cu(L}_3\text{)(Cl)}_2$.

The $\bar{\chi}$ (emu/mol) $-T$ (K) experimental data ($H = 100 \text{ G}$) for this compound are shown (dotted line) in Figure 20.

Figure 20.

When increasing the magnetic field (100 G to 10000 G), a small decrease in the $\bar{\chi}$ values with temperature is observed, but without a modification of the general magnetic response

of the sample. From the experimental curve, a Curie-Weiss behavior is observed, and so the correspondent equation was fitted to the experimental data, with excellent results and the parameters: $C = 0.2096$ emu K/mol, $\theta = -0.49$ K and $\bar{\chi}_0 = 0.01788$ emu/mol. The θ value, although very small, is in agreement with the existence of a very weak antiferromagnetic coupling in the solid product. From the $\bar{\chi}T - T$ data a continue decrease of the $\bar{\chi}T$ values with descending the temperature is observed. Starting from *ca.* 25 K, a higher slope of the line for the low-temperature region is obtained. This behavior is also suggestive of a very weak antiferromagnetic coupling in the sample.

Assuming the existence of interactions between the Cu(II) units, a linear chain arrangement was postulated. From the correspondent magnetic model, the Bonner-Fisher equation was employed for the fitting process. From this, very good results were obtained (the theoretical values are also shown in Figure 20 with a solid line). For fixed $g = 2.13$, the following parameters were obtained: $J = -11.3$ cm⁻¹, $\rho = 0.20$ and $\bar{\chi}_0 = 0.0191$ emu/mol. The J value is in concordance with a very weak antiferromagnetic coupling between the unpaired electrons of the Cu(II) units. Fitting processes considering the Bonner-Fisher equation with both the Curie-Weiss and the mean-field corrections were also exhaustively carried out, with excellent results. For example, for the mean-field correction and fixed $g = 2.13$, the parameters $J = -14.23$ cm⁻¹, $zJ' = -0.59$ cm⁻¹, $\rho = 0.219$ and $\bar{\chi}_0 = 0.01163$ emu/mol were obtained. This magnetic model, with any of the two corrections supports the existence of very weak both intrachain and interchain antiferromagnetic couplings in the solid product. By employing the dinuclear model of $S = 1/2$ coupled spins (through the Bleaney-Bowers equation) attempts of fitting to the $\bar{\chi} - T$ experimental data were made, without successful results. This supports the suggestion of a more extended (*i.e.*, polynuclear) arrangement in the Cu(II) compound under study.

With all the spectroscopic and magnetic studies for the compound in discussion, a scheme of the possible structural arrangement for the Cu(II) units and their postulated interactions can be made, which is shown in Figure 21.

Figure 21.

In this scheme, N-S represents the 6-mercaptapurine ligands bonded through the $\underline{S}(6)$ and $\underline{N}(7)$ atoms. The magnetic interactions between the Cu(II) units would be through the Cl^- atoms. In fact, these connecting units have been structurally found in $\text{Cu(II)(6-thio-9-methylpurine)}_1(\text{Cl})_2 \cdot \text{H}_2\text{O}$ [33] and $\text{Cd(II)(6-thiopurine)}_1(\text{H}_2\text{O})_1(\text{Cl})_2$ [34], and also suggested in the anhydrous analogue [35] of the former system. Very weak interchain magnetic interactions must be also considered in this structural arrangement proposition. Finally, to our knowledge there are no studies reported up to date related to this Cu(II) compound.

8) $\text{Cu(L}_3)_2(\text{Br})_2$.

The $\bar{\chi}$ (emu/mol) $-T$ (K) experimental data at $H = 100$ G for this compound are shown (dotted line) in Figure 22.

Figure 22.

When increasing the magnetic field (100 G to 10000 G), no changes both in the $\bar{\chi}$ values with temperature and in the general magnetic response of the sample were observed. From the experimental curve, a Curie-Weiss behavior is observed, and so the correspondent equation was fitted to the experimental data, with very good results and the parameters: $C = 0.079$ emu K/mol, $\theta = -0.10$ K and $\bar{\chi}_0 = 0.0020$ emu/mol. The θ value, although very small, is in agreement with the existence of a very weak antiferromagnetic coupling in the sample. From the $\bar{\chi}T - T$ data a continue decrease of the $\bar{\chi}T$ values with descending the temperature is observed. Starting from *ca.* 30K, a higher slope of the line for the low-temperature region is obtained. This behavior is also suggestive of a very weak antiferromagnetic coupling in the solid product.

Assuming, as in the previous Cu(II) system, an analogous structural arrangement, the linear chain model and the Bonner-Fisher equation were employed in the magnetic analysis. Excellent fitting results were obtained (the theoretical values are shown in Figure 22 with

a solid line) for fixed $g = 2.10$, being the parameters: $J = -46.88 \text{ cm}^{-1}$, $\rho = 0.09$ and $\bar{\chi}_0 = 7.813 \times 10^{-4} \text{ emu/mol}$. The J value supports the existence of a very weak antiferromagnetic coupling in the solid product. Also, interchain magnetic interactions were assumed in the analysis, and the Bonner- Fisher equation with both the Curie-Weiss and the mean-field corrections were respectively fitted to the experimental data. For example, for the mean-field correction and with fixed $g = 2.10$, the parameters $J = -49.68 \text{ cm}^{-1}$, $zJ' = -1.17 \text{ cm}^{-1}$, $\rho = 0.096$ and $\bar{\chi}_0 = 4.691 \times 10^{-4} \text{ emu/mol}$ were obtained. This magnetic model, with any of the two corrections, supports the existence of both very weak intrachain and interchain antiferromagnetic couplings in the solid product. Attempts to explore the experimental magnetic information with the dinuclear model of $S = 1/2$ coupled spins (through the Bleaney-Bowers equation) were made. In this process, unsuccessful results were obtained, both in the fitting quality and in the physical meaning of the magnetic parameters. These results support, as in the previously discussed Cu(II) compound, the existence of a more extended framework in the Cu(II) compound in study here.

With all the spectroscopic and magnetic studies made for this compound, a suggestion both for the possible structural features for the Cu(II) units and their interactions can be made. This resembles the general features as was firstly suggested and schematically shown for Cu(II)(allopurinol)₂(Cl)₂·H₂O, although in the case discussed here the chromophore is Cu(II)(S)₂(Br)₂. The magnetic interactions between these Cu(II) units would be through the Br⁻ ligands. The higher antiferromagnetic coupling in the compound here discussed with respect to that of Cu(L₃)(Cl)₂ let us consider the existence of a more efficient superexchange magnetic coupling pathway for the former one, in part associated to the higher polarizability of the Br⁻ ligands. Other factors (as the stereochemical features of the Cu(II) centers and the spatial dispositions of the halogen atoms) can also play a critical role in the type and intensity of the magnetic coupling. At this level of study, it is difficult to dilucidate both the single and collective contributions of these aspects.

Finally, in this linear polynuclear structural arrangement suggestion, very weak interchain magnetic interactions must also be considered. To our knowledge, there are no studies reported up to date with regard to this Cu(II) compound.

9) $\text{Cu}(\text{L}_3^{2-}) \cdot 2\text{H}_2\text{O}$.

The $\bar{\chi}$ (amu/mol) $-T$ (K) experimental data at $H = 10000$ G for this compound are shown (dotted line) in Figure 23.

Figure 23.

When increasing the magnetic field from 100 G to 10000 G, a small decrease in the $\bar{\chi}$ values with temperature but without changes in the general magnetic response of the sample were observed. From the experimental curve, a Curie-Weiss behavior is observed, which indicates a very weak magnetic coupling in the solid. When fitting the Curie-Weiss equation to the experimental data, excellent results were obtained, for which the parameters: $C = 0.3013$ emu K/mol, $\theta = -0.77$ K and $\bar{\chi}_0 = 0.00388$ emu/mol were found. The θ value indicates the existence of a very weak antiferromagnetic coupling in the solid product. From the $\bar{\chi}T - T$ data a continue increase of the slope of the line with descending the temperature is observed. Starting from *ca.* 5K and lowering T , a much higher slope of the line is obtained. This behavior is also in agreement with a very weak antiferromagnetic coupling in the solid product.

Considering the information discussed before for this compound, and in a first step of a magnetic analysis, a linear chain magnetic model was selected. The correspondent fitting of the Bonner-Fisher equation to the experimental data gave excellent results (the theoretical values are shown in Figure 23 with a solid line) for fixed $g = 2.12$, resulting the following parameters: $J = -6.96$ cm⁻¹, $\rho = 0.26$ and $\bar{\chi}_0 = 0.00188$ emu/mol. The J value is in full agreement with the suggestion of a very weak antiferromagnetic coupling between the unpaired electrons of the Cu(II) units. Further on in the magnetic analysis, and considering the structural suggestion for this compound that implies a bidimensional

polynuclear framework (a chain-type arrangement constructed by imidazolate⁻ moieties bridging Cu(II) atoms, and other one with the exocyclic $\underline{S}(6)$ atoms bridging also Cu(II) centers), the Bonner-Fisher equation with the Curie-Weiss correction was employed. Excellent results were obtained, with the following parameters for fixed $g = 2.12$: $J = -7.07$ cm⁻¹, $\theta = +0.08$ K $\rho = 0.26$ and $\bar{\chi}_0 = 0.0019$ emu/mol. However, the errors for the J and θ values obtained difficult the confidence of these parameters. Finally, employing the Bonner-Fisher equation with a mean-field correction, excellent fitting results were obtained. For fixed $g = 2.12$, $J = -11.77$ cm⁻¹, $zJ' = -0.97$ cm⁻¹, $\rho = 0.30$ and $\bar{\chi}_0 = 0.00144$ emu/mol were found. The J value is in agreement with its precedent calculation, and the zJ' value let us suggest the existence of a very weak interchain antiferromagnetic coupling. Both magnetic parameters would be in concordance with the scheme of a bidimensional polynuclear framework suggested for the Cu(II) compound in discussion.

To our knowledge, there are no studies reported up to date by other research groups about this Cu(II) compound. Under our research program, this same Cu(II) system has been synthesized both in aqueous (several pH values) and DMSO media[25].

With all the magnetic studies carried out for these Cu(II) compound containing the $\underline{S}(6)$ -purine derivative ligand, both common and different structural and magnetic features arise. With respect to the Cu(II) geometries, the spectroscopic and magnetic results support the suggestion of distorted tetracoordinated environments for the respective Cu(II) units, being Cu(II)(N)(S)(X)₂, Cu(II)(S)₂(X)₂ and Cu(II)(N)₂(S)₂ the correspondent chromophores proposed. These characteristics lead to differences in their spectral and magnetic properties. In particular and for the two first systems, the influence of the metallic bonding mode of the heterocyclic ligand and of the anion nature on the intensity of the antiferromagnetic coupling between the unpaired electrons of the Cu(II) units is clear. With respect to the last system, possibly the noticeable structural distortions on Cu(II) appear to play the major role on the very weak antiferromagnetic coupling found. For the two first cases, a polynuclear linear chain arrangement of interacting Cu(II) units through the halogen

atoms is proposed, with differences in the intensity of the intrachain antiferromagnetic coupling. Very weak interchain antiferromagnetic interactions are also suspected. For the last system, a bidimensional polynuclear framework with S and N,N groups as respective directional bridges has been previously proposed[25]. In this structural suggestion and for the magnetic model employed, both types of magnetic coupling (of very weak antiferromagnetic character) are suggested.

IV. Concluding remarks.

In the present study, both single and competitive heterocyclic ligand-Cu(II) interactions in methanolic medium were carried out. All the single reactions performed were successful, leading to new Cu(II) compounds with the respective heterocyclic ligands allopurinol, hypoxanthine and 6-mercaptapurine. For these compounds $M:(L)_2$ (for allopurinol and hypoxanthine), and $M:(L)_1$ or $M:(L)_2$ (for the 6-thiopurine ligand) stoichiometries were obtained. Also and for these systems, $Cu(II)(N)_2(X)_2$ units ($X=Cl^-$, Br^- and NO_3^-) for allopurinol and hypoxanthine were found. For the S(6)-purine derivative ligand, the $Cu(II)(N)_1(S)_1(X)_2$, $Cu(II)(S)_2(X)_2$ and $Cu(II)(N)_2(S)_2$ were obtained. Some of those single heterocycle-Cu(II) interactions ($X=Cl^-$) were also explored in DMSO solutions, leading to the same products as in methanolic medium.

The spectral and magnetic characterization of the Cu(II) compounds let us suggest the N(2) and N(7) atoms as respective metallic bonding sites for allopurinol and hypoxanthine. For the S(6)-purine derivative ligand the same characterization point the S(6)/N(7), S(6), and N(7)/N(9)/S(6) as the respective metallic bonding sites in its Cu(II) compounds.

From the competitive heterocycle-Cu(II) interactions carried out, several conclusions may be drawn. With regard to the reactions of heterocyclic ligand substitution, and for allopurinol and hypoxanthine, there was not interchange between these two ligands in the respective coordination sphere. Also, the 6-mercaptapurine as first bonded ligand was not substituted from the metallic coordination sphere. On the other hand, the S(6)-purine derivative as second and potential ligand is unsuccessful in substitution of allopurinol and

hypoxanthine for $X=\text{Cl}^-$ or Br^- , but it is successful for $X=\text{NO}_3^-$. Perhaps the lower coordination capacity of this last group contributes to its substitution and the same for allopurinol and hypoxanthine by the $\underline{\text{S}}(6)$ -purine derivative ligand.

With regard to simultaneously competitive heterocycle-Cu(II) interactions, a roughly equivalent competitiveness between allopurinol and hypoxanthine by the Cu(II) center was found. Interestingly, the $\underline{\text{S}}(6)$ -purine derivative was the heterocyclic ligand with the higher competitive coordination capacity. This behavior could be associated to the noticeable reactivity of this heterocycle through its exocyclic $\underline{\text{S}}(6)$ atom. In fact, the distinctive feature of this heterocycle in its coordination chemistry, is the preponderant involvement of that atom as metallic bonding site. This behavior has not been found for the $\underline{\text{O}}(4)$ or $\underline{\text{O}}(6)$ exocyclic atoms of allopurinol and hypoxanthine in their metallic coordination compounds. From all the competitive Heterocycle-Metal interactions carried out, no new Cu(II) compounds (and no mixed heterocyclic ligands Cu(II) compounds either) were obtained besides those yielded by the single reactions.

The spectral and magnetic studies carried out for the respective Cu(II) compounds with allopurinol, hypoxanthine and the $\underline{\text{S}}(6)$ -purine derivative obtained in this work, support the suggestion for almost all the cases of distorted tetracoordinated environments for the Cu(II) centers, and weak axial interactions with ligands from the nearest neighboring Cu(II) units. The magnetic characterization for the compounds with the neutral heterocyclic ligands is in agreement with the proposition of a structural linear chain-type arrangement through the intermolecular interactions quoted before. These intrachain interactions were found to be very weak, of antiferromagnetic character. The metallic counterions anionic ligands appear to be responsible of this magnetic behavior, through their participation in the superexchange magnetic coupling pathway. For some Cu(II) systems, the halogen nature influences the intensity of these magnetic interactions. In other cases, the possible spatial disposition of the coordinated heterocyclic ligand difficults that influence. For this structural arrangement proposition and from the correspondent magnetic model employed,

very weak interchain magnetic interactions were also detected. For the Cu(II) system with the deprotonated $\underline{\text{S}}(6)$ -purine derivative ligand, its spectral and magnetic characterization is in agreement with the suggestion of a polynuclear bidimensional framework, being the $\underline{\text{S}}(6)$ and the $\underline{\text{N}}(7)/\underline{\text{N}}(9)$ donor atoms the proposed bridging groups of the Cu(II) atoms. For this Cu(II) compound the magnetic characterization leads to the suggestion of very weak antiferromagnetic coupling between the unpaired electrons of the Cu(II) centers in the two directions proposed.

V. Acknowledgments

We are specially indebted to Prof. Roberto Escudero Derat (IIM/UNAM) for the exhaustive and carefully done magnetic measurements. We also thank Max Azomoza-Palacios (UAM-Iztapalapa) and Jorge Ramírez-Salcedo (IFC-UNAM) for the thermal results and the epr spectral determinations respectively. We also indebted to CONACyT (Grant 3170-E) for partial financial support.

Tables.

Table 1. Products obtained from both single and competitive heterocycle-Cu(II) interactions. a, See analytical results; 1, L₁-allopurinol; 2, L₂=hypoxanthine; 3, L₃=6-mercaptopurine.

Table 2. Analytical results of the Cu(II) coordination compounds with allopurinol (=L₁), hypoxanthine (=L₂) and 6-mercaptopurine (=L₃).

Table 3. IR bands and assignments for the free ligand allopurinol (=L₁) and its Cu(II) coordination compounds. Abbreviations: S, strong; M, medium; W, weak; VW, very weak; vbr, very broad; br, broad; s, sharp; sh, shoulder; d, doublet.

Table 4. IR bands and assignments for the free ligand hypoxanthine (=L₂) and its Cu(II) coordination compounds. The abbreviations are the same as in Table 3.

Table 5. IR bands and assignments for the free ligand 6-mercaptopurine (=L₃) and its Cu(II) coordination compounds. The abbreviations are the same as in Table 3.

Figure Captions.

Figure 1. Schematic drawing and numbering of allopurinol (I), hypoxanthine (II) and 6-mercaptopurine (III).

Figure 2. X-band ($\nu = 9.786$ Ghz) epr spectrum at room temperature of powdered Cu(II)(allopurinol)₂(Cl)₂·H₂O.

Figure 3. X-band ($\nu = 9.78$ Ghz) epr spectrum at room temperature of powdered Cu(II)(allopurinol)₂(Br)₂·3H₂O.

Figure 4. X-band ($\nu = 9.244$ Ghz) epr spectrum at room temperature of powdered Cu(II)(allopurinol)₂(NO₃)₂.

Figure 5. X-band ($\nu = 9.244$ Ghz) epr spectrum at room temperature of powdered Cu(II)(hypoxanthine)₂(Cl)₂.

Figure 6. X-band ($\nu = 9.244$ Ghz) epr spectrum at room temperature of powdered Cu(II)(hypoxanthine)₂(Br)₂.

Figure 7. X-band ($\nu = 9.244$ Ghz) epr spectrum at room temperature of powdered $\text{Cu(II)(hypoxanthine)}_2(\text{NO}_3)_2$.

Figure 8. X-band ($\nu = 9.244$ Ghz) epr spectrum at room temperature and 77 K of powdered $\text{Cu(II)(hypoxanthine)}_2(\text{NO}_3)_2$.

Figure 9. X-band ($\nu = 9.244$ Ghz) epr spectrum at room temperature of powdered $\text{Cu(II)(6-mercaptopurine)}_1(\text{Cl})_2$.

Figure 10. X-band ($\nu = 9.244$ Ghz) epr spectrum at room temperature of powdered $\text{Cu(II)(6-mercaptopurine)}_2(\text{Br})_2$.

Figure 11. X-band ($\nu = 9.244$ Ghz) epr spectrum at room temperature of powdered $\text{Cu(II)(6-mercaptopurinolate}^{2-}) \cdot 2\text{H}_2\text{O}$.

Figure 12. $\bar{\chi}$ (emu/mol) - T (K) values for $\text{Cu(II)(allopurinol)}_2(\text{Cl})_2 \cdot \text{H}_2\text{O}$ ($H = 10000$ G). Dotted line: experimental values; solid line: theoretical prediction from a linear chain magnetic model.

Figure 13. Schematic drawing of the structural features suggested for $\text{Cu(II)(allopurinol)}_2(\text{Cl})_2 \cdot \text{H}_2\text{O}$ and its interactions.

Figure 14. $\bar{\chi}$ (emu/mol) - T (K) values for $\text{Cu(II)(allopurinol)}_2(\text{Br})_2 \cdot 3\text{H}_2\text{O}$ ($H = 10000$ G). Dotted line: experimental values; solid line: theoretical prediction from a linear chain magnetic model.

Figure 15. $\bar{\chi}$ (emu/mol) - T (K) values for $\text{Cu(II)(allopurinol)}_2(\text{NO}_3)_2$ ($H = 100$ G). Dotted line: experimental values; solid line: theoretical prediction from a linear chain magnetic model.

Figure 16. $\bar{\chi}$ (emu/mol) - T (K) values for $\text{Cu(II)(allopurinol)}_2(\text{NO}_3)_2$ ($H = 100$ G). Dotted line: experimental values, $\rho = 0$; solid line: theoretical prediction from a linear chain magnetic model.

Figure 17. $\bar{\chi}$ (emu/mol) - T (K) values for $\text{Cu(II)(hypoxanthine)}_2(\text{Cl})_2$ ($H = 100$ G). Dotted line: experimental values; solid line: theoretical prediction from a linear chain magnetic model.

Figure 18. $\bar{\chi}$ (emu/mol) - T (K) values for $\text{Cu(II)(hypoxanthine)}_2(\text{Br})_2$ ($H = 100$ G). Dotted line: experimental values; solid line: theoretical prediction from a linear chain magnetic model.

Figure 19. $\bar{\chi}$ (emu/mol) - T (K) values for $\text{Cu(II)(hypoxanthine)}_2(\text{NO}_3)_2$ ($H = 10000$ G). Dotted line: experimental values; solid line: theoretical prediction from a linear chain magnetic model.

Figure 20. $\bar{\chi}$ (emu/mol) - T (K) values for $\text{Cu(II)(6-mercaptopurine)}_1(\text{Cl})_2$ ($H = 100$ G). Dotted line: experimental values; solid line: theoretical prediction from a linear chain magnetic model.

Figure 21. Schematic drawing of the structural features suggested for $\text{Cu(II)(6-mercaptopurine)}_1(\text{Cl})_2$ and its interactions.

Figure 22. $\bar{\chi}$ (emu/mol) - T (K) values for $\text{Cu(II)(6-mercaptopurine)}_2(\text{Br})_2$ ($H = 100$ G). Dotted line: experimental values; solid line: theoretical prediction from a linear chain magnetic model.

Figure 23. $\bar{\chi}$ (emu/mol) - T (K) values for $\text{Cu(II)(6-mercaptopurinolate}^{2-}) \cdot 2\text{H}_2\text{O}$ ($H = 10000$ G). Dotted line: experimental values; solid line: theoretical prediction from a linear chain magnetic model.

References

- [1] M.N. Hughes, *The Inorganic Chemistry of Biological Processes*, 2nd. Ed., John Wiley & Sons, USA, 1981.
- [2] R.K. Robins, G.R. Revankar, D.E. O'Brien, R.H. Springer, T. Novinson, A. Albert, K. Senga, J.P. Miller and D.G. Streeter, *J. Heterocyclic Chem.*, **22**, 601 (1985).
- [3] L. Stryer, *Biochemistry*, 3rd Ed., Freeman, New York, 1988.
- [4] R. Acevedo-Chávez, M.E. Costas and R. Escudero-Derat, *J. Solid State Chem.*, **113**, 21 (1994) and references quoted.
- [5] *CRC Handbook of Nucleobase Complexes*, Vol. I, J.R. Lusty, Ed., CRC Press, Inc., USA, 1990 and references therein.
- [6] E. Dubler and E. Gyr, *Inorg. Chem.*, **27**, 1446 (1988) and references therein.
- [7] R. Acevedo-Chávez and N. Barba-Behrens, *Transition Met. Chem.*, **15**, 434 (1990) and references therein.
- [8] M.Q. Olazábal, J.M.S. Peregrín, M.P.S. Sánchez, F.G. Vilchez and M.R. Medina, *Thermochimica Acta*, **103**, 305 (1986).
- [9] C.M. Mikulski, S. Grossman, C.J. Lee and N.M. Karayannis, *Transition Metal Chem.*, **12**, 21 (1987).
- [10] C.M. Mikulski, S. Grossman and N.M. Karayannis, *J. Less- Common Met.*, **136**, 41 (1987).
- [11] D. Mulet, A.M. Calafat, J.J. Fiol, A. Terron and V. Moreno, *Inorg. Chim. Acta.*, **138**, 199 (1987).
- [12] E. Dubler, G. Hänggi and W. Bensch, *J. Inorg. Biochem.*, **29**, 269 (1987).
- [13] C.M. Mikulski, M.K. Kurlan, M.L. Bayne, M. Gaul and N.M. Karayannis, *J. Coord. Chem.*, **18**, 297 (1988).
- [14] C.M. Mikulski, M.L. Bayne, S. Grossman, M. Gaul, A. Renn, D.L. Staley and N.M. Karayannis, *J. Coord. Chem.*, **20**, 185 (1989).

- [15] C.M. Mikulski, S. Grossman, M.L. Bayne, M. Gaul, D.L. Staley, A. Renn and N.M. Karayannis, *Inorg. Chim. Acta.*, **161**, 29 (1989).
- [16] N. Katsaros and A. Grigoratou, *J. Inorg. Biochem.*, **25**, 131 (1985).
- [17] N. Kottmair and W. Beck, *Inorg. Chim. Acta.*, **34**, 137 (1979).
- [18] J. Brigando, D. Colaitis and M. Morel, *Bull. Soc. Chim. Fr.*, **10**, 3440 (1969).
- [19] P. Piperaki, N. Katsaros and D. Katakis, *Inorg. Chim. Acta*, **67**, 37 (1982).
- [20] R. Barbieri, E. Rivarola, F. Di Bianca and F. Huber, *Inorg. Chim. Acta*, **57**, 37 (1982).
- [21] L. Perelló, J. Borrás, L. Soto, F.J. Gordo and J.C. Gordo, *Monats. Chem.*, **115**, 1377 (1984).
- [22] N. Hadjiliadis and T. Theophanides, *Inorg. Chim. Acta.*, **15**, 167 (1975).
- [23] N.B. Behrens and D.M.L. Goodgame, *Inorg. Chim. Acta*, **46**, 45 (1980).
- [24] N. Kottmair and W. Beck, *Inorg. Chim. Acta*, **34**, 137 (1979).
- [25] R. Acevedo-Chávez, M.E. Costas and R. Escudero, *6-mercaptapurine - Cu(II) interactions. The Spectral and magnetic study of the novel amorphous polynuclear compound $[Cu(II)(6\text{-mercaptapurinolate}^{2-})_n$* , Submitted for publication.
- [26] J. Foley, D. Kennefick, D. Phelan, S. Tyagi and B.J. Hathaway, *J. Chem. Soc. Dalton Trans.*, **2333** (1983).
- [27] J. Foley, S. Tyagi and B.J. Hathaway, *J. Chem. Soc. Dalton Trans.*, **1** (1984).
- [28] R. Acevedo-Chávez, M.E. Costas and R. Escudero, *Allopurinol and Hypoxanthine Cu(II) compounds. Spectral and Magnetic Studies of Novel Dinuclear Coordination Compounds with Bridging Hypoxanthine*, *Inorg. Chem.*, In press.
- [29] R.J. Fereday, P. Hodgson, S. Tyagi and B.J. Hathaway, *J. Chem. Soc. Dalton Trans.*, **2070** (1981).
- [30] M.Q. Olazábal, J.M.S. Peregrín, M.P.S. Sánchez, F.G. Vilchez and M.R. Medina, *Thermochimica Acta*, **103**, 305 (1986).
- [31] D. Sonnenfroh and R.W. Kreilick, *Inorg. Chem.*, **19**, 1259 (1980) and references therein.

- [32] T. Asakawa, M. Inoue, K.I. Hara and M. Kubo, *Bull. Chem. Soc. Jpn.*, **45**, 1054 (1972).
- [33] E. Sletten and A. Apeland, *Acta Cryst.*, **B31**, 2019 (1975).
- [34] E.A.H. Griffith and E.L. Amma, *J. Chem. Soc. Chem. Comm.*, 1013 (1979).
- [35] N.B. Behrens and D.M.L. Goodgame, *Inorg. Chim. Acta*, **46**, 45 (1980).

Reaction ¹	Cl ⁻			Br ⁻			NO ₃ ⁻		
	t (days)	Color	Prod.(s) ^a	t (days)	Color	Prod.(s) ^a	t (days)	Color	Prod.(s) ^a
M+L ₁ ⇌	5.0	pale green-blue	1	4.0	dark green	4	8.0	lilac	7
M+L ₂ ⇌	5.0	deep blue	2	7.0	deep blue	5	8.0	deep blue	8
M+L ₃ ⇌	5.0	dark green	3	9.0	ocree	6	8.0	dark green	9
[M+L ₁]+L ₂ ⇌	5.0	pale green-blue	1	5.0	dark green	4	10.0	lilac	7
[M+L ₁]+L ₃ ⇌	7.0	pale green-blue	1	9.0	dark green	4	10.0	dark green	9
[M+L ₂]+L ₁ ⇌	5.0	deep blue	2	5.0	deep blue	5	10.0	deep blue	8
[M+L ₂]+L ₃ ⇌	7.0	deep blue	2	9.0	deep blue	5	10.0	drak green	9
[M+L ₃]+L ₁ ⇌	8.0	dark green	3	7.0	ocree	6	10.0	dark green	9
[M+L ₃]+L ₂ ⇌	14.0	dark green	3	7.0	ocree	6	10.0	dark green	9
(L ₁ +L ₂)+M ⇌	8.0	deep blue-green	1/2	8.0	deep blue-green	4/5	10.0	deep blue-lilac	7/8
(L ₁ +L ₃)+M ⇌	6.0	dark green	3	7.0	ocree	6	10.0	dark green	9
(L ₂ +L ₃)+M ⇌	9.0	dark green	3	7.0	ocree	6	10.0	dark green	9
(L ₁ +L ₂ +L ₃)+M ⇌	6.0	dark green	3	7.0	ocree	6	10.0	dark green	9

Table 1.

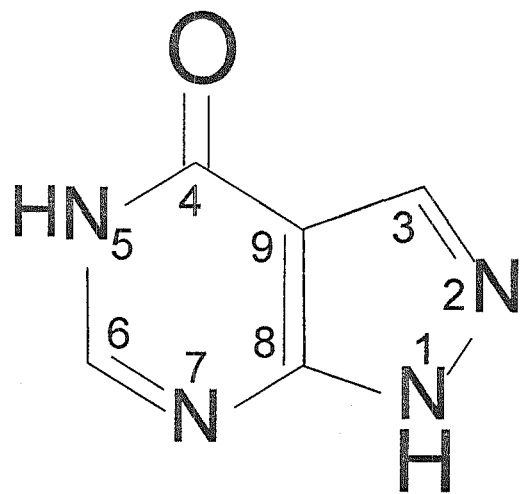
Formulation	Compound	Expected			Found		
		% C	% H	% N	% C	% H	% N
$\text{Cu}(\text{L}_1)_2(\text{Cl})_2 \cdot \text{H}_2\text{O}$	1	28.30	2.40	26.40	28.60	2.00	25.90
$\text{Cu}(\text{L}_2)_2(\text{Cl})_2$	2	29.53	1.98	27.55	29.70	1.80	27.10
$\text{Cu}(\text{L}_3)_1(\text{Cl})_2$	3	20.95	1.41	19.55	20.42	1.56	19.43
$\text{Cu}(\text{L}_1)_2(\text{Br})_2 \cdot 3\text{H}_2\text{O}$	4	21.80	2.60	20.40	21.80	2.40	19.10
$\text{Cu}(\text{L}_2)_2(\text{Br})_2$	5	24.24	1.63	22.61	25.58	1.44	23.74
$\text{Cu}(\text{L}_3)_2(\text{Br})_2$	6	22.76	1.53	21.23	23.00	1.53	21.00
$\text{Cu}(\text{L}_1)_2(\text{NO}_3)_2$	7	26.12	1.75	30.46	26.33	1.67	29.55
$\text{Cu}(\text{L}_2)_2(\text{NO}_3)_2$	8	26.12	1.75	30.46	26.23	1.94	30.59
$\text{Cu}(\text{L}_3^{2-}) \cdot 2\text{H}_2\text{O}$	9	24.05	2.42	22.43	23.76	2.71	21.72

Table 2.

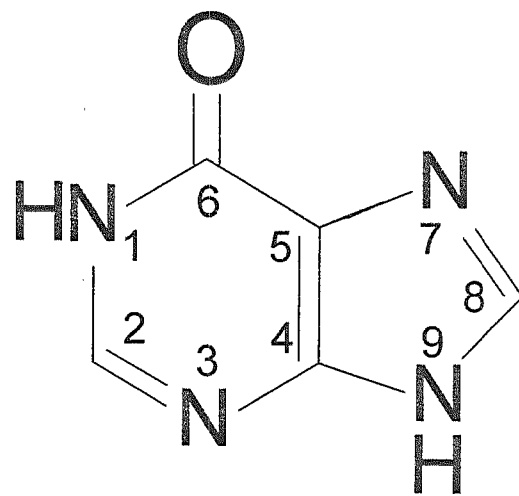
Allopurinol (=L ₁)		Cu(L ₁) ₂ (Cl) ₂ ·H ₂ O		Cu(L ₁) ₂ (Br) ₂ ·3H ₂ O		Cu(L ₁) ₂ (NO ₃) ₂		Assignments
$\bar{\nu}$ cm ⁻¹	Charac.	$\bar{\nu}$ cm ⁻¹	Charac.	$\bar{\nu}$ cm ⁻¹	Charac.	$\bar{\nu}$ cm ⁻¹	Charac.	
-	-	-	-	3500	W, vbr	-	-	ν_{OH_2}
-	-	3240	S, s	-	-	-	-	ν_{N-H} /hydrogen bonds
3170	VW, br	3160	VW, br	3170	Sh	3170	Sh	ν_{C-H} arom./ ν_{N-H}
-	-	3110	VW, br	-	-	-	-	ν_{C-H} arom./ ν_{N-H}
3080	VW, br	3070	VW, br	3080	Sh	3080	Sh	ν_{C-H} arom./ ν_{N-H}
2960	S, br	2960	Sh	2950	Sh	2960	Sh	ν_{C-H} arom./ ν_{N-H}
1700	S, br	1685	S, br	1690	S, br	1675	S, br	$\nu_{C=O}/\nu_{C=C}/\nu_{C=N}$
1595	S, br	1603	M, s	1600	M, br	1600	M, s	δ_{N_5-H} /ring vib.
-	-	1570	S, s	1560	W, br	1540	VW, br	ring vib.
-	-	-	-	1510	W, br	1505	W, br	
1390	S, br	1403	M, s	1400	W, br	1410	VW, s	ring vib.
1370	S, s	1383	M, s	1350	VW, br	1340	VW, br	pyrazolic ring vib/ ν_{C-N}
-	-	1290	W, s	-	-	-	-	ring vib./ ν_{C-N}
1240	S, br	1260	VW, s	1253	M, br	1200	M, br	A" $\delta_{C-H}/\nu_{C-C}/\nu_{C-N}$
-	-	1240	M, br	-	-	-	-	
1230	S, br	1230	M, br	1225	M, sh	-	-	A" $\delta_{C-H}/\nu_{C-C}/\nu_{C-N}$
1160	W, br	1143	W, s	1153	W, br	1165	W, s	A" $\delta_{C-H}/A"$ δ_{N-H}
-	-	1105	W, s	-	-	-	-	A" $\delta_{C-H}/A"$ δ_{N-H}
1080	M, br	1075	W, br	1090	W, br	1095	M, s	C-H vib.
-	-	-	-	1065	W, br	-	-	C-H vib.
960	S, s	975	M, s	995	VW, s	940	W, br	pyrazolic ring vib.
-	-	-	-	970	VW, s	-	-	
-	-	-	-	950	VW, s	-	-	
-	-	935	VW, br	-	-	-	-	ring vib./C-H vib.
915	S, s	915	M, s	910	W, s	910	VW, br	rin vib./A" δ_{N-H}
885	S, br	860	W, br	870	VW, s	870	W, br	γ_{C-H} /ring vib.
-	-	-	-	850	-	-	-	
815	M, br	-	-	-	-	823	W, s	γ_{C-H}
785	S, s	790	M, s	770	M, br	780	W, s	ring vib./C-H vib.
710	S, s	717	W, br	720	VW, br	700	W, s	C-H vib.
-	-	690	W, br	-	-	-	-	C-H vib.
-	-	680	W, br	-	-	-	-	
605	S, s	620	M, s	-	-	595	M, s	ring vib.
-	-	573	M, s	-	-	570	W, s	ring vib.
550	M, s	550	M, s	565	M, s	550	M, s	skelet. vib.
540	M, s	-	-	525	M, s	-	-	skelet. vib.
-	-	-	-	455	VW, br	-	-	skelet. vib.
326	M, s	390	W, s	400	M, s	400	M, s	skelet. vib.
220	VW, br	225	W, br	215	W, br	225	VW, s	skelet. vib.
210	VW, br	210	W, br	210	W, br	-	-	skelet. vib.
-	-	336	M, br	-	-	-	-	ν_{Cu} -ligand
-	-	320	M, br	326	M, s	310	M, br	ν_{Cu} -ligand
-	-	300	M, Sh	290	W, s	300	W, s	ν_{Cu} -ligand
-	-	-	-	265	M, br	285	M, br	ν_{Cu} -ligand
-	-	-	-	253	M, br	-	-	ν_{Cu} -ligand

6-oxopurine (=L ₂)		Cu(L ₂) ₂ (Cl) ₂		Cu(L ₂) ₂ (Br) ₂		Cu(L ₂) ₂ (NO ₃) ₂		Assignments
$\bar{\nu}$ cm ⁻¹	Charac.	$\bar{\nu}$ cm ⁻¹	Charac.	$\bar{\nu}$ cm ⁻¹	Charac.	$\bar{\nu}$ cm ⁻¹	Charac.	
-	-	3540	W,s	3520	W,s	-	-	n.a.
-	-	3480	W,s	3460	W,s	-	-	n.a.
-	-	-	-	-	-	3460	M,sh	n.a.
-	-	-	-	3160	Sh	-	-	ν_{C-H} arom./ ν_{N-H}
3140	W,s	3140	Sh	3120	VW,s	3200	W,br	ν_{C-H} arom./ ν_{N-H}
3050	W,br	3060	Sh	3060	VW,s	3090	W,s	ν_{C-H} arom./ ν_{N-H}
2960	S,br	2960	S,sh	2920	S,sh	2960	S,sh	ν_{C-H} arom./ ν_{N-H}
1670	S,br	1690	S,br	1670	S,br	1690	S,br	$\nu_{C=O}/\nu_{C=C}/\nu_{C=N}$
1583	M,br	1603	W,br	1585	W,br	1595	M,br	δ_{N_1-H}
1516	VW,br	1550	W,br	1530	VW,br	1520	VW,br	ring vib./ ν_{C-N}/δ_{N-H}
1424	M,s	1415	M,br	1400	M,br	1400	M,s	ring vib./ ν_{C-N}/δ_{N-H}
1380	W,s	1390	M,br	1370	M,br	-	-	ring vib./ ν_{C-N}/δ_{N-H}
1350	M,s	1330	M,br	1320	M,br	-	-	ring vib./ ν_{C-N}/δ_{N-H}
-	-	-	-	1300	M,sh	-	-	ring vib./ ν_{C-N}/δ_{N-H}
1276	M,s	1260	W,br	1250	W,br	1250	S,br	ring vib./ ν_{C-N}/δ_{N-H}
1215	S,s	1190	S,br	1175	S,br	1200	W,s	ring vib./ ν_{C-N}/δ_{N-H}
1153	M,s	1170	M,s	1155	M,br	1135	VW,s	ring vib./ ν_{C-N}/δ_{N-H}
1140	M,s	1105	M,s	1095	W,br	1110	M,br	ring vib./ ν_{C-N}/δ_{N-H}
-	-	-	-	-	-	1085	M,sh	ring vib./ ν_{C-N}/δ_{N-H}
966	M,br	970	VW,br	960	VW,br	945	VW,s	ring vib./ δ_{C-H}
910	VW,br	950	VW,s	920	VW,br	920	M,s	rin vib./C-H vib.
		935	VW,s					
893	S,s	896	VW,br	885	VW,br	870	VW,br	ring vib./C-H vib.
793	M,s	800	W,s	780	VW,br	800	M,sh	ring vib./C-H vib.
		790	M,s					
-	-	726	W,br	715	VW,br	-	-	C-H vib.
		705	W,s					
646	M,s	650	M,s	635	M,br	650	W,d	C-H vib./skeletal vib.
633	M,s	625	VW,s	-	-	610	S,br	C-H vib./skeletal vib.
-	-	596	VW,s	600	M,br	-	-	C-H vib./skeletal vib.
566	M,s	573	M,br	590	M,br	540	M,br	C-H vib./skeletal vib.
525	W,s	-	-	540	M,br	-	-	skeletal vib.
-	-	423	W,br	445	W,br	-	-	skeletal vib.
367	M,s	-	-	400	M,br	375	M,br	skeletal vib.
345	W,s	-	-	-	-	355	VW,sh	skeletal vib.
243	VW,br	250	W,s	-	-	243	VW,br	skeletal vib.
223	VW,br	225	VW,br	225	VW,br	220	VW,br	skeletal vib.
210	VW,br	210	VW,br	210	VW,br	210	VW,br	skeletal vib.
-	-	298	S,br	280	S,br	300	M,d	$\nu_{Cu-ligand}$
-	-	-	-	-	-	280	M,d	$\nu_{Cu-ligand}$

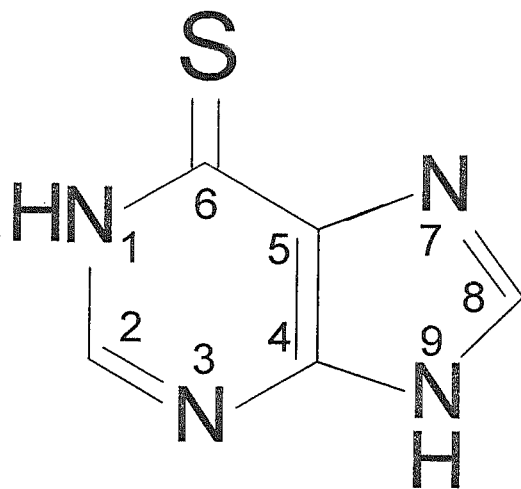
6-mercaptapurine (=L ₃)		Cu(L ₃)(Cl) ₂		Cu(L ₃) ₂ (Br) ₂		Cu(L ₃ ²⁻)·H ₂ O		Assignments
$\bar{\nu}$ cm ⁻¹	Charac.	$\bar{\nu}$ cm ⁻¹	Charac.	$\bar{\nu}$ cm ⁻¹	Charac.	$\bar{\nu}$ cm ⁻¹	Charac.	
3425	M,br	-	-	-	-	-	-	ν_{N-H} arom.
-	-	-	-	-	-	3400	W,sh	ν_{C-H} arom.
3140	W,sh	3130	Sh	-	-	-	-	ν_{C-H} arom./ ν_{N-H}
3090	W,sh	3090	Sh	3090	W,br	-	-	ν_{C-H} arom./ ν_{N-H}
2960	S,sh	2960	S,sh	2940	S,sh	-	-	ν_{C-H} arom./ ν_{N-H}
1610	S,br	1625 1600	S,d	-	-	-	-	$\delta_{N_1-H}/\nu_{C=C}/\nu_{C=N}$
-	-	-	-	1610	S,br	1580	S,br	$\nu_{C=C}/\nu_{C=N}$
1575	S,br	1580 1550	VW,d	-	-	-	-	$\nu_{R-N-C=S}$ (I)
-	-	-	-	1543	S,s	-	-	δ_{N_1-H}
1520	W,br	-	-	-	-	-	-	$\nu_{C=N}$ /ring vib.
1410	S,s	1410	Sh	1385	S,sh	1400	S,br	ν_{C-N}/ν_{C-C} /ring vib.
1345	M,s	1340	Sh	1335	M,s	-	-	$\nu_{R-N-C=S}$ (II)
-	-	-	-	1300	Sh	-	-	n.a.
1275	M,s	1250	Sh	-	-	1300	VW,br	ν_{C-N} /ring vib.
-	-	-	-	1250	Sh	1250	Sh	n.a.
1220	S,br	1215	M,br	1210	M,s	1220	M,br	$\delta_{CNC}/\delta_{NCN}$ /ring vib.
1150	W,sh	1175	W,sh	1175	M,s	1185	Sh	$\nu_{C=S}$ /ring vib.
1115	W,br	1130	W,sh	1130	W,s	-	-	$\nu_{R-N-C=S}$ (III)
-	-	1040	VW,br	-	-	-	-	n.a.
1010	M,br	970	W,br	1033	M,s	1025	VW,br	$\delta_{C-H}/\delta_{C-N}$ /ring vib.
930	M,br	900	W,br	970	W,br	960	VW,br	δ_{C-H} /imidazolic ring vib.
870	M,br	865	W,br	900	M,s	880	VW,br	δ_{C-H} /ring vib.
780	W,br	726	W,br	770	W,s	790	VW,br	δ_{C-H} /ring vib.
-	-	-	-	720	M,br	720	M,br	n.a.
675	W,s	675	Sh	-	-	-	-	ν_{C-S} /ring vib.
650	M,s	643	W,s	640	M,br	645	W,d	ν_{C-S} /ring vib.
600	M,s	606	VW,br	605	M,br	-	-	skelet. vib.
579	M,s	573	VW,br	570	M,br	575	W,br	skelet. vib.
552	W,s	555	VW,br	553 540	M,d	-	-	skelet. vib.
518	W,br	515	VW,s	505	VW,br	518	W,br	skelet. vib.
425	W,br	440	VW,br	456	M,br	425	VW,s	skelet. vib.
-	-	324	M,br	-	-	317	M,br	skelet. vib.
296	M,s	293	M,br	306	M,br	300	M,br	skelet. vib.
-	-	270 252	M,s W,br	-	-	-	-	n.a.
237	M,br	230	M,br	230	M,br	240	M,s	skelet. vib.
170	M,br	190	M,br	-	-	200	M,br	skelet. vib.
108	M,s	147	S,s	115	S,br	-	-	skelet. vib.
77	S,s	-	-	-	-	-	-	skelet. vib.
-	-	324	M,br	-	-	-	-	ν_{Cu} -ligand
-	-	293	M,br	-	-	270	M,br	ν_{Cu} -ligand
-	-	230	M,br	230	M,br	216	M,s	ν_{Cu} -ligand
-	-	-	-	115	S,br	-	-	ν_{Cu} -ligand



I

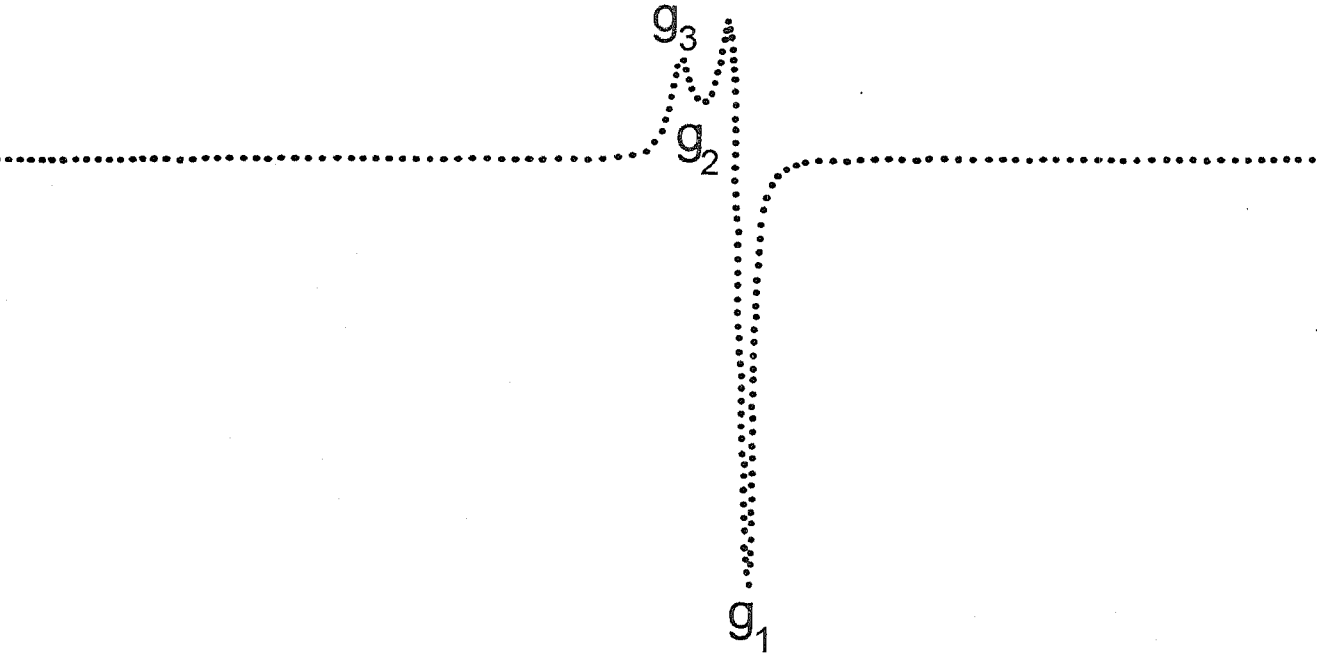


II

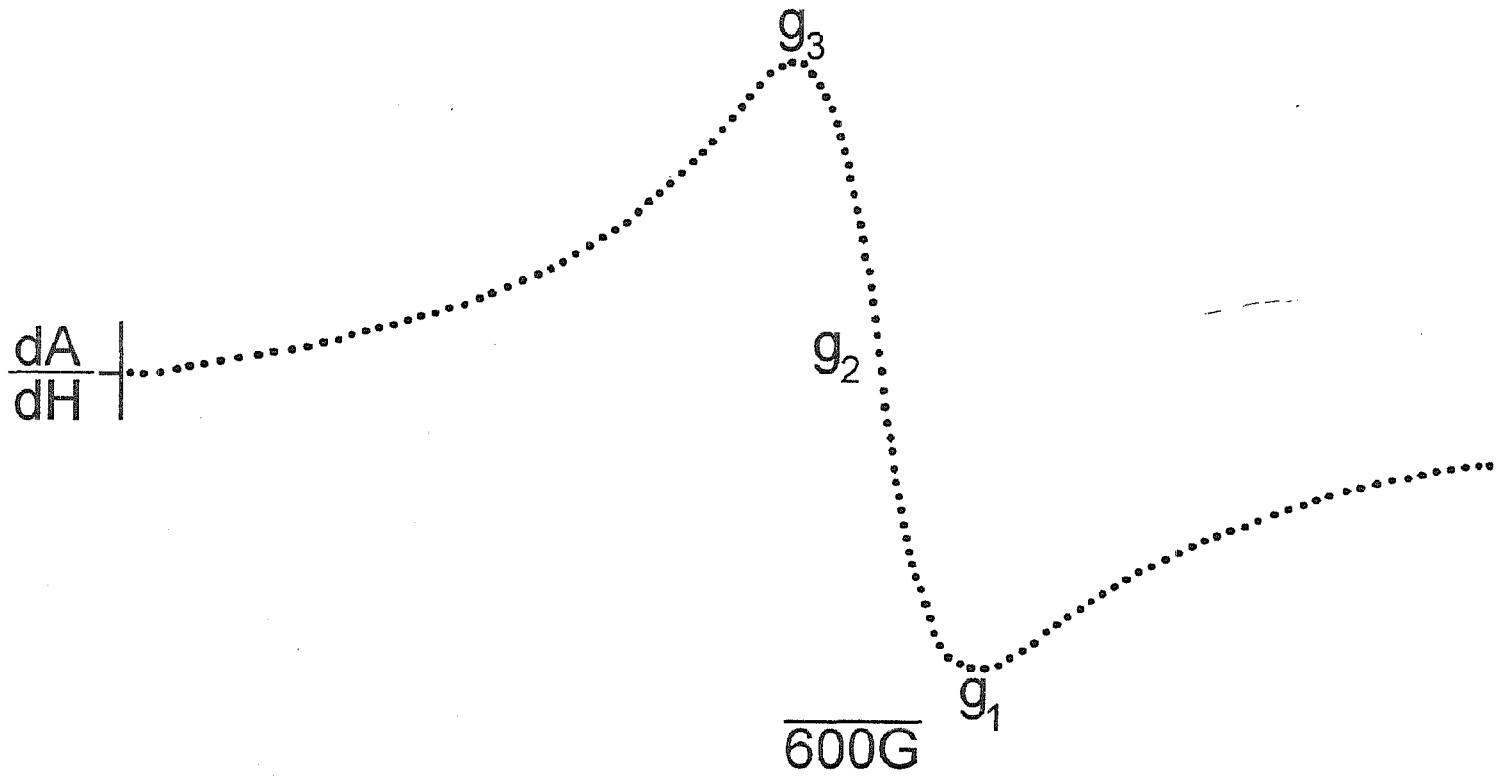


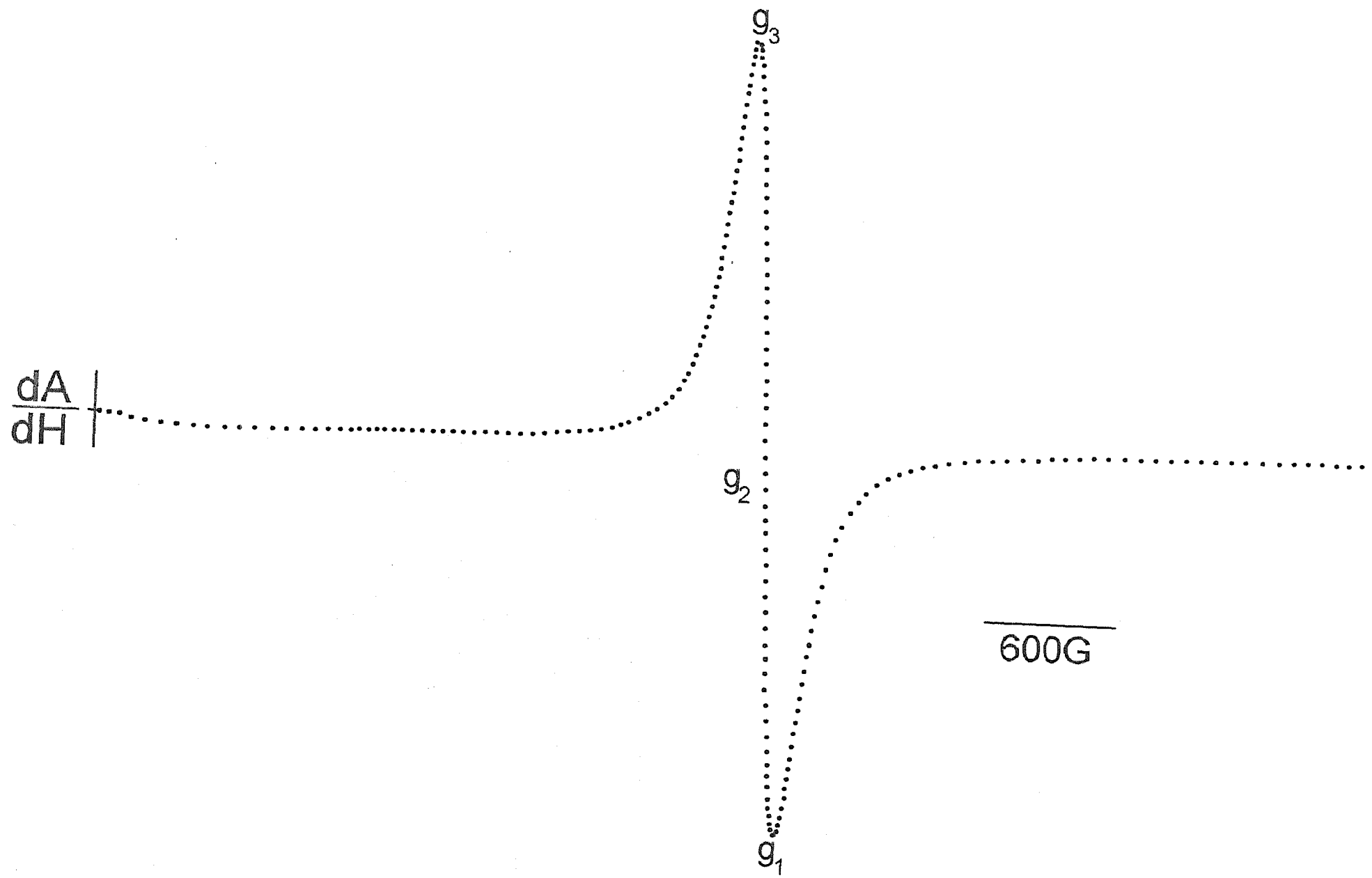
III

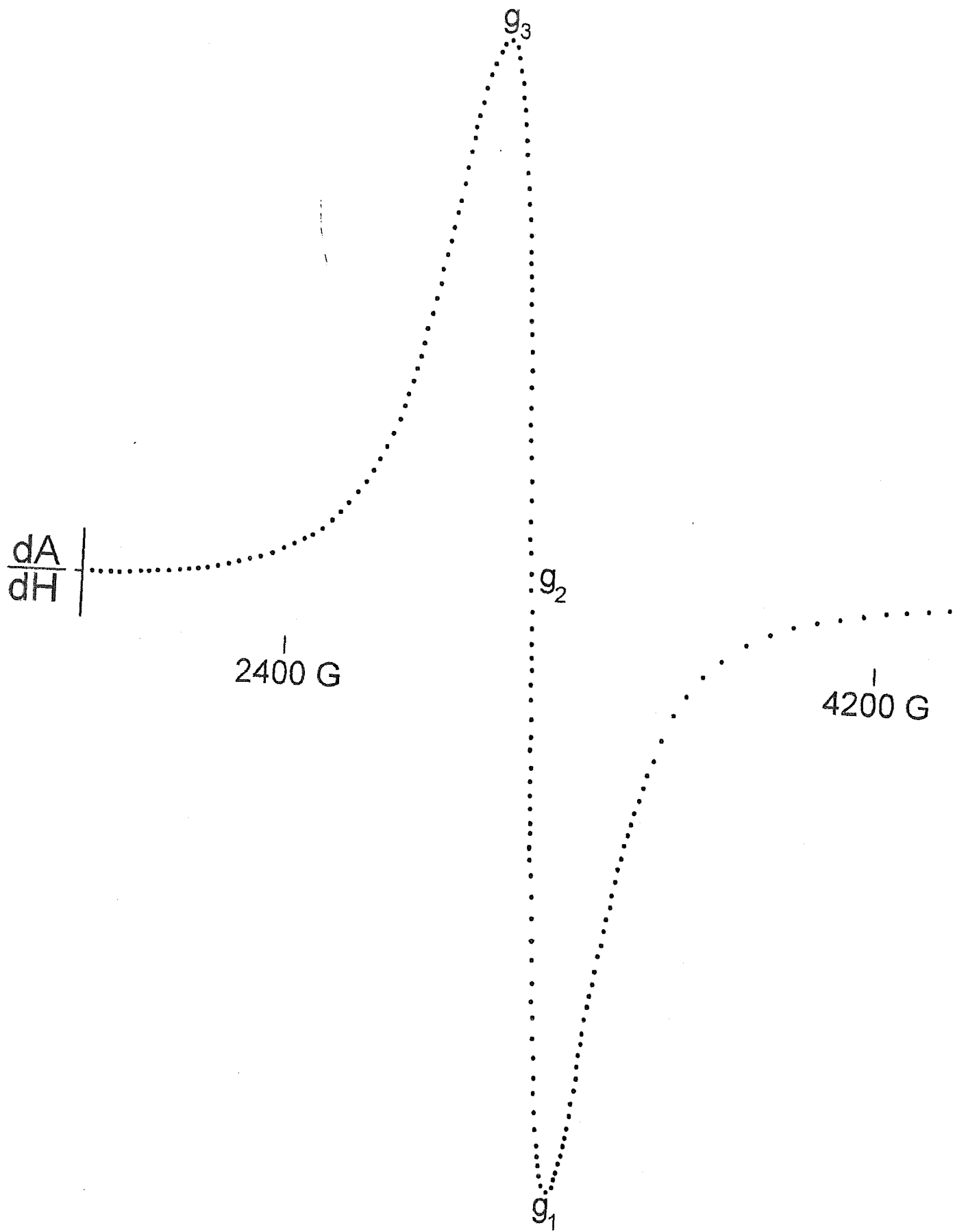
$\frac{dA}{dH}$

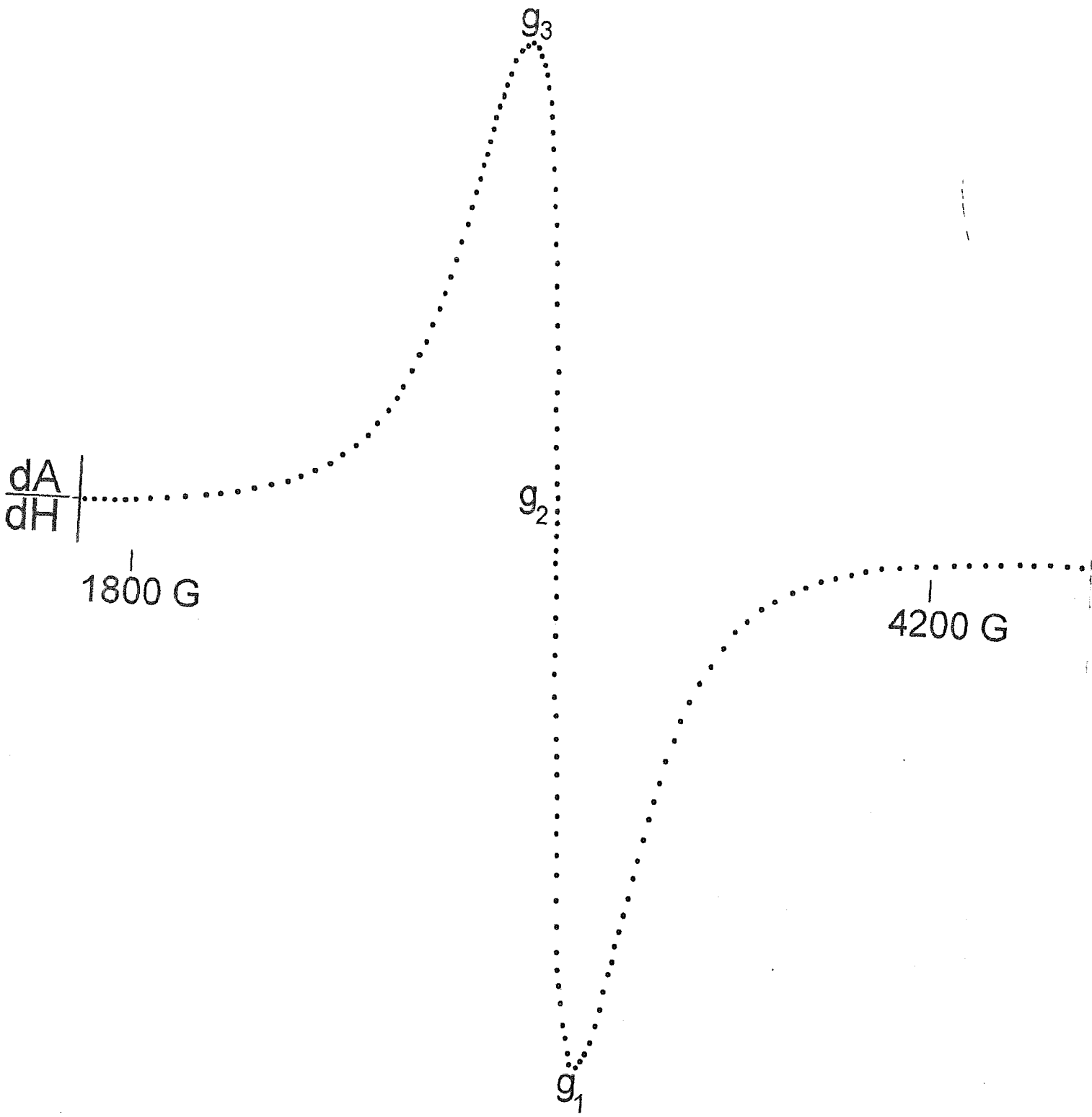


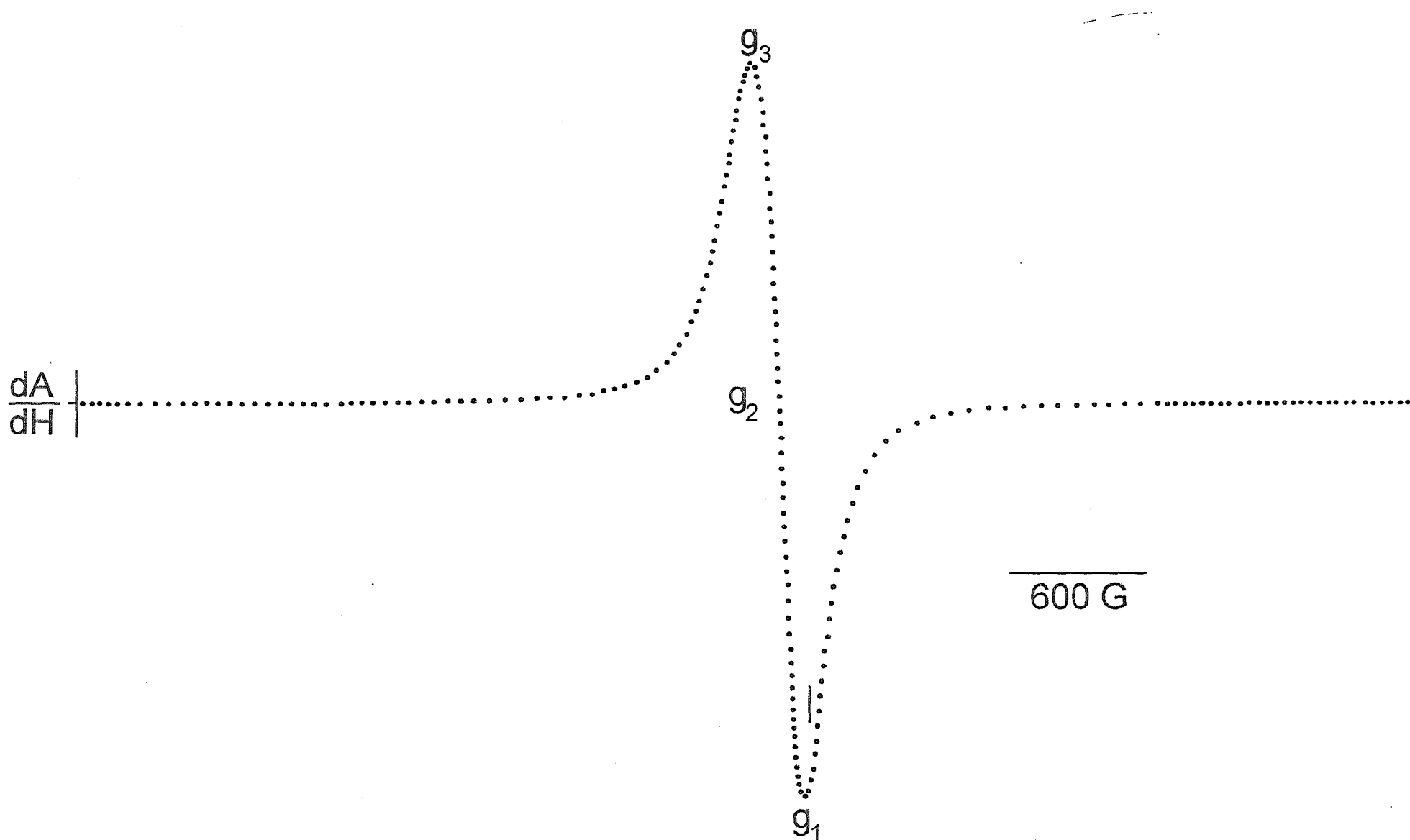
600G











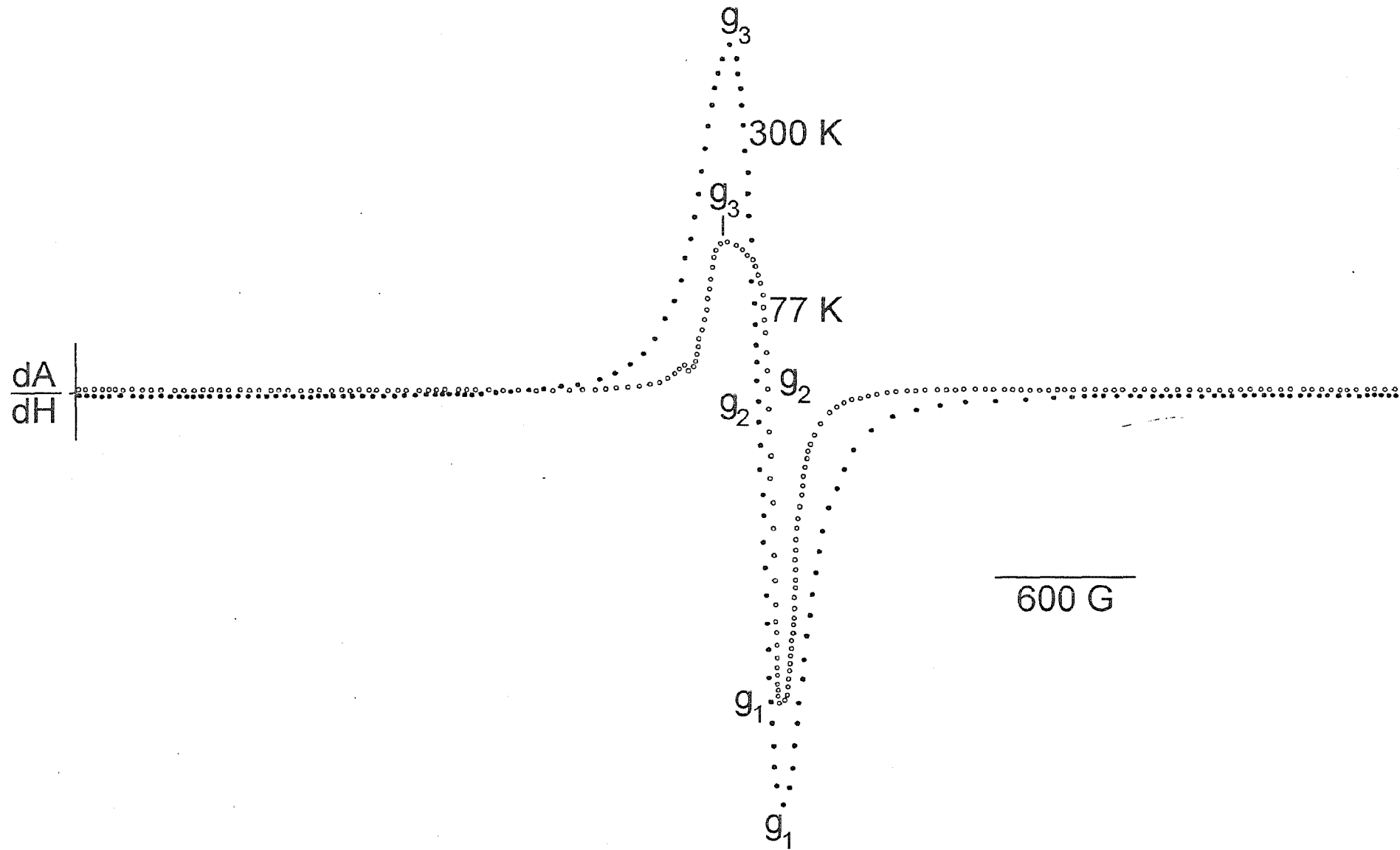
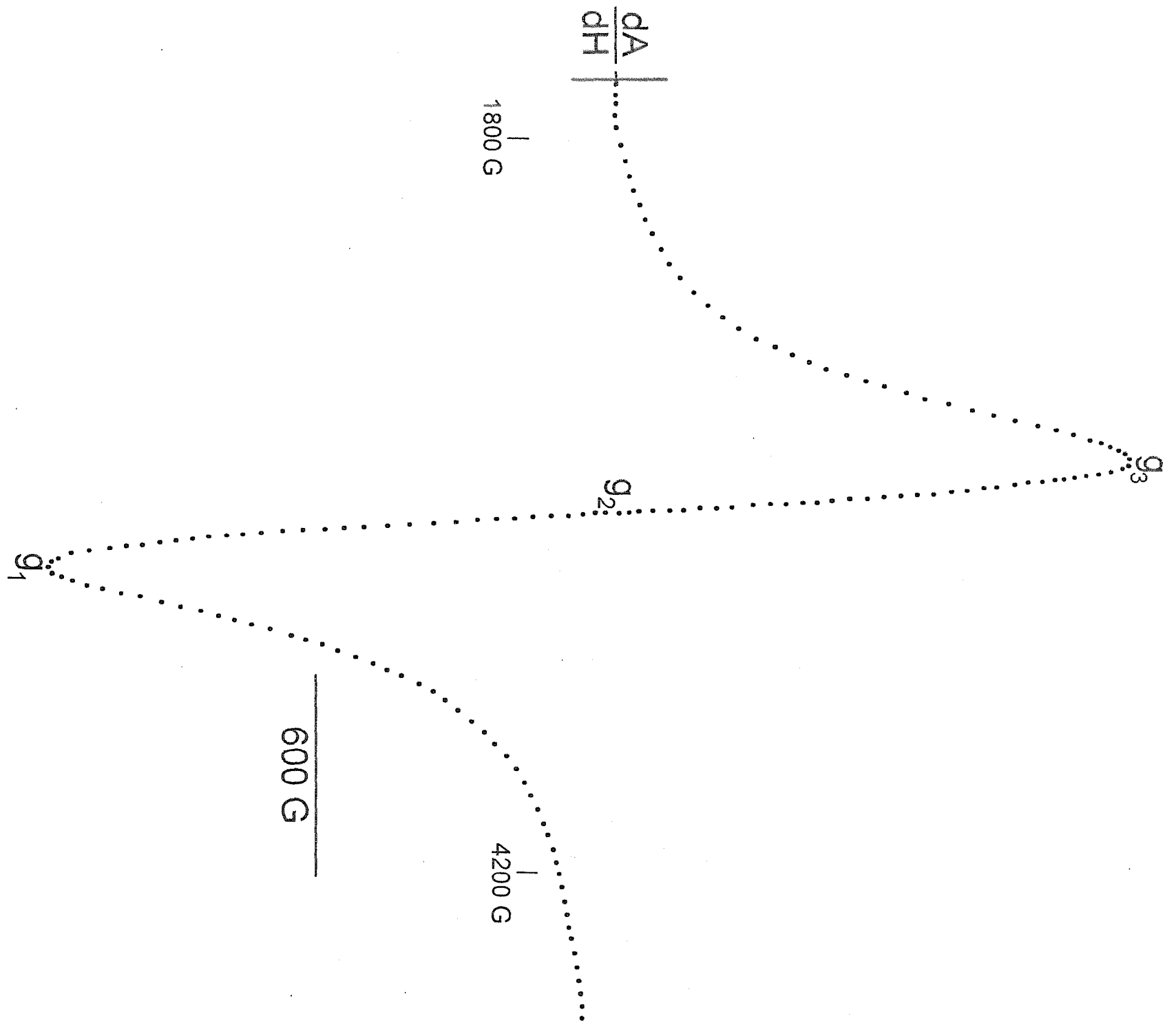
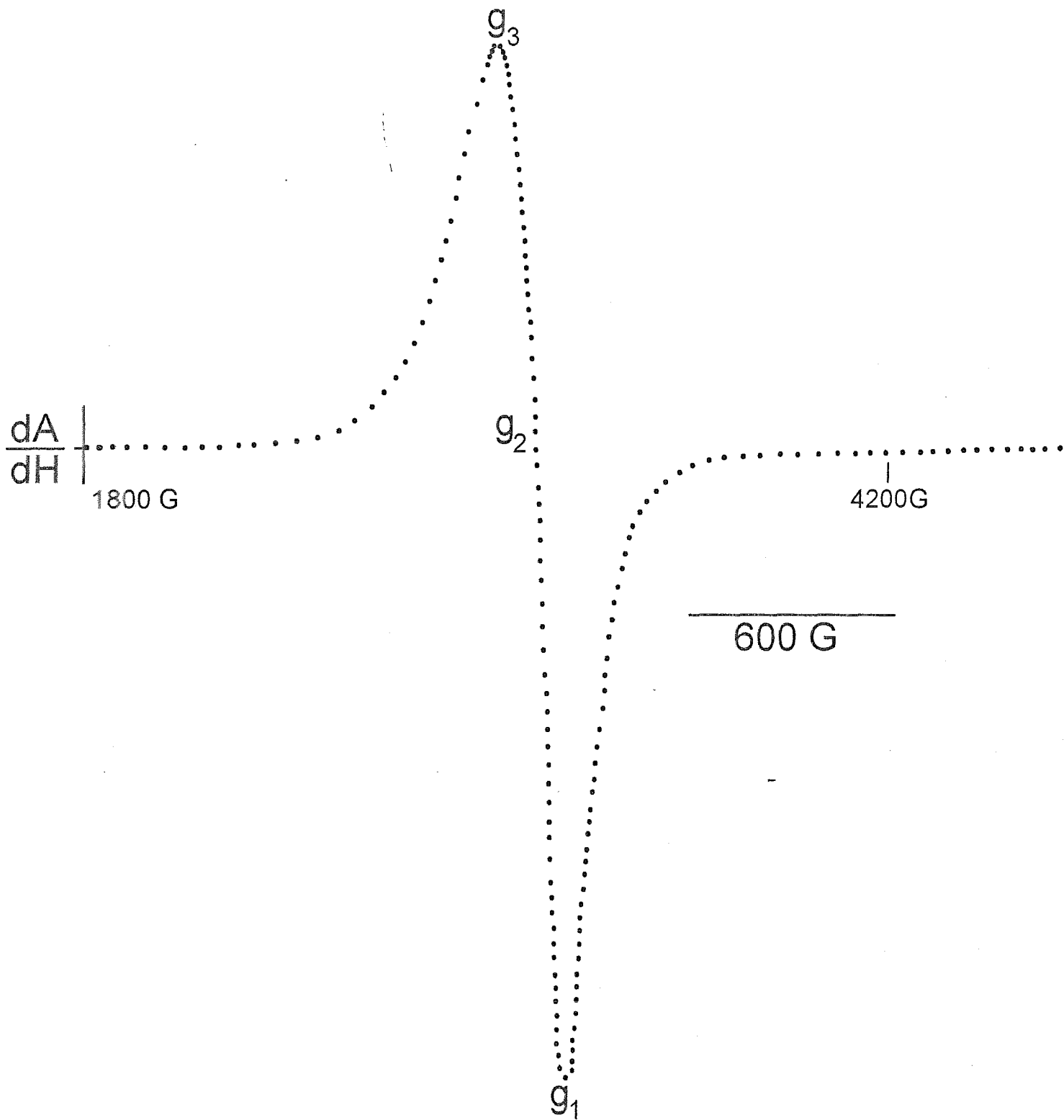


Fig. 1





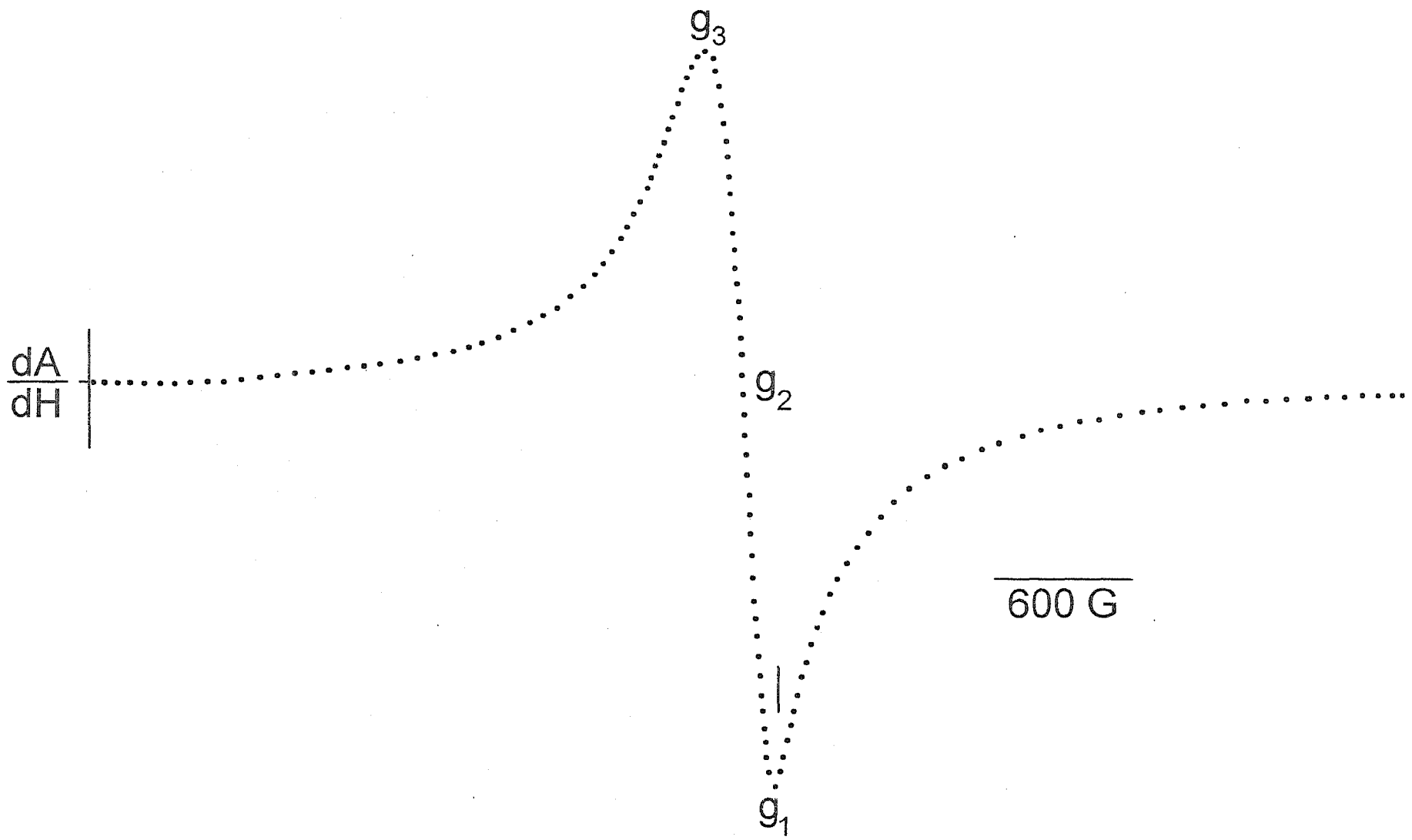
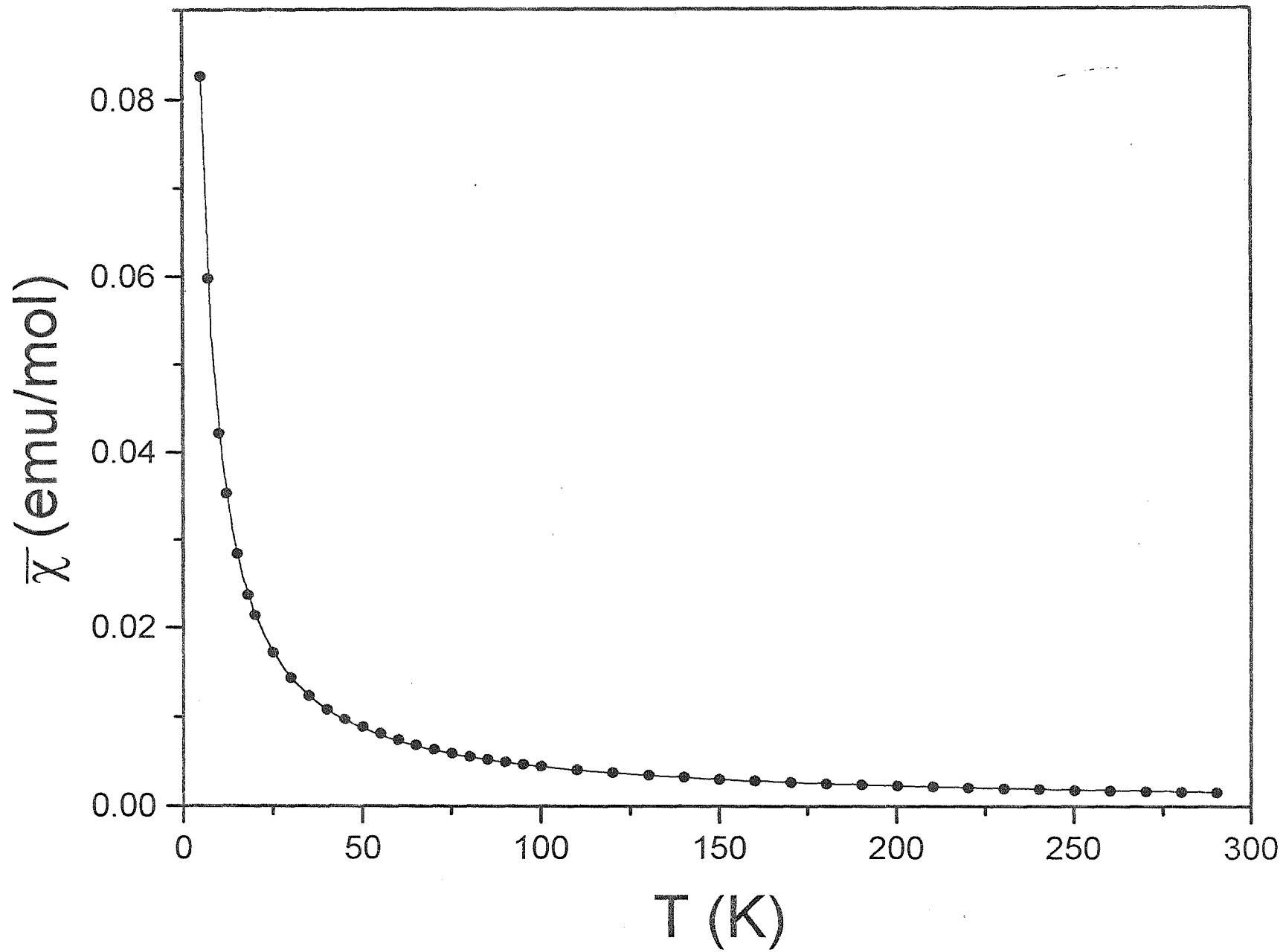


Fig. 1



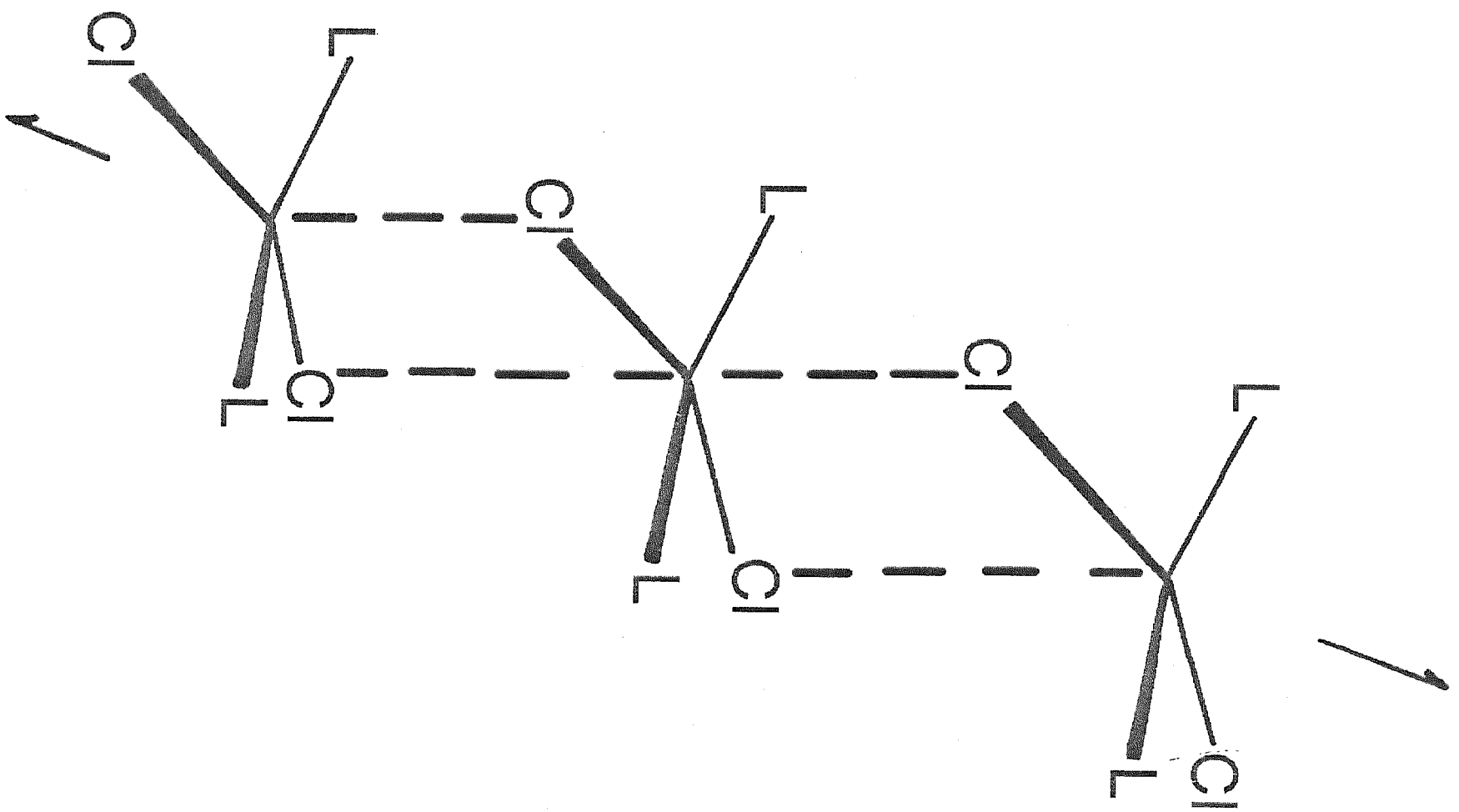
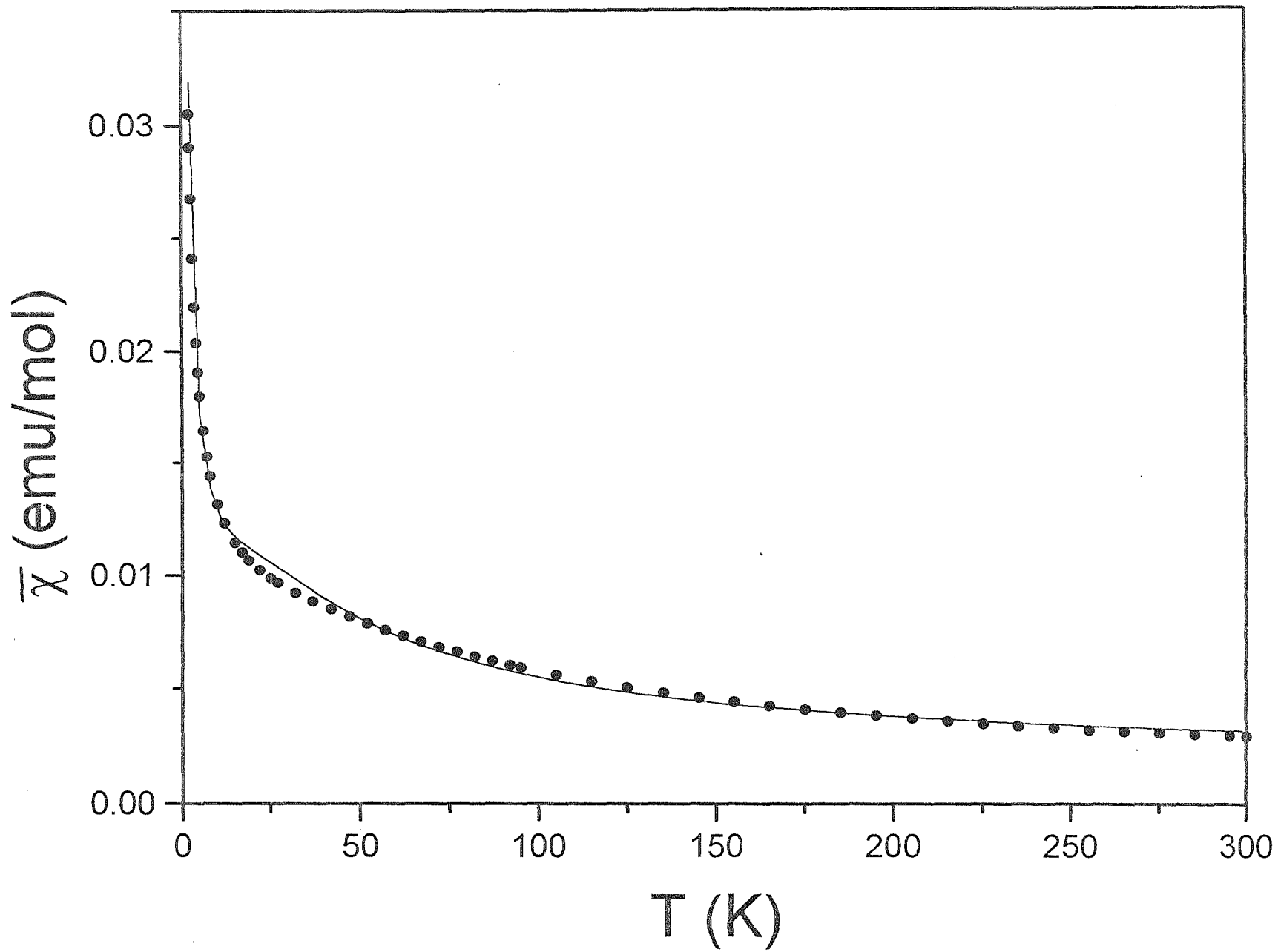
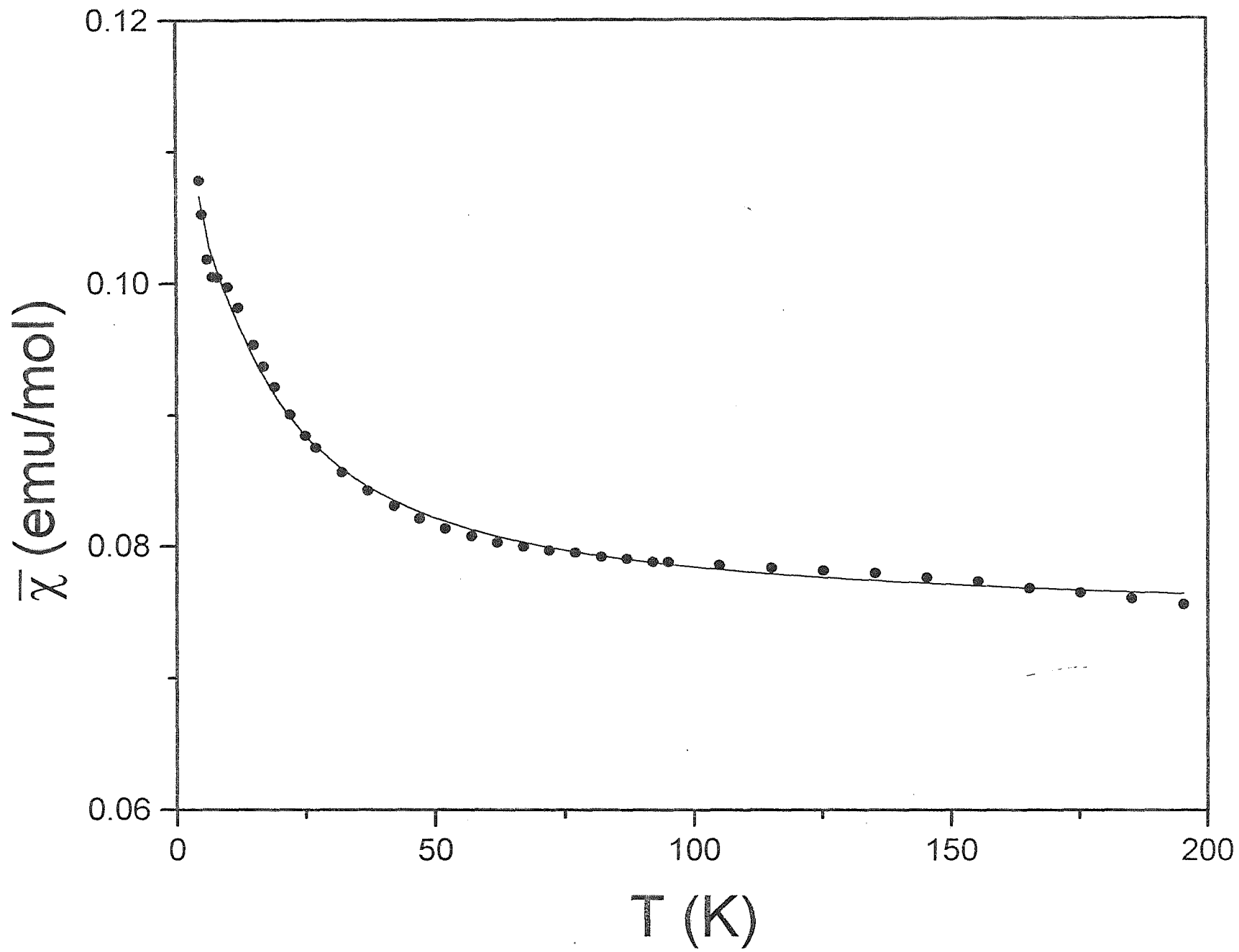
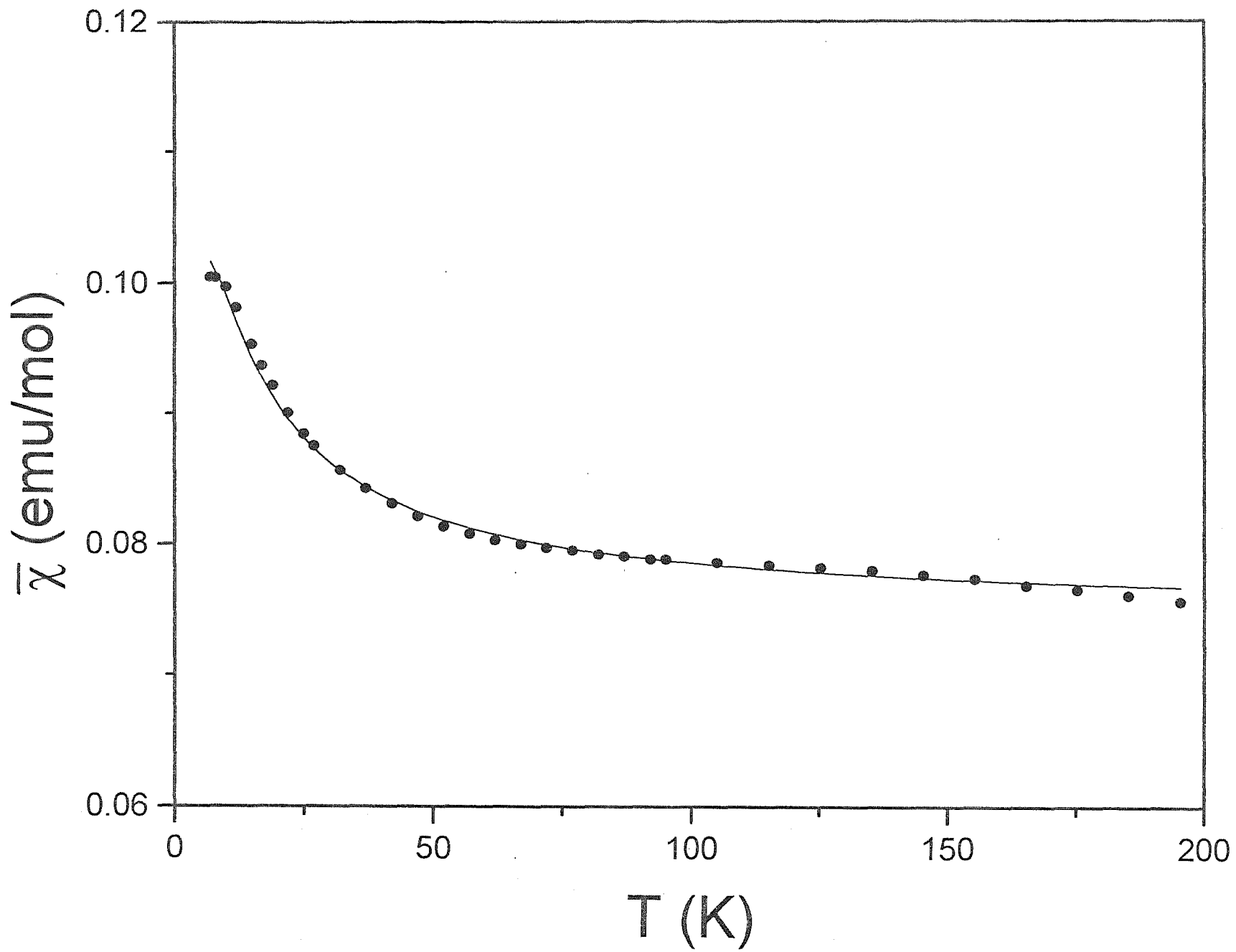
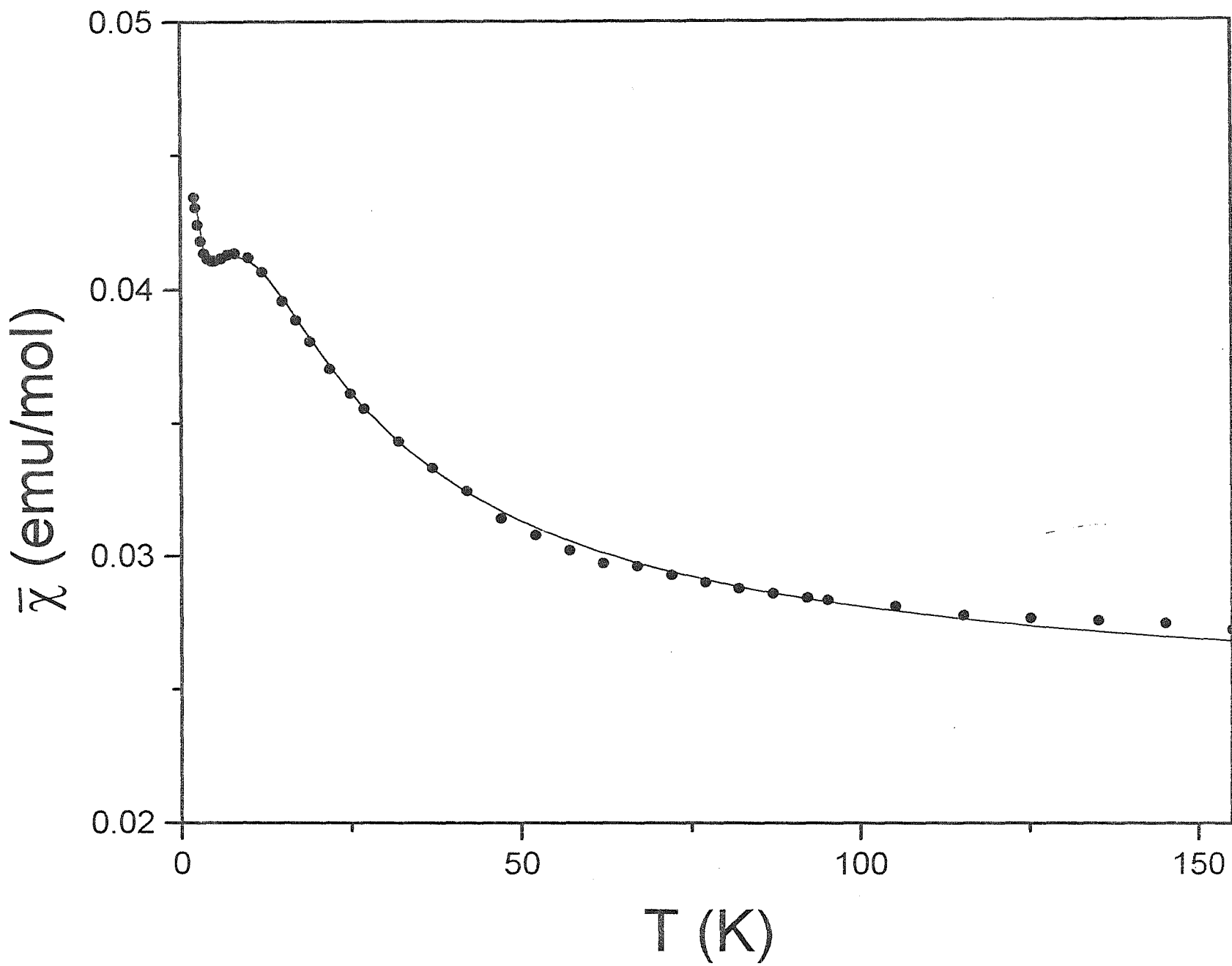


Fig 1









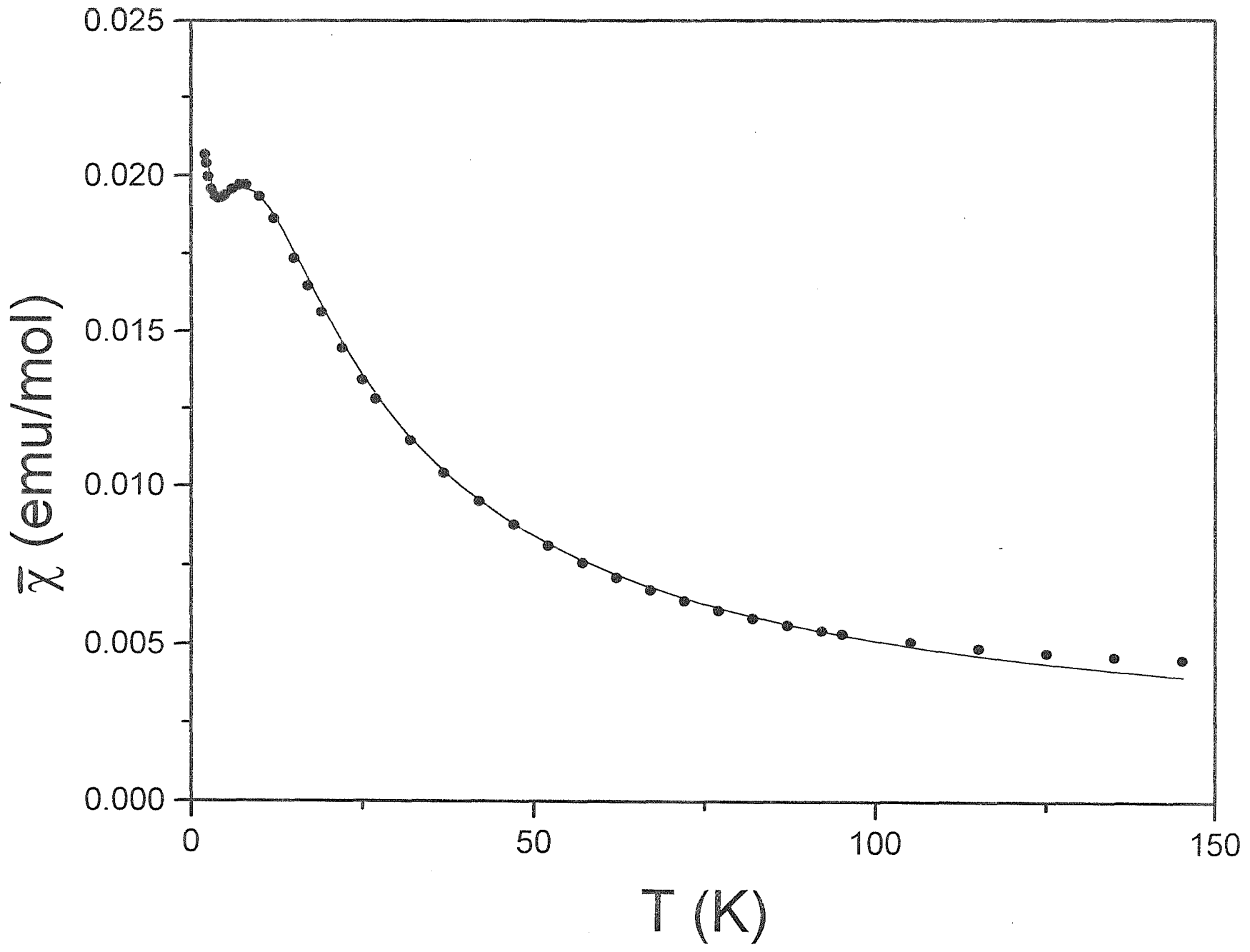
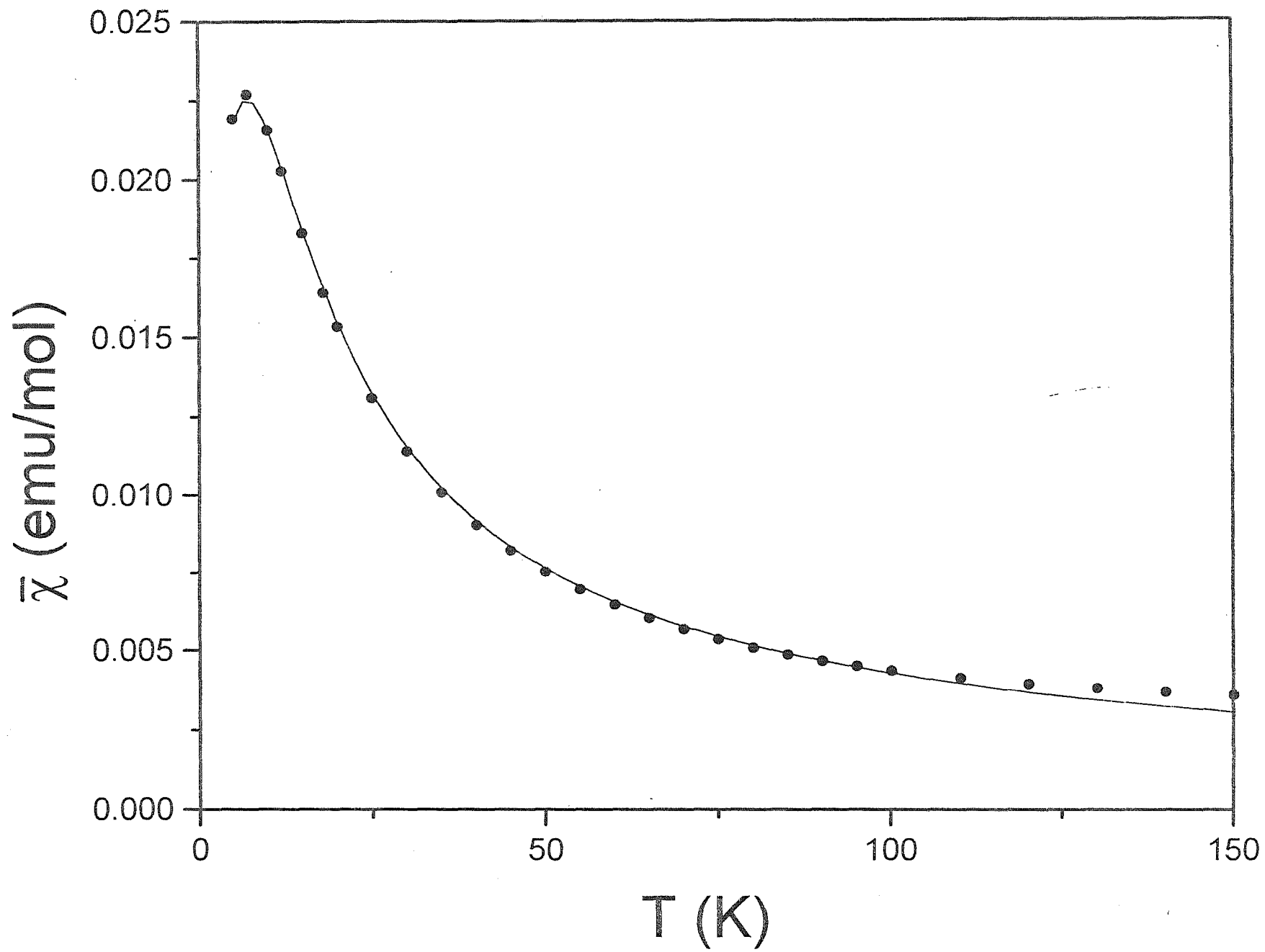
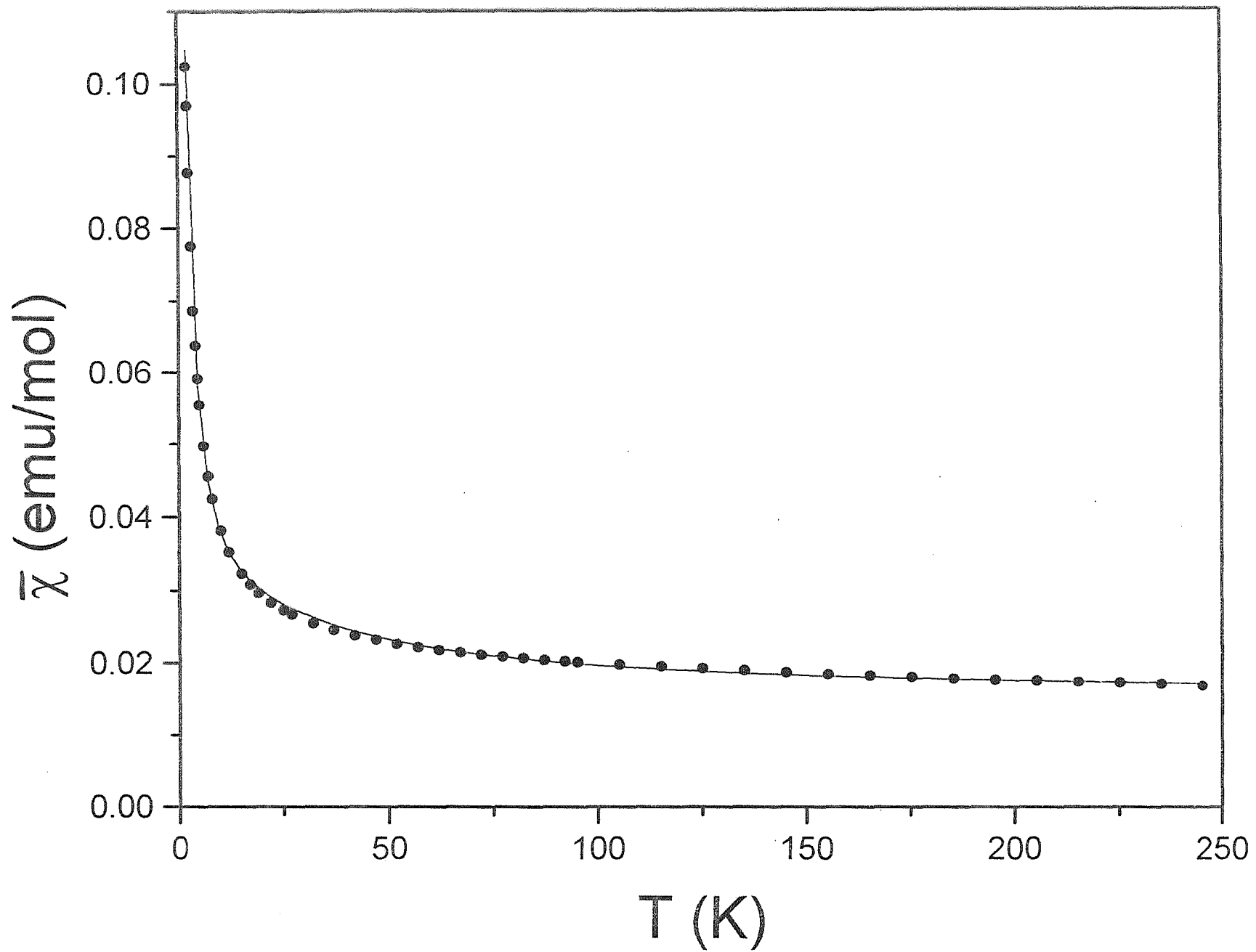
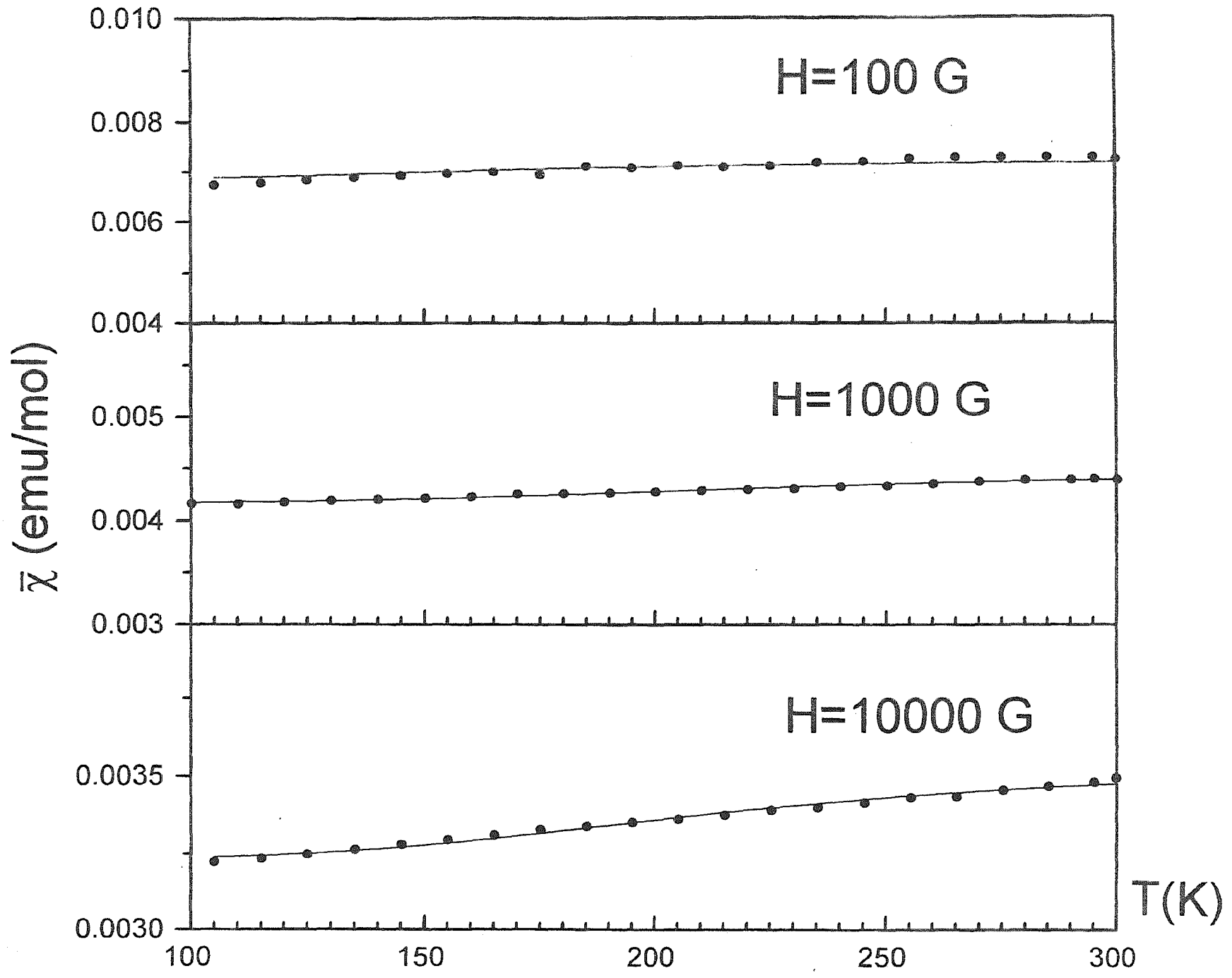
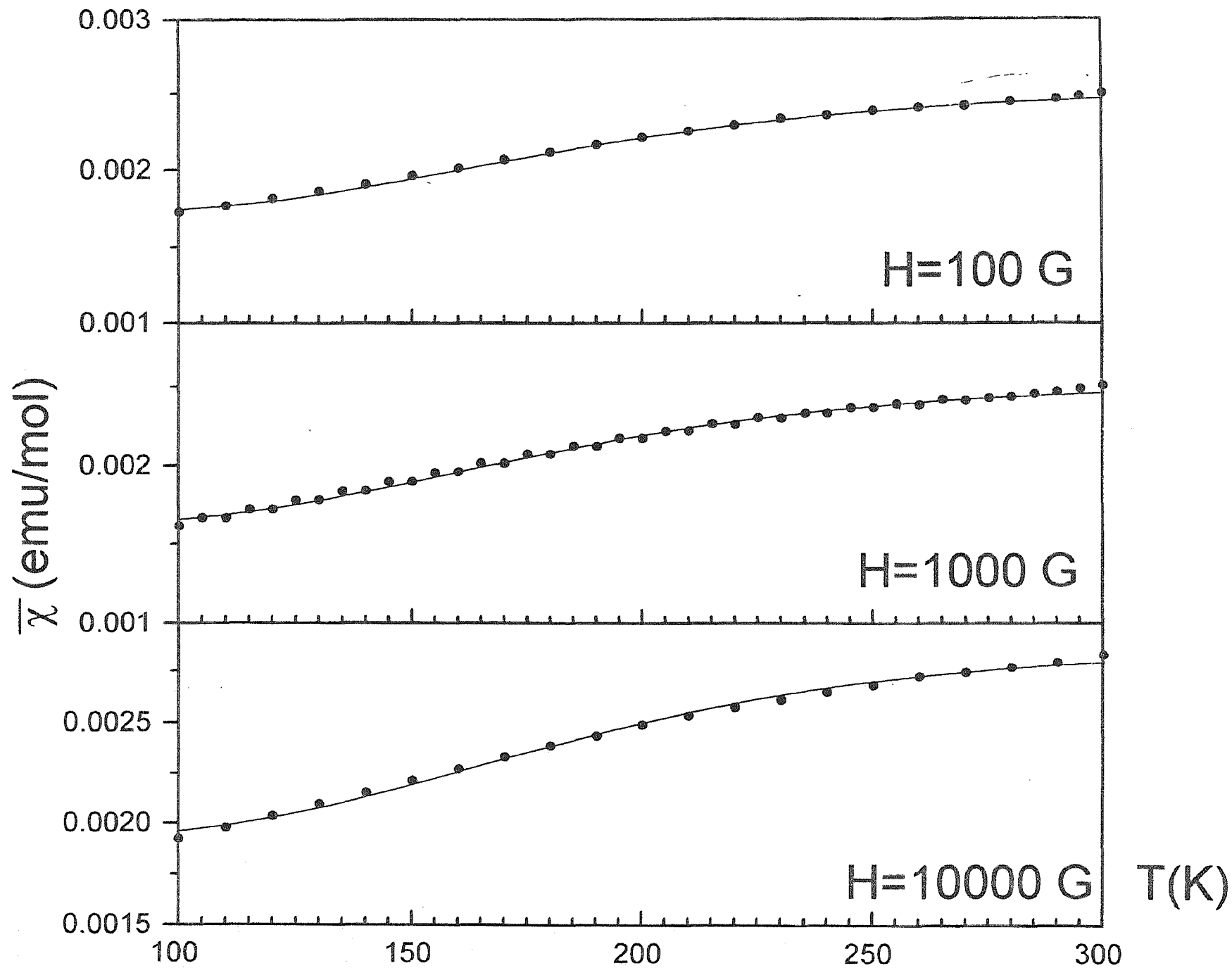


Fig. 1









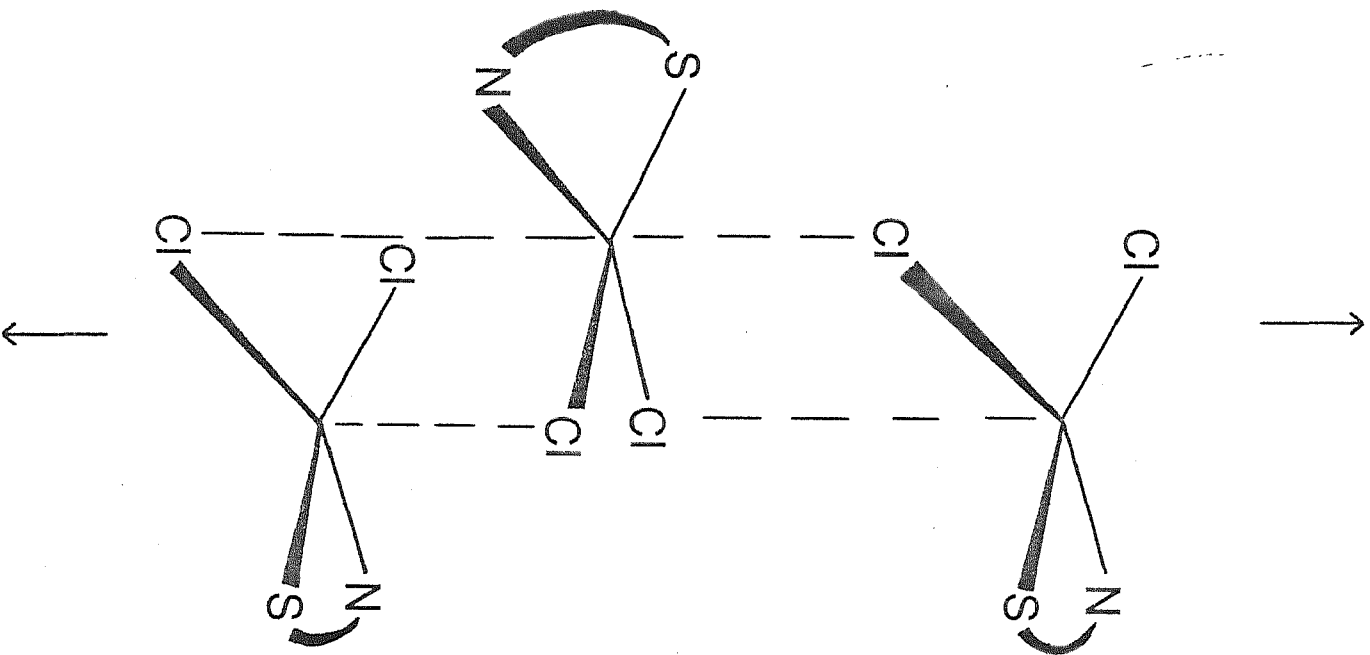
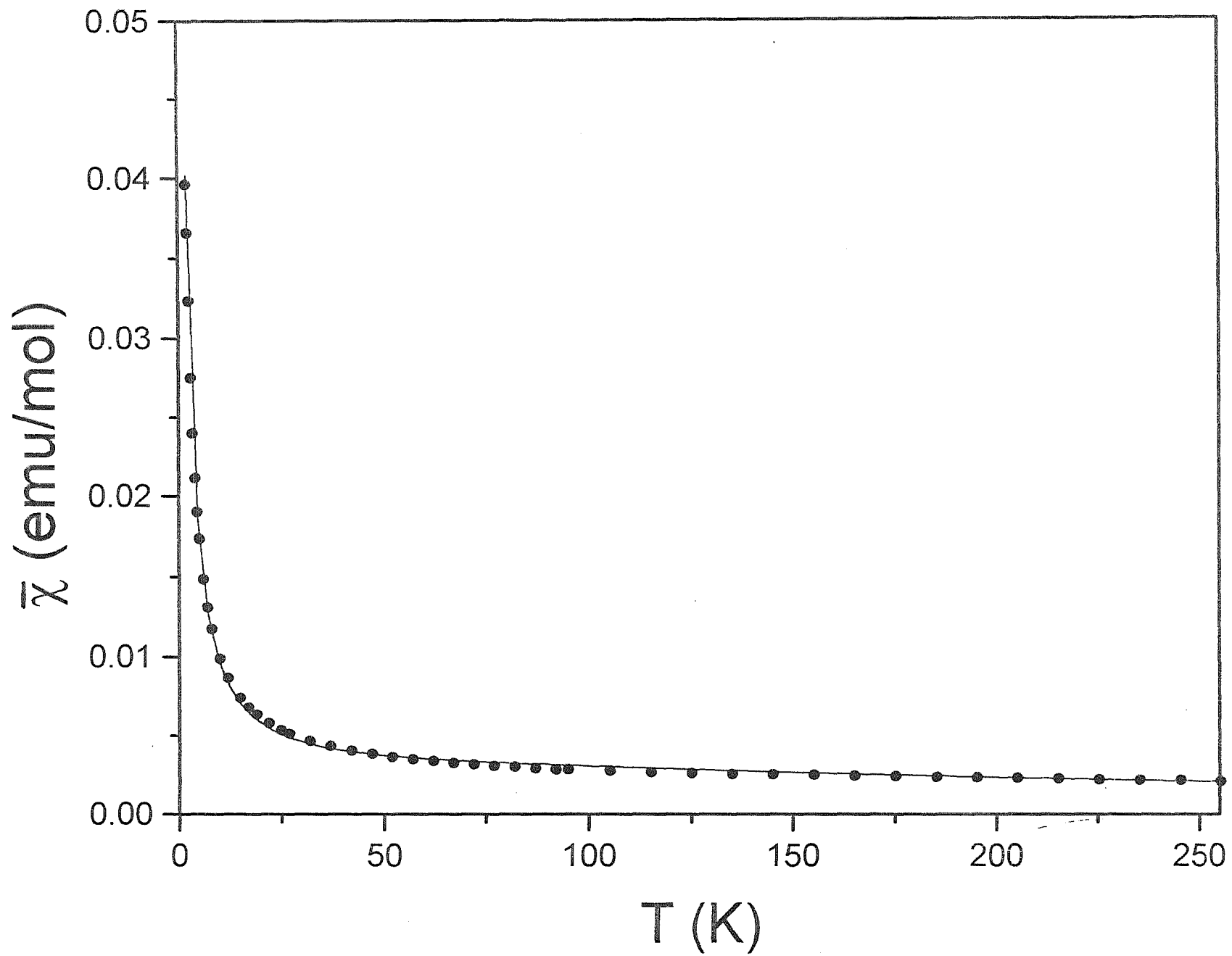
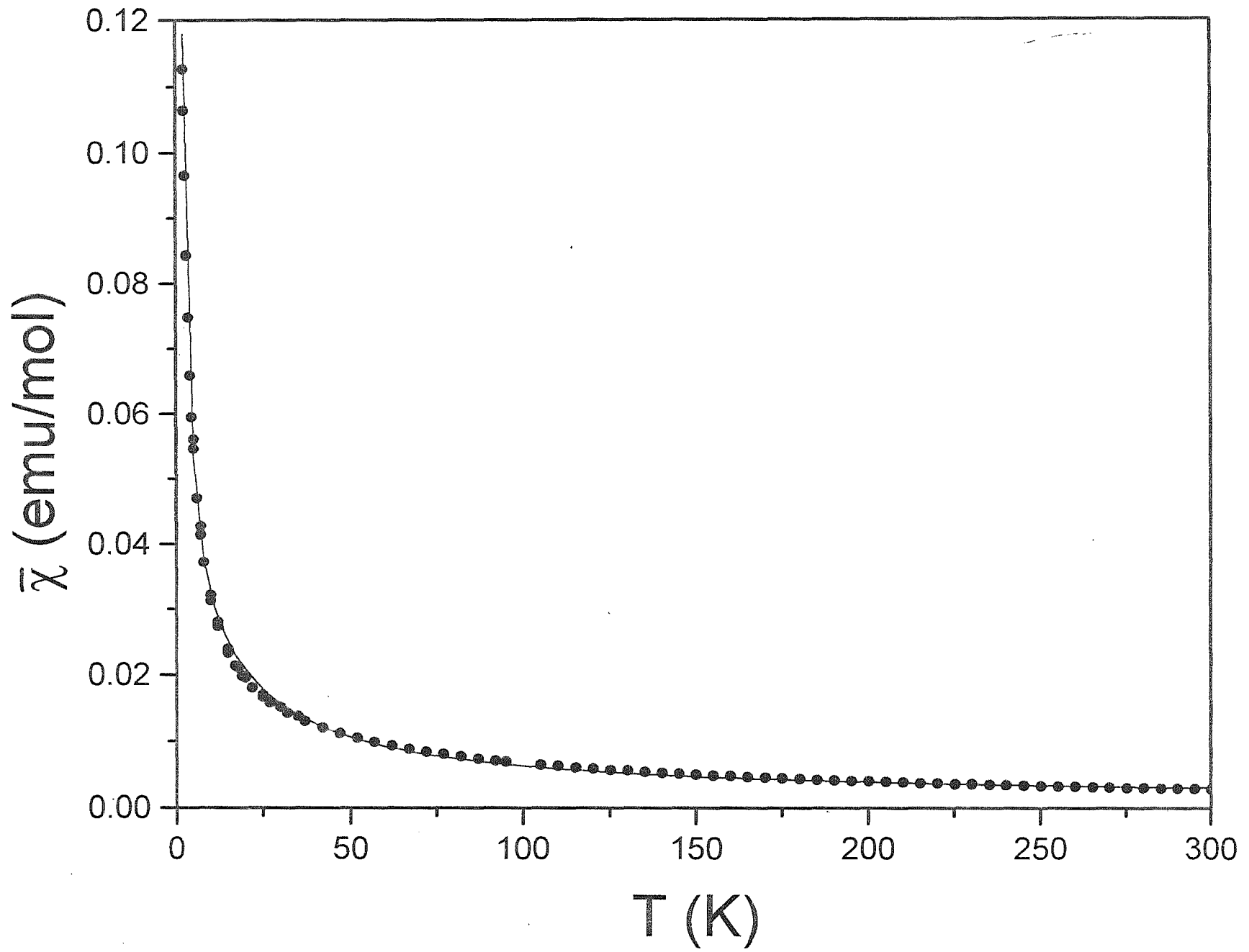


Fig. 21





ANEXO

6

Spectral and Magnetic Characterization of Novel Cu(II) Coordination Compounds Synthesized in Methanolic Medium with the Heterocycles Allopurinol, Hypoxanthine and 6-mercaptopurine. Part II.

Spectral and Magnetic Characterization of Novel Cu(II) Coordination
Compounds Synthesized in Methanolic Medium with the Heterocycles
Allopurinol, Hypoxanthine and 6-mercaptopurine. II.

Rodolfo Acevedo-Chávez.

Centro de Química, Instituto de Ciencias, B. Universidad Autónoma de Puebla,
Apartado Postal 1613, Puebla, Puebla, México.

María Eugenia Costas*.

Facultad de Química, Universidad Nacional Autónoma de México,
México 04510, D.F., México.

* To whom correspondence should be addressed.

Abstract.

Single and competitive purine derivative and isomer-Cu(II) reactions were carried out in methanolic medium. In these, the polyatomic anions SO_4^{2-} , ClO_4^- and CH_3CO_2^- as metallic counterions were employed. New Cu(II) compounds with the respective heterocyclic ligands allopurinol, hypoxanthine and 6-mercaptopurine were synthesized and characterized. In all the cases the spectral and magnetic studies are in concordance with the existence of very weak antiferromagnetic coupling in the solid products. The linear chain magnetic model of coupled $S=1/2$ spins describes successfully the respective magnetic response; the magnetic parameters obtained are associated both to intrachain and interchain magnetic couplings. In this behavior, the polyatomic anions and heterocycles appear to play the critical role in the correspondent superexchange magnetic coupling pathways.

I. Introduction.

Allopurinol (1H-pyrazolo[3,4-d]pyrimidine-4-one, I), hypoxanthine (6-oxopurine, II) and 6-mercaptopurine (III) are interesting heterocycles (Figure 1) from diverse points of view. Both pharmacological and biochemical [1-3], and their metallic bonding behavior [4-6] motivations have been detected up to date. In coordination chemistry, for example, their several metallic bonding sites, the metal:heterocycle stoichiometries, the structural characteristics and the spectral and physical properties of the respective coordination compounds show a close dependence on both the nature and characteristics of the metallic center and the experimental conditions carried out.

Figure 1

As part of our research program concerned to heterocycle-metallic center interactions, we have focused our attention on the purine derivative and isomer - Cu(II) interactions, in competitive reactions of these ligands towards the metallic center and under systematically modified reaction conditions. To our knowledge, there are no studies of this type reported in the literature, and we have considered that these studies would represent a methodology to explore some aspects of the kinetic and thermodynamic stabilities of these interactions, and their correspondent coordination compounds, and also some of their physical properties.

In this theme, we have recently explored certain heterocycle-Cu(II) interactions in methanolic medium, employing the heterocyclic ligands allopurinol, hypoxanthine and 6-mercaptopurine [7], both in single and competitive M-Ligand interactions, and also changing the nature of the metallic counterions ($X=Cl^-$, Br^- , NO_3^-). From these studies the higher reactivity of 6-mercaptopurine has been deduced, also depending on the anion employed. Continuing with the exploration of this problem, we report here the second part of these heterocycle-Cu(II) interactions, and employing SO_4^{2-} , ClO_4^- and $CH_3CO_2^-$ as

metallic counterions. Also, the spectral and magnetic characterization of the correspondent Cu(II) compounds is discussed.

II. Experimental Section.

A) Reagents.

The metallic salts, heterocyclic ligands and solvents were analytical grade and commercially acquired. All were used with no further purification.

B) Single and Competitive Heterocycle - Cu(II) interactions.

1) Single heterocycle - Cu(II) interactions.

For this type of reactions, the respective heterocyclic ligand was dissolved in 100 mL of CH₃OH under stirring and boiling at refluxing (atmospheric pressure). To the resulting solution, one mmol of the respective metallic salt (previously solvated in *ca.* 10 mL of CH₃OH) was added, and at the same experimental conditions a suspension (except for Cu(II), X=CH₃CO₂⁻ and hypoxanthine; see below) was formed. With time, and without additional changes, the respective suspension was filtered off, and the solid product was washed with boiling CH₃OH. The solid product was kept for 8 hours at 100° C (except for the reactions with X=ClO₄⁻ where 37° C and 24 hours were applied). The total reaction times and colors of the respective products obtained in this step, are shown in Table 1.

Table 1

In a typical reaction 1 mmol of solvated allopurinol and 1 mmol of solvated Cu(ClO₄⁻)₂•6H₂O were kept under the above reaction conditions. In the reaction initial step, a pale blue solution was formed, which after 12 hours evolved to a lilac suspension. 10 days after and without additional changes, the hot suspension was filtered off, and the solid product was washed with boiling CH₃OH. The product (lilac) was kept at 37° C for 24 hours, without changes.

The reaction between hypoxanthine and Cu(CH₃CO₂⁻)₂•H₂O was performed at the same above conditions, and it yields a deep green solution with time (11 days). The resulting

solution was kept at slow evaporation, resulting in a deep green oil, which was dried. The deep green solid was washed (at room temperature) with 50 mL of $\text{CH}_3\text{CO}_2(\text{C}_2\text{H}_5)$ and secondly, with several portions (each one of 50 mL) of $\text{CH}_3\text{CO}_2(\text{C}_2\text{H}_5):\text{C}_2\text{H}_5\text{OH}$ mixtures in respective ($V:V$) ratios of 8:2, 6:4, 4:6 and 2:8. Finally, the solid was washed with 50 mL of $\text{C}_2\text{H}_5\text{OH}$. The solid was suspended in 50 mL of $\text{C}_2\text{H}_5\text{OH}$, kept at boiling temperature and reflux, resulting a deep green suspension. 24 hours later and under these conditions, the suspension was filtered off, and the deep green solid was isolated and washed with hot $\text{C}_2\text{H}_5\text{OH}$. The resulting solid (deep green) was kept at 100°C for 8 hours, without changes.

Finally, in the hope to explore other experimental conditions for some Cu(II) -allopurinol interactions, which could result in other product than $\text{Cu(II)(allopurinolate}^-\text{)(OH}^-\text{)}$ (compound 1 in Table 1), one successful technique was found for the Cu(II) ($\text{X}=\text{SO}_4^{2-}$)-allopurinol interaction. This was as follows: 1 mmol of allopurinol was dissolved under heating at boiling temperature in 100 mL of dried CH_3OH , the reflux maintained at dryness conditions. At these conditions, 1 mmol of $\text{CuSO}_4\cdot 5\text{H}_2\text{O}$ was added, forming a pale green-blue suspension. At the same conditions and with no changes in the following 8 hours, the hot suspension was filtered off and the solid obtained was washed with hot CH_3OH , hot $\text{C}_2\text{H}_5\text{OH}$ and finally with hot $(\text{CH}_3)_2\text{CO}$. The pale blue solid was kept at 100°C for 8 hours, resulting in a pale green solid (this product is labeled as 7 in Table 1). No competitive heterocyclic reactions (see below) with this Cu(II) compound were explored. The correspondent characterization of this product appears in Results and Discussion.

2) Successively competitive heterocycle - Cu(II) interactions.

For this type of reactions, a Cu(II) compound was first synthesized with a specific heterocyclic ligand (reaction types in part 1). The purified compound obtained was microanalytically studied to obtain its empirical formulation. Considering a mononuclear character for this, a second interaction (coordination compound-second heterocyclic ligand) in a 1:1 molar ratio was explored at the same conditions as in 1). The correspondent solid obtained

was also treated as before (except for the reactions with $X=\text{ClO}_4^-$, for which $T = 37^\circ\text{C}$ and 24 hours were applied). The total reaction times for the second step and the colors of the respective products obtained are shown in Table 1.

In a typical reaction, 1 mmol of the product (2) (Table 1) was suspended in 100 mL of boiling CH_3OH under refluxing. To the pale blue suspension 1 mmol of the second heterocyclic ligand (6-mercaptopurine) was added, forming at these conditions a pale green suspension, which after 2 hours changed to green-yellow. Maintaining the reaction mixture for 10 days without changes at the same conditions, the hot suspension was filtered off, and the solid isolated was washed with several portions of boiling CH_3OH . The solid (dark green) was kept at 100°C for 8 hours, without changes.

3) Simultaneously competitive heterocycle - Cu(II) interactions.

For this type of competitive reactions, the respective heterocyclic ligands were previously solvated in boiling CH_3OH under refluxing. To the respective solution obtained, the correspondent metallic salt was added. The stable reaction mixture with time, was filtered in hot, and the solid product was washed with boiling CH_3OH . The solid product was kept at 100°C for 8 hours. The total reaction times and colors of the products obtained are shown in Table 1.

In a typical reaction, 1 mmol of hypoxanthine and 1 mmol of 6-mercaptopurine were solvated in 100 mL of CH_3OH under refluxing. To the solution obtained, 1 mmol of $\text{CuSO}_4 \cdot 5\text{H}_2\text{O}$ was added, forming a green suspension. 4 days after the suspension acquired a green-yellow color: 2 days after the color changed to ocree, and 5 days after it turned to brown- orange, without changes for 4 additional days. The hot suspension was filtered off, and the solid product isolated was washed with boiling CH_3OH . The solid (dark green) was kept at 100°C for 8 hours without changes.

C) Physical measurements.

-Microanalytical results (C.H.N) were obtained by the Chemistry Department at the University College of London. Analytical confirmation was performed by the Department of Chemistry, University of Sheffield (microanalysis service).

-Infrared (IR) spectra in the 4000-200 cm^{-1} range were obtained as Nujol mulls using CsI plates and employing a 599-B Perkin Elmer spectrometer. Confirmation of the low-energy IR data was carried out employing a 740 FT IR Nicolet spectrometer (high density polyethylene pellets in the 600-70 cm^{-1} range).

-Electronic spectra (200-1100 nm) of the powdered samples were measured by the specular reflectance method in a 160-A Shimadzu spectrometer, using quartz windows and BaSO_4 as reference.

-Thermogravimetric results were obtained employing both a DT-30 Shimadzu balance, and a 2100 Dupont equipment ($\text{N}_2(\text{g})$ as carrier fluid, 5 $^\circ\text{C}/\text{min}$ as heating rate).

-EPR spectra (X-band) of powdered samples were performed in a 200-D Bruker spectrometer, both at room and liquid nitrogen temperatures. The g values were standardized against the absorption of diphenylpicrylhydrazine (DPPH).

-Magnetic susceptibilities of samples at room temperature were measured using a Johnson Matthey balance and employing $\text{Hg}[\text{Co}(\text{SCN})_4]$ as calibrating agent.

-The temperature variable magnetic susceptibility measurements were carried out using a SQUID MPMS-5 Quantum Design Magnetometer, from 2- 300 K, and several magnetic fields (100 to 10000 G). The magnetic susceptibilities were corrected for the cell and sample diamagnetic contributions. The mean standard deviations of the magnetic measurements were three orders of magnitude lower than the data studied.

III Results and Discussion.

a) Analytical Results.

The analytical data and formulations of the respective coordination compounds obtained in this study, are listed in Table 2. With regard to these, the compounds (1) and (3) have been also previously obtained and characterized in related studies [4,7,8] and are only quoted here.

Table 2

b) Compounds Obtained.

1) Single heterocycle - Cu(II) interactions.

For all the reactions explored here and also for those of the precedent study[7], Cu(II) compounds with the respective heterocyclic ligands were synthesized. Also, and except for two cases, the starting metallic counterions exist in the correspondent metallic compounds. The two cases where this behavior is not found, correspond to the polynuclear systems $\text{Cu}(\text{L}_1^-)(\text{OH}^-)$ and $\text{Cu}(\text{L}_3^{2-}) \cdot 2\text{H}_2\text{O}$, for which the deprotonation of the heterocyclic ligands occur. The synthesis of the last polynuclear compound is noticeable, independently of the polyatomic metallic counterions employed. A dependence of the anion nature was also found in the previous study[7]. The formation of the first polynuclear compound quoted above, could be also related to the experimental conditions and the basic properties of the metallic counterions employed; those with higher basic character (SO_4^{2-} or CH_3CO_2^-) appear to be in part associated to the deprotonation of the heterocyclic ligand. The influence of H_2O in the solvent CH_3OH is also decisive; the absence of the former avoids the deprotonation of allopurinol, favoring product (7). Analogous attempts for the homologue reaction with the CH_3CO_2^- anion in anhydrous conditions were not tried. With regard to the Metal:Heterocycle stoichiometry, the most frequent is the 1:1 ratio. This ratio is in agreement with the polynuclear character of the compounds, both the previously studied[4,7,8] and the ones discussed in the present study (see below).

2) Successively competitive heterocycle - Cu(II) interactions.

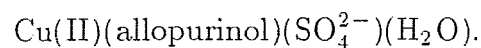
In these reactions both allopurinol and hypoxanthine do not show capability of heterocyclic ligand substitution. The heterocycle that shows this property is the $\underline{\text{S}}(6)$ -purine derivative, forming the $\text{Cu}(\text{L}_3^{2-})$ system. This product does not show reactivity towards other heterocyclic substitution reactions. As it was discussed in the previous study[8], the deprotonation of the $\underline{\text{S}}(6)$ -derivative and its metallic coordination through both the exocyclic $\underline{\text{S}}(6)$ atom and the $\underline{\text{N}}$ atoms of the five-membered ring, leads to noticeable kinetic and thermodynamic stabilities of this Cu(II) compound.

3) Simultaneously competitive heterocycle - Cu(II) interactions.

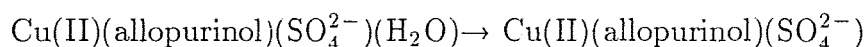
For this type of reactions the S(6)-derivative is the heterocyclic ligand with the higher metallic bonding capacity, forming the $\text{Cu}(\text{L}_3^{2-})$ system quoted before. On the other hand, allopurinol and hypoxanthine show alternate metallic bonding capabilities, being the nature of the metallic counterion employed and the deprotonation state of the heterocyclic ligands some of the main factors that play a critical role in the formation of the specific Cu(II) compound. For $\text{X}=\text{ClO}_4^-$, where the respective Cu(II) compounds with allopurinol and hypoxanthine contain the neutral heterocyclic ligands, the favored system (compound (4)) is the one that corresponds to the $\text{Cu}(\text{II})(\text{N})_4$ type (see below).

c) Thermogravimetric Results.

Cu(II) coordination compounds with allopurinol.

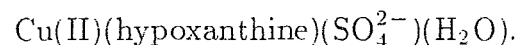


This compound shows a first mass loss step at *ca.* 167 °C. Continuing with the increase of temperature a second, noticeable and very complex path of mass loss starts at *ca.* 276°C and finishes at *ca.* 570°C. The first step is in good agreement with the process:



The temperature for this step would be in full agreement with the participation of the H_2O molecule in the coordination sphere of the Cu(II) compound. The limit of thermal stability for the resulting Cu(II) system appears to be *ca.* 276°C.

Cu(II) coordination compounds with hypoxanthine.



The compound shows a step of constant mass from room temperature until 75°C. From this temperature and until *ca.* 205°C a mass loss step is observed. Upon increasing the temperature and starting from *ca.* 265°C an abrupt, complex and noticeable mass loss step is observed until *ca.* 530°C. The first step of mass loss lies upon the 75-205°C range, and the average temperature (*ca.* 140°C) could be interpreted as that involving the loss of a H_2O molecule from the metallic coordination sphere in the original compound. The limit of thermal stability for the resulting system would be *ca.* 265°C.

$\text{Cu(II)(hypoxanthinate}^{-})(\text{CH}_3\text{CO}_2^{-})$.

The thermogravimetric data of this compounds are very complex, showing a continue mass loss with temperature. This very complex process noticeably starts above 100°C, and continues above 600°C. The shape of the mass-temperature and first derivative curves difficult a clear assignment of the steps there observed.

d) Infrared Spectral Results.

The IR data and bands assignments of both the free allopurinol [9] and hypoxanthine [10-17] and their Cu(II) compounds here reported, are listed respectively in Tables 3 and 4.

Table 3

Table 4

Cu(II) coordination compounds with allopurinol.

$\text{Cu(II)(allopurinol)}_4(\text{ClO}_4^{-})_2$.

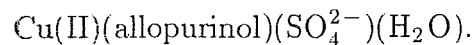
The IR spectrum shows noticeable differences with respect to the one shown by the free heterocyclic ligand. However, the spectral behavior of the bands associated to vibrational modes of the $\underline{\text{C}}(4)=\text{O}$ and $\underline{\text{N}}(5)-\text{H}$ groups let us suggest the non involvement of these in the metallic bonding. The spectral changes quoted before are related to several vibrational modes of endocyclic groups, suggesting us the participation of endocyclic atoms in the metallic coordination of the heterocycle. The remarkable perturbation of the C-H group vibrational modes could be related to its involvement as a nearest neighboring group to the metallic bonding site. Related to this, the spectral behavior of the $\underline{\text{N}}(5)-\text{H}$ group let us suggest the non participation of the $\underline{\text{N}}(7)$ atom of the pyrimidinic ring in the metallic bonding. This could lead to suggest the involvement of $\underline{\text{N}}$ atoms of the pyrazolic ring in this process. Of these, the spectral information allow us to propose the $\underline{\text{N}}(2)$ atom as the possible metallic bonding site of allopurinol.

ClO_4^- IR bands.

In the IR spectrum bands attributed to vibrational modes of the ClO_4^- group also appear. The spectral information for this group let us suggest its existence as ionic ClO_4^- . The strong and broad band centered at *ca.* 1095 cm^{-1} is assigned to (ν_3) of ClO_4^- in a T_d symmetry. Also, the weak band centered at *ca.* 645 cm^{-1} is attributed to the (ν_4) vibrational mode of ClO_4^- in the same symmetry [18-28].

In the low-energy region the spectrum shows a broad band with peaks at 285, 275 and 265 cm^{-1} . This band is associated to $\nu_{\text{Cu-N}}$.

With this spectral information, the metallic bonding of the allopurinol molecules through the $\underline{\text{N}}(2)$ atoms and the existence of ClO_4^- as ionic groups are suggested. In this proposition, the Cu(II) compound has a Cu(II)(N)_4 character.



The IR spectrum shows noticeable differences with respect to the correspondent spectrum of the free heterocycle. Differences are also due to the bands of the SO_4^{2-} group. Regarding to the coordinated heterocyclic ligand, the bands appearing at 1698 and 1606 cm^{-1} let us discard the involvement of the exocyclic $\underline{\text{O}}(4)$ atom and the $\underline{\text{N}}(5)\text{-H}$ group as coordinating sites. Several modifications of the bands associated to vibrational modes of ring and endocyclic groups (N-H and C-H) in the $1600\text{-}600\text{ cm}^{-1}$ range are evident. This spectral information would be in agreement with the metallic bonding of the heterocycle through $\underline{\text{N}}$ atoms. From these, those corresponding to the pyrazolic moiety appear to be the most probable ones, in particular the $\underline{\text{N}}(2)$ atom.

SO_4^{2-} IR bands.

In the $1200\text{-}500\text{ cm}^{-1}$ range, the bands assigned to vibrational modes of the coordinated SO_4^{2-} group appear. The three strong bands at 1196 , 1115 and 1071 cm^{-1} are attributed to (ν_3) of the SO_4^{2-} group in a C_{2v} symmetry. The band appearing at 991 cm^{-1} is assigned to (ν_1) for SO_4^{2-} in the same symmetry. The bands at 669 , 587 and 560 cm^{-1} are attributed to (ν_4). Finally, the band at 475 cm^{-1} is assigned to (ν_2). The spectral pattern of these bands

and their characterization are in full agreement with the spectral studies of coordination compounds with the bridging bidentate SO_4^{2-} ligand in a C_{2v} symmetry [28,29].

With regard to the $\nu_{\text{Cu-Ligand}}$ vibrational modes, the broad band centered at *ca.* 385 cm^{-1} is assigned to $\nu_{\text{Cu-OH}_2}$, in agreement with the thermogravimetric results. The band with peaks at 304, 296 and 286 cm^{-1} is suggested to contain the $\nu_{\text{Cu-N}}$ vibrational mode.

Cu(II) coordination compounds with hypoxanthine.

$\text{Cu(II)(hypoxanthine)(SO}_4^{2-})(\text{H}_2\text{O})$.

The IR spectrum shows noticeable differences with respect to the one shown by the free heterocyclic ligand. These correspond both to the electronic perturbation of the same heterocycle coordinated and the bands attributed to vibrational modes of the SO_4^{2-} group. The strong and broad band appearing at *ca.* 1720 cm^{-1} , which can be assigned to $\nu_{\text{C=O}}$ as the major contribution, is shifted to higher frequency than the correspondent to the free heterocycle. The shift to higher frequencies is indicative of heterocyclic metallic bonding through the $\underline{\text{N}}(3)$ atom of the pyrimidinic ring. Also, this let us discard the participation of the exocyclic $\underline{\text{O}}(6)$ atom as a metallic bonding site. The spectral information also let us discard the role of the $\underline{\text{N}}(1)\text{-H}$ group as coordination site. In the $4000\text{-}600\text{ cm}^{-1}$ range several spectral changes occur. The spectral characterization is indicative of the participation of endocyclic atoms in the metallic bonding. The noticeable changes in several bands associated to C-H group vibrational modes let us consider its participation as nearest neighboring to the metallic bonding site(s).

SO_4^{2-} IR bands.

In the $1300\text{-}900\text{ cm}^{-1}$ range, characteristic bands attributed to (ν_3) and (ν_1) vibrational modes of the bridging bidentate SO_4^{2-} group appear [28,29]. The strong bands appearing at 1180, 1160 and 1053 cm^{-1} are attributed to (ν_3) for SO_4^{2-} in the C_{2v} symmetry. The band appearing at 920 cm^{-1} is assigned to (ν_1) . The bands appearing at 640, 620 and 600 cm^{-1} are attributed to (ν_4) . Finally, the band at 485 cm^{-1} is associated to (ν_2) .

With regard to the $\nu_{\text{Cu-Ligand}}$ vibrational modes, the band at 428 cm^{-1} in the low-energy spectrum is attributed to the $\nu_{\text{Cu-OH}_2}$ vibrational mode, in concordance with the thermogravimetric studies. The band of complex structure with peaks at 285 and 275 cm^{-1} is suggested to contain the $\nu_{\text{Cu-N}}$ vibrational mode.

With the above spectral information, the metallic coordination of hypoxanthine through endocyclic sites (*e.g.*, the $\underline{\text{N}}(3)$ atom) and the participation of the SO_4^{2-} group as bridging ligand is proposed. The metallic bonding of the H_2O molecule suggested from the low-energy IR spectrum, is in concordance with the thermogravimetric results for this compound.

Comparing the IR spectrum of this compound with that of the previously reported[14] system $\text{Cu(II)}(\text{hypoxanthine})(\text{SO}_4^{2-})(\text{H}_2\text{O})$ (and for which the structural characterization as a bidimensional polynuclear network has been made) these appear to be the same. The structural characterization considers the metallic bonding of hypoxanthine as bridging ligand through the $\underline{\text{N}}(3)$ and $\underline{\text{N}}(7)$ atoms and the same bonding behavior for the SO_4^{2-} group. Coordination of the H_2O molecule is also established in that study.

The IR spectral information quoted and discussed before is in full agreement with the structural characterization. Also, it represents a complete spectral characterization of the bands both of the heterocyclic ligand and the SO_4^{2-} group as bridging ligands. The spectral information in the low-energy region also represents the IR characterization of this compound.

$\text{Cu(II)}(\text{hypoxanthine})_2(\text{ClO}_4^-)_2$.

The IR bands of hypoxanthine coordinated show remarkable changes in the patterns of frequency and intensity, related to the bands shown by the free ligand hypoxanthine. Also, noticeable changes in the IR spectrum are due to the ClO_4^- bands. With respect to the coordinated heterocycle, the characteristics of the bands at 1680 and 1600 cm^{-1} let us discard the involvement of the exocyclic $\underline{\text{Q}}(6)$ and $\underline{\text{N}}(1)$ atoms as coordinating sites. The spectral behavior of these bands also let us exclude the role of the $\underline{\text{N}}(3)$ as the metallic

bonding atom. The remarkable modifications of bands associated to ring and C-H group vibrational modes let us suggest the N atoms of the five-membered ring as the metallic bonding sites.

ClO_4^- IR bands.

The spectral behavior of the ClO_4^- bands is in full agreement with its character as monocoordinated ligand[18-28]. The strong, broad and asymmetric band with peaks at 1085 and 1050 cm^{-1} is assigned to (ν_3). The band at 925 cm^{-1} is attributed to (ν_1). The medium bands at 640 and 620 cm^{-1} are attributed to (ν_4). Finally, the weak band at 465 cm^{-1} is assigned to (ν_2). All this IR information for these ClO_4^- bands is in agreement with a C_{3v} symmetry for this monoanionic ligand.

The $\nu_{\text{Cu-Ligand}}$ vibrational modes are found in the 400-200 cm^{-1} range. The band at 300 cm^{-1} is attributed to the $\nu_{\text{Cu-OCLO}_3}$ vibrational mode. The broad band at 286 cm^{-1} is assigned to the $\nu_{\text{Cu-N}}$ vibrational mode.

$\text{Cu(II)(hypoxanthinate}^-\text{)(CH}_3\text{CO}_2^-)$.

The IR spectrum of this Cu(II) compound is very different from the free heterocyclic ligand one. Differences in the spectral pattern are also due to the CH_3CO_2^- bands. With regard to the coordinated heterocycle, drastic spectral changes are shown. For example, the strong and broad band at 1670 cm^{-1} in free hypoxanthine, it is not clearly detected in the IR spectrum under discussion. This same behavior is found for the band at 1583 cm^{-1} in the IR spectrum of free hypoxanthine. Noticeable suppression of bands attributed to several endocyclic groups vibrational modes is also found in the spectrum here discussed. The spectral pattern is in concordance with a drastic modification of all the heterocycle, related both to its deprotonation and metallic bonding.

CH_3CO_2^- IR bands.

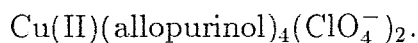
The presence of the CH_3CO_2^- group is deduced from the broad and strong bands with positions estimated at *ca.* 1625 and 1335 cm^{-1} . Their frequency would be in agreement with the spectral behavior of coordinated CH_3CO_2^- ligand[28]. The respective assignments

for these bands are $\nu_A(\text{COO}^-)$ and $\nu_S(\text{COO}^-)$. The spectral characteristics of the first band difficults the clear observation of the bands attributed respectively to the $\nu_{C(6)=O}$ and $\delta_{N(1)-H}$ vibrational modes quoted above, and also its exact frequency.

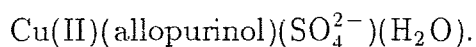
In the low-energy IR spectrum, a broad band with peaks at 303, 290 and 280 cm^{-1} appear. This band could be assigned to the $\nu_{\text{Cu}-\text{O}}(\text{CH}_3\text{CO}_2^-)$ and $\nu_{\text{Cu}-\text{N}}$ vibrational modes.

e) Electronic Spectroscopy Results.

Cu(II) coordination compounds with allopurinol.

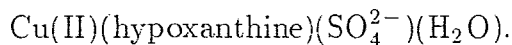


The spectrum shows in the blue region a low-energy tail of a band from the near UV region. Its minimum absorbance lies upon *ca.* 430 nm. The spectrum also shows a broad band of complex structure, with components partially resolved at *ca.* 530 and *ca.* 600 nm. The position and structure of this band would be associated to the existence of a distorted tetracoordinated geometry for Cu(II).

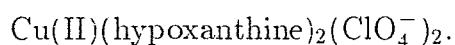


The spectrum shows a band in the blue region with a maximum of absorbance at *ca.* 350 nm. It also shows a broad and asymmetric band centered at *ca.* 690 nm. The spectral pattern could be related to the suggestion of a distorted tetracoordinated geometry for the Cu(II) metallic center.

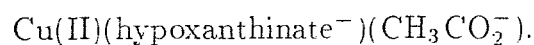
Cu(II) coordination compounds with hypoxanthine.



The spectrum shows in the blue region a low-energy tail of a band emerging from the near UV, with a minimum of absorbance at *ca.* 472 nm. The spectrum also shows an intense, broad and asymmetric band with a maximum of absorbance at *ca.* 684 nm. The characteristics of this band would be in full agreement with the suggestion of a pentacoordinated geometry for Cu(II). Using the structural characterization previously reported[14] of this compound, a square pyramidal environment for the Cu(II) center arises.



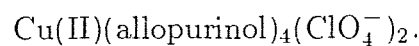
The spectrum shows in the blue region a low-energy tail of a band from the near UV region, with a minimum of absorbance that lies upon *ca.* 440 nm. It also shows a broad band centered at 585 nm. The characteristics of this last band would be in concordance with the suggestion of a roughly square geometry for Cu(II). The lower energy tail of this band, compared to the one shown by the related Cu(II) compound with allopurinol ($X=ClO_4^-$), confirms the higher ligand field intensity of the interactions for this last compound, and thus its Cu(II)(N)₄ character, compared to the Cu(II)(N)₂(O)₂ character for the system here discussed.



The spectrum shows an intense and broad band in the blue region, at *ca.* 390 nm. From the low-energy tail of this band other component centered at *ca.* 620 nm appears. The spectral pattern in full is very different from those shown by the Cu(II) compounds discussed before, illustrating the influence of the deprotonated heterocyclic ligand in the spectrum. From the data the suggestion of a distorted tetracoordinated geometry for the Cu(II) metallic center is made.

f) EPR Spectral Results.

Cu(II) coordination compounds with allopurinol.



The EPR spectrum at room temperature of this Cu(II) compound is shown in Figure 2.

Figure 2

The spectrum shows an asymmetrical absorption, with $g_1 \approx 2.06$, $g_2 \approx 2.10$ and $g_3 \approx 2.16$. From these values, $R \approx 0.66$ ($(g_2 - g_1)/(g_3 - g_2)$) is obtained. This value let us suggest a tetragonal character for the Cu(II) metallic center, possibly due to weak axial interactions. The spectral pattern in the low and high-field regions (at these conditions) let us discard the existence of noticeable Cu(II)-Cu(II) magnetic interactions.

Considering all the experimental information for this compound, a suggestion of the structural arrangement can be made, which consists of a distorted tetracoordinated environment of Cu(II), of the Cu(II)(N)₄ type. The N-bonded allopurinol molecules form the coordination sphere of the metallic center. Weak axial interactions, both from the nearest neighboring Cu(II) units or the ClO₄⁻ groups must be also considered in this proposition. This structural suggestion is in partial form schematically shown in Figure 3.

Figure 3

Cu(II)(allopurinol)(SO₄²⁻)(H₂O).

The EPR spectrum at room temperature of this Cu(II) compound (Figure 4) shows an absorption suggestive of an anisotropic *g* tensor. The components $g_1 = 2.08$, $g_2 = 2.12$ and $g_3 = 2.32$ lead to $R = (g_2 - g_1)/(g_3 - g_2) \approx 0.2$. The spectral pattern let us suspect the existence of a noticeable distorted tetracoordinated environment for Cu(II), without discarding weak axial interactions. At these conditions, there are no evidences of Cu(II)-Cu(II) magnetic interactions.

Figure 4

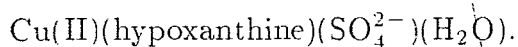
Upon decreasing the temperature (77 K, $\nu = 9.25$ GHz) there is no resolution of the absorption for the g_3 component. Also, and under these conditions there are no evidences of Cu(II)-Cu(II) magnetic interactions.

With all the experimental information related to this Cu(II) compound, a suggestion of the structural arrangement arises, consisting of a polynuclear system with bridging SO₄²⁻ ligands. In addition to these groups, H₂O and allopurinol molecules would show a distorted tetracoordinated disposition around the Cu(II) center, possibly with weak axial interactions of nearest neighboring units, as is schematically shown in Figure 5.

Figure 5

This Cu(II) compound would be, to our knowledge, the first example of a polynuclear coordination compound with allopurinol and anionic polyatomic bridging ligands. The correspondent magnetic studies (see below) would play a relevant role in the analysis of the effectiveness of the magnetic coupling pathway produced by these SO_4^{2-} groups.

Cu(II) coordination compounds with hypoxanthine.



The EPR spectrum at room temperature of this compound is shown in Figure 6.

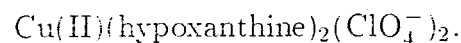
Figure 6

The spectrum corresponds to an anisotropic g tensor and is in agreement with the existence of a pentacoordinated geometry for Cu(II), in particular square-pyramidal. The components for this spectrum are $g_1 = 2.07$, $g_2 = 2.12$, $g_3 = 2.19$ and $g_4 = 2.32$. At these conditions and from the spectrum, there are no evidences of Cu(II)-Cu(II) magnetic interactions. With all the above experimental information for this compound, strong support exists for a structural arrangement proposition consisting of a square-pyramidal environment for the metallic center. The coordination sphere would be constituted by the H_2O , hypoxanthine and SO_4^{2-} ligands, the two last as bridging groups, connecting the nearest neighboring metallic units, as has been previously established[14] in the structural characterization of this compound. The structural arrangement is schematically shown in Figure 7.

Figure 7

With respect to this complex polynuclear structural arrangement, this Cu(II) compound is the first example where the metallic bonding of hypoxanthine is made through the $\underline{\text{N}}(3)$ and $\underline{\text{N}}(7)$ atoms. The existence of two types of bridging ligands across two different directions in the bidimensional network, and the non existence of Cu(II)-Cu(II) magnetic interactions

from the EPR data at room temperature, let us suppose the difficulty of these bridging ligands in the establishment of an efficient magnetic coupling pathway for the unpaired electrons of the metallic centers. At this respect, the magnetic studies (see below) would contribute to dilucidate this aspect.

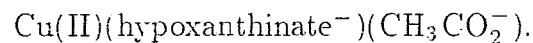


The EPR spectrum at room temperature of this compound is shown in Figure 8.

Figure 8

This shows an asymmetric absorption, with approximate values of $g_1 = 2.05$, $g_2 = 2.11$ and $g_3 = 2.21$. From these the R value is *ca.* 0.6, suggesting us a tetragonal character for the Cu(II) environment, possibly due to weak axial interactions. The spectral pattern in the low and high-field regions at these conditions, let us discard the existence of noticeable Cu(II)- Cu(II) magnetic interactions.

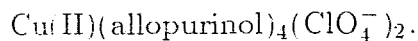
Considering all the available information for this compound, a suggestion of the correspondent structural arrangement can be made, which consists of a roughly planar tetra-coordinated environment for the Cu(II) center, of the Cu(II)(N)₂(O)₂ type. Weak axial interactions from both the Q(6) exocyclic atoms (of the hypoxanthine ligands) or the nearest Cu(II) units must be considered in this proposition. This structural suggestion is roughly related to that shown in Figure 3, for the system Cu(II)(allopurinol)₄(ClO₄⁻)₂, although in the Cu(II) system here discussed the cromophore is different.



The X-band ($\nu = 9.51953$ GHz) EPR spectrum of this Cu(II) compound at room temperature is absent of signals in the 1000-5000 G range. This spectral information is suggestive of Cu(II)-Cu(II) magnetic interactions in the solid product at these conditions. With all the above information for this compound a very complex structural arrangement is suspected, which would be of polynuclear nature.

g) Magnetic Results.

Cu(II) coordination compounds with allopurinol.



The $\bar{\chi}$ (emu/mol) *vs.* T (K) experimental data ($H = 10000\text{G}$) for this compound are shown in Figure 9.

Figure 9

From this, an antiferromagnetic coupling in the solid product is inferred. The Curie-Weiss behavior of the $\bar{\chi}$ data in the low-temperature region is suggestive of the existence of non coupled $S = 1/2$ spins, possibly as magnetic impurity. The antiferromagnetic coupling is also inferred from the $\bar{\chi}T - T$ curve, where a continue increase in the slope of the curve is observed with the temperature decrease. Considering the spectral information for this compound, two magnetic models were employed in the analysis of the magnetic response of the product. The first one was a linear chain magnetic model of $S = 1/2$ coupled spins. From this, the correspondent Bonner-Fisher equation was used for the fitting step. For fixed $g = 2.10$, a good fit was obtained, with $J = -64.20 \text{ cm}^{-1}$, $\rho = 0.011$ and $\bar{\chi}_0 = 9.58 \times 10^{-4} \text{ emu/mol}$. The J value confirms the antiferromagnetic coupling quoted before. With this magnetic model the possibility of interchain magnetic interactions was also explored, through a Curie-Weiss correction. With $g = 2.10$, the parameters obtained in the fitting process were $J = -61.02 \text{ cm}^{-1}$, $\theta = -4.69 \text{ K}$, $\rho = 0.013$ and $\bar{\chi}_0 = 9.71 \times 10^{-4} \text{ emu/mol}$. The J value corroborates the antiferromagnetic coupling, of intrachain character. The θ value let us suspect the existence of very weak antiferromagnetic coupling, of interchain type. The theoretical curve for this last treatment is also shown in Figure 9. Also and for the same magnetic model, a mean-field correction was employed; for $g = 2.10$, a good fit was obtained, which gave $J = -63.75 \text{ cm}^{-1}$, $zJ' = +8.22 \text{ cm}^{-1}$, $\rho = 0.010$ and $\bar{\chi}_0 = 5.85 \times 10^{-4} \text{ emu/mol}$. From these results, confirmation of intrachain antiferromagnetic coupling is obtained. Also, very weak interchain magnetic coupling is

deduced, although of ferromagnetic type in this case. At this level of study, it is difficult to discern about the correctness of the physical meaning for the θ and zJ' parameters.

In the magnetic study, a second model was explored. This was the dinuclear system of $S = 1/2$ coupled spins. From this, the respective Bleaney-Bowers equation was employed. In the fitting process, both the Curie-Weiss and the mean-field corrections were also explored. The fits were poor in quality; these results let us discard the dinuclear system as a structural arrangement of the Cu(II) compound in study, and let us suggest a linear chain character for this compound. With respect to the nature of the ligands connecting the Cu(II) units, at this level of spectral information, it is difficult to make a clear statement; both the ClO_4^- groups and the $\text{N}(7)$ or the $\text{O}(4)$ donor atoms (of the pyrimidinic ring in the coordinated allopurinol) could play the critical role as the correspondent intrachain magnetic coupling pathway between the unpaired electrons of the Cu(II) units.

$\text{Cu(II)(allopurinol)(SO}_4^{2-})(\text{H}_2\text{O})$.

The $\bar{\chi}$ (emu/mol) *vs.* T (K) experimental data ($H = 100\text{G}$) for this compound are shown in Figure 10.

Figure 10

From this, a shoulder of the $\bar{\chi}$ data below *ca.* 25 K is observed. This is associated to a partially masked maximum of the $\bar{\chi}$ values, for an antiferromagnetic coupling in the sample. In the low-temperature region a Curie-Weiss behavior is observed, and is associated to the presence of non coupled $S = 1/2$ spins, possibly as magnetic impurity. The position of this shoulder indicates a low intensity in the magnetic coupling, smaller than the one for the precedent Cu(II) compound. The antiferromagnetic coupling suggested above is also deduced from the $\bar{\chi}T - T$ data. From this, a continue decrease of the $\bar{\chi}T$ data with the decrease of temperature for the 300-100 K range is observed. Upon a further decrease in temperature and from *ca.* 50 K, an abrupt increase of the slope is observed. This pattern indicates an antiferromagnetic coupling in the solid product.

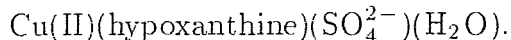
Selecting the $\bar{\chi}$ data for the 30-300 K range, and employing the Curie-Weiss equation for a fitting process to the experimental data, good results were observed, with the following parameters: $C = 0.394$ emu K/mol, $\theta = -32.00$ K and $\bar{\chi}_0 = 4.905 \times 10^{-4}$ emu/mol. The θ value supports the existence of antiferromagnetic coupling in the solid product. In the magnetic characterization of the Cu(II) compound, two models were selected. The first one was a linear chain magnetic model of $S = 1/2$ coupled spins. Employing then the Bonner-Fisher equation with fixed $g = 2.12$, from the good fit the following parameters were obtained: $J = -16.98$ cm $^{-1}$, $\rho = 0.055$ and $\bar{\chi}_0 = 1.461 \times 10^{-4}$ emu/mol. The J value is in agreement with the antiferromagnetic coupling quoted before, of intrachain type. This value is also in concordance with a lower intensity in the magnetic coupling compared with the one shown by the preceding Cu(II) compound. Further on in the magnetic analysis, the Bonner-Fisher equation with the Curie-Weiss correction was employed. From the good results in the fitting process and with $g = 2.12$, the following parameters were obtained: $J = -7.92$ cm $^{-1}$, $\theta = -24.65$ K, $\rho = 0.0639$ and $\bar{\chi}_0 = 2.799 \times 10^{-4}$ emu/mol. The J value confirms the intrachain antiferromagnetic coupling. The θ value let us suggest the existence of very weak interchain antiferromagnetic coupling. The correspondent theoretical curve is also shown in Figure 10.

Employing the Bonner-Fisher equation with a mean-field correction, good results in the fitting process for fixed g were obtained, and the resulting parameters were: $J = -16.18$ cm $^{-1}$, $zJ' = +2.86$ cm $^{-1}$, $\rho = 0.051$ and $\bar{\chi}_0 = 8.118 \times 10^{-5}$ emu/mol. The J value is in agreement with the precedent results for the intrachain antiferromagnetic coupling parameter. In this case, very weak interchain magnetic coupling (zJ') is deduced, although of ferromagnetic type. At this level of study, it is difficult to dilucidate the correctness of the physical meaning for the interchain magnetic coupling parameter. Nevertheless, the qualitative importance of this magnetic model lies in the suggestion of very weak interchain magnetic coupling.

In the magnetic study a second model was explored, which was the dinuclear system of $S = 1/2$ coupled spins. From this, the Bleaney-Bowers equation was employed, both with

the Curie-Weiss and the mean-field corrections. The fitting process had such a bad quality that it let us discard the dinuclear arrangement for the Cu(II) compound here discussed. The magnetic study carried out, supports the structural arrangement suggestion made before for this Cu(II) compound, and shown in Figure 5. In this, the SO_4^{2-} bridging ligands would play the critical role as the intrachain magnetic coupling pathway between the unpaired electrons of the Cu(II) units.

Cu(II) coordination compounds with hypoxanthine.



The magnetic measurements were carried out for this Cu(II) compound at 100, 1000 and 10000 G. From the $\bar{\chi}T$ data at these magnetic fields, a non dependence of the $\bar{\chi}$ values on the intensity of the magnetic field is observed. Figure 11 shows the $\bar{\chi}(\text{emu/mol}) - T$ (K) experimental data at 10000 G.

Figure 11

From this Figure, the maximum of the $\bar{\chi}$ values in the low-temperature region is observed, suggesting us the existence of an antiferromagnetic coupling in the solid powder. The position of the maximum is associated to a very low intensity of this magnetic coupling. Interestingly, at temperatures below this maximum, the $\bar{\chi}$ values do not increase when the temperature is decreased, suggesting us the absence of non coupled $S = 1/2$ spins, assumed as magnetic impurity. The $\bar{\chi}T - T$ data at $H = 10000\text{G}$ show a smooth decrease of the $\bar{\chi}T$ values with the decrease of temperature in the 300-50 K range. Upon further temperature decrease, an abrupt decrease of $\bar{\chi}T$ is observed. This behavior of $\bar{\chi}T$ with the temperature decrease is characteristic of an antiferromagnetic coupling in the sample. The magnetic coupling quoted before is supported by the fitting of the Curie- Weiss equation to the $\bar{\chi} - T$ experimental data ($H = 10000\text{G}$, 15- 300 K). From this, the parameters $C = 0.4151 \text{ emu K/mol}$, $\theta = -14.39 \text{ K}$ and $\bar{\chi}_0 = 4.8355 \times 10^{-5} \text{ emu/mol}$ were obtained. The θ value indicates the magnetic coupling type quoted above.

In order to study this magnetic coupling, and considering the correspondent structural information available[14], a linear chain magnetic model of $S = 1/2$ coupled spins was selected. From this, the Bonner-Fisher equation for the fitting process was employed. The very good fit obtained for $H = 10000$ G is also shown in Figure 11. With $\rho = 0$, the parameters $g = 2.007$, $J = -4.69$ cm⁻¹ and $\bar{\chi}_0 = 4.8355 \times 10^{-5}$ emu/mol were obtained. An approximate agreement between the g value here obtained and the one from the EPR data ($g = 2.12$) is observed. Besides, the J value is in good agreement with the suggestion of a very weak antiferromagnetic coupling in the product. Fixing $g = 2.12$, a good fit was obtained, with $J = -5.64$ cm⁻¹ as the parameter of intrachain superexchange magnetic coupling.

Considering the structural information previously reported[14] for this polynuclear Cu(II) compound (in which crosslinked Cu(II) chains with both bridging hypoxanthine and SO₄²⁻ groups exist), the possibility of two types of magnetic coupling in the network was established (one intrachain and other interchain). To explore this, the Bonner-Fisher equation with the Curie-Weiss correction was employed in the fitting process. A very good fit was made for $\rho = 0$ and $\bar{\chi}_0 = 1 \times 10^{-4}$ emu/mol fixed, with the resulting parameters: $g = 2.01$, $J = -5.03$ cm⁻¹ and $\theta = +0.34$ K. These results are shown in Figure 12.

Figure 12

From these, approximate concordance between the spectral and the magnetic g values is observed. The J value (assumed as the intrachain magnetic coupling parameter) is in agreement with its previous calculation. The θ value let us suspect the existence of another type of magnetic interaction, inferred as very weak ferromagnetic coupling. This would be for the unpaired electrons of the Cu(II) atoms between the nearest neighboring chains considered. These results could be associated to the crosslinked Cu(II) chains network, and to the possibility of magnetic coupling of Cu(II) atoms through the two types of bridging ligands. In order to study another approximation, the Bonner-Fisher equation

with a mean-field correction was selected. From the excellent fitting process with $\rho = 0$, and which is shown in Figure 13, the following parameters $g = 2.05$, $J = -5.28 \text{ cm}^{-1}$ and $zJ' = +26.45 \text{ cm}^{-1}$ were obtained.

Figure 13

The results for J and zJ' supports the above J and θ values, *i.e.*, the suggestion of two types of very weak magnetic coupling. Assuming as reference a linear chain with the bridging hypoxanthine molecules and considering the respective crystalline packing[14], the number of nearest neighboring chains (z) is six. For this z value, $J' = +4.4 \text{ cm}^{-1}$. The same consideration can be applied to the Cu(II) chains constructed by the bridging SO_4^{2-} groups.

Finally, assuming $\rho = 0$ and $\bar{\chi}_0 = 0 \text{ emu/mol}$, a good fit was made. From this, the parameters $g = 2.08$, $J = -5.04 \text{ cm}^{-1}$ and $zJ' = +5.15 \text{ cm}^{-1}$ were obtained. For $z = 6$, $J' = +0.86 \text{ cm}^{-1}$. The J and J' values are in qualitative agreement with the previous calculations. However and at this level of study, it is difficult to dilucidate about the contribution of each type of Cu(II) chain to the magnetic coupling of the unpaired spins. $\text{Cu(II)(hypoxanthine)}_2(\text{ClO}_4^-)_2$.

The $\bar{\chi}$ (emu/mol of tetranuclear Cu(II) unit) *vs.* T (K) experimental data ($H = 10000 \text{ G}$) for this Cu(II) compound are shown in Figure 14.

Figure 14

From the $\bar{\chi} - T$ data a continue increase of the $\bar{\chi}$ values with the temperature decrease is observed. Plotting $\bar{\chi}T - T$ a continue decrease of $\bar{\chi}T$ with the temperature decrease is observed in the 300-25 K range. Upon further lowering of the temperature, an abrupt decrease of the $\bar{\chi}T$ values is observed, which indicates a very weak antiferromagnetic coupling in the Cu(II) compound. Fitting the Curie- Weiss equation to the $\bar{\chi} - T$ data,

good results were obtained, with the following parameters: $C = 0.0989$ emu K/mol of Cu(II) unit, $\theta = -7.56$ K and $\bar{\chi}_0 = 0.00108$ emu/mol of Cu(II) unit. The θ value supports the antiferromagnetic coupling quoted before.

Considering the spectral information and the preliminary magnetic studies, two magnetic models were explored in the magnetic characterization of this Cu(II) compound. The first one was the linear chain magnetic model of $S = 1/2$ coupled spins. From this, the Bonner-Fisher equation was used for the fitting process. With fixed $g = 2.11$, the following parameters were obtained: $J = -5.22$ cm⁻¹, $\rho = 0.107$ and $\bar{\chi}_0 = 0.0040$ emu/mol of tetranuclear Cu(II) unit. The J value supports the suggestion of very weak antiferromagnetic coupling, of intrachain character. Considering the possibility of interchain magnetic coupling, the Bonner-Fisher equation with the Curie-Weiss correction was employed in the fitting process to the experimental data. With fixed $g = 2.11$ and $\rho = 0.107$, the following parameters were obtained: $J = -1.88$ cm⁻¹, $\theta = -9.16$ K and $\bar{\chi}_0 = 0.00429$ emu/mol of tetranuclear Cu(II) unit. The J value is in agreement with the suggestion of very weak intrachain magnetic coupling. The θ value let us suspect the existence of very weak interchain magnetic coupling, assumed as antiferromagnetic in character. The theoretical curve is also shown in Figure 14. Finally, and employing the Bonner-Fisher equation with a mean-field correction, the following parameters (with fixed $g = 2.11$ and $\rho = 0.107$) were obtained: $J = -5.47$ cm⁻¹, $zJ' = +2.45$ cm⁻¹ and $\bar{\chi}_0 = 0.0024$ emu/mol of tetranuclear Cu(II) unit. Here, the J value supports the existence of very weak intrachain antiferromagnetic coupling. The zJ' value let us suspect the possibility of very weak interchain magnetic coupling, although in this case of ferromagnetic character. At this level of study, it is difficult to discern the correctness of the physical meaning for the θ and zJ' values. Nevertheless, both point out to the suggestion of very weak interchain magnetic coupling. The second model selected was the dinuclear system of $S = 1/2$ coupled spins. From this, the Bleaney-Bowers equation was employed. Using both the Curie-Weiss and the mean-field corrections, good fits were obtained, but with unrealistic physical meaning of the

magnetic parameters, or appreciable errors in the values of the same parameters. These last results let us discard the dinuclear system as the possible structural arrangement of the magnetically coupled Cu(II) units, and let us propose the possibility of magnetic coupling between the unpaired electrons of Cu(II) units through a linear chain structural arrangement. In this, the coordinated ClO_4^- ligands would play the critical role as magnetic coupling pathway between the unpaired electrons of the Cu(II) units. In this structural suggestion of interacting Cu(II) units, very weak interchain magnetic coupling appears also as feasible.

$\text{Cu(II)(hypoxanthinate}^-\text{)(CH}_3\text{CO}_2^-)$.

The $\bar{\chi}$ (emu/mol of tetranuclear Cu(II) unit) vs. T (K) experimental data ($H = 10000$ G) for this Cu(II) compound are shown in Figure 15.

Figure 15

From this an increase of the $\bar{\chi}$ values with a temperature decrease is observed. Plotting $\bar{\chi}T - T$ a continue decrease of the $\bar{\chi}$ values upon a decrease in temperature is obtained in the 300-50 K range. Upon further temperature decrease, an abrupt decrease of the $\bar{\chi}T$ values is observed, which indicates a very weak antiferromagnetic coupling in the solid product. Fitting the Curie-Weiss equation to the experimental data, very good results were obtained, with the following parameters: $C = 0.245$ emu K/mol, $\theta = -11.14$ K and $\bar{\chi}_0 = 6.568 \times 10^{-4}$ emu/mol. The θ value supports the existence of very weak antiferromagnetic coupling in the sample.

Considering the precedent spectral information and the preliminary magnetic results, several magnetic models were explored in the magnetic characterization of this Cu(II) compound. The first magnetic model was the linear chain of $S = 1/2$ coupled spins. From this, the Bonner-Fisher equation was used in the fitting process. Very good results were obtained, being the parameters: $g = 2.85$, $J = -4.32$ cm $^{-1}$, $\rho = 0.094$ and $\bar{\chi}_0 = 0.00382$

emu/mol of tetranuclear Cu(II) unit. The J value supports the suggestion of very weak intrachain antiferromagnetic coupling. The theoretical curve is also shown in Figure 15. Considering the possibility of interchain magnetic coupling, the same equation with the Curie-Weiss correction was employed. From the very good fit, the following parameters were obtained: $g = 2.89$, $J = -3.28 \text{ cm}^{-1}$, $\theta = -3.23 \text{ K}$, $\rho = 0.107$ and $\bar{\chi}_0 = 0.00365$ emu/mol of tetranuclear Cu(II) unit. The J value is in agreement with its precedent calculation. The θ value let us suspect the existence of very weak interchain magnetic coupling, of antiferromagnetic type. Employing the same equation with a mean-field correction, a very good fit was obtained, with the following parameters: $g = 2.68$, $J = -5.53 \text{ cm}^{-1}$, $zJ' = -8.65 \text{ cm}^{-1}$, $\rho = 0.24$ and $\bar{\chi}_0 = 0.00166$ emu/mol of tetranuclear Cu(II) unit. The J and zJ' values are in agreement with the above calculation for J and θ . In summary, this magnetic model let us consider the existence of both very weak intrachain and interchain antiferromagnetic coupling in the solid product.

The second model selected was the dinuclear system of $S = 1/2$ coupled spins. From this, the Bleaney-Bowers equation was employed in the fitting process. Using both the Curie-Weiss and the mean-field correction, very good results were obtained, but the g values calculated were very low ($g < 2$). These last results, let us consider the non realistic character of the dinuclear magnetic model in describing the magnetic behavior of the Cu(II) compound in study.

The third type of magnetic model explored was the tetranuclear one. For this, several symmetries were considered. For the tetranuclear model with a T_d symmetry, very good results in the fitting process were obtained, with the following parameters: $J = -7.04 \text{ cm}^{-1}$, $\rho = 0.206$ and $\bar{\chi}_0 = 0.0041$ emu/mol of tetranuclear Cu(II) unit. Unfortunately, the g value was very low ($=1.60$). For lower symmetries, both unsuccessful fits and unrealistic physical meaning of the magnetic parameters, or noticeable errors in their values, were obtained. As before, these results let us consider the unsuccessful character of the tetranuclear magnetic models in the description of the magnetic behavior of the solid

product in study. At this respect, the linear chain magnetic model (considering both intrachain and interchain magnetic coupling) arises as the best in the magnetic description of this compound.

With the spectral and magnetic studies for this compound, a suggestion of its structural arrangement can be made. This consists of Cu(II) atoms bridged by CH_3CO_2^- groups, forming chains. The connection between the chains would be made through the bridges hypoxanthinate⁻ ligands, bonded to Cu(II) atoms of different chains. This structural arrangement proposition is schematically shown in Figure 16.

Figure 16

At this level of study, it is difficult to dilucidate about the origin (nature) of the two types of magnetic coupling, *i.e.*, intrachain and interchain, discussed before in the correspondent magnetic model.

IV. Concluding Remarks.

In this study, new Cu(II) coordination compounds with the respective heterocycles allopurinol and hypoxanthine were obtained and characterized. Also, alternative synthetic techniques for the polynuclear compounds $\text{Cu(II)(allopurinolate}^-\text{)(OH}^-\text{)}$ and $\text{Cu(II)(6-mercaptopurinolate}^{2-}\text{)}$ were found. For the new Cu(II) compounds with allopurinol and hypoxanthine, the correspondent starting metallic counterions form part of their formulation, almost all as groups bonded to the metallic centers.

From the studies of competitive Cu(II)-heterocycle interactions, the S(6)-purine derivative showed the higher capabilities both of heterocyclic substitution and metallic bonding. These properties appear to be strongly related to its deprotonation and the participation of several donor atoms in the metallic coordination. Also, and as in the previous study[7], Cu(II) compounds with mixed heterocyclic ligands were not synthesized.

With respect to the nature of the metallic bonding sites involved in the coordinated heterocycles, N(2) is the atom suggested for allopurinol. For hypoxanthine, the N(7) or N(9)

atoms are the suggested for $X=\text{ClO}_4^-$; $\underline{N}(3)$ and $\underline{N}(7)$ are deduced for $X=\text{SO}_4^{2-}$. For $X=\text{CH}_3\text{CO}_2^-$, a detailed suggestion cannot be made. Finally, and for 6-mercaptopurine, a previous study[8] points out the $\underline{S}(6)$, $\underline{N}(7)$ and $\underline{N}(9)$ atoms as the coordination sites of the anionic heterocyclic ligand.

The magnetic characterization reported here of the new Cu(II) coordination compounds with allopurinol and hypoxanthine, is in agreement with the existence of very weak antiferromagnetic coupling in the solid products. In this magnetic study, the linear chain magnetic model is the best in describing the magnetic behavior of the systems. In the physical meaning about the origin of the respective intrachain and interchain magnetic coupling, the polyatomic and anionic ligands SO_4^{2-} , ClO_4^- and CH_3CO_2^- and also the neutral and monoanionic hypoxanthine, contribute to the respective magnetic behavior explored. However, and at this level of study, it is difficult to discern about the type of contribution of each one of these ligands to the respective intrachain and interchain magnetic coupling, deduced from the correspondent magnetic analysis.

V. Acknowledgments

We are specially indebted to Professor Roberto Escudero Derat (IIM-UNAM) for the exhaustive and carefully done magnetic measurements. We also thank Max Azomoza-Palacios (UAM-Iztapalapa) and Carmen Vazquez-Ramos (IIM- UNAM) for the thermogravimetric data, and Jorge Ramírez-Salcedo (IFC-UNAM) for the EPR spectral determinations. We also indebted to CONACyT (Grant 3170-E) for partial financial support.

References

- [1] N.M. Hughes. *The Inorganic Chemistry of Biological Processes*. 2nd. Ed.. John Wiley & Sons, New York. 1981.
- [2] R.K. Robins. G.R. Revankar. D.E. O'Brien. R.H. Springer. T. Novinson. A. Albert. K. Senga. J.P. Miller and D.G. Streeter. *J. Heterocyclic Chem.*, **22**, 601 (1985).
- [3] L. Stryer. *Biochemistry*. 3rd Ed.. Freeman, New York. 1988.
- [4] R. Acevedo-Chávez, M.E. Costas and R. Escudero-Derat. *J. Solid State Chem.*, **113**, 21 (1994) and references quoted.
- [5] *CRC Handbook of Nucleobase Complexes*. Vol. I. J.R. Lusty, Ed.. CRC Press, Inc., USA. 1990 and references therein.
- [6] E. Dubler and E. Gyr, *Inorg. Chem.*, **27**, 1446 (1988) and references therein.
- [7] R. Acevedo-Chávez and M.E. Costas, *Spectral and Magnetic Characterization of Novel Cu(II) Coordination Compounds Synthesized in Methanolic Medium with the Heterocycles Allopurinol, Hypoxanthine and 6-mercaptopurine. I.*, Submitted for publication.
- [8] R. Acevedo-Chávez, M.E. Costas and R. Escudero. *Magnetic study of the Novel Polynuclear Compound $[Cu(II)(6\text{-mercaptopurinate}^{2-})]_n$* . Submitted for publication.
- [9] R. Acevedo-Chávez and N. Barba-Behrens. *Transition Met. Chem.*, **15**, 434 (1990) and references therein.
- [10] M.Q. Olazábal. J.M.S. Peregrín. M.P.S. Sánchez. F.G. Vilchez and M.R. Medina. *Thermochimica Acta*. **103**, 305 (1986).
- [11] C.M. Mikulski. S. Grossman. C.J. Lee and N.M. Karayannis. *Transition Met. Chem.*, **12**, 21 (1987).
- [12] C.M. Mikulski. S. Grossman. and N.M. Karayannis. *J. Less- Common Met.*, **136**, 41 (1987).
- [13] D. Mulet. A.M. Calafat, J.J. Fiol, A. Terron and V. Moreno. *Inorg. Chim. Acta.*, **138**, 199 (1987).

- [14] E. Dubler, G. Hänggi and W. Bensch. *J. Inorg. Biochem.*, **29**, 269 (1987).
- [15] C.M. Mikulski, M.K. Kurlan, M.L. Bayne, M. Gaul and N.M. Karayannis. *J. Coord. Chem.*, **18**, 297 (1988).
- [16] C.M. Mikulski, M.L. Bayne, S. Grossman, M. Gaul, A. Renn, D.L. Staley and N.M. Karayannis. *J. Coord. Chem.*, **20**, 185 (1989).
- [17] C.M. Mikulski, S. Grossman, M.L. Bayne, M. Gaul, D.L. Staley, A. Renn and N.M. Karayannis. *Inorg. Chim. Acta.*, **161**, 29 (1989).
- [18] B.J. Hathaway and A.E. Underhill. *J. Chem. Soc.*, 3091 (1961).
- [19] F.A. Cotton and D.L. Weaver. *J. Am. Chem. Soc.*, **87**, 4189 (1965).
- [20] S.F. Pavkovic and D.W. Meek. *Inorg. Chem.*, **4**, 1091 (1965).
- [21] A.E. Wickenden and R.A. Krause. *Inorg. Chem.*, **4**, 404 (1965).
- [22] M.E. Farago, J.M. James and V.C.G. Trew. *J. Chem. Soc. A*, 820 (1967).
- [23] A.N. Specca, C.M. Mikulski, F.J. Iaconianni, L.L. Pytlewski and N.M. Karayannis. *Inorg. Chem.*, **19**, 3491 (1980).
- [24] C.M. Mikulski, L. Mattucci, Y. Smith, T.B. Tran and N.M. Karayannis. *Inorg. Chim. Acta*, **66**, L71 (1982).
- [25] C.M. Mikulski, T.B. Tran, L. Mattucci and N.M. Karayannis. *Inorg. Chim. Acta*, **78**, 211 (1983).
- [26] N.M.N. Gowda, S.B. Naikar and G.K.N. Reddy. *Adv. Inorg. Chem. Radiochem.*, **28**, 255 (1984).
- [27] C.M. Mikulski, M.K. Kurlan, M. Bayne, M. Gaul and N.M. Karayannis. *Inorg. Chim. Acta*, **123**, 27 (1986).
- [28] K. Nakamoto. *Infrared Spectra of Inorganic and Coordination Compounds*; 2nd. Ed., John Wiley & Sons, Inc., USA, 1978.
- [29] J.E. Finholt, K. Caulton, K. Kimball and E. Uhlenhopp. *Inorg. Chem.*, **7**, 610 (1968).

Tables.

Table 1. Products obtained from both single and competitive heterocycle-Cu(II) reactions. *a.* see Analytical Results; *b.* see Experimental Section; L₁=allopurinol, L₂=hypoxanthine, L₃=6-mercaptopurine.

Table 2. Analytical results of the Cu(II) compounds obtained. Abbreviations are the same as in Table 1.

Table 3. IR data and bands characterization of both free and coordinated ligand allopurinol (=L₁) in its Cu(II) coordination compounds. Abbreviations: S, strong; M, medium; W, weak; VW, very weak; vbr, very broad; br, broad; s, sharp; Sh, shoulder; d, doublet.

Table 4. IR data and bands characterization of both free and coordinated ligand hypoxanthine (=L₂) in its Cu(II) coordination compounds. Same abbreviations as in Table 3.

Figure Captions.

Figure 1. Schematic drawing of the heterocycles allopurinol (I), hypoxanthine (II) and 6-mercaptopurine (III).

Figure 2. X-band ($\nu = 9.5203$ GHz) EPR spectrum at room temperature of powdered $\text{Cu(II)(allopurinol)}_4(\text{ClO}_4^-)_2$.

Figure 3. Schematic drawing of the structural arrangement suggested for $\text{Cu(II)(allopurinol)}_4(\text{ClO}_4^-)_2$.

Figure 4. X-band ($\nu = 9.25$ GHz) EPR spectrum at room temperature of powdered $\text{Cu(II)(allopurinol)(SO}_4^{2-})(\text{H}_2\text{O})$.

Figure 5. Schematic drawing of the structural arrangement suggested for $\text{Cu(II)(allopurinol)(SO}_4^{2-})(\text{H}_2\text{O})$.

Figure 6. X-band ($\nu = 9.78$ GHz) EPR spectrum at room temperature of powdered $\text{Cu(II)(hypoxanthine)(SO}_4^{2-})(\text{H}_2\text{O})$.

Figure 7. Schematic drawing of the structural arrangement suggested for $\text{Cu(II)(hypoxanthine)(SO}_4^{2-})(\text{H}_2\text{O})$.

Figure 8. X-band ($\nu = 9.5196$ GHz) EPR spectrum at room temperature of powdered $\text{Cu(II)(hypoxanthine)}_2(\text{ClO}_4^-)_2$.

Figure 9. $\bar{\chi}$ (emu/mol)- T (K) experimental data (dotted line) at $H = 10000$ G of powdered $\text{Cu(II)(allopurinol)}_4(\text{ClO}_4^-)_2$. Solid line, theoretical $\bar{\chi}$ values from the Bonner-Fisher equation with the Curie-Weiss correction.

Figure 10. $\bar{\chi}$ (emu/mol)- T (K) experimental data (dotted line) at $H = 100$ G of powdered $\text{Cu(II)(allopurinol)(SO}_4^{2-})(\text{H}_2\text{O})$. Solid line, theoretical $\bar{\chi}$ values from the Bonner-Fisher equation with the Curie-Weiss correction.

Figure 11. $\bar{\chi}$ (emu/mol)- T (K) experimental data (dotted line) at $H = 10000$ G of powdered $\text{Cu(II)(hypoxanthine)(SO}_4^{2-})(\text{H}_2\text{O})$. Solid line, theoretical $\bar{\chi}$ values from the Bonner-Fisher equation.

Figure 12. $\bar{\chi}$ (emu/mol)- T (K) experimental data (dotted line) at $H = 10000$ G of powdered Cu(II)(hypoxanthine)(SO₄²⁻)(H₂O). Solid line, theoretical $\bar{\chi}$ values from the Bonner-Fisher equation with the Curie-Weiss correction.

Figure 13. $\bar{\chi}$ (emu/mol)- T (K) experimental data (dotted line) at $H = 10000$ G of powdered Cu(II)(hypoxanthine)(SO₄²⁻)(H₂O). Solid line, theoretical $\bar{\chi}$ values from the Bonner-Fisher equation with the mean-field correction.

Figure 14. $\bar{\chi}$ (emu/mol of tetranuclear Cu(II) unit)- T (K) experimental data (dotted line) at $H = 10000$ G of powdered Cu(II)(hypoxanthine)₂(ClO₄⁻)₂. Solid line, theoretical $\bar{\chi}$ values from the Bonner-Fisher equation with the Curie-Weiss correction.

Figure 15. $\bar{\chi}$ (emu/mol of tetranuclear unit)- T (K) experimental data (dotted line) at $H = 10000$ G of powdered Cu(II)(hypoxanthinate⁻)(CH₃CO₂⁻). Solid line, theoretical $\bar{\chi}$ values from the Bonner-Fisher equation.

Figure 16. Schematic drawing of the structural arrangement suggested for Cu(II)(hypoxanthinate⁻)(CH₃CO₂⁻).

Reaction	SO_4^{2-}			ClO_4^-			CH_3CO_2^-		
	t (days)	Color	Prod.(s) ^a	t (days)	Color	Prod.(s) ^a	t (days)	Color	Prod.(s) ^a
$\text{M}+\text{L}_1 \rightleftharpoons$	11	deep blue	1	10	lilac	4	10	deep blue	1
$\text{M}+\text{L}_2 \rightleftharpoons$	13	pale blue	2	10	deep blue	5	11	deep green	6
$\text{M}+\text{L}_3 \rightleftharpoons$	8	dark green	3	8	dark green	3	9	dark green	3
$[\text{M}+\text{L}_1]+\text{L}_2 \rightleftharpoons$	10	deep blue	1	8	lilac	4	10	deep blue	1
$[\text{M}+\text{L}_1]+\text{L}_3 \rightleftharpoons$	15	dark green	3	15	dark green	3	15	dark green	3
$[\text{M}+\text{L}_2]+\text{L}_1 \rightleftharpoons$	10	pale blue	2	10	deep blue	5	7	deep green	6
$[\text{M}+\text{L}_2]+\text{L}_3 \rightleftharpoons$	10	dark green	3	10	dark green	3	15	dark green	3
$[\text{M}+\text{L}_3]+\text{L}_1 \rightleftharpoons$	10	dark green	3	10	dark green	3	10	dark green	3
$[\text{M}+\text{L}_3]+\text{L}_2 \rightleftharpoons$	10	dark green	3	10	dark green	3	15	dark green	3
$(\text{L}_1+\text{L}_2)+\text{M} \rightleftharpoons$	10	pale blue	2	7	lilac	4	8	deep blue	1
$(\text{L}_1+\text{L}_3)+\text{M} \rightleftharpoons$	15	dark green	3	15	dark green	3	15	dark green	3
$(\text{L}_2+\text{L}_3)+\text{M} \rightleftharpoons$	15	dark green	3	15	dark green	3	15	dark green	3
$(\text{L}_1+\text{L}_2+\text{L}_3)+\text{M} \rightleftharpoons$	10	dark green	3	15	dark green	3	15	dark green	3
$\text{M}+\text{L}_1 \rightleftharpoons$	0.3	pale green	7 ^b						

Table 1.

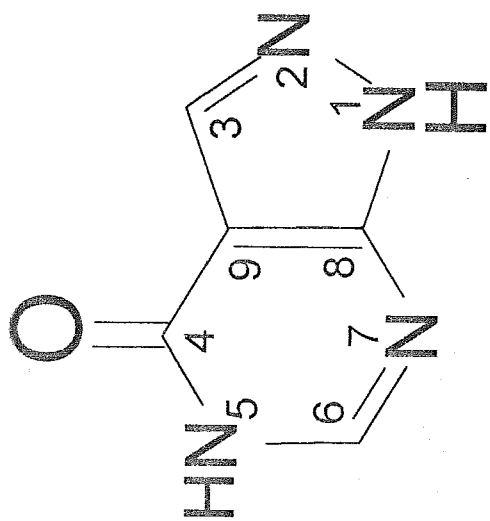
Formulation	Compound	Expected			Found		
		% C	% H	% N	% C	% H	% N
$\text{Cu}(\text{L}_1^-)(\text{OH}^-)$	1	27.80	1.90	25.90	27.50	1.90	26.00
$\text{Cu}(\text{L}_2)(\text{SO}_4^{2-})(\text{H}_2\text{O})$	2	19.14	1.93	17.86	19.58	1.93	18.08
$\text{Cu}(\text{L}_3^{2-}) \bullet 2\text{H}_2\text{O}$	3	24.05	2.42	22.43	24.17	2.36	22.59
$\text{Cu}(\text{L}_1)_4(\text{ClO}_4^-)_2$	4	29.77	2.00	27.77	31.70	2.31	29.25
$\text{Cu}(\text{L}_2)_2(\text{ClO}_4^-)_2$	5	22.46	1.51	20.96	22.56	1.40	20.69
$\text{Cu}(\text{L}_2^-)(\text{CH}_3\text{CO}_2^-)$	6	32.63	2.35	21.74	32.71	2.44	22.20
$\text{Cu}(\text{L}_1)(\text{SO}_4^{2-})(\text{H}_2\text{O})$	7	19.14	1.93	17.86	19.02	1.87	17.62

Table 2.

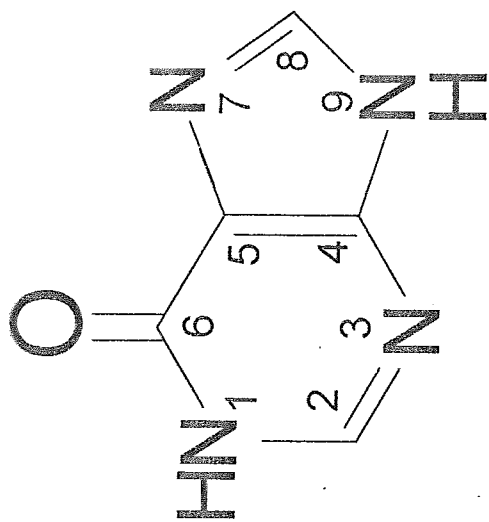
Allopurinol (=L ₁)		Cu(L ₁) ₄ (ClO ₄ ⁻) ₂		Cu(L ₁) ₁ (SO ₄ ²⁻) ₁ (H ₂ O) ₁		Assignments
$\bar{\nu}$ cm ⁻¹	Charac.	$\bar{\nu}$ cm ⁻¹	Charac.	$\bar{\nu}$ cm ⁻¹	Charac.	
-	-	3420	W,Sh	-	-	n.a.
-	-	-	-	3377	W,br	n.a.
3170	VW,br	3170	VW,br	-	-	ν_{C-H}/ν_{N-H}
3080	VW,br	3080	VW,br	3084	W,br	ν_{C-H}/ν_{N-H}
1700	S,br	1685	S,br	1698	S,br	$\nu_{C=O}/\nu_{C=C}/\nu_{C=N}$
1595	S,br	1600	M,br	1606	S,br	$\delta_{N(5)-H}/\text{ring vib.}$
-	-	1500	W,br	1578 1517	W, s M, br	$\nu_{C=C}/\nu_{C=N}$
1390	S,br	1400	W,br	1405	M,br	ring vib.
1370	S,s	-	-	1366	M,s	pyrazolic ring vib./ ν_{C-N}
1240	S,br	1250	M,br	1254	M,br	A ^{''} $\delta_{C-H}/\nu_{C-C}/\nu_{C-N}$
1230	S,br	1220	W,br	1220	VW,s	A ^{''} $\delta_{C-H}/\nu_{C-C}/\nu_{C-N}$
1160	W,br	-	-	-	-	A ^{''} $\delta_{C-H}/A^{\prime\prime}\delta_{N-H}$
1080	M,br	-	-	-	-	C-H vib.
-	-	992	W,br	-	-	n.a.
960	S,s	943	VW,br	977	W,s	pyrazolic ring vib.
915	S,s	920	VW,br	919	M,s	ring vib./A ^{''} δ_{N-H}
885	S,br	-	-	892	W,s	$\gamma_{C-H}/\text{ring vib.}$
815	M,br	-	-	-	-	γ_{C-H}
785	S,s	780	M,s	785	S,s	ring vib./C-H vib.
710	S,s	725 720	W, s W, s	725	W,s	C-H vib.
605	S,s	610	M,br	618	S,br	ring vib.
550	M,s	-	-	544	W,br	skel. vib.
540	M,s	540	W,br	525	VW,s	skel. vib.
326	M,s	363	M,br	320	M,br	skel. vib.
220	VW,br	220	W,br	216	VW,br	skel. vib.
210	VW,br	210	W,br	210	VW,br	skel. vib.
-	-	-	-	385	W,br	$\nu_{Cu-Ligand}$
-	-	285	M,br	304	M,br	$\nu_{Cu-Ligand}$
-	-	275	M,br	296	M,br	$\nu_{Cu-Ligand}$
-	-	265	M,br	286	M,br	$\nu_{Cu-Ligand}$

Table 3.

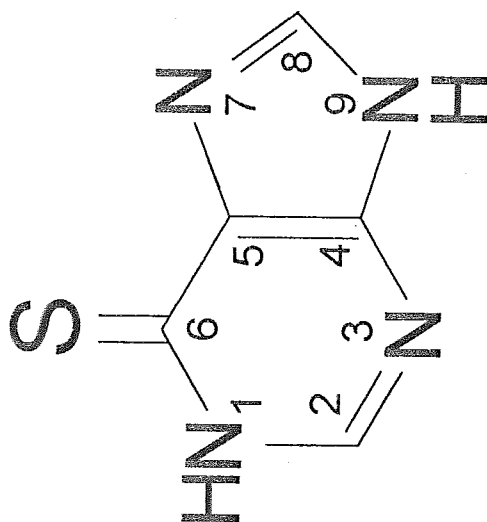
Hypoxanthine (=L ₂)		Cu(L ₂)(SO ₄) ₂ ·n(H ₂ O)		Cu(L ₂) ₂ (ClO ₄) ₂		Cu(L ₂)(CH ₃ CO ₂)		Assignments
$\tilde{\nu}$ cm ⁻¹	Charac.	$\tilde{\nu}$ cm ⁻¹	Charac.	$\tilde{\nu}$ cm ⁻¹	Charac.	$\tilde{\nu}$ cm ⁻¹	Charac.	
-	-	-	-	3390	W,br	-	-	n.a.
-	-	3200	W,br	-	-	-	-	n.a.
3140	W,s	3110	W,s	3170	VW,Sh	-	-	ν_{C-H} arom./ ν_{N-H}
3050	W,br	3060	VW,s	3070	VW,br	-	-	ν_{C-H} arom./ ν_{N-H}
1670	S,br	1720	S,br	1680	S,br	-	-	$\nu_{C=O}/\nu_{C=C}/\nu_{C=N}$
1583	M,br	1580	M,br	1600	W,br	-	-	$\delta_{N(C)-H}$
1516	VW,br	-	-	1510	W,br	-	-	ring vib./ ν_{C-N}/δ_{N-H}
-	-	-	-	1498	W,br	-	-	ring vib./ ν_{C-N}/δ_{N-H}
1424	M,s	-	-	1410	M,s	1410	W,br	ring vib./ ν_{C-N}/δ_{N-H}
1380	W,s	-	-	-	-	-	-	ring vib./ ν_{C-N}/δ_{N-H}
1350	M,s	1335	M,s	1336	W,br	-	-	ring vib./ ν_{C-N}/δ_{N-H}
-	-	-	-	1310	VW,br	-	-	ring vib./ ν_{C-N}/δ_{N-H}
1276	M,s	1303	W,br	1250	W,br	1290	W,Sh	ring vib./ ν_{C-N}/δ_{N-H}
-	-	-	-	-	-	1230	VW,s	ring vib./ ν_{C-N}/δ_{N-H}
1215	S,s	1236	M,br	1196	S,br	1180	S,br	ring vib./ ν_{C-N}/δ_{N-H}
1153	M,s	1105	M,br	1160	W,br	1100	M,br	ring vib./ ν_{C-N}/δ_{N-H}
1140	M,s	1090	M,br	-	-	-	-	ring vib./ ν_{C-N}/δ_{N-H}
966	M,br	980	M,br	940	VW,s	1015	VW,s	ring vib./ δ_{C-H}
910	VW,br	-	-	-	-	-	-	ring vib./C-H vib.
893	S,s	900	VW,s	885	VW,br	890	VW,s	ring vib./C-H vib.
793	M,s	785	W,s	780	M,br	795	M,br	ring vib./C-H vib.
-	-	-	-	-	-	720	M,br	ring vib./C-H vib.
646	M,s	730	M,br	716	W,br	650	M,s	C-H vib./skel. vib.
633	M,s	720	M,br	695	W,s	-	-	C-H vib./skel. vib.
-	-	-	-	594	W,s	-	-	C-H vib./skel. vib.
566	M,s	580	W,s	570	VW,s	570	VW,s	C-H vib./skel. vib.
525	W,s	555	W,br	546	W,br	540	VW,Sh	skelet. vib.
367	M,s	357	W,br	395	W,br	400	VW,vbr	skelet. vib.
345	W,s	323	VW,s	-	-	-	-	skelet. vib.
243	VW,br	260	VW,br	240	VW,s	246	VW,br	skelet. vib.
223	VW,br	225	VW,br	220	VW,br	223	VW,br	skelet. vib.
210	VW,br	-	-	210	VW,s	210	VW,br	skelet. vib.
-	-	428	W,br	300	M,br	303	M,br	ν_{Cu} -ligand
-	-	285	M,br	286	M,br	290	M,br	ν_{Cu} -ligand
-	-	275	M,br	-	-	280	M,br	ν_{Cu} -ligand



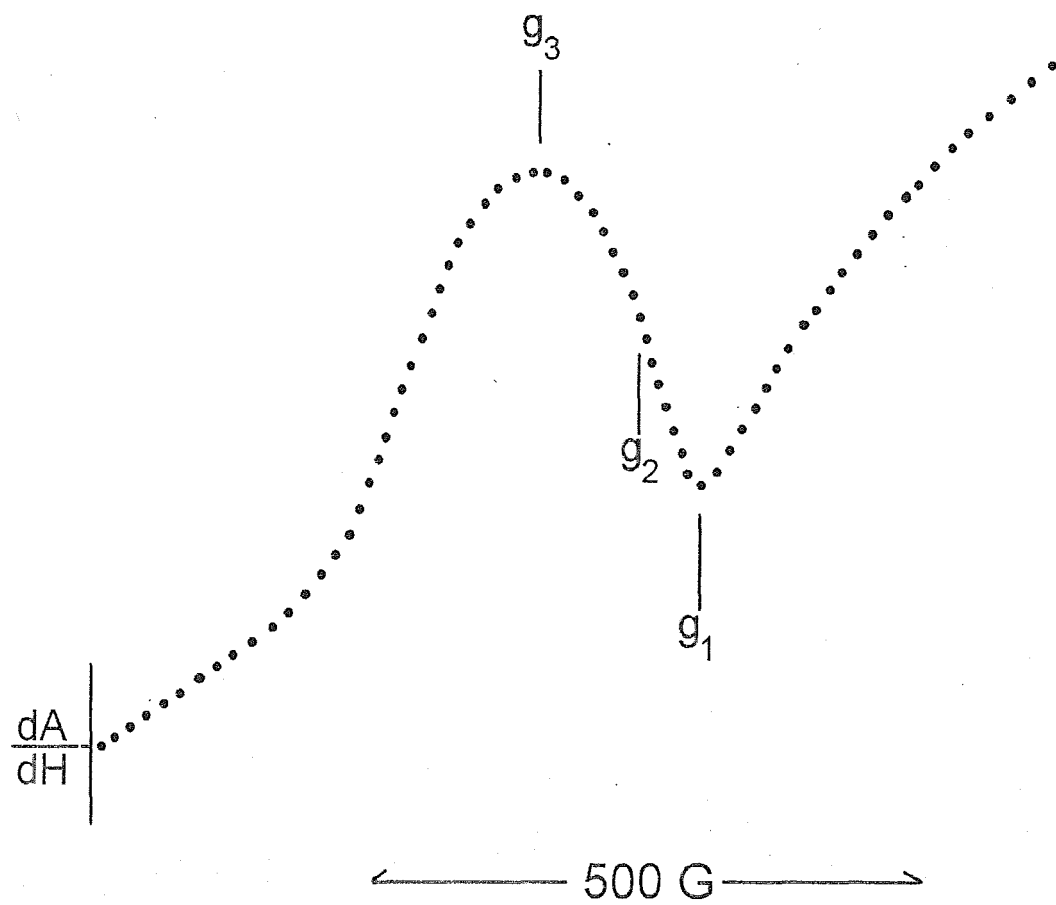
I

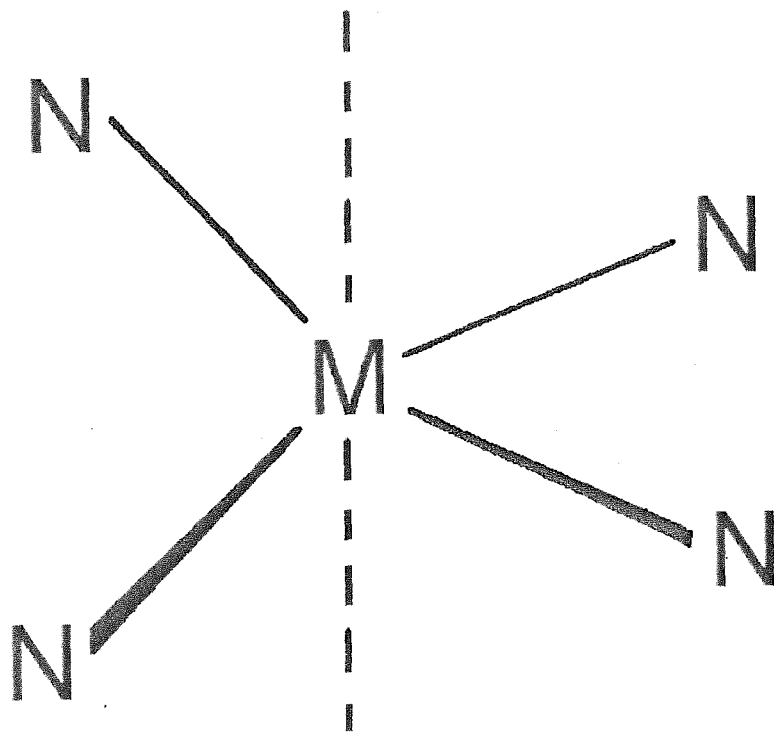


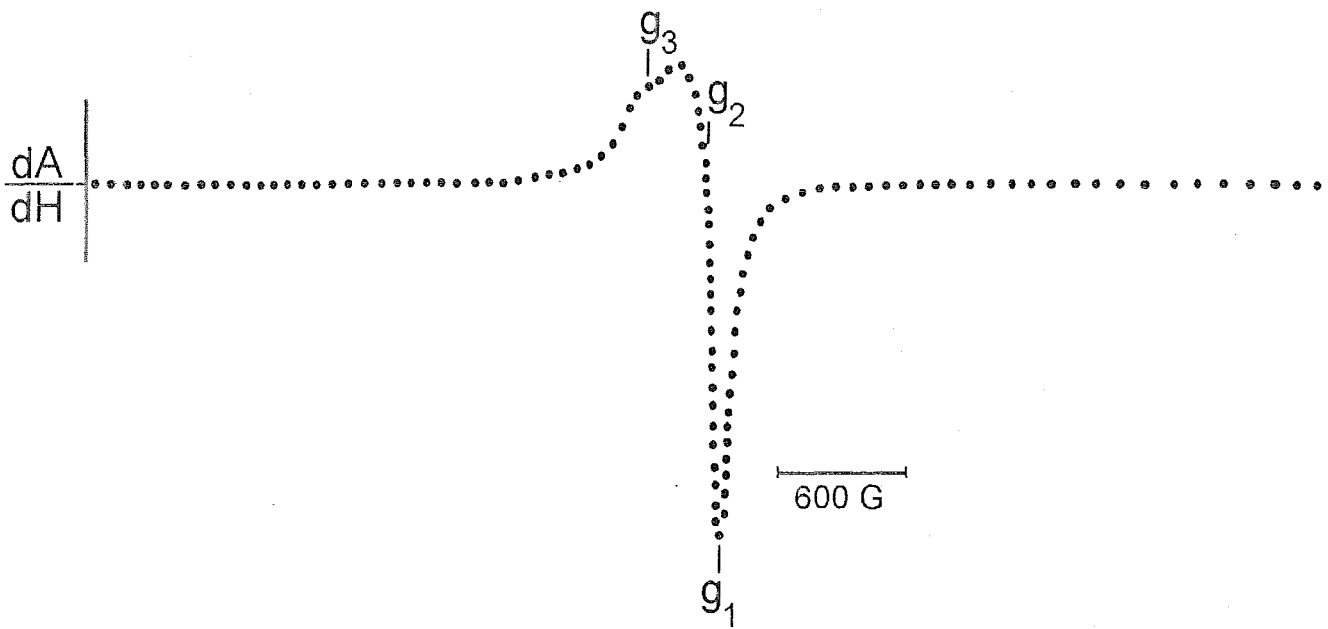
II

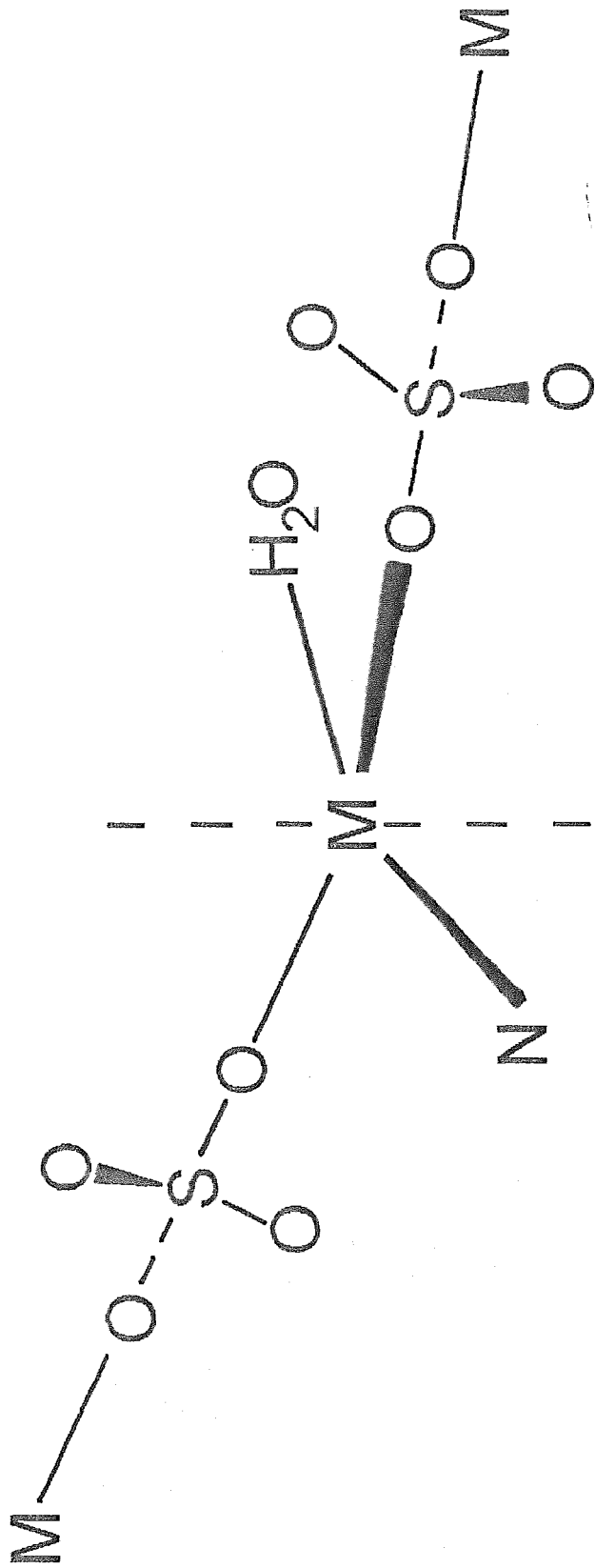


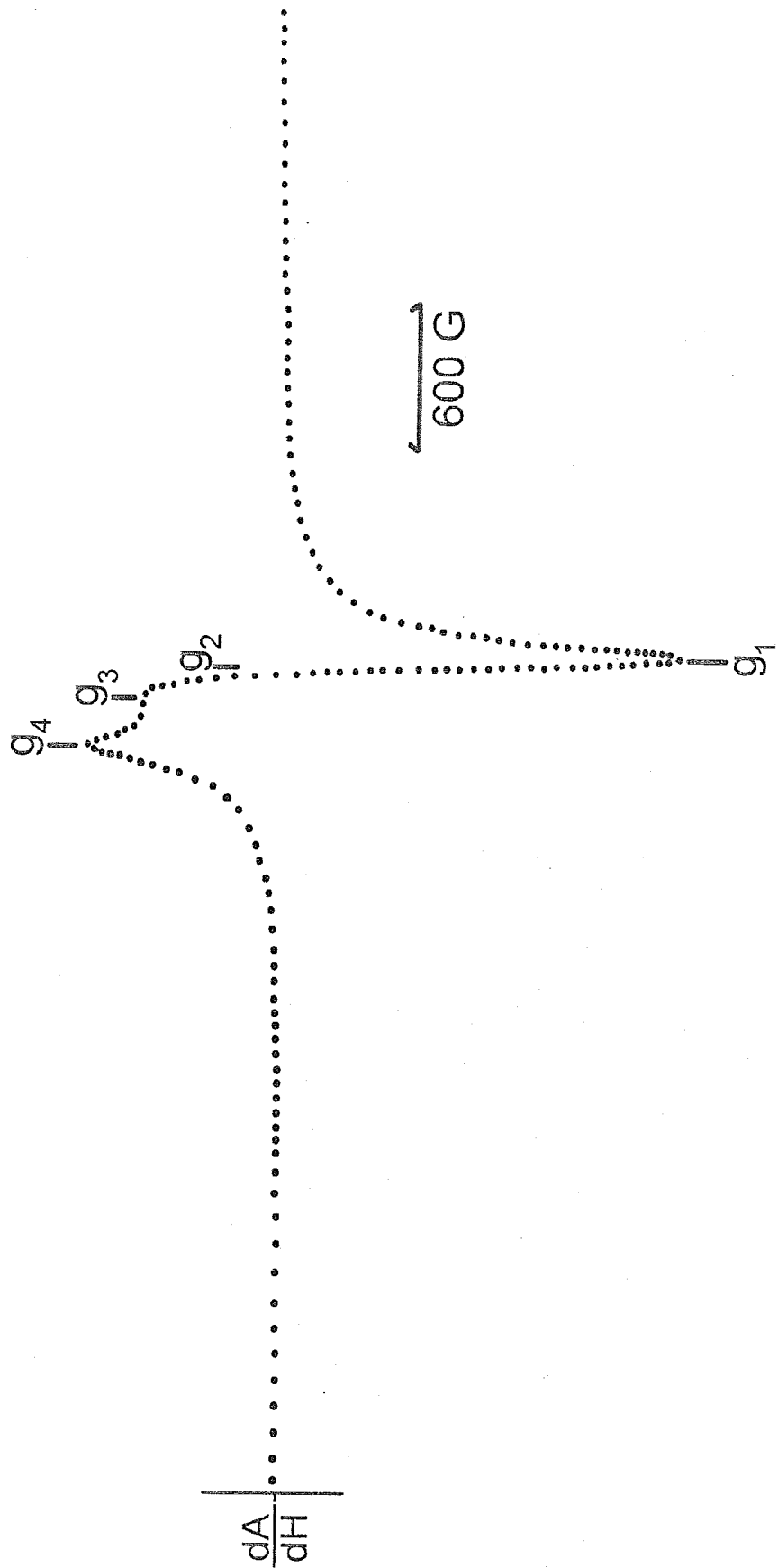
III

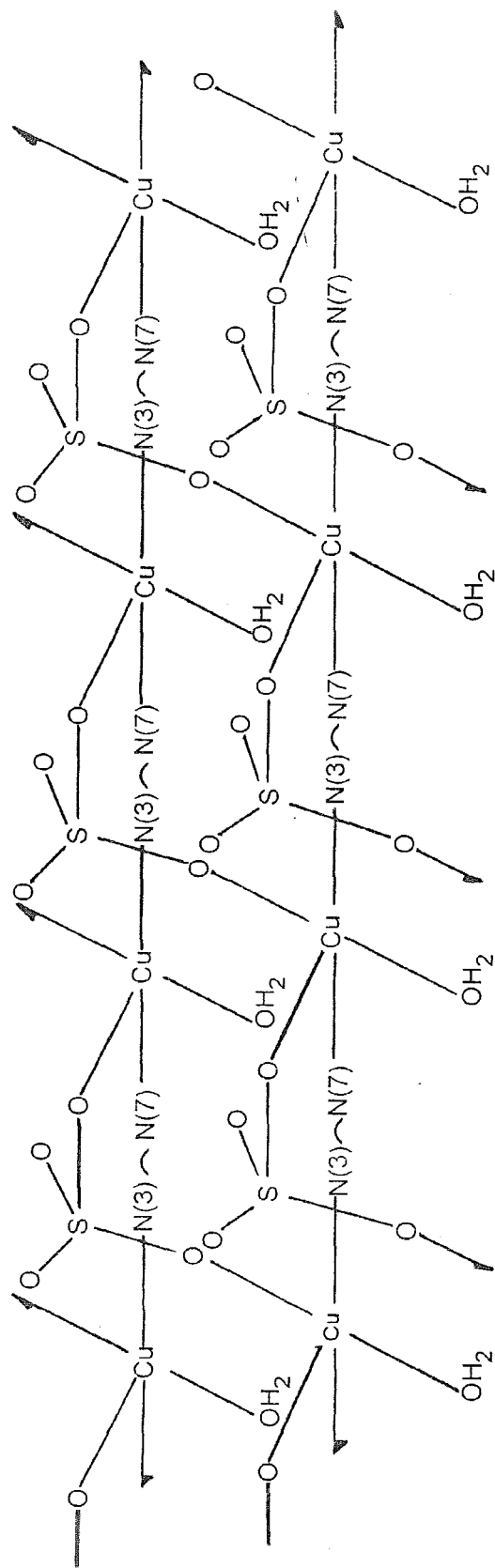


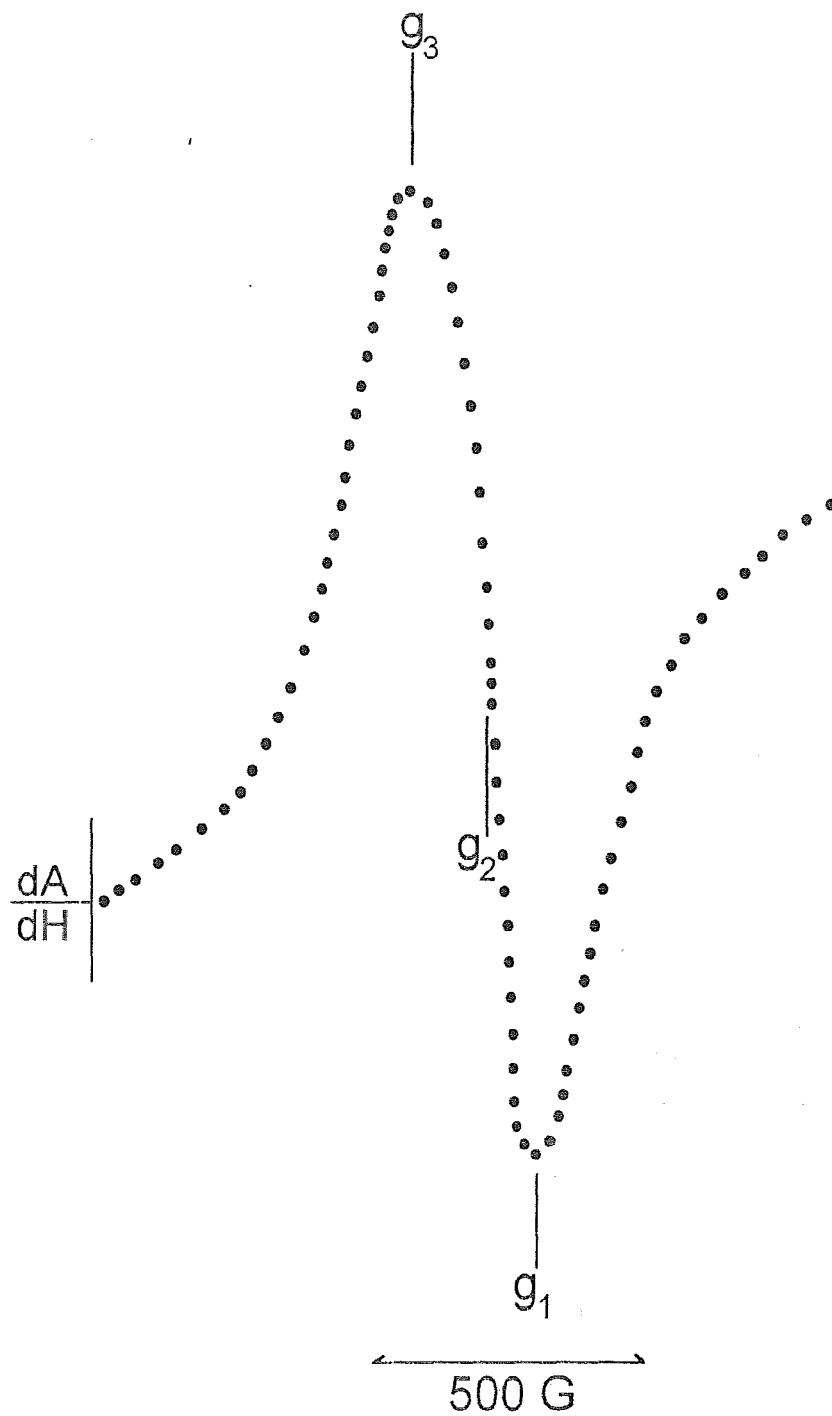


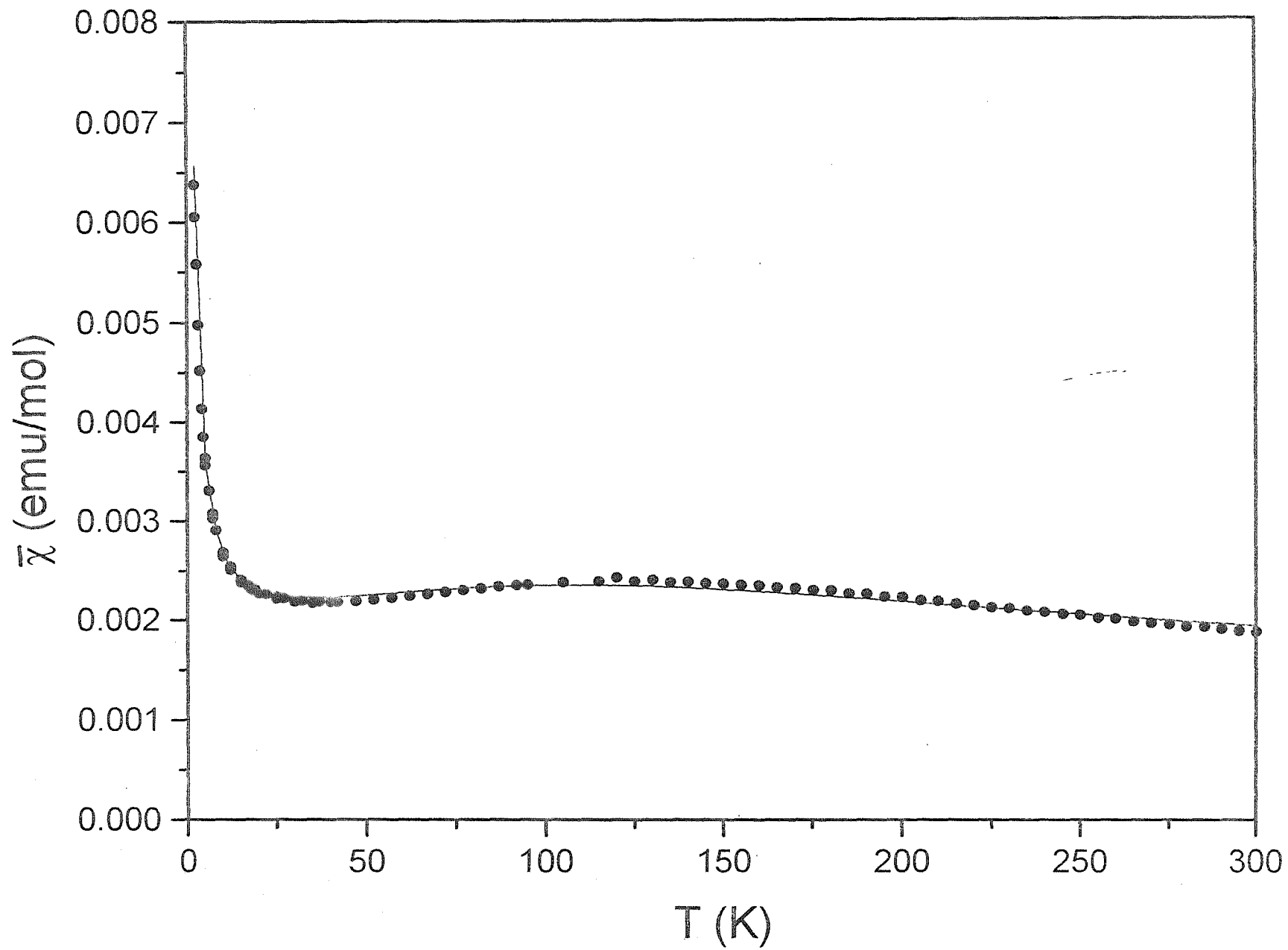


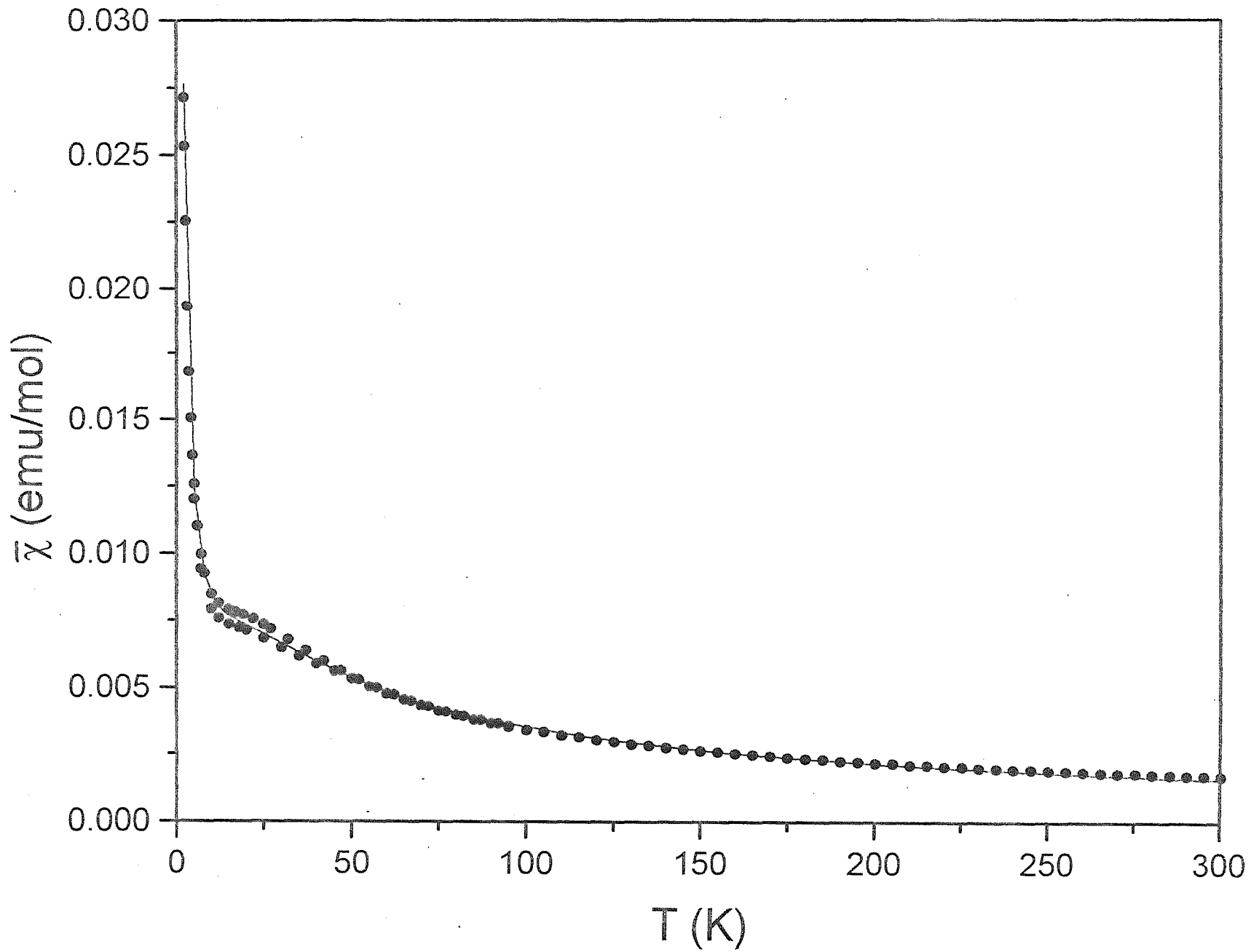


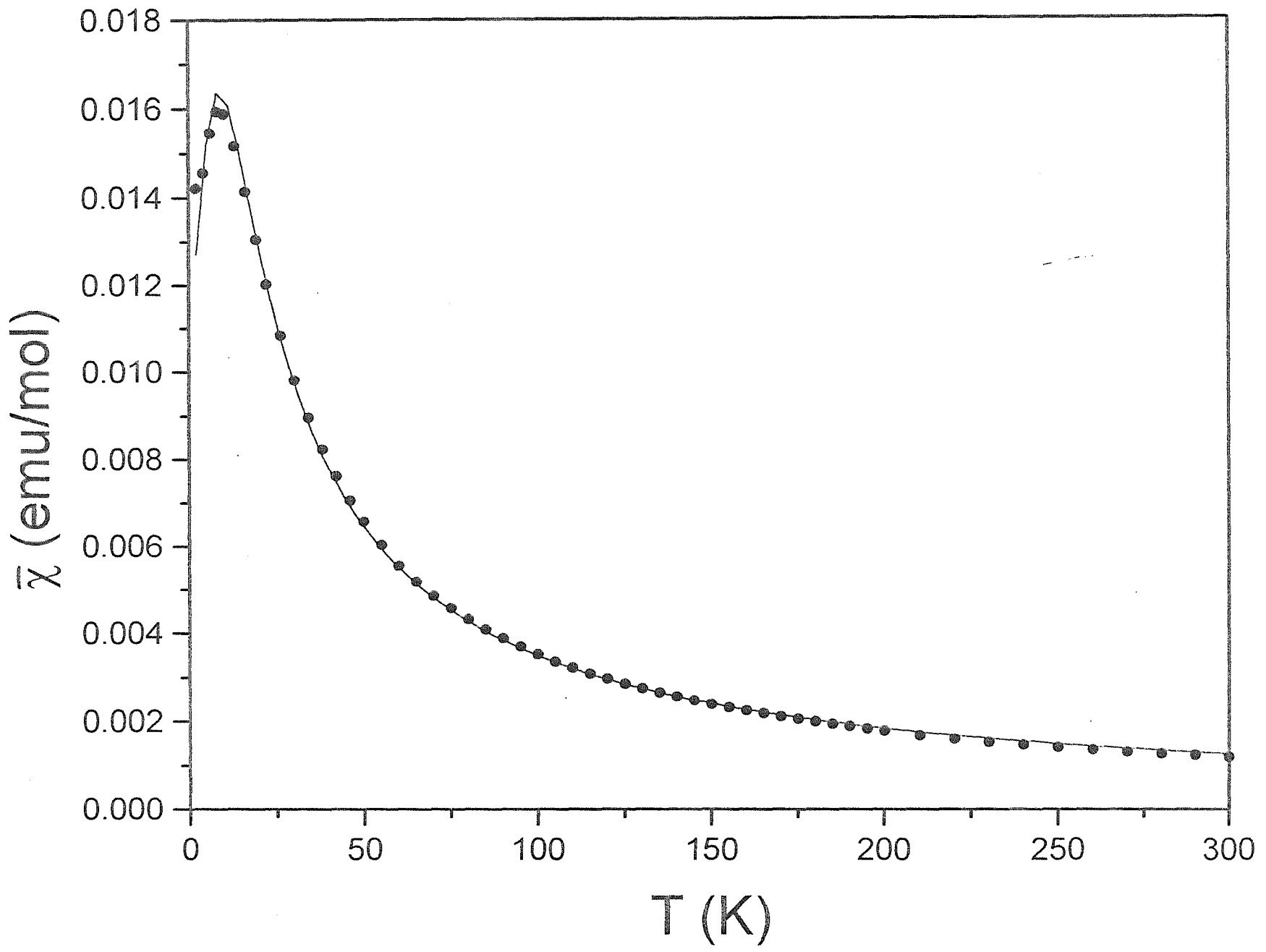


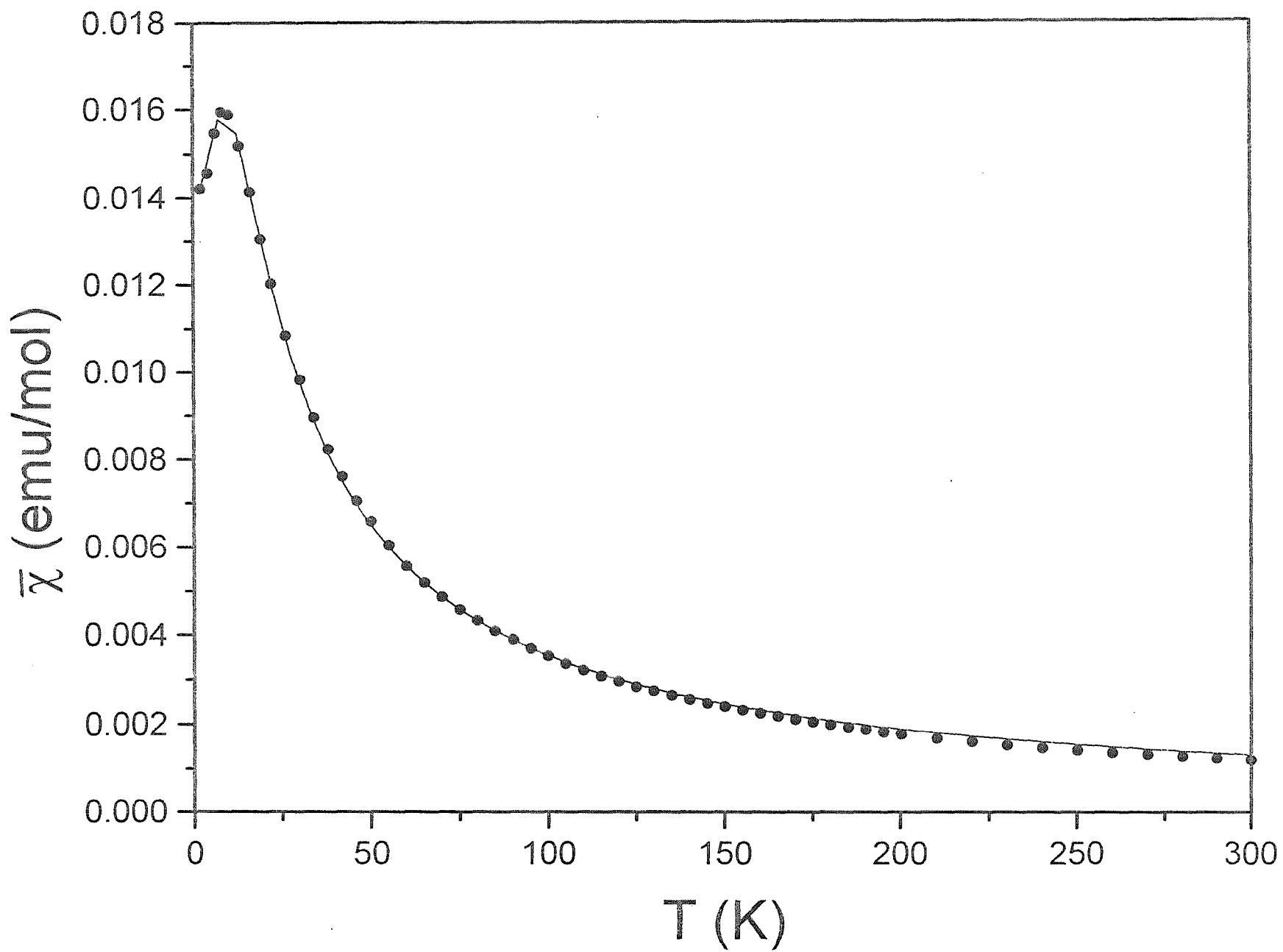


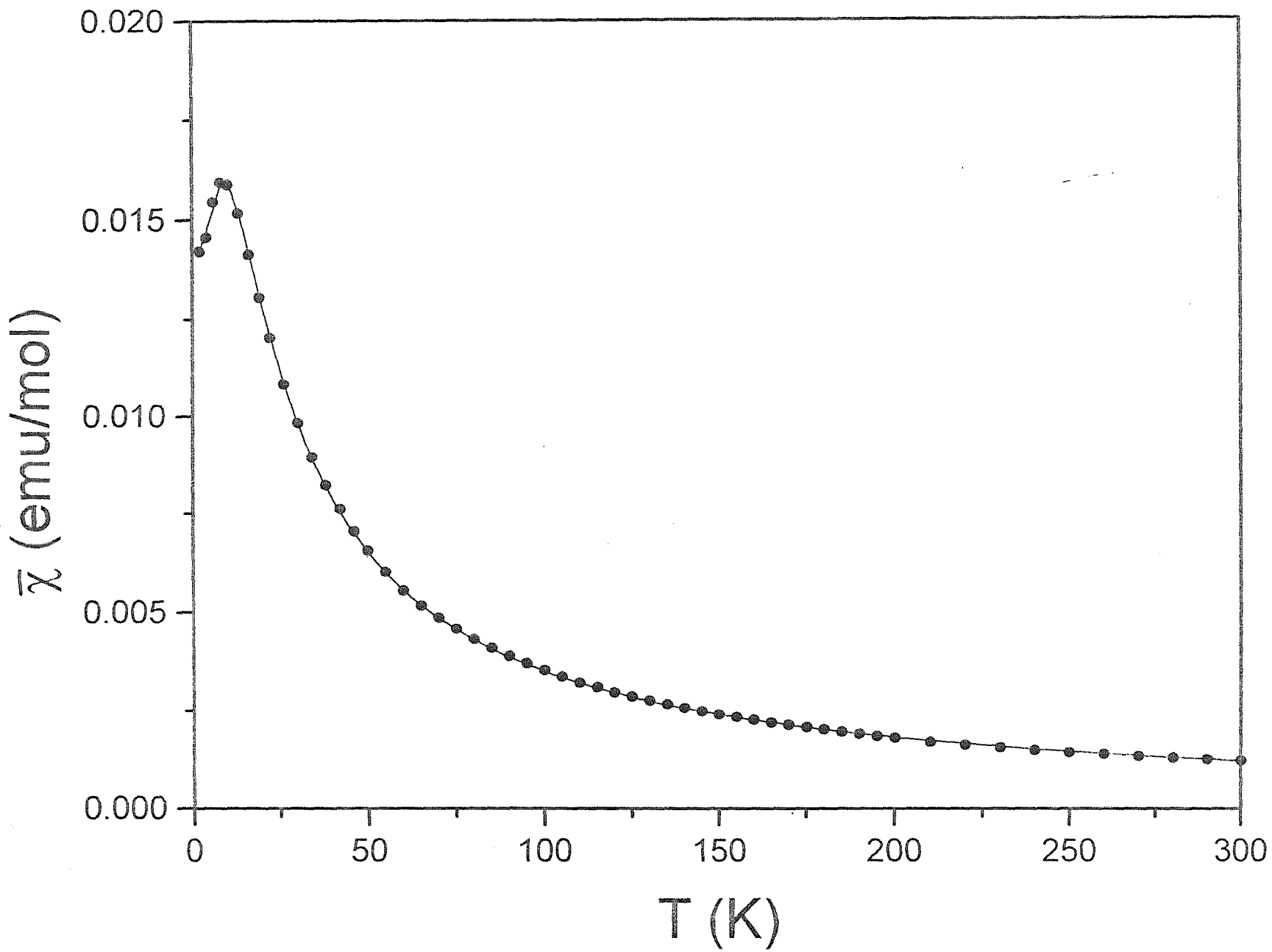












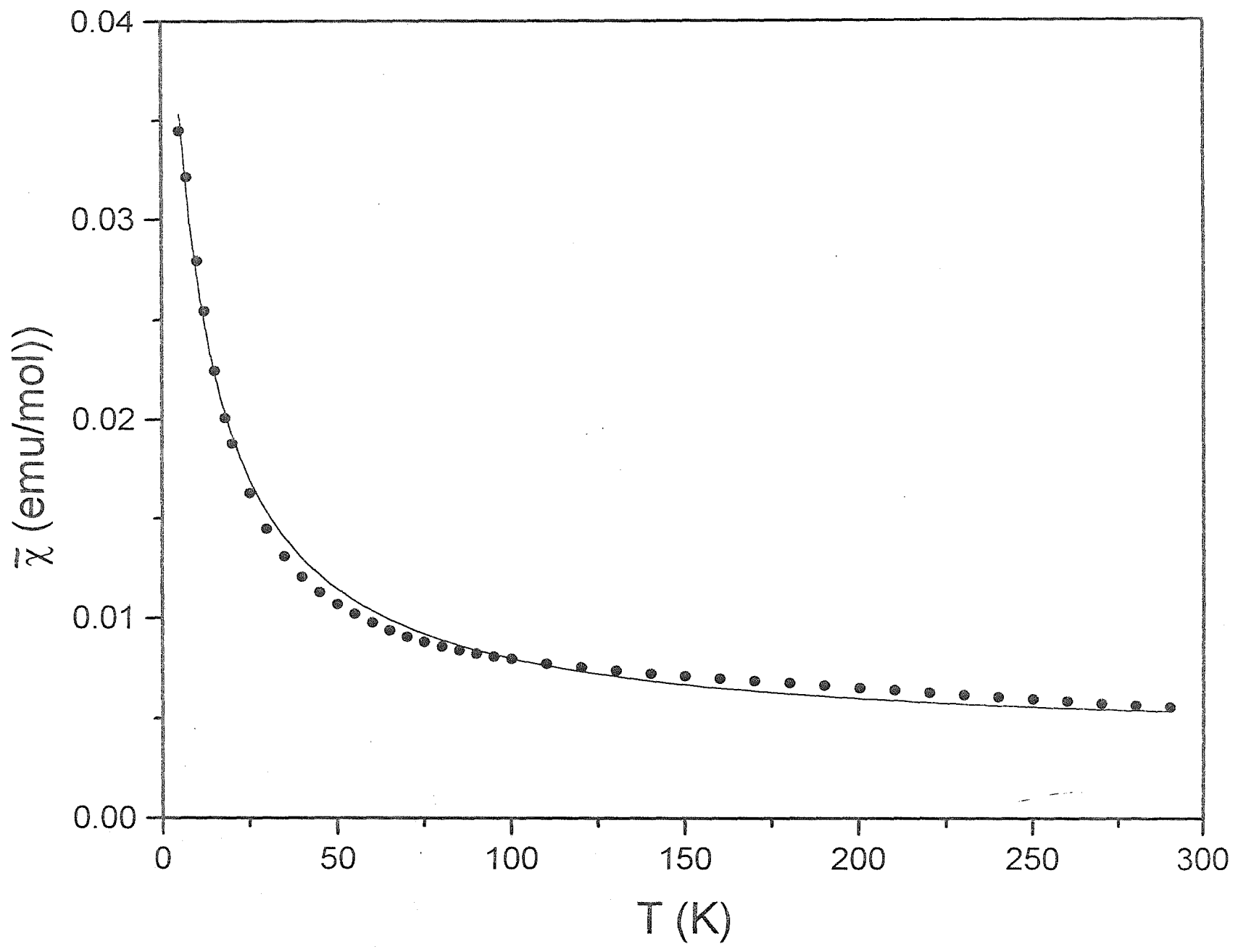
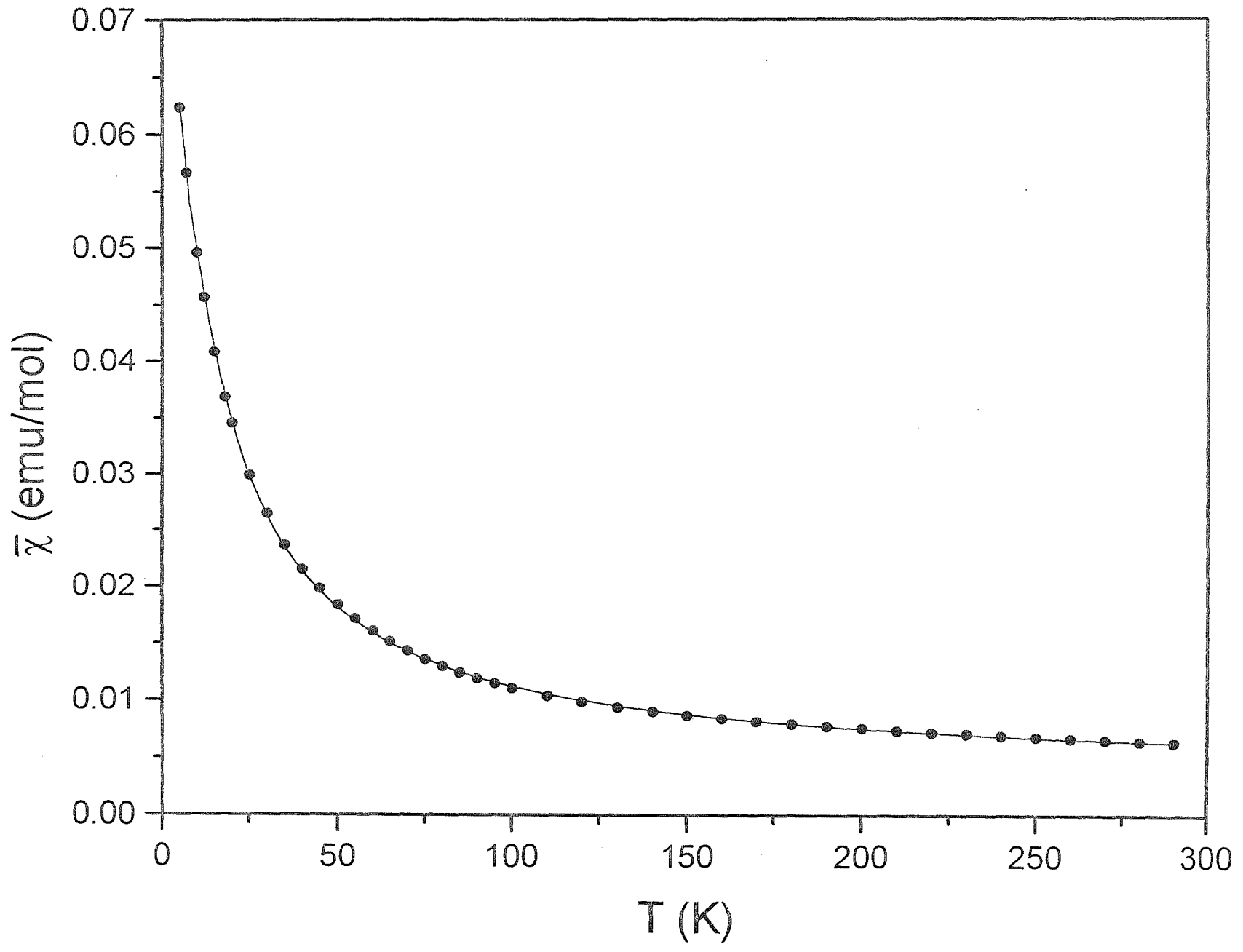


Fig. 1



ANEXO

7

*Density Functional Study of Purine-type Heterocycles:
Allopurinol and Hypoxanthine*

México D.F., a 2 de abril de 1996.

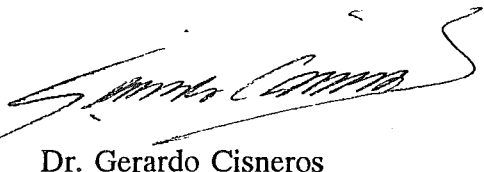
Dres. María Eugenia Costas, Estrella Ramos
y Rodolfo Acevedo Chávez
Facultad de Química
Universidad Nacional Autónoma de México
P r e s e n t e s.

Estimados Dres. Costas, Ramos y Acevedo:

La presente es para confirmar que su artículo contribuido titulado "Density Functional Study Purine-type Heterocycles: Hypoxanthine and Allopurinol" ha sido aceptado por los dos árbitros que lo examinaron, para su inclusión en el volumen de las memorias del 3er. Simposio Supercómputo UNAM-Cray, "Computational Chemistry and Chemical Engineering", el cual se publicó por World Scientific, casa editorial con la que se ha celebrado el contrato para publicación. Para fines de referencia, los editores del volumen somos el suscrito, J. Cogordán, Miguel Castro y C. Wang (en ese orden).

Sin otro particular, reciban ustedes un cordial saludo.

Atentamente,



Dr. Gerardo Cisneros
Científico Principal

Density Functional Study of Purine-type Heterocycles: Hypoxanthine and Allopurinol.

By María Eugenia Costas¹, Estrella Ramos¹ and Rodolfo Acevedo-Chávez²

¹Facultad de Química, Universidad Nacional Autónoma de México, México 04510, D.F., México.

²Centro de Química, Instituto de Ciencias, B. Universidad Autónoma de Puebla, Apartado Postal 1613, Puebla, Puebla, México.

We present the calculation of the electronic properties of the purine-type heterocycles hypoxanthine and allopurinol, which show differences both in the $\underline{\text{N}}$ atoms positions in their structures and in their metallic coordination behavior. We used the Density Functional Theory with the Becke-Perdew functional to calculate the electronic properties for all the ketonic tautomers of both heterocycles, and discuss the differences, which can be useful in chemical reactivity studies.

1. Introduction

Hypoxanthine (I) and allopurinol (II) are heterocycles (Figure 1) of interest from both pharmacological and biochemical points of view (1-3). Having several electron donor atoms in their structures, these heterocycles are interesting ligands in coordination chemistry, due to the diversity in metallic bonding sites, Metal-Ligand stoichiometries, and structural arrangements and physical properties of the respective coordination compounds.

Only a few tautomeric forms for both neutral molecules are known (4). For these, diverse metallic bonding patterns have been found (1,5), the $\underline{\text{N}}$ atoms being the coordination sites. The nature of the $\underline{\text{N}}$ sites involved in the metallic bonding are strongly related to the reaction conditions (1,5). On the other hand, the $\underline{\text{N}}$ atoms in both heterocycles show different thermodynamic stabilities towards their interaction with protons (6), and there is no correlation between the stability towards a proton and the one towards a transition metallic center for the respective $\underline{\text{N}}$ donor sites (6e,7).

In an attempt to understand these problems, a preliminary theoretical study of the energetic stability of all the different ketonic tautomers for both neutral heterocycles has been carried out. In this, the molecular and electronic structures have also been calculated, in the hope of rationalizing some aspects of both their physical chemistry properties, and their potential behavior towards Lewis acids (e.g., transition metal centers, or protons). In this communication, the theoretical study of the two most energetically stable ketonic tautomers for both neutral heterocycles is presented.

2. Methodology

Geometry optimizations and electronic structures calculations were made with the Dgauss program (8) (implemented in the YMP4/464 Cray Supercomputer), which is based on the Density Functional Theory using Gaussian-type orbitals to build the wave function. Self-consistent field calculations were performed at the Generalized Gradient Approximation level. The DZVP (Double-zeta for the valence region, plus polarization) (9) orbital basis set was used together with the auxiliary A1 basis set. Corrections for

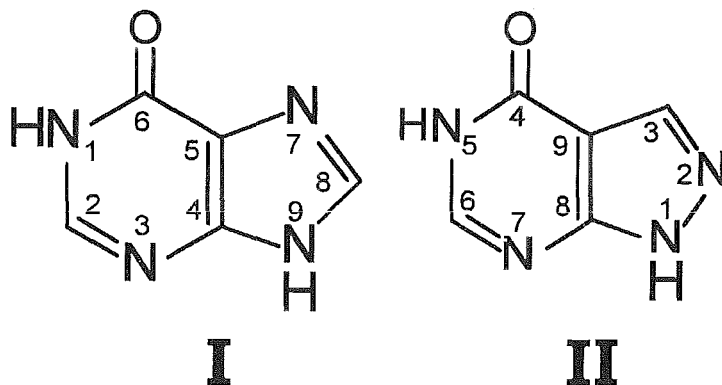


FIGURE 1. Schematic drawing of the two neutral heterocycles studied. The drawing belongs to the respective $\underline{\text{N}}(1)\text{-H}/\underline{\text{N}}(9)\text{-H}$ and $\underline{\text{N}}(1)\text{-H}/\underline{\text{N}}(5)\text{-H}$ ketonic tautomers.

exchange and correlation were made with the Becke-Perdew (10) functional included self-consistently.

The crystalline structures of the $\underline{\text{N}}(1)\text{-H}/\underline{\text{N}}(9)\text{-H}$ hypoxanthine tautomer (11) and $\underline{\text{N}}(1)\text{-H}/\underline{\text{N}}(5)\text{-H}$ allopurinol tautomer (12) were used as the initial geometry for the optimization process of these two tautomers. Their optimized structures were modified to get the initial geometry guess for the other ketonic tautomers. Total energy, bond orders, electric dipole moment, atomic charges, total electronic charge density, molecular electrostatic potential and occupied (35) and unoccupied (5) molecular orbitals (MO) wave function were calculated for all the possible tautomers of these two heterocycles in their neutral ketonic forms.

3. Results and Discussion.

I. Energetic Stability.

Table 1 shows the total molecular energy values calculated for all the possible hypoxanthine and allopurinol tautomers in their neutral ketonic forms. As can be seen from this Table, the energetically most stable hypoxanthine tautomers are those showing the prototropic protons in the 1,7 and 1,9 positions. The former is slightly higher in stability ($|\Delta E|=0.9191$ kcal/mol). For allopurinol, the most energetically favorable tautomers are the 1,5 and 2,5. The former is also slightly higher in stability ($|\Delta E|=3.54$ kcal/mol). For each heterocycle, the corresponding two ketonic tautomers quoted above as the most relatively stable ones have been found to exist in equilibrium in solution (4). In the Metallic Center-Heterocycle interactions, the same two tautomers for both neutral heterocycles have been observed as the ligands bonded to transitional metallic centers (1,5). Finally, the crystalline structures (1,9c and 1,5c) happen to be the least stable ones. As the calculations were done for the free molecules, it can be suggested that the different packing forces present in the two crystalline lattices make the structures stable in the solid state.

II. Structural Properties.

For the 1,7 (H17) and 1,9 (H19) tautomers of hypoxanthine, and the 1,5 (A15) and

2,5 (A25) tautomers of allopurinol, the internuclear distances and internal bond angles involved in the protonation or deprotonation of the N atoms show changes: for example, the protonation of N atoms is associated with bigger internuclear distances between nearest neighbors and internal bond angles in all cases. For the two pairs of tautomers the internuclear distances indicate the existence of a double bond character of both endocyclic and exocyclic types. The positions of the double bonds in the five and six-membered rings, are associated with the deprotonation of the corresponding N atoms. The four tautomers are pseudoaromatic. The Mayer valence indices are in agreement with the pseudoaromatic character (and the existence of the double bond character quoted above) for the two pairs of energetically most favorable tautomers.

HYPOXANTHINE		ALLOPURINOL	
Tautomer	Energy (Hartrees)	Tautomer	Energy (Hartrees)
1,7	-487.32412783	1,5	-487.308112834
1,9	-487.32286213	2,5	-487.302452147
3,7	-487.31266464	2,7	-487.287526930
1,3	-487.29328519	1,7	-487.278857888
3,9	-487.29000603	7,5	-487.266311176
7,9	-487.28779244	1,2	-487.256374692
1,9c	-487.22073676	1,5c	-487.254300673

Table 1. Total energy (Hartrees) for all the ketonic tautomers of hypoxanthine and allopurinol. c: crystalline structure.

This dependence of the internuclear distances and the internal bond angles on the protonation has been observed also when the same N sites for both heterocycles are involved in metallic bonding (1,5). The behavior of the internal bond angles is a general experimental pattern in pyrimidines, purines and their derivatives (1). Also, the most stable tautomers show in their optimized structures lower deviations from planarity than the corresponding ones in the solid state, suggesting that crystal packing forces induce these structural distortions.

III. Electric Dipole Moment.

The properties of the electric dipole moment vector are strongly correlated with the positions of the protonated N atoms: these regions are associated both with lower atomic charge values and to lower electronic charge density in the corresponding tautomer. Figure 2 shows the electric dipole moment for the most stable neutral and ketonic tautomers of both heterocycles.

The experimental electric dipole moment value for hypoxanthine (3.16D) has been reported (13). The 1,7/1,9 tautomeric equilibrium of hypoxanthine in solution is supported when this experimental value is compared with the mean theoretical value for the two tautomeric forms. Unfortunately, to our knowledge, there is no report of the corresponding experimental data for allopurinol.

IV. Electrostatic Potential.

Figure 3 shows the molecular electrostatic potential (-20 kcal/mol) for the two most

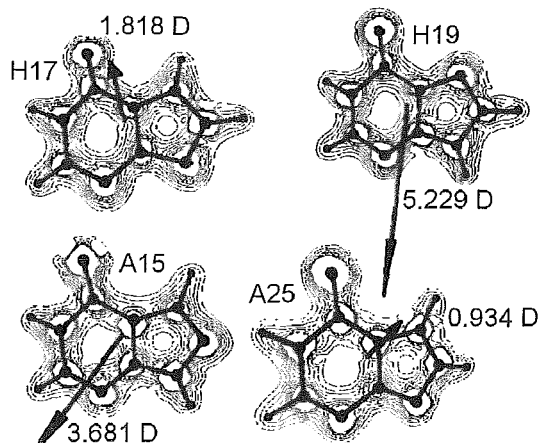


FIGURE 2. Electric dipole moment vector together with the total electronic charge density contour map on the molecular plane for the two most stable tautomers of both heterocycles.

stable tautomers of both heterocycles. This property is also strongly related to the deprotonation sites in the tautomers: those deprotonated N regions (and the exocyclic O atoms) show an attractive potential with respect to a positive charge; the N-H and C-H regions are associated with repulsive potentials.

The electric dipole moment is strongly related to the molecular electrostatic potential: those deprotonated regions are associated with bigger negative atomic charges and they are located opposite to the positive end of the electric dipole moment vector. In summary, these deprotonated regions would be potential sites for electrostatic interactions with cations. For the two respective tautomers of each heterocycle, those deprotonated regions (N atoms) have almost all been involved in chemical bonds with transition metal centers.

V. Total Electronic Charge Density.

Figure 3 shows the total electronic charge density contour maps on the molecular plane for the two most stable tautomers of both heterocycles. This property indicates the existence of atomic regions with a double bond character in the tautomers. Their molecular distribution is strongly associated with the positions of the deprotonated N atoms. In agreement with the bonding parameters, this property confirms the pseudoaromaticity of the tautomers. For these four tautomers, this property also shows the double bond character in the C-O group, supporting the experimental evidence of the predominance of the ketonic form in these type of heterocycles, both in solid state and in solution (11,12,14,15).

VI. Frontier Molecular Orbitals Wave Function.

The HOMO wave function shows (Figure 4) the same atomic contribution and molecular distribution for the two pairs of most stable tautomers. The wave function is Π -type. Interestingly, the HOMO symmetry properties do not correlate with the prototropic tautomerism in hypoxanthine or in allopurinol. From this, the symmetry properties of the molecular orbitals associated to the Π -type electron donor properties for the two pairs of tautomers are the same; the deprotonated N atoms would be favorable potential sites for Π -bonding with d -orbitals of transition metal centers, which is in general in agreement with the experimental information obtained for the interactions of both tautomers of hypoxanthine and allopurinol with these type of centers (1,5). In this respect, the ex-

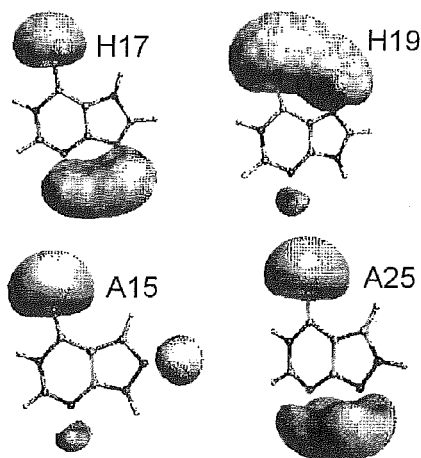


FIGURE 3. Molecular electrostatic potential surfaces (-20 kcal/mol) for the two most stable tautomers for both heterocycles.

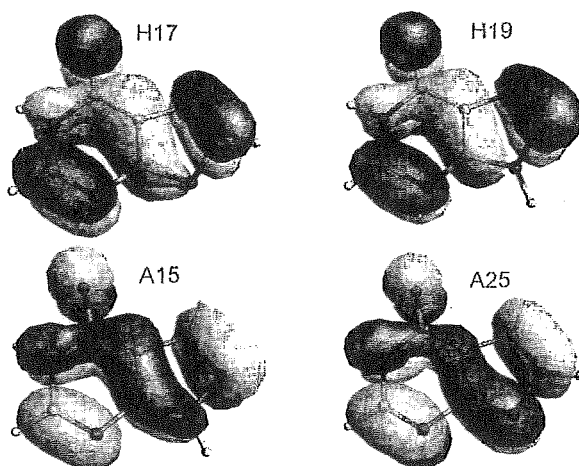


FIGURE 4. HOMO wave function (± 0.25 level) for the two most stable tautomers of both heterocycles.

perimental existence of cationic hypoxanthine and allopurinol, let us suggest that other MO's of lower energy (σ -type) are involved in the construction of the respective N-H bonds. The MO analysis (*vide infra*) supports this suggestion.

The LUMO wave functions for the same tautomers is shown in Figure 5. They are Π -type in all the cases, showing differences in the atomic contribution and molecular distribution for each pair of tautomers. By exploring the LUMO symmetry properties (atomic contributions of certain neighbors to the deprotonated \underline{N} atoms) and those of transition metal centers d -orbitals, it is possible to suspect the potential involvement of the deprotonated \underline{N} atoms in Π -backbonding processes.

VII . Molecular Orbitals Properties.

An analysis of the symmetry properties for the 35 occupied and 5 unoccupied molecular

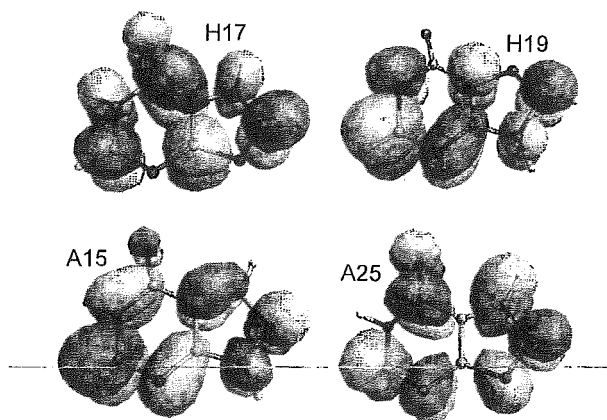


FIGURE 5. LUMO wave function (± 0.25 level) for the two most stable tautomers of both heterocycles.

orbitals of lower energy for the four tautomers was made. The first 10 occupied MO's are CORE, non bonding-type. The MO No. 11 is σ -bonding. The MO's No. 12 to No. 23 are σ -type. The MO No. 24 is Π -bonding. From the MO No. 25 to No. 35 (HOMO) the character is Π or σ -type, and the MO No. 36 (LUMO) is Π -type. All the tautomers here discussed show analogous symmetry properties for these MO's.

4. Conclusions

The theoretical study carried out indicates the existence of two energetically most favorable neutral ketonic tautomers for hypoxanthine and allopurinol. This result is in full agreement with the experimental spectral information in solution. For those tautomers, the molecular structures, bonding parameters and the majority of the molecular and atomic properties are closely related to the positions of the H atoms involved in the respective prototropic tautomeric forms. This relationship is not observed in the symmetry properties of the σ (MO No 11) and Π -type (MO No 24) molecular bonding occupied MO's, and those of the HOMO (Π -type). This last result let us propose that the MO's associated to the Π -type electron donor properties in each tautomer are independent of the ketonic tautomeric form for both hypoxanthine and allopurinol. In other words, those N atoms that are potential Π -type electron donor sites would not require its existence in deprotonated form. Finally, this study let us rationalize certain aspects of the experimental behavior of these tautomers in their interactions with protons or with transition metal centers.

Acknowledgments. We thank DGSCA-UNAM for the facilities in the use of the CRAY YMP4/464 supercomputer for the calculations.

REFERENCES.

- (1) J.R. Lusty, *Handbook of Nucleobase Complexes*, CRC Press Inc, USA, 1990 and references therein.
- (2) T.G. Spiro, Ed., *Nucleic Acid-Metal Ion Interactions*, Vol. 1, John Wiley & Sons, Inc., USA, 1980 and references therein.
- (3) L. Stryer, *Biochemistry*, 3rd Ed., Freeman, New York, 1988.

(4) a) M.T. Chenon, R.J. Pugmire, D.M. Grant, R.P. Panzica and L.B. Townsend, *J. Am. Chem. Soc.*, **97**, 4636 (1975); b) M.T. Chenon, R.J. Pugmire, D.M. Grant, R.P. Panzica and L.B. Townsend, *J. Heterocyclic Chem.*, **10**, 431 (1973); c) W.S. Sheldrick and P. Bell, *Inorg. Chim. Acta*, **137**, 181 (1987).

(5) R. Acevedo-Chávez, M.E. Costas and R. Escudero-Derat, *J. Solid State Chem.*, **113**, 21 (1994), and references therein; R. Acevedo-Chávez, M.E. Costas and R. Escudero-Derat, *Inorg. Chem.*, **35**, 7430 (1996), and references quoted.

(6) a) J.J. Christensen, J.H. Rytting and R.M. Izatt, *Biochemistry*, **9**, 4907 (1970); b) D. Lichtenberg, F. Bergmann and Z. Neiman, *Isr. J. Chem.*, **10**, 805 (1972); c) R.L. Benoit, D. Boulet, L. Séguin and M. Fréchette, *Can. J. Chem.*, **63**, 1228 (1985); d) R.L. Benoit and M. Fréchette, *Can. J. Chem.*, **63**, 3053 (1985); e) P.W. Linder, M.J. Stanford and D.R. Williams, *J. Inorg. Nucl. Chem.*, **38**, 1847 (1976); f) F. Bergmann, A. Frank and Z. Neiman, *J. Chem. Soc., Perkin Trans.*, **I**, 2795 (1979).

(7) a) R.M. Izatt, J.J. Christensen and J.H. Rytting, *Chem. Rev.*, **71**, 439 (1971); b) K.H. Scheller, B.S. Krastiger and R.B. Martin, *J. Am. Chem. Soc.*, **103**, 6833 (1981); c) W.S. Sheldrick and G. Heeb, *Inorg. Chim. Acta*, **190**, 241 (1991).

(8) DGAUSS 3.0.1/UC-3.0, Cray Research, Inc.

(9) N. Godbout, D.R. Salahub, J. Andzelm, E. Wimmer, *Can. J. Chem.*, **70**, 560 (1992).

(10) a) A.D. Becke, *Phys. Rev. A*, **38**, 3098 (1988). b) J.P. Perdew, *Phys. Rev. B*, **33**, 8822 (1986).

(11) H.W. Schmalle, G. Hänggi and E. Dubler, *Acta Cryst.*, **C44**, 732 (1988).

(12) P. Prusiner and M. Sundaralingam, *Acta Cryst.*, **B28**, 2148 (1972).

(13) J.J. Aaron, M.D. Gaye, C. Párkányi, N.S. Cho and L. Von Szentpály, *J. Mol. Struct.*, **156**, 119 (1987).

(14) V.A. Bloomfield, D.M. Crothers and I. Tinoco, Jr., *Physical Chemistry of Nucleic Acids*, Harper & Row Pub., USA, 1974 and references therein.

(15) B. Pullman and A. Pullman, *Adv. Het. Chem.*, **13**, 77 (1971) and references therein.

ANEXO

8

DFT Study of the Neutral Hypoxanthine Tautomeric Forms.

DFT Study of the Neutral Hypoxanthine Tautomeric Forms.

María Eugenia Costas.

Facultad de Química, Universidad Nacional Autónoma de México,
México 04510, D.F., México.

Rodolfo Acevedo-Chávez.

Centro de Química, Instituto de Ciencias, B. Universidad Autónoma de Puebla,
Apartado Postal 1613, Puebla, Puebla, México.

Abstract.

The theoretical study at the level of Density Functional Theory of the energetic stability, and the structural and electronic properties of all the isolated ketonic and enolic tautomers of neutral hypoxanthine is presented. We also study both the influence of temperature on the tautomeric equilibria and the IR vibrational spectrum of hypoxanthine in the gas phase in terms of the contribution of several tautomers of this heterocycle. We found that the two $\underline{\text{N}}(1)\text{-H}$ ketonic tautomers of hypoxanthine are the energetically most stable ones and they represent the main contribution to the experimental IR spectrum. The calculated properties and the potential chemical behavior suggested for hypoxanthine from the theoretical study are in reasonable agreement with the experimental data reported up to date.

I. INTRODUCTION.

Heterocycles that show in their structure the pirimidinic ring fused to azolic moieties (Figure 1) are interesting systems from the Biochemical, Pharmacological, Chemical and Physicochemical points of view (1).

Figure 1.

Among these heterocycles, hypoxanthine (Figure 2) is found as a minor purine base in transfer RNA (1b). In the purine catabolism, it is a substrate of the metalloenzyme Xanthine Oxidase in the production of uric acid (1b). Several studies have been carried out about its interactions with Lewis acids (1d,2). From these, the N atoms are the favorable metallic coordination sites, the nature depending on the experimental conditions. For the neutral coordinated hypoxanthine, two ketonic tautomeric forms have been detected (3), the N(1)-H/N(9)-H and the N(1)-H/N(7)-H, which also have been experimentally suggested as the predominant tautomers in aqueous and DMSO solutions (4).

Figure 2.

With regard to the hypoxanthine tautomerism in solution, the influence of the solvent dielectric constant in the equilibrium shift between the N(1)-H/N(7)-H and N(1)-H/N(9)-H ketonic forms (N(1)-H/N(9)-H as the predominant tautomer in aqueous solutions; N(1)-H/N(7)-H as the slightly predominant form in DMSO medium), has been inferred from experimental and theoretical studies (5). From these, the shift of the tautomeric equilibrium in a polar media favoring that tautomer which has the highest electric dipole moment in the gas phase is deduced.

To our knowledge, there are no detailed experimental studies about the exploration and detection of hypoxanthine enolic tautomers in solution, although it is difficult to discard both its existence in solution with solvents of different dielectric constants, and the influence

which they could have in the kinetic and thermodynamic stabilities of the hypoxanthine physicochemical processes carried out in those media.

Although the two $\underline{\text{N}}(1)\text{-H}$ ketonic tautomers with prototropic tautomerism in the imidazolic ring appear to be the preponderant species in solution, the tautomeric equilibria are more complicated in the gas phase because they are remarkably dependent on the temperature conditions. At this respect, the majority of the previous reported theoretical studies have been focused on some electronic properties of the two energetically most stable $\underline{\text{N}}(1)\text{-H}/\underline{\text{N}}(7)\text{-H}$ and $\underline{\text{N}}(1)\text{-H}/\underline{\text{N}}(9)\text{-H}$ ketonic tautomeric forms of hypoxanthine (4a,6-12). Theoretical studies considering some enolic tautomer of hypoxanthine in the calculation of a specific property are very scarce (13,14), and only at the semiempirical level. A theoretical study employing several levels of theory has been very recently reported (15), in which the energetic stability of the tautomers both in the gas phase and in the presence of a solvent has been studied, but without exploring the electronic properties of each one of the tautomeric forms and without comparing them with the experimental data available. Here, we present the detailed theoretical study of the energetic stability, and the structural and electronic properties of several ketonic and enolic tautomers of hypoxanthine. We also analyze the influence of temperature on the tautomeric equilibria, and the IR vibrational spectrum of hypoxanthine in the gas phase is studied in terms of the contribution of several tautomers of hypoxanthine.

II. METHODS.

Geometry optimizations, molecular and electronic properties of the fourteen possible tautomers of neutral hypoxanthine were performed at the level of Density Functional Theory with the Becke-Perdew functional (16,17), and the DZVP basis set (18) using the standard procedure in Gaussian 94 (19).

Crystalline structure (20) of hypoxanthine in its $\underline{\text{N}}(1)\text{-H}/\underline{\text{N}}(9)\text{-H}$ ketonic tautomeric form was used as starting data for geometry optimization. Its optimized structure was used to construct the initial geometry for other tautomers, by simply moving the hydrogen to

the new possible position on the molecular plane. For the enolic tautomers, a number of initial configurations for the OH group were used, and the cis and trans forms were always converged to the same structure. Criteria for geometry optimization and SCF convergence were 10^{-7} Hartree/bohr and 10^{-9} Hartrees, respectively.

For some tautomers, previous calculations were done with MNDO and DFT methods with the Dgauss program (21) with the DZVP basis and A2 auxiliary basis set and the same functional mentioned before, to get an approximate structure as starting data for the full geometry optimization performed afterwards with Gaussian-94. Frequency calculations were done to determine the nature of the stationary points found by geometry optimizations. All the tautomers were stationary points in the geometry optimization procedure, and none showed imaginary frequencies in the vibrational analysis.

The optimized geometries were used to perform single point calculations with Gaussian-92 (22) with the same functional and basis set, in order to visualize the molecular properties as the electrostatic potential, the total electronic density and the molecular orbitals wave functions. The difference in the SCF energy in doing this calculation with respect to the value obtained with Gaussian-94 was of 10^{-8} Hartrees in all the cases. Visualization of these properties were done with Unichem program (23). Single point calculations with Dgauss program for the Gaussian-94 optimized geometries were also done to obtain the Mayer valence indices.

The calculated frequencies of the IR vibrational spectra were corrected with a scaling factor of 0.9938. This factor was obtained comparing the theoretical IR frequency for the formaldehyde $\nu\text{C}=\text{O}$ vibrational mode (1756.8469 cm^{-1}) in gas phase (calculated with the same functional, basis set and methodology as the one used for hypoxanthine) with its experimental frequency (1746 cm^{-1}). Assignments to the vibrational normal modes for the different tautomers were done by visualizing them at each frequency value with the XMol 1.3.1 program. Frequency calculations were also done at 11 K, 298.15 K and 480.15 K to obtain the Gibbs free energy thermal correction, which was used to calculate the tautomeric

equilibrium constants at these temperature values. Vertical first ionization potentials and first electron affinities were obtained by calculating the SCF energy of the monocationic and monoanionic radicals restricted to the optimized structure of the respective neutral tautomers.

Calculations were done on a CRAY YMP4/464 supercomputer, a SGI Power Challenge computer (R8000-18) and a SGI workstation (R4400).

III. RESULTS AND DISCUSSION.

A. Energetic Stability.

Table 1 shows the total energy (Hartrees) for each one of the ketonic and enolic tautomers of neutral hypoxanthine, and their relative energetic stability (kcal/mol) with respect to the most stable tautomer. We also include the energy of the $\underline{\text{N}}(1)\text{-H}/\underline{\text{N}}(9)\text{-H}$ ketonic form in its crystalline structure (a single point).

Table 1.

From these results, the $\underline{\text{N}}(1)\text{-H}/\underline{\text{N}}(7)\text{-H}$ and $\underline{\text{N}}(1)\text{-H}/\underline{\text{N}}(9)\text{-H}$ ketonic tautomers are the most stable ones, being the last slightly (0.84 kcal/mol) less favorable. The higher energetic stability of the $\underline{\text{N}}(1)\text{-H}$ ketonic forms of hypoxanthine arise, being the same pattern deduced for this heterocycle in solution, as has been pointed out before. The two $\underline{\text{N}}(9)\text{-H}$ enolic forms (cis and trans) follow in descending stability. Of these, the isomer with the H atom (of the OH enolic group) in cis-configuration to the $\underline{\text{N}}(1)$ atom is relatively more stable; this allows us to suspect the possible higher basicity of $\underline{\text{N}}(1)$ with respect to $\underline{\text{N}}(7)$. From the stability of these four tautomers, the major role played by the basicity of the $\underline{\text{N}}(1)$ and $\underline{\text{O}}(10)$ atoms may be suggested. The ketonic form $\underline{\text{N}}(3)\text{-H}/\underline{\text{N}}(7)\text{-H}$ and the cis- $\underline{\text{N}}(7)\text{-H}$ enolic tautomer follow in energetic stability. For the first one, the lower basicity of $\underline{\text{N}}(3)$ with respect to $\underline{\text{N}}(1)$ can be inferred. For the second one, it is possible to suggest the influence that the deprotonation of the $\underline{\text{N}}(9)$ atom has on the energetic stability.

With respect to the other eight tautomers, the remarkable increasing energetic instability can be associated both to the presence of two interchangeable H atoms in the same heterocyclic fragment (pyrimidinic or imidazolic ring), or in different rings but with a disposition that produces considerable repulsive interatomic interactions. Finally, the $\underline{\text{N}}(1)\text{-H}/\underline{\text{N}}(9)\text{-H}$ ketonic tautomer in its crystalline structure is the most unstable one; this let us suggest the great influence that the interactions in the crystalline lattice play in the stabilization of that structure. These interactions in the gas phase are suppressed.

In the study reported by other authors (15) for the energetic stability of the hypoxanthine tautomers, the stability sequence is slightly different as the one we get. In there, some tautomers were eliminated from the final analysis by doing previous semiempirical calculations. Here, we made the complete analysis using the same method for all the tautomers, and the sequence was determined in the same level of theory. Nevertheless, the four most stable tautomers are the same as the ones they report. In what follows, only the first six most stable tautomeric forms are considered in the study of their structural and electronic properties.

B. Structural Parameters.

Table 2a shows the internuclear distances (\AA) and Table 2b shows the angles (Degrees) for each one of the six most stable tautomeric forms of hypoxanthine.

Table 2a.

Table 2b.

For the two most stable $\underline{\text{N}}(1)\text{-H}$ ketonic tautomers, a double bond character for some regions can be inferred. For $\underline{\text{N}}(1)\text{-H}/\underline{\text{N}}(7)\text{-H}$ these are $\underline{\text{C}}(2)\text{-}\underline{\text{N}}(3)$, $\underline{\text{C}}(8)\text{-}\underline{\text{N}}(9)$, $\underline{\text{C}}(4)\text{-}\underline{\text{C}}(5)$ and $\underline{\text{C}}(6)\text{-}\underline{\text{O}}(10)$. For $\underline{\text{N}}(1)\text{-H}/\underline{\text{N}}(9)\text{-H}$, they are $\underline{\text{C}}(2)\text{-}\underline{\text{N}}(3)$, $\underline{\text{N}}(7)\text{-}\underline{\text{C}}(8)$, $\underline{\text{C}}(4)\text{-}\underline{\text{C}}(5)$ and $\underline{\text{C}}(6)\text{-}\underline{\text{O}}(10)$. Noticeable differences arise for the $\underline{\text{N}}(9)\text{-H}$ enolic forms. For the cis-isomer the internuclear distances let us suggest a higher delocalization of the electronic density in

the pirimidinic ring. A double bond character is associated to $\underline{\text{N}}(7)\text{-}\underline{\text{C}}(8)$, and $\underline{\text{C}}(6)\text{-}\underline{\text{O}}(10)$ shows a lower character of that type with respect to the two ketonic forms mentioned above. An analogous behavior for the 5- and 6-membered rings, and for the $\underline{\text{C}}(6)\text{-}\underline{\text{O}}(10)$ is observed for the trans-isomer.

The $\underline{\text{N}}(3)\text{-H}/\underline{\text{N}}(7)\text{-H}$ tautomer shows double bond character associated to $\underline{\text{N}}(1)\text{-}\underline{\text{C}}(2)$, $\underline{\text{C}}(4)\text{-}\underline{\text{C}}(5)$, $\underline{\text{C}}(8)\text{-}\underline{\text{N}}(9)$ and $\underline{\text{C}}(6)\text{-}\underline{\text{O}}(10)$. Finally, the cis- $\underline{\text{N}}(7)\text{-H}$ enolic form shows a relative double bond character for $\underline{\text{C}}(2)\text{-}\underline{\text{N}}(3)$, $\underline{\text{C}}(5)\text{-}\underline{\text{C}}(6)$, $\underline{\text{C}}(6)\text{-}\underline{\text{N}}(1)$ and $\underline{\text{C}}(8)\text{-}\underline{\text{N}}(9)$. From the data, the association between the positions of the interchangeable H atoms and the internuclear distances is observed. This is also reflected in the values of the respective angles.

With regard to the internal angles of the CNC groups in the imidazolic ring and for the six tautomers, those protonated CNC groups always show higher internal angles than those deprotonated. This could be associated to a higher sp^2 -character of the atomic orbitals of the N atoms involved in the protonation, and a higher p -contribution in the corresponding atomic orbitals of the deprotonated N atoms. For the pirimidinic ring, this same structural pattern is observed in the $\underline{\text{N}}(1)\text{-H}/\underline{\text{N}}(7)\text{-H}$ and $\underline{\text{N}}(1)\text{-H}/\underline{\text{N}}(9)\text{-H}$ tautomers; the $\underline{\text{N}}(3)\text{-H}/\underline{\text{N}}(7)\text{-H}$ tautomer shows a different behavior. However, in analyzing the behavior of the CNC group which involves the $\underline{\text{N}}(3)$ atom, it systematically shows lower internal angles than those of the CNC group that contains the $\underline{\text{N}}(1)$ atom when both groups are deprotonated; the former shows an increase of the internal angle under protonation. The same assumption about the N atoms p -type atomic orbitals contribution in the protonation/deprotonation processes carried out and involving the pirimidinic ring is also considered here.

The internal angle of the $\underline{\text{N}}(1)\text{-}\underline{\text{C}}(6)\text{-}\underline{\text{C}}(5)$ group, systematically shows higher values when the tautomers are in enolic form. In these, the $\underline{\text{C}}(6)\text{-}\underline{\text{O}}(10)\text{-H}$ angles (104.99° - 106.90°) let us suggest a noticeable sp^3 -character for the O atomic orbitals.

Finally, and with respect to the planarity of the structures for these tautomers, the dihedral angles are almost all lower than 0.01° , reflecting the essentially planar nature of

the heterocyclic networks. The analysis let us consider the existence of very small out of plane-character of the H atoms in some cases.

C. Total Electronic Charge Density.

Figure 3 shows the total electronic charge density contour maps (0.15-0.50 $e/\text{\AA}^3$ range, changes in 0.05 units) in the molecular plane and for the six tautomers here studied.

Figure 3.

For each tautomer and for the 0.15 level, electronic communication in all the molecule is observed. However, for higher values of the electronic density, noticeable differences arise. The $\underline{\text{N}}(1)\text{-H}/\underline{\text{N}}(7)\text{-H}$ and $\underline{\text{N}}(1)\text{-H}/\underline{\text{N}}(9)\text{-H}$ tautomers show electronic communication in the following groups: $\underline{\text{C}}(2)\text{-}\underline{\text{N}}(3)$, $\underline{\text{C}}(4)\text{-}\underline{\text{C}}(5)$, $\underline{\text{C}}(8)\text{-}\underline{\text{N}}(9)$ and $\underline{\text{C}}(6)\text{-}\underline{\text{O}}(10)$ (for the first one) and $\underline{\text{C}}(2)\text{-}\underline{\text{N}}(3)$, $\underline{\text{C}}(4)\text{-}\underline{\text{C}}(5)$, $\underline{\text{N}}(7)\text{-}\underline{\text{C}}(8)$ and $\underline{\text{C}}(6)\text{-}\underline{\text{O}}(10)$ (for the second one). This supports the suggestion made before about the existence of double bond character in these groups.

For the $\underline{\text{N}}(9)\text{-H}$ enolic tautomers, the same analysis let us consider a higher delocalization of the electronic density in the 6-membered ring. The $\underline{\text{C}}(6)\text{-}\underline{\text{O}}(10)$ group is associated to a lower double bond character. In the imidazolic moiety, the $\underline{\text{N}}(7)\text{-}\underline{\text{C}}(8)$ group is supposed to contain in both cases a double bond character. For these two tautomers, the contour maps are in agreement with the results discussed before related to the internuclear distances.

A double bond character for the $\underline{\text{N}}(1)\text{-}\underline{\text{C}}(2)$, $\underline{\text{C}}(4)\text{-}\underline{\text{C}}(5)$, $\underline{\text{C}}(8)\text{-}\underline{\text{N}}(9)$ and $\underline{\text{C}}(6)\text{-}\underline{\text{O}}(10)$ groups is also supported for the $\underline{\text{N}}(3)\text{-H}/\underline{\text{N}}(7)\text{-H}$ tautomer. Finally, for the *cis*- $\underline{\text{N}}(7)\text{-H}$ enolic tautomer the same character is supported for the $\underline{\text{C}}(2)\text{-}\underline{\text{N}}(3)$, $\underline{\text{C}}(5)\text{-}\underline{\text{C}}(6)$, $\underline{\text{C}}(6)\text{-}\underline{\text{N}}(1)$ and $\underline{\text{C}}(8)\text{-}\underline{\text{N}}(9)$ groups; the $\underline{\text{C}}(6)\text{-}\underline{\text{O}}(10)$ group shows a lower level of double bond character.

Considering both the internuclear distances and the contour maps, and comparing them to the values of the Mayer valence indices for each atom of the tautomers, noticeable agreement both for the structural and potential physicochemical meaning is obtained, supporting again the structural properties and electronic distribution made before. As an example, for the $\underline{\text{N}}(1)\text{-H}/\underline{\text{N}}(7)\text{-H}$ tautomer, the Mayer valence indices ($\underline{\text{N}}(1)$: 3.28; $\underline{\text{C}}(2)$:3.97;

$\underline{\text{N}}(3):3.21$; $\underline{\text{C}}(4):4.00$; $\underline{\text{C}}(5):3.83$; $\underline{\text{C}}(6):4.23$; $\underline{\text{N}}(7):3.36$; $\underline{\text{C}}(8):3.95$; $\underline{\text{N}}(9):3.14$; $\underline{\text{O}}(10):2.21$ are in agreement with the double character for the $\underline{\text{C}}(2)\text{-}\underline{\text{N}}(3)$, $\underline{\text{C}}(4)\text{-}\underline{\text{C}}(5)$, $\underline{\text{C}}(8)\text{-}\underline{\text{N}}(9)$ and $\underline{\text{C}}(6)\text{-}\underline{\text{O}}(10)$ groups.

D. Molecular Electrostatic Potential and Electric Dipole Moment.

Figure 4a shows the contour maps of the molecular electrostatic potential in the molecular plane (0 to -50 kcal/mol range, with changes in 10 units, and considering a positive charge as probe), together with the electric dipole moment vector (the head of the arrow pointing to the positive end) for each one of the six most stable tautomers. Figure 4b shows the respective isopotential surfaces (-20 kcal/mol).

Figure 4a.

Figure 4b.

For the $\underline{\text{N}}(1)\text{-H}$ ketonic tautomeric forms the higher attractive (negative) electrostatic potential level lies upon two regions near the $\underline{\text{O}}(10)$ atom, and a region near each of the deprotonated N atoms. The highest level of attractive potential is distributed in a more located way around the O and N deprotonated atoms of the $\underline{\text{N}}(1)\text{-H}/\underline{\text{N}}(7)\text{-H}$ tautomer. The interchangeable H atom in the imidazolic ring appears to influence this characteristic. In both tautomers the protonated regions are associated to repulsive (positive) electrostatic potential. For these two tautomers the value and direction of the electric dipole moment into de plane (1.80 D for $\underline{\text{N}}(1)\text{-H}/\underline{\text{N}}(7)\text{-H}$ and 5.19 D for $\underline{\text{N}}(1)\text{-H}/\underline{\text{N}}(9)\text{-H}$) are in full agreement with the spatial distribution of the attractive and repulsive electrostatic potential around the heterocycles.

For the $\underline{\text{N}}(9)\text{-H}$ enolic tautomeric forms a similar pattern for the attractive electrostatic potential around the $\underline{\text{C}}(2)\text{-}\underline{\text{N}}(3)\text{-}\underline{\text{C}}(4)$ fragment is observed. In contrast, the $\underline{\text{N}}(1)$ deprotonated atom in the cis-isomer is associated to a more localized level of the highest attractive potential. The configuration of the H atom bonded to $\underline{\text{O}}(10)$, influences in a great manner

the characteristics of both the attractive and repulsive electrostatic potentials pathways: the 2-D maps clearly show differences in the “channel” of the repulsive potential that considers the OH group. As for the above two ketonic tautomers, the protonated regions are associated to repulsive electrostatic potential. Finally, the properties of the into the plane- electric dipole moment (2.52D for the cis-isomer; 4.77 D for the trans-isomer), these are also in full agreement with the distribution of the attractive and repulsive electrostatic potential around the respective heterocycles.

With respect to the last $\underline{\text{N}}(7)$ -H tautomers of the series of six, the pattern of the attractive electrostatic potential for the $\underline{\text{N}}(3)$ - H/ $\underline{\text{N}}(7)$ -H shows noticeable differences with respect to the $\underline{\text{N}}(1)$ -H/ $\underline{\text{N}}(7)$ -H tautomer. For the former, the $\underline{\text{O}}(10)$ and the $\underline{\text{N}}(1)$ atoms are associated to very localized attractive electrostatic interactions; for the $\underline{\text{N}}(9)$ atom the highest level of attractive potential is more localized than the one for the same atom in the $\underline{\text{N}}(1)$ -H/ $\underline{\text{N}}(7)$ -H tautomer, which suggests the influence that the protonated $\underline{\text{N}}(3)$ atom plays. As in the preceding cases, the protonated atoms are associated to repulsive electrostatic interactions. For the cis- $\underline{\text{N}}(7)$ -H enolic form, the pattern of the distribution of the attractive electrostatic potential around the $\underline{\text{N}}(3)$ and $\underline{\text{N}}(9)$ atoms resembles the one shown for the same atoms in the energetically most stable tautomer. The pattern of the attractive potential around the $\underline{\text{N}}(1)$ atom resembles that shown for the same site in the cis- $\underline{\text{N}}(9)$ -H enolic tautomer. However, the attractive potential for the OH group in the tautomer here discussed, shows noticeable differences with respect to the same cis- $\underline{\text{N}}(9)$ -H enolic tautomer, reflecting the great influence that the protonated $\underline{\text{N}}(7)$ atom plays in this case. As for all the above cases, the protonated atoms are associated to repulsive potentials. For these two last cases under discussion and considering the properties of the into the plane- electric dipole moment (4.92 D for the $\underline{\text{N}}(3)$ -H/ $\underline{\text{N}}(7)$ -H; 5.16 D for the cis- $\underline{\text{N}}(7)$ -H enolic tautomer), there is an agreement between its properties and the distribution of the attractive and repulsive electrostatic potentials around these heterocycles.

Finally, for the six tautomers here studied, the respective deprotonated atoms could be only suggested as potential sites in physicochemical processes mediated mainly by electrostatic

interactions (or at least in the initial steps). Nevertheless, to postulate the same sites as chemically reactive toward an electrophilic attack (processes in which the covalent contributions could be important), appears very difficult to us and related to the global chemical reactivity problem. For example, and considering the two most stable tautomeric forms, the Q(10) atom could be postulated in principle, as a site of electrophilic attack; however, there are no studies reported up to date that show categorically the existence of a direct Q(10)-transitional metal chemical bond. The same is applied for the Q(10)-N(7) fragment in the N(3)-H/N(9)-H tautomer, for which there are no reports that show categorically a simultaneous Q(10)-transition metal-N(7) chemical bond for this tautomeric form of hypoxanthine. As can be deduced from these examples, many other factors must be considered in the chemical reactivity problem, particularly in condensed phase.

E. Energy and Symmetry Properties of the Wave Function Associated to the HOMO and the LUMO.

Table 3 shows the HOMO and the LUMO energies for the six tautomers here studied, and Figure 5 shows the respective 3D-wave function (± 0.025 level) associated to the same molecular orbitals.

Table 3.

Figure 5.

As can be observed in Figure 5, noticeable trends in the symmetry for the HOMO and LUMO wave functions arise. For the two N(1)-H ketonic and the two N(9)-H enolic tautomers, the symmetry and spatial distribution of the HOMO wave functions are of the same type. From the analysis, a Π -type character for the HOMO is deduced, independently of the position of the interchangeable H atoms. It could be suggested that the potential electron donor properties of these four tautomers are non dependent on the positions of the H atoms, and that they are of the Π -type character.

For the two less energetically favorable $\underline{\text{N}}(7)$ -H tautomers here studied, the symmetry and spatial distribution properties of their HOMO wave functions are different between them and also with respect to the four above cases: they are of σ -type. Here, the σ -type potential electron donor regions are strongly dependent of the interchangeable H atoms positions. On the other hand and for the LUMO wave function, this is Π -type in all the cases. Interestingly, the wave function spatial distribution shows a relative dependence of the H atoms positions, particularly for the case of the $\underline{\text{N}}(1)$ -H ketonic tautomers. For all the tautomers, the potential electron acceptor properties lies upon Π -type molecular orbitals. The energies and properties of the 35 occupied MO and the first 5 unoccupied MO were obtained. For the two most stable tautomers ($\underline{\text{N}}(1)$ -H ketonic forms) the first 10 occupied MO are core-type; MO number 11 is σ -bonding; from MO number 12 to 23 they show σ -character (with specific atomic regions showing bonding properties); the MO number 24 is Π -bonding; from MO 25 to 34 they are σ - or Π -character (with the same characteristics as the MO 12 to 23), and the HOMO (number 35) is Π - type with atomic regions showing bonding properties. The LUMO (number 36) is Π -type.

F. Ionization Potential (I.P.) and Electron Affinity (E.A.).

Table 4 shows the first vertical I.P. and the first vertical E.A. calculated for each one of the six most stable tautomers of hypoxanthine here studied. These values belong to the processes neutral species \rightarrow monocationic radical species, and neutral species \rightarrow monoanionic radical species, respectively.

Table 4.

a) I.P. The I.P. values follow (with the exception of the $\underline{\text{N}}(3)$ -H/ $\underline{\text{N}}(7)$ -H ketonic tautomer) the same trend shown by the HOMO energy values. A gross increasing trend of the I.P. values with descending the tautomer energetic stability is inferred. The energetically most stable tautomers are associated to relatively lower I.P. values, *i.e.*, they would be the relatively stronger reductor agents. On the other hand, the experimental spectroscopic

vertical I.P. values for hypoxanthine, to our knowledge and reported up to date, ranges between 8.87 and 8.89 eV (7,24,25). With respect to the temperature experimental conditions carried out in these experiments, unfortunately only one study (7) makes a detailed description about the temperature at which hypoxanthine in the gas phase was analyzed ($T = 257^{\circ}\text{C}$). This aspect could be important, because as we will show in the next section, the gas-phase temperature influences changes in the relative population of the tautomers. In principle, we think that the experimental signals corresponding to the first I.P. of hypoxanthine, could be weighted by the ionization from the relative tautomeric contribution in the gas phase studied at a specific temperature. In fact, in one of the studies, the signal at 8.87 eV, and reported as the first I.P. is overlapped with a signal at 8.70 eV, this last being interpreted (25) as the starting of the photoionization. In this way, one can suspect that the experimental signals may be only “Iceberg peaks” of very complex processes occurring simultaneously.

With respect to the MO levels associated to the first I.P., we propose that the ionization (oxidation) process involves mainly the HOMO of each tautomer, of Π -character for the $\underline{\text{N}}(1)$ -H ketonic and the $\underline{\text{N}}(9)$ -H enolic forms, and of σ -type for the $\underline{\text{N}}(7)$ -H tautomers. We have analyzed the possible involvement of other occupied MO in the first ionization process, by looking at the their energies for each tautomer: for all the tautomeric forms the MO number 34 lies (σ -type for the $\underline{\text{N}}(1)$ - H and the $\underline{\text{N}}(9)$ -H forms; Π -type for the $\underline{\text{N}}(7)$ -H forms) around 0.01 eV below the HOMO energy. This energetic difference let us suspect that this MO could be in some measure involved in the photoionization process of each tautomer, but having this possibility important experimental implications as a consequence of the higher relative population of the tautomers energetically most stable.

E.A. The theoretical values for this property do not show a clear trend with respect to LUMO energies for the six most stable tautomers studied. However, if we take two groups of three tautomers each, one can observe some gross concordance between the E.A. values and the LUMO energies. The theoretical value of E.A. is associated to the relative

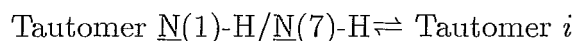
stability of the tautomer upon a reduction process. In general, the most energetically stable tautomers show higher E.A. values than the less stable ones, *i.e.*, the more stable ones would be relatively poorer oxidant agents than the less stable ones. Unfortunately and to our knowledge, experimental E.A. data are not reported up to date.

With respect to the MO associated to the first E.A., we think that the ionization (reduction) process would involve mainly the LUMO of each tautomer, of Π -type in all the cases. Analyzing the energy of the nearest unoccupied MO (number 37), only the energy difference between this and the LUMO energy for $\underline{\text{N}}(1)\text{-H}/\underline{\text{N}}(7)\text{-H}$ is close to 0.01 eV; for the other tautomers, this difference increases as the tautomer becomes energetically more unstable. In this way, and for the most stable tautomer, the possible involvement of the unoccupied MO number 37 (Π -type) in its reduction process arise.

G. Tautomeric Equilibria in Gas Phase as a Function of Temperature.

At this point, the energetic stability and the structural and electronic properties of the six most stable tautomers have been explored for each case. However, an interesting aspect of the problem about the hypoxanthine tautomers in gas phase, lies on the evaluation of the tautomeric equilibrium constants, and their behavior with temperature.

We calculated the tautomeric constants corresponding to the equilibrium:



for which

$$K_{eq} = \frac{[\text{Tautomer } i]}{[\underline{\text{N}}(1)\text{-H}/\underline{\text{N}}(7)\text{-H}]} = e^{-\Delta G^0/RT}$$

where ΔG^0 is the standard Gibbs free energy difference between tautomer i and $\underline{\text{N}}(1)\text{-H}/\underline{\text{N}}(7)\text{-H}$. Table 5 shows the equilibrium constants for all the tautomeric equilibria involving the six tautomers here studied, at three different values of temperature.

Table 5.

As can be seen, the tautomeric constant values at a certain T for the process indicated above, follows a trend of descending values, in agreement with the descending energetic stability of tautomer i with respect to the $\underline{\text{N}}(1)\text{-H}/\underline{\text{N}}(7)\text{-H}$ form. On the other hand, for a specific tautomeric equilibrium, the equilibrium constant shows an increasing behavior with temperature. This means that the hypoxanthine gas phase in thermal equilibrium at a higher temperature would have a tautomeric population remarkably different than the one at low temperature. This also can be seen considering the respective K values. For example, at 298.15 K, the relatively most important tautomeric forms of hypoxanthine in the gas phase would be the two $\underline{\text{N}}(1)\text{-H}$ ketonic forms. However, at 480.15 K, the relative contribution of initially unfavorable tautomeric forms shows a significant increase. These results could have important consequences in the process of analyzing physicochemical properties experimentally obtained and corresponding to the gas phase of hypoxanthine at different temperatures.

H. IR spectroscopy.

As part of the theoretical properties study of the six tautomers, the calculation of the respective IR vibrational spectrum was carefully done, and the correspondent assignment of the absorptions was carried out. Table 6 shows the corrected theoretical frequencies, the intensities and assignments for each one of the absorptions of the IR vibrational spectrum of the six tautomers here studied.

Table 6.

As can be deduced from this table, each one of the tautomers (both ketonic and enolic) shows characteristic absorptions that can lead to make a detailed comparison of the experimental vibrational spectrum of hypoxanthine in gas phase at any temperature below its thermal decomposition. In a previous study (26) the experimental IR vibrational spectrum of hypoxanthine in an Ar matrix measured by the low-temperature method at 11 K and in the 4000-500 cm^{-1} range was reported. In this, the experimental spectrum was assumed

to be mainly a result of the $\underline{\text{N}}(1)\text{-H}/\underline{\text{N}}(7)\text{-H}$ and $\underline{\text{N}}(1)\text{-H}/\underline{\text{N}}(9)\text{-H}$ tautomeric contributions. In addition, a estimated small contribution of a enolic tautomer was established. This was deduced from the pioneering work by Pullman *et al* (4a) on semiempirical calculations for the $\underline{\text{N}}(1)\text{-H}$ ketonic tautomers, some other semiempirical calculations carried out (26) for two enolic forms ($\underline{\text{N}}(9)\text{-H}$ and $\underline{\text{N}}(7)\text{-H}$ but without detailed information about the OH-group configuration), and from the analysis of the experimental IR data in the 4000-3400 cm^{-1} range of some model heterocycles.

For our theoretical study of the IR vibrational spectrum and its comparison with the experimental one, several assumptions were made: a) although the experimental IR spectrum was measured at 11 K in an Ar matrix, we considered that at this temperature there are no tautomeric transformations in the solid sample (in fact, the gas mixture freezes at a higher temperature); b) although the relative population of the hypoxanthine tautomers in the gas phase appears to be dependent on temperature, we assumed that the abrupt decrease of T overcomes the dynamics of the tautomeric equilibria shift; c) as a consequence of a) and b), we considered the experimental sublimation temperature of hypoxanthine (26), *i.e.*, 207°C, as a more realistic value for which the analysis of the relative population of the hypoxanthine tautomers in the gas phase should be done.

From these considerations, the relative population of the hypoxanthine tautomers used to analyze the experimental IR spectrum was the one that corresponds to the tautomeric equilibria at 480.15 K (207°C), and for which the equilibrium tautomeric constants have been previously discussed (Section G, Table 5). The respective mole fraction (x_i) of each tautomer was obtained from the K_{eq} values. The theoretical intensities of the absorptions in each spectrum were weighted by the correspondent mole fraction. After this, all the intensities were scaled relative to the signal of highest intensity value. As a result, a theoretical IR spectrum considering the relative contributions of the six most stable tautomers at 480.15 K was obtained. The experimental spectrum was carefully scanned and digitized

upon a meticulous comparison with the data in a table reported in reference 26, and the experimental absorptions were also scaled with respect to the highest intensity experimental value. Both spectra, the experimental and theoretical ones are shown in Figure 6.

Figure 6.

From their comparison, a reasonable concordance in both the frequency and intensity patterns between several groups of highest absorptions in the two spectra is found. These groups belong to the 3510-3300 cm^{-1} , 1800-1200 cm^{-1} , 1100-1000 cm^{-1} and 1000-500 cm^{-1} ranges.

In order to carry out the spectral characterization of the experimental IR spectrum from a theoretical point of view, we first constructed the theoretical spectrum by successive incorporation of each tautomer in order of descending energetic stability, and made a detailed comparison of the possible changes observed. From this procedure, a essential contribution of the $\underline{\text{N}}(1)\text{-H}/\underline{\text{N}}(7)\text{-H}$ and $\underline{\text{N}}(1)\text{-H}/\underline{\text{N}}(9)\text{-H}$ tautomers was found. This is, the resultant theoretical IR spectrum (Figure 6b) and its observable absorptions correspond to the two $\underline{\text{N}}(1)\text{-H}$ ketonic tautomers contributions. The energetically less stable ones do not have any significative spectral contributions to the theoretical IR spectrum shown in Figure 6b.

Characterization of the experimental IR spectrum of hypoxanthine from the theoretical study.

a) 3510-3300 cm^{-1} range.

The experimental IR bands with maximum absorptions at 3464 cm^{-1} (band 1) and 3428 cm^{-1} (band 2) could be assigned to the $\nu_{\text{N-H}}$ (imidazolic ring) and $\nu_{\text{N-H}}$ (pyrimidinic ring) vibrational modes respectively. Although the theoretical frequencies for these two vibrational modes in the $\underline{\text{N}}(1)\text{-H}$ ketonic tautomers lies upon slightly higher values than the experimental ones, their relative intensities are very similar. When analyzing in more detail the two experimental bands, a shoulder in both is observed. For the band at 3464

cm^{-1} , a shoulder at 3478 cm^{-1} is detected; for the band at 3428 cm^{-1} a shoulder in the low-energy side is suggested. From the comparison between these two experimental bands and their correspondent theoretical ones, the maxima absorptions at 3464 and 3428 cm^{-1} are attributed respectively to $\nu_{\underline{\text{N}}(7)\text{-H}}$ and $\nu_{\underline{\text{N}}(1)\text{-H}}$ of the $\underline{\text{N}}(1)\text{-H}/\underline{\text{N}}(7)\text{-H}$ tautomer. The two shoulders of the experimental bands are attributed respectively to $\nu_{\underline{\text{N}}(9)\text{-H}}$ (the one at higher frequency) and $\nu_{\underline{\text{N}}(1)\text{-H}}$ (the one at lower energy) of the $\underline{\text{N}}(1)\text{-H}/\underline{\text{N}}(9)\text{-H}$ tautomer.

b) $1800\text{-}1200 \text{ cm}^{-1}$ range.

The experimental bands at 1753 cm^{-1} (band 3) and 1735 cm^{-1} (band 4) are very similar in frequency and relative intensity to two theoretical absorptions of the two $\underline{\text{N}}(1)\text{-H}$ ketonic tautomers. Considering the previous assignments of the theoretical absorptions of the $\underline{\text{N}}(1)\text{-H}$ ketonic tautomers, it can be proposed that the band at 1753 cm^{-1} is due to the $\nu \text{ C=O}/\underline{\text{N}}(1)\text{-H}$ vib./rings vib. modes of the $\underline{\text{N}}(1)\text{-H}/\underline{\text{N}}(9)\text{-H}$ tautomer. The band at 1735 cm^{-1} is attributed to contain the $\nu \text{ C=O}/\text{rings vib.}/\underline{\text{N}}(1)\text{-H}$ vib. modes of the $\underline{\text{N}}(1)\text{-H}/\underline{\text{N}}(7)\text{-H}$ tautomer.

In this same range, there are three bands at 1595 cm^{-1} (band 5), 1555 cm^{-1} (band 6) and 1534 cm^{-1} (band 7). Comparing these with the absorptions of the theoretical IR spectrum, the band at 1595 cm^{-1} is associated to the modes ring vib./ $\underline{\text{C}}(2)\text{-H}$ vib./ $\underline{\text{N}}(1)\text{-H}$ vib./ $\nu \text{ C=O}$ of the $\underline{\text{N}}(1)\text{-H}/\underline{\text{N}}(7)\text{-H}$ form. The band at 1555 cm^{-1} is attributed to the modes rings vib./ $\underline{\text{C}}(2)\text{-H}/\nu \text{ C=O}$, and the one at 1534 cm^{-1} is associated to the modes rings vib./ $\underline{\text{N}}(9)\text{-H}$ vib./ $\underline{\text{C}}(8)\text{-H}$ vib. of the $\underline{\text{N}}(1)\text{-H}/\underline{\text{N}}(9)\text{-H}$ tautomer.

Finally, there are bands in this range appearing at 1433 cm^{-1} (band 8), 1384 and 1381 cm^{-1} (band 9), 1371 cm^{-1} (band 10) and 1324 cm^{-1} (band 11). When comparing them with the theoretical absorptions, we suggest for the first the contribution of the modes rings vib./ $\underline{\text{C}}(8)\text{-H}/\nu \text{ C=O}$ of the $\underline{\text{N}}(1)\text{-H}/\underline{\text{N}}(7)\text{-H}$ tautomer; the second one (doublet) is suggested to contain mainly both the rings vib./ N-H vib./ $\nu \text{ C=O}$ and the rings vib./ $\underline{\text{C}}(2)\text{-H}$ vib./ $\underline{\text{C}}(8)\text{-H}$ vib. modes of the $\underline{\text{N}}(1)\text{-H}/\underline{\text{N}}(7)\text{-H}$ form. The band at 1371 cm^{-1} could be associated mainly to the rings vib./ N-H vib./ $\nu \text{ C=O}$ modes of the same tautomer.

The band at 1324 cm^{-1} is proposed to contain both the rings vib./ $\underline{\text{C}}(2)\text{-H}$ vib./ $\underline{\text{N}}(1)\text{-H}$ vib. modes of the $\underline{\text{N}}(1)\text{-H}/\underline{\text{N}}(9)\text{-H}$ tautomer, and the rings vib./ $\underline{\text{C}}(2)\text{-H}$ vib./ $\underline{\text{N}}(7)\text{-H}$ vib./ ν C=O modes of the $\underline{\text{N}}(1)\text{-H}/\underline{\text{N}}(7)\text{-H}$ tautomer.

c) $1100\text{-}1000\text{ cm}^{-1}$ range.

In this range, the experimental IR spectrum show bands at 1100 cm^{-1} $\underline{\text{N}}(9)\text{-H}$ (band 12), 1084 cm^{-1} (band 13) and 1062 and 1054 cm^{-1} (band 14). Again, comparing them with the theoretical spectrum, the following assignments can be suggested: the band at 1100 cm^{-1} corresponds to the rings vib./ $\underline{\text{N}}(1)\text{-H}$ vib modes of the $\underline{\text{N}}(1)\text{-H}/\underline{\text{N}}(9)\text{-H}$ tautomer; the band at 1084 cm^{-1} is attributed to rings vib./ $\underline{\text{N}}(1)\text{-H}$ vib./ modes of the $\underline{\text{N}}(1)\text{-H}/\underline{\text{N}}(7)\text{-H}$ form, and the band of complex structure with absorptions at 1062 and 1055 cm^{-1} can be assigned, the first frequency to rings vib./ $\underline{\text{N}}(7)\text{-H}$ vib. modes of the $\underline{\text{N}}(1)\text{-H}/\underline{\text{N}}(7)\text{-H}$ tautomer, and the second frequency to the rings vib./ $\underline{\text{N}}(\text{imidazolic})\text{-H}$ vib. modes of both $\underline{\text{N}}(1)\text{-H}$ ketonic tautomers, without discarding some contribution of the modes $\underline{\text{C}}(2)\text{-H}$ vib./C=O vib. of the $\underline{\text{N}}(1)\text{-H}/\underline{\text{N}}(9)\text{-H}$ tautomer.

d) $1000\text{-}500\text{ cm}^{-1}$ range.

Several band of low-intensity appear in this range. Comparing carefully the frequency and intensity patterns with the theoretical ones, assignments for those were possible. These are as follows (o.m.p. means out of the molecular plane): 891 cm^{-1} (band 15): rings vib./ $\underline{\text{N}}(9)\text{-H}$ vib./ $\underline{\text{C}}(8)\text{-H}$ vib. of $\underline{\text{N}}(1)\text{-H}/\underline{\text{N}}(9)\text{-H}$; 860 cm^{-1} (band 16): $\underline{\text{C}}(2)\text{-H}$ vib./pyrimidinic ring vib. (o.m.p.) of both $\underline{\text{N}}(1)\text{-H}$ ketonic tautomers; *ca.* 775 cm^{-1} (band 17): $\underline{\text{C}}(8)\text{-H}$ vib./rings vib. (o.m.p.) of the $\underline{\text{N}}(1)\text{-H}$ ketonic tautomers; 725 cm^{-1} (band 18): $\underline{\text{N}}(1)\text{-H}$ vib./rings vib. (o.m.p.) of the $\underline{\text{N}}(1)\text{-H}$ ketonic tautomers; 691 cm^{-1} (band 19): rings vib. of the $\underline{\text{N}}(1)\text{-H}$ ketonic tautomers; 657 cm^{-1} (band 20): rings vib./ $\underline{\text{N}}\text{-H}$ vib. (o.m.p.) of the $\underline{\text{N}}(1)\text{-H}/\underline{\text{N}}(7)\text{-H}$ tautomer; 640 cm^{-1} (band 21): $\underline{\text{N}}(1)\text{-H}$ vib./rings vib. (o.m.p.) of the $\underline{\text{N}}(1)\text{-H}/\underline{\text{N}}(9)\text{-H}$ tautomer; 626 and 622 cm^{-1} (band 22): rings vib./ $\underline{\text{N}}\text{-H}$ vib. (o.m.p.) of the $\underline{\text{N}}(1)\text{-H}$ ketonic tautomers; 602 and 598 cm^{-1} (band 23): essentially rings vib. of the $\underline{\text{N}}(1)\text{-H}$ ketonic tautomers; 558 and 553 cm^{-1} (band 24): $\underline{\text{N}}(9)\text{-H}$ vib./rings vib. (o.m.p.)

of the $\underline{\text{N}}(1)\text{-H}/\underline{\text{N}}(9)\text{-H}$ tautomer and rings vib./ $\underline{\text{N}}(1)\text{-H}$ vib. (o.m.p.) of the $\underline{\text{N}}(1)\text{-H}/\underline{\text{N}}(7)\text{-H}$ tautomer respectively; 542 and 534 cm^{-1} (band 25): rings vib. of both $\underline{\text{N}}(1)\text{-H}$ ketonic tautomers; 524 cm^{-1} (band 26): imidazolic ring vib./ $\underline{\text{N}}(7)\text{-H}$ vib. (o.m.p.) of the $\underline{\text{N}}(1)\text{-H}/\underline{\text{N}}(7)\text{-H}$. Finally, the band at 508 cm^{-1} (band 27), is attributed to $\underline{\text{N}}(9)\text{-H}$ vib./rings vib. (o.m.p.) of the $\underline{\text{N}}(1)\text{-H}/\underline{\text{N}}(9)\text{-H}$ tautomer.

On the other hand, and from the same analysis, our theoretical spectral results let us propose the existence of absorptions in the experimental IR spectrum for the ranges: *ca.* 3300-3000 cm^{-1} (for the $\nu \underline{\text{C}}(8)\text{-H}$ and $\nu \underline{\text{C}}(2)\text{-H}$ modes of both $\underline{\text{N}}(1)\text{-H}$ ketonic tautomers); *ca.* 1520-1450 cm^{-1} (for the rings vib./ $\underline{\text{N}}(7)\text{-H}$ vib./ $\underline{\text{C}}(2)\text{-H}$ vib./ $\nu \text{C}=\text{O}$ modes of the $\underline{\text{N}}(1)\text{-H}/\underline{\text{N}}(7)\text{-H}$ form); and *ca.* 1200-1100 cm^{-1} (for the rings vib./ $\underline{\text{C}}(8)\text{-H}$ vib./ N-H vib. of both $\underline{\text{N}}(1)\text{-H}$ ketonic tautomers). Other theoretical absorptions (their characterization appears in Table 6), are also predicted below 500 cm^{-1} .

From the above analysis, only the vibrational modes of the two $\underline{\text{N}}(1)\text{-H}$ ketonic tautomers have shown to have significative contributions. At this respect, it is important to arise that in the experimental study (26), the spectral contribution of an enolic tautomer was established after the increase of the total intensity of the spectrum; from this, a band of extremely low-intensity was shown in the original spectrum at 3578 cm^{-1} (band a in the experimental spectrum of Figure 6a). The authors used some semiempirical results (that predict the existence of this band) and the IR data (4000-3400 cm^{-1}) of some model heterocycles to conclude that tautomeric contribution.

We attempted to make observable the theoretical absorptions associated to the νOH mode for the *cis*- and *trans*- $\underline{\text{N}}(9)\text{-H}$ enolic tautomers in the spectrum of Figure 6b, and only when multiplying by a factor of 100, they were detected. The complexity of the resulting theoretical spectrum made it very difficult to consider that in the experimental one, bands associated clearly to vibrational modes of the OH group could be detected. It is then very difficult for us to consider a significative contribution of an enolic tautomer (*i.e.*, the *cis*- or *trans*- $\underline{\text{N}}(9)\text{-H}$, or both) in the experimental IR spectrum of hypoxanthine.

These considerations could be in agreement with a mass spectra study ($T = 252^{\circ}\text{C}$) of hypoxanthine (27), from which the existence of only the $\underline{\text{N}}(1)\text{-H}$ ketonic forms was deduced.

IV. CONCLUDING REMARKS.

In the theoretical study carried out, the total energy, the structural properties, the electronic structures, some properties associated with electrostatic interactions and Redox processes, and the IR vibrational spectra of all the ketonic and enolic tautomeric forms of neutral hypoxanthine were calculated. Here, those corresponding to the six energetically most stable tautomers have been shown and discussed.

From this study, the following conclusions can be drawn:

1. The total energy values let us consider the highest relative energetic stability for the two $\underline{\text{N}}(1)\text{-H}$ ketonic tautomers, followed by the two enolic $\underline{\text{N}}(9)\text{-H}$, the $\underline{\text{N}}(3)\text{-H}/\underline{\text{N}}(7)\text{-H}$ and the *cis*- $\underline{\text{N}}(7)\text{-H}$ enolic forms. For the $\underline{\text{N}}(1)\text{-H}$ ketonic tautomers, and at this level of study, the $\underline{\text{N}}(1)\text{-H}/\underline{\text{N}}(7)\text{-H}$ form is slightly more stable than the $\underline{\text{N}}(1)\text{-H}/\underline{\text{N}}(9)\text{-H}$ one.
2. The values of the structural parameters are noticeably sensitive to the tautomeric form. The experimental trend found about the increase of the internal angle of a specific region in the heterocycles upon a protonation or a metallic coordination here has been also obtained. All the tautomeric forms here studied are remarkably planar in isolated form. Interestingly and for the enolic forms, the OH group is also found to be located into the correspondent molecular plane. The theoretical values of the same structural parameters, let us consider the existence of regions with double bond character. Endocyclically these are remarkably dependent on the position of the interchangeable H atoms involved in the prototropic tautomerism. For the ketonic forms this same character is attributed to the $\underline{\text{C}}(6)\text{-}\underline{\text{O}}(10)$ group.
3. The total electronic density distribution is also noticeably sensitive to the tautomeric form, accordingly with the values of the structural parameters and the Mayer valence indices values.
4. In agreement with the structural parameters, the total electronic density and Mayer valence indices, the attractive electrostatic potential distribution is also strongly dependent

on the tautomeric form: those endocyclic atomic regions involved in double bonds are also associated to high attractive potentials. In contrast, all the protonated regions (N-H or C-H) are associated to the repulsive ones. For the exocyclic O atom, the spatial distribution of the attractive electrostatic potential is dependent on both the tautomeric form (ketonic or enolic) and for the last one, on its configuration. We also found concordance of the electric dipole moment behavior with the above properties.

Considering all these properties, possible favorable sites for interactions with electrophilic agents and directed in the first steps (or essentially) by electrostatic contributions can be suggested, being in principle those associated to a higher total electronic density, a higher attractive electrostatic potential and the negative end of the electric dipole moment vector. Interestingly and for the N(1)-H ketonic tautomers, the most stable in solution, the metallic coordination behavior found up to date involves mainly those atomic regions with the properties rationalized before: the N(3) and N(9) atoms for the N(1)-H/N(7)-H form, and the N(7) (or the N(3) and N(7) atoms) for the N(1)-H/N(9)-H have been involved. Unfortunately, there are no reports on theoretical and experimental studies were the reactivity of other less stable tautomers here studied are considered. In spite of the above considerations and experimental evidences, one has to be cautious about the reactivity sites studies in these heterocycles. Many other factors, as for example the kinetic one, can play a critical role.

5. The properties of the wave function associated to the molecular orbitals would appear to have significative contributions and implications in the reactivity of the tautomers (mainly the most stable ones) towards Lewis acids, particularly those having Π -type frontier MO energetically accessible for electron density transfer processes. In particular, these results for the most stable tautomers of hypoxanthine, let us propose that in their respective interaction with a transitional metallic center through a specific potential coordination site (*e.g.*, the N(7) atom), the initial step of the chemical bond formation in that site could be feasible although the same N atom shows a σ -bond with an H atom. This would mean

that the protonated N atom has not necessarily filled its bonding capacity, and thus it can react with other electrophilic agent.

This let us suspect that the initial step of the protonated N atom-transition metal chemical bond formation does not necessarily requires the respective N atom protonic dissociation. In other words, the potential reactivity of an specific N atom towards a transitional metallic center does not require its existence in deprotonated form.

6. From the first I.P. and E.A. theoretical values, an approximated both increasing trend for the first one and decreasing for the second one, with descending energetic stability of the tautomers is found. These properties could have significative repercussions in the reactivity of the $\underline{\text{N}}(1)\text{-H}$ ketonic forms, because they would be the strongest reductors (*i.e.*, weakest oxidants) tautomers. For these two tautomers, the electron donor-acceptor properties are associated to the Π -type frontier MO, but without excluding the possible contribution of the respective energetically nearest MO for each one of those.

7. The theoretical tautomeric equilibrium constant calculated for the whole set of tautomers at different temperatures show a decreasing tendency for the relative contribution of the energetically less stable tautomeric forms with the temperature decrease. The equilibrium constants at the sublimation temperature ($T = 207^\circ\text{C}$) were used to obtain the relative contribution of the tautomers to the IR vibrational spectrum theoretical analysis. The theoretical spectral analysis carefully carried out has lead to the absorptions characterization of the experimental IR data, being the $\underline{\text{N}}(1)\text{-H}$ ketonic tautomers the spectroscopically observable ones. In our opinion, the enolic tautomers (*e.g.*, the $\underline{\text{N}}(9)\text{-H}$ forms) have not significative contributions at this spectroscopic level, and for the thermal conditions established.

Finally, the highest energetic stability of the $\underline{\text{N}}(1)\text{-H}$ ketonic tautomeric forms here found would appear to be in correspondence with their clear spectroscopic preponderance in solution studies. Comparing the relative population of the $\underline{\text{N}}(1)\text{-H}/\underline{\text{N}}(7)\text{-H}$ and $\underline{\text{N}}(1)\text{-H}/\underline{\text{N}}(9)\text{-H}$ tautomers, both in solution and in gas phase, the environment dielectric properties influence is clear: the tautomeric form with higher electric dipole moment shows an increasing

contribution in the relative population as the environment dielectric constant increases, as in the case of the $\underline{\text{N}}(1)\text{-H}/\underline{\text{N}}(9)\text{-H}$ ketonic tautomer.

ACKNOWLEDGMENTS.

The authors are indebted to DGSCA-UNAM and UAM-Iztapalapa for the computer service facilities. We also acknowledge Dr. Alberto Vela (UAM-I) for his advice on some aspects of the calculations.

References

- (1) See for example: a) Hughes, M.N. *The Inorganic Chemistry of Biological Processes*, 2nd. Ed.; John Wiley & Sons: New York, 1981; b) Stryer, L. *Biochemistry*, 3rd. Ed., Freeman: New York, 1988; c) *Nucleic Acid-Metal Ion Interactions*, Vol. 1, Spiro, T.G. Ed., John Wiley & Sons: New York, 1980; d) *CRC Handbook of Nucleobase Complexes*, Vol. I, Lusty, J.R. Ed., CRC Press: Boca Raton, FL, 1990; e) Kwiatkowski, J.S.; Zielinski, T.J.; Rein, R. in *Adv. Quantum Chem.* Löwdin, P.O. Ed., Academic Press, Inc.: New York, **1986**, 18, 85.
- (2) Tauler, R.; Cid, J.F.; Casassas, E. *J. Inorganic Biochemistry* **1990**, 39, 277.
- (3) Acevedo-Chávez, R.; Costas, M.E.; Escudero, R. *Inorganic Chemistry* **1996**, 35, 7430.
- (4) a) Pullman, B.; Pullman, A. *Adv. heterocyclic Chem.* **1971**, 13, 77; b) Lichtenberg, D.; Bergmann, F.; Neiman, Z. *Isr. J. Chem.* **1972**, 10, 805; c) Chenon, M.T.; Pugmire, R.J.; Grant, D.M.; Panzica, R.P.; Townsend, L.B. *J. Am. Chem. Soc.* **1975**, 97, 4636.
- (5) a) Cheng, D.M.; Kan, L.S.; Ts'o, P.O.P.; Prettre, C.G.; Pullman, B. *J. Am. Chem. Soc.* **1980**, 102, 525; b) Szczepaniak, K.; Szczespaniack, M. *J. Mol. Struct.* **1987**, 156, 29; c) Person, W.B.; Szczepaniak, K.; Szczespaniack, M.; Kwiatkowski, J.S.; Hernandez, L.; Czerminski, R. *J. Mol. Struct.* **1989**, 194, 239; d) Nowak, M.J.; Lapinski, L.; Kwiatkowski, J.S. *Chem. Phys. Lett.* **1989**, 157, 14; e) Santhosh, C.; Mishra, P.C. *Spectrochim. Acta* **1993**, 49A, 985.
- (6) Neiman, Z. *Isr. J. Chem.* **1971**, 9, 119.
- (7) Lin, J.; Yu, C.; Peng, S.; Akiyama, I.; Li, K.; Lee, L.K.; LeBreton, P.R. *J. Phys. Chem.* **1980**, 84, 1006.
- (8) Aaron, J.J.; Gaye, M.D.; Párkányi, C.; Cho, N.S.; Von Szentpály, L. *J. Mol. Struct.* **1987**, 156, 119.
- (9) Ohta, Y.; Nishimoto, K.; Tanaka, H.; Baba, Y.; Kagemoto, A. *Bull. Chem. Soc. Jpn.* **1989**, 62, 2441.
- (10) Leo, T.; Accion, F.; Escolar, D.; Tortajada, J. *An. Quim. Sp.* **1991**, 87, 14.

- (11) Nonella, M.; Hänggi, G.; Dubler, E. *J. Mol. Struct. (Theochem.)* **1993**, *279*, 173.
- (12) El-Bakali Kassimi, N.; Thakkar, A.J. *J. Mol. Struct. (Theochem.)* **1996**, *366*, 185.
- (13) Lazo, L.; Tejo, A.M.; Pousa, J.L.; Sorarrain, O.M.; Roncaglia, H.A. *Z. Phys. Chemie, Leipzig* **1985**, *266*, 143.
- (14) Sheina, G.G.; Stepanian, S.G.; Radchenko, E.D.; Blagoi, Yu.P. *J. Mol. Struct.* **1987**, *158*, 275.
- (15) Hernández, B.; Luque, F.J.; Orozco, M. *J. Org. Chem.* **1996**, *61*, 5964.
- (16) Becke, A.D. *Phys. Rev. A* **1988**, *38*, 3098.
- (17) Perdew, J.P. *Phys. Rev. B* **1986**, *33*, 8822.
- (18) Godbout, N.; Salahub, D.R.; Andzelm, J.; Wimmer, E. *Can. J. Chem.* **1992**, *70*, 560.
- (19) Frisch, M.J.; Trucks, G.W.; Schlegel, H.B.; Gill, P.M.W.; Johnson, B.G.; Robb, M.A.; Cheeseman, J.R.; Keith, T.; Petersson, G.A.; Montgomery, J.A.; Raghavachari, K.; Al-Laham, M.A.; Zakrzewski, V.G.; Ortiz, J.V.; Foresman, J.B.; Cioslowski, J.; Stefanov, B.B.; Nanayakkara, A.; Challacombe, M.; Peng, C.Y.; Ayala, P.Y.; Chen, W.; Wong, M.W.; Andres, J.L.; Replogle, E.S.; Gomperts, R.; Martin, R.L.; Fox, D.J.; Binkley, J.S.; Defrees, D.J.; Baker, J.; Stewart, J.P.; Head-Gordon, M.; Gonzalez, C.; Pople, J.A. *Gaussian 94, Revision D.4*, Gaussian, Inc., Pittsburgh PA, 1995.
- (20) Schmalle, H.W.; Hänggi G.; Dubler, E. *Acta Cryst.* **1988**, *C44*, 732.
- (21) DGAUSS 3.0.1/UC-3.0, Cray Research, Inc.
- (22) Frisch, M.J.; Trucks, G.W.; Schlegel, H.B.; Gill, P.M.W.; Johnson, B.G.; Wong, M.W.; Foresman, J.B.; Robb, M.A.; Head-Gordon, M.; Replogle, E.S.; Gomperts, R.; Andres, J.L.; Raghavachari, K.; Binkley, J.S.; Gonzalez, C.; Martin, R. L.; Fox, D.J.; Defrees, D.J.; Baker, J.; Stewart, J.J.P.; Pople, J.A. *Gaussian 92/DFT, Revision F.3*, Gaussian, Inc., Pittsburgh PA, 1993.
- (23) UNICHEM 3.0, Cray Research, Inc., 1995.
- (24) Hush, N.S.; Cheung, A.S. *Chem. Phys. Lett.* **1975**, *34*, 11.
- (25) Dougherty, D.; Younathan, E.S.; Voll, R.; Abduluur, S.; McGlynn, S.P., *J. Electron Spectrosc. Relat. Phenom.* **1978**, *13*, 379.

(26) Sheina, G.G.; Stepanian, S.G.; Rádchenko, E.D.; Blagoi, Yu. P. *J. Mol. Struct.* **1987**, *158*, 275.

(27) Rice, J.M.; Dudek, G.O. *J. Am. Chem. Soc.* **1967**, *89*, 2719.

Tables.

Table 1. DFT energy for all the tautomers and energy difference with respect to tautomer K17. K=ketonic; E=enolic; c=cis with respect to N(1); t=trans with respect to N(1); cr=crystalline structure.

Table 2. a) Internuclear distances (\AA) for the six most stable tautomers. b) Internal angles (degrees) for the six most stable tautomers.

Table 3. HOMO and LUMO energy for the six most stable tautomers.

Table 4. First vertical ionization potentials and first vertical electronic affinities for the six most stable tautomers.

Table 5. Tautomeric equilibrium constants at three different temperatures for all the tautomers in the gas phase.

Table 6. Frequency ($\bar{\nu}$, cm^{-1}), intensity (I, KM/mol) and vibrational modes assignments for the theoretical IR spectrum of the six most stable tautomers: a) $\underline{\text{N}}(1)\text{-H}/\underline{\text{N}}(7)\text{-H}$ and $\underline{\text{N}}(1)\text{-H}/\underline{\text{N}}(9)\text{-H}$ ketonic forms; b) cis- $\underline{\text{N}}(9)$ and trans- $\underline{\text{N}}(9)$ enolic forms; c) $\underline{\text{N}}(3)\text{-H}/\underline{\text{N}}(7)\text{-H}$ ketonic and cis- $\underline{\text{N}}(7)$ enolic forms. α : all the vibrational modes at the indicated frequency are out of molecular plane (o.m.p.). δ COH* means ν and δ combined modes for this group.

Figure Captions.

Figure 1. Schematic drawing of heterocycles showing pirimidinic and azolic rings fused in their structure. X,Y=H, NH_2 , O, S,...; A,B,C=C, N; R_i =possible H atoms or other substituents depending on each case and tautomeric form.

Figure 2. Schematic drawing and numbering sequence of hypoxanthine in its $\underline{\text{N}}(1)\text{-H}/\underline{\text{N}}(9)\text{-H}$ ketonic tautomeric form.

Figure 3. Total electronic charge density contour maps (0.15 to 0.50 $e/\text{\AA}^3$ range, changes in 0.05 units) for the six most stable tautomers.

Figure 4. a) Attractive electrostatic potential contour maps (0 to -50 kcal/mol range, with changes in 10 units, considering a positive charge as probe), together with the electric dipole

moment vector (the head of the arrow pointing to the positive end), and b) Isopotential electrostatic potential surfaces (-20 kcal/mol), for each one of the six most stable tautomers.

Figure 5. HOMO and LUMO 3D-wave function (± 0.025 level) for the six most stable tautomers.

Figure 6. IR vibrational spectra for hypoxanthine a) experimental (from reference 26), and b) theoretical (this study).

Tautomer	Energy (Hartrees)	ΔE (Kcal/mol)
K17	-487.2690	–
K19	-487.2677	0.84
E9c	-487.2596	5.92
E9t	-487.2576	7.17
K37	-487.2569	7.65
E7c	-487.2558	8.31
E3t	-487.2464	14.22
E3c	-487.2443	15.53
E7t	-487.2417	17.14
K13	-487.2383	19.29
E1t	-487.2364	20.48
K39	-487.2351	21.29
K79	-487.2323	23.04
E1c	-487.2194	31.13
K19cr	-487.1655	65.00

Table 1.

$d(\text{Å})$	K17	K19	E9c	E9t	K37	E7c
N1-C2	1.385	1.373	1.358	1.357	1.308	1.366
C2-N3	1.311	1.318	1.346	1.351	1.384	1.339
N3-C4	1.379	1.369	1.348	1.346	1.383	1.356
C4-C5	1.411	1.411	1.420	1.414	1.395	1.424
C5-C6	1.439	1.454	1.414	1.414	1.457	1.403
C6-N1	1.428	1.448	1.345	1.339	1.425	1.336
C5-N7	1.382	1.386	1.393	1.393	1.388	1.387
N7-C8	1.380	1.326	1.324	1.326	1.374	1.385
C8-N9	1.331	1.389	1.391	1.390	1.341	1.326
N9-C4	1.383	1.383	1.385	1.389	1.371	1.390
C6-O10	1.241	1.233	1.353	1.358	1.242	1.364
C2-H	1.097	1.096	1.097	1.097	1.099	1.097
C8-H	1.091	1.091	1.092	1.092	1.091	1.092
H-	N1 1.025	N1 1.025	O10 0.987	O10 0.985	N3 1.022	O10 0.987
H-	N7 1.022	N9 1.022	N9 1.021	N9 1.021	N7 1.022	N7 1.027

Table 2a.

Angle	K17	K19	E9c	E9t	K37	E7c
C2-N1-C6	125.49	126.75	118.46	117.75	120.95	117.63
N1-C2-N3	125.45	124.53	128.07	128.94	126.61	128.46
C2-N3-C4	113.51	111.69	111.34	111.09	117.03	113.36
N3-C4-C5	123.94	129.32	127.52	126.63	118.38	122.99
C4-C5-C6	123.54	118.91	114.29	115.55	124.08	117.96
N1-C6-C5	108.07	108.81	120.32	120.04	112.95	119.59
N1-C6-O10	122.29	119.99	118.27	117.50	122.80	119.49
C5-C6-O10	129.64	131.20	121.41	122.46	124.25	120.93
N3-C4-N9	125.58	125.86	128.03	129.17	128.55	126.86
C5-C4-N9	110.49	104.83	104.45	104.20	113.07	110.15
C4-C5-N7	105.55	111.10	111.35	111.80	103.73	105.54
C6-C5-N7	130.90	129.99	134.36	132.65	132.19	136.49
C5-N7-C8	106.21	104.38	103.83	103.67	107.13	105.84
C4-N9-C8	104.43	106.67	106.64	106.83	103.13	104.44
N7-C8-N9	113.32	113.02	113.73	113.51	112.93	114.03
N1-C2-H	115.16	116.21	115.60	115.26	119.14	114.97
N3-C2-H	119.38	119.26	116.34	115.80	114.25	116.57
N7-C8-H	121.71	125.27	124.87	125.00	122.48	121.16
N9-C8-H	124.96	121.72	121.40	121.50	124.59	124.81
H	N1 – C2 119.50	N1 – C2 119.33	O10 – C6 104.99	O10 – C6 106.90	N3 – C2 121.90	O10 – C6 105.18
H	N1 – C6 115.01	N1 – C6 113.92	–	–	N3 – C4 121.07	–
H	N7 – C5 125.74	N9 – C4 125.53	N9 – C4 125.73	N9 – C4 125.94	N7 – C5 124.69	N7 – C5 126.97
H	N7 – C8 128.05	N9 – C8 127.80	N9 – C8 127.64	N9 – C8 127.23	N7 – C8 128.18	N7 – C8 127.19

Table 2b.

Tautomer	HOMO energy (eV)	LUMO energy (eV)
K17	-0.22032	-0.07842
K19	-0.21465	-0.07810
E9c	-0.22667	-0.07722
E9t	-0.22966	-0.08033
K37	-0.20991	-0.08089
E7c	-0.22970	-0.08129

Table 3.

Tautomer	I.P. (eV)	A.E. (eV)
K17	8.73	0.50
K19	8.55	0.52
E9c	8.88	0.48
E9t	8.97	0.40
K37	8.66	0.37
E7c	9.05	0.41

Table 4.

Tautomer	K_{eq} $T = 480.15\text{K}$	K_{eq} $T = 298.15\text{K}$	K_{eq} $T = 11.0\text{K}$
K19	4.64×10^{-1}	2.85×10^{-1}	1.29×10^{-15}
E9c	1.89×10^{-3}	4.65×10^{-5}	1.31×10^{-116}
E9t	4.79×10^{-4}	5.01×10^{-6}	5.82×10^{-143}
K37	5.47×10^{-4}	4.31×10^{-6}	9.62×10^{-149}
E7c	1.99×10^{-4}	1.12×10^{-6}	3.33×10^{-161}
E3t	2.43×10^{-7}	2.64×10^{-11}	5.40×10^{-286}
E3c	7.52×10^{-8}	3.90×10^{-12}	1.65×10^{-308}
E7t	6.26×10^{-8}	1.47×10^{-12}	0.0
K13	2.75×10^{-9}	1.41×10^{-14}	0.0
E1t	5.93×10^{-10}	1.39×10^{-15}	0.0
K39	1.60×10^{-9}	2.92×10^{-15}	0.0
K79	6.04×10^{-11}	2.91×10^{-17}	0.0
E1c	1.03×10^{-13}	3.59×10^{-22}	0.0

Table 5.

K17			K19		
$\bar{\nu}$	I	Assignments	$\bar{\nu}$	I	Assignments
3504.25	81.41	$\nu \underline{\text{N}}(7)\text{-H}$	3504.93	71.07	$\nu \underline{\text{N}}(9)\text{-H}$
3456.38	57.90	$\nu \underline{\text{N}}(1)\text{-H}$	3453.30	57.17	$\nu \underline{\text{N}}(1)\text{-H}$
3166.94	1.92	$\nu \underline{\text{C}}(8)\text{-H}$	3164.79	0.81	$\nu \underline{\text{C}}(8)\text{-H}$
3094.40	9.96	$\nu \underline{\text{C}}(2)\text{-H}$	3099.68	7.09	$\nu \underline{\text{C}}(2)\text{-H}$
1715.00	652.68	$\nu \text{C} = \text{O}$ Rings vib. $\underline{\text{N}}(1) - \text{H}$ vib.	1735.53	612.37	$\nu \text{C} = \text{O}$ $\delta \underline{\text{N}}(1) - \text{H}$ Rings vib.
1570.21	63.05	Rings vib. $\underline{\text{C}}(2) - \text{H}$ vib. $\delta \underline{\text{N}}(1) - \text{H}$ $\nu \text{C} = \text{O}$	1561.97	88.39	Rings vib. $\underline{\text{C}}(2) - \text{H}$ vib. $\nu \text{C} = \text{O}$
1493.04	19.78	Rings vib. $\underline{\text{N}}(7) - \text{H}$ vib. $\nu \text{C} = \text{O}$	1532.08	51.49	Rings vib. $\underline{\text{N}}(9) - \text{H}$ vib. $\delta \underline{\text{C}}(8) - \text{H}$
1487.36	8.62	Rings vib. $\underline{\text{C}}(2) - \text{H}$ vib.	1466.90	20.31	Rings vib. $\underline{\text{C}}(8) - \text{H}$ vib. $\underline{\text{N}}(1) - \text{H}$ vib. $\nu \text{C} = \text{O}$
1413.32	35.74	Rings vib. $\underline{\text{C}}(8) - \text{H}$ vib. $\nu \text{C} = \text{O}$	1422.19	1.79	Rings vib. $\underline{\text{N}}(1) - \text{H}$ vib. $\underline{\text{C}}(8) - \text{H}$ vib. $\nu \text{C} = \text{O}$
1377.94	18.71	Rings vib. $\underline{\text{N}}(1) - \text{H}/\underline{\text{N}}(7) - \text{H}$ vib. $\nu \text{C} = \text{O}$	1377.46	7.40	Rings vib. $\underline{\text{N}}(1) - \text{H}$ vib. $\underline{\text{C}}(2) - \text{H}$ vib. $\delta \underline{\text{N}}(9) - \text{H}$
1360.70	28.02	Rings vib. $\underline{\text{C}}(2) - \text{H}$ vib. $\delta \underline{\text{C}}(8) - \text{H}$	1350.06	24.85	Rings vib. $\underline{\text{C}}(2) - \text{H}$ vib. $\underline{\text{N}}(9) - \text{H}$ vib. $\delta \underline{\text{N}}(1) - \text{H}$
1348.05	84.42	Rings vib. $\text{N} - \text{H}$ vib. $\nu \text{C} = \text{O}$	1329.15	34.89	Rings vib. $\underline{\text{C}}(2) - \text{H}$ vib. $\underline{\text{N}}(1) - \text{H}$ vib.

Table 6a.

K17			K19		
$\bar{\nu}$	I	Assignments	$\bar{\nu}$	I	Assignments
1305.06	18.42	Rings vib. <u>C</u> (2) – H vib. <u>N</u> (7) – H vib. ν C = O	1308.39	1.94	Rings vib. <u>C</u> (2) – H vib. <u>C</u> (8) – H/ <u>N</u> (9) – H vib. ν C = O
1246.36	1.08	Rings vib. <u>C</u> (8) – H vib.	1247.29	5.16	Rings vib. <u>C</u> (8) – H vib. <u>N</u> (9) – H vib. <u>N</u> (1) – H/ <u>C</u> (2) – H vib.
1155.14	67.99	Rings vib. <u>C</u> (8) – H vib. N – H vib.	1141.25	68.68	Rings vib. <u>C</u> (8) – H vib. N – H vib.
1078.21	5.14	Rings vib. <u>N</u> (1) – H vib.	1091.60	12.06	Rings vib. <u>N</u> (1) – H vib.
1053.17	46.20	Rings vib. <u>N</u> (7) – H vib.	1037.63	17.21	Rings vib. <u>N</u> (9) – H vib.
1031.23	7.82	Rings vib. <u>N</u> (7) – H vib. <u>C</u> (8) – H vib.	1016.49	37.00	Rings vib. <u>C</u> (2) – H vib. C = O vib.
916.17	1.46	Rings vib. <u>N</u> (7) – H vib. <u>C</u> (2) – H vib.	903.52	6.19	Rings vib. <u>N</u> (9) – H vib. <u>C</u> (8) – H vib.
865.76	10.71	<u>C</u> (2) – H vib. ^a Pirimidinic ring vib.	864.89	7.26	<u>C</u> (2) – H vib. ^a Pirimidinic ring vib.
858.11	2.07	Rings vib.	859.91	8.71	Rings vib.
793.94	21.14	<u>C</u> (8) – H vib. ^a Imidazolic ring vib.	777.05	17.35	<u>C</u> (8) – H vib. ^a Rings vib.
748.96	0.68	Rings vib. ^a <u>C</u> (8) – H vib.	742.34	13.58	<u>C</u> (8) – H vib. ^a Rings vib.
693.41	32.51	Rings vib. ^a <u>N</u> (1) – H vib. C = O vib.	694.68	45.86	<u>N</u> (1) – H vib. ^a Rings vib.
683.99	2.57	Rings vib.	673.05	10.54	Rings vib.
643.36	25.12	Rings vib. ^a N – H vib.	639.14	10.30	<u>N</u> (1) – H vib. ^a Rings vib.

Continuation of Table 6a.

K17			K19		
$\bar{\nu}$ (cm ⁻¹)	I (KM/mol)	Assignments	$\bar{\nu}$ (cm ⁻¹)	I (KM/mol)	Assignments
608.37	32.92	Rings vib. ^a N – H vib.	623.31	12.29	<u>N</u> (1) – H vib. ^a Rings vib.
584.25	5.12	Rings vib.	579.39	6.84	Rings vib. ν C = O
533.29	24.48	Rings vib. ^a <u>N</u> (1) – H vib.	535.93	96.70	<u>N</u> (9) – H vib. ^a Rings vib.
522.03	2.05	Rings vib.	511.53	9.48	Rings vib.
491.96	2.43	Rings vib.	488.21	31.79	<u>N</u> (9) – H vib. ^a Rings vib.
489.33	79.82	Imidazolic ring vib. ^a <u>N</u> (7) – H vib.	485.41	1.34	Rings vib.
290.16	15.48	Rings vib. C = O vib.	305.76	1.15	Rings vib. C = O vib.
258.66	6.95	Rings vib. ^a	249.47	0.09	Rings vib. ^a
186.49	13.19	Rings vib. ^a	197.20	19.63	Rings vib. ^a
147.64	11.35	Rings vib. ^a C = O vib.	141.33	0.82	Rings vib. ^a C = O vib.

Continuation of Table 6a.

E9c			E9t		
$\bar{\nu}$	I	Assignments	$\bar{\nu}$	I	Assignments
3533.95	74.20	ν OH	3566.66	65.61	ν OH
3510.96	80.75	ν <u>N</u> (9)-H	3510.49	81.26	ν <u>N</u> (9)-H
3160.87	0.94	ν <u>C</u> (8)-H	3163.89	0.56	ν <u>C</u> (8)-H
3097.44	18.09	ν <u>C</u> (2)-H	3096.94	19.02	ν <u>C</u> (2)-H
1608.88	137.45	Rings vib. δ COH* <u>N</u> (9) – H vib.	1598.19	131.88	Rings vib. δ COH* <u>N</u> (9) – H vib.
1564.79	198.93	Rings vib. ν C – O <u>N</u> (9) – H/ <u>C</u> (2) – H vib.	1567.81	333.92	Rings vib. <u>C</u> (2) – H vib. δ COH* <u>N</u> (9) – H vib.
1462.54	21.66	Rings vib. <u>C</u> (8) – H vib. δ COH*	1465.46	46.17	Rings vib. <u>C</u> (2) – H/ <u>C</u> (8) – H vib. δ COH* <u>N</u> (9) – H vib.
1446.78	141.67	Rings vib. δ COH* <u>C</u> (2) – H vib.	1457.33	11.85	Rings vib. <u>C</u> (2) – H/ <u>C</u> (8) – H vib. ν C – O
1389.03	38.49	Rings vib. δ COH*	1378.72	75.17	Rings vib. δ COH*
1365.26	7.66	<u>C</u> (2) – H/ <u>N</u> (9) – H vib. Rings vib. ν C – O	1369.40	0.44	Rings vib. <u>C</u> (2) – H vib. <u>N</u> (9) – H vib. δ COH*
1327.64	136.21	Rings vib. <u>N</u> (9) – H vib. δ COH*	1336.47	23.34	Rings vib. <u>N</u> (9) – H vib. δ COH*
1309.95	85.27	Rings vib. <u>C</u> (8) – H vib. δ COH*	1313.28	20.39	Rings vib. δ COH* <u>C</u> (8) – H vib.
1296.65	12.64	Rings vib. <u>C</u> (2) – H vib. <u>N</u> (9) – H vib. δ COH*	1292.27	67.04	Rings vib. <u>C</u> (2) – H/ <u>N</u> (9) – H/ <u>C</u> (8) – H vib. δ COH

Table 6b.

E9c			E9t		
$\bar{\nu}$	I	Assignments	$\bar{\nu}$	I	Assignments
1264.27	17.75	Rings vib. δ COH* <u>N</u> (9) – H vib.	1266.70	216.37	Rings vib. δ COH*
1218.05	22.29	Rings vib. <u>C</u> (8) – H vib. <u>N</u> (9) – H vib. ν C – O	1215.99	15.72	Rings vib. <u>C</u> (8) – H/ <u>N</u> (9) – H vib. ν C – O
1106.41	5.26	Rings vib. <u>C</u> (8) – H vib. δ COH*	1114.58	49.17	Rings vib. <u>C</u> (8) – H vib. δ COH*
1060.47	176.47	Rings vib. δ COH* <u>C</u> (8) – H vib.	1073.91	21.35	Rings vib. δ COH* <u>C</u> (8) – H vib.
1037.85	10.08	Rings vib. <u>N</u> (9) – H vib.	1043.07	16.43	Rings vib. <u>N</u> (9) – H vib. δ COH
911.04	8.52	<u>C</u> (2)-H vib. ^a	916.12	6.51	<u>C</u> (2) – H vib. ^a Pirimidinic ring vib.
899.27	15.61	Rings vib. ν C – O <u>C</u> (2) – H vib.	900.51	14.43	Rings vib. ν C – O
857.16	13.69	Rings vib. ν C – O	850.04	17.43	Rings vib. ν C – O
798.63	10.50	<u>C</u> (8) – H vib. ^a Rings vib.	794.36	10.19	<u>C</u> (8) – H vib. ^a Rings vib.
762.47	17.04	<u>C</u> (8) – H vib. ^a Rings vib.	763.18	15.84	<u>C</u> (8) – H vib. ^a Rings vib.
698.50	1.83	Rings vib. δ COH*	702.56	2.15	Rings vib. ν C – O
656.62	21.31	Rings vib. ^a δ COH*	648.69	4.49	Rings vib. ^a ν C – O <u>C</u> (8) – H vib.
639.18	6.35	Rings vib. ^a δ OH	635.10	1.71	Rings vib. ^a

Continuation of Table 6b.

E9c			E9t		
$\bar{\nu}$	I	Assignments	$\bar{\nu}$	I	Assignments
590.06	1.36	Rings vib.	603.52	9.70	Rings vib.
555.77	15.00	Rings vib. ^a N(9) – H vib. OH vib.	552.65	47.85	Rings vib. ^a N(9) – H vib.
550.58	118.61	OH vib. ^a Rings vib.	536.63	110.13	O-H vib. ^a
510.21	8.49	Rings vib.	518.71	17.26	Pirimidinic ring vib.
506.53	0.79	Rings vib.	507.61	0.41	Pirimidinic ring vib.
482.84	59.87	N(9) – H vib. ^a Rings vib. δ OH	487.53	73.18	N(9) – H vib. ^a Rings vib.
287.95	12.60	Rings vib. ν COH	286.53	0.49	Rings vib. ^a
284.43	0.45	Rings vib. ^a	269.16	7.53	Pirimidinic ring vib.
207.89	14.10	Rings vib. ^a OH vib.	205.95	1.53	Rings vib. ^a δ OH
154.44	2.96	Rings vib. ^a δ COH*	157.82	3.01	Rings vib. ^a δ COH*

Continuation of Table 6b.

K37			E7c		
$\bar{\nu}$	I	Assignments	$\bar{\nu}$	I	Assignments
3507.39	93.10	ν <u>N</u> (7)-H	3539.33	73.74	ν OH
3486.52	76.92	ν <u>N</u> (3)-H	3514.50	75.52	ν <u>N</u> (7)-H
3176.36	1.46	ν <u>C</u> (8)-H	3159.87	1.79	ν <u>C</u> (8)-H
3071.50	21.16	ν <u>C</u> (2)-H	3095.04	21.27	ν <u>C</u> (2)-H
1665.85	551.26	ν C = O Pirimidinic ring vib.	1636.47	137.29	Rings vib. δ COH*
1594.62	87.97	Pirimidinic ring vib. ν C = O	1532.92	231.41	Rings vib. δ COH*
1543.23	62.56	Rings vib. <u>N</u> (3) - H vib. <u>N</u> (7) - H vib. ν C = O	1468.34	55.48	Rings vib. <u>C</u> (8) - H/ <u>N</u> (7) - H vib. δ COH <u>C</u> (2) - H vib.
1500.05	85.81	Rings vib. <u>C</u> (2) - H vib.	1453.02	15.21	Rings vib. <u>C</u> (2) - H vib. ν C - O
1422.43	50.39	Rings vib. <u>C</u> (8) - H vib. <u>N</u> (3) - H vib.	1368.29	86.33	Rings vib. <u>N</u> (7) - H vib. δ COH* <u>C</u> (2) - H vib.
1399.32	82.81	Rings vib. <u>N</u> (7) - H/ <u>N</u> (3) - H vib.	1355.28	143.05	Rings vib. <u>C</u> (8) - H vib. δ COH*
1358.65	23.92	Rings vib. <u>C</u> (2) - H vib.	1338.38	54.50	Rings vib. <u>C</u> (2) - H/ <u>C</u> (8) - H vib. ν C - O
1328.31	11.64	Rings vib. <u>N</u> (7) - H/ <u>N</u> (3) - H vib.	1318.74	36.00	Rings vib. <u>C</u> (2) - H vib. δ COH* <u>N</u> (7) - H/ <u>C</u> (8) - H vib.
1299.82	7.34	Rings vib. <u>C</u> (2) - H/ <u>N</u> (3) - H vib.	1284.26	2.23	Rings vib. δ COH* C - H vib.
1244.80	16.21	Rings vib. <u>C</u> (8) - H/ <u>N</u> (3) - H vib.	1259.98	51.12	Rings vib. δ COH*

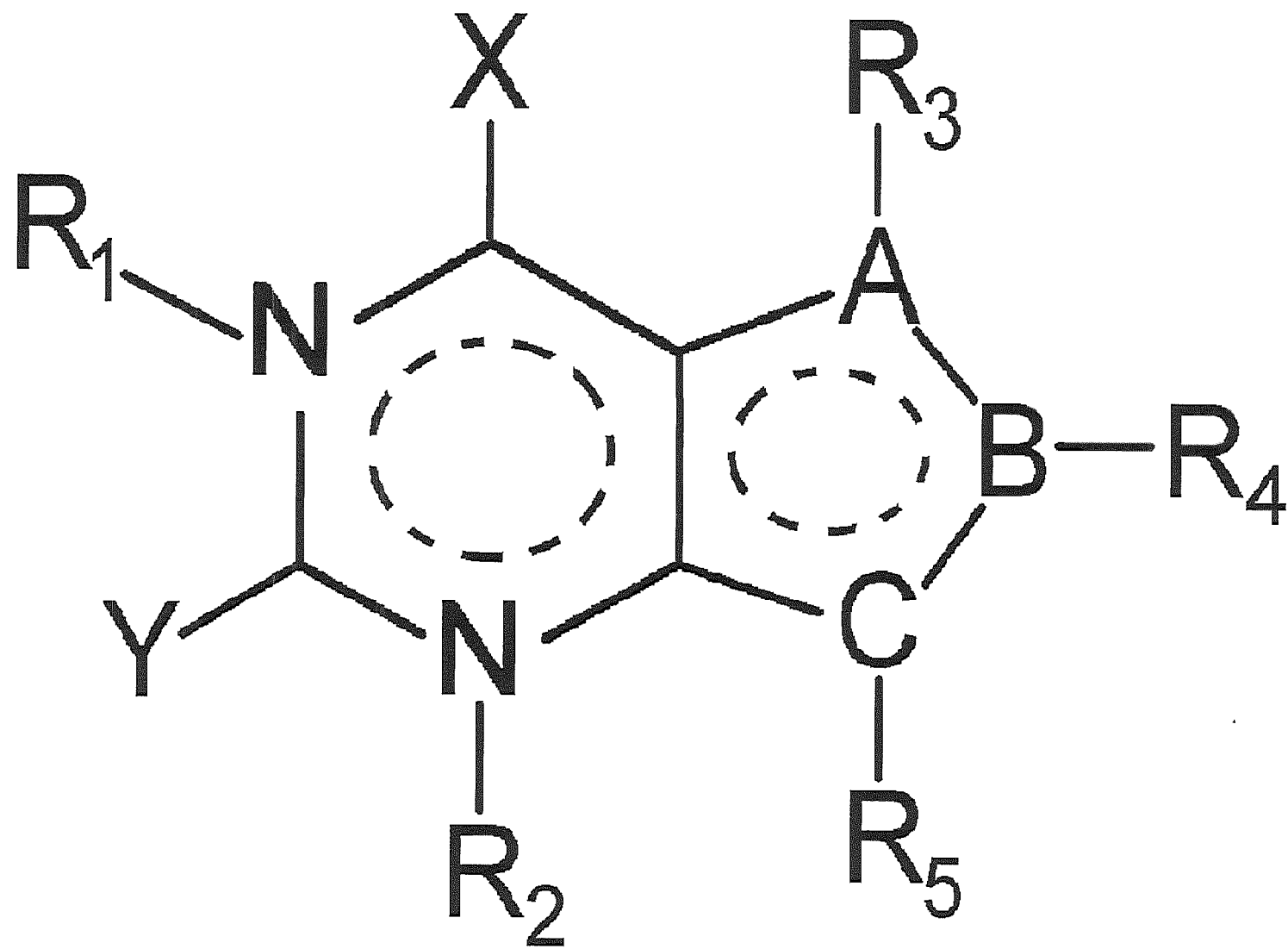
Table 6c.

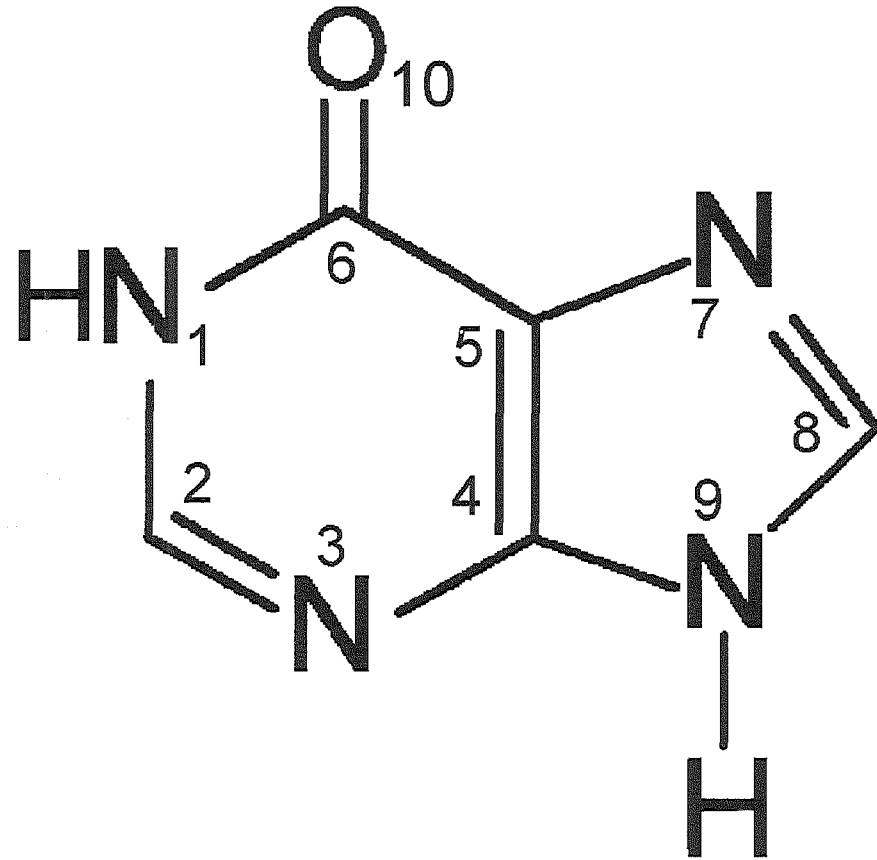
K37			E7c		
$\bar{\nu}$	I	Assignments	$\bar{\nu}$	I	Assignments
1160.29	23.37	Rings vib. $\underline{\text{C}}(8) - \text{H}/\underline{\text{N}}(7) - \text{H}$ vib.	1211.02	32.13	Rings vib. $\underline{\text{C}}(8) - \text{H}/\underline{\text{N}}(7) - \text{H}$ vib. δ COH*
1081.10	27.79	Rings vib. $\underline{\text{N}}(7) - \text{H}/\underline{\text{N}}(3) - \text{H}$ vib.	1108.34	15.42	Rings vib. δ COH*
1049.79	18.26	Rings vib. $\underline{\text{N}}(7) - \text{H}$ vib.	1063.41	69.39	Rings vib. $\underline{\text{N}}(7) - \text{H}$ vib. δ COH*
998.61	43.67	Rings vib. $\underline{\text{N}}(7) - \text{H}$ vib.	1029.02	117.08	Rings vib. $\underline{\text{N}}(7) - \text{H}/\underline{\text{C}}(8) - \text{H}$ vib. δ COH*
921.14	5.33	Rings vib.	914.07	9.55	$\underline{\text{C}}(2)$ -H vib. ^a
881.73	11.89	$\underline{\text{C}}(2)$ -H vib. ^a	907.56	2.66	Rings vib.
863.36	1.51	Rings vib.	849.18	18.09	Rings vib. ν C - O
775.49	26.41	$\underline{\text{C}}(8)$ -H vib. ^a	812.08	23.62	$\underline{\text{C}}(8)$ -H vib. ^a
749.26	0.39	$\underline{\text{C}}(8) - \text{H}$ vib. ^a Rings vib.	767.20	4.11	$\underline{\text{C}}(8) - \text{H}$ vib. ^a Rings vib.
688.44	3.45	Rings vib.	700.15	1.58	Rings vib. ν C - O
674.33	2.83	Rings vib. ^a	663.68	7.77	Rings vib. ^a
628.42	7.72	$\underline{\text{N}}(7) - \text{H}$ vib. ^a Rings vib.	613.38	5.25	Rings vib. ^a $\underline{\text{N}}(7) - \text{H}$ vib. δ OH
601.59	1.14	Rings vib.	589.37	0.73	Rings vib.
553.09	26.37	$\underline{\text{N}}(3)$ -H vib. ^a	559.04	0.12	$\underline{\text{C}}(2) - \text{H}$ vib. ^a Rings vib.
521.42	121.52	$\underline{\text{N}}(7)$ -H vib. ^a	521.33	0.30	Rings vib.
506.37	3.51	Pirimidinic ring vib.	521.10	118.68	δ OH/ ν OH ^a Imidazolic ring vib.
485.18	3.89	Pirimidinic ring vib.	503.82	0.55	Pirimidinic ring vib.

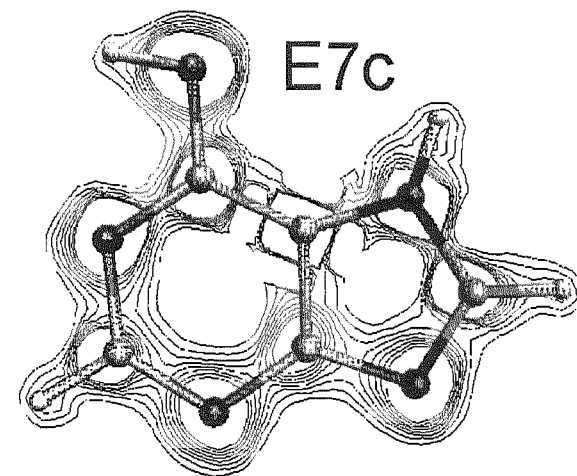
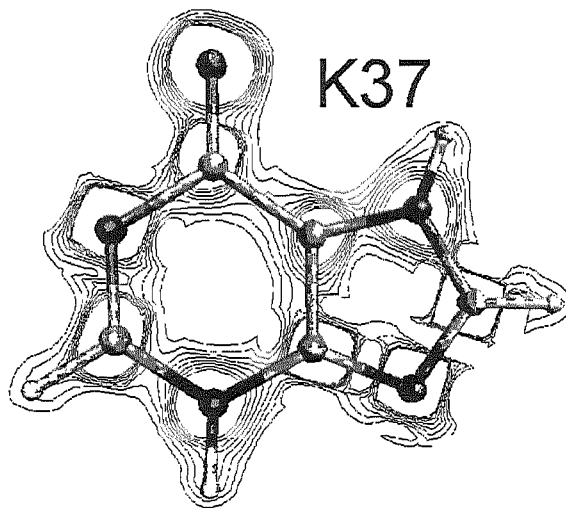
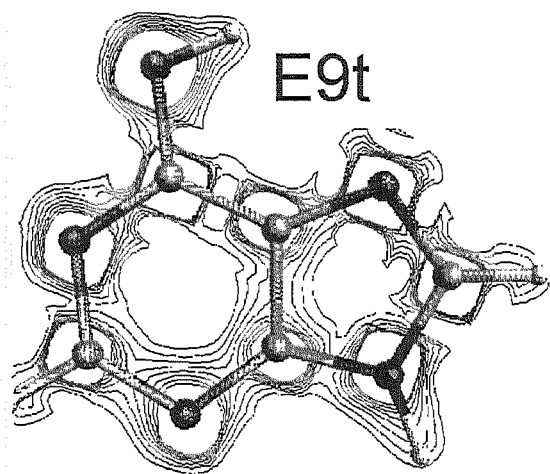
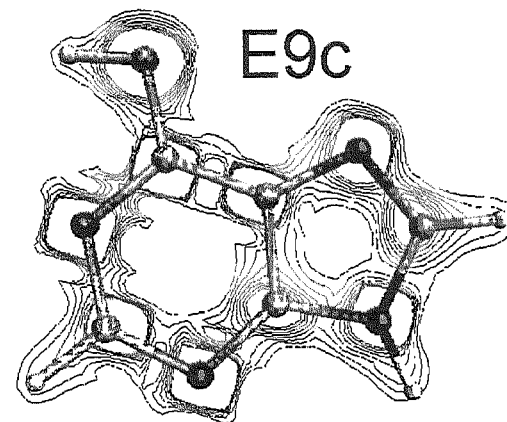
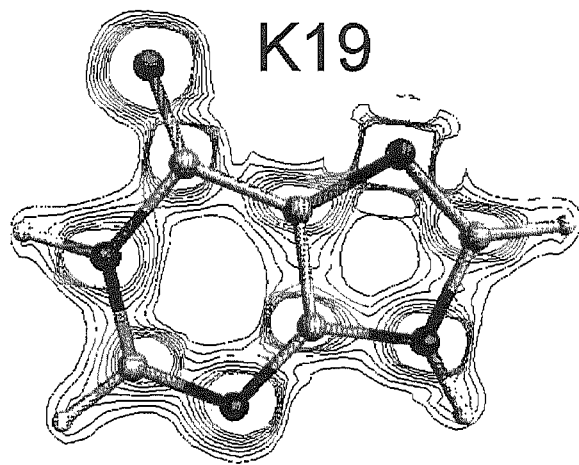
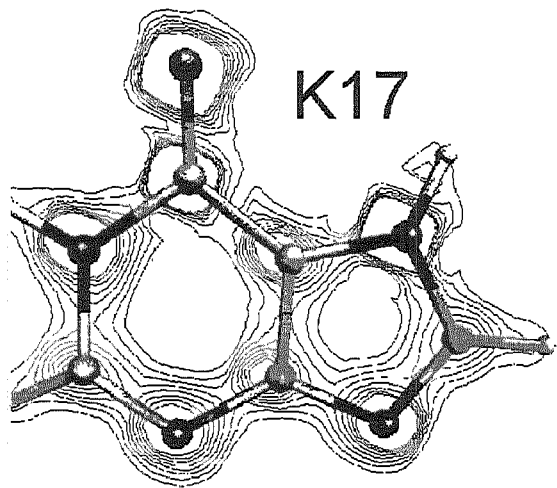
Continuation of Table 6c.

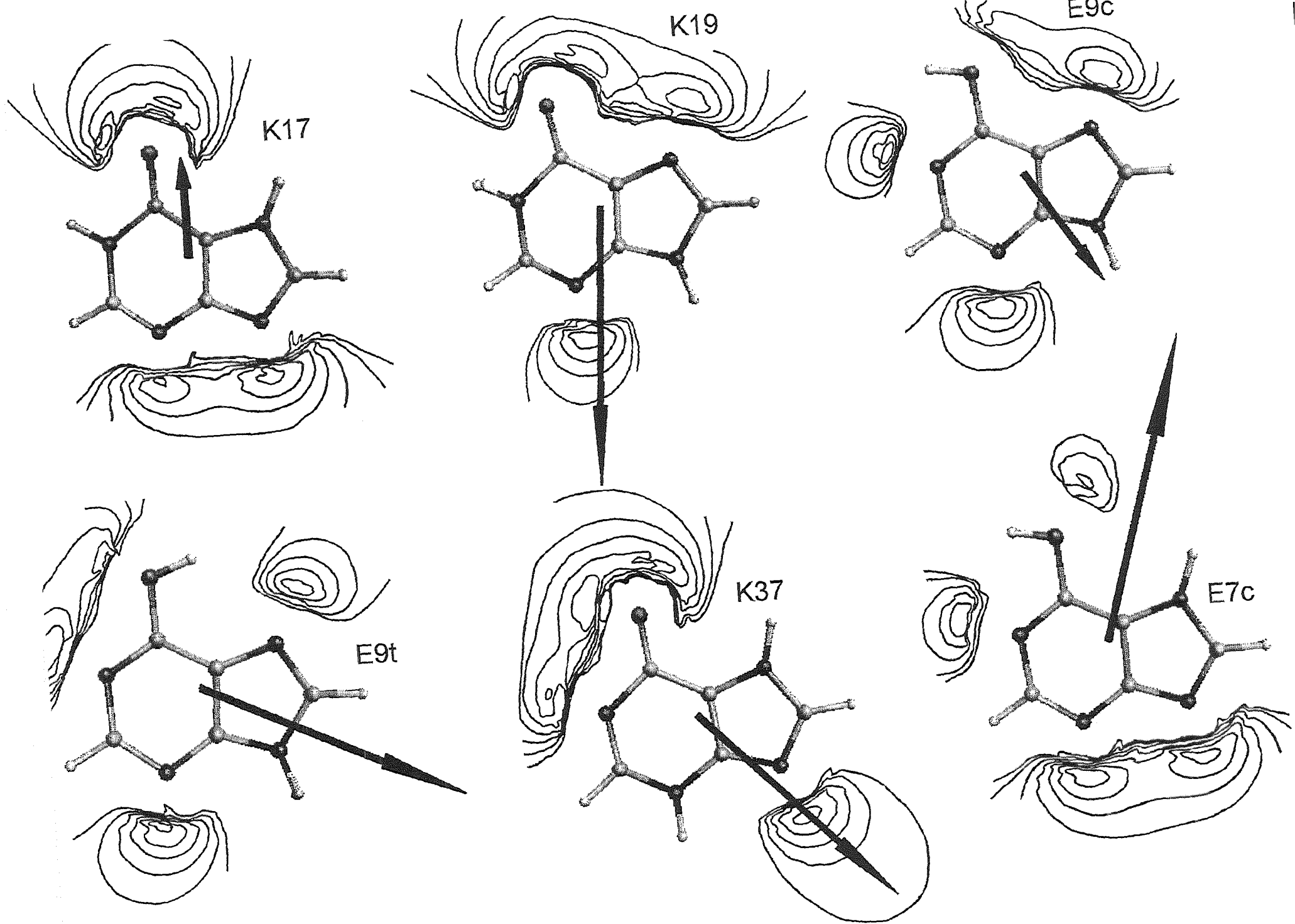
K37			E7c		
$\bar{\nu}$	I	Assignments	$\bar{\nu}$	I	Assignments
429.79	38.94	$\underline{\text{N}}(3) - \text{H}$ vib. ^a Rings vib.	425.56	88.26	$\underline{\text{N}}(7) - \text{H}$ vib. ^a Imidazolic ring vib. δ OH
287.24	21.91	Rings vib. ^a	288.08	4.49	Rings vib.
285.49	14.88	Pirimidinic ring vib. ν C = O	279.07	12.57	Rings vib. δ C - O
166.74	0.21	Rings vib. ^a	202.52	7.89	Rings vib. ^a δ OH
124.48	3.86	δ C = O ^a Rings vib.	156.56	3.01	Rings vib. ^a $\underline{\text{N}}(7) - \text{H}$ vib. δ COH

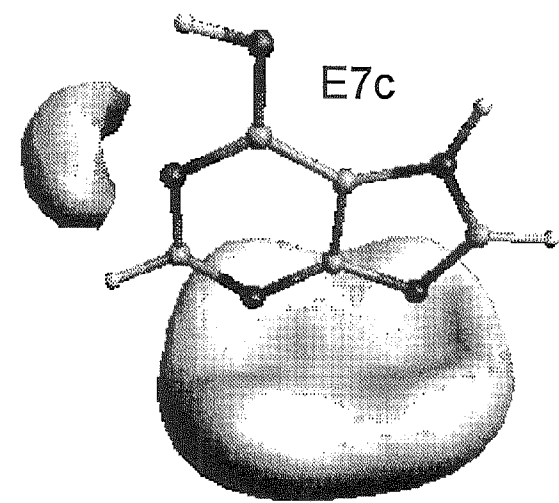
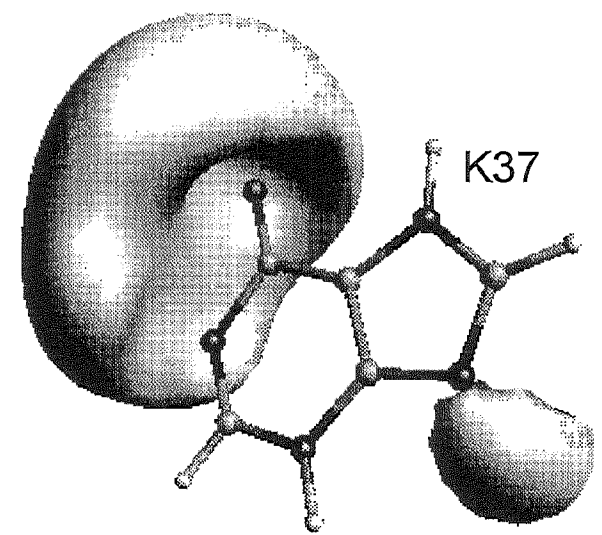
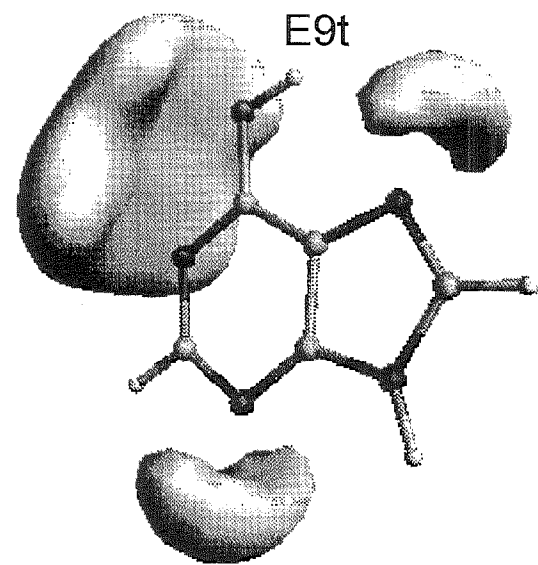
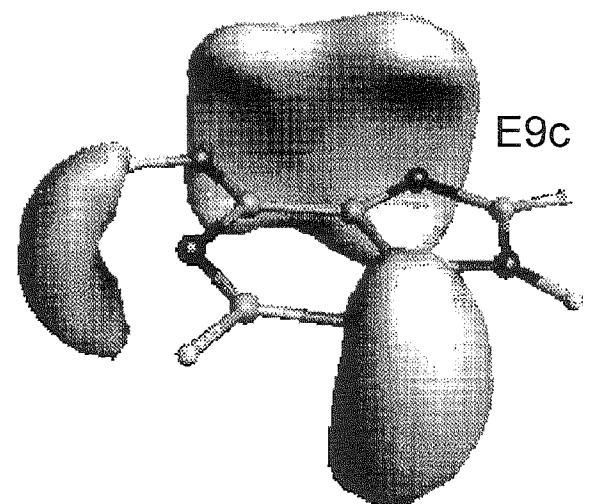
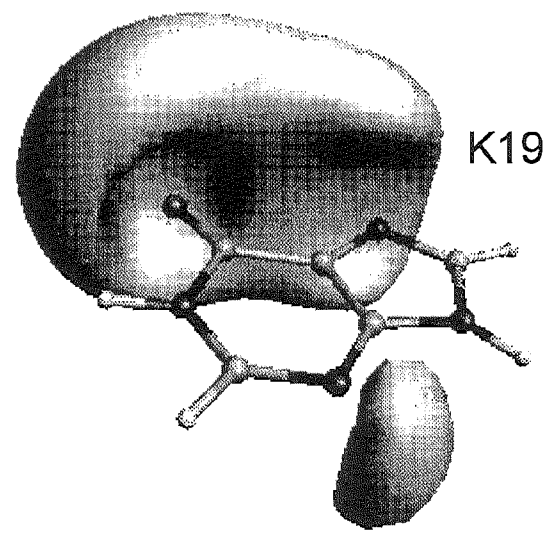
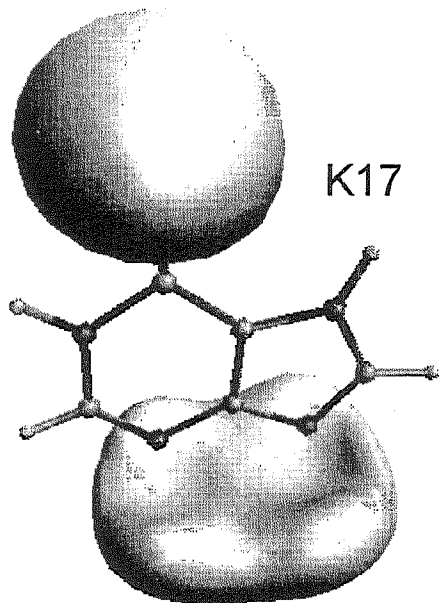
Continuation of Table 6c.

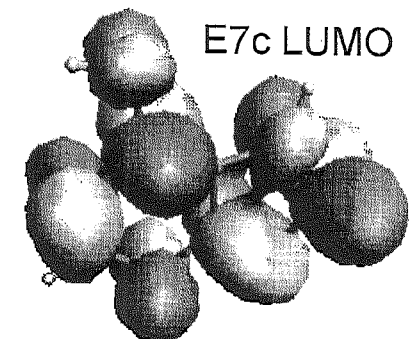
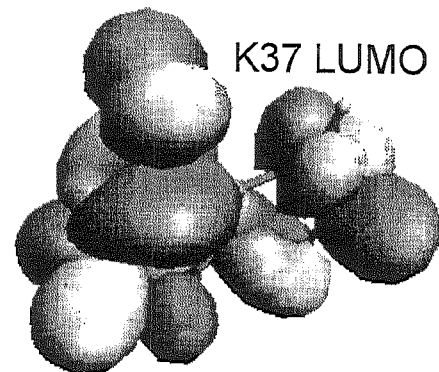
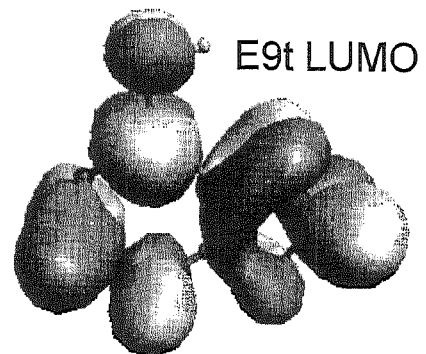
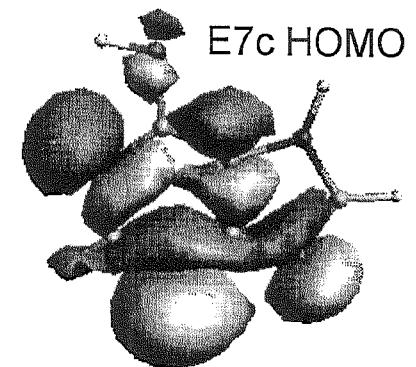
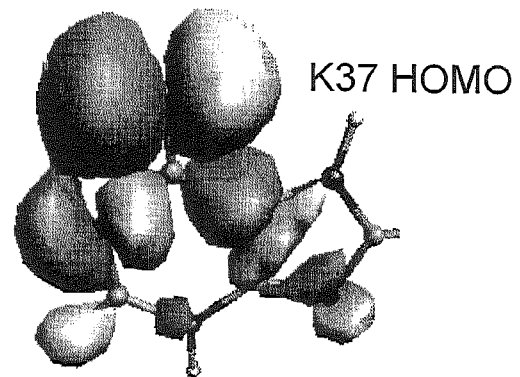
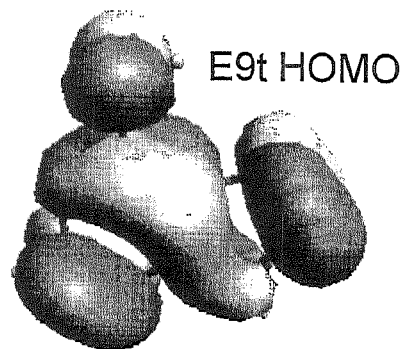
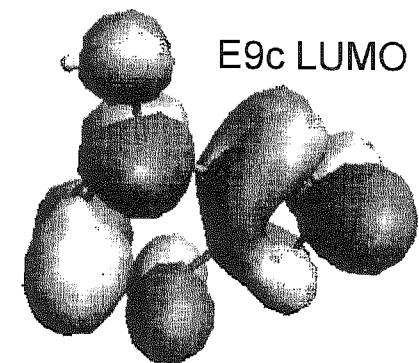
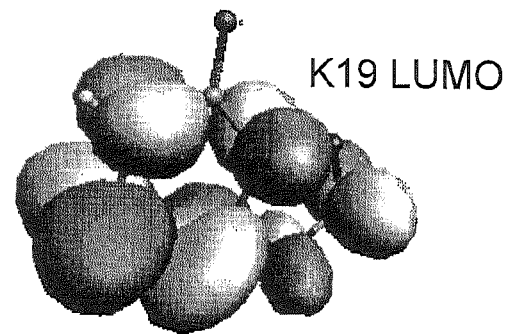
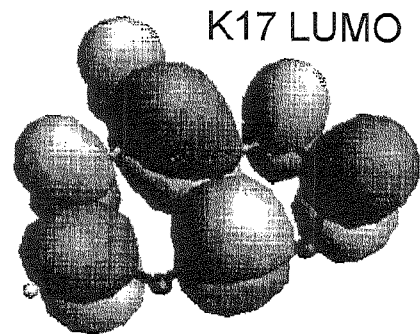
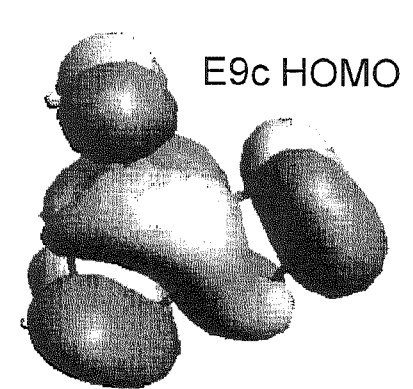
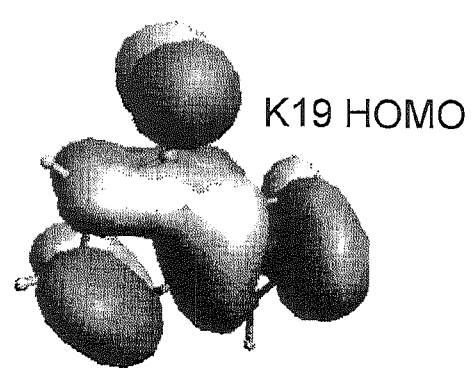
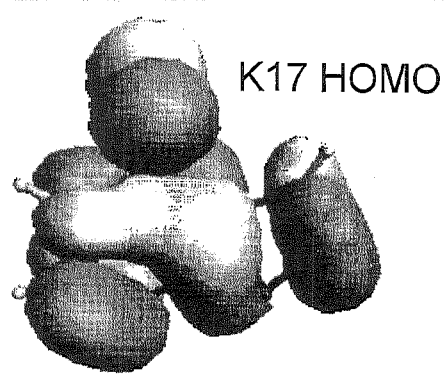


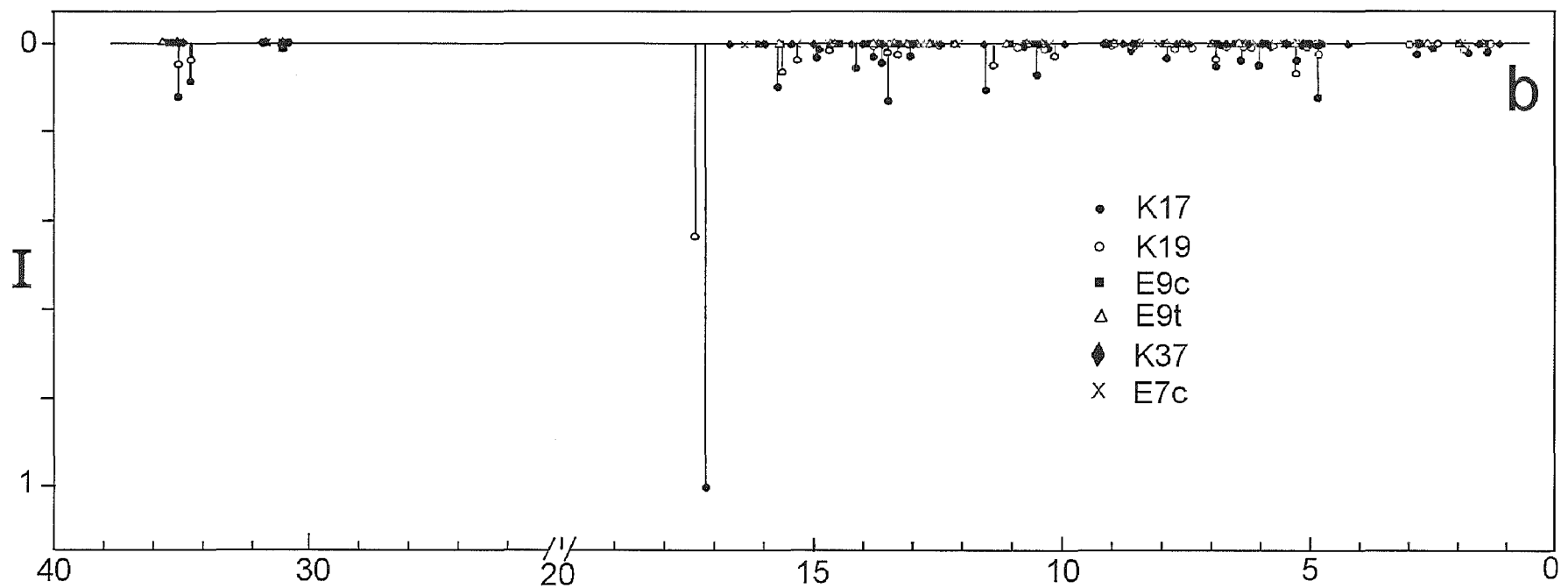
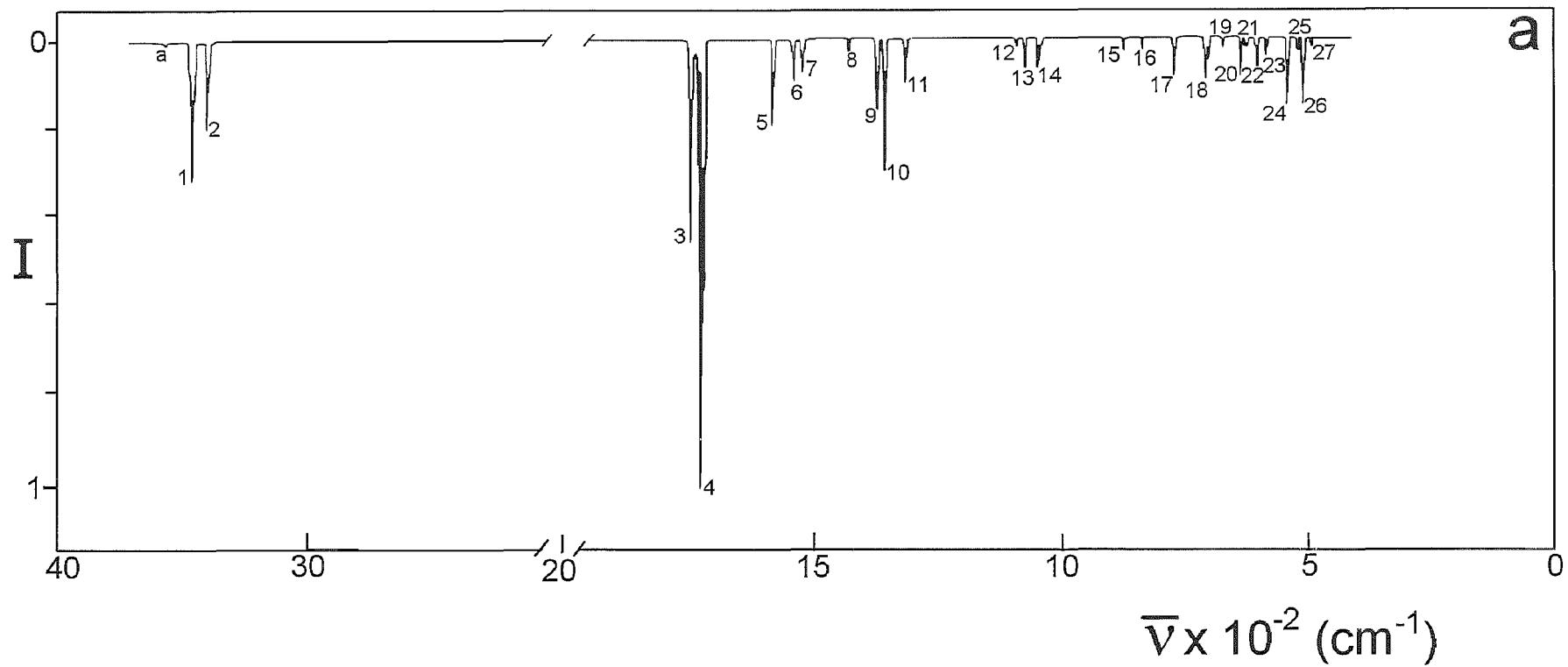












La impresión de esta edición
ha sido limitada a 15 ejemplares.